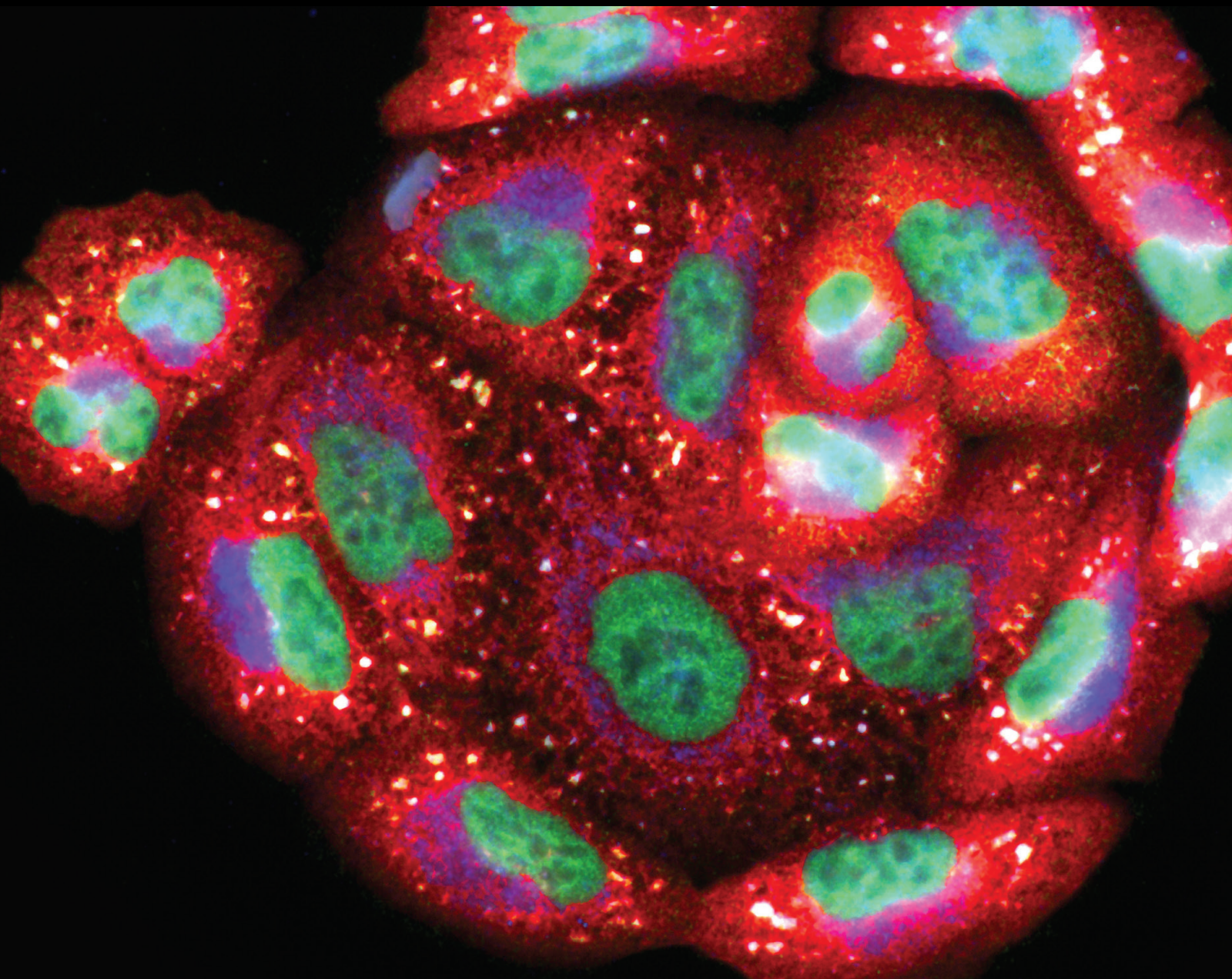# New Molecules and Mechanisms to Fight the Onset and Progression of Cardiovascular Diseases

Lead Guest Editor: Albino Carrizzo
Guest Editors: Ciccarelli Michele and Gaetano Santulli

New Molecules and Mechanisms to Fight the Onset and Progression of Cardiovascular Diseases

New Molecules and Mechanisms to Fight the Onset and Progression of Cardiovascular Diseases

Lead Guest Editor: Albino Carrizzo
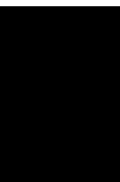Guest Editors: Ciccarelli Michele and Gaetano Santulli

Chief Editor

Jeannette Vasquez-Vivar, USA

Tim Hofer, Norway
John D. Horowitz, Australia
Silvana Hrelia, Italy
Dragan Hrncic, Serbia
Zebo Huang, China
Zhao Huang, China
Tarique Hussain, Pakistan
Stephan Immenschuh, Germany
Norsharina Ismail, Malaysia
Franco J. L, Brazil
Sedat Kacar, USA
Andleeb Khan, Saudi Arabia
Kum Kum Khanna, Australia
Neelam Khaper, Canada
Ramoji Kosuru, USA
Demetrios Kouretas, Greece
Andrey V. Kozlov, Austria
Chan-Yen Kuo, Taiwan
Gaocai Li, China
Guoping Li, USA
Jin-Long Li, China
Qiangqiang Li, China
Xin-Feng Li, China
Jialiang Liang, China
Adam Lightfoot, United Kingdom
Christopher Horst Lillig, Germany
Paloma B. Liton, USA
Ana Lloret, Spain
Lorenzo Loffredo, Italy
Camilo López-Alarcón, Chile
Daniel Lopez-Malo, Spain
Massimo Lucarini, Italy
Hai-Chun Ma, China
Nageswara Madamanchi, USA
Kenneth Maiese, USA
Marco Malaguti, Italy
Steven McAnulty, USA
Antonio Desmond McCarthy, Argentina
Sonia Medina-Escudero, Spain
Pedro Mena, Italy
Víctor M. Mendoza-Núñez, Mexico
Lidija Milkovic, Croatia
Alexandra Miller, USA
Sara Missaglia, Italy

Premysl Mladenka, Czech Republic
Sandra Moreno, Italy
Trevor A. Mori, Australia
Fabiana Morroni, Italy
Ange Mouithys-Mickalad, Belgium
Iordanis Mourouzis, Greece
Ryoji Nagai, Japan
Amit Kumar Nayak, India
Abderrahim Nemmar, United Arab Emirates
Xing Niu, China
Cristina Nocella, Italy
Susana Novella, Spain
Hassan Obied, Australia
Pál Pacher, USA
Pasquale Pagliaro, Italy
Dilipkumar Pal, India
Valentina Pallottini, Italy
Swapnil Pandey, USA
Mayur Parmar, USA
Vassilis Paschalis, Greece
Keshav Raj Paudel, Australia
Ilaria Peluso, Italy
Tiziana Persichini, Italy
Shazib Pervaiz, Singapore
Abdul Rehman Phull, Republic of Korea
Vincent Pialoux, France
Alessandro Poggi, Italy
Zsolt Radak, Hungary
Dario C. Ramirez, Argentina
Erika Ramos-Tovar, Mexico
Sid D. Ray, USA
Muneeb Rehman, Saudi Arabia
Hamid Reza Rezvani, France
Alessandra Ricelli, Italy
Francisco J. Romero, Spain
Joan Roselló-Catafau, Spain
Subhadeep Roy, India
Josep V. Rubert, The Netherlands
Sumbal Saba, Brazil
Kunihiro Sakuma, Japan
Gabriele Saretzki, United Kingdom
Luciano Saso, Italy
Nadja Schroder, Brazil

Contents

Contents

Hindawi

Research Article

Paricalcitol Attenuates Metabolic Syndrome-Associated Heart Failure through Enhanced Mitochondrial Fusion

Hina L. Nizami [ID],[1] **Parmeshwar B. Katare,**[1] **Pankaj Prabhakar** [ID],[2] **Ramu Adela,**[3] **Soumalya Sarkar,**[1] **Sudheer Arava,**[4] **Praloy Chakraborty,**[5] **Subir K. Maulik,**[2] **and Sanjay K. Banerjee** [ID][1,6]

[1]*Non-Communicable Disease Group, Translational Health Science and Technology Institute (THSTI), Faridabad 121001, India*
[2]*Department of Pharmacology, All India Institute of Medical Science (AIIMS), New Delhi 110029, India*
[3]*Department of Endocrinology, All India Institute of Medical Science (AIIMS), New Delhi 110029, India*
[4]*Department of Pathology, All India Institute of Medical Science (AIIMS), New Delhi 110029, India*
[5]*Cardiology Department, VMMC and Safdarjung Hospital, New Delhi 110029, India*
[6]*Department of Biotechnology, National Institute of Pharmaceutical Education and Research, Guwahati 781101, India*

Correspondence should be addressed to Sanjay K. Banerjee; sanjayk.banerjee@niperguwahati.ac.in

Objectives. Transition from cardiac hypertrophy to failure involves adverse metabolic reprogramming involving mitochondrial dysfunction. We have earlier shown that vitamin D deficiency induces heart failure, at least in part, through insulin resistance. However, whether activation of vitamin D receptor (VDR) can attenuate heart failure and underlying metabolic phenotype requires investigation. Thus, we aimed to assess the cardioprotective potential of paricalcitol, a vitamin D receptor-activator, against cardiac hypertrophy and failure in high-fat high-fructose-fed rats. *Methods.* Male Sprague Dawley rats were fed control (Con) or high-fat high-fructose (HFHFrD) diet for 20 weeks. After 12 weeks, rats from HFHFrD group were divided into the following: HFHFrD, HFHFrD+P (paricalcitol *i.p.* 0.08 μg/kg/day) and HFHFrD+E (enalapril maleate *i.p.* 10 mg/kg/day). Intraperitoneal glucose tolerance test, blood pressure measurement, and 2D echocardiography were performed. Cardiac fibrosis was assessed by Masson's trichrome staining of paraffin-embedded heart sections. Mitochondrial DNA and proteins, and citrate synthase activity were measured in rat hearts. VDR was silenced in H9c2 cardiomyoblasts, and immunoblotting was performed. *Results.* Paricalcitol improved glucose tolerance, serum lipid profile, and blood pressure in high-fat high-fructose-fed rats. Paricalcitol reduced cardiac wall thickness and increased ejection fraction in high-fat high-fructose-fed rats but had no effect on perivascular fibrosis. PGC1-α was upregulated in the HFHFrD+P group compared to the HFHFrD group, but there was no significant difference in mitochondrial content. Citrate synthase activity was significantly higher in the HFHFrD+P group compared to the HFHFrD group. Rat hearts of the HFHFrD+P group had significantly higher expression of mitofusins. H9c2 cells with VDR knockdown showed significantly lower expression of Mfn2. Improvement in the HFHFrD+P group was comparable with that in the HFHFrD+E group. *Conclusions.* Paricalcitol reverses cardiac dysfunction in rats with metabolic syndrome by enhancing mitochondrial fusion. We demonstrate repurposing potential of the drug currently used in end-stage kidney disease.

1. Introduction

Heart failure is a public health problem with persistently rising prevalence due to increase in ageing population [1]. Maladaptive cardiac remodeling, in response to injury or comorbid conditions such as diabetes and hypertension, and ventricular dilatation, and impaired contractility constitute systolic heart failure [2]. Its diagnosis is clinically confirmed by echocardiographic observation of impaired myocardial and valvular structure and function. Treatment

options include pharmacologic therapy, implantable devices, lifestyle changes, and surgery. Drug therapy is mainly aimed at relief of symptoms (e.g., diuretics) and improvement of residual cardiac function (e.g., ACE inhibitors, beta blockers, and aldosterone antagonists). Heart failure often coexists with other morbidities such as metabolic syndrome, renal impairment, and anemia, which further complicates the treatment.

We have earlier shown vitamin D deficiency is associated with increased prevalence of type 2 diabetes both with and without coexisting coronary artery disease, both important risk factors for heart failure [3]. We have also demonstrated the role of vitamin D deficiency as an independent risk factor for cardiac hypertrophy and heart failure in rats, through induction of myocardial insulin resistance [4]. In experimental and clinical studies, respectively, VDR knockdown or vitamin D deficiency is associated with remarkable cardiac hypertrophy, activation of the renin angiotensin system, cardiac dysfunction, and failure [5, 6]. However, experimental and clinical reports of vitamin D supplementation yield contradicting data about possible benefits [7, 8]. Reduced activation of vitamin D due to hepatic or renal dysfunction and sequestering of vitamin D in fat stores in obesity are some possible reasons for the loss of beneficial effects in disease, and hence, synthetic, nonhypercalcemic analogues might be preferable alternatives [9, 10]. Paricalcitol is an FDA-approved drug used in the management of end-stage kidney disease and has shown cardiorenal benefits in various experimental models [11, 12].

Though heart failure is essentially a decompensated state of cardiac muscle contractility, it is also marked by deficits in cardiac bioenergetics. Energy transduction in the heart depends majorly on oxidative phosphorylation in the mitochondria; excessive fatty acid oxidation in the absence of glucose leads to respiratory uncoupling and oxidative stress [13]. Mitochondrial dynamics are under control of processes such as fusion, fission, and biogenesis, and insulin is known to directly promote mitochondrial fusion through optic atrophy protein 1 (OPA1) [14]. Myocardial insulin resistance and mitochondrial dysfunction have been shown to be involved in the transition of heart from diastolic dysfunction to systolic failure in a model of pressure overload-hypertrophy in rats [15]. Successful use of therapies such as trimetazidine, omega-3 fatty acid, and perhexiline indicates that metabolic modulation might be an attractive therapeutic strategy to manage the development and progression of heart failure [16, 17].

Vitamin D receptor is a nuclear receptor conventionally known to be involved in transcription of target genes involved in calcium absorption and bone formation. However, the pleiotropic extraskeletal effects of VDR are under investigation in various tissues [18, 19]. Vitamin D has been shown to favourably affect metabolic functions such as insulin signalling and lipid metabolism in both experimental and clinical samples [20–22]. High circulating level of free fatty acidscan contribute to both insulin resistance and mitochondrial dysfunction. Regulation of mitochondrial structure, content, and bioenergetics by 1,25-OH vitamin D3 has been reported in peripheral blood mononuclear cells, adipocytes,

skeletal muscle, and various cancer cell lines [23–26]. In homocysteine-treated rat heart slices, treatment with vitamin D3 improved mitochondrial function and redox status [27]. However, the possible effect of VDR modulation on myocardial mitochondrial dynamics in metabolic syndrome-associated cardiac failure requires investigation.

We aimed to investigate the therapeutic potential of paricalcitol in cardiac dysfunction in rats with metabolic syndrome, through its possible effect on cardiac mitochondrial dynamics. Animals were fed high-fat high-fructose diet and treated with paricalcitol, and cardiometabolic outcomes were assessed. Since renin angiotensin system blockade has known clinical benefit against cardiac remodeling and failure, enalapril was used as the standard therapy in a group of high-fat high-fructose fed rats.

2. Research Designs and Methods

2.1. Animals. Male Sprague Dawley rats (200-220 g) were procured from All India Institute of Medical Sciences, New Delhi, and maintained in Small Animal facility of THSTI, Faridabad. Rats were provided food and water *ad libitum* throughout the study period, with the exception of the 12-hour fasting period preceding blood sample withdrawal and intraperitoneal glucose tolerance test. All experimental procedures involving animals were performed according to the relevant regulations and guidelines of Institutional Animal Ethical Committee (IAEC) of Translational Health Science and Technology Institute, Faridabad (IAEC/THSTI/2015-3).

2.2. Materials. Paricalcitol was purchased from Cayman Chemical Company (#17716). Enalapril maleate was procured from LKT Labs (#E5201). Antibodies against VDR (ab3508; 1 : 500), PGC1-α (ab54481; 1 : 1000), MFN1 (ab57602; 1 : 1000), and MFN2 (ab137037; 1 : 1000) were purchased from Abcam.

2.3. In Vivo Study Design and Drug Treatment. Control (65% corn starch diet; Cat. No. D11708B) and high-fat high-fructose (45% kcal% fat and 35% kcal% fructose; Cat. No. D08040105G) diets were purchased from Research Diets, USA. After an acclimatization period of one week, rats were randomized into two groups and were fed either control diet (CON) or high-fat high-fructose diet (HFHFrD) for 20 weeks. At the end of 12 weeks, intraperitoneal glucose tolerance test and echocardiography were performed, and rats from the HFHFrD group were further divided into three groups: HFHFrD, HFHFrD+P (paricalcitol *i.p.* 0.08 μg/kg/day), and HFHFrD+E (enalapril maleate *i.p.* 10 mg/kg/day). The experimental design is illustrated in Figure 1. At the end of the remaining 8 weeks, rats from all the groups were sacrificed; serum samples and heart tissues were collected and stored at a -80°C refrigerator for further analysis. Experimental methods have been adapted from our previously published work [4].

2.4. Intraperitoneal Glucose Tolerance Test. At the end of 12 and 20 weeks, after an overnight fasting period, rats were given an intraperitoneal bolus injection of glucose (2 g/kg *BW*). Blood glucose sampling was performed at 0 (just
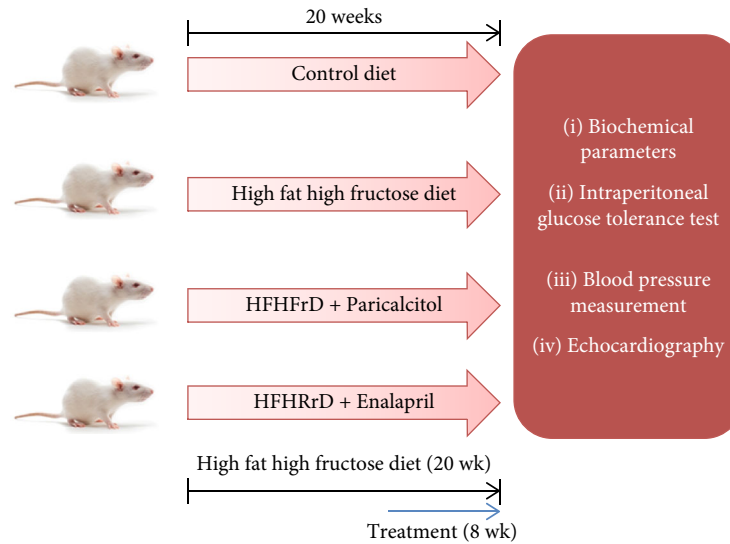
FIGURE 1: Schematic representation of experimental animal study design.

before), 15, 30, 60, and 120 minutes post glucose administration, using a commercially available blood glucose measurement system (OneTouch Select Plus, Johnson & Johnson).

2.5. Serum Biochemistry. Insulin (Crystal Chem, USA), triglycerides (BioVision, USA), HDL cholesterol (BioVision, USA), and free fatty acids (BioVision, USA) were measured in rat serum samples using commercially available assay kits.

2.6. Noninvasive Blood Pressure Measurement. Blood pressure was evaluated at the end of the study (20 weeks) using the Non-Invasive Blood Pressure System (Harvard Apparatus), complying with manufacturer's protocol. Animals were trained daily in restrainers for 4 days prior to experimental data recording. To record blood pressure, a tail cuff and sensor were placed about 2 cm from the tip of the animal's tail, and blood pressure was recorded. Five individual measurements were made and analysed as mean for each animal.

2.7. Echocardiography. Echocardiography was performed after the completion of 12 and 20 weeks. Rats were anesthetized using a cocktail of ketamine (80 mg/kg BW *i.p.*) and xylazine (8 mg/kg BW *i.p.*). Two-dimensional and M-mode echocardiograms were obtained using a fully digitized instrument (HD11 XE, Philips) with a hand-held 12 MHz neonatal cardiac probe transducer placed at a short axis view at the level of the papillary muscles of the left ventricle. Diastolic left ventricular posterior wall (LVPW) and intraventricular septum (IVS) thicknesses were recorded. Left ventricular internal diastolic dimension (LVIDd) and LV internal systolic dimension (LVIDs) were also recorded. Fractional shortening and ejection fraction values were derived from the dimensions recorded above. Image acquisition and analysis were performed by an analyst blind to the experimental groups.

2.8. Cardiac Hypertrophy Measurement. Heart weight-to-tail length ratio of rats was used to evaluate cardiac hypertrophy. Briefly, at the end of 20 weeks, animals from all groups were sacrificed, hearts were isolated, rinsed in ice-cold PBS, and

blotted, and their weight was measured. The ratio of heart weight and tail length was calculated and expressed in gcm^{-1}.

2.9. Histopathology. At the end of 20 weeks, the heart tissue was harvested and fixed in phosphate-buffered formalin (10%). Fixed samples were embedded in paraffin and sectioned for histopathological analysis. Sections of 5 μm thickness were stained with haematoxylin-eosin (H&E) and Masson's trichrome stains and examined under a light microscope.

2.10. Mitochondrial Content/Mass Measurement. Mitochondrial mass/content was estimated by analysing mitochondrial DNA expression and normalising it to nuclear DNA expression. DNA was isolated from rat hearts using the GF1-Tissue/Blood FNA Extraction kit (Vivantis) as per manufacturer's protocol. DNA concentration and quality were measured using NanoDrop spectrophotometer (Thermo Scientific). Polymerase chain reaction (PCR) was set up using EmeraldAmp PCR Mastermix (Takara, USA) on Veriti Thermal Cycler (Applied Biosystems). Nuclear beta 2-microglobin expression was used as a reference to normalise the mitochondrial CO-1 (cytochrome oxidase C subunit 1) expression data. Primer sequences are listed in Table 1.

2.11. Cell Culture. H9c2 cells, purchased from ATCC (USA), were cultured in DMEM supplemented with 10% FBS, at 37°C in a 5% CO_2 incubator. VDR was silenced by transfecting H9c2 cells with shRNA against VDR (Origene) using Xtremgene HP Transfection Reagent (Roche), and transfected cells were used to establish a stable cell line using puromycin as a selecting agent.

2.12. Western Blotting. Rat heart tissues and H9c2 cells were lysed in ice-cold RIPA buffer (Pierce) and were then centrifuged at 12000 rpm for 20 minutes at 4°C. Bicinchoninic acid (BCA) assay (Thermo Scientific) was used to measure

TABLE 1: List of primers used in mitochondrial content measurement.

Gene	Forward primer	Reverse primer
CO-1	CACATGAGCAAAAGCCCACT	ACGGCCGTAAGTGAGATGAA
Beta 2-microglobin	GATCACTTGTCCGGAGTAGAA	ACGTAGCAGTTGAGGAAGTTG

protein content. Proteins (30 μg) were resolved on 10-12% SDS-polyacrylamide gel using TGX stain free kit (Bio-Rad). After electrophoresis, proteins were blotted on to polyvinylidine difluoride (PVDF) membrane (Merck Millipore). Membrane was blocked in 3% nonfat dry milk in TBST (0.1% Tween 20) or 5% BSA solution at room temperature for an hour, followed by incubation with desired primary antibody overnight at 4°C. After three washes with TBST, the membrane was incubated with the appropriate HRP-labeled secondary antibody at room temperature for an hour. Membrane was washed with TBST (thrice for 5 min each), and the blot was visualized using Gel Doc XR system (Bio-Rad), using Roche Lumi Light substrates (Thermo Scientific). Protein expression was normalised to corresponding stain free gel (BioRad™) loading controls' expression.

3. Results

3.1. Paricalcitol Improves Glucose Tolerance in High-Fat High-Fructose-Fed Rats

3.1.1. Fasting Blood Glucose and Serum Insulin. There was a significant increase in fasting blood glucose of HFHFrD group as compared to that of the Con group, at the end of 20 weeks (Figure 2(a)). However, we did not observe any significant difference in the HFHFrD+P and HFHFrD+E groups, in comparison to the HFHFrD group (Figure 2(a)).

Similarly, there was a significant increase in fasting serum insulin of the HFHFrD group as compared to the Con group (Figure 2(b)). However, no significant difference was observed in the HFHFrD+P and HFHFrD+E groups, in comparison to the HFHFrD group (Figure 2(b)).

3.1.2. HOMA Analysis. At the end of twenty weeks, HOMA-IR of the HFHFrD group was significantly higher than that of the Con group (Figure 2(c)). However, no significant difference was observed in the HFHFrD+P and HFHFrD+E groups, in comparison to the HFHFrD group (Figure 2(c)).

No significant difference was found between HOMA-B values of different groups (Figure 2(d)).

3.1.3. Intraperitoneal Glucose Tolerance Test. In the intraperitoneal glucose tolerance test (IPGTT) performed at the end of 12 weeks, the HFHFrD group showed raised blood glucose time-profile and significantly higher area-under-curve (AUC) than the Con group (Figure 2(e)), indicating impaired blood glucose disposal in these rats.

In the IPGTT performed at the end of 20 weeks, the HFHFrD group showed impaired glucose tolerance and higher area under curve, compared to the Con group (Figures 2(f) and 2(g)). After 8 weeks of treatment with paricalcitol, the HFHFrD+P group showed significantly

improved glucose tolerance in IPGTT, with significantly lower area under curve, compared to the HFHFrD group (Figures 2(f) and 2(g)).

3.2. Paricalcitol Attenuates Dyslipidemia in High-Fat High-Fructose-Fed Rats.

We observed significantly higher serum triglycerides and free fatty acids in the HFHFrD group compared to the Con group (Figures 3(a) and 3(b)). After 8 weeks of treatment with paricalcitol, the HFHFrD+P group showed significantly decreased triglycerides and free fatty acids, compared to the HFHFrD group (Figures 3(a) and 3(b)). The HFHFrD+E group showed significant decrease in serum free fatty acids, compared to the HFHFrD group (Figure 3(b)). There were no significant changes in serum HDL cholesterol in the different groups (Figure 3(c)).

3.3. Paricalcitol Attenuates Hypertension in High-Fat High-Fructose-Fed Rats.

There were significant increases in systolic, diastolic, and mean arterial blood pressure in the HFHFrD group, compared to the Con group (Figures 3(d)–3(f)). After 8 weeks of treatment with paricalcitol or enalapril, the HFHFrD+P group showed significantly decreased blood pressure, compared to the HFHFrD group (Figures 3(d)–3(f)).

3.4. Paricalcitol Attenuates Cardiac Hypertrophy in High-Fat High-Fructose-Fed Rats.

At the end of 20 weeks, we observed significant increase in the heart weight-to-tail length ratio in the HFHFrD group, when compared to the Con group (Figure 3(g)). After treatment with paricalcitol for 8 weeks, the HFHFrD+P and HFHFrD+E groups showed significant decrease in heart weight-to-tail length, as compared to the HFHFrD group (Figure 3(g)).

3.5. Paricalcitol Attenuates Left Ventricular Hypertrophy and Systolic Dysfunction in High-Fat High-Fructose-Fed Rats

3.5.1. Cardiac Wall Thickness. To study changes in the cardiac structure and function, we performed 2D echocardiography at the end of 12 and 20 weeks. At the end of 20 weeks, there was a significant increase in the intraventricular septum thickness (IVSd) and left ventricular posterior wall thickness (LVPWd) in the HFHFrD group, compared to the control group (Figures 4(a) and 4(b)). The HFHFrD+P and HFHFrD+E groups had significantly decreased IVSd and LVPWd compared to the HFHFrD group, at the end of 20 weeks. Also, IVSd had significantly decreased in the HFHFrD+P and HFHFrD+E groups between 12 and 20 weeks, indicating curative effect of the treatment with paricalcitol and enalapril (Figures 4(a) and 4(b)).

3.5.2. Cardiac Chamber Diameters. We did not observe significant changes in the diastolic left ventricular internal diameter (LVIDd) (Figure 4(c)). However, there was a significant increase in the systolic left ventricular internal diameter
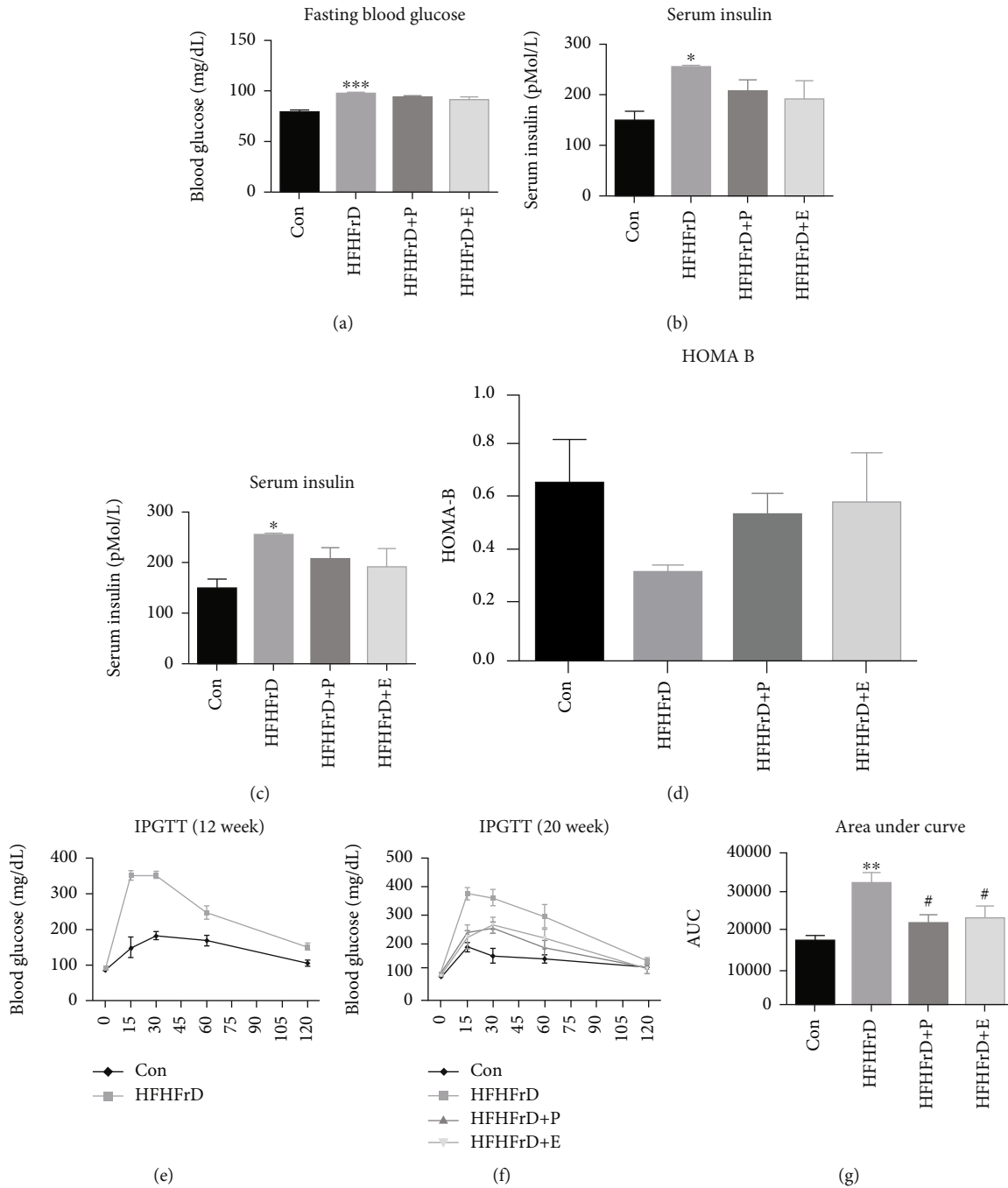
Figure 2: Paricalcitol improves glucose tolerance in high-fat high-fructose-fed rats. (a) Fasting blood glucose. (b) Fasting serum insulin. (c) HOMA IR. (d) HOMA-B. (e) Intraperitoneal glucose tolerance test (12 weeks). (f) Intraperitoneal glucose tolerance test (20 weeks). (g) Area under the curve (20 weeks IPGTT). Data expressed as mean ± SEM ($n = 6$). $^{*}p < 0.05$, $^{**}p < 0.01$, and $^{***}p < 0.001$ vs. the Con group. $^{#}p < 0.05$ vs. the HFHFrD group.

(LVIDs) of the HFHFrD group compared to the Con group, at the end of 20 weeks (Figure 4(d)). This indicated dilatation of the left ventricle in the HFHFrD group. The HFHFrD+P and HFHFrD+E groups showed significant decrease in LVIDs compared to the HFHFrD group, at the end of 20 weeks. Also, LVIDs showed significant decrease in the HFHFrD+P group between 12 and 20 weeks, indicating curative effect of the treatment with paricalcitol (Figure 4(d)).

3.5.3. Cardiac Contractile Function. At the end of 20 weeks, there was a significant decrease in the fractional shortening (FS) and ejection fraction (EF) in the HFHFrD group, compared to the control group (Figures 4(e) and 4(f)). The HFHFrD+P and HFHFrD+E groups significantly improved in FS and EF compared to the HFHFrD group, at the end of 20 weeks. Also, FS significantly improved in the HFHFrD+P and HFHFrD+E groups between 12 and 20
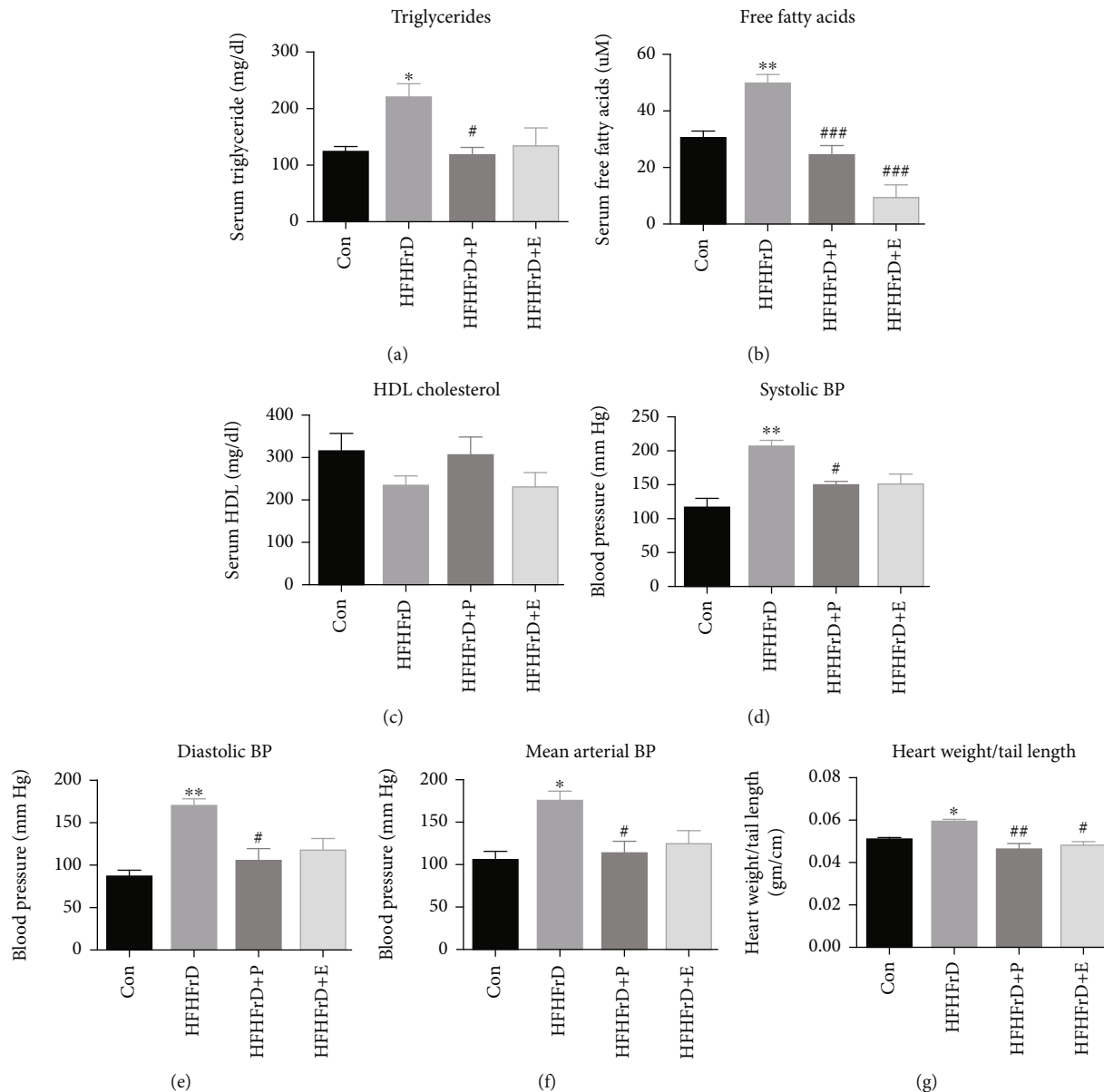
Figure 3: Paricalcitol attenuates dyslipidemia, hypertension and cardiac hypertrophy in high-fat high-fructose-fed rats. (a) Serum triglycerides. (b) Serum free fatty acids. (c) Serum HDL cholesterol. (d) Systolic blood pressure. (e) Diastolic blood pressure. (f) Mean arterial pressure. (g) Heart weight/tail length ratio. Data expressed as mean ± SEM ($n = 6$). $^{*}p < 0.05$ and $^{**}p < 0.01$ vs. the CON group, $^{#}p < 0.05$, $^{##}p < 0.01$, and $^{###}p < 0.001$ vs. the HFHFrD group.

weeks, indicating curative effect of the treatment with paricalcitol and enalapril (Figure 4(e)).

3.6. Paricalcitol Does Not Affect Myocardial Fibrosis in High-Fat High-Fructose-Fed Rats.
We observed no significant differences in histopathological features among the different groups based on haematoxylin and eosin (H&E)-stained rat heart sections (Figure 5(a)). In the Masson trichrome stained heart sections, increased perivascular fibrosis was observed in the HFHFrD group (Figure 5(b)). However, no significant improvement was observed in the HFHFrD+P and HFHFrD+E groups, compared to the HFHFrD group (Figure 5(b)).

3.7. Paricalcitol Increases Cardiac PGC1-α Expression in High-Fat High-Fructose-Fed Rats.
PGC1-α induces mitochondrial biogenesis through activation of transcription factors such as NRF-1 and NRF-2. At the end of the study, PGC1-α expression was lower in the HFHFrD group, compared to the Control group, though not statistically significant (Figure 6(b)). Treatment with paricalcitol caused significantly higher expression of PGC1-α protein in the HFHFrD+P group, compared to the HFHFrD group. The enalapril also significantly upregulated PGC1-α expression, similar to paricalcitol (Figure 6(b)).

3.8. Paricalcitol Does Not Alter Mitochondrial Mass/Content in High-Fat High-Fructose-Fed Rats.
Since we observed
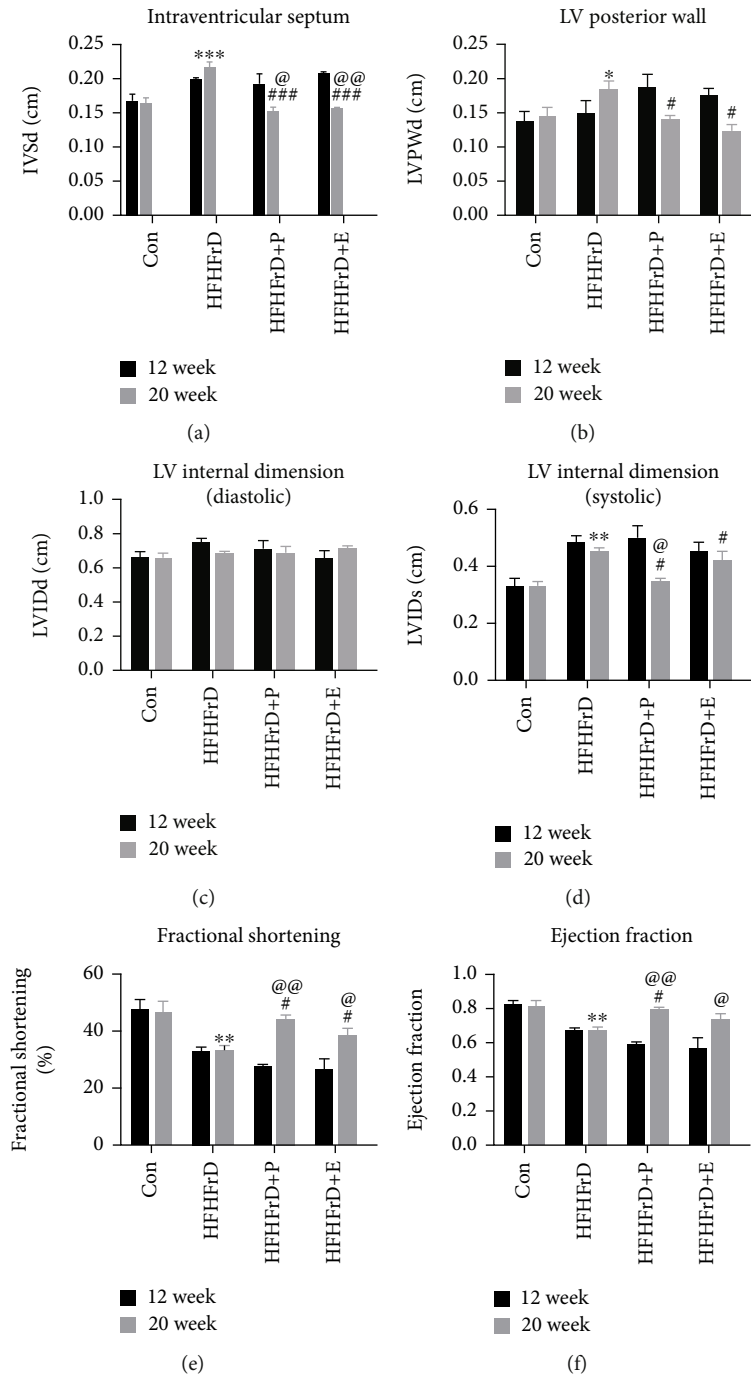
FIGURE 4: Paricalcitol reverses cardiac hypertrophy and failure in high-fat high-fructose-fed rats. (a) Intraventricular septum thickness (diastole). (b) Left ventricular posterior wall thickness (diastole). (c) Left ventricular internal dimension (diastolic). (d) Left ventricular internal dimension (systolic). (e) Fractional shortening. (f) Ejection fraction. Data expressed as mean ± SEM ($n = 4$-5). $^{*}p < 0.05$ and$^{***}p < 0.001$ vs. the CON group. $^{\#}p < 0.05$, $^{\#\#}p < 0.01$, and $^{\#\#\#}p < 0.001$ vs. the HFHFrD group.

increased expression of PGC1-α expression in the hearts of the HFHFrD+P group, we evaluated the effect of paricalcitol on mitochondrial mass/content. Change in mitochondrial DNA content is a marker of changing mitochondrial mass. We observed no significant differences in mitochondrial DNA/content between the different experimental groups, calculated from the expression of mitochondrial CO-1 normalised to beta 2-microglobin (Figure 6(d)).

3.9. Paricalcitol Increases Cardiac Citrate Synthase Activity in High-Fat High-Fructose-Fed Rats. At the end of the study, we evaluated citrate synthase activity in the rat hearts. It was significantly lower in the HFHFrD group, compared to the Con group (Figure 6(e)). Treatment with paricalcitol, but not with enalapril, significantly increased citrate synthase activity in the HFHFrD+P group, compared to the HFHFrD group.

(a)   (b)
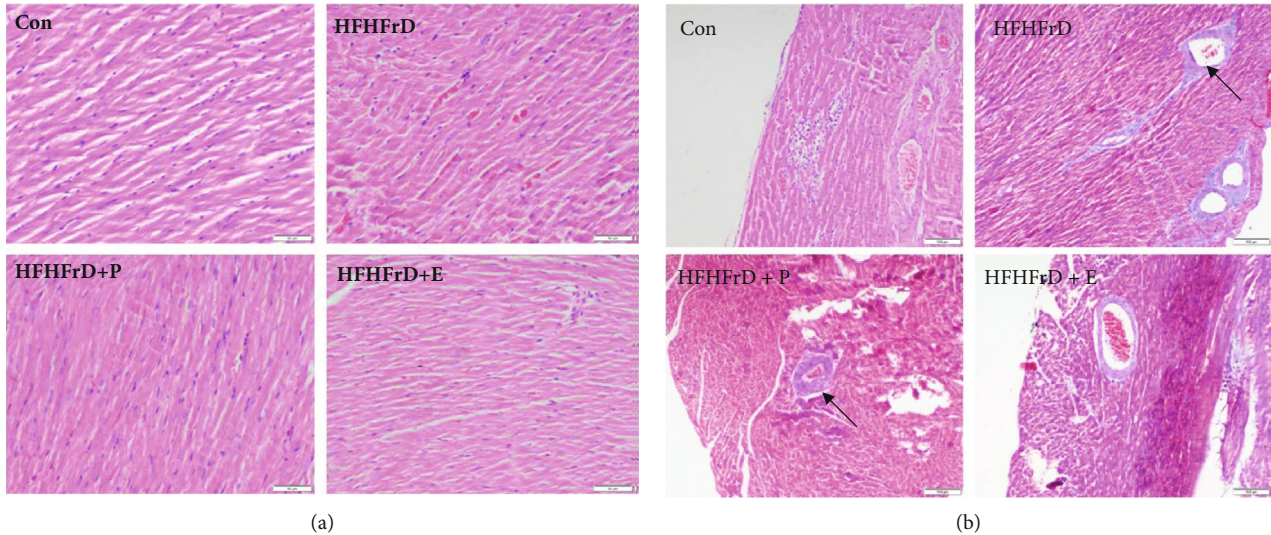
FIGURE 5: Paricalcitol does not affect myocardial fibrosis in high-fat high-fructose-fed rats. (a) Representative micrograph of haematoxylin and eosin-stained rat heart sections. (b) Representative micrograph of Masson's trichrome-stained rat heart sections.

3.10. Paricalcitol Increases Cardiac Expression of Mfn2 in High-Fat High-Fructose-Fed Rats. Since we observed an increase in citrate synthase activity with paricalcitol treatment, we next studied the expression of Mfn1 and Mfn2 that are involved in mitochondrial fusion. There was no significant change in the expression of Mfn1 and Mfn2 in the HFHFrD group compared to the Con group (Figure 7(b)). The increase in Mfn1 expression in both the HFHFrD+P and HFHFrD+E groups was not significant, compared to the HFHFrD group. Paricalcitol and enalapril significantly increased the expression of Mfn2 in the HFHFrD+P group, compared to the HFHFrD group (Figure 7(c)).

3.11. VDR Knockdown Causes Downregulation of Mfn2 in H9c2 Cardiomyoblasts. Since paricalcitol upregulated the expression of Mfn2 in a high-fat high-fructose-fed rat heart, we next investigated whether VDR is directly involved in the regulation of cardiac expression of mitofusins. We observed that VDR silencing in H9c2 cardiomyoblasts causes a significant decrease in Mfn2 expression, but not in Mfn1 expression (Figures 7(e) and 7(f)).

4. Discussion

Vitamin D has been gaining attention for nonclassical roles such as regulation of inflammation, immunity, cell cycle, and metabolism. Association between vitamin D deficiency and adverse cardiometabolic outcomes has been repeatedly shown in patients, but the therapeutic role of vitamin D supplementation remains controversial [3, 28, 29]. Clinical studies have yielded conflicting results regarding the potential benefits of vitamin D in subjects with cardiometabolic diseases [30, 31]. In view of reduced bioavailability of the active form of vitamin D in disease conditions, use of vitamin D analogues such as paricalcitol and maxacalcitol has been investigated [32]. Paricalcitol has shown therapeutic benefit in experimental models of kidney disease, diabetes,

and their cardiovascular complications [33, 34]. However, its effect on metabolic syndrome-associated heart failure remained to be investigated. In this study, we have demonstrated the cardioprotective effects of paricalcitol treatment in a high-fat high-fructose-fed rat model of metabolic syndrome.

Rats were fed diets with high fat and high fructose to induce metabolic syndrome. Hypercaloric diets containing high fat and high fructose have been shown to induce hyperinsulinemia and impaired glucose tolerance [35]. Insulin resistance is considered a principal component of diet-induced metabolic syndrome [36, 37]. In our study, animals of the HFHFrD group showed elevated blood glucose, serum insulin, and HOMA-IR values, indicating development of a prediabetes-like state. Treatment with paricalcitol for 8 weeks did not cause any significant changes in these parameters. However, paricalcitol reversed the impairment of blood glucose disposal in the intraperitoneal glucose tolerance test in the HFHFrD+P group.

High-calorie diets are known to disturb serum lipid profile with an increase in serum triglycerides and free fatty acids [38]. In this study, we observed increase in triglycerides and free fatty acids in serum of rats in the HFHFrD group. Treatment with paricalcitol attenuated these changes and improved lipid profile of the HFHFrD+P group. No significant differences were observed in the HDL cholesterol levels of the different groups. The lipid-lowering effect of paricalcitol in metabolic syndrome has not been reported earlier.

Apart from triggering metabolic derangements such as insulin resistance and dyslipidemia, high-fat high-fructose diet also causes cardiovascular perturbations [35]. At the end of the study, we observed raised systolic, diastolic, and mean arterial blood pressure in the HFHFrD group. Treatment with paricalcitol significantly reduced blood pressure in the HFHFrD+P group. Hypertension is an established predictor of cardiac hypertrophy, due to resultant increase in cardiac workload. Heart weight-to-tail length ratio, an

(a)

(b)

(c)

(d)

(e)
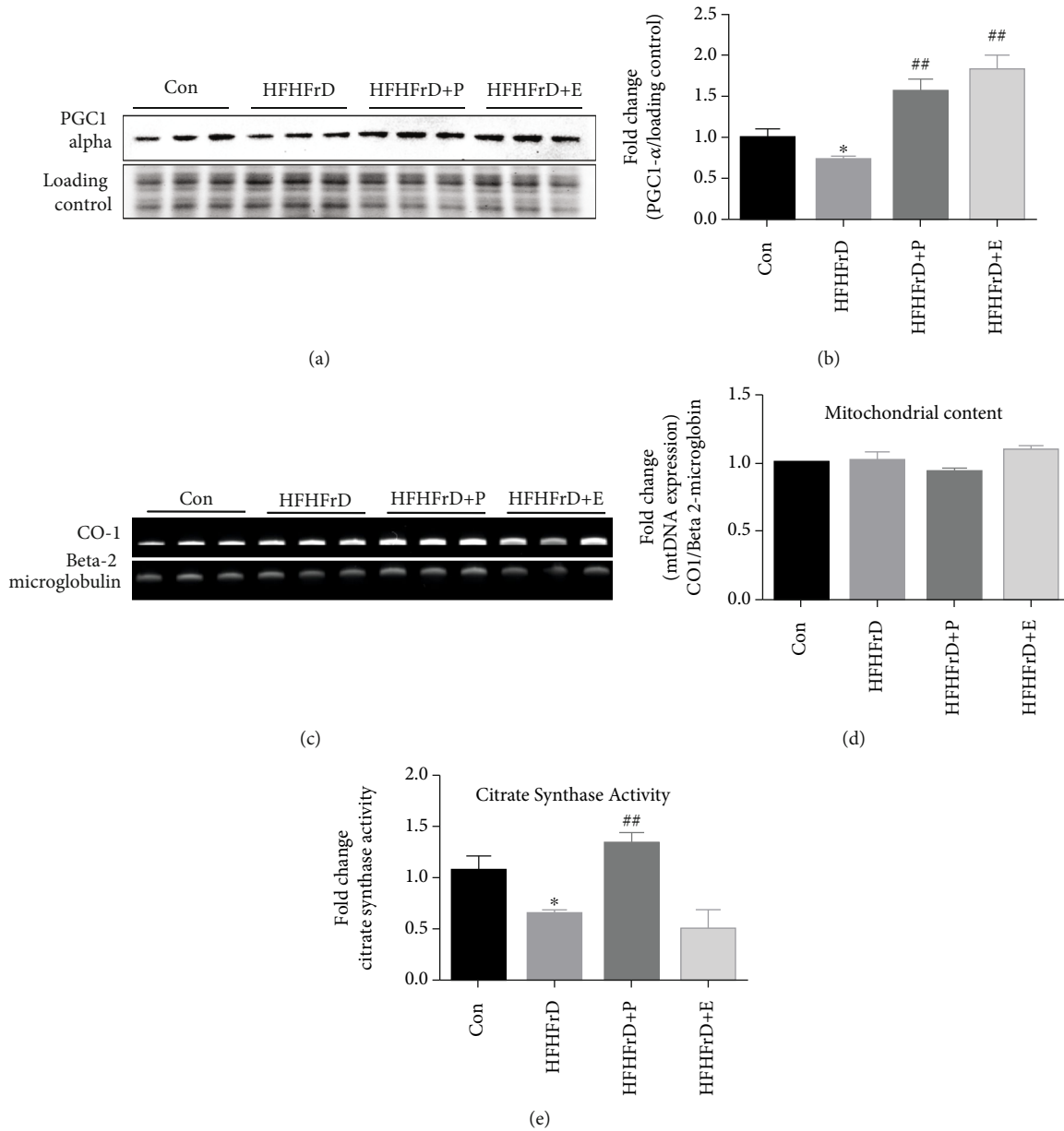
Figure 6: Paricalcitol does not alter myocardial mitochondrial content in high-fat high-fructose-fed rats. (a) Representative western blot image of PGC1-α. (b) Densitometry analysis of PGC1-α expression. (c) Representative agarose gel image of CO-1 and beta 2-microglobin PCR products. (d) Densitometry analysis of CO-1 expression. (e) Fold change in citrate synthase activity. Protein expression data were normalised to the expression of stain free gel (TGX Stain-FreeTM FastCastTM BioRadTM) image. $^{\#\#}p < 0.01$ vs. HFHFrD group. CO-1 expression data were normalised to beta 2-microglobin expression. Data expressed as mean $\pm$ SEM ($n = 3$ for Western blot and agarose gel electrophoresis; $n = 5$ for citrate synthase activity). $^{*}p < 0.05$ vs. Control; $^{\#\#}p < 0.01$ vs. HFHFrD.

index of cardiac size, was increased significantly in the HFHFrD group compared to the Con group. Treatment with paricalcitol was associated with a significant decrease in heart weight-to-tail length ratio in the HFHFrD+P group. Similar to our findings, paricalcitol has earlier been shown to attenuate cardiac hypertrophy in experimental models of pressure overload, hypertension, and uremia [39–41].

As a consequence of its metabolic effects, high-fat high-fructose diet also induces cardiac remodeling [35]. At the end of 20 weeks, there was significant increase in the intra-ventricular septum and left ventricular posterior wall thick-

nesses in the HFHFrD rats. We observed significant decrease in cardiac wall thicknesses in the HFHFrD+P group, indicating attenuation of cardiac hypertrophy. Though initially an adaptive response, unmitigated left ven-tricular hypertrophy progresses to cardiac failure. Metabolic syndrome is known to increase the risk of left ventricular systolic dysfunction by two folds [42]. Echocardiography is considered the gold-standard diagnostic technique for sys-tolic failure; hence, we used it to assess systolic function in these rats. In the HFHFrD rats, we observed increased sys-tolic internal dimension of the left ventricle, indicating

(a)

(b)

(c)

(d)

(e)

(f)
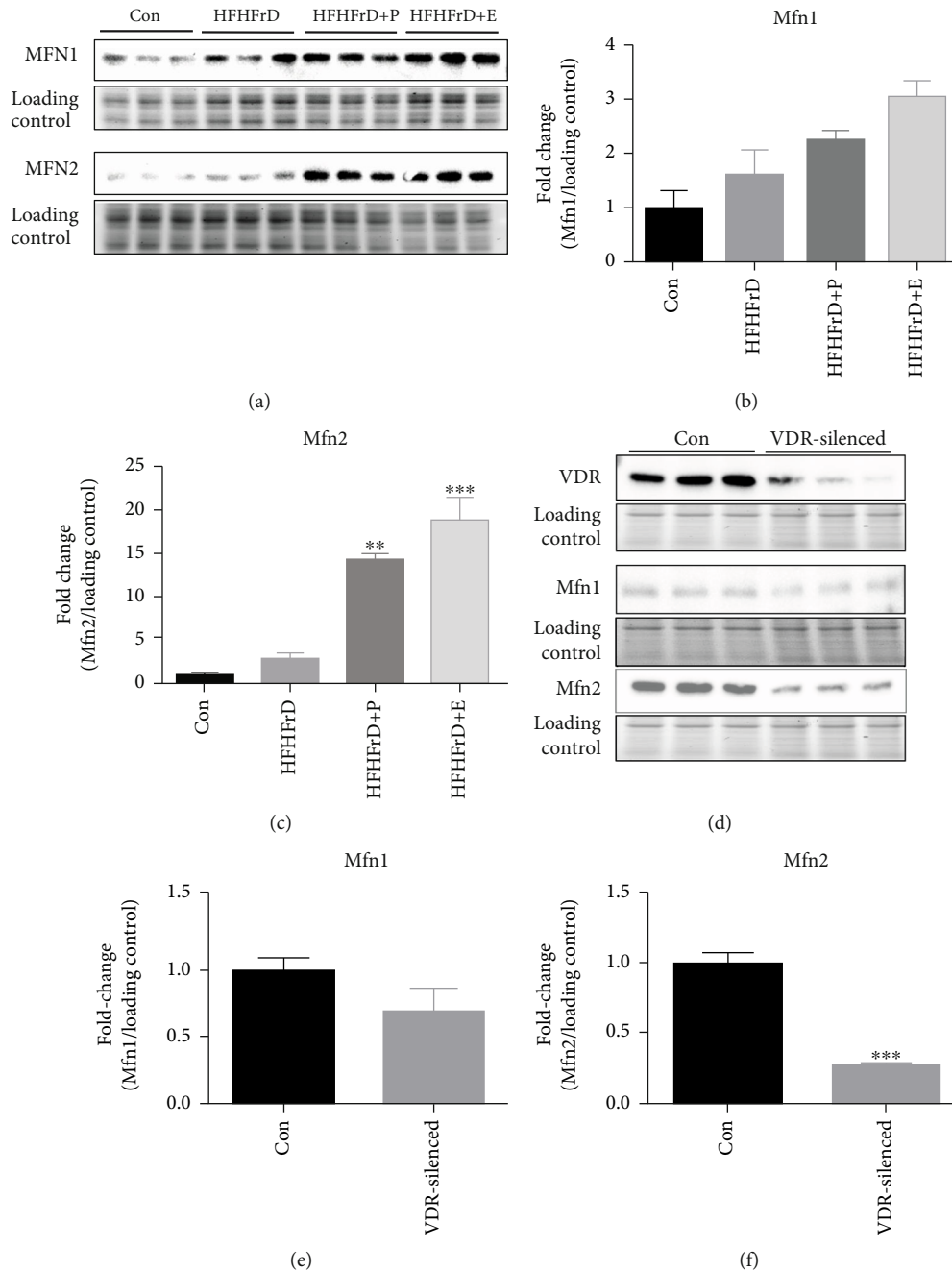
FIGURE 7: Vitamin D receptor modulates myocardial expression of mitofusin 2. (a) Representative western blot images of Mfn1 and Mfn2 in rat hearts. (b) Densitometry analysis of Mfn1 expression in rat hearts. (c) Densitometry analysis of Mfn2 expression in rat hearts. (d) Representative western blot images of VDR, Mfn1, and Mfn 2 in H9c2 cells. (e) Densitometry analysis of Mfn1 in H9c2 cells. (f) Densitometry analysis of Mfn2 in H9c2 cells. Protein expression data were normalised to the expression of stain free gel (TGX Stain-FreeTM FastCastTM BioRadTM) image. Data expressed as mean ± SEM ($n = 3$). $^{*}p < 0.05$ vs. the Control group; $^{***}p < 0.001$ vs. the Control group.

dilatation and systolic dysfunction. This led to significantly reduced fractional shortening and ejection fraction, which implies compromised cardiac contractility. In the HFHFrD +P group, systolic function was markedly improved. According to earlier studies, paricalcitol prevents the progression of hypertrophy to heart failure in Dahl salt-sensitive hypertensive rats [40].

Interestingly, paricalcitol did not only attenuate the high-fat high-fructose-induced cardiac perturbations seen at the end of 20 weeks, it also reversed the progression of cardiac dysfunction induced by high-fat high-fructose diet seen at the end of 12 weeks. The improvement in systolic function is an interesting finding because the current treatment regimens for heart failure only manage the symptoms

and do not reverse cardiac dysfunction. An important underlying pathology here is the pathological remodeling of the heart. Increased cardiac load due to factors such as hypertension, sympathetic tone, and others can trigger reactive myocardial fibrosis [43]. These fibrotic changes usually begin in the perivascular region and slowly spread into the myocardium. Perivascular fibrosis was observed in the HFHFrD group through observation of Masson's trichrome-stained heart sections. We speculated that attenuation or reversal of this fibrosis might be responsible for cardioprotective effect of paricalcitol, seen earlier. However, we did not observe any significant difference in the HFHFrD+P group, as compared to the HFHFrD group. This is similar to earlier reports where paricalcitol had no protective effect on perivascular fibrosis in rats with renal insufficiency and low vitamin D [44]. These findings warranted further investigation into the factors underlying the protective effect of paricalcitol in high-fat high-fructose-induced cardiac dysfunction.

Since there were no significant improvements in cardiac structure or remodelling status and functional improvements were observed, it indicated improvement in the functional status of the cardiac muscle. The myocardium relies on continuous supply of ATP to sustain its contractility. Mitochondria are the cellular organelles that generate the required ATP for energy transduction in heart. Defects in structure, function, or dynamics of mitochondria adversely affect cardiac function. Mitochondrial dysfunction has been shown to underlie progression of cardiac hypertrophy to heart failure [45]. Hypercaloric diets can cause mitochondrial dysfunction through increased flux of fats and glucose [46]. Mitochondrial biogenesis, which implies formation of new mitochondria, might be impaired in conditions of unmitigated stress [44]. In our study also, we observed that expression of PGC1-α was downregulated in HFHFrD rat hearts. PGC1-α drives mitochondrial biogenesis through activation of downstream transcription factors [47, 48]. In the HFHFrD+P group, increased expression of PGC1-α was observed. In earlier reports, vitamin D supplementation has been shown to upregulate PGC1-α expression in rat skeletal muscle [49].

Increased cardiac expression of PGC1-α after paricalcitol treatment led us to speculate an increase in mitochondrial mass/content in the HFHFrD group. Mitochondrial mass/content can be quantified using mitochondria-tagging fluorescent dyes or by measuring mitochondrial DNA amount. We measured the expression of CO-1 gene that is encoded in mitochondrial DNA and normalised it to expression of beta 2-microbin encoded in nuclear DNA. Surprisingly, we did not observe any significant changes between the fold changes of CO-1 expression between different groups. This indicated that there was no significant increase in mitochondrial content in HFHFrD+P rat hearts, despite upregulation of PGC1-α. This could be due to regulation of PGC1-α function by posttranslational modifications. However, activity of myocardial citrate synthase improved in the HFHFrD+P group, compared to the HFHFrD group. Acetyl CoA generated from glycolysis and fatty acid oxidation enters Kreb's cycle in the mitochondrial matrix. Citrate synthase is the first enzyme of this biochemical cycle, and its activity is thus

considered a hallmark of mitochondrial health [50]. Our findings indicate that paricalcitol improves mitochondrial function in high-fat high-fructose-fed rats.

Our next question was how mitochondrial function could improve without any changes in mitochondrial content or biogenesis. Mitochondrial dynamics are controlled not only through biogenesis but also through fusion and fission. Mitochondrial fusion improves mitochondrial function by fusing of healthy mitochondrial fractions and recycling of damaged components [51]. We examined the expression of mitofusins (Mfn2) that are the proteins involved in mitochondrial fusion. Myocardial expression of Mfn2 increased significantly in the HFHFrD+P group, compared to the HFHFrD group. Mfn2 has been earlier described as a therapeutic target for diabetic cardiomyopathy through inhibition of mitochondrial fission in db/db mice [52]. It has also been shown to be protective against angiotensin-mediated cardiomyocyte injury by induction of mitophagy and mitochondrial fusion [48].

The findings above indicate that paricalcitol improved mitochondrial function, possibly through improvement of mitochondrial dynamics. To confirm that this beneficial effect was mediated by activation of VDR by paricalcitol, we performed further experiments *in vitro*. To perform loss-of-function studies regarding the effect of VDR on mitochondrial fusion, we silenced VDR in H9c2 cardiomyoblasts. Here, we observed that the expression of Mfn2, but not Mfn1, was remarkably reduced in H9c2 cells with VDR knockdown.

5. Summary and Conclusion

In this study, we demonstrate that paricalcitol, a vitamin D receptor activator, attenuates metabolic syndrome-associated cardiac dysfunction in rats. High-fat high-fructose diet induces glucose intolerance, dyslipidemia, hypertension, fibrosis, and cardiac dysfunction in rats. Paricalcitol improves glucose tolerance, lipid profile, blood pressure, and cardiac contractility, but does not attenuate myocardial fibrosis. We demonstrate that the VDR activator paricalcitol improves cardiometabolic function in rats, possibly through improvement of mitochondrial dynamics. Despite increase in cardiac PGC1-α expression, change in mitochondrial content is not observed in paricalcitol-treated rats with metabolic syndrome. However, paricalcitol-induced increase in citrate cynthase activity and expression of Mfn2 indicates the possible role of VDR activation in mitochondrial fusion. Further investigation is warranted into the detailed mechanism of activation of Mfn2 and its effect on other mitochondrial function parameters. Decreased expression of mitofusin 2 in VDR-silenced H9c2 cells provided evidence about the positive role of VDR in mitochondrial fusion. These findings indicate potential for repurposing of paricalcitol for treatment of cardiac failure associated with conditions such as prediabetes and diabetes mellitus.

Data Availability

Data are available upon reasonable request.

Disclosure

Conflicts of Interest

The authors declare that they have no conflict of financial or non-financial interests.

Acknowledgments

References

[1] N. Conrad, A. Judge, J. Tran et al., "Temporal trends and patterns in heart failure incidence: a population-based study of 4 million individuals," *The Lancet*, vol. 391, no. 10120, pp. 572–580, 2018.

[2] J. J. McMurray, "Systolic heart failure," *New England Journal of Medicine*, vol. 362, no. 3, pp. 228–238, 2010.

[3] R. Adela, R. M. Borkar, M. M. Bhandi et al., "Lower vitamin D metabolites levels were associated with increased coronary artery diseases in type 2 diabetes patients in India," *Scientific Reports*, vol. 6, no. 1, article 37593, 2016.

[4] H. L. Nizami, P. Katare, P. Prabhakar et al., "Vitamin D deficiency in rats causes cardiac dysfunction by inducing myocardial insulin resistance," *Molecular nutrition & food research.*, vol. 63, no. 17, article 1900109, 2019.

[5] R. U. Simpson, S. H. Hershey, and K. A. Nibbelink, "Characterization of heart size and blood pressure in the vitamin D receptor knockout mouse," *The Journal of Steroid Biochemistry and Molecular Biology*, vol. 103, no. 3-5, pp. 521–524, 2007.

[6] C. M. Porto, V. D. L. Silva, J. S. B. da Luz, B. M. Filho, and V. M. da Silveira, "Association between vitamin D deficiency and heart failure risk in the elderly," *ESC heart failure*, vol. 5, no. 1, pp. 63–74, 2018.

[7] J. A. Sugden, J. I. Davies, M. D. Witham, A. D. Morris, and A. D. Struthers, "Vitamin D improves endothelial function in patients with type 2 diabetes mellitus and low vitamin D levels," *Diabetic Medicine*, vol. 25, no. 3, pp. 320–325, 2008.

[8] A. Zittermann, J. B. Ernst, S. Prokop et al., "A 3 year post-intervention follow-up on mortality in advanced heart failure (EVITA vitamin D supplementation trial)," *ESC Heart Failure*, vol. 7, no. 6, pp. 3754–3761, 2020.

[9] G. Musso, M. Cassader, S. Cohney et al., "Fatty liver and chronic kidney disease: novel mechanistic insights and therapeutic opportunities," *Diabetes Care*, vol. 39, no. 10, pp. 1830–1845, 2016.

[10] J. Wortsman, L. Y. Matsuoka, T. C. Chen, Z. Lu, and M. F. Holick, "Decreased bioavailability of vitamin D in obesity," *The American Journal of Clinical Nutrition*, vol. 72, no. 3, pp. 690–693, 2000.

[11] C. Zoccali, G. Curatola, V. Panuccio et al., "Paricalcitol and endothelial function in chronic kidney disease trial," *Hypertension*, vol. 64, no. 5, pp. 1005–1011, 2014.

[12] M. Tamayo, L. Martín-Nunes, A. Val-Blasco et al., "Beneficial effects of paricalcitol on cardiac dysfunction and remodelling

in a model of established heart failure," *British Journal of Pharmacology*, vol. 177, no. 14, pp. 3273–3290, 2020.

[13] N. Sorokina, J. M. O'Donnell, R. D. McKinney et al., "Recruitment of compensatory pathways to sustain oxidative flux with reduced carnitine palmitoyltransferase I activity characterizes inefficiency in energy metabolism in hypertrophied hearts," *Circulation*, vol. 115, no. 15, pp. 2033–2041, 2007.

[14] V. Parra, H. E. Verdejo, M. Iglewski et al., "Insulin stimulates mitochondrial fusion and function in cardiomyocytes via the Akt-mTOR-NFκB-Opa-1 signaling pathway," *Diabetes*, vol. 63, no. 1, pp. 75–88, 2014.

[15] L. Zhang, J. S. Jaswal, J. R. Ussher et al., "Cardiac insulin-resistance and decreased mitochondrial energy production precede the development of systolic heart failure after pressure-overload hypertrophy," *Heart Failure*, vol. 6, no. 5, pp. 1039–1048, 2013.

[16] X. Zhou and J. Chen, "Is treatment with trimetazidine beneficial in patients with chronic heart failure?," *PLoS One*, vol. 9, no. 5, article e94660, 2014.

[17] Y. Lopatin and Volgograd State Medical University, Volgograd Regional Cardiology Centre, Volgograd, Russia, "Metabolic therapy in heart failure," *Cardiac Failure Review*, vol. 1, no. 2, pp. 112–117, 2015.

[18] E. K. Calton, K. N. Keane, and M. J. Soares, "The potential regulatory role of vitamin D in the bioenergetics of inflammation," *Current Opinion in Clinical Nutrition & Metabolic Care*, vol. 18, no. 4, pp. 367–373, 2015.

[19] R. Adela, R. M. Borkar, N. Mishra et al., "Lower serum vitamin D metabolite levels in relation to circulating cytokines/chemokines and metabolic hormones in pregnant women with hypertensive disorders," *Frontiers in Immunology*, vol. 8, p. 273, 2017.

[20] P. Manna, A. E. Achari, and S. K. Jain, "1, 25 (OH) 2-vitamin D 3 upregulates glucose uptake mediated by SIRT1/IRS1/GLUT4 signaling cascade in C2C12 myotubes," *Molecular and Cellular Biochemistry*, vol. 444, no. 1-2, pp. 103–108, 2018.

[21] J. Marcotorchino, F. Tourniaire, J. Astier et al., "Vitamin D protects against diet-induced obesity by enhancing fatty acid oxidation," *The Journal of Nutritional Biochemistry*, vol. 25, no. 10, pp. 1077–1083, 2014.

[22] Z. Asemi, T. Hashemi, M. Karamali, M. Samimi, and A. Esmaillzadeh, "Effects of vitamin D supplementation on glucose metabolism, lipid concentrations, inflammation, and oxidative stress in gestational diabetes: a double-blind randomized controlled clinical trial," *The American Journal of Clinical Nutrition*, vol. 98, no. 6, pp. 1425–1432, 2013.

[23] E. K. Calton, K. N. Keane, M. J. Soares, J. Rowlands, and P. Newsholme, "Prevailing vitamin D status influences mitochondrial and glycolytic bioenergetics in peripheral blood mononuclear cells obtained from adults," *Redox Biology*, vol. 10, pp. 243–250, 2016.

[24] X. Peng, G. Shang, W. Wang et al., "Fatty acid oxidation in zebrafish adipose tissue is promoted by 1α,25(OH)$_2$D$_3$," *Cell Reports*, vol. 19, no. 7, pp. 1444–1455, 2017.

[25] K. M. Alkharfy, N. M. Al-Daghri, M. Ahmed, and S. M. Yakout, "Effects of vitamin D treatment on skeletal muscle histology and ultrastructural changes in a rodent model," *Molecules*, vol. 17, no. 8, pp. 9081–9089, 2012.

[26] C. Ricca, A. Aillon, L. Bergandi, D. Alotto, C. Castagnoli, and F. Silvagno, "Vitamin D receptor is necessary for mitochondrial function and cell health," *International Journal of Molecular Sciences*, vol. 19, no. 6, p. 1672, 2018.

[27] A. Longoni, J. Kolling, C. Siebert et al., "1,25-Dihydroxyvitamin D$_3$ prevents deleterious effects of homocysteine on mitochondrial function and redox status in heart slices," *Nutrition Research*, vol. 38, pp. 52–63, 2017.

[28] J. Gambardella, M. De Rosa, D. Sorriento et al., "Parathyroid hormone causes endothelial dysfunction by inducing mitochondrial ROS and specific oxidative signal transduction modifications," *Oxidative Medicine and Cellular Longevity*, vol. 2018, 18 pages, 2018.

[29] A. Aleksova, F. Ferro, G. Gagno et al., "Diabetes mellitus and vitamin D deficiency: comparable effect on survival and a deadly association after a myocardial infarction," *Journal of Clinical Medicine*, vol. 9, no. 7, p. 2127, 2020.

[30] Q. Zhang, Y. Cheng, M. He, T. Li, Z. Ma, and H. Cheng, "Effect of various doses of vitamin D supplementation on pregnant women with gestational diabetes mellitus: a randomized controlled trial," *Experimental and Therapeutic Medicine*, vol. 12, no. 3, pp. 1889–1895, 2016.

[31] K. M. Swart, P. Lips, I. A. Brouwer et al., "Effects of vitamin D supplementation on markers for cardiovascular disease and type 2 diabetes: an individual participant data meta-analysis of randomized controlled trials," *The American Journal of Clinical Nutrition*, vol. 107, no. 6, pp. 1043–1053, 2018.

[32] R. Parsanathan and S. K. Jain, "Glutathione deficiency induces epigenetic alterations of vitamin D metabolism genes in the liver of high-fat diet–induced type 2 diabetic mice," *Diabetes*, vol. 67, Supplement_1, 2018.

[33] C. C. Lai, C. P. Liu, P. W. Cheng et al., "Paricalcitol attenuates cardiac fibrosis and expression of endothelial cell transition markers in isoproterenol-induced cardiomyopathic rats," *Critical Care Medicine*, vol. 44, no. 9, pp. e866–e874, 2016.

[34] Y. Yildirim, Z. Yilmaz, A. K. Kadiroglu et al., "Mp179 pretreatment with paricalcitol attenuates oxidative stress in renal ischemia reperfusion induced nephropathy in rats," *Nephrology Dialysis Transplantation*, vol. 31, suppl_1, p. i401, 2016.

[35] J. R. Wu-Wong, "Potential for vitamin D receptor agonists in the treatment of cardiovascular disease," *British Journal of Pharmacology*, vol. 158, no. 2, pp. 395–412, 2009.

[36] S. K. Panchal, H. Poudyal, A. Iyer et al., "High-carbohydrate high-fat diet–induced metabolic syndrome and cardiovascular remodeling in rats," *Journal of Cardiovascular Pharmacology*, vol. 57, no. 1, pp. 51–64, 2011.

[37] Y. Zhang, J. R. Sowers, and J. Ren, "Pathophysiological insights into cardiovascular health in metabolic syndrome,," *Experimental Diabetes Research*, vol. 2012, Article ID 320534, 2 pages, 2012.

[38] Y. Zhang, A. T. Whaley-Connell, J. R. Sowers, and J. Ren, "Autophagy as an emerging target in cardiorenal metabolic disease: from pathophysiology to management," *Pharmacology & Therapeutics*, vol. 191, pp. 1–22, 2018.

[39] L. M. Meems, M. V. Cannon, H. Mahmud et al., "The vitamin D receptor activator paricalcitol prevents fibrosis and diastolic dysfunction in a murine model of pressure overload," *The Journal of Steroid Biochemistry and Molecular Biology*, vol. 132, no. 3-5, pp. 282–289, 2012.

[40] S. Bae, B. Yalamarti, Q. Ke et al., "Preventing progression of cardiac hypertrophy and development of heart failure by paricalcitol therapy in rats," *Cardiovascular Research*, vol. 91, no. 4, pp. 632–639, 2011.

[41] M. Freundlich, Y. C. Li, Y. Quiroz et al., "Paricalcitol downregulates myocardial renin–angiotensin and fibroblast growth factor expression and attenuates cardiac hypertrophy in uremic rats," *American Journal of Hypertension*, vol. 27, no. 5, pp. 720–726, 2014.

[42] H. P. Gong, H. W. Tan, N. N. Fang et al., "Impaired left ventricular systolic and diastolic function in patients with metabolic syndrome as assessed by strain and strain rate imaging," *Diabetes Research and Clinical Practice*, vol. 83, no. 3, pp. 300–307, 2009.

[43] H. Wu, L. Chen, J. Xie et al., "Periostin expression induced by oxidative stress contributes to myocardial fibrosis in a rat model of high salt-induced hypertension," *Molecular Medicine Reports*, vol. 14, no. 1, pp. 776–782, 2016.

[44] J. M. Repo, I. S. Rantala, T. T. Honkanen et al., "Paricalcitol aggravates perivascular fibrosis in rats with renal insufficiency and low calcitriol," *Kidney International*, vol. 72, no. 8, pp. 977–984, 2007.

[45] M. G. Rosca, B. Tandler, and C. L. Hoppel, "Mitochondria in cardiac hypertrophy and heart failure," *Journal of Molecular and Cellular Cardiology*, vol. 55, pp. 31–41, 2013.

[46] T. Jelenik and M. Roden, "Mitochondrial plasticity in obesity and diabetes mellitus," *Antioxidants & Redox Signaling*, vol. 19, no. 3, pp. 258–268, 2013.

[47] W. I. Sivitz and M. A. Yorek, "Mitochondrial dysfunction in diabetes: from molecular mechanisms to functional significance and therapeutic opportunities," *Antioxidants & Redox Signaling*, vol. 12, no. 4, pp. 537–577, 2010.

[48] R. C. Scarpulla, "Metabolic control of mitochondrial biogenesis through the PGC-1 family regulatory network," *Cell Research*, vol. 1813, no. 7, pp. 1269–1278, 2011.

[49] R. S. Savkur, K. S. Bramlett, K. R. Stayrook, S. Nagpal, and T. P. Burris, "Coactivation of the human vitamin D receptor by the peroxisome proliferator-activated receptor γ coactivator-1 α," *Molecular Pharmacology*, vol. 68, no. 2, pp. 511–517, 2005.

[50] S. J. Remington, "Structure and mechanism of citrate synthase," *Current Topics in Cellular Regulation*, vol. 33, pp. 209–229, 1992.

[51] J. N. Meyer, T. C. Leuthner, and A. L. Luz, "Mitochondrial fusion, fission, and mitochondrial toxicity," *Toxicology*, vol. 391, pp. 42–53, 2017.

[52] L. Hu, M. Ding, D. Tang et al., "Targeting mitochondrial dynamics by regulating Mfn2 for therapeutic intervention in diabetic cardiomyopathy," *Theranostics*, vol. 9, no. 13, pp. 3687–3706, 2019.

Review Article

Understanding the Stony Bridge between Osteoporosis and Vascular Calcification: Impact of the FGF23/Klotho axis

Xu Wei [ID],[1] **Xinyi Huang** [ID],[2] **Ning Liu,**[1] **Baoyu Qi,**[1] **Shengjie Fang,**[1] **and Yili Zhang** [ID][3]

[1]*Wangjing Hospital, China Academy of Chinese Medical Sciences, Beijing, China*
[2]*School of Traditional Chinese Medicine, Beijing University of Chinese Medicine, Beijing, China*
[3]*School of Traditional Chinese Medicine & School of Integrated Chinese and Western Medicine, Nanjing University of Chinese Medicine, Nanjing, China*

Correspondence should be addressed to Yili Zhang; zhangyili823@126.com

A relationship between osteoporosis (OP) and vascular calcification (VC) is now proposed. There are common mechanisms underlying the regulation of them. Fibroblast growth factor- (FGF-) 23 and Klotho are hormones associated with the metabolic axis of osteovascular metabolism. Most recently, it was suggested that the FGF23-klotho axis is associated with increasing incidence of fractures and is potentially involved in the progression of the aortic-brachial stiffness ratio. Herein, we discussed the potential role of the FGF23/Klotho axis in the pathophysiology of OP and VC. We want to provide an update review in order to allow a better understanding of the potential role of the FGF23/Klotho axis in comorbidity of OP and VC. We believe that a better understanding of the relationship between both entities can help in proposing new therapeutic targets for reducing the increasing prevalence of OP and VC in the aging population.

1. Introduction

Osteoporosis (OP) is a systemic skeletal disease, characterized by low bone mass and deterioration in the microarchitecture of the bone tissue, which has greater susceptibility to fractures [1]. The prevalence of this metabolic bone disease is very high in the population, and fractures resulting from osteoporosis are becoming frequent situations. Vascular calcification (VC) in the past was reported a passive process, traditionally considered a degenerative consequence of aging [2]. However, recent studies have identified it is an active process, which has histopathological characteristics, mineral composition, and initiation and development mechanisms characteristic of bone formation [3]. Paradoxically, patients suffering from OP exhibit many of the classic hallmarks of vascular calcifications, which are known as "calcification paradox" [4].

There has been growing researchers in studying the relationship between metabolic bone disease and cardiovascular diseases over the years. Current clinical practice evidence supports the notion that patients with OP frequently suffer from VC, which was shown as a predictor for the progression of cardiovascular morbidity/mortality and osteoporotic fractures [5]. In the famous Framingham Heart Study, a 30-year longitudinal analysis of bone loss and VC showed that cortical bone loss measured at the metacarpal was related to the progression of atherosclerotic aortic calcification in women [6]. The association between cardiovascular disease and calcium deposition in the vasculature was first described in the 19th century [7]. Traditionally, OP and VC have been considered as independent processes related to age; although, a correlation has been demonstrated between the loss of bone mass and vascular calcification through a series of recent epidemiological studies [8–10].

Another important concept that connects OP and VC is the bone-vascular axis. Growing evidence linking bone with different functional and structural characteristics of arterial tree has contributed to developing the concept of the bone-vascular axis [11]. The emerging new study results still continue to enhance the rationality of the bone-vascular axis,

which is reflected in the interpretation and discovery of the interaction mechanism [12–14]. What is more, clinical evidence demonstrated that some medications such as statins, insulin, and antihypertensives could exert protective effects on both osteoporosis and cardiovascular disease, suggesting a common pathophysiological basis [15].

Over the past decade, although there is a complex relationship between OP and VC, various research tools enabled clinicians and scientists to take a closer look at the molecular and cellular mechanisms behind these two diseases [16]. Among them, the knowledge progress of the FGF23/Klotho axis and its influence on phosphorus and calcium metabolism change our vision of the regulation of mineral metabolism in the past few years [17]. Fibroblast growth factor- (FGF-) 23 and Klotho are hormones associated with the metabolic axis of osteovascular metabolism. Klotho is known as a membrane protein in response to the effect of FGF-23 on kidney [18]. The FGF-23, which is a growth factor synthesized in the bone, acts in the renal to inhibit activation of vitamin D and to induce Pi excretion through proximal tubular epithelial cells [19]. Most recently, it was especially investigated that the FGF23-klotho axis is associated with increasing incidence of fractures and is potentially involved in the progression of aortic-brachial stiffness ratio [20]. Furthermore, an essential role of the FGF-23 is in the positively regulation and modulation of the OPG gene expression, emphasizing its role in the bone-vascular axis [21]. While in animal models, Klotho also has been reported to exert various effects on bone formation and to play a protective role in vascular calcification [22, 23].

Hence, this review provides an update in order to allow a better understanding of the potential role of the FGF23/Klotho axis in comorbidity of OP and VC. We believe that a better understanding of the relationship between both entities can help in proposing new therapeutic targets for reducing the increasing prevalence of OP and VC in the aging population.

2. Mechanism of the FGF23/Klotho axis on Osteoporosis

2.1. Vitamin D. FGF23 was later demonstrated to be involved in the decreases of $1,25(OH)_2$ D in both global and tissue-specific deletion studies [24]. The renal $1\alpha(OH)$ ase enzyme is recognized as the major source of circulating 1, $25(OH)_2$ D, which is tightly downregulated by the phosphaturic hormone FGF23. It is well established that activation of the FGF23/α-klotho signal is able to inhibit the production of $1,25(OH)_2$ D by suppression of the renal Cyp27b1 expression. In addition, diverse studies point to these active forms, including 1,25(OH) 2 D and 25(OH) D, can be metabolized largely by CYP24A1, while FGF23 could increase the expression of CYP24A1 [25]. It is well known that 1,25(OH)2 D, a steroidal hormone, acts mainly as a ligand of the widely distributed nuclear vitamin D receptor (VDR). Vitamin D compounds reduce the RANKL/OPG ratio and osteoclast differentiation by acting on VDR which is preferentially expressed in osteoblasts and osteocytes in the bone, while mineral-regulating hormones such as PTH and FGF23 plays

a complex role in the VDR-regulated expression of RANKL and OPG in osteoblast lineage cells [26]. Also, interesting results were observed in a recent animal experiment. Klotho −/− VDR Δ/Δ knockout mice, like Klotho −/− -PTH −/− mice, had complete rescue of the skeletal phenotype, while FGF23 −/− VDR Δ/Δ knockout mice did not [27]. These data provided a second line of evidence that Klotho and FGF23 effects independently in bone.

2.2. Phosphate (Pi). FGF23 reduces serum Pi by inhibiting 1,25-dihydroxyvitamin D synthesis, suppressing intestinal Pi absorption, and by downregulating the transporters NPT2a and NPT2c, suppressing Pi reabsorption in the proximal tubules [28]. Of special interest, the organ-specific expression of Klotho has been detected that is practically confined to distal tubules, which is also the site for initial FGF23 binding and signaling. The mechanism of how signals originating in the distal tubules translate into the proximal tubules to reduce Pi reabsorption remains unknown. However, recently, a novel mechanism of efflux of inorganic Pi from renal proximal tubular epithelia has been proposed: Xenotropic and polytropic retrovirus receptor 1 mediates efflux of Pi through the basolateral membrane of the renal proximal tubular epithelia [29]. Furthermore, an in vivo experiment implied a potential role for the FGF23/Klotho/PTH axis in the Pi handling in the proximal tubules [30].

It is confirmed by several studies that a high phosphorus diet decreases the α-Klotho expression. On the contrary, the expression of α-Klotho increased by a Pi-deficient diet in mature mice [31]. One recent study further explored dietary Pi exerts effects on the expression of α-klotho at different life stages, which allowed to hypothesize that there are more adverse effects in weaned mice given high Pi diet on the renal α-klotho expression and pathogenesis of renal calcification compared with periadolescent mice given the same diet [32]. Meanwhile, the main regulatory mechanism of enhanced FGF23 production by high dietary Pi is the post-translational modification of FGF23 protein through a gene product of GALNT3. Furthermore, high extracellular Pi directly activates FGFR1, and its downstream intracellular signaling pathway regulates the expression level of GALNT3 [33]. The capability of increasing FGF23 production in response to high Pi has highlighted the important role of the FGFR1c-GALNT3 axis [34].

2.3. Parathyroid Hormone (PTH). FGF23, which is a hormone synthesized mainly in mature osteoblasts and osteocytes, exerts inhibitive effects on the production of 1,25(OH) 2 D and PTH [35]. Recent clinical studies suggest a very intriguing opposite independent association between PTH and FGF23: premenopausal women exhibited a positive relationship, while FGF23 has a negative relation with PTH in men. To date, the nature of the regulation involved in the links between FGF23 and PTH is not clearly defined, as PTH administration increases circulating FGF23 in some studies, while decreasing it in others [36, 37]. A reasonable explanation is the dual antagonistic effect of FGF23 on parathyroid cells; that is to say, FGF23 directly inhibits the

secretion of PTH and simultaneously inhibits the renal vitamin D activation, thus indirectly stimulating the synthesis of PTH [38]. In addition, the FGF23/Klotho axis has been proposed that it is not essential for the phosphaturic and anabolic functions of PTH by using the novel FGF23 and Klotho knockout mice in other experiments, which further represented PTH as one of the most promising new therapeutic targets for improving the skeletal quality of patients even in the presence of abnormal serum FGF23 levels [39].

2.4. Ectonucleotide Phosphatase/Phosphodiesterase 1 (ENPP1).

ENPP1 was the first enzyme identified and is the only human enzyme capable of generating extracellular pyroPi [40]. Recently, clinical study reported a cohort of middle age men with hereditary early onset osteoporosis (EOOP) manifested by vertebral and/or radial fractures and low bone mass with heterozygous ENPP1 deficiency. Specifically, these patients exhibit mildly elevated FGF23, decreased serum phosphorous, elevated urinary Pi clearance, and radiographic evidence of osteoporosis [41]. This allowed to hypothesize the suppression of murine FGF23 and Alp by human ENPP1-Fc, which was demonstrated later by animal experiments [42]. Other study also showed that Enpp1 loss significantly downregulates the renal Klotho expression under the elevated levels of dietary Pi. Meanwhile, a progressive increase in serum Pi levels promote FGF23 production from the bone, but the FGF23 signals are altered due to the decreased Klotho expression [43].

2.5. Bone Marrow-Derived Mesenchymal Stem Cells (BMSCs).

BMSCs are primarily secreted from mesoderm with infinite expansion and differentiation into the nerve, muscle, and bone. It plays a significant role in bone formation and repair. One latest original study clarified that astragalus exerts influence on the aging BMSC model and on the vitamin D-FGF23-Klotho axis. In fact, it has been verified that changes in astragalus concentration affect diverse factors such as FGF23, Klotho, and CYP24A1. After adding serum-containing astragalus, the activity of cells and the osteogenic ability was increased; the expression levels of FGF23, Klotho, and CYP24A1 were decreased, while the expression levels of CYP27B1 were increased. The trend was more obvious with a progressive increase in astragalus concentration, which finally demonstrated that astragalus has the ability of inhibiting the aging of BMSCs and improving the osteogenesis ability by regulating the VD-FGF23-Klotho pathway. In addition, several evidences point to secreted Klotho, through the inhibition of FGFR1 and ERK phosphorylation, and can delay the differentiation of human mesenchymal stem cells into osteoblasts [44].

2.6. Wnt Signaling.

Historically, the participation of the Wnt/β-catenin pathway in bone disorders has been widely documented. WNT1 in the bone is secreted from osteocytes, and WNT1 mutations may be direct players in the process of impaired WNT/β-catenin signaling and decreased bone formation [45, 46]. However, the mechanisms involved in the direct interaction of FGF23 or Klotho with Wnt elements are not clearly defined. It has been shown that the extracellular domain of Klotho binds to multiple Wnt ligands, specifically inhibiting their ability to activate Wnt signaling [47, 48]. Carrillo et al. identified that FGF23 plays a directly role of inhibiting Wnt signaling through the increase of Dkk1 levels with the participation of soluble Klotho in the bone [49]. Recently, some studies have shown that there is a positive correlation between FGF23 and sclerostin levels in patients with rheumatic arthritis; in this sense, these indicated a direct relationship among FGF23, reduced Wnt activity, and bone demineralization in these patients [50]. In vitro studies, the link between FGF23, Klotho, and Wnt signaling in bone cells had been recently confirmed [51]. Klotho is located within osteocytes and osteoblasts, suggesting that the bone is another target organ for FGF23. Several studies indicate that Klotho as a negative modulator of bone formation [23]. Moreover, the capability of FGF23 with the assistance of klotho is to inhibit Wnt signaling and osteogenesis by enhancing the Dkk1 expression, which is supported by previous observations showing that Wnt activity is increased in Klotho knockout mice [52]. Additionally, Ma et al. observed that in UMR-106, a bone cell line, the addition of β-glycerophosphate upregulates the expression of Wnt target genes; the coadministration of β-glycerophosphate and sKlotho results in a decrease in FGF23 levels and a reduction in Wnt activation, suggesting that sKlotho may modulate osteogenesis and FGF23 production [53].

2.7. NF-κB Signaling Pathway.

In fact, it has been verified that the NF-κB overexpression can promote apoptosis of vascular smooth muscle cells and inhibit cell proliferation [54]. Additionally, NF-κB inhibition results in osteoblast differentiation and bone enhancement [55]. Furthermore, it has been described that activation of NF-κB by palmitate can induce apoptosis of MC3T3-E1 osteoblasts [56]. Growing recent evidence suggests that klotho has inhibitory effects results in the degradation of IκB and activation of nuclear NF-κB [57]. In latest article, the authors reported that the NF-κB inhibitor pyrrolidine dithiocarbamate (PDTC) participates in reducing the number of apoptotic cells and attenuating the activity of caspase-3 induced by DEX, suggesting the involvement of NF-κB in DEX-induced MC3T3-E1 apoptosis [58]. Klotho was demonstrated to be involved in the inhibition of NF-κB activation and the reduction of the DEX-induced caspase-3 expression by these researchers, in consistent with previous studies. These results indicate that NF-κB activation may mediate the antiapoptotic effect of Klotho and proapoptotic effect of DEX.

2.8. Mechanism of the FGF23/Klotho axis on Vascular Calcification.

Patients with advanced CKD were frequently found to have VCs, and at present, it is responsible for the high CVD-related mortality [59]. VC is the final consequence of a process where VSMC is transdifferentiated into osteoblast-like cells [60]. The molecular mechanisms of VC present substantial similarities with those of skeletal bone mineralization.

2.9. Phosphate.

The involvement of elevated FGF23 in the progress of VC is still under debate [61, 62]. A correlation

has been demonstrated between higher FGF23 levels and increased aortic calcification in clinical studies of 65 hemodialysis and 142 patients with CKD stages 2–5 [63]. In contrast, different results were observed in a much larger cohort study named the CRIC (Chronic Renal Insufficiency Cohort), which performed in a cohort of 1501 patients with a mean eGFR of 47 mL/min/1.73 m^2 and showed that there are no associations between FGF23 levels and the prevalence of coronary artery calcification [64]. The CRIC study was further supported by in vitro experiments. Stimulation with FGF23 did not augment phosphate-induced calcification, neither in human vascular smooth muscles cells (VSMCs) in dependence on the Pi concentration nor in aortic rings in the presence of soluble Klotho [64]. Other experimental studies even suggested that FGF23 exerts protective effects on the progression of VC [65]. Recently, Chen et al. further showed that the overexpression of FGF23 and Klotho in rat VSMCs attenuated phosphate-induced calcification by inhibiting Wnt7b/β-catenin signaling [66]. On the contrary, Jimbo et al. reported FGF23 may dedicate an enhanced phosphate-induced calcification in Klotho-overexpressing VSMCs [61]. In other studies, a remarkable aspect is that FGF23 is recognized as a protective factor, since it was observed that depletion of FGF23 levels in rodent CKD models results in a more severe VC [67].

2.10. Intermedin 1–53. Intermedin (IMD) is characterized by a potential endogenous protective peptide of the cardiovascular system, activating the cyclic adenosine monophosphate (cAMP)/protein kinase A (PKA) pathway [68]. Previous studies showed that the levels of IMD downregulated in calcified aortas in vivo and in calcified VSMCs, and IMD$_{1-53}$ treatment was later demonstrated to be involved in the alleviation of vascular calcification [69]. However, a novel mechanism behind the suppression of IMD$_{1-53}$ on VC [70] has been proposed by Chang et al. In their study, IMD$_{1-53}$ administration has been shown to attenuate VC, suppress osteoblast-like cell formation, and increase the expression of Klotho in the aorta of CKD rats. To directly examine the effect of IMD$_{1-53}$ on Klotho and calcification in VSMCs, IMD$_{1-53}$ was applied to cultured VSMCs. An interesting and more importantly aspect is that IMD$_{1-53}$ increased the level of vitro Klotho protein in calcified VSMCs. Klotho knockdown blocked the inhibitory effect of IMD$_{1-53}$ on calcification in VMSCs and transformation of VMSCs into osteoblast-like cells [71]. Taken together, in the basis of the vivo and vitro findings, we consider the numerous processes in which IMD$_{1-53}$ is involved, including as stimulator to upregulate renal, vascular, and plasma Klotho protein levels.

2.11. Peroxisome Proliferator-Activated Receptor γ (PPAR γ). It has been indicated that mice lack Klotho promoted calcification and osteoblastic differentiation of VSMCs [72], whereas Klotho transgenic mice were observed a significant decrease in the incidence of calcifications and have better preserved renal function compared to wild-type mice with CKD [73]. It has been suggested that Klotho suppresses osteoblastic transdifferentiation and calcification of VSMCs by inhibiting PiT-1/2-dependent Pi uptake, thus repressing the expression of Cbfa1/Runx2. Klotho has been identified as a target for nuclear receptor peroxisome proliferator-activated receptor (PPAR) γ [74]. Thiazolidinediones, which act as PPAR γ agonists, participate in the upregulated Klotho expression in HEK293 cells and several renal epithelial cell lines at the mRNA and protein level. This induction was blocked by siRNA-mediated gene silencing of PPAR γ or PPAR γ antagonists, which have been shown to attenuate high glucose-induced VSMC calcification [75]. The latest findings suggested that Klotho plays a modulatory role in the regulation of Pi-induced vascular calcification by PPAR γ, since it has recently been shown that knockdown of Klotho abolished the ability of activated PPAR γ to inhibit calcification in VSMCs. These findings suggested a potential mechanism of PPAR γ in the regulation of Pi-induced vascular calcification [76].

2.12. Salusin-β. Salusins are characterized as two related peptides: salusin-α and salusin-β [77]. In contrast to salusin-α, associations traditionally considered are salusin-β referred to the regulation of cardiovascular and the accelerated development of atherosclerosis [78]. Salusin-β was expressed at high levels in macrophage foam cells, VSMCs, and fibroblasts within atherosclerotic lesions in coronary arteries [79]. CD36 lymphocytes have also been confirmed to play a key role in the formation of foam cells and participate in the uptake of oxidized low-density lipoprotein by macrophages. The interaction between these two key molecules is a hot research topic at present [80]. Moreover, existing evidence demonstrated that salusin-β increased the expressions and activity of acyl coenzyme A-cholesterol acyltransferase-1 (ACAT-1), and silencing of ACAT-1 abolished the salusin-β-induced lipid accumulation. Salusin-β also stimulates the proliferation of VSMCs and fibroblasts and induces the expression of growth-associated genes, such as c-myc and c-fos [77]. These phenomena are regarded as important characteristics of atherosclerosis.

In addition, in light of oxidative stress, salusin-β is widely accepted as an oxidation inducer in cardiac tissues, VSMCs, and endothelial cells in multiple disease scenarios [81]. Klotho is characterized for antiaging that protects cells from inflammation and oxidative stress [82]. Klotho treatment exerts protective effects on the heart from hyperglycemia-induced injury by inactivating the reactive oxygen species (ROS) signaling pathway [83]. In particular, oxidative stress is a significant regulator in the expression of the Klotho gene, and an essential role of the associations of oxidative stress with klotho is in the process of VC [84]. However, the direct evidence involved in the links between salusin-β and Klotho is not clearly defined, and they might target the same oxidative stress signaling pathway. As demonstrated by recent study, Salusin-β regulates VC through activation of NAD(-P)H/ROS-mediated Klotho downregulation, suggesting that salusin-β may represent one of promising new therapeutic targets for the treatment of VC [85].

2.13. Wnt7b/β-Catenin Pathway. The Wnt/β-catenin pathway is accepted as a family of proteins that is implicated in the regulation of many vital functions such as vascular
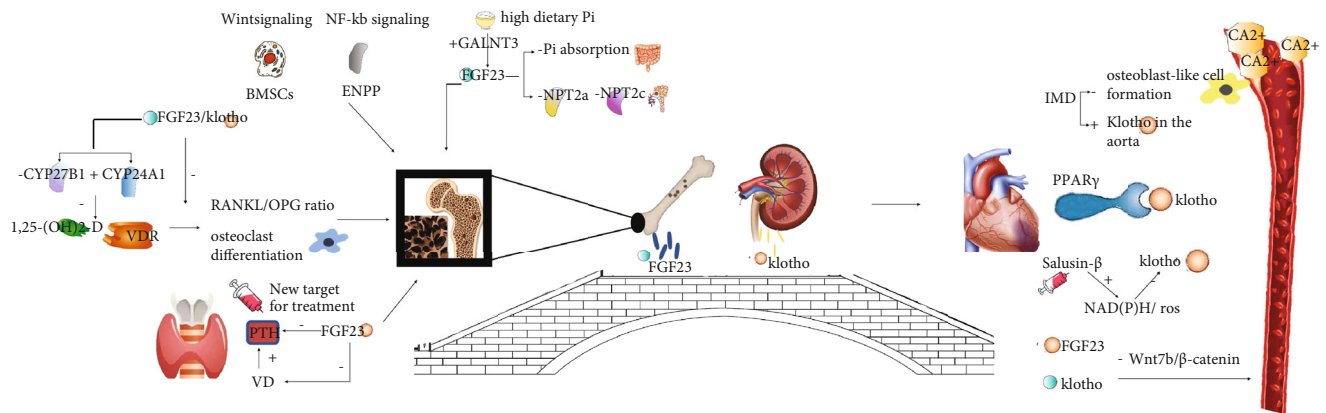
Figure 1: The common mechanism by which the FGF23/Klotho axis affects OP and VC.

calcification [86]. More recently, Yao et al. in a study revealed that high phosphorus level leads to aortic calcification via β-catenin in CKD [87]. Besides, VC in CKD was also reported to be induced via a mechanism involving the Wnt/β-catenin pathway. However, additional studies are needed to specifically address the mechanisms by which the Klotho/FGF23 axis could influence the relevant signaling molecules in Wnt/β-catenin signaling. Recent study demonstrated that both Klotho and FGF23 have opposite effects on the VSMC calcification induced by high phosphate. In addition, Klotho and FGF23 impaired phosphate-induced vascular calcification by inhibiting the Wnt7b/β-catenin pathway [66]. Other studies have shown that inhibition of the Wnt/β-catenin pathway is able to prevent VSMC calcification by Klotho supplementation [88].

The common mechanism by which the FGF23/Klotho axis affects OP and VC was shown in Figure 1.

3. Discussion

The link between OP and VC had been recently confirmed. Patients with OP frequently suffer from VC. Several studies have demonstrated that VC presents substantial similarities with OP, for example, they share several cardiovascular risk factors such as age, hypertension, dyslipidemia, diabetes, and cigarette smoking [5], the majority of studies of our review suggested that this relationship is not only due to the presence of common clinical risk factors but most probably also to underlying biological factors that connect them. Furthermore, a recent retrospective observational study promoted that it seems unlikely that VC could be secondary only to the catabolic processes in the osteoporotic bone, considering the lack of any significant impact of bisphosphonate therapy in the progression of VC [89, 90]. The existence of underlying biohumoral mechanisms indicates that the connection of the two pathological conditions is probable. In support of this, it has been proposed that vitamin D plays a modulatory role in the regulation of both bone metabolism and valve calcification [91]. Vitamin D is the precursor to the active steroid hormone of 1,25-dihydroxyvitamin D (1,25[OH]$_2$ D), known as calcitriol, a key regulator of calcium and phosphorous homeostasis through actions in the intestine, kidneys, and bones. Activated vitamin D binding

to the vitamin D receptor regulates transcription of hundreds of genes, including those involved in cell cycling, proliferation, differentiation, and apoptosis [92]. But interestingly, the results of studies [93, 94] exploring the association between bone mineral density and vascular calcification are inconsistent in terms of race. A study in different races revealed that vitamin D and/or vitamin D precursor levels in European Americans was correlated with BMD and negatively associated in African American [95]. In addition, positive correlations in African Americans between calcified atherosclerotic plaque and 25(OH)D levels have been reported; instead, the associations in European Americans were negatively [96]. Some researchers suppose that there are differences in terms of the appropriate "normal" range for 25(OH)D levels among racial and ethnic groups [97].

Nowadays, the FGF23/Klotho system is considered as a principal regulator of phosphate homeostasis, exerting its effects independently of the two classic endocrine regulating factors: PTH and calcitriol. PTH and calcitriol synthesis is also actively regulated by this system. Overall, the important role of the endocrine bone–kidney–parathyroid gland axis was highlighted by FGF23 to control serum phosphate levels by negative feedbacks over kidney and parathyroid glands [98]. In addition, the relationship between the FGF23/Klotho axis and Wnt signaling pathway has also been revealed [99]. Herein, we discussed the potential role of the FGF23/Klotho axis in the pathophysiology of OP and VC, which we believe that has great clinical value in the context of an aging society.

Although the preliminary basic research on VC hvs shown evidence of pathological mechanisms similar to OP, how will these findings from experimental bench benefit patients with OP and VC? Clearly, animal models have some immanent peculiarities, including differences in bone growth pattern and a relative resistance against atherosclerosis and arterial calcification; thus, further studies are needed to evaluate whether these results can be extrapolated from animal to human. However, progress in imaging techniques will allow higher resolution, shorter acquisition time, and more reasonable radiation exposure in noninvasive preclinical evaluation [100]. With the improvement of techniques, these are becoming more accessible and affordable and should be employed in clinical studies to assess simultaneously OP and VC. Additionally, intervention studies addressing the

question whether treatment of OP benefits VC or vice versa would be desirable, based on the molecular and cellular concepts of VC.

To sum up, studies have revealed common pathogenesis underlying these two frequent age-related disorders by the combined skeletal and vascular phenotypes of animal models. However, additional studies are needed to demonstrate whether these findings can be directly extrapolated to the human OP/VC syndrome. Thus, these data highlight the need of clinicians to employ an open-minded approach with integrative thinking, with the aim to benefit patients with OP and VC.

Data Availability

The data used to support the findings of this study are included within the article.

Conflicts of Interest

The authors declare that there is no conflict of interest regarding the publication of this paper.

Authors' Contributions

Xu Wei, Xinyi Huang and Ning Liu contributed equally to this work.

Acknowledgments

References

[1] M. De Martinis, M. Sirufo, and L. Ginaldi, "Osteoporosis: current and emerging therapies targeted to immunological checkpoints," *Current Medicinal Chemistry*, vol. 26, 2019.

[2] E. Shantsila and G. Y. H. Lip, "Systemic inflammation as a driver of vascular calcification: a proof of concept," *Journal of Internal Medicine*, vol. 266, no. 5, pp. 453–456, 2009.

[3] L. Demer Linda, "Tintut yin, inflammatory, metabolic, and genetic mechanisms of vascular calcification," *Arteriosclerosis, Thrombosis, and Vascular Biology*, vol. 34, pp. 715–723, 2014.

[4] P. Sage Andrew, T. Yin, and L. Demer Linda, "Regulatory mechanisms in vascular calcification," *Nature Reviews. Cardiology*, vol. 7, pp. 528–536, 2010.

[5] L. C. Hofbauer, C. C. Brueck, C. M. Shanahan, M. Schoppet, and H. Dobnig, "Vascular calcification and osteoporosis–from clinical observation towards molecular understanding," *Osteoporosis International*, vol. 18, no. 3, pp. 251–259, 2007.

[6] D. P. Kiel, L. I. Kauppila, L. A. Cupples, M. T. Hannan, C. J. O'Donnell, and P. W. F. Wilson, "Bone loss and the progression of abdominal aortic calcification over a 25 year period: the Framingham heart study," *Calcified Tissue International*, vol. 68, no. 5, pp. 271–276, 2001.

[7] R. Virchow, "As based upon physiological and pathological histology. Lecture XVI–atheromatous affection of arteries," *Nutrition Reviews*, vol. 47, pp. 23–25, 1989.

[8] A. Zengin, L. M. Jarjou, R. E. Janha et al., "Sex-specific associations between cardiac workload, peripheral vascular calcification, and bone mineral density: the Gambian bone and muscle aging study," *Journal of Bone and Mineral Research*, vol. 36, article BF02390833, pp. 227–235, 2021.

[9] X. Xu, M. Zhang, Z. Fei, H. Sheng, S. Qu, and R. Cui, "Calcification of lower extremity arteries is related to the presence of osteoporosis in postmenopausal women with type 2 diabetes mellitus: a cross-sectional observational study," *Osteoporosis International*, vol. 32, no. 6, pp. 1185–1193, 2021.

[10] R. Cui, S. Q. Sun, N. Zhong et al., "The relationship between atherosclerosis and bone mineral density in patients with type 2 diabetes depends on vascular calcifications and sex," *Osteoporosis International*, vol. 31, no. 6, pp. 1135–1143, 2020.

[11] D. Hamerman, "Osteoporosis and atherosclerosis: biological linkage and the emergence of dual-purpose therapies," *The Quarterly Journal of Medicine*, vol. 98, pp. 467–484, 2005.

[12] N. Carrillo-López, On behalf of the European Renal Osteodystrophy (EUROD) Workgroup, L. Martínez-Arias et al., "Role of the RANK/RANKL/OPG and Wnt/β-catenin systems in CKD bone and cardiovascular disorders," *Calcified Tissue International*, vol. 108, no. 4, pp. 439–451, 2021.

[13] C. G. Sotomayor, S. Benjamens, A. W. Gomes-Neto et al., "Bone mineral density and aortic calcification: evidence for a bone-vascular Axis after kidney transplantation," *Transplantation*, vol. 105, pp. 231–239, 2021.

[14] P. Luciano and M. Frazão João, "The bone-vessel axis in chronic kidney disease: an update on biochemical players and its future role in laboratory medicine," *Clinica Chimica Acta*, vol. 508, pp. 221–227, 2020.

[15] S. Delia, "Correlation between osteoporosis and cardiovascular disease," *Clinical Cases in Mineral and Bone Metabolism*, vol. 11, pp. 117–119, 2014.

[16] L. L. Demer and Y. Tintut, "The leading edge of vascular calcification," *Trends in Cardiovascular Medicine*, vol. 25, no. 4, pp. 275–277, 2015.

[17] J. Donate-Correa, M. Muros-de-Fuentes, C. Mora-Fernández, and J. F. Navarro-González, "FGF23/Klotho axis: phosphorus, mineral metabolism and beyond," *Cytokine & Growth Factor Reviews*, vol. 23, pp. 37–46, 2012.

[18] M. S. Razzaque, "Fgf23-mediated regulation of systemic phosphate homeostasis: is klotho an essential player?," *American Journal of Physiology - Renal Physiology*, vol. 296, pp. F470–F476, 2009.

[19] M. Baum, S. Schiavi, V. Dwarakanath, and R. Quigley, "Effect of fibroblast growth factor-23 on phosphate transport in proximal tubules," *Kidney International*, vol. 68, pp. 1148–1153, 2005.

[20] L.-C. Desbiens, A. Sidibé, R.-V. Ung et al., "FGF23-klotho axis, bone fractures, and arterial stiffness in dialysis: a case-control study," *Osteoporosis International*, vol. 29, no. 10, pp. 2345–2353, 2018.

[21] T. Nakahara, K. Kawai-Kowase, H. Matsui et al., "Fibroblast growth factor 23 inhibits osteoblastic gene expression and induces osteoprotegerin in vascular smooth muscle cells," *Atherosclerosis*, vol. 253, pp. 102–110, 2016.

[22] S. Yamada and C. M. Giachelli, "Vascular calcification in CKD-MBD: roles for phosphate, FGF23, and klotho," *Bone*, vol. 100, pp. 87–93, 2017.

[23] H. Komaba, J. Kaludjerovic, D. Z. Hu et al., "Klotho expression in osteocytes regulates bone metabolism and controls bone formation," *Kidney International*, vol. 92, pp. 599–611, 2017.

[24] M. Dengshun and G. David, "Probing the scope and mechanisms of calcitriol actions using genetically modified mouse models," *JBMR Plus*, vol. 5, article e10434, 2021.

[25] T. Shimada, H. Hasegawa, Y. Yamazaki et al., "FGF-23 is a potent regulator of vitamin D metabolism and phosphate homeostasis," *Journal of Bone and Mineral Research*, vol. 19, no. 3, pp. 429–435, 2004.

[26] Y. Nakamichi, N. Udagawa, T. Suda, and N. Takahashi, "Mechanisms involved in bone resorption regulated by vitamin D," *The Journal of Steroid Biochemistry and Molecular Biology*, vol. 177, pp. 70–76, 2018.

[27] P. Ostergaard, E. Andersen, B. J. Sellevold, and T. Solheim, "The occurrence of denticles in the craniums of Norwegian Samis (Lapps)," *Tandlaegebladet*, vol. 93, no. 3, pp. 88–91, 1989.

[28] B. Ho Bryan and B. Clemens, "FGF23 signalling and physiology," *Journal of Molecular Endocrinology*, vol. 66, pp. R23–R32, 2021.

[29] C. Ansermet, M. B. Moor, G. Centeno et al., "Renal fanconi syndrome and hypophosphatemic rickets in the absence of xenotropic and polytropic retroviral receptor in the nephron," *Journal of the American Society of Nephrology*, vol. 28, pp. 1073–1078, 2017.

[30] N. Ide, R. Ye, M. Courbebaisse et al., "In vivo evidence for an interplay of FGF23/Klotho/PTH axis on the phosphate handling in renal proximal tubules," *American Journal of Physiology. Renal Physiology*, vol. 315, pp. F1261–F1270, 2018.

[31] K. Morishita, A. Shirai, M. Kubota et al., "The progression of aging in klotho mutant mice can be modified by dietary phosphorus and zinc," *The Journal of Nutrition*, vol. 131, pp. 3182–3188, 2001.

[32] S. Fukuda-Tatano, H. Yamamoto, O. Nakahashi et al., "Regulation of α-Klotho expression by dietary phosphate during growth periods," *Calcified Tissue International*, vol. 104, pp. 667–678, 2019.

[33] Y. Takashi and S. Fukumoto, "Phosphate-sensing and regulatory mechanism of FGF23 production," *Journal of Endocrinological Investigation*, vol. 43, pp. 877–883, 2020.

[34] T. Yuichi and F. Seiji, "Fibroblast growth factor receptor as a potential candidate for phosphate sensing," *Current Opinion in Nephrology and Hypertension*, vol. 29, pp. 446–452, 2020.

[35] J. Bacchetta, C. Bardet, and D. Prié, "Physiology of FGF23 and overview of genetic diseases associated with renal phosphate wasting," *Metabolism*, vol. 103S, p. 153865, 2020.

[36] M. Sridharan, J. Cheung, A. E. Moore et al., "Circulating fibroblast growth factor-23 increases following intermittent parathyroid hormone (1-34) in postmenopausal osteoporosis: association with biomarker of bone formation," *Calcified Tissue International*, vol. 87, no. 5, pp. 398–405, 2010.

[37] R. Samadfam, C. Richard, L. Nguyen-Yamamoto, I. Bolivar, and D. Goltzman, "Bone formation regulates circulating concentrations of fibroblast growth factor 23," *Endocrinology*, vol. 150, no. 11, pp. 4835–4845, 2009.

[38] H. Juppner, M. Wolf, and I. B. Salusky, "FGF-23: more than a regulator of renal phosphate handling?," *Journal of Bone and Mineral Research*, vol. 25, pp. 2091–2097, 2010.

[39] Q. Yuan, T. Sato, M. Densmore et al., "Fgf23/klotho signaling is not essential for the phosphaturic and anabolic functions of PTH," *Journal of Bone and Mineral Research*, vol. 26, no. 9, pp. 2026–2035, 2011.

[40] F. Rutsch, S. Vaingankar, K. Johnson et al., "PC-1 Nucleoside Triphosphate Pyrophosphohydrolase Deficiency in Idiopathic Infantile Arterial Calcification," *The American journal of pathology*, vol. 158, no. 2, pp. 543–554, 2001.

[41] R. Oheim, K. Zimmerman, N. D. Maulding et al., "Human heterozygous ENPP1 deficiency is associated with early onset osteoporosis, a phenotype recapitulated in a mouse model of Enpp1 deficiency," *Journal of Bone and Mineral Research*, 2019.

[42] N. D. Maulding, D. Kavanagh, K. Zimmerman et al., "Genetic pathways disrupted by ENPP1 deficiency provide insight into mechanisms of osteoporosis, osteomalacia, and paradoxical mineralization," *Bone*, vol. 142, p. 115656, 2021.

[43] R. Watanabe, N. Fujita, Y. Sato et al., "Enpp1 is an anti-aging factor that regulates Klotho under phosphate overload conditions," *Scientific Reports*, vol. 7, p. 7786, 2017.

[44] W. Zhang, D. Xue, D. Hu et al., "Secreted klotho protein attenuates osteogenic differentiation of human bone marrow mesenchymal stem cells in vitro via inactivation of the FGFR1/ERK signaling pathway," *Growth Factors*, vol. 33, pp. 356–365, 2015.

[45] K. S. Joeng, Y.-C. Lee, J. Lim et al., "Osteocyte-specific WNT1 regulates osteoblast function during bone homeostasis," *The Journal of Clinical Investigation*, vol. 127, pp. 2678–2688, 2017.

[46] J. Luther, T. A. Yorgan, T. Rolvien et al., "Wnt1 is an Lrp5-independent bone-anabolic Wnt ligand," *Science Translational Medicine*, vol. 10, no. 466, p. eaau7137, 2018.

[47] Y. Wang and Z. Sun, "Current understanding of klotho," *Ageing Research Reviews*, vol. 8, pp. 43–51, 2009.

[48] L. Zhou, Y. Li, D. Zhou et al., "Loss of Klotho contributes to kidney injury by derepression of Wnt/β-catenin signaling," *Journal of the American Society of Nephrology*, vol. 24, pp. 771–785, 2013.

[49] N. Carrillo-López, S. Panizo, C. Alonso-Montes et al., "Direct inhibition of osteoblastic Wnt pathway by fibroblast growth factor 23 contributes to bone loss in chronic kidney disease," *Kidney International*, vol. 90, pp. 77–89, 2016.

[50] A. Fayed, R. Elgohary, and M. Fawzy, "Evaluating the role of serum sclerostin as an indicator of activity and damage in Egyptian patients with rheumatoid arthritis: university hospital experience," *Clinical Rheumatology*, vol. 39, no. 4, pp. 1121–1130, 2020.

[51] A. Raimann, D. A. Ertl, M. Helmreich, S. Sagmeister, M. Egerbacher, and G. Haeusler, "Fibroblast growth factor 23 and Klotho are present in the growth plate," *Connective Tissue Research*, vol. 54, pp. 108–117, 2013.

[52] Q. Yuan, T. Sato, M. Densmore et al., "Deletion of PTH rescues skeletal abnormalities and high osteopontin levels in Klotho-/- mice," *PLoS Genetics*, vol. 8, no. 5, article e1002726, 2012.

[53] L. Ma, M. Gao, L. Wu, X. Zhao, H. Mao, and C. Xing, "The suppressive effect of soluble Klotho on fibroblastic growth factor 23 synthesis in UMR-106 osteoblast-like cells," *Cell Biology International*, vol. 42, no. 9, pp. 1270–1274, 2018.

[54] L. Jiao, M. Jiang, J. Liu, L. Wei, and M. Wu, "Nuclear factor-kappa B activation inhibits proliferation and promotes apoptosis of vascular smooth muscle cells," *Vascular*, vol. 3, p. 170853811878712, 2018.

[55] A. Rauch, S. Seitz, U. Baschant et al., "Glucocorticoids suppress bone formation by attenuating osteoblast

differentiation via the monomeric glucocorticoid receptor," *Cell Metabolism*, vol. 11, no. 6, p. 517e531, 2010.

[56] J.-W. Gu, E. Young, B. Busby, J. Covington, and J. W. Johnson, "Oral administration of pyrrolidine dithiocarbamate (PDTC) inhibits VEGF expression, tumor angiogenesis, and growth of breast cancer in female mice," *Cancer Biology & Therapy*, vol. 8, no. 6, p. 514e521, 2009.

[57] P. Buendía, R. Ramírez, P. Aljama, and J. Carracedo, "Klotho prevents translocation of NF-κB," *Vitamins & Hormones*, vol. 101, p. 119e150, 2016.

[58] X. Liang, B. Li, Q. Huang, D. Liu, and H. Ma, "Klotho prevents DEX-induced apoptosis in MC3T3-E1 osteoblasts through the NF-κB signaling pathway," *Biochemical and Biophysical Research Communications*, vol. 507, no. 1-4, pp. 355–361, 2018.

[59] G. M. London, S. J. Marchais, A. P. Guérin, and F. Métivier, "arteriosclerosis, vascular calcifications and cardiovascular disease in uremia," *Current opinion in nephrology and hypertension*, vol. 14, pp. 525–531, 2005.

[60] C. M. Shanahan, M. H. Crouthamel, A. Kapustin, and C. M. Giachelli, "Arterial calcification in chronic kidney disease: key roles for calcium and phosphate," *Circulation Research*, vol. 109, no. 6, pp. 697–711, 2011.

[61] R. Jimbo, F. Kawakami-Mori, S. Mu et al., "Fibroblast growth factor 23 accelerates phosphate-induced vascular calcification in the absence of Klotho deficiency," *Kidney International*, vol. 85, no. 5, pp. 1103–1111, 2014.

[62] D. Zhu, N. C. Mackenzie, J. L. Millan, C. Farquharson, and V. E. MacRae, "A protective role for FGF-23 in local Defence against disrupted Arterial Wall integrity?," *Molecular and Cellular Endocrinology*, vol. 372, no. 1-2, pp. 1–11, 2013.

[63] M. M. Nasrallah, A. R. El-Shehaby, M. M. Salem, N. A. Osman, E. El Sheikh, and U. A. S. El Din, "Fibroblast growth Factor-23 (FGF-23) is independently correlated to aortic calcification in haemodialysis patients," *Nephrology, Dialysis, Transplantation*, vol. 25, pp. 2679–2685, 2010.

[64] J. J. Scialla, W. L. Lau, M. P. Reilly et al., "Fibroblast growth factor 23 is not associated with and does not induce arterial calcification," *Kidney International*, vol. 83, pp. 1159–1168, 2013.

[65] E. L. Clinkenbeard, M. L. Noonan, J. C. Thomas et al., "Increased FGF23 protects against detrimental cardio-renal consequences during elevated blood phosphate in CKD," *JCI Insight*, vol. 4, p. 123817, 2019.

[66] Y. Chen, C. Huang, Z. Duan, C. Y. Xu, and Y. Chen, "Klotho/FGF23 axis mediates high phosphate-induced vascular calcification in vascular smooth muscle cells via Wnt7b/β-catenin pathway," *The Kaohsiung Journal of Medical Sciences*, vol. 35, no. 7, pp. 393–400, 2019.

[67] V. Shalhoub, E. M. Shatzen, S. C. Ward et al., "FGF23 neutralization improves chronic kidney disease–associated hyperparathyroidism yet increases mortality," *Journal of Clinical Investigation*, vol. 122, no. 7, pp. 2543–2553, 2012.

[68] Y. Hong, D. L. Hay, R. Quirion, and D. R. Poyner, "The pharmacology of adrenomedullin 2/intermedin," *British Journal of Pharmacology*, vol. 166, no. 1, pp. 110–120, 2012.

[69] Y. Cai, M. J. Xu, X. Teng et al., "Intermedin inhibits vascular calcification by increasing the level of matrix gamma-carboxyglutamic acid protein," *Cardiovascular Research*, vol. 85, no. 4, pp. 864–873, 2010.

[70] J. R. Chang, J. Guo, Y. Wang et al., "Intermedin$_{1-53}$ attenuates vascular calcification in rats with chronic kidney disease by

[71] M. C. Hu, K. Shiizaki, M. Kuro-o, and O. W. Moe, "Fibroblast growth factor 23 and Klotho: physiology and pathophysiology of an endocrine network of mineral metabolism," *Annual Review of Physiology*, vol. 75, no. 1, pp. 503–533, 2013.

[72] K. Lim, T. S. Lu, G. Molostvov et al., "Vascular Klotho deficiency potentiates the development of human artery calcification and mediates resistance to fibroblast growth factor 23," *Circulation*, vol. 125, no. 18, pp. 2243–2255, 2012.

[73] M. C. Hu, M. Shi, J. Zhang et al., "Klotho deficiency causes vascular calcification in chronic kidney disease," *Journal of the American Society of Nephrology*, vol. 22, no. 1, pp. 124–136, 2011.

[74] H. Zhang, Y. Li, Y. Fan et al., "Klotho is a target gene of PPAR-γ," *Kidney International*, vol. 74, no. 6, pp. 732–739, 2008.

[75] Y. B. Zhou, J. Zhang, D. Q. Peng et al., "Peroxisome proliferator-activated receptor γ ligands retard cultured vascular smooth muscle cells calcification induced by high glucose," *Cell Biochemistry and Biophysics*, vol. 66, no. 3, pp. 421–429, 2013.

[76] L. Cheng, L. Zhang, J. Yang, and L. Hao, "Activation of peroxisome proliferator-activated receptor γ inhibits vascular calcification by upregulating klotho," *Experimental and Therapeutic Medicine*, vol. 13, no. 2, pp. 467–474, 2017.

[77] M. Shichiri, S. Ishimaru, T. Ota, T. Nishikawa, T. Isogai, and Y. Hirata, "Salusins: newly identified bioactive peptides with hemodynamic and mitogenic activities," *Nature Medicine*, vol. 9, no. 9, pp. 1166–1172, 2003.

[78] M. Nagashima, T. Watanabe, Y. Shiraishi et al., "Chronic infusion of salusin-α and -β exerts opposite effects on atherosclerotic lesion development in apolipoprotein E-deficient mice," *Atherosclerosis*, vol. 212, no. 1, pp. 70–77, 2010.

[79] T. Watanabe, K. Nishio, T. Kanome et al., "Impact of salusin-α and -β on human macrophage foam cell formation and coronary atherosclerosis," *Circulation*, vol. 117, no. 5, pp. 638–648, 2008.

[80] F. J. O. Rios, M. Ferracini, M. Pecenin et al., "Uptake of oxLDL and IL-10 production by macrophages requires PAFR and CD36 recruitment into the same lipid rafts," *PLoS One*, A. Cignarella, Ed., vol. 8, no. 10, article e76893, 2013.

[81] H.-J. Sun, D. Chen, P.-Y. Wang et al., "Salusin-beta is involved in diabetes mellitus-induced endothelial dysfunction via degradation of peroxisome proliferator-activated receptor gamma," *Oxidative Medicine and Cellular Longevity*, vol. 2017, 2017.

[82] G. Jia, A. R. Aroor, C. Jia, and J. R. Sowers, "Endothelial cell senescence in aging-related vascular dysfunction," *Biochimica et Biophysica Acta - Molecular Basis of Disease*, vol. 1865, pp. 1802–1809, 2019.

[83] Y. Guo, X. Zhuang, Z. Huang et al., "Klotho protects the heart from hyperglycemia-induced injury by inactivating ROS and NF-kappa B-mediated inflammation both in vitro and in vivo," *Biochimica et Biophysica Acta - Molecular Basis of Disease*, vol. 1864, pp. 238–251, 2018.

[84] R. Mencke and J. L. Hillebrands, "The role of the anti-ageing protein klotho in vascular physiology and pathophysiology," *Ageing Research Reviews*, vol. 35, pp. 124–146, 2017.

[85] H. Sun, F. Zhang, Y. Xu et al., "Salusin-β promotes vascular calcification via nicotinamide adenine dinucleotide phosphate/reactive oxygen species-mediated klotho downregulation,"

Antioxidants & Redox Signaling, vol. 31, pp. 1352–1370, 2019.

[86] S. Rong, X. Zhao, X. Jin et al., "Vascular calcification in chronic kidney disease is induced by bone morphogenetic protein-2 via a mechanism involving the Wnt/β-catenin pathway," *Cellular Physiology and Biochemistry*, vol. 34, no. 6, pp. 2049–2060, 2014.

[87] L. Yao, Y. T. Sun, W. Sun et al., "High phosphorus level leads to aortic calcification via β-Catenin in chronic kidney disease," *American Journal of Nephrology*, vol. 41, no. 1, pp. 28–36, 2015.

[88] T. Chen, H. Mao, C. Chen et al., "The Role and Mechanism of α-Klotho in the Calcification of Rat Aortic Vascular Smooth Muscle Cells," *BioMed Research International*, vol. 2015, 7 pages, 2015.

[89] O. Aksoy, A. Cam, S. S. Goel et al., "Do bisphosphonates slow the progression of aortic stenosis?," *Journal of the American College of Cardiology*, vol. 59, no. 16, pp. 1452–1459, 2012.

[90] S. R. K. EttaPK, "Gupta a. study of chronic kidney disease-mineral bone disorders in newly detected advanced renal failure patients: a hospital-based cross-sectional study," *Saudi Journal of Kidney Diseases and Transplantation*, vol. 28, no. 4, pp. 874–885, 2017.

[91] D. Bellavia, V. Costa, A. de Luca et al., "Vitamin D level between calcium-phosphorus homeostasis and immune system: new perspective in osteoporosis," *Current Osteoporosis Reports*, 2016.

[92] H. A. Morris and P. H. Anderson, "Autocrine and paracrine actions of vitamin D," *Clinical Biochemist Reviews*, vol. 31, pp. 129–138, 2010.

[93] L. S. Acheson, "Bone density and the risk of fractures: should treatment thresholds vary by race?," *JAMA*, vol. 293, no. 17, pp. 2151–2154, 2005.

[94] J. F. Aloia, "African Americans, 25-hydroxyvitamin D, and osteoporosis: a paradox," *The American Journal of Clinical Nutrition*, vol. 88, no. 2, pp. 545S–550S, 2008.

[95] B. I. Freedman, L. E. Wagenknecht, K. G. Hairston et al., "vitamin D, adiposity, and calcified atherosclerotic plaque in African Americans," *The Journal of Clinical Endocrinology & Metabolism*, vol. 95, no. 3, pp. 1076–1083, 2010.

[96] R. Detrano, A. D. Guerci, J. J. Carr et al., "Coronary calcium as a predictor of coronary events in four racial or ethnic groups," *The New England Journal of Medicine*, vol. 358, no. 13, pp. 1336–1345, 2008.

[97] A. C. Ross, J. E. Manson, S. A. Abrams et al., "The 2011 report on dietary reference intakes for calcium and vitamin D from the Institute of Medicine: what clinicians need to know," *The Journal of Clinical Endocrinology & Metabolism*, vol. 96, no. 1, pp. 53–58, 2011.

[98] M. Kuro-o, "Klotho in chronic kidney disease—what's new?," *Nephrology, Dialysis, Transplantation*, vol. 24, pp. 1705–1708, 2009.

[99] J. R. Muñoz-Castañeda, C. Rodelo-Haad, M. V. Pendon-Ruiz de Mier, A. Martin-Malo, R. Santamaria, and M. Rodriguez, "Klotho/FGF23 and Wnt signaling as important players in the comorbidities associated with chronic kidney disease," *Toxins*, vol. 12, pp. 1–17, 2020.

[100] G. R. Thompson and J. Partridge, "Coronary calcification score: the coronary-risk impact factor," *Lancet*, vol. 363, pp. 557–559, 2004.

Review Article

COVID-19 and Acute Coronary Syndromes: From Pathophysiology to Clinical Perspectives

Luca Esposito [ID],[1] **Francesco Paolo Cancro** [ID],[1] **Angelo Silverio** [ID],[1] **Marco Di Maio,**[1]
Patrizia Iannece,[2] **Antonio Damato,**[3] **Carmine Alfano,**[1] **Giuseppe De Luca,**[4]
Carmine Vecchione,[1,3] **and Gennaro Galasso** [ID][1]

[1]*Department of Medicine, Surgery and Dentistry, University of Salerno, Baronissi, Salerno, Italy*
[2]*Department of Chemistry and Biology, University of Salerno, Fisciano, Italy*
[3]*Vascular Pathophysiology Unit, IRCCS Neuromed, Pozzilli, Isernia, Italy*
[4]*Division of Cardiology, Azienda Ospedaliera-Universitaria "Maggiore della Carità," Eastern Piedmont University, Novara, Italy*

Correspondence should be addressed to Gennaro Galasso; ggalasso@unisa.it

Academic Editor: John D. Horowitz

Acute coronary syndromes (ACS) are frequently reported in patients with coronavirus disease 2019 (COVID-19) and may impact patient clinical course and mortality. Although the underlying pathogenesis remains unclear, several potential mechanisms have been hypothesized, including oxygen supply/demand imbalance, direct viral cellular damage, systemic inflammatory response with cytokine-mediated injury, microvascular thrombosis, and endothelial dysfunction. The severe hypoxic state, combined with other conditions frequently reported in COVID-19, namely sepsis, tachyarrhythmias, anemia, hypotension, and shock, can induce a myocardial damage due to the mismatch between oxygen supply and demand and results in type 2 myocardial infarction (MI). In addition, COVID-19 promotes atherosclerotic plaque instability and thrombus formation and may precipitate type 1 MI. Patients with severe disease often show decrease in platelets count, higher levels of d-dimer, ultralarge von Willebrand factor multimers, tissue factor, and prolongation of prothrombin time, which reflects a prothrombotic state. An endothelial dysfunction has been described as a consequence of the direct viral effects and of the hyperinflammatory environment. The expression of tissue factor, von Willebrand factor, thromboxane, and plasminogen activator inhibitor-1 promotes the prothrombotic status. In addition, endothelial cells generate superoxide anions, with enhanced local oxidative stress, and endothelin-1, which affects the vasodilator/vasoconstrictor balance and platelet aggregation. The optimal management of COVID-19 patients is a challenge both for logistic and clinical reasons. A deeper understanding of ACS pathophysiology may yield novel research insights and therapeutic perspectives in higher cardiovascular risk subjects with COVID-19.

1. Introduction

After the identifications of the first cases in Wuhan, China, coronavirus disease 2019 (COVID-19) rapidly spread worldwide and took on pandemic proportions [1, 2].

Although primarily affecting the respiratory tract, the clinical course of COVID-19 may be complicated by several systemic and potentially life-threatening conditions, with a reported inhospital mortality rate ranging from 9% to 15% [3].

Cardiovascular (CV) involvement is frequently reported in COVID-19 and may impact on patient clinical outcome and mortality risk [4–7].

Acute coronary syndrome (ACS) has been reported in a substantial proportion of patients with COVID-19 [8, 9]. Although the underlying pathogenesis remains unclear, several potential mechanisms have been hypothesized, including direct viral cellular damage, systemic inflammatory response with cytokine-mediated injury, microvascular thrombosis, endothelial dysfunction, and oxygen supply/demand

imbalance due to the severe hypoxic state [10–14]. Moreover, as described in other infective diseases, COVID-19 may promote atherosclerotic plaque instability and thrombus formation and precipitate type 1 myocardial infarction (MI) [15, 16].

In this review, we aimed at describing the pathophysiological mechanisms of ACS in patients with COVID-19, with a focus on the translational perspectives and potential clinical applications.

2. Pathogenesis and Transmission of COVID-19

COVID-19 is caused by severe acute respiratory syndrome coronavirus-2 (SARS-CoV-2), a novel β-coronavirus infecting human cells of the respiratory tract, vascular endothelium, heart, gut, and immune system [17]. The virus binds the angiotensin-converting enzyme 2 (ACE2) receptor, highly expressed on the target host cells, through a spike (S) protein that enables the fusion of membranes and viral internalization [18, 19]. In particular, endothelial cells and cardiac pericytes express abundant ACE2, making them highly susceptible to SARS-CoV-2 interaction and internalization.

The interferon-mediated upregulation of ACE2 may facilitate the involvement of adjacent pneumocytes and the development of an uncontrolled inflammatory reaction, microvascular thrombosis, interstitial and alveolar edema, and eventual progression toward acute respiratory distress syndrome (ARDS) [20], Moreover, it has been hypothesized that SARS-CoV-2, by interacting with ACE2 for the cell entry, causes a downregulation of the bound ACE2 and increases the circulating level of soluble ACE2. This deregulation affects the activity of bound ACE2, which is associated with several beneficial effects by regulating the inflammatory response, reducing oxidative stress, and promoting vessel relaxation via the production of angiotensin1-7 (Ang1-7) [17, 21]. It seems reasonable to hypothesize that, similarly to SARS-CoV-1, SARS-CoV-2 promotes the cleavage of ACE2 receptors leading to lower Ang1-7 serum levels [22]. However, only one in vitro study has showed that SARS-CoV-2 downregulates the ACE2 expression, and further studies are needed to confirm this pathophysiological pathway [23]. SARS-CoV-2 is transmitted from person to person via close contact through respiratory droplets and viral particles inhalation, with a mean incubation of about five days [24]. Viral load detected in the asymptomatic and symptomatic subjects appears to be similar, suggesting that asymptomatic subjects can transmit the virus as well as the symptomatic ones [25].

The initial symptoms are very similar to other viral respiratory syndromes and include fever, cough, shortness of breath, fatigue, myalgias, headache and gastrointestinal involvement. [1] The clinical spectrum of COVID-19 manifestations is particularly wide, ranging from asymptomatic or minimally symptomatic to life-threatening or fatal forms, characterized by systemic inflammatory response syndrome, ARDS, multiple organ failures, and death [26]. CV involvement has been frequently reported in hospitalized patients with COVID-19 and may impacts the length of hospitalization, clinical severity, rate of admission in intensive care unit, and probability of survival [4, 9].

3. The Epidemiology Paradox of ACS in COVID-19

Although COVID-19 may be complicated by coronary plaque instability and myocardial oxygen supply/demand imbalance, multiple investigators worldwide have reported a marked reduction in the rate of hospitalization for ACS during the peak of pandemic. Data from the ISACS-STEMI COVID-19 registry showed a significant drop in the number of ST-elevation MI (STEMI) patients invasively treated from 2019 to 2020, with a 18.9% reduction of admissions for STEMI in the last year. Patients treated in 2020 also had longer ischemia and door-to-balloon time [27]. Another study conducted in China showed that the number of primary percutaneous coronary intervention (PCI) dropped by more than a half in the first three months of 2020 compared to 2018 and 2019, while the number of patients treated with fibrinolysis increased by 2 to 3 times. Also in this study, a longer time to reperfusion was reported among patients treated in 2020 [28].

The significant reduction of hospitalization for ACS registered all over the world has been associated with a substantial reduction in the total number of urgent and emergent coronary angiography performed [29–33]. Despite the delay in the reperfusion time, most of STEMI patients without COVID-19 underwent emergent coronary angiography and primary PCI as per standard of care [34]. Conversely, COVID-19 patients with STEMI frequently did not receive guideline-recommended treatments, and the use of fibrinolysis over PCI has been reported in a high number of cases [27, 28, 35, 36]. In a cohort of 78 COVID-19 patients with STEMI, noninvasive treatment with fibrinolysis, instead of primary PCI, was reported as the most performed strategy in 3 out of 4 cases [27].

Changes in the epidemiology of STEMI may have several potential interpretations. First, social distancing, the fear of contagion, and the prominent media attention on the uncontrolled spread of the disease might have reduced the awareness of the population towards other life-threatening conditions, such as ACS. Second, the redistribution of healthcare resources in the struggle against the overwhelming pandemic could have weaken the local emergency networks, as highlighted by the reported system delays. Additionally, although seemingly contradictory given the risk of COVID-19-related thrombotic complications, the contribution of an actual reduction of ACS due to less emotional and physical triggering cannot be excluded, a plausible phenomenon after the prompt adoption of national lockdowns during the first period of the pandemic [37].

The lower rate of admission for STEMI has been associated with the increased incidence of out-of-hospital cardiac arrest and mechanical complications reported in this period [38–40]. This has raised the attention of health organizations worldwide and calls for caution and further investigations.

4. Mechanisms of ACS in COVID-19

The potential underlying mechanisms of ACS in COVID-19 may be multiple and to date are not fully understood. The spectrum of pathophysiological mechanisms reflects the distinctive clinical features of patients with confirmed MI diagnosis, such as the angiographic evidence of non-obstructed coronary arteries, stent thrombosis, multiple thrombotic culprit lesions, and high thrombus burden [27, 41, 42]. Sometimes, MI has been the first manifestation of the disease, suggesting that ACS should be considered as a specific thrombotic complication of SARS-CoV-2 infection [41, 43]. The most recognized mechanisms include cytokine-mediated systemic inflammatory response, prothrombotic activation of the coagulation cascade, endothelial dysfunction, and hypoxic injury due to oxygen supply/demand imbalance (Figure 1).

4.1. Hemostatic Abnormalities.
Several hemostatic abnormalities have been reported in COVID-19. Patients with severe disease often show decrease in platelets count, higher levels of d-dimer, and prolongation of prothrombin time [44, 45]; these abnormalities have showed negative prognostic impact in cohorts of hospitalized patients with COVID-19. In an observational study conducted in Wuhan, China, patients admitted to the intensive care unit (ICU) had significant higher plasma levels of d-dimer than patients who did not need ICU care [46]. Similarly, Tang et al. reported increased levels of d-dimer and fibrinogen degradation products and a mild prolongation of prothrombin time in fatal cases, compared with patients who survived [47]. The reason for this prothrombotic state is not completely understood; moreover, it is unclear whether these abnormalities are imputable to direct viral effects on the coagulation cascade or to the cytokine-mediated inflammatory response [48]. A recent prospective study comparing laboratory findings in cases with COVID-19-related ARDS with a historic cohort of patient with nonCOVID-19-related ARDS showed a significant increase in procoagulant factors in patients with SARS-CoV-2 infection, correlated with the elevation of the acute phase reactants. These findings suggest a major role of the cytokine storm (CS) in COVID-19-related coagulopathy [49]. Cytokines produced during the systemic inflammatory response induce the overexpression of ultralarge von Willebrand factor multimers (ULVWF) and tissue factor (TF), which are involved in the primary and secondary hemostatic mechanisms, respectively [47, 50, 51]. These factors may act as major triggers in the activation of the coagulation cascade, resulting in a hypercoagulability status characterized by increased production of thrombin [52]. In addition, the presence of a positive lupus anticoagulant (LA) might further contribute to SARS-CoV-2- related coagulopathy [50]. LA antibodies are produced in clinical circumstances characterized by high cellular lysis, such as infectious, inflammatory, and immune diseases; in such cases, the occurrence of cellular damage, caused by the oxidative stress on the endothelium, exposes phospholipids usually not accessible to the immune system, with consequent induction of thrombus formation [53].

This multifactorial coagulopathy justifies the common incidence of life-threatening thrombotic complications, such as venous thromboembolism (VTE), pulmonary embolism (PE), and ACS [7, 10, 14, 41]. More specifically, patients with ACS and concurrent COVID-19 represent a distinctive clinical setting characterized by hallmarks of heightened thrombogenicity. Choudry et al. compared COVID-19 patients with STEMI with a control group of SARS-CoV-2-negative STEMI and reported a higher incidence of multiple thrombotic culprit lesions, higher thrombus grade, and lower rate of procedural success of primary PCI procedures as assessed by myocardial blush grade (a marker of myocardial perfusion) [42, 54]. Notably, high coronary thrombus burden and low myocardial blush grade were associated with higher d-dimer plasma levels. Eventually, in a population of 91 COVID-19 patients with STEMI, Rodriguez-Leor et al. reported a high rate of stent thromboses (4.1%) [30], a potentially catastrophic event with lower than 1% incidence at one year in contemporary STEMI cohorts [55, 56].

4.2. Endothelial Dysfunction.
Vascular endothelium is a central interface between circulatory apparatus and tissues and plays a key role in vascular homeostasis. A functional endothelium possesses several valuable properties for regulating vasomotion, inflammation, platelet reactivity, coagulation, vascular permeability, and host defense. Traditional CV risk factors such as diabetes, hypertension, older age, and smoking may damage the endothelium through several mechanisms, including oxidative stress related to the increased intracellular levels of superoxide anions. All these mechanisms shift towards a vasoconstrictive and procoagulant status typical of the dysfunctional endothelium, which is a distinctive feature of patients with coronary artery disease (CAD) [57, 58].

Recent findings indicate that endothelial dysfunction represents one of the most detrimental mechanisms of COVID-19 pathophysiology [59, 60]. The endothelial injury may be induced by both direct viral effects, as demonstrated by the presence of viral elements within the endothelium and inflammatory cell accumulation, resulting in venous, arterial, and microvascular thrombosis [13, 61]. Several pathways seem to be involved in the development of endothelial-mediated complications of COVID-19. While in physiological conditions, the endothelium maintains anticoagulant, antithrombotic, and profibrinolytic characteristics, when stimulated by inflammatory and infectious triggers, it can shift toward an opposite array of functions through the expression of tissue factor, the release of von Willebrand factor (vWf), and the production of thromboxane and plasminogen activator inhibitor-1 (PAI-1) [62–64]. Under normal conditions, a functional endothelium is able to limit oxidative stress, a recognized contributor to the progression of atherosclerosis, through the expression of superoxide dismutase and glutathione [65, 66]. In contrast, when activated by inflammatory cytokines, endothelial cells generate superoxide anions with consequent enhancement of local oxidative stress, which has been associated with a higher risk of MI and other CV consequences [67–69]. The enhanced production of endothelin-1, a potent vasoconstrictor and
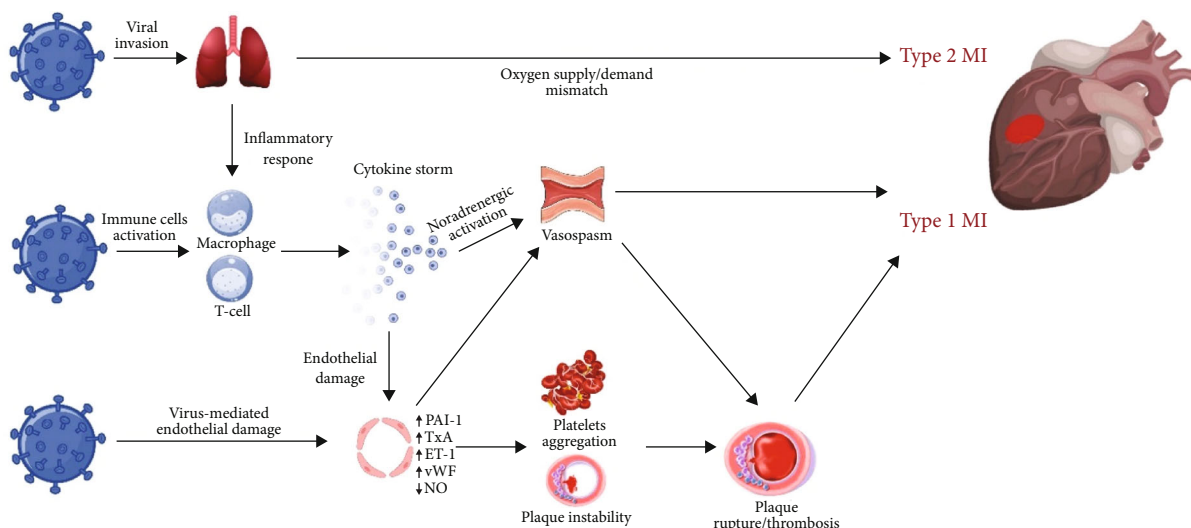
FIGURE 1: Pathophysiology of ACS in COVID-19. Mechanisms involved in the pathophysiology of ACS in patients with COVID-19. SARS-CoV-2, by binding the ACE2 receptors expressed on the surface of the host cell, may infect pneumocytes, macrophages, and endothelial cells. The respiratory impairment related to the pulmonary involvement, ranging from pneumonia to ARDS in severe forms, causes hypoxia and type 2 MI due to the oxygen supply/demand mismatch. Also, the infection promotes an aberrant inflammatory response resulting in the release of cytokines and proinflammatory molecules such as IL-1, IL-6, IL-7, TNFα, and IFNγ. Cytokines have the potential to damage the endothelial function with increased production of oxidative stress agents and prothrombotic factors. SARS-CoV-2 may also exert a direct cellular effect by interacting with molecules expressed on the surface of the endothelial cells. In turn, the inflammatory environment enhances the instability of preexisting atheromatous plaques, promotes platelets activation and aggregation, and upregulates the sympathetic nervous system resulting in increased vasomotility and coronary spasm. The interplay of all these mechanisms may favor plaque rupture and thrombosis leading to type 1 MI. ACS: acute coronary syndrome; ACE2: angiotensin-converting enzyme 2; COVID-19: coronavirus disease 2019; IFNγ: interferon γ; IL-1: interleukin 1; IL-6: interleukin 6; IL-7: interleukin 7; MI: myocardial infarction; SARS-CoV-2: severe acute respiratory syndrome coronavirus 2; TNFα: tumor necrosis factor α.

prothrombotic agent, may also favor the vasodilator/vaso-constrictor imbalance, platelet aggregation and, finally, myocardial ischemia [70]. Recent findings from a single-centre study also reported higher levels of thrombomodulin, a specific marker of endothelial injury, which resulted associated with poor inhospital outcome [60].

Another pathway of endothelial dysfunction may be vascular endothelial glycocalyx (VEGLX) SARS-CoV-2-mediated damage. VEGLX is composed by glycosylated lipid-protein mixtures that covers vascular endothelium and plays an important role in maintaining vascular homeostasis [71]. A variety of conditions, including inflammatory response, hypoxia, hyperglycemia, and ischemia/reperfusion injury, are known to be associated with VEGLX damage through several degradation pathways [72–74]. Moreover, high circulating levels of VEGLX components are associated with poor outcomes in critically hill patients [75]. Severe COVID-19 forms represent the typical scenario in which glycocalyx damage might occur. Several reports observed high concentrations of VEGLX injury biomarkers in patients hospitalized for COVID-19, including syndecan-1, hyaluronic acid, and sTie-2 [75–78]. Moreover, Stahl et al. found a severe depletion of heparanase-2, an enzyme with protective effects on VEGLX structure and functions [76].

Despite the paucity of data, it is possible to hypothesize that VEGLX damage might contribute to the progression of endothelial dysfunction in severe COVID-19, with anticipated consequences on the development of thrombotic and vascular complications.

All these mechanisms might be amplified in case of preexisting endothelial dysfunction, such as in patients with CV risk factors and CAD, leading to a heightened risk of ACS and other thrombotic complications. Advances in the understanding of SARS-CoV-2-related endothelial dysfunction, beyond the pathophysiological insights, would encourages the assessment of the utility of pharmacological therapies targeting the endothelium, such as ACE-inhibitors (ACEi) and statins, in large prospective randomized studies [79–82].

4.3. Inflammatory Response and Cytokine Storm. Immune and inflammatory response is chronically involved in the progression of atherosclerotic disease. [83] In the context of viral infection, the inflammation may spoil the regular homeostasis and trigger a prothrombotic state by activating platelets and promoting endothelial dysfunction [15]. Moreover, infections can increase the sympathetic activity with consequent vasoconstriction in the coronary tree [84]. The interplay between all these biological and mechanical conditions can induce atheromatous plaque erosion or rupture, resulting in coronary thrombosis and ACS [85, 86].

The clinical course of severe forms of COVID-19 is characterized by an aberrant inflammatory response and CS [46, 48]. CS is a process primed by the primordial inflammatory cytokine interleukin-1 (IL-1), which has the ability to induce its own gene expression and to endorse a self-powered inflammatory response [87]. IL-1 stimulates the production of other proinflammatory mediators such as tumor necrosis factor (TNFα), interleukin-6 (IL-6), and chemoattractant

molecules, involved in tissue penetration of inflammatory cells [88–90]. In addition to the local effects, IL-6 induces the synthesis of acute phase reactants, such as fibrinogen, plasminogen activator inhibitor-1 (PAI-1), and favor a prothrombotic and antifibrinolytic imbalance. SARS-CoV-2-related CS is confirmed by several studies showing increased level of proinflammatory factors, such as IL-1, IL-6, IL-10, IFNγ, granulocyte colony stimulating factor (G-CSF), monocyte chemoattractant protein (MCP1), macrophage inflammatory protein 1 alpha (MIP1A), platelet-derived growth factor (PDGF), TNFα, and vascular endothelial growth factor (VEGF) [46, 91]. The extensive production of proinflammatory cytokines disrupts the physiological homeostasis guaranteed by the functional endothelium, thus contributing to thrombosis and local tissue injury [47, 50, 92]. The pathophysiological relationship between COVID-related CS and thrombotic events suggests the implementation of targeted therapy for prevention and treatment of ACS in this setting [93].

4.4. Oxygen Supply/Demand Imbalance. Hypoxemic respiratory failure is the leading cause of death in COVID-19, accounting for nearly 60% of cases with fatal outcome [94]. The severe hypoxic state, combined with other mechanisms observed in COVID-19, such as sepsis, tachyarrhythmias, anemia, hypotension, and shock, can induce a myocardial damage due to the mismatch between oxygen supply and demand in absence of atherothrombotic lesions, findings consistent with the diagnosis of type 2 MI [95]. Compared with type 1 MI, patients with type 2 MI show distinct clinical features and poorer prognosis, largely related to the higher prevalence of coexisting systemic diseases [96]. Given their high complexity and vulnerability, critically ill patients with COVID-19 are particularly prone to the occurrence of type 2 MI, which strongly contributes to the reported high rate of inhospital mortality [4].

5. Myocardial Infarction with Nonobstructive Coronary Arteries

Myocardial infarction with nonobstructive coronary arteries (MINOCA) has been frequently reported in patients with COVID-19 [30, 97]. In an Italian series of 28 STEMI patients with COVID-19, 11 patients (39.3%) did not have obstructive CAD [43]. In another series of 18 COVID-19 patients with STEMI from New York, coronary angiography did not detect obstructive CAD in 33% of cases [41]. Several mechanisms have been proposed for these cases, including plaque erosion, microthrombi, or coronary vasospasm [41, 98, 99]. The pathophysiology seems to be multifactorial and encompasses inflammatory activation, oxidative stress, and endothelial dysfunction in the context of COVID-19-related CS [100, 101]. The underlying mechanisms of MINOCA, albeit theoretical, are largely underinvestigated due to difficulties in performing invasive and noninvasive diagnostic work-up including intravascular imaging, pharmacological provocative test, and cardiac magnetic resonance [102–104].

Takotsubo syndrome (TTS), a condition that simulates an ACS at presentation, has been frequently reported during COVID-19 pandemic [105]. Observational studies on hospitalized patients with COVID-19 and laboratory evidence of myocardial injury have estimated an incidence of TTS ranging from 2% to 4% of cases [9, 106, 107]. Although TTS has been proposed as a direct manifestation of COVID-19, it may be also the consequence of the physical and emotional stress related to the SARS-CoV-2 infection leading to sympathetic overdrive [108]. A higher risk of TTS has also been described in the context of pandemic, irrespective of SARS-CoV-2 infection. In a cohort study of consecutive patients admitted for suspected ACS at Cleveland Clinic, TTS diagnosis was reported in 7.8% of patients during the first wave of the pandemic, being significantly higher than in prepandemic timelines [109]. These findings have been considered the consequence of growing psychological stress related to the pandemic context (e.g., fear of contagion, social distancing, and isolation), but need confirmation in larger prospective studies [110].

6. Therapeutic Perspectives

The optimal management of ACS in COVID-19 patients is a demanding challenge, both for logistic and clinical reasons. During the first wave of the pandemic, in order to reduce healthcare workers exposure and the risk of contagion, several scientific societies suggested the use of fibrinolysis as first-line therapy in STEMI patients with COVID [111–113]. However, the delay in reperfusion time, the increased risk of mortality and left ventricular dysfunction, and frequent absence of a coronary culprit lesion do not seem to support such an approach as an alternative to the guideline-recommended treatment with primary PCI and optimal antithrombotic therapy, currently considered as the standard of care [34, 42, 114].

Antithrombotic therapy in COVID-19 is an active area of investigation, with multiple ongoing randomized clinical trials evaluating a variety of regimens with antiplatelet, anticoagulant, or their combinations (Table 1). Antiplatelet agents, besides being the cornerstone of pharmacological treatment of ACS, may deserve a remarkable role in the setting of COVID-related endothelial injury and thromboinflammation. Their anti-inflammatory and antithrombotic effects, indeed, provide the pathophysiological rationale for a systematic use in this clinical setting. Activated platelets release several inflammatory mediators, such as cytokines, chemokines, and metalloproteinases, further contributing to the sustainment of a systemic inflammatory response [115]. Moreover, the interaction between activated platelets and neutrophils induces neutrophil activations, extracellular matrix protein degradation, and prothrombotic endothelium activation [116, 117].

Several antiplatelet agents, such as glycoprotein IIb/IIIa antagonists and P2Y12 inhibitors, also showed protective effects on lung injury in patients with viral respiratory infections, due to the limitation of neutrophil recruitment [118]. Although all P2Y12 inhibitors have the potential to reduce platelet–leukocyte aggregates and platelet-derived

TABLE 1: Ongoing randomized clinical trials investigating antithrombotic regimens in patients with COVID-19.

Study name	Registration number	Population	Treatments	Design	Estimated enrollement (n)	Primary endpoint	Time of FU (days)
PARTISAN	NCT04445623	Non-ICU patients	Prasugrel 10 mg	Randomized, double blind	128	P/F ratio	7
PEAC	NCT04365309	Non-ICU patients	Aspirin 100 mg	Randomized, open label	128	Clinical recovery time	14
						The time of SARS-CoV2 overcasting	37
						Colchicine vs. control; aspirin and rivaroxaban vs. control:	
						(i) Composite of invasive mechanical ventilation	
ACT-COVID19	NCT04324463	Non-ICU patients	Aspirin Rivaroxaban Colchicine	Randomized, open label, factorial	4000	or death	45
						(ii) Disease progression of 2 points on a 7-point scale	
						Aspirin and rivaroxaban vs. control:	
						(i) Composite of MACE (MI, stroke, acute limb ischemia, VTE, death)	
			Aspirin 75 mg Clopidogrel 75 mg				
C-19-ACS	NCT04333407	Non-ICU patients	Rivaroxaban 2.5 mg Atorvastatin 40 mg Omeprazole 20 mg	Randomized, open label	3170	All-cause mortality	30
RESIST	CTRI/2020/07/026791	Non-ICU patients	Aspirin 75 mg Atorvastatin 40 mg	Randomized, open label	800	Clinical deterioration expressed as progression of WHO clinical improvement ordinal score ≥ 6	10
			UFH iv enoxaparin 1 mg/kg			Hierarchical composite: death due to venous or arterial thrombosis, pulmonary embolism, clinically	
COVID-PACT	NCT04409834	ICU patients	Clopidogrel 75 mg UFH sc Enoxaparin 40 mg/ 0.4 mL	Randomized, open label, factorial	750	evident DVT, type 1 MI, ischemic stroke, systemic embolism, or acute limb ischemia or clinically silent DVT	28

COVID-19: coronavirus disease 2019; DVT: deep vein thrombosis; ECMO: extra corporeal membrane oxygenation; ICU: intensive care unit; MACE: major adverse cardiovascular events; MI: myocardial infarction; P/F: PaO2/FiO2; RRT: renal replacement therapy; SARS-CoV2: severe acute respiratory syndrome coronavirus 2; UFH: unfractionated heparin; VTE: venous thromboembolism.

proinflammatory cytokines, ticagrelor is unique in the inhibition of ENT1 (equilibrative nucleoside transporter 1), resulting in higher antiplatelet, but also antibacterial activity [119]. Previous data from non-COVID-19 cohorts showed the reduction of lung injury and the prevention of septic complications in patients with pneumonia treated with ticagrelor, resulting in a significant survival benefit [120, 121]. However, to counterbalance the well-documented risk of thrombotic complications, diffuse alveolar hemorrhage was reported as a possible autoptic finding in COVID-19 and severe acute respiratory syndrome [122, 123]. The extensive thrombosis of pulmonary capillary bed, if left uncontrolled, leads to secondary fibrinolysis, consumption coagulopathy, disseminated intravascular coagulation, and diffuse alveolar hemorrhage. Also, considering the high bleeding risk profile of frail patients hospitalized for severe COVID-19, some authors hypothesized the possibility of a shorter duration dual antiplatelet therapy after an ACS [124, 125].

Thus, the selection of the proper antiplatelet regimen in COVID-19 patients with ACS remains an open clinical issue; it should be based on the careful assessment of ischemic and bleeding risk and tailored to the individual patient.

Anticoagulant agents might yield clinical benefits in COVID-19, not only for their antithrombotic action but also for additional anti-inflammatory effects. Unfractionated heparin (UFH) and low-molecular-weight heparin (LMWH) have pleiotropic anti-inflammatory effects, including the inhibition of the interaction between platelets and neutrophils and the reduction of the release of inflammatory mediators like IL-1β, IL-6, E-selectin, and ICAM-1 [126–128]. Heparins have also direct antiviral effects mediated by their interaction with heparan sulfate, a component of cell surface identified as the initial contact point between human cells and several viruses, including SARS-CoV-2 [129–131]. Heparins compete with heparan sulfate and hamper the interaction between virus and target cells.

Additional antiviral effects of heparin may be related to the interaction with SARS-CoV-2S proteins. Each S protein is characterized by two subunits, S1 and S2; S1 presents the binding domain which interacts with ACE2 receptor on host cells. Heparin has been demonstrated to bind the S1 subunit, causing a structural change that jeopardizes the viral entry mechanism into the target cells. [129] After the interaction with ACE2, the cleavage of S1-S2 subunits is needed to expose S2 for adhesion of cell membrane and to finalize the virus entrance into the target cell. This step is permitted by several proteases, including factor Xa, cathepsin, thrombin, and furin. The anticoagulant agents that inhibit these proteases, including heparins and oral anticoagulants, might exert antiviral effects due to the interference with SARS-CoV-2 in host cell infection.

Although the pathophysiology of COVID-19 seems to provide a rationale for the use of anticoagulant drugs in routine clinical practice, also in patients without clinically evident thrombotic complications, there are still controversial data on what is the best anticoagulant agent and on the optimal dosing [132, 133]. An observational study on 4,389 patients showed a lower rate of mortality in patients treated with anticoagulants; there was no incremental benefit of therapeutic over prophylactic regimens, but an increased risk of bleeding in patients treated with therapeutic doses [134]. Results from randomized clinical trials, currently ongoing, are urgently needed to clarify these controversies. In the meantime, the choice of the optimal anticoagulation strategy should be individually considered, particularly in patients with COVID-19 and life-threatening thrombotic complications, like ACS [135, 136]. The optimal antithrombotic therapy in COVID-19 patients with ACS and indication for chronic oral anticoagulation therapy (e.g., atrial fibrillation and mechanical valvular prosthesis) is a poorly explored clinical scenario. The choice of type and duration of antithrombotic therapy should be tailored on patients' characteristics taking into account the trade-off between ischemic and bleeding risks, which varies on an individual basis. Due to the higher risk of thrombotic events, some authors have suggested a more aggressive treatment in COVID-19 patients at higher risk of thromboembolic events, such as those with an indication for combined antiplatelet and anticoagulation therapy. However, there are no evidence supporting such an approach and to date seems reasonable to follow the general recommendations proposed for patients with ACS and indication for concomitant oral anticoagulation.

The progressive understanding of COVID-19 pathophysiology provides us a conceptual framework for treatment of endothelial dysfunction. ACEi and statins, two widely used drugs in CV diseases, have robust evidence on their ability to improve endothelial function [80, 82].

The renin-angiotensin-aldosterone system, a key regulator of vascular homeostasis, effectively participates in COVID-19 CV manifestations. Given the central role of ACE2 in COVID-19 pathophysiology, its interaction with SARS-CoV2 might represent a potential therapeutic target [17, 19]. ACE2, unlike ACE, is not antagonized by ACEi, and its expression and activity provide beneficial effects through different pathways [137]. Most of these properties are related to the production of angiotensin1-7, a molecule with multiple anti-inflammatory, antioxidant, vasodilatory, and natriuretic effects, exerted through the G-protein coupled receptor Mas [138]. Ang1-7 production can be obtained by several mechanisms: ACE2 can convert angiotensin II (Ang II) directly into Ang1-7 via C-terminus cleavage, representing the most efficient way of production of Ang1-7. Ang1-7 can also be produced from the Ang I via an alternative pathway mediated by the metallopeptidase neprilysin. In addition, ACE2 can convert Ang I into the Angiotensin1-9 (Ang1-9) intermediate, which itself is converted into Ang1-7 by ACE; however, the latter two pathways are less efficient [137]. Conversely, SARS-CoV-2, similarly to other coronaviruses, limits ACE2 expression by promoting its cleavage by the specialized proteinase A disintegrin and metalloproteinase 17 (ADAM17), leading to a reduction in ACE2's protective effects [22]. Previous studies showed that ACEi increases the transcription of ACE2 mRNA and plasma levels of Ang1-7, therefore suggesting an ACEi-mediated upregulation of the ACE2/Ang1-7/Mas pathway [139]. In light of this evidence, the use of ACEi

might lead to anti-inflammatory, antifibrotic, and anti-thrombotic effects, providing a valuable protection against ACS in patients with COVID-19.

Statins, beyond their effect on circulating lipids, exert pleiotropic effects on the immune response by modulating immune cell adhesion and migration, antigen presentation, and cytokine production. These effects are mediated by their capability of inhibiting the production of small GTPases (Ras, Rho, Rac) and modulate the plasma level of the myeloid differentiation primary response 88 (MYD88), leading to the downregulation of inflammatory transcriptional factors, like NF-κB [140, 141]. Statins also reduce reactive oxygen species and increase the production of antioxidants, restoring the normal endothelial function and integrity by upregulating eNOS and consequently increasing the production of NO by the endothelium [142]. Statin-mediated NO production has been associated with a reduction of platelets reactivity; [143] additional antithrombotic properties of statins are related to the inhibition of thromboxane A2 and isoprostane formation, the downregulation of TF production, and the increase of thrombomodulin levels [144]. Like ACEi, statins can upregulate the expression of ACE2 via epigenetic histone modification, favoring the beneficial effects of the upregulation of the ACE2/Ang1-7/Mas axis [145]. This wide range of pharmacodynamic properties would support the use of statins in COVID-19, aiming to antagonize the proinflammatory and prothrombotic endothelial modifications of the disease [146]. A recent propensity-matched observational study on 13,981 patients has showed a reduction in all-cause mortality in patients hospitalized for COVID-19 and treated with statins [147]. Albeit, these findings from general COVID-19 population need confirmation by large randomized clinical trials, and the rationale for the use of statins would be stronger in patients with multiple risk factors for ACS.

Beta-blockers (β-blockers) are widely used in different cardiovascular diseases, including ACS. They have been proposed in patients with COVID-19 to antagonize the disease-related hyperinflammatory response [148, 149]. In fact, beta2-adrenergic receptors are widely expressed on immune cells such as macrophages, dendritic cells, and T and B lymphocytes and seem to play a relevant role in promoting macrophage activation and proinflammatory cytokine production (IL-6, TNF-α, and NFκB) [150–153].

Since CS is involved in the pathogenesis of vascular complications in COVID-19, the reduction of circulating cytokines driven by β-blockers could mitigate their systemic detrimental effects. The rationale for the use of β-blockers is reinforced in COVID-19 patients who develop left ventricular systolic dysfunction and heart failure (HF) after STEMI. Rodriguez-Leor et al. reported a higher percentage of HF on admission in STEMI patients with vs. those without COVID-19 (31.9% vs. 18.4%) [30]. Consistently, Choudry et al. showed that left ventricular ejection fraction after PCI was lower in STEMI patients with COVID-19 than in those without (42.5% vs. 45%) [42]. The potentially beneficial anti-inflammatory and cardiac effects of β-blockers need to be confirmed by large multi-center studies.

7. Conclusions

Despite the overall reduction in cases admitted at the emergency departments during the early phase of the pandemic, ACS is a potential life-threatening complication of COVID-19. The pathophysiological mechanisms are multiple and include atherosclerotic plaque rupture, overactivation of the coagulation system, platelet hyperreactivity, abnormal systemic inflammatory response, and oxygen supply/demand imbalance. When compared to non-COVID-19 cases, patients with ACS and SARS-CoV-2 infection present distinctive clinical and anatomical features including the absence of obstructive CAD, the higher burden of thrombus, and the angiographic evidence of multiple thrombotic lesions. Deeper understanding of the ACS pathophysiology in COVID-19 may allow the application of translational notions in daily clinical practice. The use of pharmacological agents, namely, antiplatelets, anticoagulants, ACEi, β-blockers, and statins, seems a valuable strategy not only in the treatment of ACS but also as a preventive strategy in higher CV risk subjects with COVID-19.

Conflicts of Interest

The authors declare that they have no conflicts of interest. The authors have no commercial or financial relationships that could be construed as a potential conflict of interest.

References

[1] W. J. Guan, Z. Y. Ni, Y. Hu et al., "Clinical characteristics of coronavirus disease 2019 in China," *The New England journal of medicine*, vol. 382, no. 18, pp. 1708–1720, 2020.

[2] "Progress report on the coronavirus pandemic," *Nature*, vol. 584, 2020.

[3] A. Silverio, M. di Maio, R. Citro et al., "Cardiovascular risk factors and mortality in hospitalized patients with COVID-19: systematic review and meta-analysis of 45 studies and 18,300 patients," *BMC cardiovascular disorders*, vol. 21, no. 1, p. 23, 2021.

[4] S. Shi, M. Qin, B. Shen et al., "Association of cardiac injury with mortality in hospitalized patients with COVID-19 in Wuhan, China," *JAMA cardiology*, vol. 5, no. 7, pp. 802–810, 2020.

[5] R. Citro, G. Pontone, M. Bellino et al., "Role of multimodality imaging in evaluation of cardiovascular involvement in COVID-19," *Trends in cardiovascular medicine*, vol. 31, no. 1, pp. 8–16, 2021.

[6] V. Russo, M. di Maio, F. F. Mottola et al., "Clinical characteristics and prognosis of hospitalized COVID-19 patients with incident sustained tachyarrhythmias: a multicenter observational study," *European journal of clinical investigation*, vol. 50, no. 12, article e13387, 2020.

[7] F. Scudiero, A. Silverio, M. di Maio et al., "Pulmonary embolism in COVID-19 patients: prevalence, predictors and clinical outcome," *Thrombosis research*, vol. 198, pp. 34–39, 2021.

[8] G. Piazza, U. Campia, S. Hurwitz et al., "Registry of arterial and venous thromboembolic complications in patients with COVID-19," *Journal of the American College of Cardiology*, vol. 76, no. 18, pp. 2060–2072, 2020.

[9] G. Giustino, L. B. Croft, G. G. Stefanini et al., "Characterization of myocardial injury in patients with COVID-19," *Journal of the American College of Cardiology*, vol. 76, no. 18, pp. 2043–2055, 2020.

[10] K. J. Clerkin, J. A. Fried, J. Raikhelkar et al., "COVID-19 and cardiovascular disease," *Circulation*, vol. 141, no. 20, pp. 1648–1655, 2020.

[11] M. Madjid, P. Safavi-Naeini, S. D. Solomon, and O. Vardeny, "Potential effects of coronaviruses on the cardiovascular system: a review," *JAMA cardiology*, vol. 5, no. 7, pp. 831–840, 2020.

[12] G. Guagliumi, A. Sonzogni, I. Pescetelli, D. Pellegrini, and A. V. Finn, "Microthrombi and ST-segment-elevation myocardial infarction in COVID-19," *Circulation*, vol. 142, no. 8, pp. 804–809, 2020.

[13] Z. Varga, A. J. Flammer, P. Steiger et al., "Endothelial cell infection and endotheliitis in COVID-19," *The Lancet*, vol. 395, no. 10234, pp. 1417-1418, 2020.

[14] B. Bikdeli, M. V. Madhavan, D. Jimenez et al., "COVID-19 and Thrombotic or Thromboembolic Disease: Implications for Prevention, Antithrombotic Therapy, and Follow-Up;," *Journal of the American College of Cardiology*, vol. 75, no. 23, pp. 2950–2973, 2020.

[15] V. F. Corrales-Medina, M. Madjid, and D. M. Musher, "Role of acute infection in triggering acute coronary syndromes," *The Lancet Infectious diseases*, vol. 10, no. 2, pp. 83–92, 2010.

[16] J. C. Kwong, K. L. Schwartz, M. A. Campitelli et al., "Acute myocardial infarction after laboratory-confirmed influenza infection," *The New England journal of medicine*, vol. 378, no. 4, pp. 345–353, 2018.

[17] H. Zhang, J. M. Penninger, Y. Li, N. Zhong, and A. S. Slutsky, "Angiotensin-converting enzyme 2 (ACE2) as a SARS-CoV-2 receptor: molecular mechanisms and potential therapeutic target," *Intensive care medicine*, vol. 46, no. 4, pp. 586–590, 2020.

[18] P. Wu, X. Hao, E. H. Y. Lau et al., "Real-time tentative assessment of the epidemiological characteristics of novel coronavirus infections in Wuhan, China, as at 22 January 2020," *Eurosurveillance*, vol. 25, no. 3, 2020.

[19] Y. Wan, J. Shang, R. Graham, R. S. Baric, and F. Li, "Receptor recognition by the novel coronavirus from Wuhan: an analysis based on decade-long structural studies of SARS Coronavirus," *Journal of virology*, vol. 94, no. 7, 2020.

[20] C. G. K. Ziegler, S. J. Allon, S. K. Nyquist et al., "SARS-CoV-2 Receptor ACE2 Is an Interferon-Stimulated Gene in Human Airway Epithelial Cells and Is Detected in Specific Cell Subsets across Tissues," *Cell*, vol. 181, no. 5, pp. 1016–1035.e19, 2020.

[21] Y. Imai, K. Kuba, S. Rao et al., "Angiotensin-converting enzyme 2 protects from severe acute lung failure," *Nature*, vol. 436, no. 7047, pp. 112–116, 2005.

[22] K. Kuba, Y. Imai, S. Rao et al., "A crucial role of angiotensin converting enzyme 2 (ACE2) in SARS coronavirus-induced lung injury," *Nature medicine*, vol. 11, no. 8, pp. 875–879, 2005.

[23] Y. Lei, J. Zhang, C. R. Schiavon et al., "SARS-CoV-2 spike protein impairs endothelial function via downregulation of ACE 2," *Circulation research*, vol. 128, no. 9, pp. 1323–1326, 2021.

[24] Q. Li, X. Guan, P. Wu et al., "Early transmission dynamics in Wuhan, China, of novel coronavirus-infected pneumonia," *The New England journal of medicine*, vol. 382, no. 13, pp. 1199–1207, 2020.

[25] L. Zou, F. Ruan, M. Huang et al., "SARS-CoV-2 viral load in upper respiratory specimens of infected patients," *The New England journal of medicine*, vol. 382, no. 12, pp. 1177–1179, 2020.

[26] Z. Wu and J. M. McGoogan, "Characteristics of and important lessons from the coronavirus disease 2019 (COVID-19) outbreak in China," *Journal of the American Medical Association*, vol. 323, no. 13, pp. 1239–1242, 2020.

[27] A. Hamadeh, A. Aldujeli, K. Briedis et al., "Characteristics and Outcomes in Patients Presenting With COVID-19 and ST- Segment Elevation Myocardial Infarction," *The American journal of cardiology*, vol. 131, pp. 1–6, 2020.

[28] F. Zhang, X. Song, and Y. Dang, "Experience of ST segment elevation myocardial infarction management during COVID-19 pandemic from the mainland of China," *Cardiovascular revascularization medicine*, vol. 28, pp. 92–94, 2021.

[29] S. Garcia, M. S. Albaghdadi, P. M. Meraj et al., "Reduction in ST-segment elevation cardiac catheterization laboratory activations in the United States during COVID-19 pandemic," *Journal of the American College of Cardiology*, vol. 75, no. 22, pp. 2871-2872, 2020.

[30] O. Rodriguez-Leor, A. B. Cid Alvarez, A. Pérez de Prado et al., "in-hospital outcomes of COVID-19 ST-elevation myocardial infarction patients," *Euro Intervention*, vol. 16, no. 17, pp. 1426–1433, 2021.

[31] G. Bonnet, V. Panagides, M. Becker et al., "Infarctus du myocarde avec sus-decalage du segment ST : prise en charge et association au pronostic lors de la pandemie de COVID-19 en France," *Archives of Cardiovascular Diseases*, vol. 114, no. 5, pp. 340–351, 2021.

[32] T. J. Gluckman, M. A. Wilson, S. T. Chiu et al., "Case rates, treatment approaches, and outcomes in acute myocardial infarction during the coronavirus disease 2019 pandemic," *JAMA Cardiology*, vol. 5, no. 12, pp. 1419–1424, 2020.

[33] M. M. Mafham, E. Spata, R. Goldacre et al., "COVID-19 pandemic and admission rates for and management of acute coronary syndromes in England," *Lancet*, vol. 396, no. 10248, pp. 381–389, 2020.

[34] E. Mahmud, H. L. Dauerman, F. G. P. Welt et al., "Management of acute myocardial infarction during the COVID-19 pandemic: a consensus statement from the Society for Cardiovascular Angiography and Interventions (SCAI), the American College of Cardiology (ACC), and the American College of Emergency Physicians (ACEP)," *Catheterization and cardiovascular interventions: official journal of the Society for Cardiac Angiography & Interventions.*, vol. 96, no. 2, pp. 336–345, 2020.

[35] M. Rashid, J. Wu, A. Timmis et al., "Outcomes of COVID-19-positive acute coronary syndrome patients: a multisource electronic healthcare records study from England," *Journal of Internal Medicine*, vol. 290, no. 1, pp. 88–100, 2021.

[36] D. Xiang, X. Xiang, W. Zhang et al., "Management and outcomes of patients with STEMI during the COVID-19 pandemic in China," *Journal of the American College of Cardiology*, vol. 76, no. 11, pp. 1318–1324, 2020.

[37] A. Silverio, M. Di Maio, M. Ciccarelli, A. Carrizzo, C. Vecchione, and G. Galasso, "Timing of national lockdown and mortality in COVID-19: the Italian experience," *International journal of infectious diseases: IJID*, vol. 100, pp. 193–195, 2020.

[38] G. de Luca, M. Verdoia, M. Cercek et al., "Impact of COVID-19 pandemic on mechanical reperfusion for patients with STEMI," *Journal of the American College of Cardiology*, vol. 76, no. 20, pp. 2321–2330, 2020.

[39] E. Baldi, G. M. Sechi, C. Mare et al., "Out-of-hospital cardiac arrest during the COVID-19 outbreak in Italy," *The New England journal of medicine*, vol. 383, no. 5, pp. 496–498, 2020.

[40] G. De Luca, H. Suryapranata, J. P. Ottervanger, and E. M. Antman, "Time delay to treatment and mortality in primary angioplasty for acute myocardial infarction: every minute of delay counts," *Circulation*, vol. 109, no. 10, pp. 1223–1225, 2004.

[41] S. Bangalore, A. Sharma, A. Slotwiner et al., "ST-segment elevation in patients with Covid-19 — a case series," *The New England journal of medicine*, vol. 382, no. 25, pp. 2478–2480, 2020.

[42] F. A. Choudry, S. M. Hamshere, K. S. Rathod et al., "High Thrombus burden in patients with COVID-19 presenting with ST-segment elevation myocardial infarction," *Journal of the American College of Cardiology*, vol. 76, no. 10, pp. 1168–1176, 2020.

[43] G. G. Stefanini, M. Montorfano, D. Trabattoni et al., "ST-elevation myocardial infarction in patients with COVID-19: clinical and angiographic outcomes," *Circulation*, vol. 141, no. 25, pp. 2113–2116, 2020.

[44] G. Lippi and E. J. Favaloro, "D-dimer is associated with severity of coronavirus disease 2019: a pooled analysis," *Thrombosis and Haemostasis*, vol. 120, no. 5, pp. 876–878, 2020.

[45] G. Lippi, M. Plebani, and B. M. Henry, "Thrombocytopenia is associated with severe coronavirus disease 2019 (COVID-19) infections: A *meta* -analysis," *Clinica chimica acta*, vol. 506, pp. 145–148, 2020.

[46] C. Huang, Y. Wang, X. Li et al., "Clinical features of patients infected with 2019 novel coronavirus in Wuhan, China," *The Lancet*, vol. 395, no. 10223, pp. 497–506, 2020.

[47] N. Tang, D. Li, X. Wang, and Z. Sun, "Abnormal coagulation parameters are associated with poor prognosis in patients with novel coronavirus pneumonia," *Journal of thrombosis and haemostasis*, vol. 18, no. 4, pp. 844–847, 2020.

[48] P. Mehta, D. F. McAuley, M. Brown et al., "COVID-19: consider cytokine storm syndromes and immunosuppression," *The Lancet*, vol. 395, no. 10229, pp. 1033-1034, 2020.

[49] P. Masi, G. Hékimian, M. Lejeune et al., "Systemic inflammatory response syndrome is a major contributor to COVID-19-associated coagulopathy: insights from a prospective, single-center cohort study," *Circulation*, vol. 142, no. 6, pp. 611–614, 2020.

[50] CRICS TRIGGERSEP Group (Clinical Research in Intensive Care and Sepsis Trial Group for Global Evaluation and Research in Sepsis), J. Helms, C. Tacquard et al., "High risk of thrombosis in patients with severe SARS-CoV-2 infection: a multicenter prospective cohort study," *Intensive care medicine*, vol. 46, no. 6, pp. 1089–1098, 2020.

[51] W. Zhang, Y. Zhao, F. Zhang et al., "The use of anti-inflammatory drugs in the treatment of people with severe coronavirus disease 2019 (COVID-19): The Perspectives of clinical immunologists from China," *Clinical immunology*, vol. 214, p. 108393, 2020.

[52] M. Panigada, N. Bottino, P. Tagliabue et al., "Hypercoagulability of COVID-19 patients in intensive care unit: a report of thromboelastography findings and other parameters of hemostasis," *Journal of thrombosis and haemostasis*, vol. 18, no. 7, pp. 1738–1742, 2020.

[53] B. Giannakopoulos and S. A. Krilis, "The pathogenesis of the antiphospholipid syndrome," *The New England journal of medicine*, vol. 368, no. 11, pp. 1033–1044, 2013.

[54] A. W. J. van't Hof, A. Liem, H. Suryapranata, J. C. A. Hoorntje, M.-J. de Boer, and F. Zijlstra, "Angiographic assessment of myocardial reperfusion in patients treated with primary angioplasty for acute myocardial infarction: myocardial blush grade," *Circulation*, vol. 97, no. 23, pp. 2302–2306, 1998.

[55] G. Souteyrand, N. Amabile, L. Mangin et al., "Mechanisms of stent thrombosis analysed by optical coherence tomography: insights from the national PESTO French registry," *European heart journal*, vol. 37, no. 15, pp. 1208–1216, 2016.

[56] T. Kimura, T. Morimoto, K. Kozuma et al., "Comparisons of baseline demographics, clinical presentation, and long-term outcome among patients with early, late, and very late stent thrombosis of sirolimus-eluting stents: observations from the registry of stent thrombosis for review and reevaluation (RESTART)," *Circulation*, vol. 122, no. 1, pp. 52–61, 2010.

[57] E. Gutiérrez, A. J. Flammer, L. O. Lerman, J. Elízaga, A. Lerman, and F. Fernández-Avilés, "Endothelial dysfunction over the course of coronary artery disease," *European heart journal*, vol. 34, no. 41, pp. 3175–3181, 2013.

[58] Y. Kitta, J. E. Obata, T. Nakamura et al., "Persistent impairment of endothelial vasomotor function has a negative impact on outcome in patients with coronary artery disease," *Journal of the American College of Cardiology*, vol. 53, no. 4, pp. 323–330, 2009.

[59] P. Libby and T. Lüscher, "COVID-19 is, in the end, an endothelial disease," *European heart journal*, vol. 41, no. 32, pp. 3038–3044, 2020.

[60] G. Goshua, A. B. Pine, M. L. Meizlish et al., "Endotheliopathy in COVID-19-associated coagulopathy: evidence from a single-centre, cross-sectional study," *The Lancet Haematology*, vol. 7, no. 8, pp. e575–e582, 2020.

[61] F. A. Klok, M. Kruip, N. J. M. van der Meer et al., "Confirmation of the high cumulative incidence of thrombotic complications in critically ill ICU patients with COVID-19: an updated analysis," *Thrombosis research*, vol. 191, pp. 148–150, 2020.

[62] K. Croce and P. Libby, "Intertwining of thrombosis and inflammation in atherosclerosis," *Current opinion in hematology*, vol. 14, no. 1, pp. 55–61, 2007.

[63] T. F. Lüscher and P. M. Vanhoutte, "Endothelium-dependent contractions to acetylcholine in the aorta of the spontaneously hypertensive rat," *Hypertension*, vol. 8, no. 4, pp. 344–348, 1986.

[64] D. D. Wagner, "The Weibel-Palade body: the storage granule for von Willebrand factor and P-selectin," *Thrombosis and Haemostasis*, vol. 70, no. 1, pp. 105–110, 1993.

[65] M. A. Gimbrone Jr. and G. García-Cardeña, "Endothelial cell dysfunction and the pathobiology of atherosclerosis," *Circulation research*, vol. 118, no. 4, pp. 620–636, 2016.

[66] E. Lubos, N. J. Kelly, S. R. Oldebeken et al., "Glutathione Peroxidase-1 Deficiency Augments Proinflammatory Cytokine-induced Redox Signaling and Human Endothelial Cell Activation," *The Journal of biological chemistry*, vol. 286, no. 41, pp. 35407–35417, 2011.

[67] L. Loffredo, F. Martino, A. M. Zicari et al., "Enhanced NOX-2 derived oxidative stress in offspring of patients with early myocardial infarction," *International journal of cardiology*, vol. 293, pp. 56–59, 2019.

[68] Y. Xuan, X. Gào, B. Holleczek, H. Brenner, and B. Schöttker, "Prediction of myocardial infarction, stroke and cardiovascular mortality with urinary biomarkers of oxidative stress: results from a large cohort study," *International journal of cardiology*, vol. 273, pp. 223–229, 2018.

[69] S. Pennathur and J. W. Heinecke, "Oxidative stress and endothelial dysfunction in vascular disease," *Current diabetes reports*, vol. 7, no. 4, pp. 257–264, 2007.

[70] A. Rafnsson, L. P. Matic, M. Lengquist et al., "Endothelin-1 increases expression and activity of arginase 2 via ETB receptors and is co-expressed with arginase 2 in human atherosclerotic plaques," *Atherosclerosis*, vol. 292, pp. 215–223, 2020.

[71] C. S. Alphonsus and R. N. Rodseth, "The endothelial glycocalyx: a review of the vascular barrier," *Anaesthesia*, vol. 69, no. 7, pp. 777–784, 2014.

[72] I. Rubio-Gayosso, S. H. Platts, and B. R. Duling, "Reactive oxygen species mediate modification of glycocalyx during ischemia-reperfusion injury," *American journal of physiology Heart and circulatory physiology*, vol. 290, no. 6, pp. H2247–H2256, 2006.

[73] M. Nieuwdorp, M. C. Meuwese, H. L. Mooij et al., "Tumor necrosis factor-α inhibition protects against endotoxin-induced endothelial glycocalyx perturbation," *Atherosclerosis*, vol. 202, no. 1, pp. 296–303, 2009.

[74] C. J. Zuurbier, C. Demirci, A. Koeman, H. Vink, and C. Ince, "Short-term hyperglycemia increases endothelial glycocalyx permeability and acutely decreases lineal density of capillaries with flowing red blood cells," *Journal of applied physiology*, vol. 99, no. 4, pp. 1471–1476, 2005.

[75] R. Uchimido, E. P. Schmidt, and N. I. Shapiro, "The glycocalyx: a novel diagnostic and therapeutic target in sepsis," *Critical care*, vol. 23, no. 1, p. 16, 2019.

[76] K. Stahl, P. A. Gronski, Y. Kiyan et al., "Injury to the endothelial glycocalyx in critically ill patients with COVID-19," *American journal of respiratory and critical care medicine*, vol. 202, no. 8, pp. 1178–1181, 2020.

[77] A. Rovas, I. Osiaevi, K. Buscher et al., "Microvascular dysfunction in COVID-19: the MYSTIC study," *Angiogenesis*, vol. 24, no. 1, pp. 145–157, 2021.

[78] B. Buijsers, C. Yanginlar, A. de Nooijer et al., "Increased plasma heparanase activity in COVID-19 patients," *Frontiers in immunology*, vol. 11, p. 575047, 2020.

[79] T. J. Anderson, I. T. Meredith, A. C. Yeung, B. Frei, A. P. Selwyn, and P. Ganz, "The effect of cholesterol-lowering and antioxidant therapy on endothelium-dependent coronary vasomotion," *The New England journal of medicine*, vol. 332, no. 8, pp. 488–493, 1995.

[80] Y. Shahin, J. A. Khan, N. Samuel, and I. Chetter, "Angiotensin converting enzyme inhibitors effect on endothelial dysfunction: a meta-analysis of randomised controlled trials," *Atherosclerosis*, vol. 216, no. 1, pp. 7–16, 2011.

[81] A. J. Flammer, I. Sudano, F. Hermann et al., "Angiotensin-converting enzyme inhibition improves vascular function in rheumatoid arthritis," *Circulation*, vol. 117, no. 17, pp. 2262–2269, 2008.

[82] W. F. Penny, O. Ben-Yehuda, K. Kuroe et al., "Improvement of coronary artery endothelial dysfunction with lipid-lowering therapy: heterogeneity of segmental response and correlation with plasma- oxidized low density lipoprotein," *Journal of the American College of Cardiology*, vol. 37, no. 3, pp. 766–774, 2001.

[83] P. Libby, P. M. Ridker, G. K. Hansson, and Leducq Transatlantic Network on Atherothrombosis, "Inflammation in atherosclerosis: from pathophysiology to practice," *Journal of the American College of Cardiology*, vol. 54, no. 23, pp. 2129–2138, 2009.

[84] N. G. Ardlie, J. A. McGuiness, and J. J. Garrett, "Effect on human platelets of catecholamines at levels achieved in the circulation," *Atherosclerosis*, vol. 58, no. 1-3, pp. 251–259, 1985.

[85] P. H. Stone, "Triggering myocardial infarction," *The New England journal of medicine*, vol. 351, no. 17, pp. 1716–1718, 2004.

[86] D. G. Katritsis, J. Pantos, and E. Efstathopoulos, "Hemodynamic factors and atheromatic plaque rupture in the coronary arteries: from vulnerable plaque to vulnerable coronary segment," *Coronary Artery Disease*, vol. 18, no. 3, pp. 229–237, 2007.

[87] S. J. Warner, K. R. Auger, and P. Libby, "Human interleukin 1 induces interleukin 1 gene expression in human vascular smooth muscle cells," *The Journal of experimental medicine*, vol. 165, no. 5, pp. 1316–1331, 1987.

[88] S. J. Warner and P. Libby, "Human vascular smooth muscle cells. Target for and source of tumor necrosis factor," *Journal of immunology*, vol. 142, no. 1, pp. 100–109, 1989.

[89] J. M. Wang, A. Sica, G. Peri et al., "Expression of monocyte chemotactic protein and interleukin-8 by cytokine-activated human vascular smooth muscle cells," *Arteriosclerosis and thrombosis: a journal of vascular biology*, vol. 11, no. 5, pp. 1166–1174, 1991.

[90] H. Loppnow and P. Libby, "Adult human vascular endothelial cells express the IL6 gene differentially in response to LPS or IL1," *Cellular immunology*, vol. 122, no. 2, pp. 493–503, 1989.

[91] N. Chen, M. Zhou, X. Dong et al., "Epidemiological and clinical characteristics of 99 cases of 2019 novel coronavirus pneumonia in Wuhan, China: a descriptive study," *Lancet*, vol. 395, no. 10223, pp. 507–513, 2020.

[92] S. Pons, M. Arnaud, M. Loiselle, E. Arrii, E. Azoulay, and L. Zafrani, "Immune consequences of endothelial cells' activation and dysfunction during sepsis," *Critical care clinics*, vol. 36, no. 2, pp. 401–413, 2020.

[93] B. Bikdeli, M. V. Madhavan, A. Gupta et al., "Pharmacological agents targeting thromboinflammation in COVID-19: review and implications for future research," *Thrombosis and Haemostasis*, vol. 120, no. 7, pp. 1004–1024, 2020.

[94] Q. Ruan, K. Yang, W. Wang, L. Jiang, and J. Song, "Clinical predictors of mortality due to COVID-19 based on an analysis of data of 150 patients from Wuhan, China," *Intensive care medicine*, vol. 46, no. 5, pp. 846–848, 2020.

[95] K. Thygesen, J. S. Alpert, A. S. Jaffe et al., "Fourth universal definition of myocardial infarction (2018)," *Circulation*, vol. 138, no. 20, pp. e618–e651, 2018.

[96] A. R. Chapman, A. S. V. Shah, K. K. Lee et al., "Long-term outcomes in patients with type 2 myocardial infarction and myocardial injury," *Circulation*, vol. 137, no. 12, pp. 1236–1245, 2018.

[97] B. Popovic, J. Varlot, P. A. Metzdorf, H. Jeulin, F. Goehringer, and E. Camenzind, "Changes in characteristics and

management among patients with ST-elevation myocardial infarction due to COVID-19 infection," *Catheterization and cardiovascular interventions*, vol. 97, no. 3, pp. E319–E326, 2021.

[98] F. Rivero, P. Antuña, J. Cuesta, and F. Alfonso, "Severe coronary spasm in a COVID-19 patient," *Catheterization and cardiovascular interventions*, vol. 97, no. 5, pp. E670–E672, 2021.

[99] M. Nakao, J. Matsuda, M. Iwai et al., "Coronary spasm and optical coherence tomography defined plaque erosion causing ST-segment-elevation acute myocardial infarction in a patient with COVID-19 pneumonia," *Journal of cardiology cases*, vol. 23, no. 2, pp. 87–89, 2021.

[100] Y. Murase, Y. Yamada, A. Hirashiki et al., "Genetic risk and gene-environment interaction in coronary artery spasm in Japanese men and women," *European heart journal*, vol. 25, no. 11, pp. 970–977, 2004.

[101] A. Matta, F. Bouisset, T. Lhermusier et al., "Coronary artery spasm: new insights," *Journal of Interventional Cardiology*, vol. 2020, article 5894586, 10 pages, 2020.

[102] H. R. Reynolds, A. Maehara, R. Y. Kwong et al., "Coronary optical coherence tomography and cardiac magnetic resonance imaging to determine underlying causes of myocardial infarction with nonobstructive coronary arteries in women," *Circulation*, vol. 143, no. 7, pp. 624–640, 2021.

[103] A. G. Dastidar, A. Baritussio, E. De Garate, Z. Drobni, G. Biglino, P. Singhal et al., "Prognostic role of CMR and conventional risk factors in myocardial infarction with nonobstructed coronary arteries," *JACC Cardiovascular imaging*, vol. 12, no. 10, pp. 1973–1982, 2019.

[104] J. P. Collet, H. Thiele, E. Barbato et al., "2020 ESC guidelines for the management of acute coronary syndromes in patients presenting without persistent ST-segment elevation," *European heart journal*, vol. 42, no. 14, pp. 1289–1367, 2021.

[105] J. P. Lang, X. Wang, F. A. Moura, H. K. Siddiqi, D. A. Morrow, and E. A. Bohula, "A current review of COVID-19 for the cardiovascular specialist," *American Heart Journal*, vol. 226, pp. 29–44, 2020.

[106] S. Hegde, R. Khan, M. Zordok, and M. Maysky, "Characteristics and outcome of patients with COVID-19 complicated by Takotsubo cardiomyopathy: case series with literature review," *Open Heart*, vol. 7, no. 2, 2020.

[107] M. R. Dweck, A. Bularga, R. T. Hahn et al., "Global evaluation of echocardiography in patients with COVID-19," *European heart journal Cardiovascular Imaging*, vol. 21, no. 9, pp. 949–958, 2020.

[108] G. Moady and S. Atar, "Takotsubo syndrome during the COVID-19 pandemic, state-of -the- art review.," *CJC open*, 2021.

[109] A. Jabri, A. Kalra, A. Kumar, A. Alameh, S. Adroja, H. Bashir et al., "Incidence of stress cardiomyopathy during the coronavirus disease 2019 pandemic," *JAMA network open*, vol. 3, no. 7, article e2014780, 2020.

[110] J. R. Ghadri, I. S. Wittstein, A. Prasad et al., "International expert consensus document on Takotsubo syndrome (part I): clinical characteristics, diagnostic criteria, and pathophysiology," *European heart journal*, vol. 39, no. 22, pp. 2032–2046, 2018.

[111] Z. C. Jing, H. D. Zhu, X. W. Yan, W. Z. Chai, and S. Zhang, "Recommendations from the Peking union medical college hospital for the management of acute myocardial infarction during the COVID-19 outbreak," *European heart journal*, vol. 41, no. 19, pp. 1791–1794, 2020.

[112] F. G. P. Welt, P. B. Shah, H. D. Aronow et al., "Catheterization laboratory considerations during the coronavirus (COVID-19) pandemic: from the ACC's interventional council and SCAI," *Journal of the American College of Cardiology*, vol. 75, no. 18, pp. 2372–2375, 2020.

[113] M. J. Daniels, M. G. Cohen, A. A. Bavry, and D. J. Kumbhani, "Reperfusion of ST-segment-elevation myocardial infarction in the COVID-19 era: business as usual?," *Circulation*, vol. 141, no. 24, pp. 1948–1950, 2020.

[114] B. Ibanez, S. James, S. Agewall et al., "2017 ESC guidelines for the management of acute myocardial infarction in patients presenting with ST-segment elevation: the task force for the management of acute myocardial infarction in patients presenting with ST-segment elevation of the European Society of Cardiology (ESC)," *European heart journal*, vol. 39, no. 2, pp. 119–177, 2018.

[115] A. A. Manfredi, G. A. Ramirez, P. Rovere-Querini, and N. Maugeri, "The Neutrophil's choice: phagocytose vs make neutrophil extracellular traps," *Frontiers in immunology*, vol. 9, 2018.

[116] E. D. Hottz, I. M. Medeiros-de-Moraes, A. Vieira-de-Abreu et al., "Platelet activation and apoptosis modulate monocyte inflammatory responses in dengue," *Journal of immunology*, vol. 193, no. 4, pp. 1864–1872, 2014.

[117] A. Zarbock, R. K. Polanowska-Grabowska, and K. Ley, "Platelet-neutrophil-interactions: linking hemostasis and inflammation," *Blood reviews*, vol. 21, no. 2, pp. 99–111, 2007.

[118] V. B. Lê, J. G. Schneider, Y. Boergeling et al., "Platelet activation and aggregation promote lung inflammation and influenza virus pathogenesis," *American journal of respiratory and critical care medicine*, vol. 191, no. 7, pp. 804–819, 2015.

[119] P. Lancellotti, L. Musumeci, N. Jacques et al., "Antibacterial activity of Ticagrelor in conventional antiplatelet dosages against antibiotic-resistant gram-positive Bacteria," *JAMA Cardiology*, vol. 4, no. 6, pp. 596–599, 2019.

[120] T. R. Sexton, G. Zhang, T. E. Macaulay et al., "Ticagrelor reduces thromboinflammatory markers in patients with pneumonia," *JACC Basic to translational science*, vol. 3, no. 4, pp. 435–449, 2018.

[121] R. F. Storey, S. K. James, A. Siegbahn et al., "Lower mortality following pulmonary adverse events and sepsis with ticagrelor compared to clopidogrel in the PLATO study," *Platelets*, vol. 25, no. 7, pp. 517–525, 2014.

[122] T. Menter, J. D. Haslbauer, R. Nienhold et al., "Postmortem examination of COVID-19 patients reveals diffuse alveolar damage with severe capillary congestion and variegated findings in lungs and other organs suggesting vascular dysfunction," *Histopathology*, vol. 77, no. 2, pp. 198–209, 2020.

[123] Z. W. Lang, L. J. Zhang, S. J. Zhang et al., "A clinicopathological study of three cases of severe acute respiratory syndrome (SARS)," *Pathology*, vol. 35, no. 6, pp. 526–531, 2003.

[124] D. Giacoppo, Y. Matsuda, L. N. Fovino et al., "Short dual antiplatelet therapy followed by P2Y12 inhibitor monotherapy vs. prolonged dual antiplatelet therapy after percutaneous coronary intervention with second-generation drug-eluting stents: a systematic review and meta-analysis of randomized clinical trials," *European heart journal*, vol. 42, no. 4, pp. 308–319, 2021.

[125] U. Baber, G. Dangas, D. J. Angiolillo et al., "Ticagrelor alone vs. ticagrelor plus aspirin following percutaneous coronary intervention in patients with non-ST-segment elevation acute coronary syndromes: TWILIGHT-ACS," *European heart journal*, vol. 41, no. 37, pp. 3533–3545, 2020.

[126] X. Li, Z. Zheng, X. Li, and X. Ma, "Unfractionated heparin inhibits lipopolysaccharide-induced inflammatory response through blocking p38 MAPK and NF-κB activation on endothelial cell," *Cytokine*, vol. 60, no. 1, pp. 114–121, 2012.

[127] N. Maugeri, G. de Gaetano, M. Barbanti, M. B. Donati, and C. Cerletti, "Prevention of platelet-polymorphonuclear leukocyte interactions: new clues to the antithrombotic properties of parnaparin, a low molecular weight heparin," *Haematologica*, vol. 90, no. 6, pp. 833–839, 2005.

[128] Y. Qian, H. Xie, R. Tian, K. Yu, and R. Wang, "Efficacy of low molecular weight heparin in patients with acute exacerbation of chronic obstructive pulmonary disease receiving ventilatory support," *COPD*, vol. 11, no. 2, pp. 171–176, 2014.

[129] C. Mycroft-West, D. Su, S. Elli et al., "The 2019 coronavirus (SARS-CoV-2) surface protein (Spike) S1 Receptor Binding Domain undergoes conformational change upon heparin binding," *bioRxiv*, 2020.

[130] E. Trybala, J. A. Liljeqvist, B. Svennerholm, and T. Bergström, "Herpes simplex virus types 1 and 2 differ in their interaction with heparan sulfate," *Journal of virology*, vol. 74, no. 19, pp. 9106–9114, 2000.

[131] A. Y. Simon, M. R. Sutherland, and E. L. Pryzdial, "Dengue virus binding and replication by platelets," *Blood*, vol. 126, no. 3, pp. 378–385, 2015.

[132] V. Russo, R. Bottino, A. D'Andrea et al., "Chronic Oral anticoagulation and clinical outcome in hospitalized COVID-19 patients," *Cardiovascular Drugs and Therapy*, pp. 1–8, 2021.

[133] V. Russo, M. di Maio, E. Attena et al., "Clinical impact of preadmission antithrombotic therapy in hospitalized patients with COVID-19: a multicenter observational study," *Pharmacological Research*, vol. 159, 2020.

[134] G. N. Nadkarni, A. Lala, E. Bagiella et al., "Anticoagulation, bleeding, mortality, and pathology in hospitalized patients with COVID-19," *Journal of the American College of Cardiology*, vol. 76, no. 16, pp. 1815–1826, 2020.

[135] A. Silverio, G. Galasso, and G. De Luca, "Consolidating the value of fondaparinux for current treatment of non-ST- elevation acute coronary syndromes," *International Journal of Cardiology*, vol. 335, pp. 21–23, 2021.

[136] A. Silverio, M. Di Maio, C. Prota et al., "Safety and efficacy of non-vitamin K antagonist oral anticoagulants in elderly patients with atrial fibrillation," *European Heart Journal-Cardiovascular Pharmacotherapy*, vol. 7, 2019.

[137] G. I. Rice, D. A. Thomas, P. J. Grant, A. J. Turner, and N. M. Hooper, "Evaluation of angiotensin-converting enzyme (ACE), its homologue ACE2 and neprilysin in angiotensin peptide metabolism," *The Biochemical journal*, vol. 383, no. 1, pp. 45–51, 2004.

[138] A. C. S. e Silva, K. D. Silveira, A. J. Ferreira, and M. M. Teixeira, "ACE2, angiotensin-(1-7) and mas receptor axis in inflammation and fibrosis," *British journal of pharmacology*, vol. 169, no. 3, pp. 477–492, 2013.

[139] S. N. Iyer, M. C. Chappell, D. B. Averill, D. I. Diz, and C. M. Ferrario, "Vasodepressor actions of angiotensin-(1-7) unmasked during combined treatment with lisinopril and losartan," *Hypertension*, vol. 31, no. 2, pp. 699–705, 1998.

[140] R. Zeiser, "Immune modulatory effects of statins," *Immunology*, vol. 154, no. 1, pp. 69–75, 2018.

[141] V. Castiglione, M. Chiriacò, M. Emdin, S. Taddei, and G. Vergaro, "Statin therapy in COVID-19 infection," *European heart journal Cardiovascular pharmacotherapy*, vol. 6, no. 4, pp. 258-259, 2020.

[142] U. Laufs, V. La Fata, J. Plutzky, and J. K. Liao, "Upregulation of endothelial nitric oxide synthase by HMG CoA reductase inhibitors," *Circulation*, vol. 97, no. 12, pp. 1129–1135, 1998.

[143] U. Laufs, K. Gertz, P. Huang et al., "Atorvastatin upregulates type III nitric oxide synthase in thrombocytes, decreases platelet activation, and protects from cerebral ischemia in normocholesterolemic mice," *Stroke*, vol. 31, no. 10, pp. 2442–2449, 2000.

[144] F. Violi, C. Calvieri, D. Ferro, and P. Pignatelli, "Statins as antithrombotic drugs," *Circulation*, vol. 127, no. 2, pp. 251–257, 2013.

[145] K. Tikoo, G. Patel, S. Kumar et al., "Tissue specific up regulation of ACE2 in rabbit model of atherosclerosis by atorvastatin: role of epigenetic histone modifications," *Biochemical Pharmacology*, vol. 93, no. 3, pp. 343–351, 2015.

[146] A. Gupta, M. V. Madhavan, T. J. Poterucha et al., "Association between antecedent statin use and decreased mortality in hospitalized patients with COVID-19," *Nature Communications*, vol. 12, no. 1, p. 1325, 2021.

[147] X. J. Zhang, J. J. Qin, X. Cheng et al., "In-hospital use of statins is associated with a reduced risk of mortality among individuals with COVID-19," *Cell Metabolism*, vol. 32, no. 2, pp. 176–87.e4, 2020.

[148] A. Barbieri, N. Robinson, G. Palma, N. Maurea, V. Desiderio, and G. Botti, "Can beta-2-adrenergic pathway be a new target to combat SARS-CoV-2 hyperinflammatory syndrome?-lessons learned from cancer," *Frontiers in immunology*, vol. 11, 2020.

[149] N. Vasanthakumar, "Beta-adrenergic blockers as a potential treatment for COVID-19 patients," *BioEssays*, vol. 42, no. 11, 2020.

[150] L. Wu, Y. Tai, S. Hu et al., "Bidirectional role of β2-adrenergic receptor in autoimmune diseases," *Frontiers in Pharmacology*, vol. 9, 2018.

[151] M. Manni, R. D. Granstein, and G. Maestroni, "β2-adrenergic agonists bias TLR-2 and NOD2 activated dendritic cells towards inducing an IL-17 immune response," *Cytokine*, vol. 55, no. 3, pp. 380–386, 2011.

[152] R. Haldar, L. Shaashua, H. Lavon et al., "Perioperative inhibition of β-adrenergic and COX2 signaling in a clinical trial in breast cancer patients improves tumor Ki-67 expression, serum cytokine levels, and PBMCs transcriptome," *Brain, Behavior, and Immunity*, vol. 73, pp. 294–309, 2018.

[153] L. Zhou, Y. Li, X. Li et al., "Propranolol attenuates surgical stress–induced elevation of the regulatory T cell response in patients undergoing radical mastectomy," *The Journal of Immunology*, vol. 196, no. 8, pp. 3460–3469, 2016.

Review Article

Exploring Functional Differences between the Right and Left Ventricles to Better Understand Right Ventricular Dysfunction

Judith Bernal-Ramirez [iD],[1] **Magda C. Díaz-Vesga** [iD],[2,3,4,5,6] **Matias Talamilla,**[2]
Andrea Méndez,[2,5,7,8] **Clara Quiroga** [iD],[3,9] **Javier A. Garza-Cervantes** [iD],[1]
Anay Lázaro-Alfaro [iD],[1] **Carlos Jerjes-Sanchez** [iD],[1,10] **Mauricio Henríquez** [iD],[2,5]
Gerardo García-Rivas [iD],[1,10] **and Zully Pedrozo** [iD][2,3,4,5]

[1]*Tecnológico de Monterrey, Escuela de Medicina y Ciencias de la Salud, Ave. Morones Prieto 3000, Monterrey, NL 64710, Mexico*
[2]*Programa de Fisiología y Biofísica, Instituto de Ciencias Biomédicas, Facultad de Medicina, Universidad de Chile,*
Santiago de Chile, Chile
[3]*Advanced Center for Chronic Diseases, Facultad de Ciencias Químicas y Farmacéuticas & Facultad Medicina, Universidad de Chile,*
Santiago de Chile, Chile
[4]*Centro de Estudios en Ejercicio, Metabolismo y Cáncer (CEMC), Facultad de Medicina, Universidad de Chile,*
Santiago de Chile, Chile
[5]*Red para el Estudio de Enfermedades Cardiopulmonares de Alta Letalidad (REECPAL), Universidad de Chile,*
Santiago de Chile, Chile
[6]*Grupo de Investigación en Ciencias Básicas y Clínicas de la Salud, Pontificia Universidad Javeriana de Cali, Colombia*
[7]*Escuela de Kinesiología, Facultad de Salud y Ciencias Sociales, Campus Providencia, Sede Santiago,*
Universidad de las Américas, Chile
[8]*Centro de Investigación e Innovación Biopsicosocial en Enfermedades Crónicas, Facultad de Salud y Ciencias Sociales,*
Universidad de las Américas, Chile
[9]*División de Enfermedades Cardiovasculares, Facultad de Medicina, Pontificia Universidad Católica de Chile, Santiago, Chile*
[10]*Tecnológico de Monterrey, Centro de Investigación Biomédica, Hospital Zambrano Hellion, TecSalud, San Pedro Garza Garcia,*
NL 66278, Mexico

Correspondence should be addressed to Gerardo García-Rivas; gdejesus@itesm.mx and Zully Pedrozo; zpedrozo@uchile.cl

The right and left ventricles have traditionally been studied as individual entities. Furthermore, modifications found in diseased left ventricles are assumed to influence on right ventricle alterations, but the connection is poorly understood. In this review, we describe the differences between ventricles under physiological and pathological conditions. Understanding the mechanisms that differentiate both ventricles would facilitate a more effective use of therapeutics and broaden our knowledge of right ventricle (RV) dysfunction. RV failure is the strongest predictor of mortality in pulmonary arterial hypertension, but at present, there are no definitive therapies directly targeting RV failure. We further explore the current state of drugs and molecules that improve RV failure in experimental therapeutics and clinical trials to treat pulmonary arterial hypertension and provide evidence of their potential benefits in heart failure.

1. Introduction

Pulmonary arterial hypertension (PAH) is an incurable life-limiting disease characterized by increased pulmonary hypertension secondary to pulmonary vasculature remodeling [1]. The increased pressure overloads the right ventricle (RV), inducing adaptive RV remodeling. In the initial stages, RV hypertrophy decreases wall tension, but maladaptive remodeling induces RV dysfunction and right heart failure syndrome in the end stages [2]. Specific treatment includes therapies targeting endothelin, nitric oxide, and prostacyclin pathways in pulmonary arteries to decrease pulmonary pressure and prevent RV stress [3]. The available therapeutic approaches improve quality of life and reduce the incidence of clinical worsening [4]. Although RV dysfunction and the patient's response to PAH-specific treatment determine survival [5, 6], there are no therapeutic aims to improve RV dysfunction [7]. Left ventricular (LV) dysfunction mechanisms have been widely studied, and multiple therapies to improve LV failure survival are available [8]; however, treatment for RV dysfunction is less robust [9]. Notably, beta-blockers and drugs that target the renin-angiotensin-aldosterone system (RAAS), which are standard therapies for LV failure, are potentially contraindicated in RV dysfunction [8]. Thus, understanding the differences between the RV and LV and describing RV dysfunction's underlying mechanism may be essential to outline an RV-directed therapy and improve PAH patient outcomes. This review focuses on the underlying mechanisms that differentiate left and right ventricles in both physiological conditions and disease development.

2. Structural and Functional Differences between the Right and Left Ventricles

The heart is a muscular pump whose primary function is to supply blood to the body, allowing oxygen and nutrients to reach each cell while removing carbon dioxide and metabolic waste. The ventricles propel blood from the heart to either high-pressure systemic circulation by the thick-walled conic-shaped LV or pulmonary circulation by the thin-walled, crescent-shaped RV, which is capable of maintaining low pressure levels even under changes in volume [10, 11]. Both ventricles adapt their mechanisms at the cellular and tissue levels to meet the whole organism's needs and their development into adulthood to accomplish the heart's function. This section summarizes the differences in development and adaptations of each ventricle to maintain its proper function.

2.1. Structural Differences between Ventricles. Embryonic development of the human cardiovascular system occurs between the third and eighth weeks of gestation [12]. Specifically, heart development begins on the 16th day of gestation; however, it is not a uniform process. Ventricles show differences in development, cellular origin, and molecular and genetic markers. These differences begin with the movement of cardiac progenitor cells that originate in gastrulation, from the mesoderm to the anterior of the primitive vein [13],

where two structures are differentiated: the first cardiac field (FHF) and the second cardiac field (SHF) [14]. The FHF will give origin to the crescent-shaped cardiac tube and the LV, which begins development before the RV. The SHF will give origin to the outflow tract and the RV. It is essential to note that these processes develop successively and under genetic control, including the Paired-Like Homeodomain 2 (*PITX2*) gene, which determines left and right asymmetry [13], and the Heart and Neural Crest Derivatives Expressed (*HAND1* and *HAND2*) genes, which influence the development of the left and right ventricles, respectively, [14]. Contrary to what happens in adulthood, where cardiac output is the same for both ventricles, during embryological development, the RV produces 60% of total cardiac output [11]. Likewise, during embryological development, the thickness and strength generated by the LV and RV are the same [12].

An organ's structure serves its function; thus, differences in the pressure of pulmonary and systemic circuits determine several structural differences between ventricles. Noting the anatomical muscle arrangement in both ventricles helps to understand how blood is pumped through different parts of the circulatory system. Most of the muscle fibers in the RV free wall are transverse fibers with a small portion of subendocardial longitudinal fibers [15]. However, the LV is composed of endocardial and epicardial fibers, which form a helical structure, and circumferential fibers located at the midwall [16]. Therefore, RV needs fewer muscle fibers and is much thinner than the LV, and it has about one-third of LV's thickness [10]. This fiber arrangement contributes differently to ventricle contraction. LV contraction involves the septum, presenting a radial constriction and longitudinal shortening, contributing 67% and 33% to the LV ejection fraction (LVEF), respectively [16]. Simultaneously, longitudinal fibers in the RV free wall account for 20–30% of the RV ejection fraction (RVEF). In comparison, approximately 80% of RV systolic function is attributed to the septum's helical fibers, which twist and shorten the longitudinal axis in the RV [15]. Along with differences in fiber arrangement and muscle contraction, the RV has a higher extracellular matrix content than the LV [17].

2.2. Physiological Difference between Ventricles. Anatomical differences between the ventricles are also reflected in their perfusion system. The lower pulmonary arterial pressure and pulmonary vascular resistance are 20% and 10% of systemic arterial pressure and systemic vascular resistance, respectively [18], leading to lower oxygen consumption by the RV [19]. While the LV has a higher oxygen demand, its perfusion predominantly occurs during diastole due to the fact that increased intramural pressure during systole impedes the flow supply [19]. The low pressures handled by the RV allow the perfusion of blood flow throughout the entire cardiac cycle, allowing it to maintain an appropriate myocardial oxygen level [19]. Moreover, the collateral vessels of the RV are denser than those of the LV [10]. The lower oxygen consumption and blood flow in the RV result in an oxygen extraction reserve, making the RV less vulnerable to myocardial ischemia [19]. However, the RV is highly susceptible to acute increases in afterload, unlike the LV [20, 21].

Increases in pulmonary arterial pressure increase intramural pressure, impeding blood supply during systole, which increases blood flow demands during diastole, like LV perfusion [19]. After the blood flow fails to meet an acute or chronic increased oxygen demand caused by an increased afterload, it results in RV ischemia and RV failure [19, 22].

2.3. Differences in Cell Shortening and Relaxation between Cardiac Cells. The cardiac muscle's functional unit is the cardiomyocyte, whose primary function is to accomplish the cell contraction-relaxation cycle, leading to synchronized organ contraction and relaxation [23]. This synchronization is made possible by cardiac excitation-contraction coupling (ECC), which is the physiological process of converting an electrical stimulus to a mechanical response [24]. ECC refers to everything from the activation of the calcium ion (Ca^{2+}) transient by initial membrane depolarization, through the action potential (AP), to myofilament contraction in response to increased intracellular Ca^{2+}. The initial AP promotes the entry of extracellular Ca^{2+} through voltage-dependent Ca^{2+} channels at the plasma membrane or sarcolemma, which promotes the release of Ca^{2+} from the sarcoplasmic reticulum (SR) in a process known as calcium-induced calcium release (CICR), causing a significant transient increase in intracellular Ca^{2+} [24], which interacts with the proteins in myofilaments to produce cellular contraction. Cell relaxation occurs by removing cytosolic Ca^{2+} in a highly energy-dependent process [25]. This section will focus on describing the differences between left and right cardiomyocytes during ECC, especially the differential characteristics of AP, components of Ca^{2+} handling in myocytes, and energetic and mitochondria-dependent process in excitation energetic coupling.

By definition, AP involves a reversible change in membrane potential due to the sequential activation and inhibition of several ionic channels, which allow ions to flow in favor of their electrochemical gradient through the cell membrane [26]. Sodium ion (Na^+) and Ca^{2+} inward currents and different potassium ion (K^+) outward currents are described in this section. Differences in AP form and duration (APD) are explained by changes in the expression and function of these ions' channels (Table 1). Figure 1 highlights the main differences between the right and left AP shape and currents. Membrane depolarization by AP starts with a sodium inward current (I_{Na}) through voltage-sensitive Na^+ channels. Higher I_{Na} densities and larger Na^+ currents have been found in the LV than in the RV. In the LV, Na^+ channels also have more negative steady-state inactivation, $V_{1/2}$, and slower recovery from inactivation than in the RV, without changes in the activation threshold [26]. The lower I_{Na} density causes a slower conduction time in the RV, resulting in a lower upstroke velocity [26]. Despite the lower density, higher [27] or unchanged [26] Na^+ channel expression has been reported.

The movement of different ions through the cell membrane shapes the AP, organizing it in well-defined membrane depolarization and repolarization phases. The main difference between LV's and RV's AP is during phase 1, which corresponds to the synchronized opening of K^+ channels after the initial Na^+ inward current [28, 29]. The RV has a deeper notch

than the LV due to an increase in outward K^+ current density [28, 30, 31]. This increase is due to the larger amplitude of the transient outward current (I_{to}) in the RV than in the LV [28, 30–32]. In some studies, no changes were observed in protein expression [31, 33] or in the inactivation constant [30, 32]. APD differences between the LV and RV have been described in several species, with some studies finding more prolonged APD in the LV than the RV [29, 30, 32, 34–36], even in human hearts [37]. However, a lack of changes in APD was reported in Langendorff-perfused guinea pig hearts [38], and 2-9% RV longer APD has been observed in dogs [26]. The K^+ repolarization currents can explain the shorter APD present in the RV. The RV's steeper repolarization phase's significant contribution is partially due to a higher density in the RV of the slowly activating component (I_{Ks}) of the delayed rectifier $K1$ current [32]. In contrast, a rapidly activating component (I_{Kr}), the inward rectifier current (I_{K1}), and the sustained current (I_{SS}) do not show changes in expression, density, or inactivation [29–33]. The ATP-activated K^+ current (I_{KATP}) has been identified as a determinant factor of APD in ischemia, and its expression is higher in the LV than in the RV [38].

Changes in AP duration and shape may be considered since the cardiac AP's immediate consequence is the generation of an intracellular Ca^{2+} transient and differences observed between the APs of the LV and RV may influence intracellular Ca^{2+} dynamics. The initial membrane depolarization triggers the activation of L-type Ca^{2+} channels (LTCC), allowing an inward current of Ca^{2+}, which, in turn, promotes the release of Ca^{2+} from the SR through the ryanodine receptors (RyR) by CICR, originating the Ca^{2+} transient [24]. Figure 1 shows the main differences between the RV and LV in the Ca^{2+} transient.

The link between the initial membrane depolarization and the Ca^{2+} transient is the LTCC. There is a clear difference between the AP in both ventricles; however, the initial phase of the Ca^{2+} transient is not affected by these changes. Indeed, while some reports show an increase in LTCC protein expression in the RV [27], others report unchanged gene expression between ventricles [29]. Moreover, the Ca^{2+} currents (I_{Ca}) do not show differences between ventricles [29].

Regarding RyR, there are no differences in Ca^{2+} concentration for half-maximal activation, the Hill coefficient, caffeine-sensitive ryanodine binding, or current density [39]. However, there are discrepancies in RyR expression in the RV, since some studies show unchanged protein expression, while others refer to lower expression [40]. More studies will be required to clarify these discrepancies.

At rest, there is no difference in diastolic Ca^{2+} between the right and left ventricles [29, 41]. However, although it seems that RyR expression and function are unchanged, it has been reported an increase in Ca^{2+} transient amplitude during systole in the LV [29, 42], indicating a major Ca^{2+} release by the SR due to primary Ca^{2+} content [42]. A higher contraction force [36] and greater sarcomere shortening have been found in the LV than in the RV [29, 36, 41, 43], which coincides with the increase in the transient amplitude since the more significant the Ca^{2+} release, the greater the contraction force. However, two previous studies found no changes

TABLE 1: Physiological differences between ventricles in myocyte function.

Process	Component	Level	RV change (Compared to LV)	Model	Reference
Action potential	INa	Density	Lower	Dog	[26]
		Expression (SCN5A,SCN1B and 4B)	NC	Dog	
		Steady-state inactivation	Higher	Dog	
		Recovery from inactivation	Higher	Dog	
	AP	Duration	Higher	Human, Dog, Rat, Mice, Human	[29, 30, 32, 34–37]
			NC	Guinea pig	[38]
	Ito	Current	Higher	Dog, Mice, Rat, Dog	[28, 30–32]
		Expression	NC	Rabbit, Mice	[31, 33]
		Inactivation constant	NC	Dog, Dog	[30, 32]
	ICa	Current	NC	Mice	[29]
	IKs	Density	Higher	Dog	[32]
		Expression	NC	Rabbit	[33]
	IKr	Density	NC	Dog	[32]
	IK1	Expression	NC	Mice, Dog	[30, 31]
		Density	NC	Mice	[29]
	ISS	Density	NC	Dog, Mice	[30, 31]
	IKATP	Expression	Lower	Guinea pig	[38]
CIRC	LTCC	Expression	Higher	Rabbit	[27]
			NC	Mice	[29]
		Current	NC	Mice	[29]
		Activity	NC	Human	[39]
		Sensitivity	NC	Human	[39]
	RyR	Density	NC	Human	[39]
		Expression	NC	Rabbit, Human	[27, 154]
			Lower	Dog	[40]
	Ca^{2+} transient	Amplitude	Lower	Rat, Mice	[29, 42]
		Time to decay	Higher	Rat	[36]
	SR	Volume	NC	Pig	[54]
		Ca^{2+} load	Lower	Rat	[42]
	Diastolic Ca^{2+}	Level	NC	Mice, Rat	[29, 41]
Cell contraction	Contraction force		Lower	Dog	[36]
	Sarcomere shortening		Lower	Rat, Mice, Dog, Rat	[29, 36, 41, 43]
	Troponin I	Phosphorylation	NC	Mice	[46]
	Troponin T	Phosphorylation	NC	Mice	[46]
	MyBP-C	Phosphorylation	NC	Mice	[46]
	MRLC	Phosphorylation	NC	Mice	[46]
	Actin-Myosin binding	Mobility	Lower	Mice, Rabbit	[44, 45]
	Maximal shortening velocity		Lower	Mice	[29]
	Myofilaments Ca^{2+} sensitivity		Lower	Rat, Mice	[46–48]
	Myosine ATPase activity		Higher	Rat, Rat	[49, 50]
	Myosine heavy chain	Alfa: beta proportion	Higher	Rat	[49]

TABLE 1: Continued.

Process	Component	Level	RV change (Compared to LV)	Model	Reference
Cell relaxation	SERCA	Activity	Lower	Rat, Rat	[41, 42]
			Higher	Rat	[36]
			NC	Mice	[29]
		Expression	Lower	Rat	[41]
			NC	Rat, Rabbit	[27, 42]
		Phosphorylation	Lower	Rat	[41]
		Affinity to Ca^{2+}	Lower	Rat	[41]
	SERCA-PBL	Ratio	NC	Rat	[41]
		Stability complex	Higher	Rat	
	NCX	Expression	Higher	Rabbit	[27]
		Rest-potentiation phenomenon	Higher	Rat, Mice	[29, 36]
Cell energetics	Mitochondria respiration	Expression	NC	Rat	[53]
		Activity	NC	Dog	[52]
	Oxidative metabolism	Expression	NC	Rat	[53]
	Fatty acid oxidation	Expression	NC	Rat	[53]
	Rate of oxidation	Activity	Lower	Rat	[53]
		Citrate synthase activity	Lower	Rat	[53]
	Mitochondria content	Mitochondria-myofibrils ratio	Lower	Pig	[54]
		Mitochondria volume	NC	Pig	[54]

NC: no change.
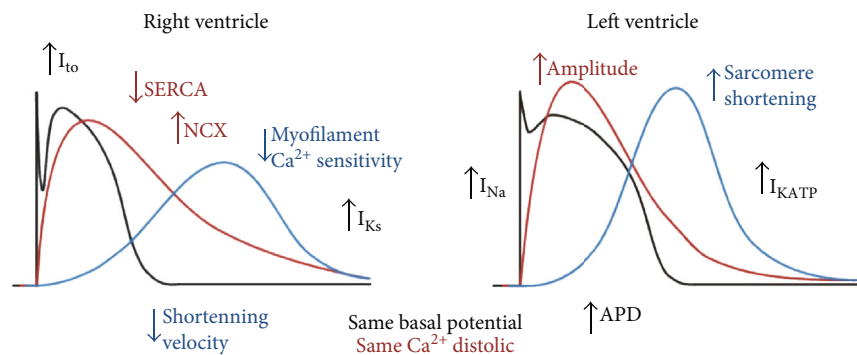
FIGURE 1: Physiological differences in excitation-contraction coupling between ventricles. Black lines, letters and arrows represent the action potential; red lines, letters and arrows represent Ca^{2+} transient; blue line, letters and arrows represent cellular shortening. I_{to}: transient outward current; I_{Ks}: slowly activating component; I_{Na}: sodium inward current; I_{KATP}: ATP-activated K^+ current; ADP: action potential duration; SERCA: sarcoendoplasmic reticulum Ca^{2+} ATPase; NCX: sodium-calcium exchanger. The figure was created with BioRender.com.

in sarcomere shortening in rats [41, 42]. Furthermore, at the molecular level, actin interacts differently with myosin cross-bridges in the LV, allowing greater mobility of actin monomers and, hence, greater contractility [44, 45], without changes in troponin I and T, myosin-binding protein C (MyBP-C), or the myosin regulatory light chain phosphorylation, between LV and RV [46]. On the other hand, the maximal shortening velocity is also slower in RV myocytes [29],

which is related to decreased Ca^{2+} sensitivity in RV myofilaments [46–48]. However, greater myosin ATPase activity [49, 50] and a faster cellular contraction in the RV have also been reported due to a larger proportion of heavy α-chain-containing myosin isozyme in the RV compared to the LV, which has a larger proportion of the slower β-chain [49]. All the expression changes between ventricles are summarized in Table 1.

For relaxation to occur during diastole, intracellular Ca^{2+} must decline, and the sarco/endoplasmic reticulum Ca^{2+}-ATPase (SERCA) pump is the primary removal mechanism [24]. As illustrated in Figure 1, a more prolonged Ca^{2+} transient has been reported in RV myocytes than in LV myocytes [41, 42], accompanied by decreased SERCA activity [41, 42] and expression, as well as affinity to Ca^{2+} in the RV [41]. Phospholamban (PLB) is a critical SERCA inhibitor, but PLB phosphorylation relieves SERCA of its inhibition [51]. A previous study found that LV and RV present similar SERCA/PLB ratios but the RV's SERCA-PLB complex is more stable than in LV [41]. The decreased SERCA activity in RV myocytes may allow more active participation of other Ca^{2+} removal mechanisms, leading to lower Ca^{2+} availability in the SR. This phenomenon might explain the decreased transient amplitudes and SR content [42] observed in RV myocytes when compared to LV myocytes. However, there are some discrepancies since faster relaxation has been reported in the RV [36] than in the LV, as well as no differences in SERCA and PBL activity [29] and expression [27, 42] between LV and RV.

Another important Ca^{2+} removal mechanism in cardiomyocytes is the Na^+/Ca^{2+} exchanger (NCX). Higher NCX protein expression has been found in RV than in LV [27] (Table 1), which might also explain the decreased SR Ca^{2+} availability, resulting in a decreased Ca^{2+} transient amplitude without changes in SERCA activity. However, regardless of its expression, NCX is more active in LV than in RV [36], promoting Ca^{2+} overload in the SR during the rest-potentiation phenomenon, which is more prominent in the LV than in the RV [36]; thus, there are differences in the balance between Ca^{2+} entry and SR loading in the right and left ventricles. Notably, the mitochondrial Ca^{2+} uniporter and mitochondrial NCX contribute to Ca^{2+} handling in cardiac cells [25], but the function and expression of these systems remain unknown in RV cardiomyocytes.

Otherwise, cell relaxation is a high energy-dependent process. Ca^{2+} removal against its concentration gradient by SERCA and the detachment of myosin heads from actin require an adequate ATP supply [24]. Mitochondria are the organelle responsible for energy production in ATP form. There is no change in respiratory components, oxidative metabolism, fatty acid oxidation, or mitochondria respiration between the right and left ventricles [52, 53]. However, the LV has a higher rate of oxidation and mitochondrial membrane potential. This finding has been understood as higher mitochondrial content, supported by a higher citrate synthase activity [53], a higher mitochondria-myofibril ratio [54], and higher nitrosylated protein content in LV than in RV [53]. The mechanism that induces differential levels of mitochondrial biogenesis between the LV and RV is entirely unknown and could be a fertile research area in the future.

3. Distinctions between Right and Left Ventricle Dysfunction

In the vascular system, the RV has not received much research attention since 1943, when cauterization of the RV free wall in canine hearts did not change venous pressure [55]. Furthermore, the LV is more severely affected than the RV in heart disease. However, the medical field's perception of the RV is changing from it being considered unimportant to it being an essential component of normal hemodynamics [56]. More recently, significant differences have been recognized in right and left heart failure progression [11]. Although changes in the left ventricles of failing hearts have been thoroughly described, the assumption that the same mechanism is involved in LV and RV failure has been challenged in recent decades. Physiological and structural differences between the two ventricles may explain the differences in the pathologies each ventricle faces, giving importance to underlying mechanisms that make them more susceptible or resistant to diverse insults.

3.1. Differences between Right and Left Ventricular Infarction. The compromised coronary artery predominantly determines the size and location of the infarction. Acute right ventricular infarction (RVMI) can occur when there is occlusion of the right coronary artery (RCA), proximally to the takeoff of RV branches [57]. The RVMI is an infrequent event, occurring in one-third to one-half of patients presenting with inferior myocardial infarction; very rarely, it can occur in isolation [58].

The term RV infarction may be somewhat misleading since acute RV ischemic dysfunction frequently has a faster recovery than LV infarction. Indeed, there is a deep contrast between the effects of ischemia and reperfusion in RV and in LV, in which prolonged ischemia often leads to myocardial infarction. Levin and Goldstein proposed diverse reasons to explain LV's lower vulnerability to infarction. First, oxygen demand is undoubtedly lower in the RV than in the LV, because of its much smaller muscle mass and lower afterload. Second, in the absence of severe RV hypertrophy or pressure overload, the coronary artery flow in the RV is given in both diastole and systole. Third, chronic RV failure attributable to RV myocardial infarction is infrequent. Fourth, there is greater availability of blood perfusion in the RV through the collateral flow from the left to right coronary arteries [59]. However, Heresi et al. used a sensitive assay to measure cardiac troponin I (cTnI), a myocardial infarction biomarker, and found a significant positive association between cTnI and a more severe PAH and worse clinical outcomes in patients with PAH [60], suggesting that the susceptibility of the RV to ischemic events is not completely understood.

3.2. Differential Mechanisms of Right versus Left Pathological Remodeling. Cardiac hypertrophy is defined as an increase in cardiac mass manifested by increasing size, as well as morphological and functional alterations attributed to a physiological or pathological stimulus. Physical exercise is an example of a physiological stimulus, while a pathological stimulus is found in hypertension, diabetes, myocardial ischemia, and other conditions [61]. Cardiac hypertrophy is considered an adaptive response to increased activity or functional overload, and it is classified as eccentric or concentric. An increase in preload due to high blood volumes reaching the heart, usually observed in aortic regurgitation or endurance exercise, leads to eccentric hypertrophy. This

represents a serial addition of sarcomeres, which increases of the ventricular chamber volume and the wall thickness. A higher afterload due to pressure overload in the ventricle leads to concentric hypertrophy. This represents a parallel addition of sarcomeres, which increases myocardial thickness and reduces the diameter of the ventricular chamber [61].

Concentric hypertrophy is generally accompanied by remodeling to adapt to pressure overload and maintain a stable cardiac output. Next, remodeling progresses from an adaptive to a maladaptive phenotype, with altered contractility that leads to cardiac failure [62]. Differences in LV and RV responses to pressure overload have been described [63, 64]. The compensatory remodeling is restricted in RV versus LV. Inhibition of nitric oxide with L-NAME generates LV and RV hypertrophy, but the RV responds with dilation, dysfunction, and an increase in reactive oxygen species (ROS), which causes the inhibition of hypoxia-inducible factor 1-α (HIF1α) and the suppression of angiogenesis, inducing chronic ischemia in the RV [64, 65]. Moreover, a reduction in superoxide dismutase in the RV versus its increase in the LV has been observed [64]. Additionally, pressure overload in the RV in pulmonary artery banding (PAB) models leads to higher mortality and oxidative stress than pressure overload in the LV by aortic constriction. PAB models also produce more elevated hypoxia in the RV after surgery, with less capillary density and ischemia [66].

Furthermore, mechanical stress on the ventricular wall due to pressure overload stimulates fibroblasts to differentiate into myofibroblasts that produce type II and III collagen in the LV and RV, contributing to cardiac failure [67, 68]. However, differences in the distribution of extracellular matrix (ECM) protein and metalloproteinases in the LV and RV may be explained by a further ECM degradation pattern between ventricles [69], which could explain why effective antifibrotic therapies in LV failure are not effective in RV failure [70]. On the other hand, in chronic thromboembolic pulmonary hypertension, to adjust the RV afterload and wall stress, RV pathological remodeling and wall hypertrophy occur [71], and ECM biomarkers, such as matrix metalloproteinases 2 and 9, decrease, while tissue inhibitor of metalloproteinases-1 (TIMP-1) increases significantly [72]. Notably, treatment with a massive pulmonary embolus is applied to relieve the RV afterload (e.g., pulmonary artery endarterectomy, systemic thrombolytics, or percutaneous intervention), resulting in significant regression of pathological remodeling and RV hypertrophy [71].

Studies have shown shared molecular pathways to hypertrophy and fibrosis between the LV and RV, such as TGF-β, Rho-ROCK, and MAPKs. However, differences in signaling have been observed in MAPKs [61, 65]. Phosphorylated p38 (p-p38) MAPK increases in RV fibroblasts and mediates fibrosis induced by TGF-β and ventricular dysfunction; however, hypertrophy and changes in proinflammatory genes are not mediated by p-p38 MAPK [73]. In the LV, the role of p38 MAPK, specifically p38α, has been also described as a mediator of fibrosis and hypertrophy, but conversely, interleukin-6 is involved as a probable pathway to induce hypertrophy [74]. Furthermore, while the apelin receptor (APJ) partici-

pates in hypertrophy induced by pressure overload and apelin prevents hypertrophy in the LV [75–77], the role of APJ in RV has not been elucidated [78].

Difference between RV and LV responses also depends on the stimulus. ROCK signaling mediates hypertrophy induced by metabolic alterations in the LV and by hypoxia in the RV [61], but also, it induces hypertrophy in the LV and RV in pressure overload models, inducing p-ERK1/2 and GATA4 [66, 79]. Studies have demonstrated angiotensin II's role through AT1R in LV hypertrophy due to pressure overload [80–82], whereas an increase in mRNA levels of angiotensin in the monocrotaline (MCT) model has been reported [83]; however, its role in RV has not been fully demonstrated. Angiotensin II is also involved in the induction of autophagy [81]. The role of autophagy in cardiac hypertrophy is controversial; however, basal autophagy would be essential for the preservation of cellular homeostasis, whereas excessive autophagy or its inhibition could aggravate hypertrophy. In different models, such as LV hypertrophy induced by pressure overload or metabolic dysfunction [84, 85] and RV hypertrophy induced by monocrotaline-induced pulmonary arterial hypertension (MCT-PAH) or hypoxia [86, 87], hypertrophy would be mediated by the induction of autophagy, while its inhibition could prevent hypertrophy [85].

On the other hand, activation of proteasome has been observed in LVs exposed to pressure overload, which produces hypertrophy [88], similar to findings obtained in RVs [89]. However, another study performed using the pressure overload model in RVs observed a reduction in proteasome activity [90]; this study was conducted 8-10 days after surgery contrarily to the previous study performed three weeks after surgery [89].

Epigenetic mechanisms have also been identified in cardiac hypertrophy. Class I histone deacetylase inhibitors (HDACs) induce hypertrophy in the LV and RV [91, 92], whereas class IIa HDACs prevent hypertrophy [91, 93]. Unlike findings in the LV [94], inhibitors of HDACs aggravate RV hypertrophy induced by pressure overload [93, 95]. Therefore, further studies are needed to better understand hypertrophy mechanisms in the LV and, mainly, in the RV.

The inflammatory response also plays an essential role in heart failure progression by the activation of proinflammatory cytokines [96]. The increase in inflammatory mediators that can interfere with cardiac contractility and remodeling in PAH correlates to RV dysfunction [97]. While the effects of anti-inflammatory therapies in LV failure are unclear [98, 99], they might be useful in preventing RV failure since perivascular inflammation triggers RV inflammation in a vicious cycle that leads to RV failure [97].

3.3. An Overview of the Similarities and Differences between Right and Left Ventricular Failure.
The increase in LV afterload by an overload of pressure or volume is considered a determining cause of left heart failure (LHF). In contrast, pulmonary hypertension, pulmonary stenosis, chronic obstructive pulmonary disease, and tricuspid valve pathology produce similar consequences on the right side, inducing right heart failure (RHF) [100–102]. RHF could be acute or chronic. Acute RHF is caused by a suddenly increased RV

afterload due to hypoxia or a pulmonary embolus [102, 103] or decreased RV contractility in RV ischemia, myocarditis, or postcardiotomy shock [104]. On the other hand, chronic RHF results from the gradual increases in RV afterload produced by pulmonary hypertension [101, 102], which promotes cardiac remodeling with increased RV mass, fibrosis, and hypertrophy of cardiomyocytes, analogous to the remodeling observed in LHF [105].

As a further example of the interconnection between both ventricles, the prevalence of RV dysfunction increases with LHF progression [106], and RV function and RV–pulmonary artery coupling fail progressively across HF stages [107]. In a community-based cohort study, subclinical RV dysfunction was present in nearly 20% of elderly people and was associated with common HF risk factors. Among people without HF, lower RVEF was associated with HF and death independent of LVEF or N-terminal pro-brain natriuretic peptide (pro-BNP) [107], suggesting that RV dysfunction plays a crucial and underestimated role in HF progression. RV dysfunction was observed in 48% [108] and 33% [109] of heart failure with reduced ejection fraction (HFrEF) and with preserved ejection fraction (HFpEF) patients, respectively, and HFpEF patients displayed greater right-sided chamber enlargement, higher RV diastolic pressure, and more severe contractile dysfunction compared to controls [109].

Furthermore, in patients with LHF, the development of pulmonary hypertension and RV dysfunction is common, and they play an essential role in disease progression, morbidity, and mortality. The diagnosis of pulmonary hypertension aggravates the prognosis in HFpEF and HFrEF patients, and pulmonary hypertension is observed in approximately 75% of patients with HFpEF. Thereby, this prevalence is higher than in patients with HFrEF [100, 110]. In a large community-based prospective cohort of 1,049 subjects with HF, pulmonary hypertension was described as an independent and strong predictor of mortality [110]. Pulmonary hypertension was also defined as a decisive factor in posttransplant mortality because the significantly elevated levels of pulmonary vascular resistance in the postoperative period to which the donor's heart is exposed could trigger RV dysfunction [111].

The requirements of oxygen, glucose absorption, and the glycolytic rate increase in both the LV and RV, reducing fatty acid metabolism [112]. An increased hemodynamic load causes the activation of a pattern of early response or the immediate-early genes c-fos and c-jun, followed by the induction of a "fetal gene program" for the sarcomeric proteins and natriuretic peptides: atrial natriuretic peptide (ANP) and BNP, whose expression is observed also in both ventricles [66, 113].

Mitochondrial dysfunction is an important and crucial mechanism in the development of heart failure [114]. Hypertrophy triggers the Warburg effect in the RV, shifting metabolism from aerobic to anaerobic, showing a decrease in glucose oxidation and increased uncoupled glycolysis and glucose uptake [115], as well as decreasing mitochondrial membrane potential and compromising ATP production [116]. Therefore, protecting mitochondrial function and

metabolism has shown positive results in preserving RV function. On the other hand, glutamine antagonist [117] and sodium-glucose cotransporter 2 (SGLT2) inhibitors [118] positively affect cardiac performance, RV hypertrophy, and survival. Regarding fatty acid oxidation (FAO), the information is controversial since RV function improvement has been observed following FAO inhibition [119] and stimulation [120]. Improvement in mitochondrial fragility and membrane potential by activating SIRT3 through stilbene resveratrol administration improves RV function and decreases fibrosis and hypertrophy [43, 121].

In LV and RV failure, alterations in ECC and relaxation are observed. In the LV, diastolic dysfunction with a slower contraction-relaxation kinetic is produced, as well as loss of T-tubules, reduced SR density, and altered Ca^{2+} release from the SR. These changes were also described in RV failure, where loss of T-tubules, smaller and slower intracellular Ca^{2+} transients, reduction and disorganization of the RyR2 network, and reduction of SERCA have been observed in severe hypertrophy caused by MCT-PAH [62]. However, it has been reported that remodeling of the LV wall, which causes diastolic dysfunction, is compensated by an increase in the contraction-relaxation kinetic in cardiomyocytes [122]. PAH-RV treated with resveratrol significantly improves cell relaxation dynamics by enhancing SERCA activity and maintaining the mitochondrial energy supply [121].

The role of Ca^{2+} signaling has been well demonstrated. Ca^{2+} binds to calmodulin (CaM), which activates calcineurin, a phosphatase that dephosphorylates NFAT in the cytosol, allowing its nuclear translocation to regulate the expression of prohypertrophic genes, such as the β-myosin heavy chain (β-MHC). Additionally, Ca^{2+}/CaM activates Ca^{2+}/CaM kinase II (CaMKII), which induces the nuclear export of histone deacetylase 5 (HDAC5), derepressing the prohypertrophic transcription factor Mef2 [123]. Mef2 has been implicated in the underlying mechanisms that cause a switch from compensated to decompensated hypertrophy in the RV; Mef2 increases in compensated hypertrophy and decreases during decompensation [124]. In the LV, the role of TGF-β and its signaling pathway as a molecular switch has also been reported [65].

4. A Clinical and Experimental Therapeutic Approach to RV Dysfunction

As mentioned previously, patients with PAH develop RV remodeling due to the progressive increase in pulmonary vascular resistance and pulmonary artery pressure, leading to RV failure. Although RV failure is the leading cause of death in PAH patients, most PAH treatments (e.g., prostaglandin analogs, Ca^{2+}-antagonists, endothelin receptor antagonists, and nitric oxide) target vascular abnormalities. Therefore, the amelioration of RV remodeling and dysfunction may represent an essential aspect of PAH therapy, but unfortunately, current therapies do not improve RV function.

Under the experimental therapeutic side, different research groups have focused on observing the effects of PAH treatment directly on RV function, mostly using the *in vivo* induction of PAH by MCT, PAB, or hypoxia. Three

main action mechanisms are identified. The first and most common mechanism is the blocking of surface receptor signaling, in which the compounds tend to act on multiple receptors. Second, the reduction of cytosolic ROS production by trapidil and pterostilbene at different levels of signaling prevents RV remodeling. The third mechanism is the preservation of the metabolic capacity of the cell, where ursolic acid prevents lipotoxicity, while CsA and RES preserve mitochondrial function. Table 2 and Figure 2 summarize the effects of different PAH treatments on RV remodeling and protection. Using recombinant human neuregulin (rhNRG-1), Adão et al. observed attenuation in the increased PLB phosphorylation and decreased mRNA expression of Col1a2, Col3a1, and ACTA1 caused by MCT-PAH in Wistar rats, as well as decreased passive tension in the rats' isolated RV cardiomyocytes [125]. Treatment with rhNGR-1 also decreased the Fulton index scores, the cardiomyocyte cross-sectional area, and fibrosis caused by PAB-induced PAH in Wistar rats [125]. During treatment of PAH caused by MCT in Sprague-Dawley rats, An et al. [126] observed that a maxingxiongting mixture (MXXTM, an effective Chinese medicine compound prescribed for pulmonary hypertension) reduced the protein expression of RhoA and ROCK II, suggesting that it might improve RV hypertrophy by inhibiting the Rho-kinase signaling pathway in the treatment of pulmonary hypertension. Using a hypoxia-induced PAH in vivo model, Dang et al. observed decreased myocardial and RV hypertrophy and collagen deposition, as well as the downregulation of collagen I and III genes and ACE, AngII, and AT1R proteins, when Sprague-Dawley rats were treated with Tsantan Sumtang, a traditional and commonly prescribed Tibetan medicine. Treatment with Tsantan Sumtang attenuated RV remodeling and fibrosis, likely through disruption of the ACE-AngII-AT1R equilibrium in the RV [127].

After treating of PAH caused by an MCT in vivo model with ursolic acid, Gao et al. observed the preservation of RV function and the attenuation of hypertrophy indexes. The expression of Col1a1, Col3a1, TGFβ1, and Bax, as well as fibrosis and apoptosis markers, also decreased [128]. Similarly, when using resveratrol, a phenolic compound with known cardioprotective effects, in an MCT-PAH in vivo model, Vázquez-Garza et al. observed improved RV function measured by tricuspid annular plane systolic excursion (TAPSE) technique and RV free wall thickness and contractility and decreased RV fibrosis and cardiomyocyte area and volume, caused by the low mRNA expression of BNP, Tnnc1, and Col1a1, as well as increased IL-10 and SIRT1 mRNA levels [43]. These mRNA markers were also decreased after using nintedanib to treat PAH in a SU5416+hypoxia in vivo model. Rol et al. observed a decrease in RV hypertrophy and collagen content, accompanied by reduced mRNA levels of Col1a1, BNP, and OPN [129]. Furthermore, Leong et al. observed reduced cardiac remodeling biomarker BNP mRNA levels and serum-NT-pro-BNP levels after treating Wistar-Imamichi rats with imatinib and sunitinib in an MCT-PAH in vivo model [130].

On the other hand, in a PAB in vivo model, Rai et al. observed the preservation of RV function by the attenuation of the increase in RV end-diastolic/systolic volume and colla-

gen content after C57Bl/6J mice were treated with riociguat or sildenafil [131]. These compounds also reduced collagen production and secretion and the phosphorylation of Smad2 and Smad3 proteins when used to treat RV cardiac fibroblast stimulated with TGFβ1 in vitro. Therapy with macitentan also improved RV function and hypertrophy caused by PAB in Wistar-Tokyo rats [132].

In a hypoxia-induced PAH model, Schmuck et al. observed that mesenchymal stem cells had a protective effect on RV function. A reduction in RV hypertrophy was observed, with an attenuated RV stroke volume and cardiac output, maintained RV contractility, reduced RV collagen content, and slowed cardiomyocyte enlargement [133].

Poststress conditions could increase ROS in the RV, a determinant factor in many diseases' progression and severity. Pterostilbene complexed with hydroxypropyl-β-cyclodextrin (HPβCD) to treat PAH induced by MCT in vivo, Lacerda et al. observed an increase in GSH concentrations and GSH/GSSG ratio, accompanied by restored glutathione reductase, glutathione-S-transferase, and glutaredoxin enzyme activity [134]. This treatment also increased the expression of SERCA. Similarly, using trapidil to treat PAH in a MCT in vivo model, Türck et al. observed increased GSH/total glutathione ratio, decreased NADPH oxidase activity, and increased RV SERCA and RyR protein content [135]. The results of these studies suggest that oxidative stress and improving the RV's Ca^{2+} handling mechanisms may represent valuable targets to treat PAH.

As mitochondria play a key role in heart pathophysiology, Lee et al. investigated the effect of cyclosporine A (CsA) in MCT-PAH in vivo [114]. Despite the increase in RV mass, CsA prevented the mitochondrial disruption caused by MCT and attenuated the increases in apoptotic protein Casp3 and Apoptosis-Inducing Factor (AIF) levels. Similarly, Bernal-Ramírez et al. [121] showed that resveratrol treatment in MC-induced PAH rat model avoids mitochondrial permeability and transition pore formation by decreasing cyclophilin D (CypD) hyperacetylation via SIRT3 activation. The combinatorial treatment with macitentan and tadalafil used by Mamazhakypov et al. in Wistar-Kyoto rats with PAH induced by SU5416+hypoxia improved RV function and decreased the expression of hypertrophy A-type natriuretic peptide precursor (NPPA), B-type natriuretic peptide precursor (NPPB), and fibrosis Col1a1 markers [132]. The results of these studies suggest that the use of combinatorial treatments or the addition of an RV-targeted therapy, such as CsA, might be a new therapeutic strategy in the treatment of PAH.

Various clinical trials have been conducted to better understand or more effectively treat PAH. However, most of them managed cardiac improvement secondary to reduced pulmonary artery pressure instead of managing it as a primary objective. Clinical trials aimed at RV function have studied functional and structural improvement by measuring various parameters. Table 3 summarizes the available clinical trial results with measures focused on RV function through RVEF, RV end-diastolic, end-systolic volume (RVEDV and RVESV), mass, longitudinal strain, TAPSE, or Tei index parameters.

Table 2: Treatment of PAH focused on RV remodeling and protection of its function.

Biological subject	Treatment	Experimental model	Effect on RV compared with the model group	Reference
Isolated skinned cardiomyocytes (Wistar rats)	Recombinant human neuregulin-1 (rhNRG-1)	MC-induced PAH	Decreased RV isolated cardiomyocyte passive tension	[125]
Wistar rats	Recombinant human neuregulin-1 (rhNRG-1)	MC-induced PAH	Attenuate the increase of phospholamban phosphorylation Attenuate the upregulated mRNA expression of *Col1a2*, *Col3a1*, and *ACTA1*	[125]
		PAB-induced pressure overload	Decreased Fulton index, cardiomyocyte CSA, and fibrosis	
Sprague-Dawley rats	Maxingxiongting mixture	MC-induced PAH	Attenuate the upregulated protein expression of RhoA and ROCK II	[126]
Sprague-Dawley rats	Tsantan Sumtang	Hx-induced PAH	Decrease RVHI, RV/TL, myocardial hypertrophy, and collagen deposition Downregulate collagen I and III levels and hydroxyproline content Downregulated levels of ACE, AngII, and AT1R proteins	[127]
Sprague-Dawley rats	Ursolic acid	MC-induced PAH	Higher TAPSE and PAT/PET Prevented increase in RVSP Attenuated the increase of RVHI, RV myocardial cell size, and cross-sectional area Attenuated the increased expression of *Col1a1*, *Col3a1*, *TGFβ1*, and *Bax*	[128]
Sprague-Dawley rats	Resveratrol	MC-induced PAH	Improved TAPSE, RV free wall thickness, and contractility Decreased RV fibrosis and cardiomyocyte area and volume Decreased BNP, Tnnc1, and Col1a1 mRNA levels Increased IL-10 and SIRT1 mRNA levels	[43]
Sprague-Dawley rats	Nintedanib	SU5416+Hx-induced PAH	Decreased RV hypertrophy Reduced RV total collagen content Reduced *Col1a1*, *BNP*, and *OPN* mRNA levels	[129]
Wistar-Imamichi rats	Imatinib	MC-induced PAH	Reduced RVH Reduced RV BNP mRNA expression and serum NT-pro-BNP levels	[130]
	Sunitinib		Reduced RVH Reduced RV BNP mRNA expression and serum NT-pro-BNP levels	
C57Bl/6J mice	Riociguat	PAB-induced pressure overload	Attenuated the increase of RV end-diastolic/systolic volume Reduced RV collagen content	[131]
	Sildenafil		Attenuated the increase of RV end-diastolic/systolic volume	
Sprague-Dawley rats	Mesenchymal stem cells	SU5416+Hx-induced PAH	Reduced RV hypertrophy Attenuated the reduction of RV stroke volume and cardiac output Maintained RV contractility Reduced RV collagen content and cardiomyocyte enlargement	[133]

TABLE 2: Continued.

Biological subject	Treatment	Experimental model	Effect on RV compared with the model group	Reference
	Macitentan	SU5416+Hx-induced PAH	Reduced RVSP, TPVR, and RV hypertrophy Increased cardiac output, TAPSE, and RV dilatation Attenuated the increase of NPPA and NPPB expression Attenuated the increase of *Col1a1*	[132]
Wistar-Kyoto rats	Tadalafil		Reduced RVSP, TPVR, and RV hypertrophy Increased cardiac output, TAPSE, and RV dilatation Attenuated the increase of NPPA and NPPB expression Attenuated the increase of *Col1a1*	
	Macitentan+tadalafil		Reduced RVSP, TPVR, and RV hypertrophy Increased cardiac output, TAPSE, and RV dilatation Attenuated the increase of NPPA and NPPB expression Attenuated the increase of *Col1a1* and *Col3a1*	
Wistar rats	Pterostilbene complexed with HPβCD	MC-induced PAH	Increased concentration of GSH and GSH/GSSG ratio Restored the activity of GSR, GST, and GRx Reduced TBARS levels Increased expression of SERCA	[134]
Wistar rats	Trapidil	MC-induced PAH	Increased GSH/total glutathione ratio Decreased NADPH oxidase activity Increased RV SERCA and ryanodine receptor protein content	[135]
Sprague-Dawley rats	Cyclosporine A	MC-induced PAH	Increased RV mass Prevented mitochondrial disruptions Attenuated the increase of Casp3 and AIF protein levels	[114]
Sprague-Dawley rats	17β-Estradiol	MC-induced PAH	Reduced RV diameter, wall thickness, fibrosis, RV/LV+IVS, and RV/BW ratio Improvement of TAPSE, RVFAC, and RIMP Decreased serum BNP levels	[155]

Among the therapeutic compounds studied for PAH treatment at clinical trials are anti-ischemic agents (e.g., trimetazidine and ranolazine), vasodilators (e.g., treprostinil, sildenafil, tadalafil, and riociguat), endothelin receptor antagonists (e.g., ambrisentan, macitentan, and ambrisentan), beta-blockers (e.g., bisoprolol and carvedilol), stem cells (allogeneic human cardiosphere-derived stem cells), and others. Some of these clinical trials report improvements in RVEF at different percentages: 3.9% after three months of trimetazidine treatment (NCT03273387), 10.4% after six months of carvedilol (NCT00964678) oral treatment, 10.14% after six months of macitentan (NCT02310672) oral treatment, 7.65% and 5.8% after six months of ranolazine (NCT02829034, NCT01839110) oral treatments, and 7.54% after six months of treprostinil inhalations combined with oral tadalafil treatment (NCT01305252). Besides, some clinical trials describe changes in TAPSE such as 7% from baseline after three months of anastrozole treatment (NCT01545336), a decrease from 1.88 to 1.79 cm after four months of QCC374 therapy (NCT02927366), and a decrease from 2.2 to 1.65 cm after nine months of tadalafil and ambrisentan combinational treatment (NCT01042158). These

changes reported in RVEF and TAPSE suggest an improvement of the RV function.

Changes in RV volume parameters were also observed in different clinical trials. Treatment with macitentan caused changes in RVSV of 15.17 mL, RVEDV of -6.22 mL, and RVESV of 16.39 mL (NCT02310672); besides, treatment with carvedilol caused a difference of 22.6 mL in RVESV (NCT00964678); these results were observed after six months of treatment with each compound. Along with these changes, improvements in RV mass were reported. Treatment with macitentan for six months caused a reduction of 10.10 g in RV mass (NCT02310672). Similarly, the combinatorial treatment with tadalafil and ambrisentan caused a change in RV mass from 32.5 to 28 g after nine months of treatment (NCT01042158), indicating an improvement in right ventricular remodeling.

As mentioned, most of the conducted clinical trials focus on enhancing cardiac function as a consequence of an improvement in pulmonary artery condition. The clinical trials mentioned here reported improvement in cardiac function with RV function parameters. Unfortunately, these clinical trials aimed at measuring RV function are not primarily
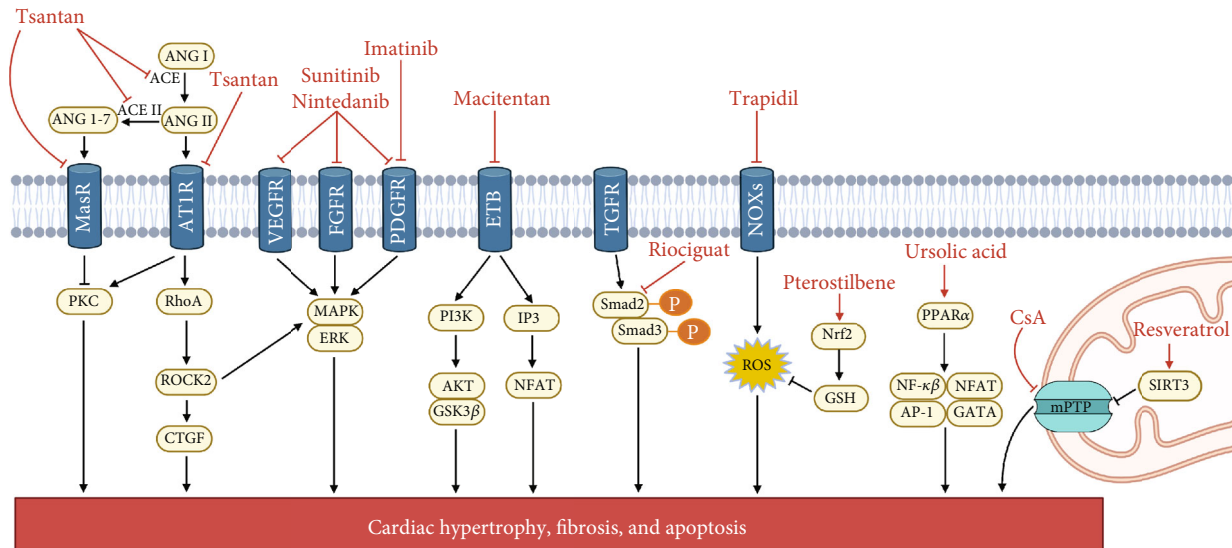
Figure 2: Mechanisms of cardioprotection in *in vivo* therapeutic approaches. Molecules and their effects are shown in red. Lines with arrows indicate activation/stimulation; lines with blunt ends indicate inhibition. Mechanism involved (1) surface receptors blockade: tsantan, sunitinib, nintedanib, imatinib, macitentan, and riociguat; (2) reactive oxygen species inhibition: trapidil and pterostilbene; (3) metabolic capacity preservation: ursolic acid, cyclosporin A (CsA), and resveratrol. ANG: angiotensin; ACE: angiotensin-converting enzyme; MasR: Mas receptor; AT1R: angiotensin II type 1 receptor; VEGFR: vascular endothelial growth factor receptor; FGFR: epidermal growth factor receptor; PDGFR: platelet-derived growth factor receptors; ETB: endothelin receptor type B; TGFR: transforming growth factor receptor; NOXs: nicotinamide adenine dinucleotide phosphate-oxidases; PKC: protein kinase C; ROCK: rho-associated protein kinase; CTGF: connective tissue growth factor; MAPK: mitogen-activated protein kinases; ERK: extracellular signal-regulated kinase; PI3K: phosphatidylinositol 3-kinase; AKT: protein kinase B; GSK3β: glycogen synthase kinase 3 beta; IP3: inositol trisphosphate; NFAT: nuclear factor of activated T cells; ROS: reactive oxygen species; Nrf2: nuclear factor E2-related factor 2; GSH: glutathione; PPARα: peroxisome proliferator-activated receptor alpha; NF-$\kappa\beta$: nuclear factor kappa-light-chain-enhancer of activated B cells; AP-1: activator protein 1; mPTP: mitochondrial permeability and transition pore; SIRT3: sirtuin 3. The figure was created with BioRender.com.

focused on molecular parameters, such as mRNA or protein markers of RV damage, which could be helpful in achieving a better understanding of PAH improvement in humans.

4.1. Biomarkers in Right Ventricular Dysfunction. Although the clinical trials described above focus on evaluating improvement in the functional parameters of the RV after administering treatment, some studies have evaluated molecular parameters that could be taken into account when evaluating the results of these treatments. Although most of these molecular parameters are not exclusive to right ventricular dysfunction, they could be used as a complementary tool in functional evaluations to determine the diagnosis and prognosis of RV dysfunction. For example, myocardial fibrosis is a hallmark of ventricular remodeling and can be detected by assessing myocardial interstitial collagen content. Although endocardial tissue biopsy is the gold standard in the diagnosis of myocardial fibrosis, researchers have proposed assessing a number of circulating biomarkers with serum analysis markers of collage type I and III turnover, such as procollagen type III amino-terminal propeptide (PIIINP), collagen type I carboxy-terminal telopeptide (CITP), and procollagen type I N-terminal propeptide (PINP), which might serve as surrogate estimates in approximating the intensity of fibrosis in the myocardium. PIIINP may also be a good indicator for right ventricular (SRV) remodeling [136, 137]. Furthermore, cartilage intermediate layer protein 1 (CILP1), an extracellular matrix (ECM) pro-

tein involved in profibrotic signaling in the myocardium [138], was recently described as a novel biomarker of RV and LV pathological remodeling in patients with pulmonary hypertension. In one study, maladaptive RV patients had higher CILP1 concentrations than controls and those with LV hypertrophy and dilated cardiac myopathy in [139]. Previously, expression at the RNA level in heart mouse models was shown to be more pronounced in RV pressure overload than in LV pressure overload [140]. Another novel biomarker has been reported; fetal tenascin-C (Tn-C) variants (B+ and C+) are significantly elevated in patients with pulmonary hypertension and can be used to estimate both pulmonary vascular remodeling and RV load in patients with pulmonary hypertension [141]. Furthermore, in an animal model with monocrotaline-induced PAH, Tn-C overexpression has been demonstrated in cardiac tissue [142, 143]. Moreover, it has been reported that elevated serum Interlukin-6 (IL-6) levels in pulmonary hypertension patients are associated with RV dysfunction, regardless of the burden of pulmonary vascular disease. The association between serum IL-6 levels and RV dysfunction may explain the increased mortality in pulmonary hypertension patients with elevated serum IL6 levels, but it is important to clarify that IL6 levels are also related to functional impairment in patients with left ventricular systolic heart failure[144]. BNP and N-terminal pro-BNP are the most commonly used biomarkers in PAH. Both hormones are measurable in plasma and serve as biomarkers of RV dysfunction [145].

TABLE 3: Clinical trials with aim in measuring RV function.

Clinicaltrials.gov identifier	Trial status	Intervention	RV outcome measures	Results
NCT03273387	Completed	Trimetazidine	Changes in RV ejection fraction after 3 months	Improvement of RVEF (3.9%) from baseline
NCT03835676	Recruiting	Treprostinil	Effects on right ventricular structure and function using echocardiography Effects on right ventricular structure and function using cardiac magnetic resonance imaging	No results reported
NCT02253394	Terminated (low enrollment)	Ambrisentan plus spironolactone	Effect on cardiac output	No results reported
NCT04435782	Not yet recruiting	JNJ-67896049	Change from baseline to week 26 in RVSV, RVEDV, RVESV, RVEF, mass, and RVGLS in participants will be assessed by pulmonary artery flow MRI	No results reported
NCT02074449	Completed	Treprostinil	Change in RV coupling index between baseline, titration at 48-72 hours, and 3 months	No results reported
NCT01545336	Completed	Anastrozole	Tricuspid annular plane systolic excursion (TAPSE) from baseline to 3 months	7% change from baseline
NCT02310672	Completed	Macitentan	Change from baseline in RVSV, RVEDV, RVESV, RVEF, and mass to week 26	Change of 15.17 mL of RVSV, -6.22 mL of RVEDV, -16.39 mL of RVESV, 10.14% of RVEF, and -10.10 g to week 26
NCT02169752	Terminated (PI left National Jewish Health)	Ambrisentan	Improvement in RV myocardial strain from baseline to 1, 3, and 6 months	No results reported
NCT03236818	Unknown	ERA and PDE-5I (sildenafil, tadalafil, bosentan, macitentan)	Change in RVEF	No results reported
NCT01083524	Completed	Dichloroacetate sodium	Changes in RV size/function	No results reported
NCT01246037	Unknown	Bisoprolol	Improvement of maladaptive remodeling of the RV wall and diastolic properties of RV	No results reported
NCT00742014	Suspended (absorption of oral sildenafil not consistent)	Sildenafil	Increase in end-systolic elastance of the right ventricle from baseline	No results reported
NCT01148836	Completed	Coenzyme Q-10 Dietary supplement	RV outflow and myocardial performance from baseline to 3 months	RV outflow from 11.3 to 13.5 cm and performance ratio from 0.9 to 0.7
NCT01757808	Completed	Ranolazine	Change in RV echo parameters	No results reported
NCT03617458	Recruiting	Metformin	Change from baseline to week 12 in RV myocardial muscle triglyceride content, TAPSE, RVEF, RV fractional area, RV diastolic function, and RV free wall longitudinal strain	No results reported
NCT04062565	Recruiting	Treprostinil	Change in RV diastolic stiffness	No results reported
NCT02829034	Completed	Ranolazine	Change from baseline in RVEF to 26 weeks	Change of 7.56% from baseline
NCT01839110	Completed	Ranolazine	Changes from baseline in RVEF to 6 months	Change of 5.8% from baseline

TABLE 3: Continued.

Clinicaltrials.gov identifier	Trial status	Intervention	RV outcome measures	Results
NCT02939599	Terminated (study was terminated early for strategic reasons; only part I of the study was completed)	QCC374	Change from baseline in RV Tei index and RV fractional area at week 16	Tei index change of 0.84 and fractional area of 23.91%
NCT02927366	Terminated (study was terminated early for strategic reasons; only part I of the study was completed)	QCC374	Change from baseline in RV fractional area, Tei index, and TAPSE	Change from 20.17 to 20.70% of fractional area, 0.92 to 0.89 of Tei index, and TAPSE from 1.88 to 1.79 cm
NCT00964678	Completed	Carvedilol	Change from baseline in RVEF and RVESV to 6 months	Change in RVEF of 10.4% and RVESV of 22.6 mL
NCT03344159	Suspended (COVID-19 pandemic)	Spironolactone	Change from baseline of RV wall stress, structure, function, and area of fibrosis	No results reported
NCT02507011	Terminated	Carvedilol	Mean change in RVEF	Change in RVEF of 10%
NCT01174173	Completed	Ranolazine	Change from baseline in absolute RV longitudinal strain to 3 months	Change in RV longitudinal strain from -1.4 to 1.0%
NCT02744339	Completed	Riociguat	Change from baseline in RVEF and RV volume to 26 weeks	No results reported
NCT02102672	Unknown	Trimetazidine	Change from baseline in RV function to 3 months	No results reported
NCT03648385	Recruiting	Dehydroepiandrosterone	Chance from baseline in RV longitudinal strain and RVEF to 40 weeks	No results reported
NCT01042158	Completed	Tadalafil and ambrisentan	Change from baseline in RV mass and TAPSE to 36 weeks	Change in RV mass from 32.5 to 28 g and TAPSE from 2.2 to 1.65 cm
NCT03145298	Recruiting	Allogeneic human cardiosphere-derived stem cells	Change in RV ventricular function	No results reported
NCT03362047	Recruiting	Riociguat and macitentan	Change from baseline in RV function and contractility to 12 weeks	No results reported
NCT03449524	Terminated	CXA-10	Change from baseline in RVEF to 6 months	No results reported
NCT01305252	Completed	Treprostinil inhalations and tadalafil	Change from baseline in RVEF to 24 weeks	Change of 7.45% in RVEF
NCT01917136	Completed	11C-acetate and [18F]fluoro-2-deoxy-2-D-glucose	Change from baseline in RVEF to 6 months	Change of 7.56% of RVEF
NCT00772135	Unknown	Sildenafil citrate	Change from baseline in RV pressure	No results reported

However, they are not specific to RV damage and can be elevated in almost all heart diseases [146].

Additionally, cardiac troponin T (cTnT) is used less frequently but has been identified as an independent marker of mortality in patients with PAH [147]; cTnT levels must be correlated with functional and hemodynamic measures [148]. Currently, miRNAs are also important candidate biomarkers. Notwithstanding, most of the upregulated miRNAs in RV failure are similar to those in LV afterload stress. In a murine model of right ventricular hypertrophy (RVH) and right ventricular failure (RVF) using pulmonary artery con-striction, RV-specific miRNAs 34a, 28, 93, and 148a were found; however, none of these are increased in LV hypertrophy and failure induced by transverse aortic constriction [149]. Interestingly, a transcriptomic study of human RVH via RNA expression and network analysis using exclusively freshly isolated myocardium of pediatric patients with tetralogy of Fallot/pulmonary stenosis found that miR-371a and miR-372 are differentially expressed when compared to controls. The authors suggest that these miRNAs are potential biomarkers for diseases associated with RV pressure overload [150]. In a study with 40 patients with RV pressure overload

TABLE 4: Possible therapeutic strategies to address key alterations in RV versus LV dysfunction.

	Possible therapeutic strategies	Ref.
Fibrosis	Current antifibrotic therapies effective in LV do not reverse RV fibrosis, possibly due to differences in ECM composition.	[69, 70, 156–159]
Myocyte contraction	There is improvement of sarcomere function by PKA activators since RV myofilaments have lower Ca^{2+} sensitivity.	[46–48, 160, 161]
Inflammation	RV has more macrophages and dendritic cells, which could mean inflammation plays a more important role.	[162, 163]
Mitochondrial dynamics	PAH presents excessive RV mitochondrial fission, which could indicate significant mitochondrial quality control impairment.	[164–166]
Mitochondrial function	RV has less mitochondrial content and a lower rate of oxidation; thus, the preservation of mitochondrial integrity and membrane potential improves RV function.	[43, 53, 121, 167]

by pulmonary hypertension, it was reported that circulating levels of miR-21, miR-130a, miR-133b, miR-191, miR-204, and miR-208b were higher, while the levels of miR-1, miR26a, miR-29c, miR-34b, miR-451, and miR-1246 were lower in comparison to matched controls. This study also confirmed that a correlation exists between the severity of PAH and circulating levels of miR-133b and miR-208b with [151]. It was also shown that long noncoding RNA H19 is upregulated in decompensated RV from PAH patients and correlates with RV hypertrophy and fibrosis. These findings were corroborated in a rat model of monocrotaline and pulmonary artery banding. The authors propose that H19 is a promising biomarker for the prognosis and severity of RV dysfunction by PAH [152].

Additional research is needed to identify new biomarkers that can further improve diagnostic accuracy. It is important to define standard operating procedures for blood and tissue collection, processing, and storage, as well as miRNA analysis, to ensure precise quantification. Additionally, it is necessary to correlate all emerging biomarkers with right ventricular function for robust validation.

5. Final Thoughts

The ventricles have commonly been studied as individual entities; however, each ventricle must adapt its function to perform its respective role in coordination with each other. Structural differences between ventricles determine their physiological differences in function at the organ level. LV contraction involves radially constricting and longitudinally shortening the septum, while RV contraction is more passive since the RV's free wall lies flat against the septum when LV contracts. The prolonged AP in the LV and the slower contraction velocity in the RV may be a mechanism to coordinate whole-organ contraction. Changes in ECC may compensate for the differences in muscle thickness and ejection pressure to allow ventricles to synchronize at the end of the systole. Furthermore, the discrepancies reported in changes at different stages of the ECC may be due to the heterogeneity within and between ventricles [26, 31, 153]. Physiological differences in the structure, function, and molecular adaptations of the LV and RV result in different responses to stressful stimuli. While LV thickness helps to support higher pressures, a thin RV wall is highly susceptible to increases in

vascular resistance. A better understanding of the differences in cellular and molecular alterations in the LV and RV due to remodeling and failure may facilitate the development of more effective therapeutic approaches. This understanding is especially important for the RV, given that the mechanisms related to its dysfunction are not as widely studied as those related to LV's dysfunction.

Advances in RV dysfunction diagnostics and therapeutics are needed to improve the early detection of the disease and improve prognosis. The determination and validation of new, less-invasive, and more accurate biomarkers is an important research area that has been strengthened by the description of ventricle differences in dysfunction. Additionally, the search for new therapeutic approaches that target RV has been fueled by the variation in response between the two ventricles. Some diverse therapeutic strategies could be beneficial in improving current treatments (Table 4), but they require further investigation to estimate their contribution to patient morbidity and mortality.

Data Availability

The data used to support the findings of this study are available from the corresponding authors upon request.

Conflicts of Interest

No conflicts of interest, financial or otherwise, are declared by the authors.

Authors' Contributions

Judith Bernal-Ramirez and Magda C. Díaz-Vesga contribute equally to this work.

Acknowledgments

References

[1] D. Santos-Ribeiro, P. Mendes-Ferreira, C. Maia-Rocha, R. Adão, A. F. Leite-Moreira, and C. Brás-Silva, "Hypertension arterielle pulmonaire : connaissances de base pour les cliniciens," *Archives of Cardiovascular Diseases*, vol. 109, no. 10, pp. 550–561, 2016.

[2] F. S. de Man, M. L. Handoko, and A. Vonk-Noordegraaf, "The unknown pathophysiological relevance of right ventricular hypertrophy in pulmonary arterial hypertension," *European Respiratory Journal*, vol. 53, article 1900255, no. 4, 2019.

[3] N. Galiè, R. N. Channick, R. P. Frantz et al., "Risk stratification and medical therapy of pulmonary arterial hypertension," *European Respiratory Journal*, vol. 53, no. 1, article 1801889, 2019.

[4] A. Hemnes, A. M. K. Rothman, A. J. Swift, and L. S. Zisman, "role of biomarkers in evaluation, treatment and clinical studies of pulmonary arterial hypertension," *Pulmonary Circulation*, vol. 10, no. 4, 2020.

[5] R. L. Benza, D. P. Miller, M. Gomberg-Maitland et al., "Predicting survival in pulmonary arterial hypertension: insights from the Registry to Evaluate Early and Long-Term Pulmonary Arterial Hypertension Disease Management (REVEAL)," *Circulation*, vol. 122, no. 2, pp. 164–172, 2010.

[6] J. A. Mazurek, A. Vaidya, S. C. Mathai, J. D. Roberts, and P. R. Forfia, "Follow-up tricuspid annular plane systolic excursion predicts survival in pulmonary arterial hypertension," *Pulmonary circulation*, vol. 7, no. 2, pp. 361–371, 2017.

[7] A. Huertas, L. Tu, M. Humbert, and C. Guignabert, "Chronic inflammation within the vascular wall in pulmonary arterial hypertension: more than a spectator," *Cardiovascular Research*, vol. 116, no. 5, pp. 885–893, 2020.

[8] C. W. Yancy, M. Jessup, B. Bozkurt et al., "2016 ACC/AHA/HFSA Focused Update on New Pharmacological Therapy for Heart Failure: An Update of the 2013 ACCF/AHA Guideline for the Management of Heart Failure: A Report of the American College of Cardiology/American Heart Association Task Force on Clinical Practice Guidelines and the Heart Failure Society of America," *Journal of cardiac failure*, vol. 22, no. 9, pp. 659–669, 2016.

[9] M. A. Simon, "Assessment and treatment of right ventricular failure," *Nature Reviews. Cardiology*, vol. 10, no. 4, pp. 204–218, 2013.

[10] F. Haddad, S. A. Hunt, D. N. Rosenthal, and D. J. Murphy, "Right ventricular function in cardiovascular disease, part I: anatomy, physiology, aging, and functional assessment of the right ventricle," *Circulation*, vol. 117, no. 11, pp. 1436–1448, 2008.

[11] D. J. Penny and A. N. Redington, "Function of the left and right ventricles and the interactions between them," *Pediatric Critical Care Medicine*, vol. 17, 8 Supplement 1, pp. S112–S118, 2016.

[12] J. Sanz, D. Sánchez-Quintana, E. Bossone, H. J. Bogaard, and R. Naeije, "Anatomy, Function, and Dysfunction of the Right Ventricle;," *Journal of the American College of Cardiology*, vol. 73, no. 12, pp. 1463–1482, 2019.

[13] P. Delgado-Olguin, "Embryological origins: how does the right ventricle form," in *Right Ventricular Physiology, Adaptation and Failure in Congenital and Acquired Heart Disease*, pp. 1–17, Springer, 2018.

[14] F. Radu-Ioniţă, E. Bontaş, V. Goleanu et al., "Heart embryology: overview," in *Right Heart Pathology*, pp. 3–24, Springer, 2018.

[15] G. Buckberg and J. I. E. Hoffman, "Right ventricular architecture responsible for mechanical performance: unifying role of ventricular septum," *The Journal of Thoracic and Cardiovascular Surgery*, vol. 148, no. 6, pp. 3166–3171.e4, 2014.

[16] D. H. MacIver, "The relative impact of circumferential and longitudinal shortening on left ventricular ejection fraction and stroke volume," *Experimental and Clinical Cardiology*, vol. 17, no. 1, pp. 5–11, 2012.

[17] D. Oken and R. Boucek, "Quantitation of collagen in human myocardium," *Circulation Research*, vol. 5, no. 4, pp. 357–361, 1957.

[18] D. Sidebotham, "Pulmonary Hypertension," in *Cardiothoracic Critical Care*, D. Sidebotham, A. Mckee, M. Gillham, and L. JHBT-CCC, Eds., pp. 374–382, Elsevier, 2007.

[19] G. J. Crystal and P. S. Pagel, "Right ventricular perfusion: physiology and clinical implications," *Anesthesiology*, vol. 128, no. 1, pp. 202–218, 2018.

[20] K. M. Chin, N. H. S. Kim, and L. J. Rubin, "The right ventricle in pulmonary hypertension," *Coronary Artery Disease*, vol. 16, no. 1, pp. 13–18, 2005.

[21] J. C. Matthews and V. McLaughlin, "Acute right ventricular failure in the setting of acute pulmonary embolism or chronic pulmonary hypertension: a detailed review of the pathophysiology, diagnosis, and management," *Current Cardiology Reviews*, vol. 4, no. 1, pp. 49–59, 2008.

[22] F. Haddad, R. Doyle, D. J. Murphy, and S. A. Hunt, "Right ventricular function in cardiovascular disease, part II: pathophysiology, clinical importance, and management of right ventricular failure," *Circulation*, vol. 117, no. 13, pp. 1717–1731, 2008.

[23] J. M. Cordeiro, K. Calloe, R. Aschar-Sobbi et al., "Physiological roles of the transient outward current i I i sub to sub in normal and diseased hearts," *Frontiers in Bioscience*, vol. 8, no. 1, pp. 143–159, 2016.

[24] D. M. Bers, "Cardiac excitation-contraction coupling," *Nature*, vol. 415, no. 6868, pp. 198–205, 2002.

[25] E. Fernández-Sada, C. Silva-Platas, C. A. Villegas et al., "Cardiac responses to β-adrenoceptor stimulation is partly dependent on mitochondrial calcium uniporter activity," *British Journal of Pharmacology*, vol. 171, no. 18, pp. 4207–4221, 2014.

[26] K. Calloe, G. L. Aistrup, J. M. Di Diego, R. J. Goodrow, J. A. Treat, and J. M. Cordeiro, "Interventricular differences in sodium current and its potential role in Brugada syndrome," *Physiological reports*, vol. 6, no. 14, article e13787, 2018.

[27] J. J. Kim, J. Nemec, R. Papp, R. Strongin, J. J. Abramson, and G. Salama, "Bradycardia alters Ca(2+) dynamics enhancing dispersion of repolarization and arrhythmia risk," *American Journal of Physiology. Heart and Circulatory Physiology*, vol. 304, no. 6, pp. H848–H860, 2013.

[28] J. M. Di Diego, Z. Q. Sun, and C. Antzelevitch, "I(to) and action potential notch are smaller in left vs. right canine ventricular epicardium," *The American Journal of Physiology*, vol. 271, no. 2, pp. H548–H561, 1996.

[29] R. P. Kondo, D. A. Dederko, C. Teutsch et al., "Comparison of contraction and calcium handling between right and left ventricular myocytes from adult mouse heart: a role for repolarization waveform," *The Journal of Physiology*, vol. 571, no. 1, pp. 131–146, 2006.

[30] O. Casis, M. Iriarte, M. Gallego, and J. A. Sanchez-Chapula, "Differences in regional distribution of K$^+$ current densities in rat ventricle," *Life Sciences*, vol. 63, no. 5, pp. 391–400, 1998.

[31] S. Brunet, F. Aimond, H. Li et al., "Heterogeneous expression of repolarizing, voltage-gated K+ currents in adult mouse ventricles," *The Journal of Physiology*, vol. 559, no. 1, pp. 103–120, 2004.

[32] P. G. Volders, K. R. Sipido, E. Carmeliet, R. L. H. M. G. Spätjens, H. J. Wellens, and M. A. Vos, "Repolarizing K+ currents ITO1 and IKs are larger in right than left canine ventricular midmyocardium," *Circulation*, vol. 99, no. 2, pp. 206–210, 1999.

[33] Y. Tsuji, S. Zicha, X.-Y. Qi, I. Kodama, and S. Nattel, "Potassium channel subunit remodeling in rabbits exposed to longterm bradycardia or Tachycardia," *Circulation*, vol. 113, no. 3, pp. 345–355, 2006.

[34] T. Watanabe, L. M. Delbridge, J. O. Bustamante, and T. F. McDonald, "Heterogeneity of the action potential in isolated rat ventricular myocytes and tissue," *Circulation Research*, vol. 52, no. 3, pp. 280–290, 1983.

[35] A. Bueno-Orovio, B. M. Hanson, J. S. Gill, P. Taggart, and B. Rodriguez, "In vivo human left-to-right ventricular differences in rate adaptation transiently increase pro-arrhythmic risk following rate acceleration," *PLoS One*, vol. 7, no. 12, article e52234, 2012.

[36] J. Švíglerová, J. Kuncová, L. Nalos et al., "Cardiac remodeling in rats with renal failure shows interventricular differences," *Experimental Biology and Medicine (Maywood, N.J.)*, vol. 237, no. 9, pp. 1056–1067, 2012.

[37] C. Ramanathan, P. Jia, R. Ghanem, K. Ryu, and Y. Rudy, "Activation and repolarization of the normal human heart under complete physiological conditions," *Proceedings of the National Academy of Sciences of the United States of America*, vol. 103, no. 16, pp. 6309–6314, 2006.

[38] S. V. Pandit, K. Kaur, S. Zlochiver et al., "Left-to-right ventricular differences in I$_{KATP}$ underlie epicardial repolarization gradient during global ischemia," *Heart rhythm*, vol. 8, no. 11, pp. 1732–1739, 2011.

[39] V. Ramesh, M. J. Kresch, A. M. Katz, and D. H. Kim, "Characterization of Ca(2+)-release channels in fetal and adult rat hearts," *The American Journal of Physiology*, vol. 269, no. 3, pp. H778–H782, 1995.

[40] K. M. Meurs, V. A. Lacombe, K. Dryburgh, P. R. Fox, P. R. Reiser, and M. D. Kittleson, "Differential expression of the cardiac ryanodine receptor in normal and arrhythmogenic right ventricular cardiomyopathy canine hearts," *Human Genetics*, vol. 120, no. 1, pp. 111–118, 2006.

[41] V. Sathish, A. Xu, M. Karmazyn, S. M. Sims, and N. Narayanan, "Mechanistic basis of differences in Ca2+ -handling properties of sarcoplasmic reticulum in right and left ventricles of normal rat myocardium," *American Journal of Physiology. Heart and Circulatory Physiology*, vol. 291, no. 1, pp. H88–H96, 2006.

[42] J. Sabourin, A. Boet, C. Rucker-Martin et al., "Ca^{2+} handling remodeling and STIM1L/Orai1/TRPC1/TRPC4 upregulation in monocrotaline-induced right ventricular hypertrophy," *Journal of Molecular and Cellular Cardiology*, vol. 118, pp. 208–224, 2018.

[43] E. Vázquez-Garza, J. Bernal-Ramírez, C. Jerjes-Sánchez et al., "Resveratrol prevents right ventricle remodeling and dysfunction in monocrotaline-induced pulmonary arterial hypertension with a limited improvement in the lung vasculature," *Oxidative medicine and cellular longevity*, vol. 2020, Article ID 1841527, 13 pages, 2020.

[44] J. Nagwekar, D. Duggal, R. Rich et al., "The spatial distribution of actin and mechanical cycle of myosin are different in right and left ventricles of healthy mouse hearts," *Biochemistry*, vol. 53, no. 48, pp. 7641–7649, 2014.

[45] J. Nagwekar, D. Duggal, R. Rich et al., "Differences in the spatial distribution of actin in the left and right ventricles of functioning rabbit hearts," *Medical Photonics*, vol. 27, pp. 1–8, 2018.

[46] J. Liang, K. Kazmierczak, A. I. Rojas, Y. Wang, and D. Szczesna-Cordary, "The R21C mutation in cardiac troponin I imposes differences in contractile force generation between the left and right ventricles of knock-in mice," *BioMed Research International*, vol. 2015, Article ID 742536, 9 pages, 2015.

[47] C. L. Perreault, O. H. Bing, W. W. Brooks, B. J. Ransil, and J. P. Morgan, "Differential effects of cardiac hypertrophy and failure on right versus left ventricular calcium activation," *Circulation Research*, vol. 67, no. 3, pp. 707–712, 1990.

[48] R. J. Belin, M. P. Sumandea, G. A. Sievert et al., "Interventricular differences in myofilament function in experimental congestive heart failure," *Pflügers Archiv*, vol. 462, no. 6, pp. 795–809, 2011.

[49] W. Brooks, O. Bing, A. Blaustein, and P. Allen, "Comparison of contractile state and myosin isozymes of rat right and left ventricular myocardium," *Journal of Molecular and Cellular Cardiology*, vol. 19, no. 5, pp. 433–440, 1987.

[50] H. Krug, K. Punkt, and L. Bittorf, "The higher myosin ATPase activity in the right heart ventricle of the rat, proved by histophotometry," *Acta Histochemica*, vol. 82, no. 1, pp. 115–119, 1987.

[51] R. A. Bassani, J. W. Bassani, and D. M. Bers, "Relaxation in ferret ventricular myocytes: unusual interplay among calcium transport systems," *The Journal of Physiology*, vol. 476, no. 2, pp. 295–308, 1994.

[52] V. G. Sharov, A. Goussev, M. Lesch, S. Goldstein, and H. N. Sabbah, "Abnormal mitochondrial function in myocardium of dogs with chronic heart failure," *Journal of Molecular and Cellular Cardiology*, vol. 30, no. 9, pp. 1757–1762, 1998.

[53] R. Nogueira-Ferreira, R. Ferreira, A. I. Padrão et al., "One year of exercise training promotes distinct adaptations in right and left ventricle of female Sprague-Dawley rats," *Journal of Physiology and Biochemistry*, vol. 75, no. 4, pp. 561–572, 2019.

[54] S. Singh, F. C. White, and C. M. Bloor, "Myocardial morphometric characteristics in swine," *Circulation Research*, vol. 49, no. 2, pp. 434–441, 1981.

[55] I. Starr, W. A. Jeffers, and R. H. Meade Jr., "The absence of conspicuous increments of venous pressure after severe damage to the right ventricle of the dog, with a discussion of the relation between clinical congestive failure and heart disease," *American Heart Journal*, vol. 26, no. 3, pp. 291–301, 1943.

[56] N. H. Guiha, C. J. Limas, and J. N. Cohn, "Predominant right ventricular dysfunction after right ventricular destruction in the dog," *The American Journal of Cardiology*, vol. 33, no. 2, pp. 254–258, 1974.

[57] J. M. Isner and W. C. Roberts, "Right ventricular infarction complicating left ventricular infarction secondary to coronary heart disease: Frequency, location, associated findings and significance from analysis of 236 necropsy patients with acute or healed myocardial infarction," *The American Journal of Cardiology*, vol. 42, no. 6, pp. 885–894, 1978.

[58] S. Turkoglu, M. Erden, and M. Ozdemir, "Un infarctus ventriculaire droit isole cause par une occlusion de la branche ventriculaire droite en l'absence d'intervention coronaire percutanee," *The Canadian Journal of Cardiology*, vol. 24, no. 10, pp. 793-794, 2008.

[59] T. Levin and J. A. Goldstein, "Right ventricular myocardial infarction - UpToDate," https://www.uptodate.com/contents/right-ventricular-myocardial-infarction/.

[60] G. A. Heresi, W. H. W. Tang, M. Aytekin, J. Hammel, S. L. Hazen, and R. A. Dweik, "Sensitive cardiac troponin I predicts poor outcomes in pulmonary arterial hypertension," *The European Respiratory Journal*, vol. 39, no. 4, pp. 939–944, 2012.

[61] C. P. Anaruma, R. M. Pereira, K. Cristina da Cruz Rodrigues et al., "Rock protein as cardiac hypertrophy modulator in obesity and physical exercise," *Life sciences*, vol. 254, article 116955, 2020.

[62] F. Antigny, O. Mercier, M. Humbert, and J. Sabourin, "Alteration du couplage excitation-contraction et relaxation dans le remodelage ventriculaire droit due a une hypertension arterielle pulmonaire," *Archives of Cardiovascular Diseases*, vol. 113, no. 1, pp. 70–84, 2020.

[63] I. Friehs, D. B. Cowan, Y.-H. Choi et al., "Pressure-overload hypertrophy of the developing heart reveals activation of divergent gene and protein pathways in the left and right ventricular myocardium," *American Journal of Physiology. Heart and Circulatory Physiology*, vol. 304, no. 5, pp. H697–H708, 2013.

[64] R. Schreckenberg, M. Rebelo, A. Deten et al., "Specific mechanisms underlying right heart failure: the missing upregulation of superoxide dismutase-2 and its decisive role in antioxidative defense," *Antioxidants & Redox Signaling*, vol. 23, no. 15, pp. 1220–1232, 2015.

[65] J. Heger, R. Schulz, and G. Euler, "Molecular switches under TGFβ signalling during progression from cardiac hypertrophy to heart failure," *British Journal of Pharmacology*, vol. 173, no. 1, pp. 3–14, 2016.

[66] S. Ikeda, K. Satoh, N. Kikuchi et al., "Crucial role of rho-kinase in pressure overload-induced right ventricular hypertrophy and dysfunction in mice," *Arteriosclerosis, Thrombosis, and Vascular Biology*, vol. 34, no. 6, pp. 1260–1271, 2014.

[67] S. Minegishi, K. Kitahori, A. Murakami, and M. Ono, "Mechanism of pressure-overload right ventricular hypertrophy in infant rabbits," *International Heart Journal*, vol. 52, no. 1, pp. 56–60, 2011.

[68] M. Yildiz, A. A. Oktay, M. H. Stewart, R. V. Milani, H. O. Ventura, and C. J. Lavie, "Left ventricular hypertrophy and hypertension," *Progress in Cardiovascular Diseases*, vol. 63, no. 1, pp. 10–21, 2020.

[69] E. Herpel, S. Singer, C. Flechtenmacher et al., "Extracellular matrix proteins and matrix metalloproteinases differ between various right and left ventricular sites in end-stage cardiomyopathies," *Virchows Archiv*, vol. 446, no. 4, article 1177, pp. 369–378, 2005.

[70] S. Andersen, J. Birkmose Axelsen, S. Ringgaard et al., "Pressure overload induced right ventricular remodeling is not attenuated by the anti-fibrotic agent pirfenidone," *Pulmonary circulation*, vol. 9, no. 2, 2019.

[71] Y. C. Bryce, R. Perez-Johnston, E. B. Bryce, B. Homayoon, and E. G. Santos-Martin, "Pathophysiology of right ventricular failure in acute pulmonary embolism and chronic thromboembolic pulmonary hypertension: a pictorial essay for the interventional radiologist," *Insights Into Imaging*, vol. 10, no. 1, p. 18, 2019.

[72] W. Pang, Z. Zhang, Y. Zhang et al., "Extracellular matrix collagen biomarkers levels in patients with chronic thromboembolic pulmonary hypertension," *Journal of Thrombosis and Thrombolysis*, vol. 52, no. 1, pp. 48–58, 2021.

[73] B. Kojonazarov, T. Novoyatleva, M. Boehm et al., "p38 MAPK inhibition improves heart function in pressure-loaded right ventricular hypertrophy," *American Journal of Respiratory Cell and Molecular Biology*, vol. 57, no. 5, pp. 603–614, 2017.

[74] S. A. Bageghni, K. E. Hemmings, N. Zava et al., "Cardiac fibroblast-specific p38α MAP kinase promotes cardiac hypertrophy via a putative paracrine interleukin-6 signaling mechanism," *The FASEB Journal*, vol. 32, no. 9, pp. 4941–4954, 2018.

[75] L. Lu, D. Wu, L. Li, and L. Chen, "Apelin/APJ system: a bifunctional target for cardiac hypertrophy," *International Journal of Cardiology*, vol. 230, pp. 164–170, 2017.

[76] D. Wu, F. Xie, L. Xiao et al., "Caveolin-1-autophagy pathway mediated cardiomyocyte hypertrophy induced by apelin-13," *DNA and Cell Biology*, vol. 36, no. 8, pp. 611–618, 2017.

[77] V. N. Parikh, J. Liu, C. Shang et al., "Apelin and APJ orchestrate complex tissue-specific control of cardiomyocyte hypertrophy and contractility in the hypertrophy-heart failure transition," *American Journal of Physiology. Heart and Circulatory Physiology*, vol. 315, no. 2, pp. H348–H356, 2018.

[78] I. Falcão-Pires, N. Gonçalves, T. Henriques-Coelho, D. Moreira-Gonçalves, R. J. Roncon-Albuquerque, and A. F. Leite-Moreira, "Apelin decreases myocardial injury and improves right ventricular function in monocrotaline-induced pulmonary hypertension," *American Journal of Physiology. Heart and Circulatory Physiology*, vol. 296, no. 6, pp. H2007–H2014, 2009.

[79] Y. Olgar, M. C. Celen, B. E. Yamasan, N. Ozturk, B. Turan, and S. Ozdemir, "Rho-kinase inhibition reverses impaired Ca^{2+} handling and associated left ventricular dysfunction in pressure overload-induced cardiac hypertrophy," *Cell Calcium*, vol. 67, pp. 81–90, 2017.

[80] B. R. Cowan and A. A. Young, "Left ventricular hypertrophy and renin-angiotensin system blockade," *Current Hypertension Reports*, vol. 11, no. 3, pp. 167–172, 2009.

[81] L. Zhou, B. Ma, and X. Han, "The role of autophagy in angiotensin II-induced pathological cardiac hypertrophy," *Journal of Molecular Endocrinology*, vol. 57, no. 4, pp. R143–R152, 2016.

[82] S. Gallo, A. Vitacolonna, A. Bonzano, P. Comoglio, and T. Crepaldi, "ERK: a key player in the pathophysiology of cardiac hypertrophy," *International journal of molecular sciences*, vol. 20, no. 9, p. 2164, 2019.

[83] H. K. Park, S. J. Park, C. S. Kim, Y. W. Paek, J. U. Lee, and W. J. Lee, "Enhanced gene expression of renin-angiotensin system, TGF-beta1, endothelin-1 and nitric oxide synthase in right-ventricular hypertrophy," *Pharmacological Research*, vol. 43, no. 3, pp. 265–273, 2001.

[84] I.-P. Chou, Y.-P. Chiu, S.-T. Ding, B.-H. Liu, Y. Y. Lin, and C.-Y. Chen, "Adiponectin receptor 1 overexpression reduces lipid accumulation and hypertrophy in the heart of diet-induced obese mice–possible involvement of oxidative stress and autophagy," *Endocrine Research*, vol. 39, no. 4, pp. 173–179, 2014.

[85] L. Weng, W. Zhang, Y. Ye et al., "Aliskiren ameliorates pressure overload-induced heart hypertrophy and fibrosis in mice," *Acta Pharmacologica Sinica*, vol. 35, no. 8, pp. 1005–1014, 2014.

[86] L. Long, X. Yang, M. Southwood et al., "Chloroquine prevents progression of experimental pulmonary hypertension via inhibition of autophagy and lysosomal bone morphogenetic protein type II receptor degradation," *Circulation Research*, vol. 112, no. 8, pp. 1159–1170, 2013.

[87] D. K. Rawat, A. Alzoubi, R. Gupte et al., "Increased reactive oxygen species, metabolic maladaptation, and autophagy contribute to pulmonary arterial hypertension-induced ventricular hypertrophy and diastolic heart failure," *Hypertens (Dallas, Tex 1979)*, vol. 64, no. 6, pp. 1266–1274, 2014.

[88] F. Cacciapuoti, "Role of ubiquitin-proteasome system (UPS) in left ventricular hypertrophy (LVH)," *American journal of cardiovascular disease*, vol. 4, no. 1, pp. 1–5, 2014.

[89] T. Heitmeier, A. Sydykov, C. Lukas et al., "Altered proteasome function in right ventricular hypertrophy," *Cardiovascular Research*, vol. 116, no. 2, pp. 406–415, 2020.

[90] V. Rajagopalan, M. Zhao, S. Reddy et al., "Altered ubiquitin-proteasome signaling in right ventricular hypertrophy and failure," *American Journal of Physiology. Heart and Circulatory Physiology*, vol. 305, no. 4, pp. H551–H562, 2013.

[91] R. Kerkela and T. Force, "Recent insights into cardiac hypertrophy and left ventricular remodeling," *Current Heart Failure Reports*, vol. 3, no. 1, pp. 14–18, 2006.

[92] B. S. Ferguson, B. C. Harrison, M. Y. Jeong et al., "Signal-dependent repression of DUSP5 by class I HDACs controls nuclear ERK activity and cardiomyocyte hypertrophy," *Proceedings of the National Academy of Sciences of the United States of America*, vol. 110, no. 24, pp. 9806–9811, 2013.

[93] P. Chelladurai, O. Boucherat, K. Stenmark et al., "Targeting histone acetylation in pulmonary hypertension and right ventricular hypertrophy," *British Journal of Pharmacology*, vol. 178, no. 1, pp. 54–71, 2021.

[94] J. Y. Y. Ooi, N. K. Tuano, H. Rafehi et al., "HDAC inhibition attenuates cardiac hypertrophy by acetylation and deacetylation of target genes," *Epigenetics*, vol. 10, no. 5, pp. 418–430, 2015.

[95] H. J. Bogaard, S. Mizuno, A. A. Hussaini et al., "Suppression of histone deacetylases worsens right ventricular dysfunction after pulmonary artery banding in rats," *American Journal of Respiratory and Critical Care Medicine*, vol. 183, no. 10, pp. 1402–1410, 2011.

[96] Y. Seta, K. Shan, B. Bozkurt, H. Oral, and D. L. Mann, "Basic mechanisms in heart failure: the cytokine hypothesis," *Journal of Cardiac Failure*, vol. 2, no. 3, pp. 243–249, 1996.

[97] X.-Q. Sun, A. Abbate, and H.-J. Bogaard, "Role of cardiac inflammation in right ventricular failure," *Cardiovascular Research*, vol. 113, no. 12, pp. 1441–1452, 2017.

[98] E. S. Chung, M. Packer, K. H. Lo, A. A. Fasanmade, J. T. Willerson, and Anti-TNF Therapy Against Congestive Heart Failure Investigators, "Randomized, double-blind, placebo-controlled, pilot trial of infliximab, a chimeric monoclonal antibody to tumor necrosis factor-α, in patients with moderate-to-severe heart failure," *Circulation*, vol. 107, no. 25, pp. 3133–3140, 2003.

[99] B. W. van Tassell, N. A. Abouzaki, C. Oddi Erdle et al., "Interleukin-1 blockade in acute decompensated heart failure: a randomized, double-blinded, placebo-controlled pilot study," *Journal of Cardiovascular Pharmacology*, vol. 67, no. 6, pp. 544–551, 2016.

[100] C. S. P. Lam, V. L. Roger, R. J. Rodeheffer, B. A. Borlaug, F. T. Enders, and M. M. Redfield, "Pulmonary hypertension in heart failure with preserved ejection fraction: a community-based study," *Journal of the American College of Cardiology*, vol. 53, no. 13, pp. 1119–1126, 2009.

[101] M. Guazzi and R. Naeije, "Pulmonary hypertension in heart failure: pathophysiology, pathobiology, and emerging clinical perspectives," *Journal of the American College of Cardiology*, vol. 69, no. 13, pp. 1718–1734, 2017.

[102] A. Kemdem, F. Lemaitre, R. Lovat, V. Siraux, P. Dillien, and F. Dive, "Acute hypoxic pulmonary hypertension associated with right heart failure," *Acta Cardiologica*, vol. 75, no. 6, pp. 544–548, 2020.

[103] C. E. Ventetuolo and J. R. Klinger, "Management of acute right ventricular failure in the intensive care unit," *Annals of the American Thoracic Society*, vol. 11, no. 5, pp. 811–822, 2014.

[104] S. Ghio, C. Raineri, L. Scelsi, M. Ašanin, M. Polovina, and P. Seferovic, "Pulmonary hypertension and right ventricular remodeling in HFpEF and HFrEF," *Heart Failure Reviews*, vol. 25, no. 1, pp. 85–91, 2020.

[105] J. J. Ryan, J. Huston, S. Kutty et al., "Right ventricular adaptation and failure in pulmonary arterial hypertension," *The Canadian Journal of Cardiology*, vol. 31, no. 4, pp. 391–406, 2015.

[106] S. Rosenkranz, J. S. R. Gibbs, R. Wachter, T. de Marco, A. Vonk-Noordegraaf, and J.-L. Vachiéry, "Left ventricular heart failure and pulmonary hypertension," *European Heart Journal*, vol. 37, no. 12, pp. 942–954, 2016.

[107] K. Nochioka, G. Querejeta Roca, B. Claggett et al., "Right ventricular function, right ventricular-pulmonary artery coupling, and heart failure risk in 4 US communities: the atherosclerosis risk in communities (ARIC) study," *JAMA Cardiology*, vol. 3, no. 10, pp. 939–948, 2018.

[108] I. Iglesias-Garriz, C. Olalla-Gómez, C. Garrote et al., "Contribution of right ventricular dysfunction to heart failure mortality: a meta-analysis," *Reviews in Cardiovascular Medicine*, vol. 13, no. 2-3, pp. e62–e69, 2012.

[109] V. Melenovsky, S.-J. Hwang, G. Lin, M. M. Redfield, and B. A. Borlaug, "Right heart dysfunction in heart failure with preserved ejection fraction," *European Heart Journal*, vol. 35, no. 48, pp. 3452–3462, 2014.

[110] F. Bursi, S. M. McNallan, M. M. Redfield et al., "Pulmonary pressures and death in heart failure: a community study," *Journal of the American College of Cardiology*, vol. 59, no. 3, pp. 222–231, 2012.

[111] M. A. Konstam, M. S. Kiernan, D. Bernstein et al., "Evaluation and management of right-sided heart failure: a scientific statement from the American Heart Association," *Circulation*, vol. 137, no. 20, pp. e578–e622, 2018.

[112] S. E. Altin and P. C. Schulze, "Metabolism of the right ventricle and the response to hypertrophy and failure," *Progress in Cardiovascular Diseases*, vol. 55, no. 2, pp. 229–233, 2012.

[113] N. Saadane, L. Alpert, and L. E. Chalifour, "Expression of immediate early genes, GATA-4, and Nkx-2.5 in adrenergic-induced cardiac hypertrophy and during regression in adult mice," *British Journal of Pharmacology*, vol. 127, no. 5, pp. 1165–1176, 1999.

[114] D. S. Lee and Y. W. Jung, "Protective effect of right ventricular mitochondrial damage by cyclosporine a in monocrotaline-induced pulmonary hypertension," *Korean circulation journal*, vol. 48, no. 12, pp. 1135–1144, 2018.

[115] J. J. Ryan and S. L. Archer, "The right ventricle in pulmonary arterial hypertension: disorders of metabolism, angiogenesis and adrenergic signaling in right ventricular failure," *Circulation Research*, vol. 115, no. 1, pp. 176–188, 2014.

[116] T. A. Karim, N. T. Boardman, and M. C. Sanchez, "Mitochondrial respiratory states and rates," 2019.

[117] L. Piao, Y.-H. Fang, K. Parikh, J. J. Ryan, P. T. Toth, and S. L. Archer, "Cardiac glutaminolysis: a maladaptive cancer metabolism pathway in the right ventricle in pulmonary hypertension," *Journal of Molecular Medicine*, vol. 91, no. 10, pp. 1185–1197, 2013.

[118] B. Chowdhury, A. Z. Luu, V. Z. Luu et al., "The SGLT2 inhibitor empagliflozin reduces mortality and prevents progression in experimental pulmonary hypertension," *Biochemical and Biophysical Research Communications*, vol. 524, no. 1, pp. 50–56, 2020.

[119] Y.-H. Fang, L. Piao, Z. Hong et al., "Therapeutic inhibition of fatty acid oxidation in right ventricular hypertrophy: exploiting Randle's cycle," *Journal of Molecular Medicine*, vol. 90, no. 1, pp. 31–43, 2012.

[120] E. Legchenko, P. Chouvarine, P. Borchert et al., "PPARγ agonist pioglitazone reverses pulmonary hypertension and prevents right heart failure via fatty acid oxidation," *Science translational medicine*, vol. 10, no. 438, p. eaao0303, 2018.

[121] J. Bernal-Ramírez, C. Silva-Platas, C. Jerjes-Sánchez et al., "Resveratrol Prevents Right Ventricle Dysfunction, Calcium Mishandling, and Energetic Failure via SIRT3 Stimulation in Pulmonary Arterial Hypertension," *Oxidative Medicine and Cellular Longevity*, vol. 2021, Article ID 9912434, 15 pages, 2021.

[122] Å. T. Røe, J. M. Aronsen, K. Skårdal et al., "Increased passive stiffness promotes diastolic dysfunction despite improved Ca2+ handling during left ventricular concentric hypertrophy," *Cardiovascular Research*, vol. 113, no. 10, pp. 1161–1172, 2017.

[123] A. M. Gómez, G. Ruiz-Hurtado, J.-P. Benitah, and A. Domínguez-Rodríguez, "Ca(2+) fluxes involvement in gene expression during cardiac hypertrophy," *Current Vascular Pharmacology*, vol. 11, no. 4, pp. 497–506, 2013.

[124] R. Paulin, G. Sutendra, V. Gurtu et al., "A miR-208-Mef2 axis drives the decompensation of right ventricular function in pulmonary hypertension," *Circulation Research*, vol. 116, no. 1, pp. 56–69, 2015.

[125] R. Adão, P. Mendes-Ferreira, C. Maia-Rocha et al., "Neuregulin-1 attenuates right ventricular diastolic stiffness in experimental pulmonary hypertension," *Clinical and Experimental Pharmacology & Physiology*, vol. 46, no. 3, pp. 255–265, 2019.

[126] X. An, S. Li, X. Weng et al., "Maxingxiongting mixture attenuates hypoxia pulmonary arterial hypertension to improve right ventricular hypertrophy by inhibiting the rho-kinase signaling pathway," *Journal of Traditional Chinese Medicine= Chung i tsa Chih Ying wen pan*, vol. 40, no. 6, pp. 992–998, 2020.

[127] Z. Dang, S. Su, G. Jin et al., "Tsantan Sumtang attenuated chronic hypoxia-induced right ventricular structure remodeling and fibrosis by equilibrating local ACE-AngII-AT1R/ACE2-Ang1-7-Mas axis in rat," *Journal of Ethnopharmacology*, vol. 250, p. 112470, 2020.

[128] X. Gao, Z. Zhang, X. Li et al., "Ursolic acid improves monocrotaline-induced right ventricular remodeling by regulating metabolism," *Journal of Cardiovascular Pharmacology*, vol. 75, no. 6, pp. 545–555, 2020.

[129] N. Rol, M. A. de Raaf, X. Q. Sun et al., "Nintedanib improves cardiac fibrosis but leaves pulmonary vascular remodelling unaltered in experimental pulmonary hypertension," *Cardiovascular Research*, vol. 115, no. 2, pp. 432–439, 2019.

[130] Z. P. Leong, A. Okida, M. Higuchi, Y. Yamano, and Y. Hikasa, "Reversal effects of low-dose imatinib compared with sunitinib on monocrotaline-induced pulmonary and right ventricular remodeling in rats," *Vascular Pharmacology*, vol. 100, pp. 41–50, 2018.

[131] N. Rai, S. Veeroju, Y. Schymura et al., "Effect of riociguat and sildenafil on right heart remodeling and function in pressure overload induced model of pulmonary arterial banding," *BioMed Research International*, vol. 2018, Article ID 3293584, 9 pages, 2018.

[132] A. Mamazhakypov, A. Weiß, S. Zukunft et al., "Effects of macitentan and tadalafil monotherapy or their combination on the right ventricle and plasma metabolites in pulmonary hypertensive rats," *Pulmonary circulation*, vol. 10, no. 4, p. 204589402094728, 2020.

[133] E. G. Schmuck, T. A. Hacker, D. A. Schreier, N. C. Chesler, and Z. Wang, "Beneficial effects of mesenchymal stem cell delivery via a novel cardiac bioscaffold on right ventricles of pulmonary arterial hypertensive rats," *American Journal of Physiology-Heart and Circulatory Physiology*, vol. 316, no. 5, pp. H1005–H1013, 2019.

[134] D. Lacerda, P. Türck, C. Campos-Carraro et al., "Pterostilbene improves cardiac function in a rat model of right heart failure through modulation of calcium handling proteins and oxidative stress," *Applied Physiology, Nutrition, and Metabolism*, vol. 45, no. 9, pp. 987–995, 2020.

[135] P. Türck, D. S. Lacerda, C. C. Carraro et al., "Trapidil improves hemodynamic, echocardiographic and redox state parameters of right ventricle in monocrotaline-induced pulmonary arterial hypertension model," *Biomedicine & Pharmacotherapy*, vol. 103, pp. 182–190, 2018.

[136] M. Lipczyńska, P. Szymański, M. Kumor, A. Klisiewicz, and P. Hoffman, "Collagen turnover biomarkers and systemic right ventricle remodeling in adults with previous atrial switch procedure for transposition of the great arteries," *PLoS One*, vol. 12, no. 8, article e0180629, 2017.

[137] B̆. López, A. González, and J. Díez, "Circulating biomarkers of collagen metabolism in cardiac diseases," *Circulation*, vol. 121, no. 14, pp. 1645–1654, 2010.

[138] F. A. van Nieuwenhoven, C. Munts, R. C. op't Veld et al., "Cartilage intermediate layer protein 1 (CILP1): a novel mediator of cardiac extracellular matrix remodelling," *Scientific Reports*, vol. 7, no. 1, article 16201, p. 16042, 2017.

[139] S. Keranov, O. Dörr, L. Jafari et al., "CILP1 as a biomarker for right ventricular maladaptation in pulmonary hypertension," *European Respiratory Journal*, vol. 57, no. 4, p. 1901192, 2021.

[140] K. Kreymborg, S. Uchida, P. Gellert et al., "Identification of right heart-enriched genes in a murine model of chronic outflow tract obstruction," *Journal of Molecular and Cellular Cardiology*, vol. 49, no. 4, pp. 598–605, 2010.

[141] I. Rohm, K. Grün, L. M. Müller et al., "Increased serum levels of fetal tenascin-C variants in patients with pulmonary hypertension: novel biomarkers reflecting vascular remodeling and right ventricular dysfunction?," *International journal of molecular sciences*, vol. 18, no. 11, p. 2371, 2017.

[142] J. Correia-Pinto, T. Henriques-Coelho, R. J. Roncon-Albuquerque et al., "Time course and mechanisms of left ventricular systolic and diastolic dysfunction in monocrotaline-induced pulmonary hypertension," *Basic Research in Cardiology*, vol. 104, no. 5, pp. 535–545, 2009.

[143] M. Hessel, P. Steendijk, B. den Adel, C. Schutte, and A. van der Laarse, "Pressure overload-induced right ventricular failure is associated with re-expression of myocardial tenascin-C and elevated plasma tenascin-C levels," *Cellular Physiology and Biochemistry*, vol. 24, no. 3-4, pp. 201–210, 2009.

[144] K. W. Prins, S. L. Archer, M. Pritzker et al., "Interleukin-6 is independently associated with right ventricular function in pulmonary arterial hypertension," *The Journal of Heart and Lung Transplantation*, vol. 37, no. 3, pp. 376–384, 2018.

[145] N. M. Pradhan, C. Mullin, and H. D. Poor, "Biomarkers and right ventricular dysfunction," *Critical Care Clinics*, vol. 36, no. 1, pp. 141–153, 2020.

[146] N. Galiè, M. Humbert, J.-L. Vachiery et al., "2015 ESC/ERS guidelines for the diagnosis and treatment of pulmonary Hypertension," *European Heart Journal*, vol. 37, no. 1, pp. 67–119, 2016.

[147] A. Torbicki, M. Kurzyna, P. Kuca et al., "Detectable serum cardiac troponin T as a marker of poor prognosis among patients with chronic precapillary pulmonary hypertension," *Circulation*, vol. 108, no. 7, pp. 844–848, 2003.

[148] M. Wilkins, "Pulmonary hypertension: proteins in the blood," *Global Cardiology Science & Practice*, vol. 2020, no. 1, article e202007, 2020.

[149] S. Reddy, M. Zhao, D.-Q. Hu et al., "Dynamic microRNA expression during the transition from right ventricular hypertrophy to failure," *Physiological Genomics*, vol. 44, no. 10, pp. 562–575, 2012.

[150] P. Chouvarine, J. Photiadis, R. Cesnjevar et al., "RNA expression profiles and regulatory networks in human right ventricular hypertrophy due to high pressure load," *iScience*, vol. 24, no. 3, article 102232, 2021.

[151] C. Wei, H. Henderson, C. Spradley et al., "Circulating miR-NAs as potential marker for pulmonary hypertension," *PLoS One*, vol. 8, no. 5, article e64396, 2013.

[152] J. Omura, K. Habbout, T. Shimauchi et al., "Identification of long noncoding RNA H19 as a new biomarker and therapeutic target in right ventricular failure in pulmonary arterial hypertension," *Circulation*, vol. 142, no. 15, pp. 1464–1484, 2020.

[153] B. C. Knollmann, A. N. Katchman, and M. R. Franz, "Monophasic action potential recordings from intact mouse heart: validation, regional heterogeneity, and relation to refractoriness," *Journal of Cardiovascular Electrophysiology*, vol. 12, no. 11, pp. 1286–1294, 2001.

[154] G. Münch, B. Bölck, A. Sugaru, and R. H. Schwinger, "Isoform expression of the sarcoplasmic reticulum Ca2+ release channel (ryanodine channel) in human myocardium," *Jour-*

[155] Y. D. Wang, Y. D. Li, X. Y. Ding et al., "17β-Estradiol preserves right ventricular function in rats with pulmonary arterial hypertension: an echocardiographic and histochemical study," *The International Journal of Cardiovascular Imaging*, vol. 35, no. 3, pp. 441–450, 2019.

[156] M. J. Overbeek, K. T. B. Mouchaers, H. M. Niessen et al., "Characteristics of interstitial fibrosis and inflammatory cell infiltration in right ventricles of systemic sclerosis-associated pulmonary arterial hypertension," *International Journal of Rheumatology*, vol. 2010, Article ID 604615, 10 pages, 2010.

[157] M. Boehm, N. Arnold, A. Braithwaite et al., "Eplerenone attenuates pathological pulmonary vascular rather than right ventricular remodeling in pulmonary arterial hypertension," *BMC Pulmonary Medicine*, vol. 18, no. 1, p. 41, 2018.

[158] S. Rain, D. S. G. Bos, M. L. Handoko et al., "Protein changes contributing to right ventricular cardiomyocyte Diastolic Dysfunction in Pulmonary Arterial Hypertension," *Journal of the American Heart Association*, vol. 3, no. 3, article e000716, 2014.

[159] D. Sacks, B. Baxter, B. C. V. Campbell et al., "Multisociety consensus quality improvement revised consensus statement for endovascular therapy of acute ischemic stroke," *International journal of stroke*, vol. 13, no. 6, pp. 612–632, 2018.

[160] S. Hsu, K. M. Kokkonen-Simon, J. A. Kirk et al., "Right ventricular myofilament functional differences in humans with systemic sclerosis-associated versus idiopathic pulmonary arterial hypertension," *Circulation*, vol. 137, no. 22, pp. 2360–2370, 2018.

[161] S. Rain, S. Andersen, A. Najafi et al., "Right ventricular myocardial stiffness in experimental pulmonary arterial hypertension: relative contribution of fibrosis and myofibril stiffness," *Circulation. Heart Failure*, vol. 9, no. 7, article e002636, 2016.

[162] M. W. Gorr, K. Sriram, A. M. Chinn, A. Muthusamy, and P. A. Insel, "Transcriptomic profiles reveal differences between the right and left ventricle in normoxia and hypoxia," *Physiological reports*, vol. 8, no. 2, article e14344, 2020.

[163] J. A. Watts, J. Zagorski, M. A. Gellar, B. G. Stevinson, and J. A. Kline, "Cardiac inflammation contributes to right ventricular dysfunction following experimental pulmonary embolism in rats," *Journal of Molecular and Cellular Cardiology*, vol. 41, no. 2, pp. 296–307, 2006.

[164] L. Tian, F. Potus, D. Wu et al., "Increased Drp1-mediated mitochondrial fission promotes proliferation and collagen production by right ventricular fibroblasts in experimental pulmonary arterial hypertension," *Frontiers in Physiology*, vol. 9, p. 828, 2018.

[165] H. V. Hwang, N. Sandeep, R. V. Nair et al., "Transcriptomic and functional analyses of mitochondrial dysfunction in pressure overload-induced right ventricular failure," *Journal of the American Heart Association*, vol. 10, no. 4, article e017835, 2021.

[166] U. K. Ihenacho, K. A. Meacham, M. C. Harwig, M. E. Widlansky, and R. B. Hill, "Mitochondrial fission protein 1: emerging roles in organellar form and function in health and disease," *Frontiers in Endocrinology*, vol. 12, article 660095, 2021.

[167] J. Nagendran, V. Gurtu, D. Z. Fu et al., "A dynamic and chamber-specific mitochondrial remodeling in right ventricular hypertrophy can be therapeutically targeted," *the Journal of thoracic and cardiovascular surgery*, vol. 136, no. 1, pp. 168–178.e3, 2008.

Research Article

Endogenous Taurine Downregulation Is Required for Renal Injury in Salt-Sensitive Hypertensive Rats via CBS/H$_2$S Inhibition

Pan Huang,[1] Yaqian Huang ![ORCID],[1] Boyang Lv,[1] Heng Zhang,[2] Jia Liu,[1] Guosheng Yang,[3] Yinghong Tao,[3] Dingfang Bu,[4] Guang Wang ![ORCID],[2] Junbao Du ![ORCID],[1,5] and Hongfang Jin ![ORCID][1]

[1]*Department of Pediatrics, Peking University First Hospital, Beijing 100034, China*
[2]*Department of Endocrinology, Beijing Chaoyang Hospital, Capital Medical University, Beijing 100020, China*
[3]*Animal Center, Peking University First Hospital, Beijing 100034, China*
[4]*Research Center, Peking University First Hospital, Beijing 100034, China*
[5]*Key Laboratory of Molecular Cardiology, Ministry of Education, Beijing, China*

Correspondence should be addressed to Yaqian Huang; yaqianhuang@126.com, Guang Wang; drwg6688@aliyun.com, Junbao Du; junbaodu1@126.com, and Hongfang Jin; jinhongfang51@126.com

Although taurine is known to exert an antihypertensive effect, it is unclear whether it is involved in the mechanism for hypertension-related target organ injury. To reveal the role of endogenous taurine in renal injury formation during salt-sensitive hypertension and clarify its mechanisms, both salt-sensitive Dahl rats and salt-resistant SS-13BN rats were fed a high-salt diet (8% NaCl) and given 2% taurine for 6 weeks. Rat systolic blood pressure (SBP) was measured by the tail-cuff method and artery catheterization. Kidney ultrastructure was observed under an electron microscope. Taurine content and mRNA and protein levels of taurine synthases, cysteine dioxygenase type 1 (CDO1) and cysteine sulfinic acid decarboxylase (CSAD), were decreased in Dahl rats fed a high-salt diet. However, taurine supplementation and the resulting increase in renal taurine content reduced the increased SBP and improved renal function and structural damage in high-salt diet-fed Dahl rats. In contrast, taurine did not affect SS-13BN SBP and renal function and structure. Taurine intervention increased the renal H$_2$S content and enhanced cystathionine-β-synthase (CBS) expression and activity in Dahl rats fed a high-salt diet. Taurine reduced the renin, angiotensin II, and aldosterone contents and the levels of oxidative stress indices in Dahl rat renal tissues but increased antioxidant capacity, antioxidant enzyme activity, and protein expression. However, taurine failed to achieve this effect in the renal tissue of SS-13BN rats fed a high-salt diet. Pretreatment with the CBS inhibitor HA or renal CBS knockdown inhibited H$_2$S generation and subsequently blocked the effect of taurine on renin, superoxide dismutase 1 (SOD1), and superoxide dismutase 2 (SOD2) levels in high-salt-stimulated Dahl renal slices. In conclusion, the downregulation of endogenous taurine production resulted in a decrease in the renal CBS/H$_2$S pathway. This decrease subsequently promoted renin-angiotensin-aldosterone system (RAAS) activation and oxidative stress in the kidney, ultimately contributing to renal injury in salt-sensitive Dahl rats.

1. Introduction

The kidney is the main target of organ damage due to hypertension. A chronic increase in arterial pressure leads to a decrease in the glomerular filtration rate, proteinuria, and ultimately renal failure [1]. Chronic kidney disease, which is caused by hypertension, is a powerful independent risk factor for adverse cardiovascular outcomes [2]. However,

the pathogenesis of hypertensive renal injury is still poorly understood. Dietary habits are closely related to the incidence of hypertension [3]. Up to 50% of patients with essential hypertension have high salt-induced hypertension, also known as salt-sensitive hypertension [4]. Notably, salt-sensitive hypertensive patients are more likely to develop end-stage renal disease compared with salt-resistant hypertensive patients [5]. High salt intake also directly causes

renal damage [6]. The activation of the renin-angiotensin-aldosterone system (RAAS), oxidative stress, and inflammation are all related to high salt-induced renal damage [7]. However, the mechanism for endogenous regulation of salt-sensitive hypertensive renal injury has not been fully elucidated.

Taurine is a nonprotein free amino acid produced endogenously from cysteine by the oxidation of cysteine dioxygenase (CDO) and decarboxylation of cysteine sulfinic acid decarboxylase (CSAD) [8]. Taurine has a variety of biological effects, including the inhibition of RAAS activation, antioxidant stress, and vasodilation, promotion of water and sodium metabolism, and suppression of sympathetic nerve excitation [9, 10]. Taurine supplementation can decrease blood pressure in various hypertensive animal models, including L-NAME-induced hypertensive rats [11], stroke-prone spontaneously hypertensive rats [12], cyclosporine A-induced hypertensive rats [13], and DOCA-salt rats [14]. Oral taurine has been shown to significantly lower blood pressure and protect vascular function and responsiveness in clinical hypertensive patients [15]. These studies suggest that taurine is of great potential value in the mechanism and clinical treatment of hypertension. However, the changes in endogenous taurine during high salt-induced hypertensive renal injury and the possible mechanisms by which it impacts renal injury are unclear and warrant further exploration.

In the past, hydrogen sulfide (H_2S) was considered a waste gas. However, over the past two decades, it has been found that there is a complete H_2S-generating pathway in mammals [16]. L-cysteine produces H_2S under the catalysis of cystathionine-β-synthase (CBS) and cystathionine-γ-lyase (CSE) [17]. Moreover, 3-mercaptopyruvate, which can be produced either from L-cysteine catalyzed by cysteine aminotransferase or from D-cysteine catalyzed by D-amino-acid oxidase (DAO), also generates H_2S under the catalysis of mercaptopyruvate sulfurtransferase (MPST) [17–19]. CBS, CSE, and MPST are all expressed in the brain, heart, lung, artery, and kidney [17, 18, 20]. An increasing number of studies have revealed that endogenous H_2S is an important gasotransmitter and exerts various physiological and pathophysiological effects [17–22]. Endogenous H_2S generation was reportedly downregulated in several hypertensive animal models including spontaneously hypertensive rats (SHRs) [23] and models of salt-sensitive hypertension [24], L-NAME-induced hypertension [25], and two-kidney one-clip hypertension [26]. Furthermore, supplementation of the H_2S donor sodium hydrosulfide (NaHS) significantly alleviated hypertension [27] and suppressed renal oxidative stress [28, 29], implying that the downregulated endogenous H_2S pathway might be important in the mechanism underlying hypertensive renal damage. Sun et al. [15] found that taurine could reduce the blood pressure of patients with prehypertension, improve vasodilation, and impact the plasma H_2S content. However, whether endogenous taurine participates in the development of salt-sensitive hypertensive renal injury through regulating the H_2S-generating pathway remains to be clarified.

In this study, the change in and role of the endogenous taurine pathway during salt-sensitive hypertensive renal damage and the role of the renal H_2S-generating pathway in controlling renal damage via taurine were examined.

2. Materials and Methods

2.1. Materials. High-salt (HS) feed containing 8% sodium chloride (NaCl) was purchased from Beijing Keao Xieli Feed Company (Beijing, China), taurine was purchased from Beijing Puboxin Biotechnology Company (Beijing, China), and horseradish peroxidase-labeled secondary antibodies, NaHS, and the CBS inhibitor hydroxylamine hydrochloride (HA) were purchased from Sigma-Aldrich (St. Louis, MO, USA) [30]. Antibodies against CBS , MPST, gp91phox, p47phox, p22phox and CD31 were purchased from Santa Cruz (Dallas, TX, USA); CSE antibody was purchased from Sigma-Aldrich; antibodies against CSAD, CDO1, CD31 and renin were purchased from Abcam (Waltham, MA, USA); β-actin antibody was purchased from Beijing Zhongshan Golden Bridge Biotechnology Co., Ltd. (Beijing, China); GAPDH antibody was from Shanghai Kangcheng Biological Engineering Company (Shanghai, China), and antibodies against SOD1 and SOD2 were purchased from Enzo Life (Farmingdale, NY, USA).

2.2. Animal Experiments. Animal experiments were approved by the Animal Research Ethics Committee of Peking University First Hospital (approval number: j201205) and strictly abided by the regulations of the Animal Experiment Center of Peking University First Hospital and the laboratory animal welfare rules. Male salt-sensitive (Dahl) and salt-resistant (SS-13BN) rats ($n = 30$ per group, 5 weeks old, and weighing 180–200 g) were obtained from Beijing Vital River Laboratory Animal Technology Company (Beijing, China). These two types of rats were further randomly divided into three groups ($n = 10$ per group) and given a normal diet containing 0.5% NaCl (Dahl+normal salt (NS), SS-13BN+NS), an HS diet containing 8% NaCl [31] (Dahl+HS, SS-13BN+HS), or an HS diet combined with 2% taurine [11] in drinking water (Dahl+HS+Tau, SS-13BN+HS+Tau) for 6 weeks.

2.3. Blood Pressure Measurement. The tail arterial pressure of awake rats was measured using an intelligent noninvasive blood pressure monitor [32]. After the experiment, rat systolic blood pressure (SBP) was also determined using the carotid artery catheter method [33]. Briefly, the rat was anesthetized with 25% urethane and then intubated through the right common carotid artery. Rat SBP was recorded using a PT-100 biological blood pressure sensor and a BL-420F multichannel physiological signal acquisition and recording system (Chengdu Techman Instrument Co., Ltd., Sichuan, China).

2.4. Determination of Biochemical Indicators. After the experiment, 24-h urine samples were collected using a metabolic cage. After rat SBP measurement, the blood sample was collected by puncture of the inferior vena cava. After centrifugation, the serum was collected. The serum urea and creatinine content and 24-h urinary protein level were

determined using an automatic biochemical analyzer (Hitachi 7600, Tokyo, Japan) [28].

2.5. Ultrastructure of Renal Tissue.
Renal cortex tissue ($2 \times 2 \times 2 \, mm^3$) was fixed with 3% glutaraldehyde solution and then prepared into sections for electron microscopy [28]. The ultrastructure of renal sections was observed under a JEM-1230 transmission electron microscope (JEOL, Tokyo, Japan).

2.6. Ex Vivo Incubation Experiments of Renal Tissue Slices.
After the rats were anesthetized with 25% urethane, the abdominal cavity was quickly opened. The kidney was removed and stored in aerated sterile Krebs buffer (pH 7.4) on ice. The kidney cross-section was placed in a tissue microtome with 0.1% low-melting-point agarose in ice-cold phosphate-buffered saline (PBS) to prepare renal cortex slices ($300 \pm 50 \, \mu m$). The slices were incubated in continuously aerated (95% O_2 : 5% CO_2) Dulbecco's modified Eagle medium (DMEM)/F12 medium at 37°C for 3 h. Finally, the incubation medium and renal slices were collected and tested.

2.7. Inhibition of CBS Activity in Renal Slices.
HA was used in the *ex vivo* incubation experiments to suppress renal CBS activity. The Dahl renal slices were divided into the NS (incubation medium with 137 mM NaCl) [34], HS, HS +Tau, and HS+Tau+HA groups. HS incubation medium contained 200 mM NaCl [34, 35]. The concentrations of taurine and HA in the incubation medium were 10 mM and 50 μM, respectively [36, 37].

2.8. CBS Knockdown in Rat Renal Tissue.
Lentivirus containing CBS-small hairpin RNA (shRNA) or scramble-shRNA was purchased from Cyagen Biosciences Inc. (Guangzhou, China). After four-week-old male Dahl rats (weighing about 150 g) were anesthetized, a small incision was made in the renal area on the back of the rats to expose the kidney. Each kidney was administrated with 100 μL of scramble-shRNA or CBS-shRNA lentivirus (1×10^9 TU/mL) through kidney puncture. The same procedure was used for both kidneys. After two weeks of lentivirus infection, the *ex vivo* incubation experiments were performed using the renal tissue slices. Dahl rats transfected with scramble-shRNA lentivirus were divided into three groups ($n = 8$ per group): the Dahl +NS+scramble-shRNA, Dahl+HS+scramble-shRNA, and Dahl+HS+Tau+scramble-shRNA groups. Dahl rats transfected with CBS-shRNA lentivirus were also divided into three groups ($n = 8$ per group): the Dahl+NS+CBS-shRNA, Dahl+HS+CBS-shRNA, and Dahl+HS+Tau+CBS-shRNA groups. The NS and HS incubation medium contained 137 mM and 200 mM NaCl, respectively. The incubation medium contained a taurine concentration of 10 mM.

2.9. Taurine Content Determination.
Taurine content was determined by Beijing Mass Spectrometry Medical Research Co., Ltd (Beijing, China). The renal tissue was homogenized in deionized water on ice. The homogenate (50 μL) was mixed with 50 μL of protein precipitation agent and centrifuged at 13,200 rpm for 4 min. The supernatant (10 μL) was mixed with 50 μL labeling buffer and centrifuged for a few seconds. Derivatization solution (20 μL) was added and centrifuged for a few seconds, then reacted for 15 min at 55°C. The above mixture (50 μL) was analyzed using a high-performance liquid chromatographer (AB Company, Carlsbad, CA, USA). The liquid chromatography column was MSLAB 45+AA-C18 ($150 \times 4.6 \, mm$, 5 μm). The mobile phase included the water phase (water containing 1‰ formic acid) and organic phase (acrylonitrile containing 1‰ formic acid). The methanol elution gradient was 90% (0–1 min), 90–30% (1–12 min), 30–0% (12–12.1 min), 0% (12.1–15 min), 0–90% (15–15.1 min), and 90% (15.1–20 min). The taurine content in the renal tissue was determined in the positive ionization mode.

2.10. H₂S Content Determination.
H_2S levels in serum and renal tissue were measured by the sensitive sulfur electrode method [37]. The renal tissue was homogenized with PBS and centrifuged, and the supernatant was collected to measure the protein and H_2S concentrations. The front end (10 mm) of the polarized H_2S electrode (WPI, Shanghai, China) was inserted into the sample at room temperature, and the current output (pA) increased. After reaching a plateau, the pA was recorded. A standard curve was drawn based on the concentration of sodium sulfide and pA. The H_2S content in the sample was calculated based on this standard curve. The H_2S content in the tissue homogenate was then corrected for protein concentration.

2.11. Real-Time Quantitative Polymerase Chain Reaction (RT-qPCR).
The rat renal tissues were ground into powder in liquid nitrogen, followed by the addition of TRIzol for homogenization and lysis. Chloroform was added to remove protein and DNA. RNA was selectively precipitated by isopropanol, washed with ethanol, dissolved in ribozyme-free water, and finally reverse-transcribed into cDNA [38]. RT-qPCR was carried out on an Applied Biosystems 7300 system (Carlsbad, CA, USA). Each reaction contained a mixture of $2 \times$ mix, primers (7.5 μM), TaqMan probe (5 μM), cDNA, and purified water. The PCR program was 10 min at 95°C, followed by 40 cycles of 15 s at 95°C and 1 min at 60°C. Data were compared quantitatively with the relative CT value ($2^{-\Delta\Delta CT}$). β-Actin was used as the internal reference. Table 1 shows the primer and TaqMan probe sequences.

2.12. Western Blot.
Renal protein was extracted using lysis buffer containing 50 mM Tris base, 150 mM NaCl, 1 mM EDTA, 6 mM sodium deoxycholate, 1% NP-40, protease inhibitor, phosphatase inhibitor, and phenylmethylsulfonyl fluoride (PMSF). After centrifugation, the supernatants were used for protein quantification and Western blot [39]. The proteins were separated by polyacrylamide electrophoresis and transferred to a nitrocellulose membrane, which was then blocked and incubated with antibodies. ECL luminescent solution was added to the membrane which was then placed in a gel imaging instrument (Gene Company Limited Company, Hong Kong, China) for exposure. Optical density values of protein bands were determined by AlphaEase FC software. The optical density of the corresponding internal reference β-actin or GAPDH was used for correction.

TABLE 1: Sequence of primer and TaqMan probe for rat target genes and β-actin.

Target		Sequence (5′-3′)	Product
CSAD	Forward	CTGGAGTGGCGCATCGA	80 bp
	Reverse	AACTCAAATCCTTCCCGCTTTT	
	TaqMan	CAGGCCTTTGCTCTCACTCGGTACTTGG	
CDO1	Forward	GGGAAAATCAGTGTGCCTACATT	121 bp
	Reverse	GCATGGCATGTATCGAAAGGT	
	TaqMan	TTACATCGAGTAGAGAACGTCAGCCACACAGAG	
CBS	Forward	CTCCGGGAGAAGGGTTTTGA	81 bp
	Reverse	CATGTTCCCGAGAGTCACCAT	
	TaqMan	AGGCACCTGTGGTCAACGAGTCTGG	
CSE	Forward	GCTGAGAGCCTGGGAGGATA	92 bp
	Reverse	TCACTGATCCCGAGGGTAGCT	
	TaqMan	CTGAGCTTCCAGCAATCATGACCCATG	
MPST	Forward	CGGCGCTTCCAGGTAGTG	131 bp
	Reverse	CTGGTCAGGAATTCAGTGAATGG	
	TaqMan	CCGCGCAGCTGGCCGTTT	
β-Actin	Forward	ACCCGCGAGTACAACCTTCTT	80 bp
	Reverse	TATCGTCATCCATGGCGAACT	
	TaqMan	CCTCCGTCGCCGGTCCACAC	

Note: the 5′ end of the TaqMan probe is labeled with FAM, and the 3′ end is labeled with TAMRA.

2.13. Detection of CBS, MPST, and CSE Activity in Renal Tissues.

Renal homogenate was incubated with protein A/G at 4°C for 1 h and centrifuged at 8,000 g for 10 min. Supernatant was incubated with primary antibody against corresponding protein overnight. Protein A/G was then added, and the mixture was incubated for 4 h. After centrifugation, precipitated protein was eluted.

According to Stipanuk's method in the published literature [40], 10 μg of protein was added to 1 mL of reaction solution containing 100 mM potassium phosphate buffer, 10 mM L-cysteine, and 2 mM pyridoxal 5′-phosphate and incubated at 37°C for 2 h. Renal H_2S contents were measured using the free radical detection analyzer TBR4100. The rate of H_2S production was calculated to reflect the CBS and CSE activity (nmol/h/μg).

To detect MPST activity, 10 μg of protein was added into 1 mL of reaction solution including PBS and 2 mM β-mercaptopyruvate and incubated for 2 h. H_2S contents were measured using the free radical detection analyzer TBR4100, and the rate of H_2S production was calculated to reflect the MPST activity (nmol/h/μg) [41].

2.14. Determination of Renin, Angiotensin II (AngII), and Aldosterone Content by Enzyme-Linked Immunosorbent Assay (ELISA).

ELISA kits for renin, AngII, and aldosterone were purchased from Shanghai Bogu Biotechnology Co., Ltd (Shanghai, China). The concentrations of renin, AngII, and aldosterone in the rat renal tissue were determined by ELISA and standardized with total protein content according to the manufacturer's instructions.

2.15. Determination of Oxidative Stress Indicators in Renal Tissue.

The renal tissues were homogenized in PBS and centrifuged at 10,000 g for 10 min to obtain supernatant. According to the manufacturer's instructions provided in the kits (Nanjing Jiancheng Bioengineering Institute, Nanjing, China), the biochemical colorimetry method [42] was used to determine the activities of superoxide dismutase (SOD), catalase (CAT), glutathione peroxidase (GSH-PX), and myeloperoxidase (MPO); the contents of oxidized glutathione (GSSG), reduced glutathione (GSH), malondialdehyde (MDA), hydrogen peroxide (H_2O_2), hydroxyl radical ('OH), and carbon monoxide (CO); and total antioxidant capacity (T-AOC).

2.16. Immunofluorescence Staining.

The frozen sections of rat aorta were washed with PBS, blocked with 5% BSA, and then incubated with primary antibodies overnight at 4°C. The sections were then washed with PBS three times and incubated with secondary antibodies (Invitrogen, Carlsbad, CA, USA) for 1.5 h at room temperature away from light. After washing, sections were stained with DAPI (ZSGB-Bio, ZLI-9557). The fluorescence signals were captured under an Olympus confocal laser scanning microscope.

2.17. Statistical Analysis.

Statistical analysis was performed using IBM SPSS 13.0 software. Data are expressed as the mean ± standard error (mean ± SE). Comparisons among multiple groups were performed using one-way analysis of variance (ANOVA) with Bonferroni's post hoc test. P values less than 0.05 are considered statistically significant.

3. Results

3.1. The Renal Endogenous Taurine Pathway Was Significantly Downregulated during Salt-Sensitive Hypertensive Renal Injury.

To examine the role of the endogenous taurine
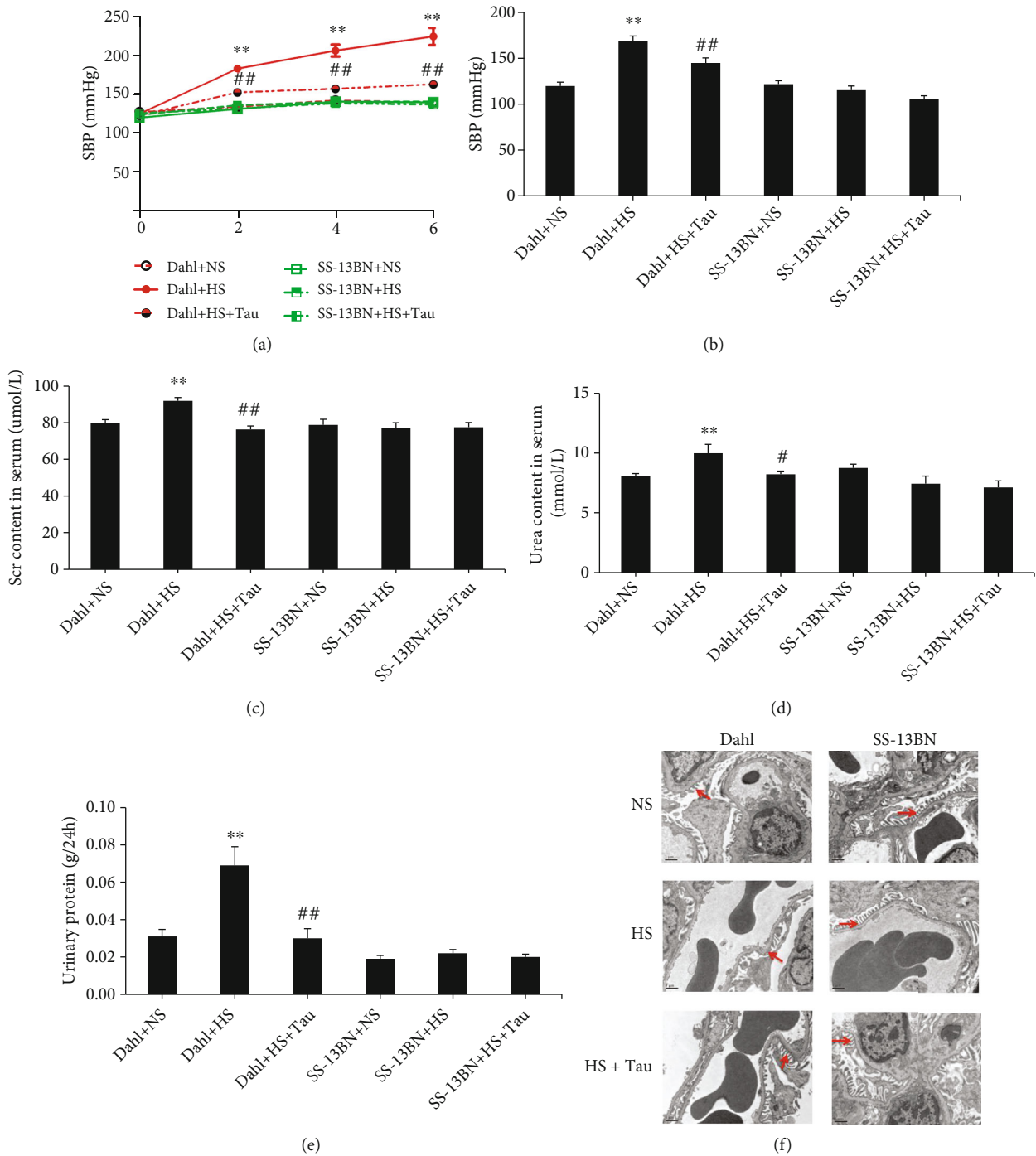
Figure 1: Taurine increment inhibited high-salt (HS) diet-induced renal damage in Dahl rats. (a) Changes of tail arterial systolic blood pressure (SBP) of Dahl and SS-13BN rats treated with normal salt (NS) diet, HS diet, or HS feeding supplemented with 2% taurine in drinking water (HS+Tau) for 2, 4, and 6 weeks, measured using an intelligent noninvasive blood pressure monitor. (b) Changes in SBP after 6 weeks of HS diet feeding measured by the carotid artery catheter method. (c–e) Changes of serum creatinine (Scr) content (c), serum urea content (d), and the 24 h urinary protein level (e) in rats. (f) Electron microscope examination of rat renal ultrastructure (transmission electron microscopy, magnification: 8000x). $\rightarrow$ indicates foot process of glomerular podocytes. $n = 10$ for each group. $**P < 0.01$ vs. Dahl+NS; $^{\#}P < 0.05$ and $^{\#\#}P < 0.01$ vs. Dahl+HS.

pathway in salt-sensitive hypertensive renal damage, both salt-sensitive Dahl rats and salt-resistant SS-13BN rats were given NS and HS diets. Compared with the Dahl+NS group, the tail arterial SBP of the Dahl+HS group was consistently and mark-

edly increased after 2, 4, and 6 weeks of HS feeding according to the tail-cuff method (Figure 1(a)). The results of the carotid artery catheterization method also revealed a significant increase in arterial SBP after 6 weeks of HS feeding

(a)

(b)

(c)

(d)

Figure 2: Continued.

(e)

(f)
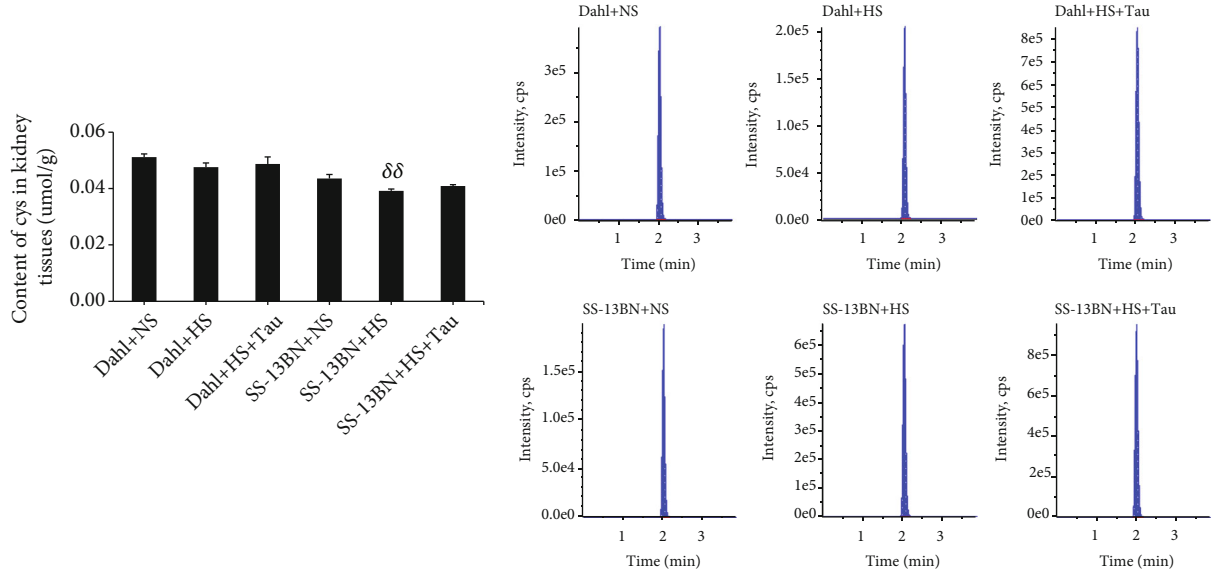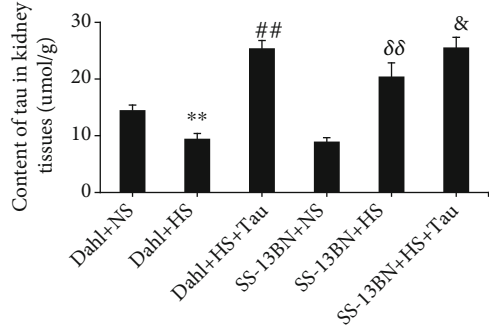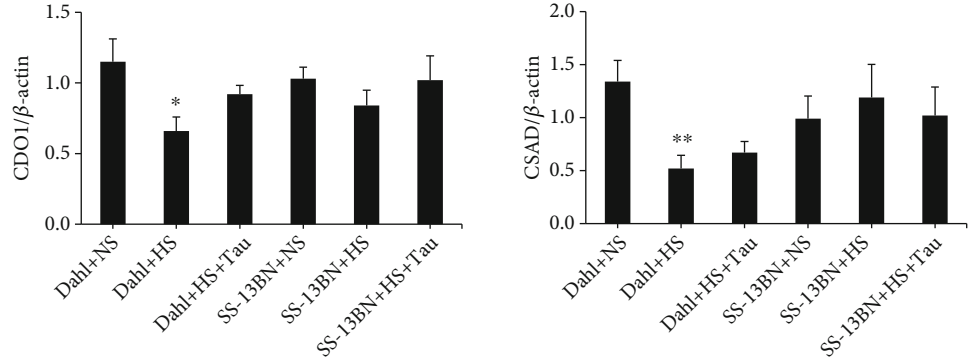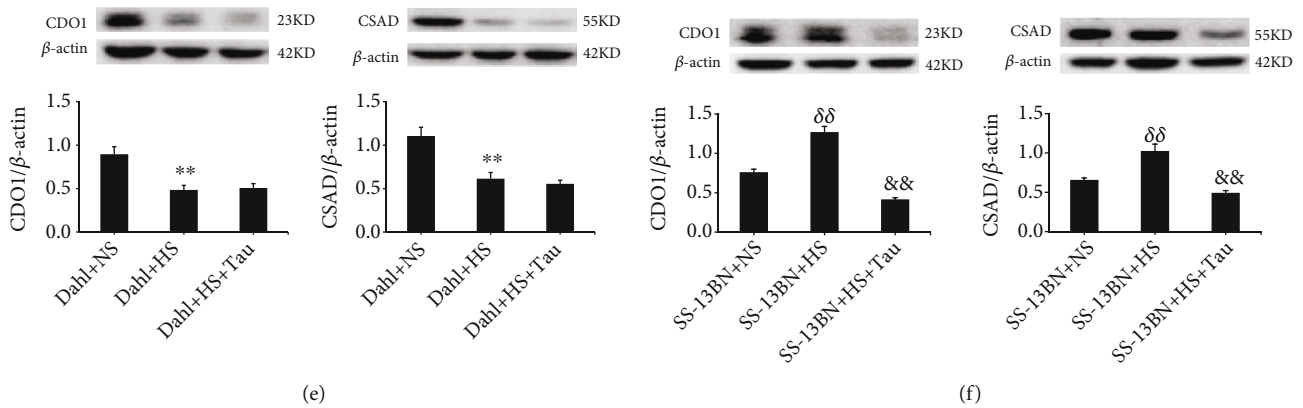
Figure 2: High-salt (HS) diet downregulated renal endogenous taurine-generating pathway in Dahl rats. (a) Changes of cysteine (Cys) contents in rat renal tissues. (b) The representative high-performance liquid chromatograms of taurine (Tau) in rat renal tissues. (c) Changes in Tau contents in rat renal tissues. (d) CDO1 and CSAD mRNA levels in rat renal tissues. (e) Protein levels and quantification of CDO1 and CSAD in the kidneys of Dahl rats. (f) Protein levels and quantification of CDO1 and CSAD in the kidneys of SS-13BN rats. $n = 10$ for each group. $^*P < 0.05$ and $^{**}P < 0.01$ vs. Dahl+normal salt (NS); $^{\#\#}P < 0.01$ vs. Dahl+HS; $^{\delta\delta}P < 0.01$ vs. SS-13BN+NS; $^{\&}P < 0.05$ and $^{\&\&}P < 0.01$ vs. SS-13BN+HS.

(Figure 1(b)). Serum contents of creatinine and urea and the 24-h urinary protein level were elevated in HS Dahl rats (Figures 1(c)–1(e)). The results of electron microscopy showed that glomerular podocytes were fused in the Dahl +HS group (Figure 1(f)). These data demonstrate that the salt-sensitive hypertensive renal injury rat model was successfully established. Interestingly, the taurine content and mRNA and protein levels of CDO1 and CSAD were significantly downregulated in the kidneys of HS-fed Dahl rats compared with NS-fed rats (Figures 2(b)–2(e)), while the renal cysteine content remained unchanged (Figure 2(a)).

However, the taurine content and CDO1 and CSAD protein levels were higher in the kidneys of SS-13BN+HS rats than those in SS-13BN+NS rats (Figures 2(b), 2(c), and 2(f)), while the CDO1 and CSAD mRNA expression in the renal tissues did not differ between the two groups (Figure 2(d)). Furthermore, the renal cysteine content decreased in the SS-13BN+HS group (Figure 2(a)). HS diet did not affect the blood pressure and renal function of SS-13BN rats (Figure 1). These results suggest that the HS diet downregulated the endogenous taurine pathway and impaired renal function in salt-sensitive hypertensive Dahl rats.

3.2. Downregulation of Renal Taurine Promoted Renal Damage in Salt-Sensitive Hypertension.
To investigate the functional significance of renal taurine downregulation during salt-sensitive hypertensive renal injury, the HS diet of both the SS-13BN rats and Dahl rats was supplemented with or without 2% taurine in drinking water (HS+Tau or HS). The renal taurine content was increased in the Dahl+HS +Tau group compared with the Dahl+HS group (Figures 2(b) and 2(c)). This upregulation of the renal taurine contents was associated with a marked decrease in the SBP (Figures 1(a) and 1(b)), serum creatinine content (Figure 1(c)), serum urea content (Figure 1(d)), and 24 h urinary protein level (Figure 1(e)). Electron microscopy results

showed that the fusion of glomerular podocytes was significantly reduced in the Dahl+HS+Tau group compared with the Dahl+HS group (Figure 1(f)). Taurine supplementation in SS-13BN rats given the HS diet increased the taurine content in the renal tissues (Figures 2(b) and 2(c)) and decreased CDO1 and CSAD protein expression (Figure 2(f)); however, it did not change the CDO and CSAD mRNA expression (Figure 2(d)), the SBP level of rats, or the function and structure of the kidney compared to the HS-fed SS-13BN rats without taurine treatment (Figure 1). These data suggest that exogenous taurine supplementation restored the renal taurine of Dahl rats to normal levels, which could antagonize HS-induced hypertensive renal damage. These findings imply that high salt downregulated the endogenous taurine pathway to cause renal injury during salt-sensitive hypertension.

3.3. Endogenous Taurine Reduction Suppressed the Renal CBS/H_2S Pathway in Rats with Salt-Sensitive Hypertensive Renal Damage.
Taurine treatment is known to increase plasma H_2S levels in prehypertensive patients [15], and previous studies have shown the possible renoprotective effect of H_2S [28]. Therefore, the changes in the endogenous H_2S-producing pathway were analyzed to aid in understanding the mechanism by which downregulated taurine contributed to renal injury in HS diet-fed Dahl rats. HS diet-fed Dahl rats exhibited a significant decrease in renal H_2S content (Figure 3(a)), CBS mRNA, protein levels, and activity, MPST mRNA levels and activity, and renal CSE mRNA levels compared with those fed an NS diet (Figures 3(b)–3(d)). Meanwhile, MPST protein expression and CSE protein expression and activity in the renal tissues were not significantly different between the Dahl+NS and Dahl+HS groups (Figures 3(d) and 3(e)). Notably, renal H_2S content (Figure 3(a)), CBS mRNA, protein expression, and activity (Figures 3(b) and 3(c)), MPST mRNA levels (Figure 3(b)), and CSE mRNA and protein levels (Figures 3(b) and 3(e)) in

(a)

(b)

(c)

(d)

(e)

(f)

(g)

(h)
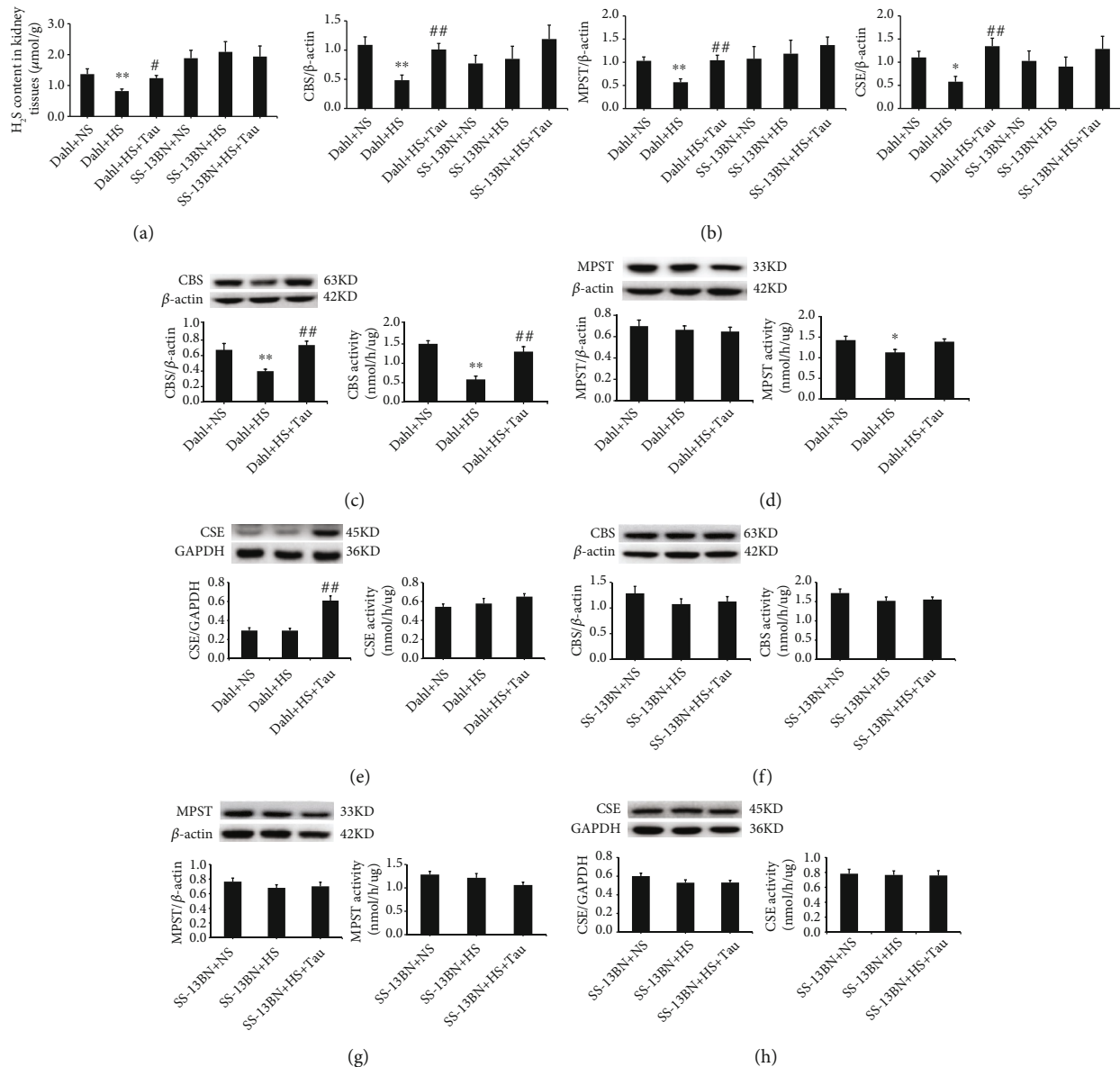
Figure 3: Taurine downregulation induced by high-salt (HS) diet reduced the cystathionine-β-synthase (CBS)/hydrogen sulfide (H_2S) pathway in Dahl kidneys. (a) H_2S content in rat renal tissues. (b) Renal mRNA levels of CBS, mercaptopyruvate sulfurtransferase (MPST), and cystathionine-γ-lyase (CSE). (c–e) Protein expression and activity of CBS (c), MPST (d), and CSE (e) in Dahl rat kidneys. (f–h) Protein expression and activity of CBS (f), MPST (g), and CSE (h) in SS-13BN rat kidneys. $n = 10$ for each group. $^*P < 0.05$ and $^{**}P < 0.01$ vs. Dahl+normal salt (NS); $^#P < 0.05$ and $^{##}P < 0.01$ vs. Dahl+HS.

renal tissues were markedly elevated by taurine supplementation in HS-induced Dahl rats; meanwhile, MPST activity and protein expression (Figure 3(d)) and CSE activity (Figure 3(e)) did not change.

There were no differences in the renal H_2S content, CBS mRNA and protein expression, and CBS, MPST, and CSE activity among the SS-13BN+NS, SS-13BN+HS, and SS-13BN+HS+Tau groups (Figures 3(a), 3(b), and 3(f)–3(h)). These data suggest that taurine supplementation upregulated the HS diet-inhibited renal CBS/H_2S levels in Dahl rats. Furthermore, the decrease in taurine caused by the HS diet suppressed the renal H_2S-generating pathway during salt-sensitive hypertensive renal damage.

3.4. Taurine Downregulation Facilitated Renal Oxidative Stress in Salt-Sensitive Hypertensive Rats. Oxidative stress is crucial in the pathogenesis of renal damage. Therefore, the impact of taurine on various oxidative damage substances and antioxidant substances in the rat renal tissues was examined. The renal contents of MDA, H_2O_2, ·OH, and GSSG and the MPO activity were higher in Dahl rats fed an HS diet than those fed an NS diet (Figures 4(a)–4(e)); meanwhile, the T-AOC (Figure 4(f)), CO, and GSH contents (Figures 4(g) and 4(i)), CAT, GSH-PX, and SOD activities (Figures 4(h), 4(j), and 4(k)), and SOD1 and SOD2 protein expression (Figure 4(l)) were lower in the kidneys of HS diet-fed Dahl rats than in those fed an NS diet. More

(a)

(b)

(c)

(d)

(e)

(f)

(g)

(h)

(i)

(j)

Figure 4: Continued.

(k)   (l)

(m)
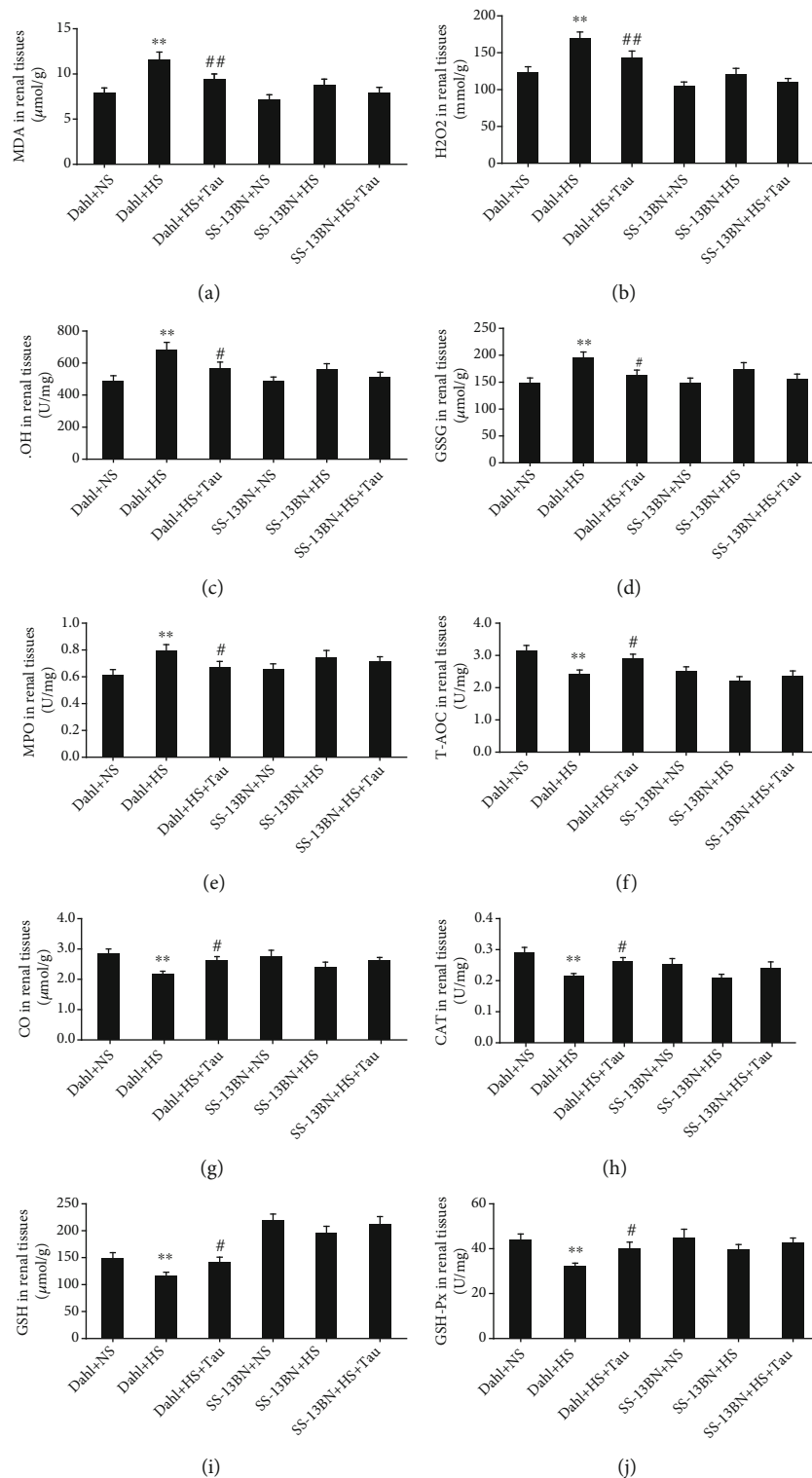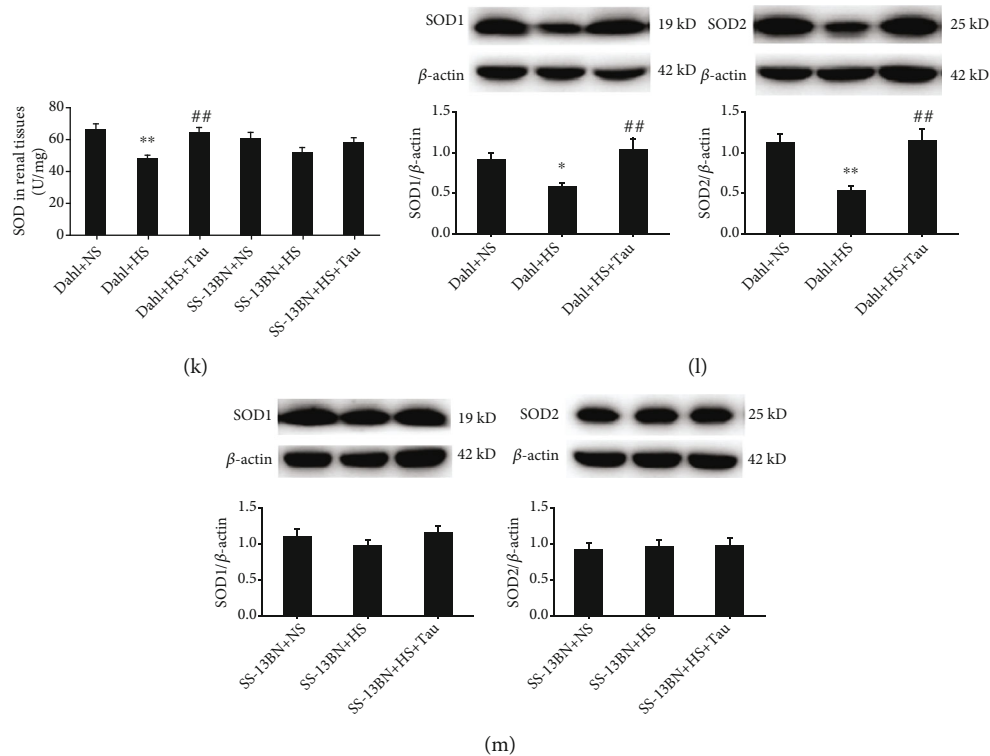
FIGURE 4: High-salt (HS) diet-caused decrease in taurine promoted oxidative stress and impaired antioxidative capacity in Dahl rat kidneys. (a–d) Malondialdehyde (MDA) (a), H_2O_2 (b), $\cdot OH$ (c), and oxidized glutathione (GSSG) contents (d) in rat renal tissues. (e) Myeloperoxidase (MPO) activity in rat renal tissues. (f) Total antioxidant capacity (T-AOC) in renal tissues. (g) Carbon monoxide (CO) content in rat renal tissues. (h) Catalase (CAT) activity in rat renal tissues. (i) Reduced glutathione (GSH) content. (j) Glutathione peroxidase (GSH-PX) activity. (k) Superoxide dismutase (SOD) activity. (l) SOD1/2 protein levels in Dahl kidneys. (m) SOD1/2 protein levels in SS-13BN kidneys. $n = 10$ for each group. $^*P < 0.05$ and $^{**}P < 0.01$ vs. Dahl+normal salt (NS); $^#P < 0.05$ and $^{##}P < 0.01$ vs. Dahl+HS.

importantly, oxidative damage index levels significantly decreased (Figures 4(a)–4(e)), and antioxidant index levels significantly increased (Figures 4(f)–4(k)) in the kidneys of Dahl+HS+Tau group rats.

However, the renal contents of MDA, H_2O_2, $\cdot OH$, GSSG, T-AOC, CO, and GSH (Figures 4(a)–4(d), 4(f), 4(g), and 4(i)), the activities of MPO, CAT, GSH-PX, and SOD (Figures 4(e), 4(h), 4(j), and 4(k)), and the SOD1 and SOD2 protein levels (Figure 4(m)) did not differ among the SS-13BN+NS, SS-13BN+HS, and SS-13BN+HS+Tau groups. These data indicated that taurine supplementation inhibited oxidative stress and promoted antioxidant capacity in the kidneys of HS diet-fed Dahl rats. Furthermore, the decrease in taurine caused by the HS diet promoted renal oxidative stress.

3.5. Taurine Downregulation Enhanced Renal RAAS Activation in Salt-Sensitive Hypertensive Rats.
The RAAS is also known to be activated by high salt and acts as another important factor in the pathogenesis of salt-sensitive hypertensive renal damage. As such, we investigated the influence of taurine on renal RAAS activation in HS diet-fed Dahl rats. High salt activated renal RAAS in Dahl rats, and renin, AngII, and aldosterone contents and renin protein expression were increased (Figures 5(a)–5(d)). Meanwhile, the administration of taurine to HS diet-fed

Dahl rats significantly reduced renal contents of renin, AngII, and aldosterone and renin protein expression (Figures 5(a)–5(d)).

In SS-13BN rats, the renal contents of renin, AngII, and aldosterone and renin protein expression were not markedly different among the NS, HS, and HS+Tau groups (Figures 5(a)–5(c) and 5(e)). These data suggest that the decreased taurine caused by the HS diet promoted renal RAAS activation in Dahl rats.

3.6. Endogenous Taurine Reduction Caused by High Salt Contributed to Renal Injury through CBS/H_2S Pathway Inhibition in Dahl Rats.
To explore whether taurine down-regulation promoted renal injury through the endogenous H_2S pathway, the Dahl renal slices were treated with HA, an inhibitor of CBS activity, in *ex vivo* experiments. The renal slices with HS medium incubation exhibited a decrease in H_2S content (Figure 6(a)) and SOD1 and SOD2 protein expression (Figures 6(c) and 6(d)), but an increase in renin expression (Figure 6(b)). Meanwhile, supplementation of HS-treated renal slices with taurine upregulated H_2S content (Figure 6(a)) and SOD1 and SOD2 protein expression (Figures 6(c) and 6(d)) but downregulated renin protein expression (Figure 6(b)). However, treatment with HA blocked taurine-induced H_2S production, the inhibition of renin protein expression, and taurine-facilitated SOD1 and

(a)

(b)

(c)

(d)

(e)
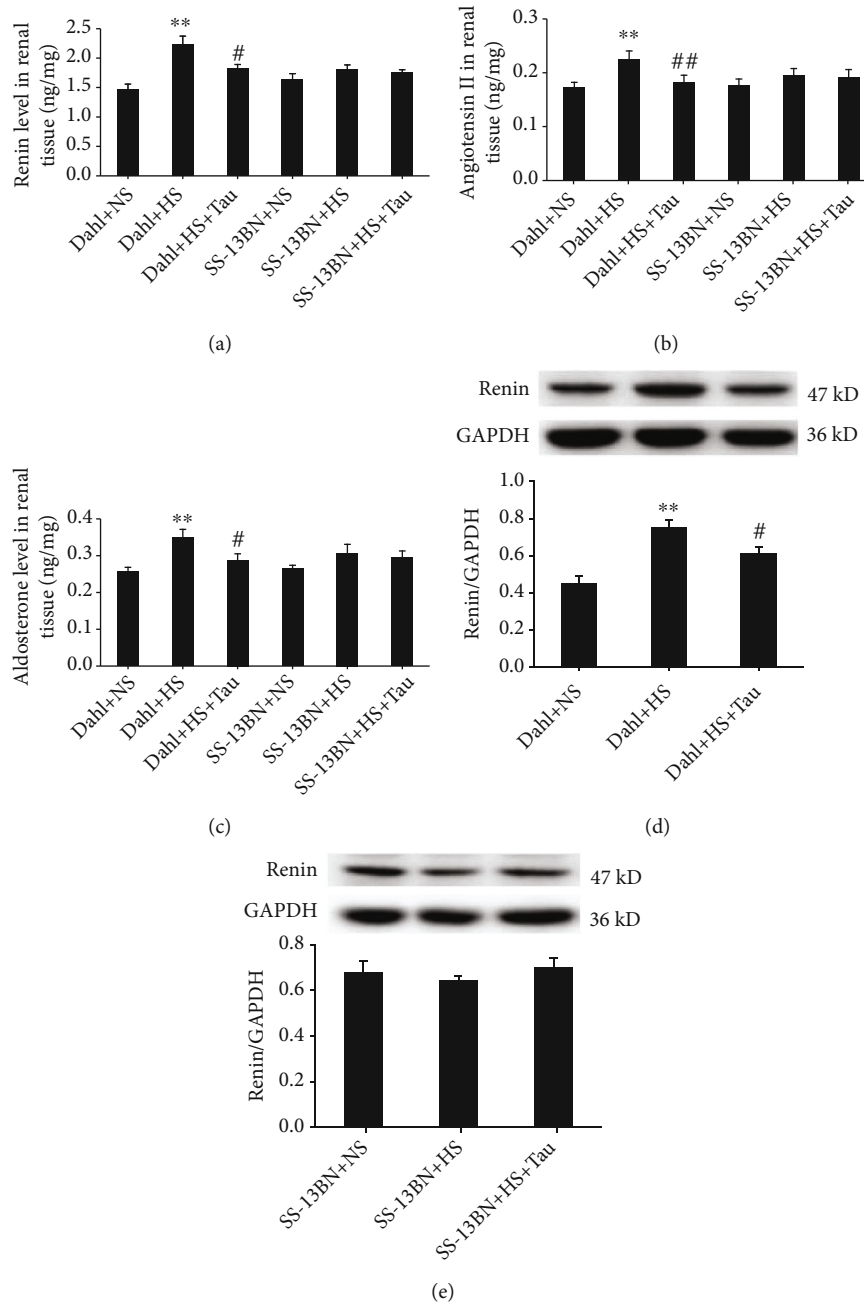
FIGURE 5: Taurine reduction by the high-salt (HS) diet activated the renin-angiotensin-aldosterone system (RAAS) in Dahl rat kidneys. (a–c) Renal contents of renin (a), angiotensin II (b), and aldosterone (c). (d, e) Protein levels of renin in Dahl rat kidneys (d) and SS-13BN rat kidneys (e). $n = 10$ for each group. $**P < 0.01$ vs. Dahl+normal salt (NS); $^{\#}P < 0.05$ and $^{\#\#}P < 0.01$ vs. Dahl+HS.

SOD2 levels in the Dahl renal slices incubated with HS (Figures 6(a)–6(d)).

To further confirm whether CBS mediated the effects of taurine on renal RAAS activation and oxidative stress, the kidneys of Dahl rats were transfected with CBS-shRNA lentivirus to knock down renal CBS (Figure 6(e)). Scramble-shRNA was used as a control. The Dahl renal slices were treated with normal medium, HS medium, and HS medium containing taurine after transfection with each lentivirus. The H₂S content (Figure 6(f)) and CBS (Figure 6(g)), SOD1 (Figure 6(i)), and SOD2 (Figure 6(j)) protein expression were decreased in the renal slices of Dahl rats trans-

fected with scramble-shRNA and incubated with HS medium, but renin protein expression was increased (Figure 6(h)). Meanwhile, taurine administration rescued the rats from this effect (Figures 6(f)–6(j)). The renal H₂S content and CBS protein expression were significantly downregulated in the Dahl rats whose kidneys were transfected with CBS-shRNA lentivirus compared with those whose kidneys were transfected with scramble-shRNA lentivirus (Figures 6(f) and 6(g)). Notably, the H₂S content and CBS, renin, SOD1, and SOD2 levels in Dahl rat renal slices transfected with CBS-shRNA were not affected by HS treatment or HS and taurine treatment (Figures 6(f)–6(j)). These

Figure 6: Continued.

(i)

(j)
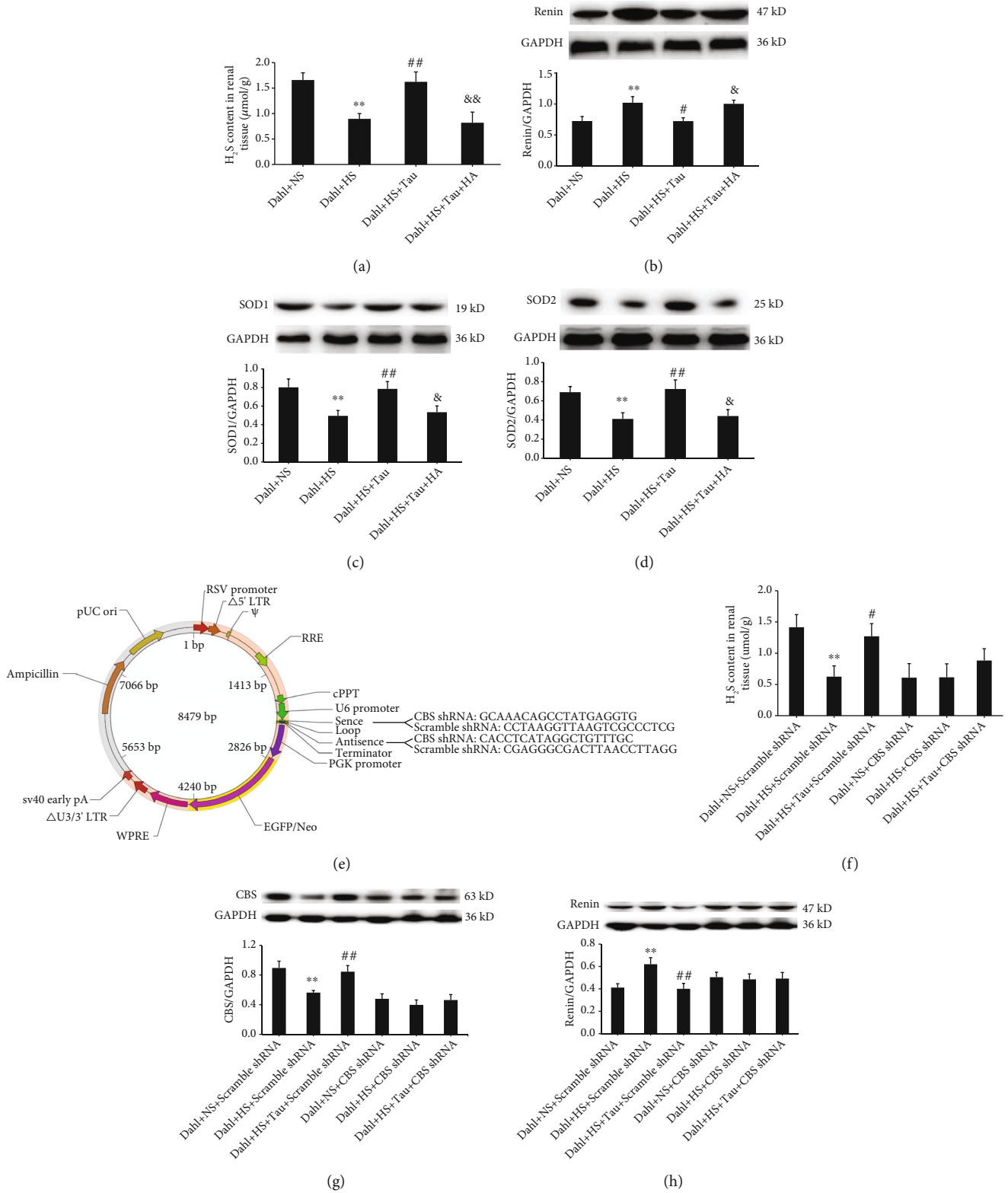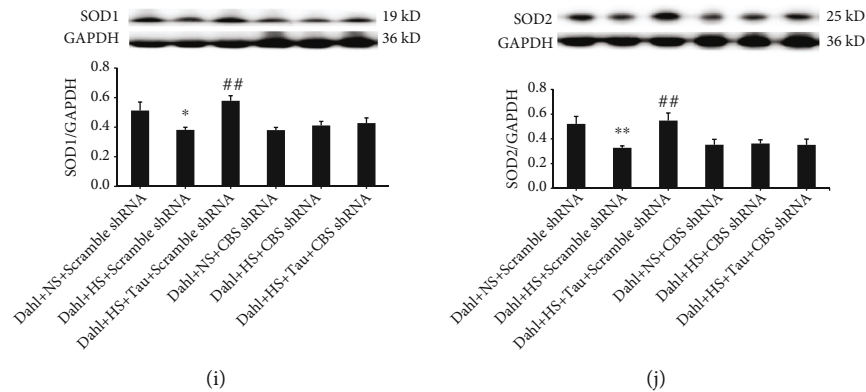
FIGURE 6: Inhibition of cystathionine-β-synthase (CBS) activity or knockdown of CBS expression abolished the action of high-salt treatment or taurine increment on the RAAS and oxidative stress in Dahl rat renal slices *ex vivo*. (a–d) H_2S content (a) and renin (b), SOD1 (c), and SOD2 (d) levels in the renal slices of Dahl rats incubated with medium containing normal salt (NS, 137 mM), high salt (HS, 200 mM), high salt (200 mM) plus taurine (10 mM) (HS+Tau), or high salt (200 mM) plus taurine (10 mM) and HA (50 μM) (HS+Tau+HA). (e) The original sequence of scramble-shRNA and target sequence of CBS-shRNA and lentivirus vector map. (f–j) H_2S content (f) and protein expressions of CBS (g), renin (h), SOD1 (i), and SOD2 (j) in the renal slices of Dahl rats transfected with scramble-shRNA or CBS-shRNA lentivirus and incubated with medium containing NS (137 mM), HS (200 mM), or HS (200 mM)+Tau (10 mM). $n = 8$ for each group. $^*P < 0.05$ and $^{**}P < 0.01$ vs. Dahl+NS; $^{\#}P < 0.01$ and $^{\#\#}P < 0.01$ vs. Dahl+HS; $^{\&}P < 0.05$ and $^{\&\&}P < 0.01$ vs. Dahl+HS+Tau.

data suggested that downregulation of endogenous taurine caused by the HS treatment promoted RAAS activation and oxidative stress in the kidneys of Dahl rats by inhibiting the renal CBS/H_2S pathway.

3.7. High-Salt Diet Caused a Reduction in Endogenous Taurine in association with Endothelial Dysfunction in Dahl Rats. Considering that taurine could improve the repair of damaged endothelial function in SHRs through its antioxidant effect [43], we investigated the contribution of taurine downregulation by the HS diet to endothelial dysfunction. The results showed that the HS diet downregulated CBS, SOD1, and SOD2 protein expression but upregulated renin, gp91phox, p22phox, and p47phox protein expression in the aortic endothelial cells of Dahl rats. Meanwhile, taurine supplementation increased CBS, SOD1, and SOD2 expression but decreased renin, gp91phox, p22phox, and p47phox levels in the aortic endothelial cells of HS diet-fed Dahl rats (Figure 7). There were no differences in these indicators in aortic endothelial cells among the SS-13BN+NS, SS-13BN+HS, and SS-13BN+HS+Tau groups (Figure 7). These data suggest that taurine downregulation caused by the HS diet is associated with endothelial dysfunction.

4. Discussion

In the present study, we first revealed a novel mechanism for salt-sensitive hypertensive renal injury. This mechanism shows that downregulation of the endogenous taurine pathway is a crucial mechanism for renal injury in salt-sensitive hypertension. Furthermore, our study clarified that the decrease in taurine caused by an HS diet suppresses endogenous H_2S production by downregulating renal CBS expression and activity. This process subsequently promotes the activation of the RAAS and oxidative stress in renal tissue, thereby leading to renal damage in Dahl rats (Figure 8).

Taurine can be produced by CDO oxidation and CSAD decarboxylation in organisms with cysteine as the substrate [8]. Taurine exerts a variety of biological effects, including the inhibition of RAAS activity and oxidative stress, vasorelaxation, and the facilitation of water and sodium metabolism [9, 10, 44]. Taurine is closely related to the occurrence of HS-induced hypertension. Taurine can lower blood pressure, reduce the levels of vasoconstrictor active substances, and upregulate vasodilator substance content in Wistar rats with hypertension induced by abdominal aortic stenosis and HS [45]; these results suggest that taurine inhibits the occurrence of renal hypertension possibly through regulating the levels of vasoactive substances. Ideishi et al. later found that exogenous taurine supplementation inhibited the development of hypertension and protected against heart damage associated with increased kallikrein in salt-sensitive Dahl rats [46]. In the stroke-prone SHRs fed an HS diet, taurine supplementation significantly reduced blood pressure and alleviated ventricular hypertrophy [47]. Furthermore, the administration of taurine inhibited LOX-1 expression and exerted an antioxidant effect in the renal tissue of Dahl rats [48]. These studies suggest that exogenous taurine supplementation could prevent the development of hypertension and might have a possible protective effect on hypertension-related target organ damage. However, it is currently unclear how sulfur-containing amino acid metabolism-produced taurine is involved in the mechanism underlying salt-sensitive hypertensive renal damage.

To address this gap, Dahl rats were herein administrated with an HS diet as an animal model of hypertensive renal injury. Salt-resistant SS-13BN rats were used as experimental controls. First, the changes in endogenous taurine and its key enzymes were detected. The results showed that the blood pressure of Dahl rats continued to rise after HS diet administration and increased dramatically at 6 weeks, accompanied by impaired renal function and structure.

(a)

(b)

(c)

(d)

Figure 7: Continued.

(e)

(f)

(g)
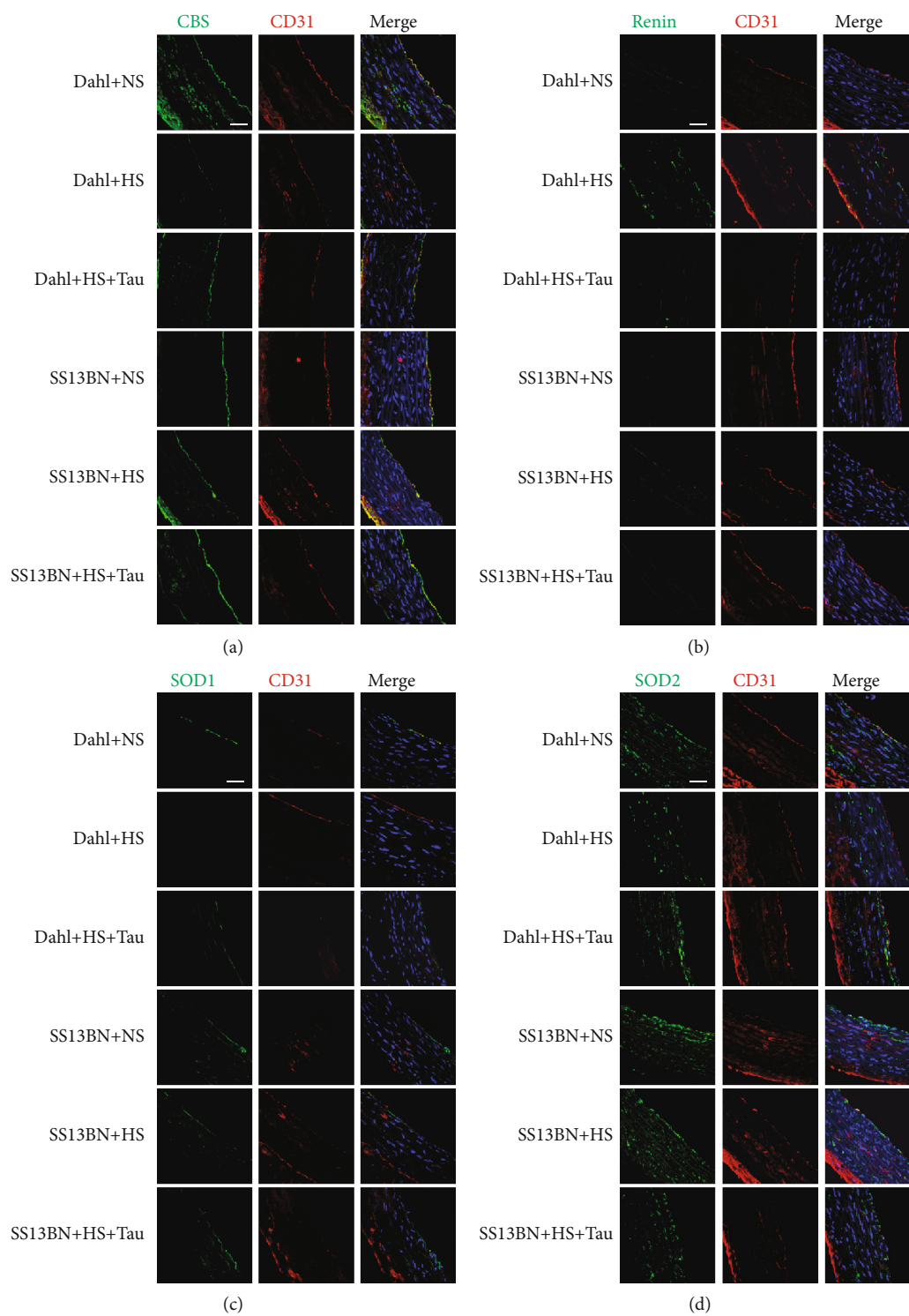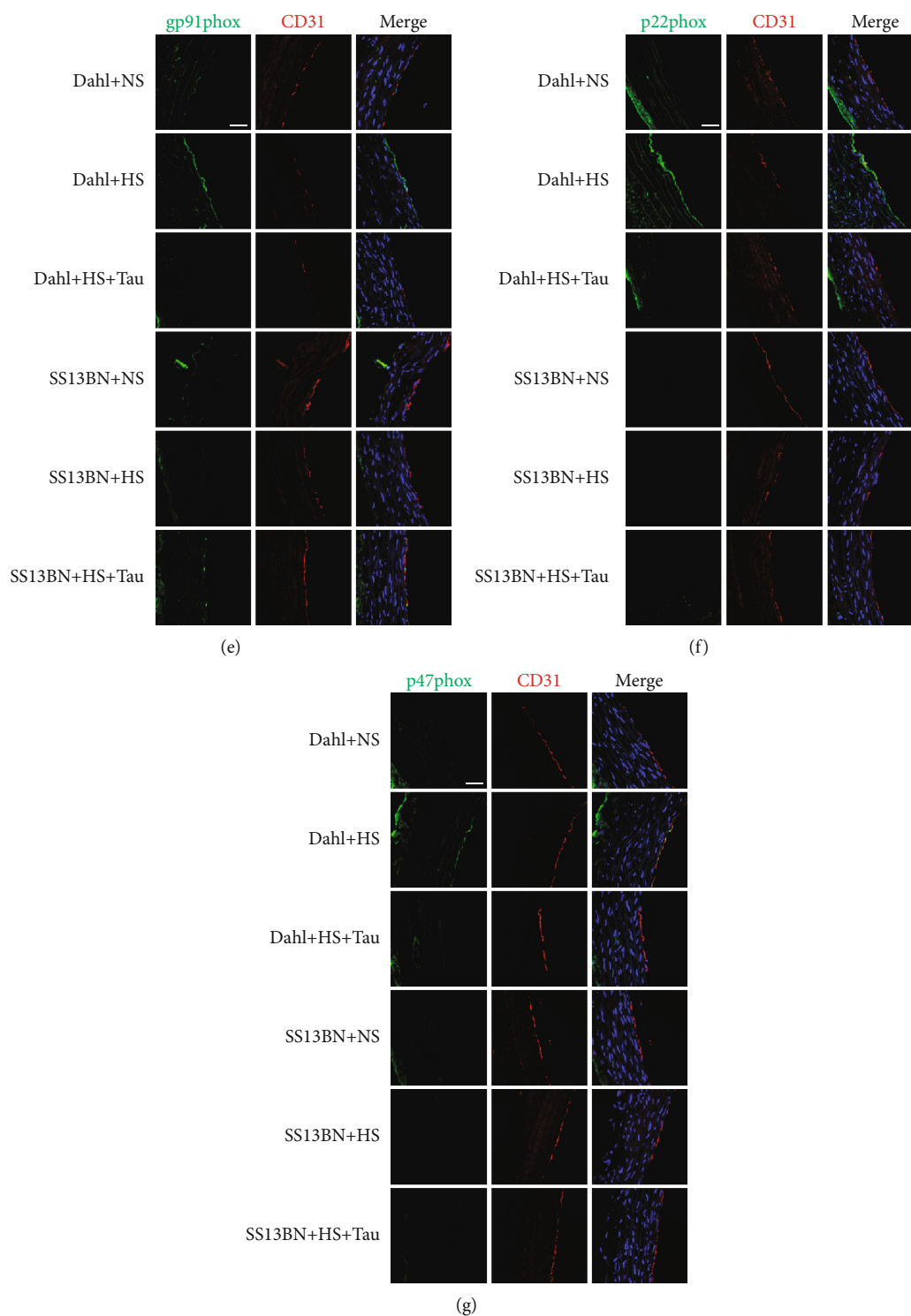
FIGURE 7: Endogenous taurine reduction by high-salt (HS) diet in Dahl rats is associated with endothelial dysfunction. (a–d) Immunofluorescence detection of protein expressions (green fluorescence) of CBS (a), renin (b), SOD1 (c), SOD2 (d), gp91phox (e), p22phox (f), and p47phox (g) in rat aortic endothelial cells. Red fluorescence represents CD31, a marker for endothelial cells. Blue fluorescence represents the nuclei. Scale bars: 40 μm.

Meanwhile, blood pressure was stable, and renal function and structure were normal in SS-13BN rats fed with an HS diet. These results confirmed that the salt-sensitive hypertensive renal injury model was successfully established. In this model, we found that the endogenous taurine content in the renal tissue was significantly reduced and the mRNA and protein expressions of the taurine-producing enzymes, CDO1 and CSAD, were downregulated. Meanwhile, the level of cysteine, the substrate for taurine synthesis, remained unchanged. The HS diet upregulated taurine
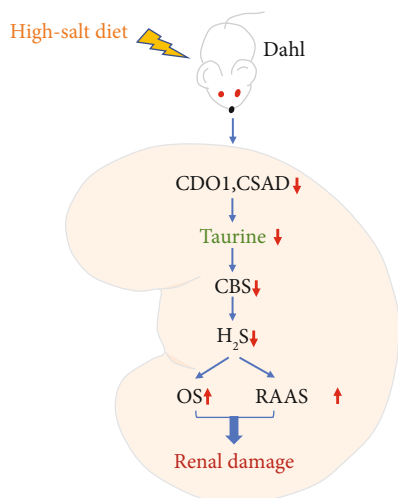
FIGURE 8: A schematic diagram. Downregulation of the endogenous taurine pathway is an important mechanism for renal injury during salt-sensitive hypertension. High salt downregulated endogenous taurine production to reduce renal cystathionine-β-synthase (CBS) expression and activity, subsequently decreasing renal H$_2$S generation, facilitating renin-angiotensin-aldosterone system (RAAS) activation and oxidative stress, and ultimately leading to renal damage in salt-sensitive Dahl rats.

content and CDO1 and CSAD protein expression but downregulated cysteine levels in the renal tissue of SS-13BN rats. These results indicate that endogenous taurine and its key enzymes were significantly downregulated during salt-sensitive hypertensive renal damage.

To further explore the significance of endogenous taurine downregulation in renal injury, we supplemented taurine to HS diet-fed Dahl rats from the perspective of "gain-of-function." Results showed that the taurine content in the HS-administrated Dahl renal tissue was increased after exogenous taurine supplementation, rat SBP was reduced, and the renal functional and structural damage were alleviated. These results suggest that downregulation of the endogenous taurine pathway is an important part of the pathogenesis of salt-sensitive hypertensive renal damage.

The mechanism by which the downregulation of endogenous taurine leads to salt-sensitive hypertensive renal injury is currently unclear. A previous study showed that the plasma H$_2$S level was increased after taurine supplementation in SHRs [15]. The H$_2$S donor NaHS increased renin protein expression in As4.1 cells [49], and CSE overexpression promoted H$_2$S production and inhibited isoproterenol-induced renin release [49]. The serum levels of ACE, AngI, and AngII were significantly increased in L-NAME-induced hypertensive rats, while exogenous taurine supplementation reduced them; these results indicate that the RAAS might mediate the antihypertensive effect of taurine [11]. Chiba et al. [48] found that taurine inhibited LOX-1 expression to protect against salt-sensitive hypertension, and the kidney is an important organ for maintaining blood pressure. These results suggest that oxidative stress might be involved in the mechanism by which taurine regulates salt-sensitive hypertension. Our group previously found that H$_2$S inhibited superoxide anion generation in

human umbilical vein endothelial cells exposed to high salt [34], indicating that H$_2$S could inhibit oxidative stress stimulated by high salt in endothelial cells. It was also found that H$_2$S reduced renin, AngII, and aldosterone contents, decreased the generation of free oxygen radicals, and enhanced antioxidant enzyme activity and expression in the renal tissue of HS diet-fed Dahl rats [24, 28]. Therefore, we hypothesized that the decreased endogenous taurine might reduce endogenous H$_2$S production in the kidney to promote renal RAAS activation and oxidative stress damage, thereby leading to salt-sensitive hypertensive renal damage. Thus, we conducted the following research to examine whether endogenous taurine downregulation contributed to renal damage in salt-sensitive hypertension and its possible mechanisms.

This study suggested that an HS diet reduced renal taurine levels and increased the renin, AngII, and aldosterone contents and renin protein levels in Dahl rat renal tissue; meanwhile, exogenous taurine supplementation increases taurine levels in the kidney significantly inhibiting RAAS activation. However, the HS diet did not activate the RAAS in the renal tissue of SS-13BN rats, which exhibited an increase in renal taurine content. Furthermore, the HS diet promoted renal oxidative stress, while an increase in taurine levels inhibited this oxidative stress in Dahl rats. The MDA, H$_2$O$_2$, ˙OH, and GSSG contents and MPO activity reflect the degree of oxidative stress damage [50]; meanwhile, T-AOC and the CO, GSH, CAT, GSH-PX, SOD1, and SOD2 contents represent antioxidant capacity [51]. This study showed that supplementing HS diet-fed Dahl rats with taurine significantly reduced the renal MDA, H$_2$O$_2$, ˙OH, GSSG, CO, and GSH contents and MPO activity but enhanced renal T-AOC, CAT, GSH-PX, and SOD activity. However, the HS diet could not induce oxidative stress in SS-13BN renal tissue with increased taurine levels. These results demonstrated that the downregulation of taurine caused by the HS diet promoted renal RAAS activation and oxidative stress in Dahl rats.

Interestingly, this study indicated that endogenous taurine reduction inhibited the renal H$_2$S-generating pathway in salt-sensitive hypertensive Dahl rats. CBS, CSE, and MPST, which catalyze endogenous H$_2$S production, are expressed in the kidney [18]. This study revealed that an HS diet downregulated H$_2$S levels, CBS expression and activity, MPST mRNA levels and activity, and CSE mRNA levels in the renal tissue of Dahl rats, while taurine increment restored the renal H$_2$S-generating pathway. The renal endogenous H$_2$S pathway was not altered in the HS or HS +Tau groups of SS-13BN rats.

To determine whether a decrease in the renal H$_2$S pathway could mediate the contribution of endogenous taurine reduction to renal damage, Dahl rat renal slices were treated with the CBS activity inhibitor HA in the *ex vivo* experiments. The results showed that HA treatment could significantly reduce renal H$_2$S content, block the suppressive effect of taurine on renin protein levels, and abolish the enhancement effect of taurine on SOD1 and SOD2 contents in the presence of high salt. These data implied that taurine reduction by high salt promoted the activation of the RAAS and oxidative stress in Dahl renal tissue by inhibiting CBS activity.

Furthermore, Dahl rat kidneys were transfected with CBS-shRNA by using renal puncture to inhibit CBS expression. The kidneys were then isolated and cut into slices for *ex vivo* experiments. Taurine inhibited renin protein expression and promoted SOD1 and SOD2 levels in the scramble-shRNA-transfected Dahl rat kidneys incubated with high salt, which was abolished in renal slices with CBS knockdown. These results suggest that the endogenous CBS/H_2S pathway mediated the action of taurine on RAAS activation and oxidative stress in Dahl rat renal slices exposed to high salt.

The concentration of NaCl in cell buffers such as PBS is 137 mM, and the control group in previous literature was mostly incubated with 137 mM NaCl [24, 34, 52]. Therefore, the NS group in this study was incubated with 137 mmol/L NaCl. Clinical studies have reported that hypernatremia patients developed renal impairment when the serum sodium concentration was close to 200 mM [53]. Many studies also used 200 mM NaCl as a high salinity stimulus [24, 34, 35, 54–56]. Moreover, our previous studies showed that 200 mM NaCl treatment could reduce the level of H_2S in endothelial cells and kidney tissues [24, 34]. Therefore, the HS group in this study was treated with 200 mM NaCl. In a variety of isolated tissue and cell experiments including isolated rat heart, canine kidney cells, vascular smooth muscle cells, rat pancreatic islet cells, retinal glial cells, and Müller cells, 10 mM is the most common dose of taurine used to exert its effects [36, 57–64]. Our previous study has shown that 50 μM HA could significantly inhibit H_2S contents [37]; thus, a dose of 50 μM HA was used in this study.

Trachtman et al. [65] found that 1% taurine in drinking water decreased blood pressure and reduced kidney and heart damage in SHRs; furthermore, its antihypertensive mechanism was independent of catecholamine, indicating that taurine might reduce blood pressure in SHRs by interacting with hormone systems involved in blood pressure regulation. Adedara et al. [66] reported that oral taurine (100 and 200 mg/kg) could significantly reduce blood pressure and ameliorate renal histological damage in L-NAME-induced hypertensive rats. The mechanism was related to the improvement of thyroid system function, an increase in nitric oxide levels, a decrease in myeloperoxidase activity, the enhancement of renal antioxidant enzyme activity, and the inhibition of renal oxidative stress. It was suggested that the evaluation of nitric oxide and the RAAS in the future would help to further explain the possible renal protective mechanism for taurine in L-NAME-induced hypertensive rats. In the present study, we revealed that endogenous taurine inhibited RAAS activation and oxidative stress through increasing the CBS/H_2S pathway in renal tissue, ultimately alleviating renal injury and reducing blood pressure in salt-sensitive hypertensive rats. Previous studies reported that the downregulation of the endogenous H_2S pathway was also an important factor in the pathogenesis of spontaneous hypertension [23] and L-NAME-induced hypertension [25]. These findings indicate that H_2S pathway upregulation might also participate in the renal protection mecha-

nism for taurine in these two models of hypertension; however, this mechanism still requires further study.

Previous studies have reported that 2% taurine in drinking water could significantly decrease blood pressure in L-NAME-induced hypertensive rats [11] and high fructose-induced hypertensive rats [67], upregulate CBS and CSE expression in the aorta of SHRs [15], alleviate kidney damage in hyperuricemia rats [68], and inhibit oxidative stress in the kidneys of diabetic rats [69]. Therefore, a 2% taurine supplementation scheme was chosen for this study. Previous studies have reported that 1% taurine in drinking water had only slight antihypertensive effects on Dahl rats fed with an HS (8%) diet [48], while 3% taurine in drinking water prevented hypertension in Dahl rats fed with an HS (4%) diet [46]. These two taurine supplementation schemes could reduce urinary protein [46, 48] and have antioxidant effects [11, 43, 70], indicating that they have renal protective effects.

Hypertensive chronic renal failure is a huge clinical burden. Lowering blood pressure is an important and widely used method to delay the progression of chronic kidney disease. Currently, there is almost no effective cure or prevention strategy for chronic kidney disease. Due to the lack of symptoms in the early stage of the disease, timely treatment is very challenging. An interesting clinical trial has confirmed that the change in blood pressure was negatively correlated with plasma taurine levels in prehypertensive patients treated with taurine [15]. Our present study suggested that taurine levels in the kidney tissue of salt-sensitive hypertensive rats were significantly reduced, which is an important factor in the pathogenesis of kidney injury. Therefore, taurine may be used as a new biomarker to predict the patient prognosis. Since taurine is an endogenous semiessential amino acid, the side effects of taurine treatment are expected to be small. As such, taurine supplementation may be a promising strategy for the treatment of hypertension and chronic kidney disease.

5. Conclusions

In summary, this study demonstrates that the downregulation of endogenous taurine in the renal tissue of Dahl rats is the main mechanism for salt-sensitive hypertensive renal damage. The decrease in endogenous taurine caused by an HS diet could reduce renal H_2S production via the inhibition of CBS activity and the expression to promote RAAS activation and oxidative stress damage in the kidney, thereby resulting in renal damage in salt-sensitive Dahl rats. Our findings not only deepen the knowledge of the mechanism underlying salt-sensitive hypertensive renal injury but also provide new research ideas and potential therapeutic targets for renal injury. In the future, taurine-based drugs or foods will be expected to be developed for use in the treatment of renal damage.

Data Availability

All data and materials supporting the findings of the current study are available within this article or from the corresponding authors on reasonable request.

Conflicts of Interest

The authors declare that there is no conflict of interest regarding the publication of this paper.

Authors' Contributions

Pan Huang, Yaqian Huang, and Boyang Lv contributed equally to this work.

Acknowledgments

References

[1] G. J. Ko, C. M. Rhee, K. Kalantar-Zadeh, and S. Joshi, "The effects of high-protein diets on kidney health and longevity," *Journal of the American Society of Nephrology*, vol. 31, no. 8, pp. 1667–1679, 2020.

[2] K. A. Griffin, "Hypertensive kidney injury and the progression of chronic kidney disease," *Hypertension*, vol. 70, no. 4, pp. 687–694, 2017.

[3] G. Howard, M. Cushman, C. S. Moy et al., "Association of clinical and social factors with excess hypertension risk in black compared with white US Adults," *JAMA*, vol. 320, no. 13, pp. 1338–1348, 2018.

[4] X. Jiang, X. Liu, X. Liu et al., "Low-dose aspirin treatment attenuates male rat salt-sensitive hypertension via platelet cyclooxygenase 1 and complement cascade pathway," *Journal of the American Heart Association*, vol. 9, no. 1, article e013470, 2020.

[5] N. Tian, K. D. Thrasher, P. D. Gundy, M. D. Hughson, and R. D. Manning Jr., "Antioxidant treatment prevents renal damage and dysfunction and reduces arterial pressure in salt-sensitive hypertension," *Hypertension*, vol. 45, no. 5, pp. 934–939, 2005.

[6] A. T. Robinson, D. G. Edwards, and W. B. Farquhar, "The influence of dietary salt beyond blood pressure," *Current Hypertension Reports*, vol. 21, no. 6, p. 42, 2019.

[7] F. J. He, M. Tan, Y. Ma, and G. A. MacGregor, "Salt Reduction to Prevent Hypertension and Cardiovascular Disease:," *Journal of the American College of Cardiology*, vol. 75, no. 6, pp. 632–647, 2020.

[8] Q. Ma, J. Zhao, W. Cao, J. Liu, and S. Cui, "Estradiol decreases taurine level by reducing cysteine sulfinic acid decarboxylase via the estrogen receptor-α in female mice liver," *American Journal of Physiology. Gastrointestinal and Liver Physiology*, vol. 308, no. 4, pp. G277–G286, 2015.

[9] M. Jakaria, S. Azam, M. E. Haque et al., "Taurine and its analogs in neurological disorders: focus on therapeutic potential and molecular mechanisms," *Redox Biology*, vol. 24, p. 101223, 2019.

[10] M. S. Mozaffari, R. Abdelsayed, C. Patel, H. Wimborne, J. Liu, and S. W. Schaffer, "Differential effects of taurine treatment and taurine deficiency on the outcome of renal ischemia reperfusion injury," *Journal of Biomedical Science*, vol. 17, Supplement 1, p. S32, 2010.

[11] J. Hu, X. Xu, J. Yang, G. Wu, C. Sun, and Q. Lv, "Antihypertensive effect of taurine in rat," *Advances in Experimental Medicine and Biology*, vol. 643, pp. 75–84, 2009.

[12] Y. Nara, Y. Yamori, and W. Lovenberg, "Effect of dietary taurine on blood pressure in spontaneously hypertensive rats," *Biochemical Pharmacology*, vol. 27, no. 23, pp. 2689–2692, 1978.

[13] H. H. Hagar, E. El Etter, and M. Arafa, "Taurine attenuates hypertension and renal dysfunction induced by cyclosporine A in rats," *Clinical and Experimental Pharmacology & Physiology*, vol. 33, no. 3, pp. 189–196, 2006.

[14] A. Inoue, H. Takahashi, L. C. Lee et al., "Retardation of the development of hypertension in DOCA salt rats by taurine supplement," *Cardiovascular Research*, vol. 22, no. 5, pp. 351–358, 1988.

[15] Q. Sun, B. Wang, Y. Li et al., "Taurine supplementation lowers blood pressure and improves vascular function in prehypertension: randomized, double-blind, placebo-controlled study," *Hypertension*, vol. 67, no. 3, pp. 541–549, 2016.

[16] R. Hosoki, N. Matsuki, and H. Kimura, "The possible role of hydrogen sulfide as an endogenous smooth muscle relaxant in synergy with nitric oxide," *Biochemical and Biophysical Research Communications*, vol. 237, no. 3, pp. 527–531, 1997.

[17] B. Lv, S. Chen, C. Tang, H. Jin, J. Du, and Y. Huang, "Hydrogen sulfide and vascular regulation - an update," *Journal of Advanced Research*, vol. 27, pp. 85–97, 2021.

[18] X. Cao and J. S. Bian, "The role of hydrogen sulfide in renal system," *Frontiers in Pharmacology*, vol. 7, p. 385, 2016.

[19] N. Shibuya, S. Koike, M. Tanaka et al., "A novel pathway for the production of hydrogen sulfide from D-cysteine in mammalian cells," *Nature Communications*, vol. 4, no. 1, p. 1366, 2013.

[20] H. Kimura, "The physiological role of hydrogen sulfide and beyond," *Nitric Oxide*, vol. 41, pp. 4–10, 2014.

[21] Y. Zhang, Y. Wang, E. Read et al., "Golgi stress response, hydrogen sulfide metabolism, and intracellular calcium homeostasis," *Antioxidants & Redox Signaling*, vol. 32, no. 9, pp. 583–601, 2020.

[22] Y. Wang, R. Yu, L. Wu, and G. Yang, "Hydrogen sulfide signaling in regulation of cell behaviors," *Nitric Oxide*, vol. 103, pp. 9–19, 2020.

[23] H. Yan, J. Du, and C. Tang, "The possible role of hydrogen sulfide on the pathogenesis of spontaneous hypertension in rats," *Biochemical and Biophysical Research Communications*, vol. 313, no. 1, pp. 22–27, 2004.

[24] P. Huang, S. Chen, Y. Wang et al., "Down-regulated CBS/H_2S pathway is involved in high-salt- induced hypertension in Dahl rats," *Nitric Oxide*, vol. 46, pp. 192–203, 2015.

[25] G. Zhong, F. Chen, Y. Cheng, C. S. Tang, and J. B. Du, "The role of hydrogen sulfide generation in the pathogenesis of hypertension in rats induced by inhibition of nitric oxide synthase," *Journal of Hypertension*, vol. 21, no. 10, pp. 1879–1885, 2003.

[26] M. Lu, Y. H. Liu, H. S. Goh et al., "Hydrogen sulfide inhibits plasma renin activity," *Journal of the American Society of Nephrology*, vol. 21, no. 6, pp. 993–1002, 2010.

[27] J. Li, X. Teng, S. Jin et al., "Hydrogen sulfide improves endothelial dysfunction by inhibiting the vicious cycle of NLRP3 inflammasome and oxidative stress in spontaneously hypertensive rats," *Journal of Hypertension*, vol. 37, no. 8, pp. 1633–1643, 2019.

[28] P. Huang, Z. Shen, J. Liu et al., "Hydrogen sulfide inhibits high-salt diet-induced renal oxidative stress and kidney injury in Dahl rats," *Oxidative Medicine and Cellular Longevity*, vol. 2016, Article ID 2807490, 15 pages, 2016.

[29] Y. Chen, S. Jin, X. Teng et al., "Hydrogen sulfide attenuates LPS-induced acute kidney injury by inhibiting inflammation and oxidative stress," *Oxidative Medicine and Cellular Longevity*, vol. 2018, Article ID 6717212, 10 pages, 2018.

[30] F. Lin, C. Liao, Y. Sun et al., "Hydrogen sulfide inhibits cigarette smoke-induced endoplasmic reticulum stress and apoptosis in bronchial epithelial cells," *Frontiers in Pharmacology*, vol. 8, p. 675, 2017.

[31] M. M. Diaz Encarnacion, G. M. Warner, C. E. Gray et al., "Signaling pathways modulated by fish oil in salt-sensitive hypertension," *American Journal of Physiology. Renal Physiology*, vol. 294, no. 6, pp. F1323–F1335, 2008.

[32] H. Z. Chen, F. Wang, P. Gao et al., "Age-associated sirtuin 1 reduction in vascular smooth muscle links vascular senescence and inflammation to abdominal aortic aneurysm," *Circulation Research*, vol. 119, no. 10, pp. 1076–1088, 2016.

[33] H. Xu, S. Du, B. Fang et al., "VSMC-specific EP4 deletion exacerbates angiotensin II-induced aortic dissection by increasing vascular inflammation and blood pressure," *Proceedings of the National Academy of Sciences of the United States of America*, vol. 116, no. 17, pp. 8457–8462, 2019.

[34] Y. Zong, Y. Huang, S. Chen et al., "Downregulation of endogenous hydrogen sulfide pathway is involved in mitochondrion-related endothelial cell apoptosis induced by high salt," *Oxidative Medicine and Cellular Longevity*, vol. 2015, Article ID 754670, 11 pages, 2015.

[35] W. Mariem, B. R. Kilani, G. Benet et al., "How does NaCl improve tolerance to cadmium in the halophyte *Sesuvium portulacastrum*?," *Chemosphere*, vol. 117, pp. 243–250, 2014.

[36] L. Chang, J. X. Xu, J. Zhao, Y. Z. Pang, C. S. Tang, and Y. F. Qi, "Taurine antagonized oxidative stress injury induced by homocysteine in rat vascular smooth muscle cells," *Acta Pharmacologica Sinica*, vol. 25, no. 3, pp. 341–346, 2004.

[37] J. Du, Y. Huang, H. Yan et al., "Hydrogen sulfide suppresses oxidized low-density lipoprotein (Ox- LDL)-stimulated monocyte chemoattractant protein 1 generation from macrophages via the nuclear factor κB (NF-κB) pathway," *The Journal of Biological Chemistry*, vol. 289, no. 14, pp. 9741–9753, 2014.

[38] J. F. Pei, X. K. Li, W. Q. Li et al., "Diurnal oscillations of endogenous H_2O_2 sustained by p66^{Shc} regulate circadian clocks," *Nature Cell Biology*, vol. 21, no. 12, pp. 1553–1564, 2019.

[39] G. Jia, S. Yu, W. Sun et al., "Hydrogen sulfide attenuates particulate matter-induced emphysema and airway inflammation through Nrf2-dependent manner," *Frontiers in Pharmacology*, vol. 11, p. 29, 2020.

[40] M. H. Stipanuk, "Effect of excess dietary methionine on the catabolism of cysteine in rats," *The Journal of Nutrition*, vol. 109, no. 12, pp. 2126–2139, 1979.

[41] P. Singh, P. Rao, and R. Bhattacharya, "Dose and time-dependent effects of cyanide on thiosulfate sulfurtransferase, 3-mercaptopyruvate sulfurtransferase, and cystathionine λ-lyase activities," *Journal of Biochemical and Molecular Toxicology*, vol. 27, no. 12, pp. 499–507, 2013.

[42] Z. Luan, Y. Wei, X. Huo et al., "Pregnane X receptor (PXR) protects against cisplatin-induced acute kidney injury in mice," *Biochimica et Biophysica Acta (BBA) - Molecular Basis of Disease*, vol. 1867, no. 3, article 165996, 2021.

[43] M. Katakawa, N. Fukuda, A. Tsunemi et al., "Taurine and magnesium supplementation enhances the function of endothelial progenitor cells through antioxidation in healthy men and spontaneously hypertensive rats," *Hypertension Research*, vol. 39, no. 12, pp. 848–856, 2016.

[44] Q. Lv, Q. Yang, Y. Cui et al., "Effects of taurine on ACE, ACE2 and HSP70 expression of hypothalamic-pituitary-adrenal axis in stress-induced hypertensive rats," *Advances in Experimental Medicine and Biology*, vol. 975, Part 2, pp. 871–886, 2017.

[45] G. Dong, L. Zhang, J. Tang, J. Su, and C. Tang, "The effect of taurine on hypertension in rats," *Chinese Pharmacological Bulletin*, vol. 8, no. 5, pp. 403–406, 1992.

[46] M. Ideishi, S. Miura, T. Sakai, M. Sasaguri, Y. Misumi, and K. Arakawa, "Taurine amplifies renal kallikrein and prevents salt-induced hypertension in dahl rats," *Journal of Hypertension*, vol. 12, no. 6, pp. 653–661, 1994.

[47] R. Dawson Jr., S. Liu, B. Jung, S. Messina, and B. Eppler, "Effects of high salt diets and taurine on the development of hypertension in the stroke-prone spontaneously hypertensive rat," *Amino Acids*, vol. 19, no. 3-4, pp. 643–665, 2000.

[48] Y. Chiba, K. Ando, and T. Fujita, "The protective effects of taurine against renal damage by salt loading in Dahl salt-sensitive rats," *Journal of Hypertension*, vol. 20, no. 11, pp. 2269–2274, 2002.

[49] M. Lu, Y. H. Liu, C. Y. Ho, C. X. Tiong, and J. S. Bian, "Hydrogen sulfide regulates cAMP homeostasis and renin degranulation in As4.1 and rat renin-rich kidney cells," *American Journal of Physiology. Cell Physiology*, vol. 302, no. 1, pp. C59–C66, 2012.

[50] B. L. Tan, M. E. Norhaizan, and W. P. Liew, "Nutrients and oxidative stress: friend or foe?," *Oxidative Medicine and Cellular Longevity*, vol. 2018, Article ID 9719584, 24 pages, 2018.

[51] I. Marrocco, F. Altieri, and I. Peluso, "Measurement and clinical significance of biomarkers of oxidative stress in humans," *Oxidative Medicine and Cellular Longevity*, vol. 2017, Article ID 6501046, 32 pages, 2017.

[52] J. Li, J. White, L. Guo et al., "Salt inactivates endothelial nitric oxide synthase in endothelial cells," *The Journal of Nutrition*, vol. 139, no. 3, pp. 447–451, 2009.

[53] J. Jeffery, R. M. Ayling, and R. J. McGonigle, "Successful rescue of severe hypernatraemia (196 mmol/L) by treatment with hypotonic fluid," *Annals of Clinical Biochemistry*, vol. 44, no. 5, pp. 491–494, 2007.

[54] N. Xu, S. Liu, Z. Lu et al., "Gene expression profiles and flavonoid accumulation during salt stress in Ginkgo biloba seedlings," *Plants*, vol. 9, no. 9, p. 1162, 2020.

[55] N. A. Tejera, E. Ortega, J. Gonzalez-Lopez, and C. Lluch, "Effect of some abiotic factors on the biological activity of Gluconacetobacter diazotrophicus," *Journal of Applied Microbiology*, vol. 95, no. 3, pp. 528–535, 2003.

[56] U. Katz, G. Zaccone, S. Fasulo, A. Mauceri, and S. Gabbay, "Lectin binding pattern and band 3 localization in toad skin epithelium and the effect of salt acclimation," *Biology of the Cell*, vol. 89, no. 2, pp. 141–152, 1997.

[57] H. Nonaka, T. Tsujino, Y. Watari, N. Emoto, and M. Yokoyama, "Taurine prevents the decrease in expression and secretion of extracellular superoxide dismutase induced by homocysteine: amelioration of homocysteine-induced endoplasmic reticulum stress by taurine," *Circulation*, vol. 104, no. 10, pp. 1165–1170, 2001.

[58] J. Bustamante, M. V. Lobo, F. J. Alonso et al., "An osmotic-sensitive taurine pool is localized in rat pancreatic islet cells containing glucagon and somatostatin," *American Journal of Physiology. Endocrinology and Metabolism*, vol. 281, no. 6, pp. E1275–E1285, 2001.

[59] I. Hizoh and C. Haller, "Radiocontrast-induced renal tubular cell apoptosis: hypertonic versus oxidative stress," *Investigative Radiology*, vol. 37, no. 8, pp. 428–434, 2002.

[60] L. Chang, J. Zhao, J. Xu, W. Jiang, C. S. Tang, and Y. F. Qi, "Effects of taurine and homocysteine on calcium homeostasis and hydrogen peroxide and superoxide anions in rat myocardial mitochondria," *Clinical and Experimental Pharmacology & Physiology*, vol. 31, no. 4, pp. 237–243, 2004.

[61] T. Ueno, Y. Iguro, G. Yotsumoto et al., "Taurine at early reperfusion significantly reduces myocardial damage and preserves cardiac function in the isolated rat heart," *Resuscitation*, vol. 73, no. 2, pp. 287–295, 2007.

[62] K. Zeng, H. Xu, M. Mi et al., "Effects of taurine on glial cells apoptosis and taurine transporter expression in retina under diabetic conditions," *Neurochemical Research*, vol. 35, no. 10, pp. 1566–1574, 2010.

[63] K. Zeng, H. Xu, K. Chen et al., "Effects of taurine on glutamate uptake and degradation in Muller cells under diabetic conditions via antioxidant mechanism," *Molecular and Cellular Neurosciences*, vol. 45, no. 2, pp. 192–199, 2010.

[64] S. Lin, G. Wu, D. Zhao et al., "Taurine increases insulin expression in STZ-treated rat islet cells in vitro," *Advances in Experimental Medicine and Biology*, vol. 975, Part 1, pp. 319–328, 2017.

[65] H. Trachtman, R. Del Pizzo, P. Rao, N. Rujikarn, and J. A. Sturman, "Taurine lowers blood pressure in the spontaneously hypertensive rat by a catecholamine independent mechanism," *American Journal of Hypertension*, vol. 2, 12, Part 1, pp. 909–912, 1989.

[66] I. A. Adedara, S. E. Alake, L. O. Olajide, M. O. Adeyemo, T. O. Ajibade, and E. O. Farombi, "Taurine ameliorates thyroid hypofunction and renal injury in L-NAME-induced hypertensive rats," *Drug Research*, vol. 69, no. 2, pp. 83–92, 2019.

[67] A. T. Nandhini and C. V. Anuradha, "Hoe 140 abolishes the blood pressure lowering effect of taurine in high fructose-fed rats," *Amino Acids*, vol. 26, no. 3, pp. 299–303, 2004.

[68] Y. Feng, F. Sun, Y. Gao et al., "Taurine decreased uric acid levels in hyperuricemic rats and alleviated kidney injury," *Biochemical and Biophysical Research Communications*, vol. 489, no. 3, pp. 312–318, 2017.

[69] H. T. Yao, P. Lin, Y. W. Chang et al., "Effect of taurine supplementation on cytochrome P450 2E1 and oxidative stress in the liver and kidneys of rats with streptozotocin-induced diabetes," *Food and Chemical Toxicology*, vol. 47, no. 7, pp. 1703–1709, 2009.

[70] S. Murakami, T. Sakurai, Y. Toda, A. Morito, M. Sakono, and N. Fukuda, "Prevention of neointima formation by taurine ingestion after carotid balloon injury," *Vascular Pharmacology*, vol. 53, no. 3-4, pp. 177–184, 2010.

Research Article

Ameliorative Effects and Mechanism of Buyang Huanwu Decoction on Pulmonary Vascular Remodeling: Network and Experimental Analyses

Yucai Chen [ID],[1] **Lidan Cui** [ID],[1] **Can Wang** [ID],[2] **Jianing Liu** [ID],[2] and **Jian Guo** [ID][1]

[1]*School of Traditional Chinese Medicine, Beijing University of Chinese Medicine, Beijing 100029, China*
[2]*School of Chinese Pharmacy, Beijing University of Chinese Medicine, Beijing 100029, China*

Correspondence should be addressed to Yucai Chen; 201801009@bucm.edu.cn and Jian Guo; guojian@bucm.edu.cn

Pulmonary hypertension (PH) is a severe and progressive cardiovascular disease. Its pathological mechanism is complex, and the common pathological feature is pulmonary vascular remodeling. The efficacy of existing therapeutic agents is limited. Traditional Chinese medicine (TCM) has its unique advantages in the prevention and treatment of complex diseases. In this study, the approaches of network pharmacology combined with biological verification are employed to explore the role of Buyang huanwu decoction (BYHWD) in the treatment of PH. The active ingredients in BYHWD were first screened based on the ADME properties of the compounds. In turn, the mean of data mining was utilized to analyze the potential targets of BYHWD for the treatment of PH. On this basis, a series of interaction networks were constructed for searching the core targets. The genes including AKT1, MMP9, NOS3/eNOS, and EGFR were found to be possible key targets in BYHWD. The results of enrichment analysis showed that the targets of BYHWD focused on smooth muscle cell proliferation, migration, and apoptosis, which are classic biological processes involved in pulmonary vascular remodeling and are closely related to the PI3K-Akt-eNOS pathway. The methods of biological experiments were adopted to verify the above results. The present study elucidated the mechanism of BYHWD in the treatment of PH and provided new ideas for the clinical use of TCM in the treatment of PH.

1. Introduction

Pulmonary hypertension (PH) is a progressive vascular disease that affects the small pulmonary arteries and is characterized by heightened proliferation and apoptosis resistance of pulmonary arterial smooth muscle cells (PASMCs) [1]. Elevated pulmonary vascular resistance results in increased pulmonary arterial pressure, right ventricular failure, and ultimately death [2]. Current therapeutics for PH in clinic mainly include endothelin receptor antagonists, prostacyclin analogs, and phosphodiesterase-5 (PDE-5) inhibitors [3]. The aetiology of PH is complex, involving vasoconstriction/-diastolic imbalance, gene mutation, in situ thrombosis, inflammatory response, and oxidative stress [4]. However, most drugs highlight the effect on one kind of cell, one cytokine, or one gene, without considering the complex process of PH [5].

Various kinds of complementary and/or alternative medicines have attracted growing interest in the long-term treatment of complex diseases with approved curative therapeutic effects. Relevant studies have shown that the traditional Chinese medicine (TCM) and active natural products generate attractive effects on PH treatment and rehabilitation. Maxingxiongting mixture, composed of four herbs, could attenuate hypoxia-induced PH and improve right ventricular hypertrophy by inhibiting the rho-kinase signaling pathway [6]. The Qishen Yiqi formula may play a therapeutic role in PH through the PI3K-Akt, MAPK, and HIF-1 signaling pathways [7]. The Qiliqiangxin formula could inhibit PH-induced right ventricular remodeling by reducing mitochondrial-related apoptosis pathway and reversing mitochondrial-related metabolic transition [8]. Therefore, the TCM has its unique advantages in the treatment of complex diseases such as PH because of its multicomponent,

multitarget, and multipathway mechanism characteristics. It is particularly important to explore the underlying mechanisms of these TCM formulas that have been widely used and are highly effective in the clinic for their promotion and optimization. But just using traditional biological experimental methods to explore the mechanism of TCM has its limitation. Network pharmacology provides a new way to solve this problem. By constructing the compounds-targets-diseases network as well as the subsequent topological parameter analysis, the key targets and signaling pathways through which drugs exert their effects can be extracted from the complex interaction relationships, providing new ideas for investigating the multitarget drug treatment as well as mechanism [9, 10].

Buyang huanwu decoction (BYHWD) is a well-known traditional Chinese medicine formula. The BYHWD is composed of seven kinds of Chinese medicine: Huangqi (Radix Astragali seu Hedysari), Danggui (Radix Angelicae Sinensis), Chishao (Radix Paeoniae Rubra), Chuanxiong (Rhizoma Ligustici Chuanxiong), Taoren (Semen Persicae), Honghua (Flos Carthami), and Dilong (Pheretima), and all of which are recorded in the Chinese Pharmacopoeia. Clinical and preclinical studies indicate the protective functions of BYHWD on cardiocerebrovascular disease [11–13]. Despite its clinical effectiveness, the mechanism of BYHWD on pulmonary vascular diseases has not been fully investigated.

In the present study, network pharmacology approaches were employed to investigate potential pharmacological mechanisms of BYHWD as a therapy for PH. Targets of compounds in BYHWD and PH-related genes were acquired from public databases. Then, the protein-protein interaction (PPI) was obtained to analyze the key targets, and Gene Ontology (GO) and Kyoto Encyclopedia of Genes and Genomes (KEGG) enrichment was performed to find the potential mechanism of BYHWD against PH. In addition, *in vivo* experiments were conducted to verify the key targets and pathway predicted in the network. Figure 1 illustrates the workflow.

2. Materials and Methods

2.1. Screening the Components of BYHWD and Predicting Targets of the Components.
The components of seven herbs were collected through the traditional Chinese medicine systems pharmacology platform (TCMSP, http://old.tcmsp-e.com/tcmsp.php) and TCM Taiwan database (http://tcm.cmu.edu.tw/zh-tw/) [14, 15]. Oral bioavailability (OB), Caco-2 permeability, and drug like availability (DL) are important pharmacokinetic parameters to evaluate the drugability of compounds in the ADME process. The parameters of active compounds for selection were set as follows: OB > 30%, DL > 0.18, and Caco-2 > −0.4 [16]. Some compounds were extremely high in content or were reported to have strong pharmacological activities; then, they were included in further evaluation, even if they did not completely meet the above screening principles. Totally, we collected 93 compounds in BYHWD. The detailed information about chemical constituents of each herb in BYHWD is showed in Table S1. The obtained Mol2 type files of ingredients were retrieved using the TCMSP database. Next, potential targets

were predicted by importing each Mol2 formatted file into the Pharmmapper online tool (http://www.lilab-ecust.cn/pharmmapper/) [17]. Based on the normalized fit score, the top 10 highly matching targets of each were selected. In addition, the SMILES structural information of compounds was obtained through the PubChem database, and targets with a match score greater than 0.5 for each compound were retrieved in the SwissTargetPrediction database based on the principle of structural similarity (http://www.swisstargetprediction.ch/) [18].

2.2. Collecting the PH-Related Targets.
With "pulmonary hypertension" as the keyword, the genes associated with PH were collected from the DisGeNET database (http://www.disgenet.org) and the Comparative Toxicogenomics Database (http://ctdbase.org/) [19]. Duplicate genes in the search results were discarded. The UniProt database (http://www.uniprot.org/) was used to acquire the standard gene symbol with the organism selected as "Homo sapiens." Finally, a total of 901 genes associated with PH was obtained. The intersection of targets of active components and PH-related targets was considered to be potential therapeutic targets of BYHWD against PH. The details are described in Table S2.

2.3. Construction of the PPI Network.
The STRING database (https://www.string-db.org/) includes both direct physical interactions and indirect functional correlations between proteins. It contains not only experimental data, results from PubMed abstracts, and other database data but also the results predicted by bioinformatics methods [20]. Using this platform, the interaction relationship network among potential targets of BYHWD was constructed. Network visualization was performed using Cytoscape 3.8.2. Topological parameters of these nodes such as the degree, betweenness centrality, closeness centrality, and average shortest path were analyzed by Network Analyzer in Cytoscape software. Among them, the degree value, one of the most predominant topological parameters in the network, was used to characterize the degree of nodes. The larger the value of the degree parameter of a node, the more central the node was considered in the topological network.

2.4. Gene-Phenotype Correlation Analysis.
The VarElect online platform (https://varelect.genecards.org/), which is an integral part of the GeneCards database, can analyze the correlation of a large number of input genes with a certain clinical phenotype [21]. The input genes were divided into phenotype-directly related genes and phenotype-indirectly related genes, and the score of correlation was obtained. According to VarElect's calculation method, the correlation score in the result is derived from the frequency of a specific phenotype in individual GeneCards. The higher the score, the higher the correlation between the gene and a specific phenotype [21]. In this study, this tool was used to analyze the correlation between the potential targets of BYHWD and the phenotype of "pulmonary hypertension."

2.5. GO and KEGG Enrichment.
The Database for Annotation, Visualization, and Integrated Discovery (DAVID, https://david.ncifcrf.gov/home.jsp, ver. 6.8) was applied for
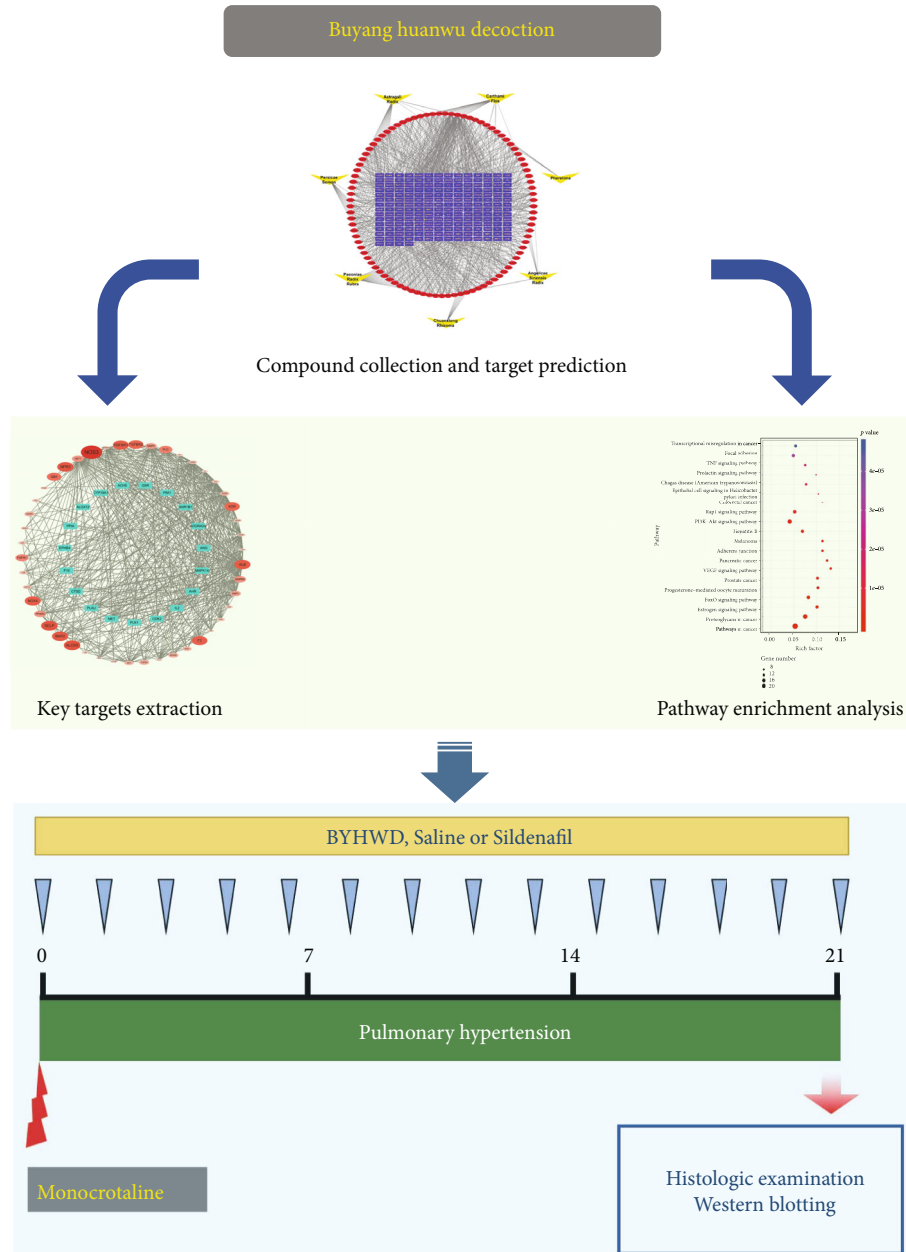
FIGURE 1: A schematic diagram of the integrative strategy combining network pharmacology analysis and biological experiments for investigation of the effect and mechanisms of BYHWD against PH.

GO and KEGG enrichment analysis [22]. The potential therapeutic targets of BYHWD against PH were input into the DAVID platform, and the species was set as "Homo sapiens." The biological processes (BP), molecular functions (MF), and KEGG pathway enrichment analysis were carried out, respectively. Only GO terms and KEGG pathways with P values < 0.01 were included. Not only that, the potential therapeutic targets of BYHWD against PH were entered into the KEGG Mapper (https://www.genome.jp/kegg/mapper.html) for further analysis of genes included in key pathways. Based on these results, the top 20 terms with the smallest P value and their parameters are uploaded to Omicshare (https://www.omicshare.com/) online tools for further visual analysis.

2.6. PH Animal Model and Drug Treatment. The adult male Sprague-Dawley rats (180–220 g) were supplied by the Vital River Laboratory Animal Center (Beijing, China). The animals were housed under a 12 h light-dark cycle at the condition with a temperature at 21–25°C and the humidity of 55%–65%. The rats were allowed access to water and commercial food. All the animal procedures were performed in accordance with the *Guide for the Care and Use of Laboratory Animals* (National Institutes of Health (NIH), USA). The monocrotaline (MCT) was purchased from Sigma-Aldrich, St. Louis, MO. The sildenafil was purchased from Yuanye Bio-Technology Co., Ltd (Shanghai, China). The BYHWD concentrated granules were obtained from Beijing Tcmages Pharmaceutical Co., Ltd (Beijing, China). Rats in the MCT-
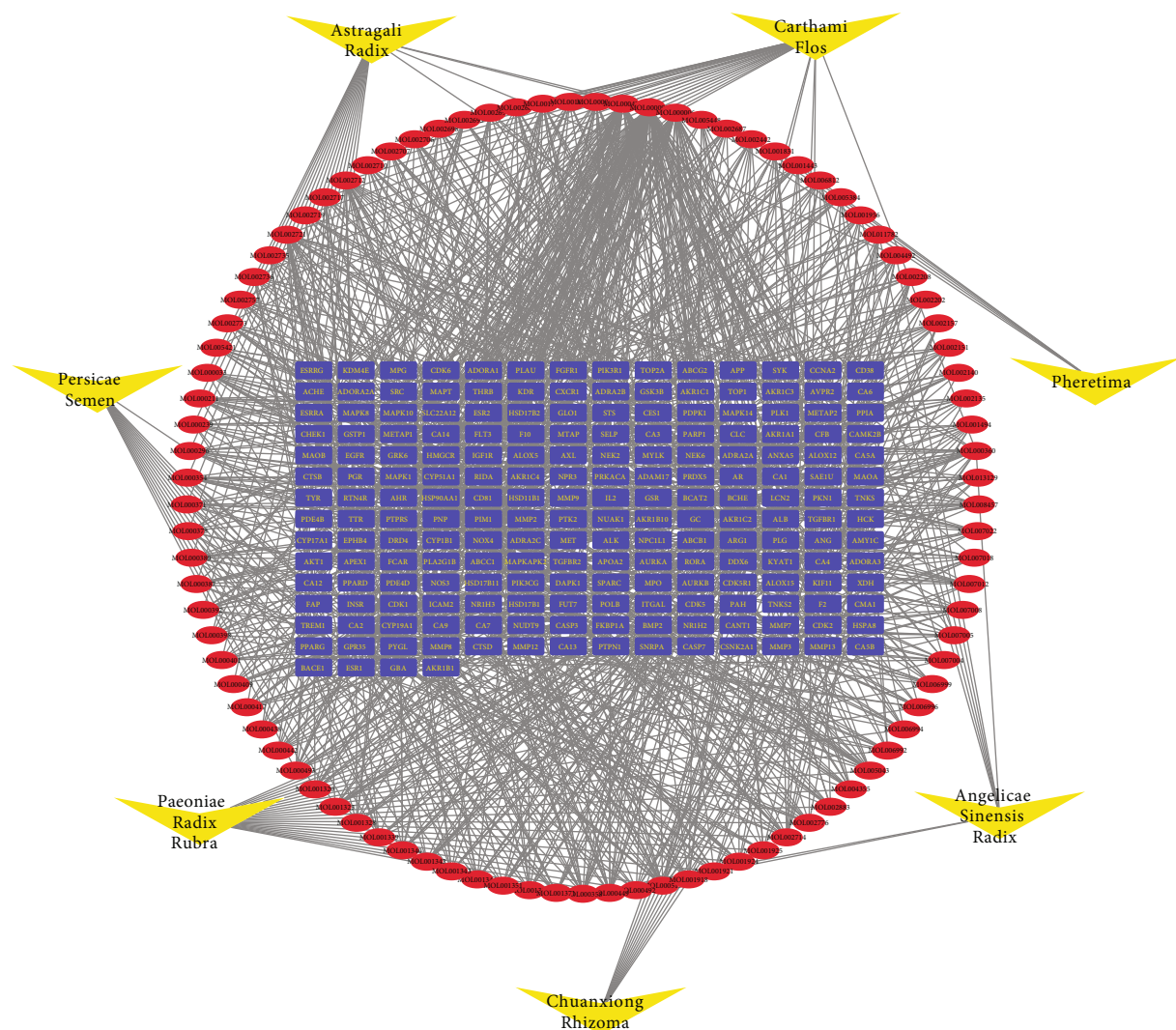
Figure 2: Global herbs-compounds-targets network in the BYHWD. Yellow nodes represent herb components in the formula, 93 red nodes represent compound components in each herb, 200 blue nodes remark the targets of BYHWD from prediction and literature mining, and edges represent interactions between them.

induced PH groups received a single subcutaneous injection of MCT (50 mg/kg) on day 1. The animals were further treated with either saline (MCT group), BYHWD solution (20 g/kg daily for 21 days, the BYHWD groups), or sildenafil solution (20 mg/kg daily for 21 days, the sildenafil groups, as the positive drug group). The control group was treated with saline but did not receive MCT injection.

2.7. Histologic Examination. By the experimental endpoint, the rats were euthanized. The left lung was removed and formalin-fixed and paraffin-embedded. Serial sections (5μm) were routinely stained using Masson's trichrome staining. Digital images were obtained at 200x magnification by microscopy (Olympus, Tokyo, Japan). The medial wall thickness was measured as described previously [23].

2.8. Western Blot. To separate the protein of lungs, the left lung samples were homogenized with whole lysis buffer (con-

taining 0.02 mol/L Tris-HCl, 1% Triton X-100, 0.15 mol/L NaCl, 1 mmol/L ethylenediamine tetraacetic acid, 1 mmol/L EGTA, 2.5 mmol/L sodium pyrophosphate, 1 mmol/L β-glycerophosphate, and 1 mmol/L sodium orthovanadate). Western blot assays of PI3K, Akt, and eNOS were carried out by standard protocols based on the previous study [24]. In brief, the supernatants were fractionated by 8% or 10% SDS-PAGE and then electrotransferred onto a PVDF membrane. The membranes were blocked with 5% BSA in Tris-buffered saline plus 0.1% Tween-20 (TBST) for 1 h at 37°C. Then, they were subjected to an immunoblotting assay using primary antibodies to PI3K (Abcam, ab40755, 1 : 1000), phospho-Akt (Abcam, ab81283, 1 : 1000), total-Akt (Abcam, ab179463, 1 : 2000), and eNOS (CST, 32027, 1 : 1000) as well as β-actin (Proteintech, 66009, 1 : 2000) as an internal reference. After incubation with a properly titrated second antibody, the immunoblot on the membrane was visible after development with an enhanced chemiluminescence (ECL) system.
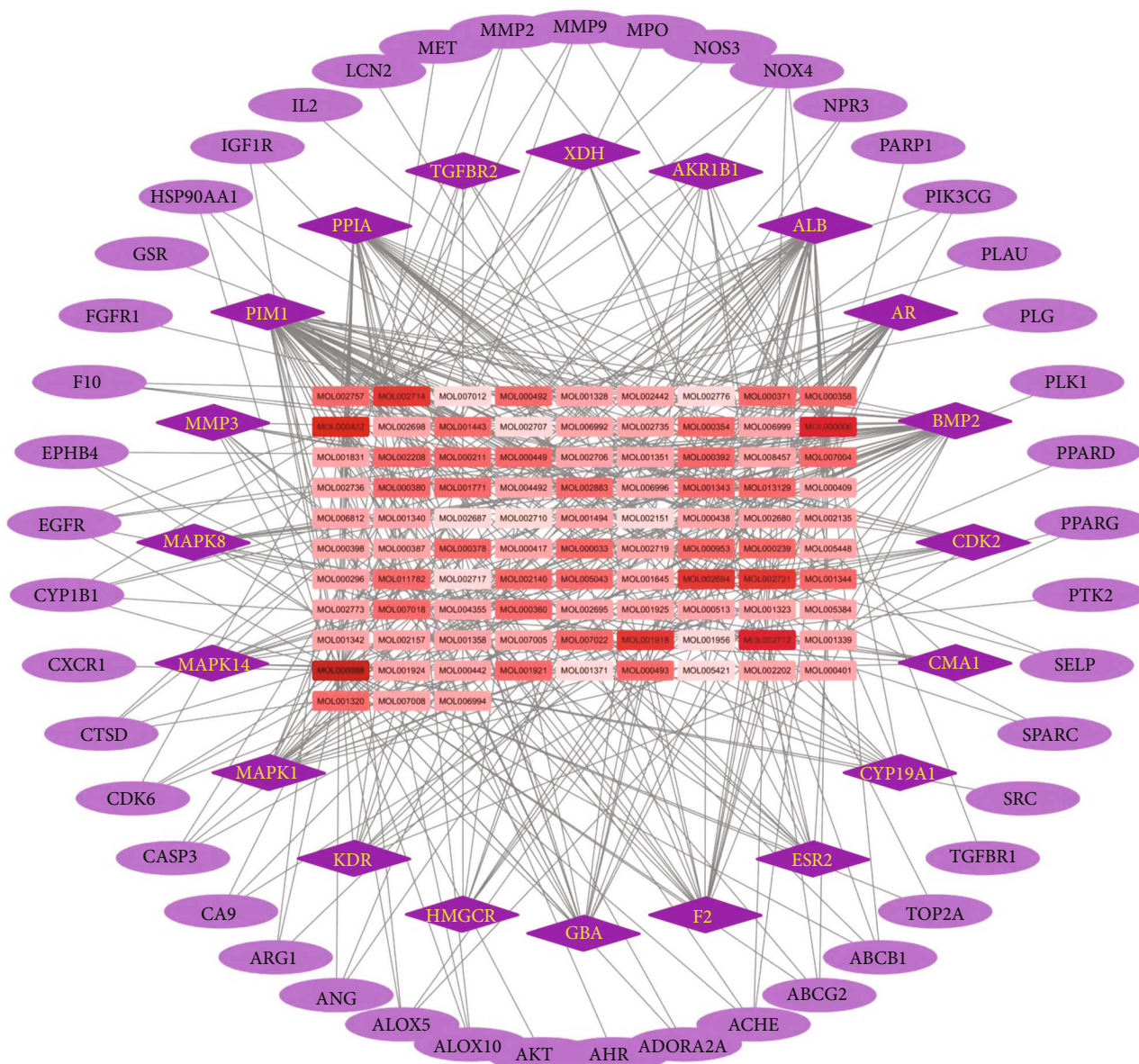
Figure 3: Specific compounds-targets network of ingredients against PH in the BYHWD. The purple nodes represent the potential therapeutic targets of BYHWD against pH, among which the 20 nodes in dark purple were the core nodes in the network. The red square nodes remark the compounds that are linked to the therapeutic targets, and the darker the red color, the higher its degree value in the network.

2.9. Statistical Analysis. Data are expressed as the mean ± SEM of at least three independent experiments and analyzed by GraphPad Prism 7 (GraphPad Software, San Diego, CA, USA). Statistical analysis was performed using one-way analysis of variance (ANOVA) followed by Dunnett's multiple comparison test. A *P* value less than 0.05 was regarded as significant.

3. Results

3.1. Screening of Active Ingredients and Targets of BYHWD. According to the properties of compounds such as OB and DL, 93 components were screened out from seven herbs. Part of the compounds, such as ferulic acid (MOL000360), chrysanthemaxanthin (MOL004492), and stigmasterol (MOL000449), are present simultaneously in multiple herbs. Based on structural similarity prediction and reverse molecular docking, a total of 200 predicted targets of the compounds were collected (Figure 2). The above results partly illustrate that there is a common effect for the individual constituent components in the formula.

3.2. Interaction Analysis of Anti-PH-Related Ingredients and Targets in BYHWD. Through further analysis, 65 targets associated with PH among all targets of BYHWD were obtained. Ingredients in BYHWD associated with these 65
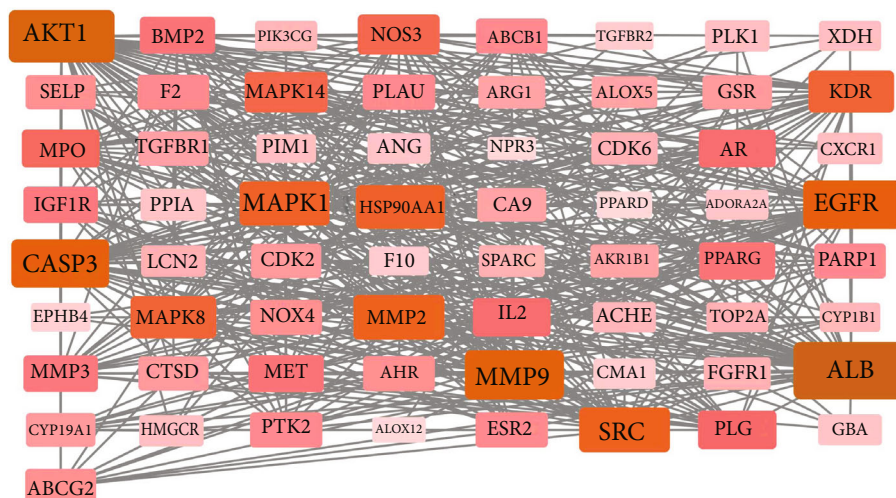
FIGURE 4: Network biology analysis for PPI constructed with potential targets of BYHWD against PH. In the network, nodes represent targets. Edges (gray) represent PPI interactions. The color intensity of a node is proportional to the value of a degree in the network.

targets were acquired. The compounds-targets network was constructed by Cytoscape software. As shown in Figure 3, the C-T network consists of 158 nodes (93 compounds and 65 PH-related targets) and 904 C-T interactions. In order to find the main active compounds, the topological parameters of the network were further analyzed. The results indicated that the compounds with the highest degree parameter in the network included quercetin, kaempferol, luteolin, 6-hydroxykaempferol, quercetagetin, and baicalein. These compounds may play a more important role in the anti-PH effects of BYHWD.

3.3. Constructing PPI Networks and Analyzing Network Topological Features.
The degree is one of the important topological parameters, which equals the number of links connected to and also the number of neighbors of the node. The value of the degree reflects the importance of the node in the network. Using the STRING online tool, the PPI network of BYHWD's potential targets for the treatment of PH was constructed. As shown in Figure 4, the targets with higher degree values in the network included AKT1, ALB, and MMP9. These key targets were more interconnected with the other targets and were also involved in multiple signaling pathways. So, these core targets may play a more critical role in the anti-PH effects of BYHWD.

3.4. Gene-Phenotype Correlation Analysis of the Targets of BYHWD.
PH is a kind of disease with complex pathogenesis. A large number of genes are implicated in the development and progression of PH. These genes vary in the level of significance of the role they are involved in. With the VarElect online tool, potential targets to the PH phenotype correlations were analyzed. Among the 65 analyzed genes, 46 were directly associated with the disease phenotype and 19 were indirectly associated (Figure 5). Among the genes directly associated with PH, the 10 most strongly associated genes were NOS3, ALOX5, SELP, NPR3, BMP2, ALB, NOX4,

TGFBR1, F2, and KDR (Table 1). Many of these genes also coincide with the core genes in the PPI network.

3.5. Gene Ontology Analysis.
The enrichment analysis of potential targets of BYHWD in the treatment of PH was performed using the DAVID platform to explore the BP and MF in which these targets were involved. As shown in Figure 6 and Tables S3 and S4, potential therapeutic targets are involved in many biological processes, including "negative regulation of apoptotic process," "positive regulation of cell migration," "angiogenesis," "positive regulation of cell promotion," "positive regulation of protein kinase b signaling," "positive regulation of smooth muscle cell promotion," "response to hypoxia," and "positive regulation of phosphatidylinositol 3-kinase signaling." The molecular function terms involved in these targets included "ATP binding," "enzyme binding," "protein tyrosine kinase activity," and "protein binding." Obviously, many of the biological processes enriched were closely related to the mechanism of vascular remodeling in PH.

3.6. Pathway Enrichment Analysis.
To further clarify the relationship between targets and the pathways, as described previously, the KEGG databases and the KEGG Mapper online tool were used for pathway enrichment analysis. The top 20 pathways involving 65 targets were screened. The results showed that the targets were mainly involved in the FoxO signaling pathway, VEGF signaling pathway, PI3K-Akt signaling pathway, TNF signaling pathway, and so on (Figure 7 and Figure 8).

3.7. Experimental Validation.
To further investigate the effect of BYHWD on pulmonary vascular remodeling, a MCT-induced PH model was constructed. The Masson trichrome staining was used to observe the thickness of small pulmonary vessels. Pulmonary vessels with a diameter less than $150 \, \mu m$ were included to calculate vessel wall thickening. The results showed that the thickness of pulmonary small vessels was significantly increased after administration of
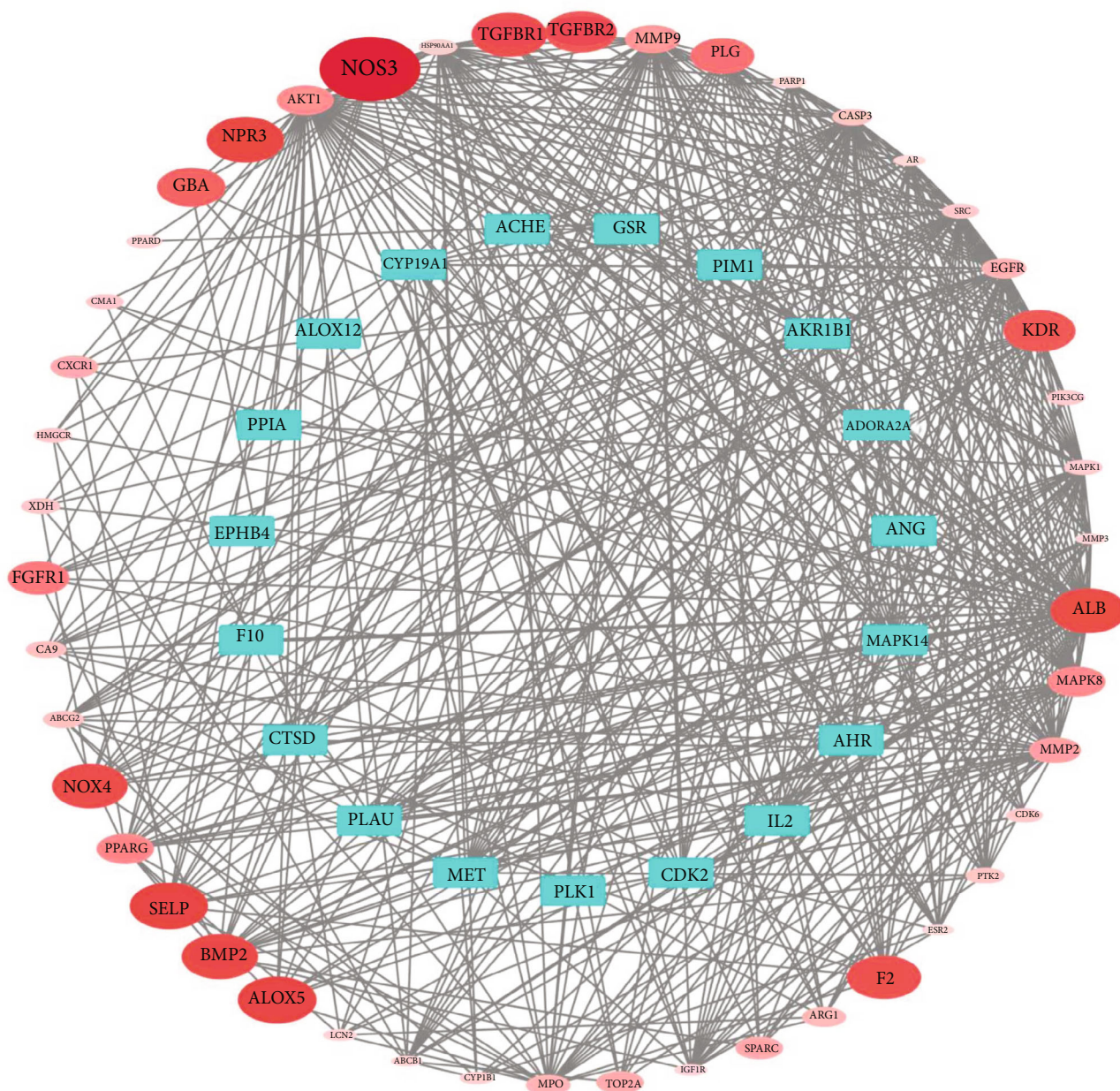
FIGURE 5: Correlation between target genes and the PH phenotypes. Green nodes located on the inner circle represent genes that are indirectly associated with PH. The red nodes located on the outer ring represent the directly related genes. The degree of darkness of node color is proportional to its phenotypic relevance.

MCT and was significantly decreased by both BYHWD treatment and positive drug sildenafil treatment (Figure 9). According to the above mechanistic analysis, the eNOS and PI3K-Akt pathway may be the key targets of BYHWD in the treatment of PH. The approach of the biological experiment was taken to validate the obtained key targets and pathways. The results of western blot showed that the activation of the PI3K-Akt pathway was significantly reduced and the expression level of eNOS was decreased in MCT-treated rats. After administration with BYHWD, the levels of the PI3K-Akt-eNOS pathway were significantly upregulated (Figure 10).

4. Discussion

The prevalence of PH and the incapability of existing vasodilation therapy in confronting the complex feature disorder make the present treatment strategies controversial. TCM formulas produce synergistic effects by potentially active ingredients acting in a multitarget and multipathway biological network, thereby interfering with the occurrence and development of diseases and finally achieving therapeutic effects. BYHWD has been widely used in the treatment of many cardiovascular and cerebrovascular diseases. A recent study reported that BYHWD could promote neurological

TABLE 1: Top 10 targets directly associated with PH phenotype.

Gene symbol	Description	Score
NOS3	Nitric oxide synthase 3	21.08
ALOX5	Arachidonate 5-lipoxygenase	14.37
SELP	Selectin P	14.25
NPR3	Natriuretic peptide receptor 3	13.96
BMP2	Bone morphogenetic protein 2	13.68
ALB	Albumin	13.56
NOX4	NADPH oxidase 4	13.42
TGFBR1	Transforming growth factor beta receptor 1	13.32
F2	Coagulation factor II, thrombin	12.99
KDR	Kinase insert domain receptor	12.33

recovery and after intracerebral hemorrhage by activating VEGFR2 through the PI3K/Akt signaling pathway [11]. The active components of BYHWD have multitarget neuroprotective effects on ischemic stroke, and its mechanism may be closely related to the improvement of blood supply [25]. A study based on a tag-based digital gene expression profiling (DGE) system showed that the mechanism of ventricular remodeling induced by myocardial infarction by BYHWD treatment may be closely related to transforming growth factor beta receptor-1, junctophilin-2, and monocyte [26]. In this study, network pharmacology-based approaches were conducted to explore the underlying mechanism of BYHWD in PH.

Firstly, we predicted the potential targets of BYHWD for the treatment of PH combining potential active ingredients, putative targets of compounds in BYHWD, and targets of PH. Through constructing the herbs-compounds-targets network as well as analyzing topological parameters, the active compounds in BYHWD for the treatment of PH were extracted, including quercetin, kaempferol, luteolin, 6-hydroxykaempferol, quercetagetin, and baicalein. Many studies have reported the anti-PH effects of these compounds *in vitro* and *in vivo*. Studies demonstrate that quercetin can inhibit pulmonary arterial endothelial cell transdifferentiation into smooth muscle-like cells by regulating Akt and ERK1/2 pathways and enhance the autophagy of PASMCs induced by hypoxia through the FoxO1-SENS3-mTOR pathway [27, 28]. Quercetin can also interfere with the IRE1α-XBP1 pathway and TrkA/kt pathway, leading to reduced PASMC migration and cell cycle arrest, which in turn ameliorates hypoxia-induced PH [29, 30]. Luteolin can inhibit PDGF-induced proliferation and migration of PASMCs in a dose-dependent manner via regulating the Hippo-YAP/PI3-K/Akt signaling pathway [31]. The role of baicalein in the treatment of PH is the focus of numerous investigators. Baicalein can delay the progression of pulmonary vascular remodeling by inhibiting the NF-κB pathway and the catenin/ET-1/ETR pathway [32, 33]. Baicalein also could attenuate MCT-induced PH by inhibiting endothelial-to-mesenchymal transition [34]. The above results suggest that numerous active ingredients in BYHWD exert effects against pulmonary vascular remodeling by regulating multiple signal transduction pathways.

Furthermore, the PPI network and gene-disease phenotype correlation of potential therapeutic targets were analyzed to find the core targets of BYHWD. AKT1, MMP9, NOS3/e-NOS, and EGFR may play critical roles in the anti-PH effects of BYHWD. Impaired availability of NO is a key underlying feature in most forms of PH. NO is produced catalytically from L-arginine by the PI3K-Akt-eNOS pathway and regulates pulmonary vascular function and structure. The decrease of eNOS expression and dysfunction will lead to the inhibition of the NO signal in the lung and the disruption of pulmonary vasoconstriction/relaxation balance [35]. Dacomitinib, an EGFR inhibitor, can significantly inhibit vascular thickening, collagen deposition, and right ventricular remodeling in PH rats [36]. Many studies have shown that matrix metalloproteinases (MMP) play a key role in the disease state, especially in extracellular matrix remodeling and vascular homeostasis [37]. Increased expression of extracellular matrix proteins is closely associated with MMP activation in pulmonary arteries [38]. There are also close interactions between these targets. Vascular remodeling progression involves cell migration and invasion as well as protein degradation of the ECM in which it participates. Upon activation of the PI3K/Akt pathway, phosphorylated Akt can further activate MMP9, thereby playing a role in cell migration and invasion [39]. Dacomitinib could inhibit cell cycle progression, proliferation, and migration and enhance cell autophagy in PASMCs induced by hypoxia via the PI3K-Akt-mTOR signaling pathway [36].

The approaches of enrichment analysis were further adopted to analyze the biological processes and signaling pathways involved in potential targets of BYHWD. Multiple canonical biological processes closely associated with PH, such as "negative regulation of apoptotic process," "positive regulation of cell migration," "angiogenesis," "positive regulation of smooth muscle cell proliferation," and "positive regulation of phosphatidylinositol 3-kinase signaling," were discovered in the study. The KEGG enrichment results showed that the signaling pathways that play therapeutic roles by BYHWD may include "VEGF signaling pathway," "PI3K-Akt signaling pathway," "TNF signaling pathway," and "FoxO signaling pathway." VEGF is one of the strongest activators of angiogenesis, which stimulates the migration and proliferation of vascular endothelial cells, thereby promoting angiogenesis. There is a close relationship between the overexpression of VEGF and the pathological process of PH. Under hypoxic conditions, VEGF is released under the regulation of hypoxia-inducible factor (HIF-1), which in turn causes pulmonary vascular inflammation [40]. Akt mediates cell proliferation induced by various growth factors, which have been widely demonstrated. As an upstream regulatory pathway, Akt could be activated by several stimuli, including VEGF and PDGF. VEGF-induced endothelial migration is mediated through the Akt pathway. In terms of vascular smooth muscle cell apoptosis, FoxOs could induce the expression of the proapoptotic Bcl-2 family of proteins or upregulated the expression of death receptor ligands such as Fas ligand and TNFα. Akt can promote the phosphorylation of FoxO, which in turn inhibits the transcriptional function of FoxO, downregulates Bcl-2 levels, and regulates cell apoptosis [41]. It can be seen that BYHWD could exert

(a)

(b)
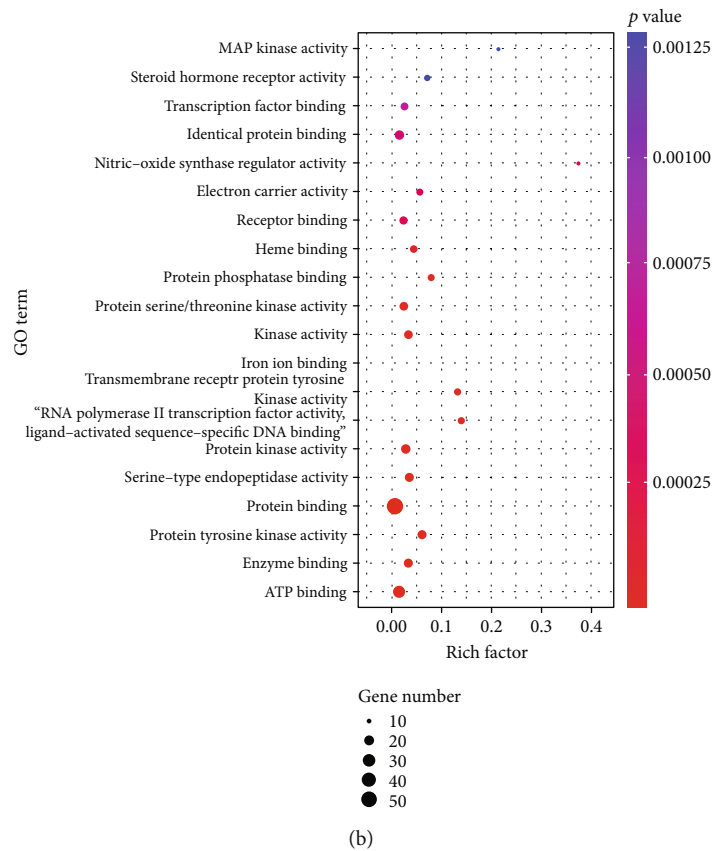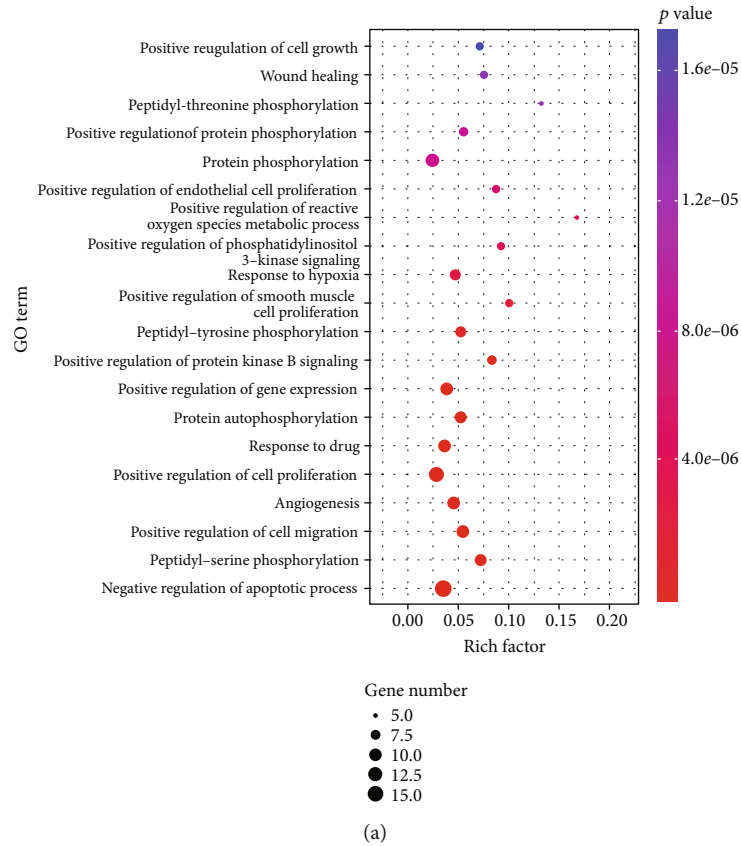
Figure 6: GO enrichment analysis map, containing (a) biological process and (b) molecular function. The size of the dots indicated the number of enriched targets, and the color of the dots represented the degree of significance based on the P value.
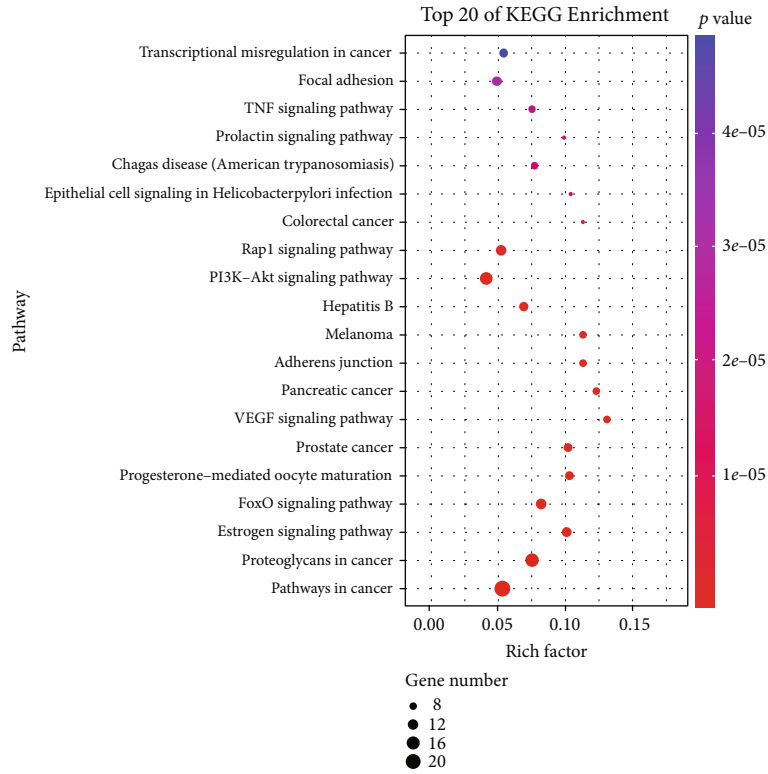
FIGURE 7: The KEGG analysis for the potential targets of BYHWD against PH. The color represents the different P values (<0.05), while the size of the circle represents the count.
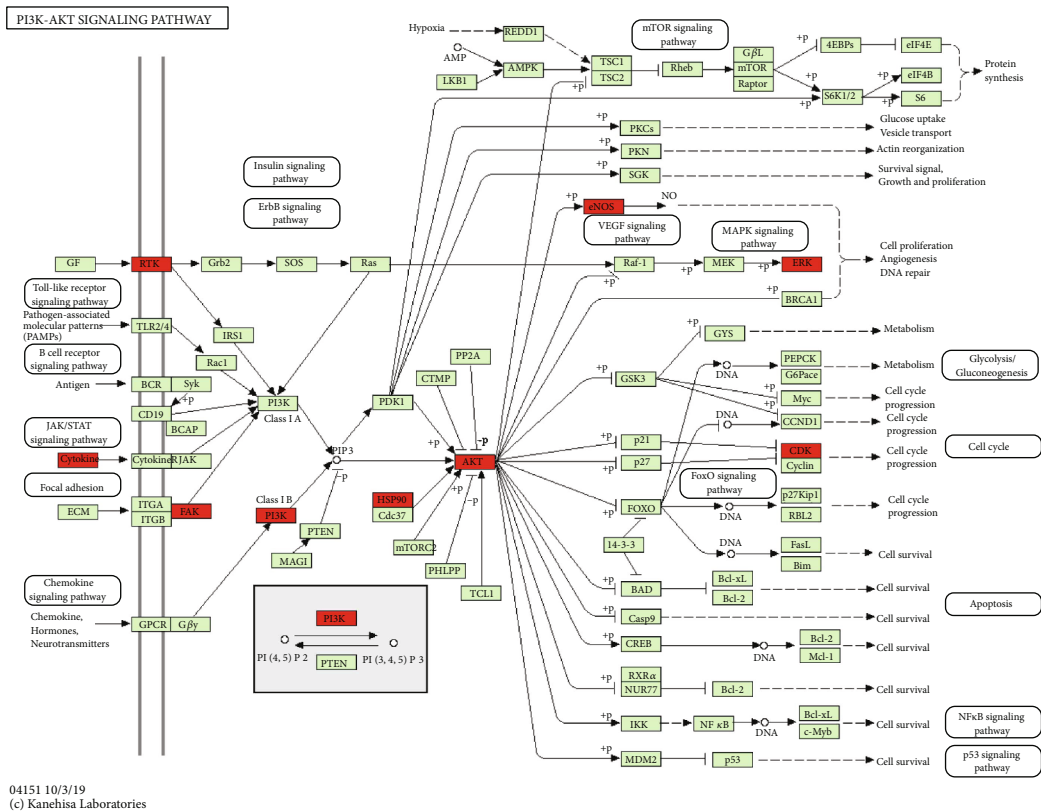
FIGURE 8: Distribution of the target proteins of BYHWD on the PI3K-Akt pathway. The red nodes are potential target proteins of BYHWD against PH, while the green nodes are relevant targets in the pathway.

(a)

(b)
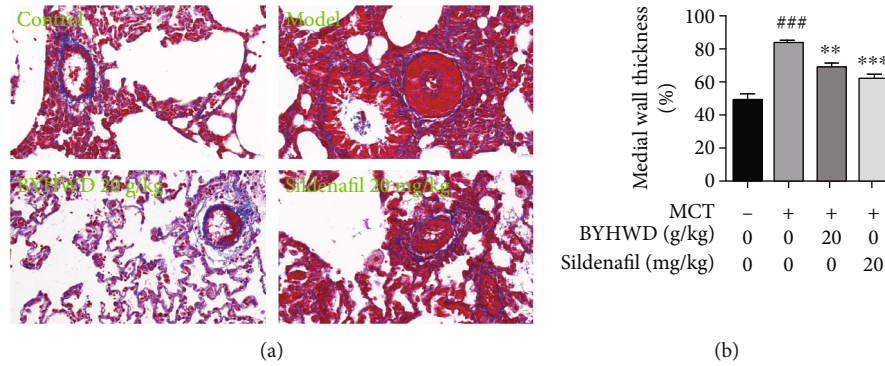
FIGURE 9: BYHWD prevents the development of small pulmonary artery hypertrophy in MCT-treated rats. (a) Representative images of the lung sections for intrapulmonary arteries stained with Masson's trichrome (original magnification ×200). (b) Medial wall thickness (%) of intrapulmonary arteries was calculated and shown in the bar graph. The results were expressed as the mean ± SEM of three independent experiments ($n = 3$). $^{###}P < 0.001$ vs. the control group; $^{**}P < 0.01$ and $^{***}P < 0.001$ vs. the model group.

(a)

(b)

(c)
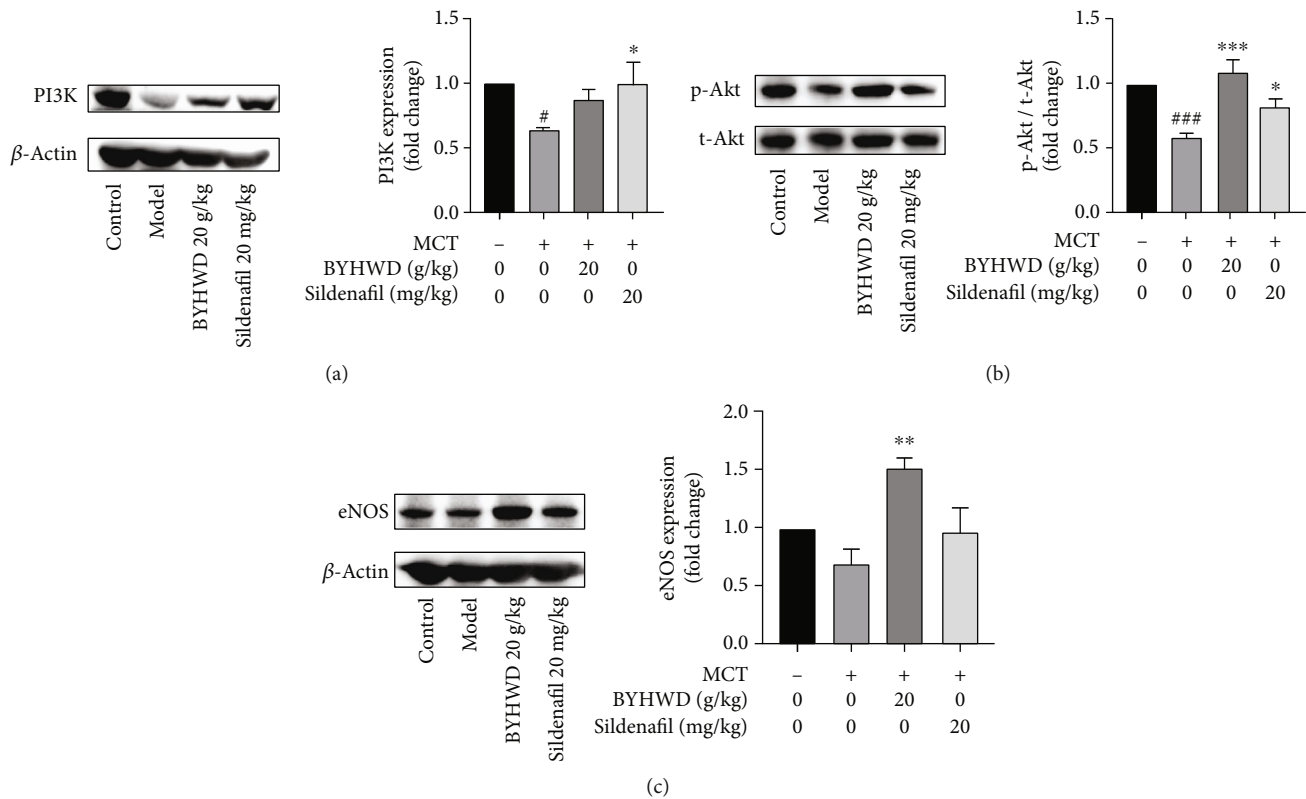
FIGURE 10: Effects of BYHWD on the PI3K/Akt/eNOS pathway. Expression of PI3K and eNOS and phosphorylation of Akt were measured by western blot analysis. Data are expressed as X-fold induction compared to normal control. The results were expressed as the mean ± SEM ($n = 3$-4). $^{#}P < 0.05$ and $^{###}P < 0.001$ vs. the control group; $^{*}P < 0.05$, $^{**}P < 0.01$, and $^{***}P < 0.001$ vs. the model group.

therapeutic effects on PH by acting on multiple targets and multiple signaling pathways. While in the analysis of topological parameters of the PPI network, it was found that Akt was in the central position in the target network. The results of gene-phenotype correlation analysis suggest that NOS3/eNOS may be one of the most critical genes in which BYHWD functions. As can be seen in the GO enrichment analysis results, the potential targets of BYHWD in the treatment of PH were significantly enriched in "positive regulation of protein kinase b signaling" and "positive regulation of phosphatidylinositol 3-kinase signaling." And in the KEGG enrichment analysis results, the term "PI3K-Akt signaling pathway" also appeared. As mentioned above, there is also a tight connection between the PI3K-Akt-eNOS pathway and other core potential targets, such as VEGF and MMP2. Based on the above experimental results of core target analysis and enrichment analysis, combined with previous studies, we speculate that the PI3K-Akt-eNOS pathway may be one of the crucial signaling pathways through which BYHWD exerts therapeutic effects on PH.

On the basis of network pharmacology analysis, the MCT-induced PH model was then constructed to preliminarily explore the efficacy and verify the mechanism of BYHWD in treating PH. Masson's trichrome staining results showed that the thickening of the pulmonary small vessel was noticeable after rats were stimulated with MCT for 21 days. BYHWD treatment can significantly inhibit the vascular remodeling process, which illustrates that BYHWD could ameliorate the PH development from the key pathological mechanism. This is also consistent with the conclusion from network pharmacology analysis that BYHWD may exert effects against PH by regulating the proliferation, apoptosis, and migration of vascular smooth muscles. Network pharmacology results revealed that the PI3K-Akt-eNOS signaling pathway may play a central role in the therapeutic effects of BYHWD. Then, western blotting was designed to validate the changes of the PI3K-Akt-eNOS pathway in lung tissues of PH rats and the effects of BYHWD treatment. Results indicated that BYHWD increased the expression and the phosphorylation of Akt. Collectively, BYHWD repressed pulmonary arterial remodeling partially by modulating the expression of the PI3K-Akt-eNOS pathway.

5. Conclusion

In conclusion, the present study demonstrated that BYHWD can exert its effects on inhibiting pulmonary vascular remodeling through multitargets and multipathways by the approach of network pharmacology as well as biological experimental verification. The most prominent mechanism may be related to the activation of the PI3K-Akt-eNOS pathway.

Data Availability

The data used to support the findings of this study are available from the corresponding authors upon request.

Conflicts of Interest

The authors declare no conflict of interest.

Authors' Contributions

Yucai Chen designed the research; Yucai Chen, Lidan Cui, Can Wang, and Jianing Liu performed the experimental work; Yucai Chen, Can Wang, and Jianing Liu wrote the manuscript; Yucai Chen and Jian Guo were responsible for the supervision and project administration.

Acknowledgments

Supplementary Materials

Table S1: 93 compounds in BYHWD. Table S2: the potential therapeutic targets of BYHWD against PH. Table S3: the result of top 20 GO (biological process) enrichment analysis. Table S4: the result of top 20 GO (molecular function) enrichment analysis. (Supplementary Materials)

References

[1] S. Fazal, M. Bisserier, and L. Hadri, "Molecular and genetic profiling for precision medicines in pulmonary arterial hypertension," *Cells*, vol. 10, no. 3, p. 638, 2021.

[2] S. A. Mandras, H. S. Mehta, and A. Vaidya, "Pulmonary hypertension: a brief guide for clinicians," *Mayo Clinic Proceedings*, vol. 95, no. 9, pp. 1978–1988, 2020.

[3] D. Gajecki, J. Gawrys, E. Szahidewicz-Krupska, and A. Doroszko, "Novel Molecular Mechanisms of Pulmonary Hypertension: A Search for Biomarkers and Novel Drug Targets—From Bench to Bed Site," *Oxidative Medicine and Cellular Longevity*, vol. 2020, Article ID 7265487, 17 pages, 2020.

[4] N. Sommer, H. A. Ghofrani, O. Pak et al., "Current and future treatments of pulmonary arterial hypertension," *British Journal of Pharmacology*, vol. 178, no. 1, pp. 6–30, 2021.

[5] K. Kearney, E. Kotlyar, and E. M. T. Lau, "Pulmonary vascular disease as a systemic and multisystem disease," *Clinics in Chest Medicine*, vol. 42, no. 1, pp. 167–177, 2021.

[6] X. An, S. Li, X. Weng et al., "Maxingxiongting mixture attenuates hypoxia pulmonary arterial hypertension to improve right ventricular hypertrophy by inhibiting the rho-kinase signaling pathway," *Journal of traditional Chinese medicine*, vol. 40, no. 6, pp. 992–998, 2020.

[7] P. Wu, X. Xie, M. Chen et al., "Elucidation of the mechanisms and molecular targets of Qishen Yiqi formula for the treatment of pulmonary arterial hypertension using a bioinformatics/network topology-based strategy," *Combinatorial Chemistry & High Throughput Screening*, vol. 24, no. 5, pp. 701–715, 2021.

[8] Y. Lu, J. Wu, Y. Sun et al., "Qiliqiangxin prevents right ventricular remodeling by inhibiting apoptosis and improving metabolism reprogramming with pulmonary arterial hypertension," *American Journal of Translational Research*, vol. 12, no. 9, pp. 5655–5669, 2020.

[9] T. T. Luo, Y. Lu, S. K. Yan, X. Xiao, X. L. Rong, and J. Guo, "Network pharmacology in research of Chinese medicine formula: methodology, application and prospective," *Chinese Journal of Integrative Medicine*, vol. 26, no. 1, pp. 72–80, 2020.

[10] B. Boezio, K. Audouze, P. Ducrot, and O. Taboureau, "Network-based approaches in pharmacology," *Molecular informatics*, vol. 36, no. 10, article 1700048, 2017.

[11] H. J. Cui, A. L. Yang, H. J. Zhou et al., "Buyang huanwu decoction promotes angiogenesis via vascular endothelial growth factor receptor-2 activation through the PI3K/Akt pathway in a mouse model of intracerebral hemorrhage," *BMC Complementary and Alternative Medicine*, vol. 15, no. 1, 2015.

[12] Y. Jin, L. Dong, C. Wu et al., "Buyang Huanwu Decoction fraction protects against cerebral ischemia/reperfusion injury by attenuating the inflammatory response and cellular apoptosis," *Neural Regeneration Research*, vol. 8, no. 3, pp. 197–207, 2013.

[13] X. Kong, X. Su, J. Zhu et al., "Neuroprotective effect of buyang huanwu decoction on rat ischemic/reperfusion brain damage

by promoting migration of neural precursor cells," *Rejuvenation Research*, vol. 17, no. 3, pp. 264–275, 2014.

[14] C. Y. Chen, "TCM Database@Taiwan: the world's largest traditional Chinese medicine database for drug screening in silico," *PLoS One*, vol. 6, no. 1, article e15939, 2011.

[15] J. Ru, P. Li, J. Wang et al., "TCMSP: a database of systems pharmacology for drug discovery from herbal medicines," *Journal of Cheminformatics*, vol. 6, no. 1, 2014.

[16] L. Zeng, K. Yang, and J. Ge, "Uncovering the pharmacological mechanism of Astragalus Salvia compound on pregnancy-induced hypertension syndrome by a network pharmacology approach," *Scientific Reports*, vol. 7, no. 1, 2017.

[17] X. Wang, Y. Shen, S. Wang et al., "PharmMapper 2017 update: a web server for potential drug target identification with a comprehensive target pharmacophore database," *Nucleic Acids Research*, vol. 45, no. W1, pp. W356–W360, 2017.

[18] A. Daina, O. Michielin, and V. Zoete, "SwissTargetPrediction: updated data and new features for efficient prediction of protein targets of small molecules," *Nucleic Acids Research*, vol. 47, no. W1, pp. W357–W364, 2019.

[19] J. Piñero, J. M. Ramírez-Anguita, J. Saüch-Pitarch et al., "The DisGeNET knowledge platform for disease genomics: 2019 update," *Nucleic Acids Research*, vol. 48, no. D1, pp. D845–D855, 2020.

[20] D. Szklarczyk, A. L. Gable, D. Lyon et al., "STRING v11: protein-protein association networks with increased coverage, supporting functional discovery in genome-wide experimental datasets," *Nucleic Acids Research*, vol. 47, no. D1, pp. D607–D613, 2019.

[21] G. Stelzer, I. Plaschkes, D. Oz-Levi et al., "VarElect: the phenotype-based variation prioritizer of the GeneCards Suite," *BMC genomics*, vol. 17, Supplement 2, 2016.

[22] D. W. Huang, B. T. Sherman, and R. A. Lempicki, "Systematic and integrative analysis of large gene lists using DAVID bioinformatics resources," *Nature Protocols*, vol. 4, no. 1, pp. 44–57, 2009.

[23] J. H. Lee, B. K. Park, K. S. Oh et al., "A urotensin II receptor antagonist, KR36676, decreases vascular remodeling and inflammation in experimental pulmonary hypertension," *International Immunopharmacology*, vol. 40, pp. 196–202, 2016.

[24] Y. Chen, T. Yuan, H. Zhang et al., "Activation of Nrf2 attenuates pulmonary vascular remodeling via inhibiting endothelial-to-mesenchymal transition: an insight from a plant polyphenol," *International Journal of Biological Sciences*, vol. 13, no. 8, pp. 1067–1081, 2017.

[25] J. Zhang, H. Zou, Q. Zhang et al., "Effects of Xiaoshuan enteric-coated capsule on neurovascular functions assessed by quantitative multiparametric MRI in a rat model of permanent cerebral ischemia," *BMC Complementary and Alternative Medicine*, vol. 16, no. 1, 2016.

[26] Z. Tao, H. Yue, L. Hao et al., "Differential gene expression profile of Buyanghuanwu decoction in rats with ventricular remodeling post-myocardial infarction," *Journal of traditional Chinese medicine*, vol. 37, no. 3, pp. 341–354, 2017.

[27] S. Huang, X. Zhu, W. Huang et al., "Quercetin inhibits pulmonary arterial endothelial cell transdifferentiation possibly by Akt and Erk1/2 pathways," *BioMed Research International*, vol. 2017, Article ID 6147294, 8 pages, 2017.

[28] Y. He, X. Cao, P. Guo et al., "Quercetin induces autophagy *via* FOXO1-dependent pathways and autophagy suppression enhances quercetin-induced apoptosis in PASMCs in hypoxia," *Free Radical Biology & Medicine*, vol. 103, pp. 165–176, 2017.

[29] X. Cao, Y. He, X. Li, Y. Xu, and X. Liu, "The IRE1α-XBP1 pathway function in hypoxia-induced pulmonary vascular remodeling, is upregulated by quercetin, inhibits apoptosis and partially reverses the effect of quercetin in PASMCs," *American Journal of Translational Research*, vol. 11, no. 2, pp. 641–654, 2019.

[30] Y. He, X. Cao, X. Liu et al., "Quercetin reverses experimental pulmonary arterial hypertension by modulating the TrkA pathway," *Experimental Cell Research*, vol. 339, no. 1, pp. 122–134, 2015.

[31] W. Zuo, N. Liu, Y. Zeng et al., "Luteolin ameliorates experimental pulmonary arterial hypertension via suppressing Hippo-YAP/PI3K/AKT signaling pathway," *Frontiers in Pharmacology*, vol. 12, article 663551, 2021.

[32] W. L. Hsu, Y. C. Lin, J. R. Jeng, H. Y. Chang, and T. C. Chou, "Baicalein ameliorates pulmonary arterial hypertension caused by monocrotaline through downregulation of ET-1 and ETAR in pneumonectomized rats," *The American Journal of Chinese Medicine*, vol. 46, no. 4, pp. 769–783, 2018.

[33] R. Shi, Z. Wei, D. Zhu et al., "Baicalein attenuates monocrotaline-induced pulmonary arterial hypertension by inhibiting vascular remodeling in rats," *Pulmonary Pharmacology & Therapeutics*, vol. 48, pp. 124–135, 2018.

[34] R. Shi, D. Zhu, Z. Wei et al., "Baicalein attenuates monocrotaline-induced pulmonary arterial hypertension by inhibiting endothelial-to-mesenchymal transition," *Life Sciences*, vol. 207, pp. 442–450, 2018.

[35] Z. Lázár, M. Mészáros, and A. Bikov, "The nitric oxide pathway in pulmonary arterial hypertension: pathomechanism, biomarkers and drug targets," *Current Medicinal Chemistry*, vol. 27, no. 42, pp. 7168–7188, 2020.

[36] X. Yu, X. Zhao, J. Zhang et al., "Dacomitinib, a new pan-EGFR inhibitor, is effective in attenuating pulmonary vascular remodeling and pulmonary hypertension," *European Journal of Pharmacology*, vol. 850, pp. 97–108, 2019.

[37] P. Chelladurai, W. Seeger, and S. S. Pullamsetti, "Matrix metalloproteinases and their inhibitors in pulmonary hypertension," *The European Respiratory Journal*, vol. 40, no. 3, pp. 766–782, 2012.

[38] P. Bai, L. Lyu, T. Yu et al., "Macrophage-derived legumain promotes pulmonary hypertension by activating the MMP (matrix metalloproteinase)-2/TGF (transforming growth factor)-β1 signaling," *Arteriosclerosis, Thrombosis, and Vascular Biology*, vol. 39, no. 4, 2019.

[39] C. Li, Y. Qin, Y. Zhong et al., "Fentanyl inhibits the progression of gastric cancer through the suppression of MMP-9 via the PI3K/Akt signaling pathway," *Annals of Translational Medicine*, vol. 8, no. 4, p. 118, 2020.

[40] A. P. Laddha and Y. A. Kulkarni, "VEGF and FGF-2: promising targets for the treatment of respiratory disorders," *Respiratory Medicine*, vol. 156, pp. 33–46, 2019.

[41] P. Abeyrathna and Y. Su, "The critical role of Akt in cardiovascular function," *Vascular Pharmacology*, vol. 74, pp. 38–48, 2015.

Research Article

Dynamic Patterns of N6-Methyladenosine Profiles of Messenger RNA Correlated with the Cardiomyocyte Regenerability during the Early Heart Development in Mice

Yuhui Yang [iD],[1,2] **Siman Shen,**[1,2] **Yin Cai,**[3,4] **Kejun Zeng,**[1,2] **Keyu Liu,**[1,2] **Simeng Li,**[1,2] **Lanfen Zeng,**[1,2] **Linming Chen,**[1,2] **Jing Tang,**[1,2] **Zhe Hu,**[1,2] **Zhengyuan Xia** [iD],[1,2,3] **and Liangqing Zhang** [iD][1,2]

[1]*Department of Anesthesiology, Affiliated Hospital of Guangdong Medical University, Zhanjiang, China*
[2]*Key Laboratory of Organ Functional Injury and Protection and Department of Translational Medicine of Zhanjiang, Zhanjiang, China*
[3]*State Key Laboratory of Pharmaceutical Biotechnology and Department of Medicine, University of Hong Kong, Hong Kong SAR, China*
[4]*Department of Health Technology and Informatics, The Hong Kong Polytechnic University, Hong Kong SAR, China*

Correspondence should be addressed to Zhengyuan Xia; zyxia@hku.hk and Liangqing Zhang; zhanglq1970@163.com

N6-Methyladenosine (m6A) plays important roles in regulating mRNA processing. Despite rapid progress in this field, little is known about the role and mechanism of m6A modification in myocardial development and cardiomyocyte regeneration. Existing studies have shown that the heart tissues of newborn mice have the capability of proliferation and regeneration, but its mechanism, particularly its relation to m6A methylation, remains unknown. *Methods*. To systematically profile the mRNA m6A modification pattern in the heart tissues of mice at different developmental stages, we jointly performed methylated RNA immunoprecipitation sequencing (MeRIP-seq) and RNA sequencing (RNA-seq) of heart tissues of mice, respectively, aged 1 day old, 7 days old, and 28 days old. *Results*. We identified the linkages and association between differentially expressed mRNA transcripts and hyper or hypomethylated m6A peaks in C57BL/6J mice at different heart developmental stages. Results showed that the amount of m6A peaks and the level of m6A modification were the lowest in the heart of mice at 1 day old. By contrast, heart tissues from 7-day-old mice tended to possess the most m6A peaks and the highest global m6A level. However, the m6A characteristics of myocardial tissue changed little after 7 days old as compared to that of 1 day old. Specifically, we found 1269 downmethylated genes of 1434 methylated genes in 7-day-old mouse heart tissues as compared to those in 1-day-old mice. Hypermethylation of some specific genes may correlate with the heart's strong proliferative and regenerative capability at the first day after birth. In terms of m6A density, the tendency shifted from coding sequences (CDS) to $3'$-untranslated regions ($3'$ UTR) and stop codon with the progression of heart development. In addition, some genes demonstrated remarkable changes both in methylation and expression, like kiss1, plekha6, and megf6, which may play important roles in proliferation. Furthermore, signaling pathways highly related to proliferation such as "Wnt signaling pathway," "ECM-receptor interaction," and "cardiac chamber formation" were significantly enriched in 1-day-old methylated genes. *Conclusions*. Our results reveal a pattern that different m6A modifications are distributed in C57BL/6J heart tissue at different developmental stages, which provides new insights into a novel function of m6A methylation of mRNA in myocardial development and regeneration.

1. Background

The adult human heart does not have sufficient ability to renovate the damaged cardiac cardiomyocytes (CMs), which is the critical factor leading to the high mortality of cardiovascular diseases [1]. Although many approaches are designed to repopulate the damaged CMs, like transplanting various sources of exogenous stem cells with differential potential [2, 3], these therapies have various limitations in treating myocardial infarction (MI) or heart failure efficaciously, such as immune response [4] and epigenetic influence [5, 6]. Interestingly, extensive recent studies show that targeting mechanisms that govern endogenous repair and proliferation to cardiomyocytes may prove to be a valid therapy for heart disease [7–9]. The adult mammalian heart has been traditionally regarded as an organ of terminal differentiation capability. Recent studies, however, discovered that several species, including neonatal mice, 1-day-old pigs, and adult zebrafish, could stimulate a robust regenerative response during cardiac injury [10, 11]. Unlike the adult zebrafish, the CMs of neonatal mice possess the proliferative capability and maintain the competence to renovate their damaged cardiac muscle tissue during the first 7 days of life [11, 12]. Convincing evidence shows that heart regeneration in neonatal mice is achieved by cardiomyocyte proliferation and the cardiac developmental program for self-renewal [12–14]. The underlying mechanisms of neonatal cardiac proliferation remain largely unclear, but the related research is of crucial significance for discovering therapeutic targets for cardiomyocyte regeneration and cardiac repair.

N6-Methyladenosine (m6A), the most common internal modification of messenger RNA (mRNA) and noncoding RNAs (ncRNA) in eukaryotes identified in the 1970s, is dynamically regulated by a set of enzymes classified into methyltransferases ("writers"), demethylases ("erasers"), and m6A binding proteins ("readers") [15]. Over the last decade, several studies have characterized the m6A mRNA landscape in multiple organisms, such as mammals [16], yeast [17], and plants [18], and these studies have identified the consensus sequence RRACH (in which R represents A or G and H represents A, C, or U), which suggests the significance of m6A modification in multispecies conservatism. Thus, imbalance in m6A modification may impact on various diseases and biochemical progress, like regulating plant embryonic development [19], immune cell homeostasis and function [20], and cancer in various organs [21], and contribute to human disease heritability [22]. Transcriptome-wide analyses have shown that m6A modified over one-third of the mRNA in humans and mice [16]. The m6A possesses 1-3 modification sites in each particular mRNA that enrich in near stop codons, 3′UTRs, and RRACH sequence of mRNA. These studies also suggested that m6A modification has a crucial effect on various cellular pathways and processes, including developmental regulation, the cell cycle, fate determination, and the heat-shock stress response by regulating the splicing, expression, stability, and translation efficiency of mRNAs [23, 24].

Recently, the regulatory role of m6A in heart diseases has been increasingly recognized [25]. In addition, the effects of m6A modification on embryonic neural stem cells (NSCs) have been demonstrated during early brain development in newborn mice [26]. It follows that the function and correlation of m6A modifications in biological physiology and disease progression have become of great interest [25, 26]. Technical advances in mammalian studies, such as transcriptome-wide analysis, open up a novel method for revealing the distribution and function of this modification through the biotechnologies of RNA-seq, RIP-seq, and m6A-seq. To date, however, study about the m6A modification of mRNAs in mammals' myocardial proliferation is rare. And researches focusing on the development of therapies that may stimulate myocardial regeneration by mining and interfering related regulating molecules with different m6A modification during cardiac development are lacking.

The proliferative ability of mouse cardiomyocytes can only be maintained for a short period after birth. The ability of DNA synthesis is an intuitive index to reflect proliferation ability, and the activity of the enzymes needed for DNA synthesis in mice decreases significantly to the level of adult at about one week after birth [27, 28]. Current researches indicated that the heart of mice aged up to 7 days old has the ability to proliferate and regenerate, while hearts from 28-day-old mice could hardly proliferate and regenerate which is similar to that seen in adult hearts [12, 29]. So most researchers usually choose 1-day-old, 7-day-old, and 28-day-old mice (hereafter referred to as P1, P7, and P28) to study the phenomenon and mechanisms of myocardial regeneration [30, 31]. We hypothesized that m6A might play a significant role in regulating and affecting the development and regeneration of rodent hearts. Thus, in the present study, we conducted an m6A-specific analysis and bioinformatics analysis in mRNAs of mouse hearts at the three stages, including P1, P7, and P28, in an effort to provide clinical and therapeutic insights and reveal the role and mechanism of m6A in myocardial development.

2. Materials and Methods

2.1. Animal Studies. The study protocol was reviewed and approved by the animal care committees of both Southern Medical University and Guangdong Medical University. Male C57BL/6J mice were randomly assigned to three groups according to different ages (P1, P7, and P28). Groups P1 and P7 consisted of 12 animals, respectively, and group P28 consisted of 3, providing 3 biological replicates to be analyzed. Given that the heart sizes for animals in groups P1 and P7 were small, the samples from every 4 hearts were pooled for analyses. All mice in each group were deep anesthetized with ketamine (80 mg/kg, IP.) + xylazine (10 mg/kg, IP.) and were executed by cervical dislocation. Subsequently, the cardiac tissues were collected and frozen in liquid nitrogen at -80°C for further RNA extraction. Animals were obtained from the Animal Research Center of Southern Medical University. The Guide for the Care and Use of Laboratory Animals and Animal Welfare Act are followed to guide 3M's animal research program.

2.2. Total RNA Preparation. RNA isolation was performed with Trizol Reagent (Thermo Fisher Scientific, Waltham, MA, USA) according to the manufacturer's instructions. The ratio of OD260/280 to OD260/230 of the product was detected by NanoDrop (Thermo Fisher Scientific, Waltham, MA, USA) as the sample purity index. And the degree of RNA degradation was detected by agarose gel electrophoresis and Agilent 2100 Bioanalyzer (Agilent, Santa Clara, CA, USA). If the OD260/280 value was between 1.8 and 2.2, OD 260/230 ≥ 2.0, and RIN ≥ 7, the RNA purity and integrity were qualified and marked as "Pass".

2.3. RNA Purification and Fragmentation. The rRNA probe with specific species (mouse) was incubated with total RNA, and then, the captured rRNA probe was modified with biotin (Thermo Fisher Scientific, Waltham, MA, USA). The magnetic beads (Thermo Fisher Scientific, Waltham, MA, USA) coated with streptavidin were combined with the probe-rRNA complex to remove rRNA. After another purification of AMPure XP magnetic beads (Beckman Coulter, Brea, CA), the RNA without rRNA was extracted. The purified RNA was diluted in fragmentation buffer for elution, fragmentation, and random primers; then, the product was incubated at 94°C for thermal fracture and lysed into fragments between 100 and 300 bp.

2.4. cDNA Library Construction and Sequencing. The fragmented RNA was divided into two parts. One part was added with premixed m6A antibody immunomagnetic beads to enrich the m6A methylated mRNA fragments. Then, the enriched m6A antibody immunomagnetic beads and the recovered m6A-containing mRNA fragment were used to construct a conventional sequencing library according to the transcriptome library construction process. The other part was used as a control to construct a conventional transcriptome sequencing library directly. These two sequenced libraries, m6A-seq library and RNA-seq library, were sequenced with high throughput, respectively.

2.5. Sequencing Data Analysis. Libraries were sequenced and visualized on Illumina NovaSeq™ 6000 (Illumina, San Diego, CA). First, the software Cutadapt and local Perl scripts removed the low-quality, contaminated, and sequencer connector sequences to obtain clean data [32]. Next, Fastp was used to perform quality control on clean data. Then, the reads were aligned to the referential genome using the default parameters of HISAT2 [33] and peak calling analysis and peak annotation were performed by ExomePeak and ChIPseeker [34]. After that, Homer (or MEME) was applied to perform motif analysis on enriched sites and StringTie to perform transcriptome analysis and gene quantification. Finally, the R package "Edge R" was used for genetic difference analysis [35].

2.6. GO and KEGG Pathway Database Analysis. We used Gene Ontology (GO; http://www.geneontology.org/) to perform functional enrichment and applied GO annotation to describe the functions of the differentially methylated genes, which were classified into three major categories: biological process (BP), cellular component (CC), and molecular func-

tion (MF). In the meantime, Kyoto Encyclopedia of Genes and Genomes (KEGG; http://www.kegg.jp/) analysis was also conducted and the major terms of signal transduction pathways and biochemical metabolic pathways were identified that participated for the DEGs. When the corrected P value was less than 0.05, the GO terms and KEGG analysis were regarded as significantly enriched, as previously described [36, 37].

2.7. Quantitative Real-Time PCR. Q-PCR was performed on Roche LightCycler 480 system (Roche Applied Science, IN, USA). Relative expressions of genes were compared by the 2-$\Delta\Delta$Ct method, and GAPDH served as the internal housekeeping gene. The sequences of all the specific primers were designed to span extron-intron to prevent the improper amplification of mRNA. The primer sequences were as follows: IGF2BP1, 5′-GGCGACTCATTGGCAAGGAAGG-3′ (forward) and 5′-TGAGGTCCTGGAGCGATGAGATG-3′ (reverse); IGF2BP3, 5′-CATCTGTTTATTCCCGCCCTGT CC-3′ (forward) and 5′-TCACCATCCGCACTTTAGCAT CTG-3′ (reverse); ALKBH5, 5′-TTCTTCAGCGACTCGG CACTTTG-3′ (forward) and 5′-CGGCAGAGAAAGCA CAGGTTCC-3′ (reverse); Hist1h2ao, 5′-GCTCCGCAAGG GCAACTACTC-3′ (forward) and 5′-CCCGCCAGCTC CAGGATCTC-3′ (reverse); Tet2, 5′-CTGCTGTTTGGGT CTGAAGGAAGG-3′ (forward) and 5′-GTTCTGCTGGTC TCTGTGGGAATG-3′ (reverse); GATA4, 5′-CGAGATGG GACGGGACACTACC-3′ (forward) and 5′-TGGCAGTT GGCACAGGAGAGG-3′ (reverse); and MEGF6, 5′-TGCG ACCCTGAGACTGGAACC-3′ (forward) and 5′-TTGGCA CAAGCACACCTCATCTG-3′ (reverse).

2.8. Western Blot. Proteins were harvested and dissolved in RIPA lysis buffer, and protein concentrations were detected by enhanced Bicinchoninic Acid (BCA) protein assay kit (Beyotime, China). And the equivalent amounts of protein were separated by SDS-PAGE on 10% acrylamide gels at 60 v for 2.5 h and transferred to PVDF membranes under a constant current of 340 mA for 1.5 h. Quantitative analysis was performed by ImageJ. The primary antibodies were anti-ALKBH5 (ab195377, Abcam, MA, USA), anti-METTL3 (86132S, CST, MA, USA), anti-YTHDF1 (ab252346, Abcam, MA, USA), anti-IGF2BP3 (ab179807, Abcam, MA, USA), anti-FTO (31687S, CST, MA, USA), and anti-GAPDH (ab8227, Abcam, MA, USA). The secondary antibodies were goat polyclonal anti-Rabbit-IgG (14708S, CST, MA, USA).

2.9. Statistical Analysis. One-way ANOVA with Tukey's post hoc tests was carried out for comparison of multiple groups. All experiments were performed at least three times independently. Data are shown as mean ± S.D. A P value less than 0.05 was considered statistically significantly different.

3. Results

3.1. General Features of Cardiac m6A Methylation in Mouse during Heart Development. In order to investigate the potential targets contributing to heart development in C57BL/6J

(a)

(b)

(c)

(d)

(e)

(f)
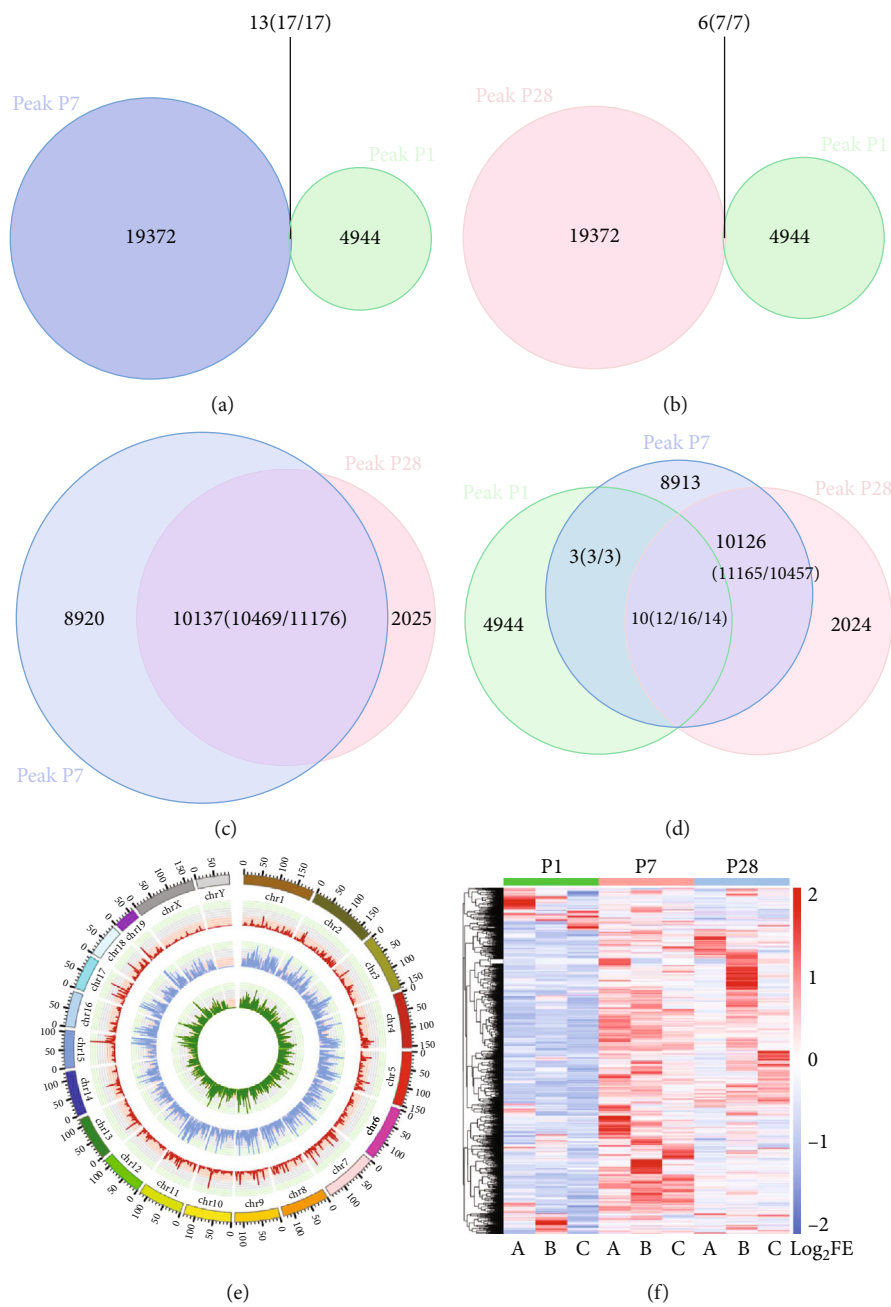
Figure 1: Continued.
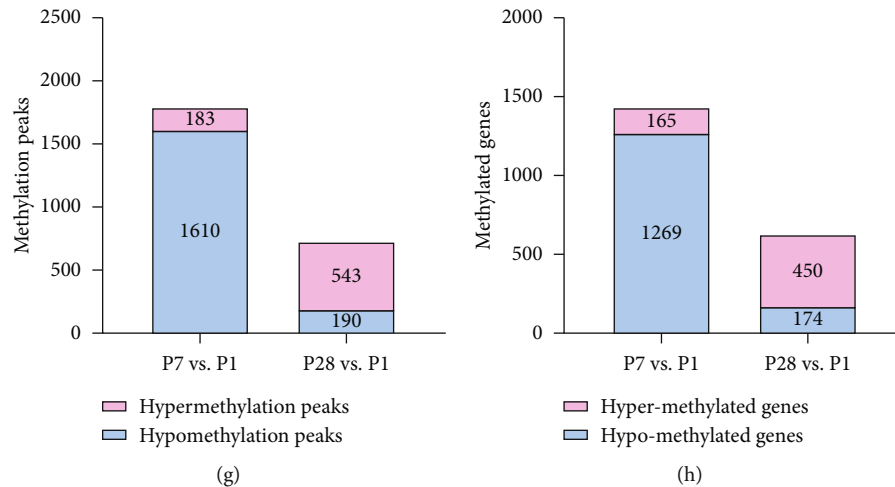
FIGURE 1: General features of m6A methylation in mouse heart development. (a) Venn diagram of m6A peaks in P7 and P1 heart tissues. (b) Venn diagram of m6A peaks in P28 and P1 heart tissues. (c) Venn diagram of m6A peaks in P28 and P7 heart tissues. (d) Venn diagram of m6A peaks in all 3 groups. (e) Distribution of m6A methylation sites on chromosome by Circos plot. Red represents P1, blue represents P7, and green represents P28. (f) Cluster analysis of m6A in P1, P7, and P28 heart tissues. The color represents the degree of the log fold enrichment (FE) value: the larger the LogFE value, the closer the color is to red ($P < 0.05$). (g) Histogram showing the methylation peaks. P7 possessed more peaks, but the levels of methylation were mostly decreased. (h) Histogram showing the methylation peaks' corresponding genes. Same as the methylation peaks, P7 genes were mostly hypomethylated as compared to P1.

mice, we performed m6A sequencing to compare the gene methylation profile grouped by P1, P7, and P28. We mapped up to 4961 methylation peaks in 3062 annotated genes of P1 heart tissues, 19389 peaks in 7404 annotated genes of P7, and 13201 peaks in 5712 annotated genes of P28, respectively (all $P < 0.05$, $\mathrm{Log_2FC} > 1$). Then, we calculated their pairwise intersection by using Venn diagram. Some redundancy data would be merged in statistical mapping. For instance, suppose group A was compared with group B and one peak in A may overlap with two or more peaks in B, which was called redundancy, so the number inside the parentheses in the overlap of the Venn diagram is the total amount of intersections that actually occurred, while the number outside the parentheses indicates the amount of intersections after duplicates are excluded. Of the 4961 methylation peaks in P1, only 13 reappeared in P7, and still fewer peaks (6 peaks) reappeared in P28. However, up to 10137 methylation peaks overlapped between P7 and P28 methylation peaks (Figures 1(a)–1(c)). In general, we found that 10 specific methylation peaks simultaneously appeared among P1, P7, and P28 mouse heart tissue (Figure 1(d)). There were noticeable differences in the number of m6A peaks in either P7 or P28 as compared to P1, while this characteristic difference was inconspicuous between P7 and P28; thus, we could presume that the m6A modification was significantly altered in early heart development, but tended to stabilize after day 7.

When using Circos software to analyze the distribution of mRNA m6A peaks on the chromosomes, it was found that the distribution and number of m6A peaks on each chromosome were diverse among P1, P7, and P28' s mouse heart tissue, with the diversity on chromosome 3 being the most apparent (Figure 1(e)). The results revealed that the methylation level of whole genome was significantly upregulated when cardiomyocytes developed to P7 and then dropped to

medium levels at P28. Furthermore, the autosomes in the mouse heart of each age group were more profoundly methylated compared with the sex chromosomes. Interestingly, the methylation degree of sex chromosome Y was barely noticeable.

3.2. Cluster Analysis. The analysis of the methylation cluster and heat map showed that the methylation differences could obviously be distinguished from each group: there were marked differences among the groups but there existed relative consistencies within the groups (Figure 1(f)). To sum up, the peaks of methylation in the P1 heart tissues were the lowest, while those in the P7 heart tissues were the highest and reduced over time. By P28, the peaks of methylation were reduced as compared to P7 but they remained high as compared to P1. In total, 1610 of 1793 methylation peaks in P7 were detected as hypomethylation, and 543 hypermethylation peaks of 733 methylation peaks in P28 were identified (Figures 1(g) and 1(h)), all $P < 0.05$, $\mathrm{Log_2FE} > 1$). By comparison, more hypomethylation peaks were seen in P7 heart tissues. However, 1793 methylation peaks with significant differences accounted for only approximately 8% of the methylation peaks in P7. The rest of the peaks were unique to P7, but not in P1. This interesting trend of methylation over time suggests that specific methylation sites may have an underlying network with the strong proliferative and regenerative capability of the heart at the very first day after birth, and subsequent studies are needed to investigate the mechanism.

3.3. Motif Analysis. While mapping the m6A methylome motif by scanning the peaks, we found that RRACH was a conserved sequence motif for m6A-containing regions among all the 3 groups, which is consistent with previous studies

(a)   (b)   (c)

(d)   (e)   (f)

(g)   (h)
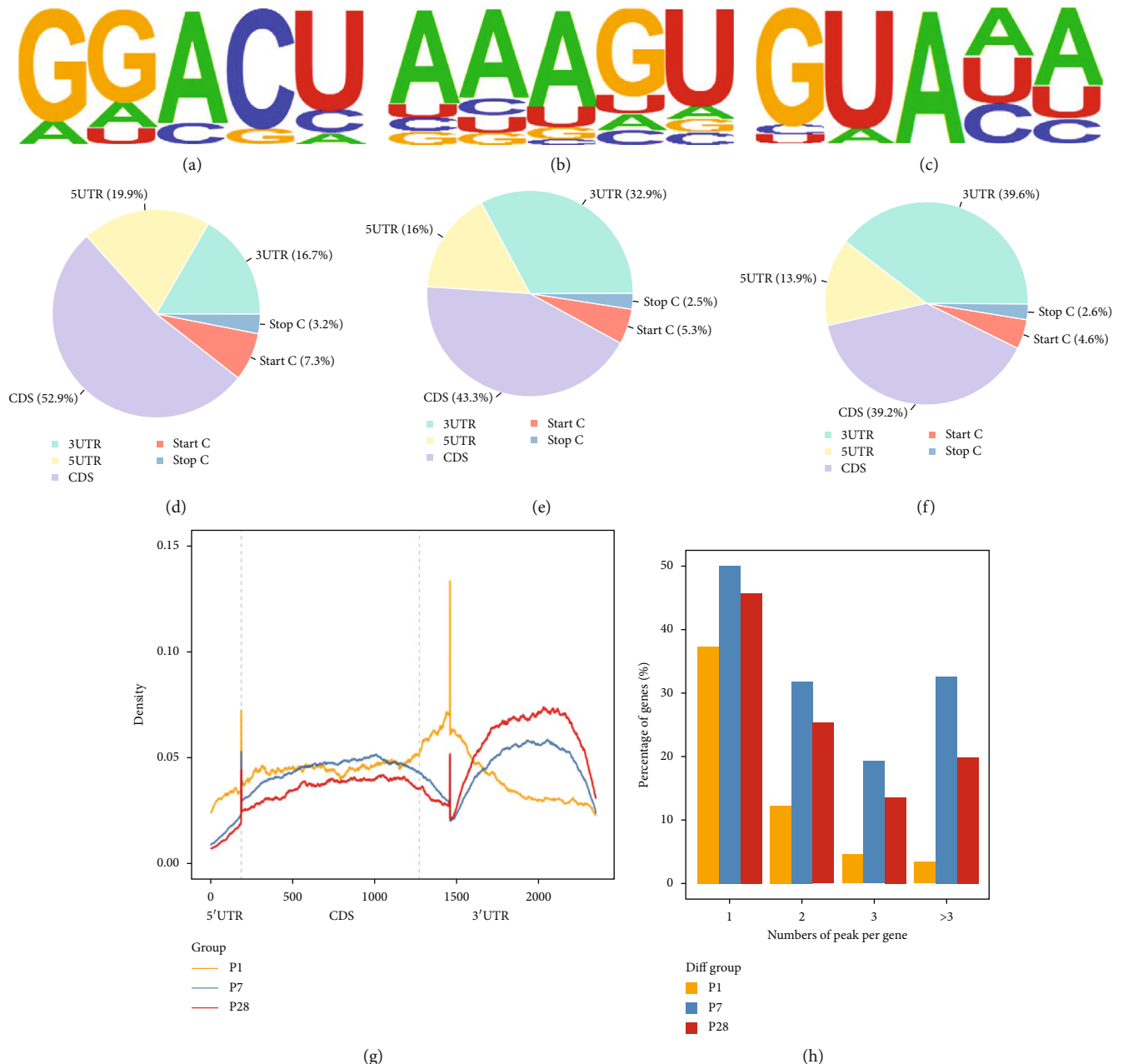
Figure 2: The profiles of m6A peaks and the joint analysis of m6A-seq and RNA-seq. (a–c) Motif with maximum P value of m6a in the P1, P7, and P28 heart tissues. (d–f) Pie chart of m6A peaks in different regions of P1, P7, and P28 heart tissues mRNA. (g) The m6A density distribution of P1, P7, and P28 heart tissues. All groups appeared at 3′UTR mostly. (h) The number of m6A peaks in P1, P7, and P28 heart tissues on each mRNA. Only one methylation peak appears among most mRNAs in each of the three groups.

[11, 24]. GGACU ($P = 1e − 93$), AAAGU ($P = 1e − 87$), and GUAAA ($P = 1e − 63$) were the most common and reliable among the motifs in P1, P7, and P28 heart tissues, respectively (Figures 2(a)–2(c)). We, thus, speculated that difference in motifs might be one of the factors that caused m6A differences.

3.4. Analysis of Regions of mRNA Methylation in Different Developmental Stages of Heart Tissues. The analysis of the regions of mRNA methylation peaks showed that m6A was distributed in all regions of the mRNA (Figures 2(d)–2(f)).

We observed that m6A was mostly distributed at the CDS region and 3′UTR near the stop codon in each group, which is suggestive of the direction of translational regulation, as previously described [16, 38]. Furthermore, we found that with the progression of heart development, the distribution of m6A in 5′UTR (P1: 19.9%, P7: 16%, and P28: 13.9%), CDS (P1: 52.9%, P7: 43.3%, and P28: 39.2%), and start codon (P1: 7.3%, P7: 5.3%, and P28: 4.6%) decreased gradually, but increased at 3′UTR (P1: 16.7%, P7: 32.9%, and P28: 39.6%). Nevertheless, the stop codon remained the lowest distribution in each group of heart tissues (P1: 3.2%, P7: 2.5%, and P28:

2.6%) (all $P < 0.05$, $\text{Log}_2\text{FC} > 1.5$). As shown in Figure 2(g), the m6A density shifted to $3'\text{UTR}$ and stop codon regions from P1 to P28. These findings are consistent with previous research in Homo sapiens' mRNA methylation characteristic between neonate and adult [39], indicating that the m6A landscape of humans and mice was highly homologous.

3.5. Density Distribution of m6A Peaks across mRNA Transcripts.
In each of the three groups, most of the m6A-modified mRNAs contained only one m6A peak, whereas a small number of them contained two or more peaks (Figure 2(h)), which was in accordance with previous studies [38]. And this characteristic in the P7 heart tissues was particularly high (~50%, $P < 0.05$). Likewise, the quantities of mRNAs with two or more m6A peaks were the largest in day 7 heart tissues.

3.6. Effect of RNA m6A Modifications on Gene Transcriptional Expression.
We performed a joint analysis of the gene transcriptome and methylation (all $P < 0.05$, $\text{Log}_2\text{FC} > 1$). The result demonstrated that there were more upregulated methylated mRNAs in the P28 heart tissues than in P1 and more downregulated methylated mRNAs in P7 than in P1 heart tissues (Figures 3(a) and 3(b)). Among the 450 P28 heart tissue genes that were upmethylated, 162 genes were upregulated and 50 genes were downregulated as compared to P1. Among the 1269 genes that were downmethylated in P7 heart tissues, a total of 246 genes were upregulated and 194 genes were downregulated as compared to P1. However, barely any methylation difference appeared in DEGs between P7 and P28 (Figure 3(c)). The differences in the transcription level of hyper- and hypomethylation peaks and their corresponding genes are shown in Tables 1–4. Moreover, we noticed that some genes that were highly expressed, respectively, in both the P1 and the P7 heart tissues were rarely expressed in the P28 heart tissues, such as plekaha6 and megf6. Taken together, it may indicate that m6A-modified genes tended to have a positive regulation of expression in developing heart tissues, but further validation is required to verify this hypothesis.

Furthermore, we performed a heat map by Z-score analysis ($P < 0.05$) on the expression of various methylases in different developmental stages of mouse hearts. The result showed that there was no significant difference in the expression of "writers" at different developmental stages. By contrast, in "erasers," the expression of ALKBH5 was more abundant than that of FTO, the expression of ALKBH5 was higher at P1 than at P7 and P28, and IGF2BP3 was the most highly differentially expressed "reader" protein and it decreased gradually from P1 to P28. These findings implied that "eraser" and "reader" seem to play a more important regulatory role as compared to "writers" in the development of mouse heart, especially when some methylases are highly expressed at P1. According to previous reports, the mouse heart at P1 has the strongest proliferative and regenerative capability [12], but whether these methylases highly expressed in P1 mouse heart tissues could regulate the proliferation and regeneration of mouse heart needs further work to explore.

3.7. Bioinformatics Analysis of Functional Genomics.
Given that the 7th day of heart development is being considered a watershed in myocardial regeneration and proliferation, we divided the results into two parts for bioinformatics analysis as follows.

3.7.1. P7 Compared to P1.
For the GO terms of BP category, genes with hypermethylated m6A sites were significantly enriched in the "intracellular protein transmembrane transport," "negative regulation of cytosolic calcium ion concentration," and "vesicle-mediated transmembrane transport," while hypomethylated genes were highly enriched in "glycerophospholipid metabolic process" and "phospholipid biosynthetic process." For the CC part, genes with hypermethylated m6A sites were mainly related to "Golgi stack" and "nuclear transcriptional repressor complex," while hypomethylated genes were primarily enriched in "trans-Golgi network" and "extracellular matrix." As for the analysis of MF, it revealed that the "transmembrane receptor protein tyrosine kinase activity," "ATP-dependent helicase activity," and "ligand-gated cation channel activity" were mostly enriched in genes with hypermethylated m6A sites, while the hypomethylated genes were primarily enriched in "guanyl-nucleotide exchange factor activity" and "active transmembrane transporter activity" (Figures 4(a) and 4(b), all $P < 0.05$).

KEGG pathway analysis revealed that the most significantly overrepresented pathways among upmethylated transcripts were the "AMPK signaling pathway," "longevity regulation pathway," and "insulin signaling pathway" (Figure 4(e), $P < 0.05$), while the downmethylated mRNAs were significantly enriched in "glycerophospholipid metabolism," "ECM-receptor interaction," and "microRNAs in cancer" (Figure 4(f), $P < 0.05$).

3.7.2. P28 Compared to P1.
The GO analysis of BP showed that the genes with hypermethylated m6A sites were significantly enriched in "regulation of protein exit from endoplasmic reticulum," "macromolecule methylation," and "protein methylation," while the hypomethylated genes were significantly detected in "cell surface receptor signaling pathway involved in cell-cell signaling," "Wnt signaling pathway," and "cardiac chamber formation." The CC part indicated that the genes with hypermethylated m6A sites were mainly related to "intercellular canaliculus" and "integral component of endoplasmic reticulum membrane," and the hypomethylated genes were mostly related to "lamellipodium" and "contractile actin filament bundle." The analysis of MF revealed that the genes with hypermethylated m6A sites were mostly enriched in the "active transmembrane transporter activity," "transcription factor activity," and "direct ligand-regulated sequence-specific DNA binding," whereas the hypomethylated genes were primarily related to "proximal promoter DNA-binding transcription activator activity," "RNA polymerase II-specific," and "transmembrane receptor protein tyrosine kinase activity" (Figures 4(c) and 4(d), all $P < 0.05$).

Pathway analysis revealed that upmethylated transcripts were involved in "ABC transporter," "cell motility," and "cell adhesion molecules" (Figure 4(g), $P < 0.05$), whereas downregulated transcripts included "Wnt signaling pathway,"

(a)

(b)

(c)

(d)
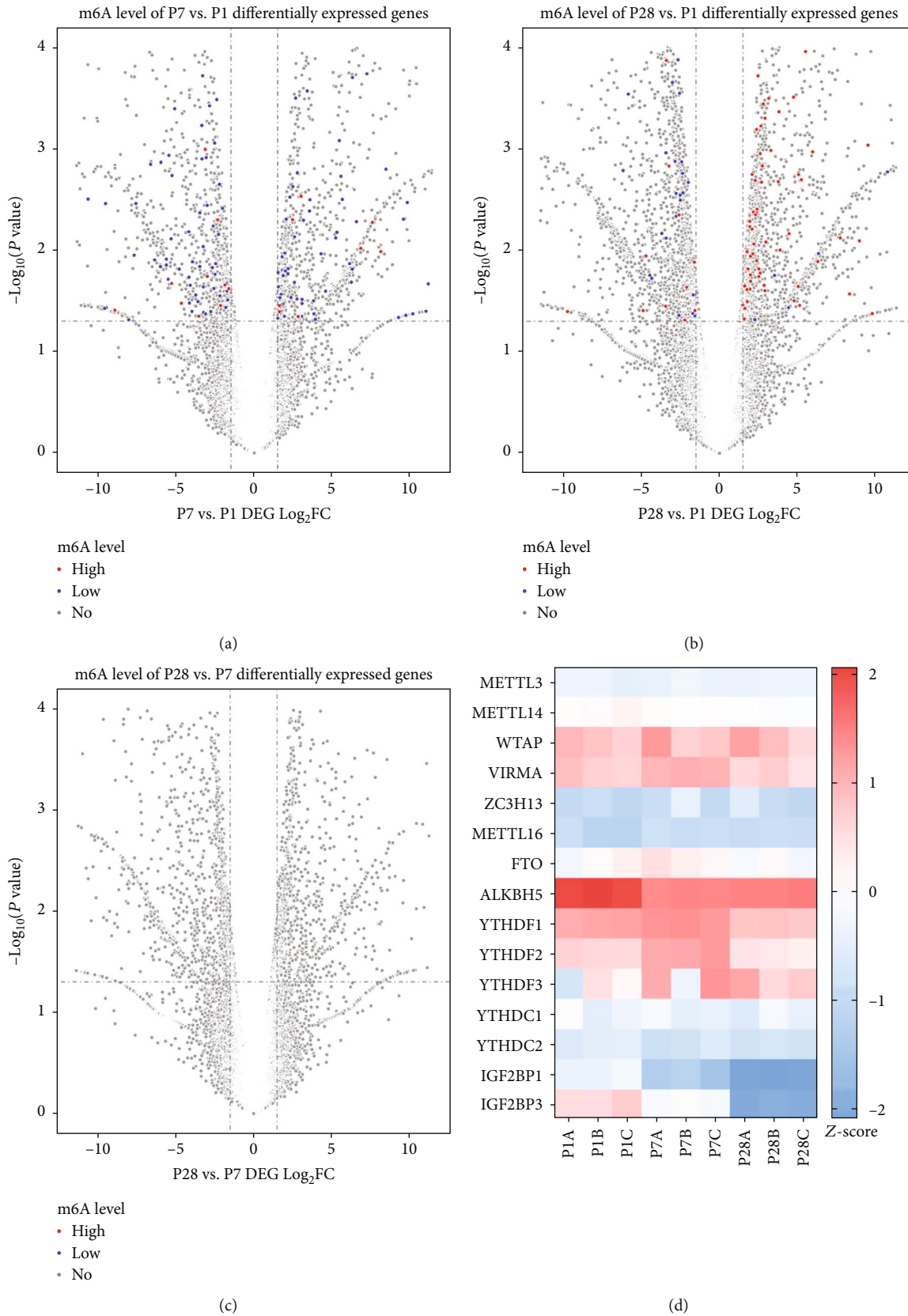
FIGURE 3: Joint analysis of gene transcriptome and methylation. (a) Different gene expressions combining with methylation level in P7 and P1 heart tissues. (b) Different gene expressions combining with methylation level in P28 and P1 heart tissues. (c) Different gene expressions combining with methylation level in P28 and P7 heart tissues. (d) Heat map of a series of methylase expression ($P < 0.05$, $-2 \leq Z\text{-score} \leq 2$).

TABLE 1: Top ten upmethylation peaks and their corresponding genes (P7 *vs.* P1).

Chromosome	TxStart	TxEnd	Gene name	Fold change
4	88760543	88760643	**Gm13283 ↑**	349.8
13	21810736	21810849	**Gm19658 ↑**	38.3
16	17209752	17209927	**Rimbp3**	15.3
13	21810739	21810864	**Hist1h2ao**	13.9
3	96240117	96240167	**Gm20632**	9.1
3	96240098	96240173	**H2ac19**	8.5
17	47468660	47468760	**AI661453 ↑**	7.9
7	83935631	83935681	**Cemip ↓**	7.1
7	109752344	109752444	**4930431P19Rik ↑**	6.9
7	131341694	131341794	**2310057M21Rik**	5.5

Top ten upmethylation peaks and their corresponding genes (P7 *vs.* P1). Fold change represents methylation peak's degree. Arrow represents up or down regulation of gene expression, $\mathrm{Log_2FC} > 1.5$, $P < 0.05$ (no arrow means no statistically significant change).

TABLE 2: Top ten downmethylation peaks and their corresponding genes (P7 *vs.* P1).

Chromosome	TxStart	TxEnd	Gene name	Fold change
7	131391143	131391193	**Pstk ↑**	81.6
2	53218067	53218117	**Arl6ip6**	60.7
X	71315056	71315181	**Mtm1 ↓**	58.0
12	69963717	69963767	**Atl1**	27.7
2	122447916	122452011	**Slc28a2**	20.6
4	139962219	139962419	**Klhdc7a ↑**	20.0
2	122452036	122452531	**Slc28a2**	19.70
2	23507969	23508019	**Spopl**	18.1
5	149186468	149186518	**Uspl1 ↓**	17.4
17	84184705	84184805	**Zfp36l2**	15

Top ten downmethylation peaks and their corresponding genes (P7 *vs.* P1). Fold change represents methylation peak's degree. Arrow represents up or down regulation of gene expression, $\mathrm{Log_2FC} > 1.5$, $P < 0.05$ (no arrow means no statistically significant change).

TABLE 3: Top ten upmethylation peaks and their corresponding gene (P28 *vs.* P1).

Chromosome	TxStart	TxEnd	Gene name	Fold change
2	86042835	86043035	**Olfr1033**	59.9
7	74359749	74359849	**Slco3a1 ↑**	28.3
4	139962244	139962419	**Klhdc7a ↑**	26.1
11	55179387	55180723	**Slc36a2**	24.5
19	10450168	10450218	**Syt7 ↑**	21.8
8	83572497	83572547	**Tecr ↓**	20.2
6	24570892	24571067	**Asb15 ↓**	19.5
14	101442734	101442859	**Tbc1d4 ↑**	19.4
12	91633008	91633133	**Ston2 ↑**	19.3
8	83572397	83572472	**Nr1d2**	16.4

Top ten upmethylation peaks and their corresponding genes (P28 *vs.* P1). Fold change represents methylation peak's degree. Arrow represents up or down regulation of gene expression, $\mathrm{Log_2FC} > 1.5$, $P < 0.05$ (no arrow means no statistically significant change).

TABLE 4: Top ten downmethylation peaks and their corresponding genes (P28 *vs.* P1).

Chromosome	TxStart	TxEnd	Gene name	Fold change
12	27342363	27342463	**Sox11 ↓**	48.5
3	96240098	96240173	**H2ac19**	17.7
3	96240092	96240192	**Gm20632**	16.7
3	96268599	96268899	**Gm20628**	13.3
11	62648384	62648484	**Lrrc75a**	13.1
7	143460986	143461050	**Cdkn1c ↓**	12.8
4	109666053	109666103	**Cdkn2c**	11.9
3	96268653	96268903	**H3c13 ↓**	11.4
13	23533930	23534005	**H2ac10 ↓**	11.1
13	23574380	23574680	**H2ac7 ↓**	10.8

Top ten downmethylation peaks and their corresponding genes (P28 *vs.* P1). Fold change represents methylation peak's degree. Arrow represents up or down regulation of gene expression, $\mathrm{Log_2FC} > 1.5$, $P < 0.05$ (no arrow means no statistically significant change).

"gastric cancer," and "alcoholism" mostly (Figure 4(h), $P < 0.05$).

To sum up, there were differences between the results of these two parts. What mainly be methylated in the P7 heart tissues were genes governing cell-to-cell transport and signal transduction, while in the P28 heart tissues were genes more related to the function of macromolecules such as organelle formation. However, the overlaps that were identified in both parts, such as the "ABC transporters" and "ECM-receptor interaction pathway" of KEGG, most likely play significant roles in myocardial development process.

3.8. Verification of Significant Genes and Proteins. On the basis of the m6A methylation analysis results described above, we further validated at the gene or protein levels of the major m6A methylases and genes with noteworthy differences both in methylation and expression using qPCR and western blot analysis. The qPCR results showed significant increases of GAT4and Tet2, but decreases of IGF2BP3and MEGF6 (Figure 5(a)), which were in general in agreement with the findings obtained using gene profiling. Similarly, western blot results showed that the expression of "writer"
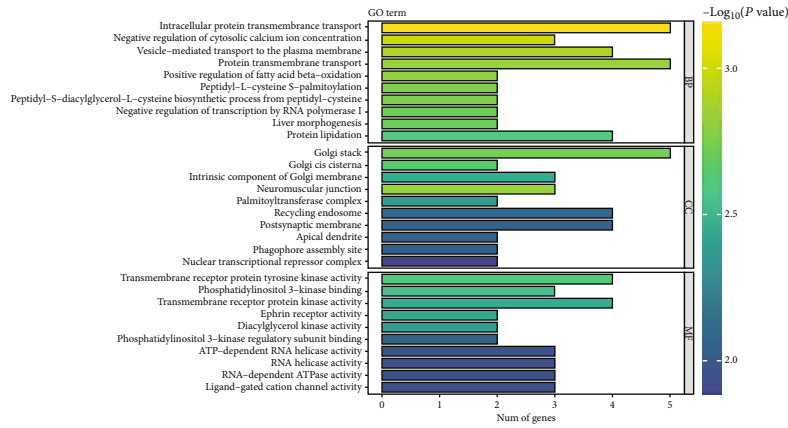
(a)
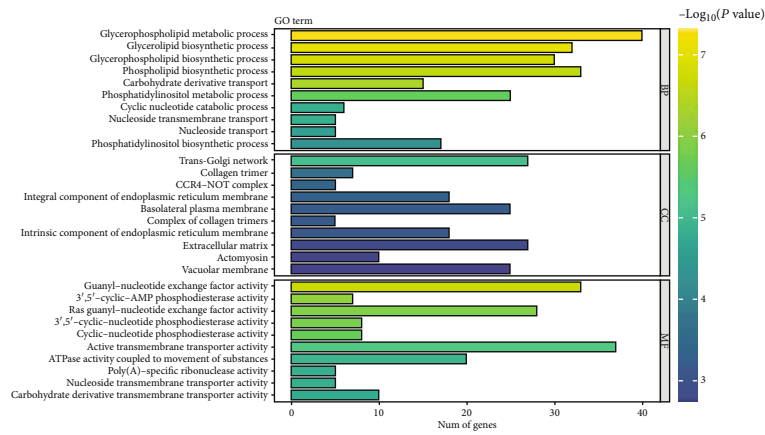
(b)
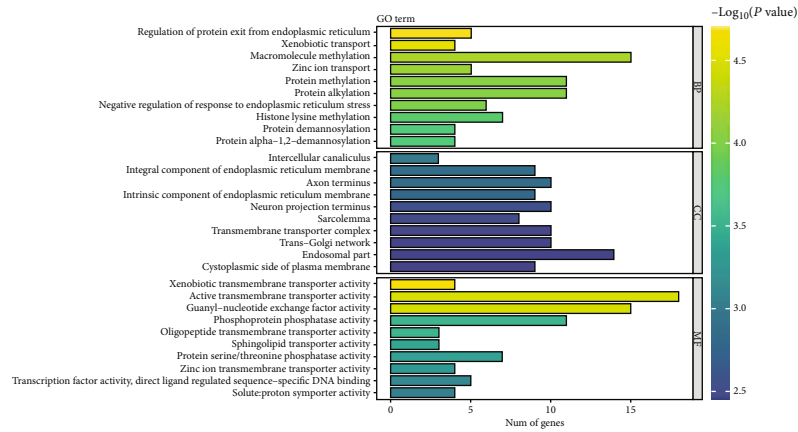
(c)

FIGURE 4: Continued.

(d)

(e)

(f)

(g)

(h)
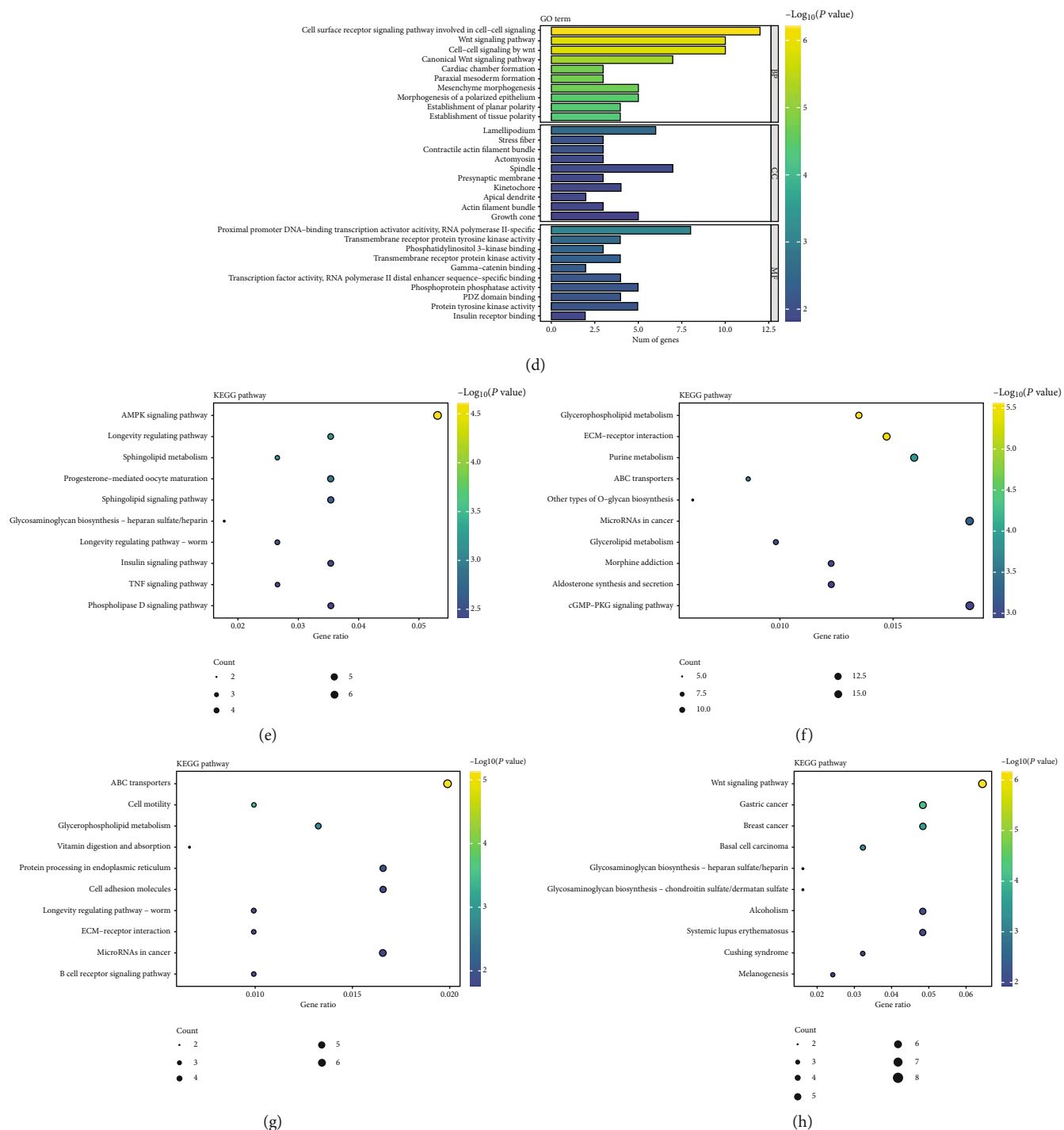
FIGURE 4: Gene Ontology and KEGG analysis of comparing C57B/L different day-old heart tissues. (a, b) Biological processes (BP), cell component (CC), and molecular functions (MF) of hyper- and hypomethylated genes in P7 as compared to P1. (c, d) Biological processes (BP), cell component (CC), and molecular functions (MF) of hyper- and hypomethylated genes in P28 as compared to P1. (e, f) KEGG pathway analysis of hyper- and hypomethylated genes in P7 as compared to P1. (g, h) KEGG pathway analysis of hyper- and hypomethylated genes in P28 as compared to P1.

METTL 3 was upregulated in the P7 heart tissues and then dropped down in the P28 heart tissue, but still higher than that in the P1 heart tissue, which was consistent with the distribution of m6A methylation sites on the chromosome (Figures 5(b), 5(c), and 1(e)). The high expression of "eraser" FTO may exert synergistic action on the hypomethylation in

P1. However, YTHDC1 and IGF2BP3, as the representative of "YTH" and "IGF" family of "reader," changed differently over time from P1 to P28, with increased YTHDC1 and decreased IGF2BP3 (Figures 5(b) and 5(c)), which may be related to the regulation of different downstream target proteins at different times.
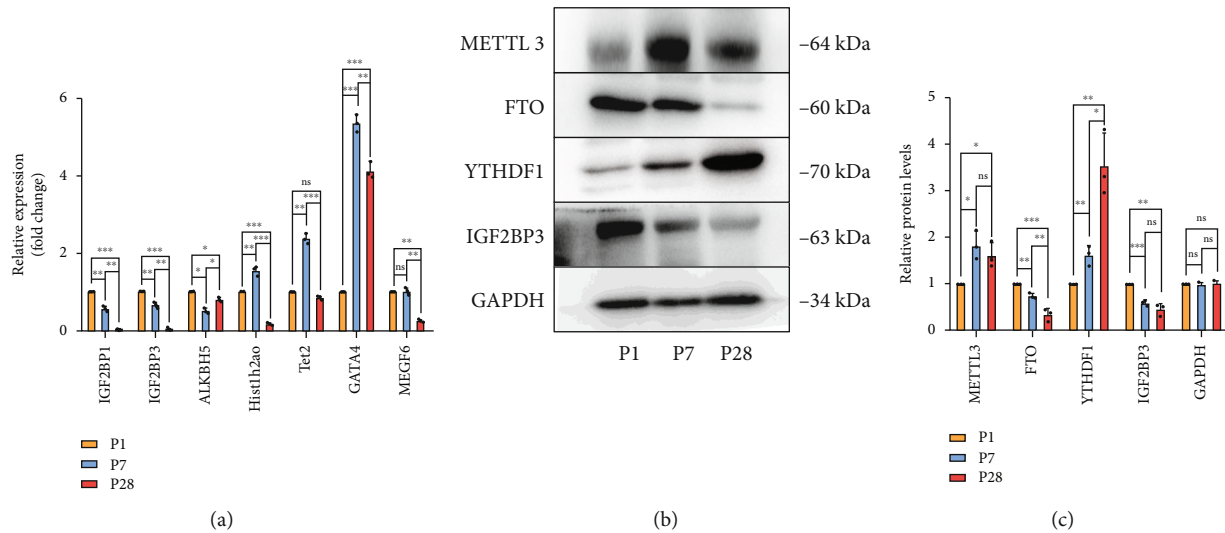
FIGURE 5: Verification of significant genes. (a) qPCR result of noteworthy methylases and genes in mouse heart tissues. (b, c) Western blot showing the representative methylases in mouse heart tissues, quantitated by ImageJ. Values are the mean ± S.D. of $n = 3$ independent experiments. $^{*}P < 0.05$; $^{**}P < 0.01$; $^{***}P < 001$; ns: not significant.

4. Discussion

m6A, a dynamic and reversible modification among different species, is one of the most common and functional RNA modifications [16–18, 40, 41]. More and more studies showed that m6A RNA methylation plays a critical role in regulating RNA metabolic processes, which was increasingly found in mammalian failing hearts and hypoxic cardiomyocytes [31, 42, 43]. In the current study, we reported the m6A distribution and differences of mRNA in C57BL/6J hearts over time during the early development stages by illustrating global m6A modification patterns and analyzing gene expression, function, and related pathways.

We revealed that the pattern of m6A modification in the neonatal mouse heart tissue was distinct from that of the adult mice. Interestingly, in the P1 heart tissues, the amount and level of global m6A peaks detected were the lowest. But when compared with the P7 heart tissues in which it possessed the largest amount and highest level of m6A peaks, it was found that most of the peaks in P1 were hypermethylated. These specific and critical genes with aberrant hypermethylation against the globally low m6A modification tendency in P1 may be the key why neonates possess the efficient proliferative and regenerative capability. Thus, we presumed that some hypermethylated genes functioned at P1 and then misfunctioned after demethylation over time. By analyzing different methylated transcripts and peaks, various biological processes and pathways that control cardiomyocyte proliferation, such as the Wnt signaling pathway [44], were found to be significantly enriched, suggesting that there exists a relationship between abnormal m6A modification and cardiac tissue regeneration and proliferation. The global change of m6A modification spectrum may be caused by the abnormal expression of m6A key enzymes [40, 45]. According to the result of the RNA-seq, differences in the expression levels of "writers," "erasers," and "readers" of m6A do exist in

the heart tissues from mice at different days during their early life stage.

Previous studies have shown that the proliferation and regeneration ability of heart tissue basically disappears around the 7th day of development, and the cell cycle of cardiomyocytes no longer exists, with only a very small proliferation rate remaining [12–14]. The underlying mechanism is still unclear. It is the terminal differentiation and nonrenewability of myocardial tissue in adulthood that prevent the heart from proliferating and repairing itself after the heart injuries, such as ischemia reperfusion injury (IRI) and MI [10–14]. The response of the mammalian heart to MI and the concomitant cell death is the substitution of fibroblasts, extracellular matrix reticulum, and proliferating cells for the damaged myocardium, thereby the scar-forming, called ventricular remodeling [46, 47]. Extensive cell therapy studies have used embryonic stem cells (ESC) and induced pluripotent stem cells (iPSC) as exogenous sources of new cardiomyocytes for treatment [9, 48]. After being transplanted into the infarcted heart, they can play a beneficial role in the repair of local and global cardiac regeneration function [49]. However, before being used clinically, some potential adverse effects need to be resolved, such as unstable phenotypes [50], low efficient cardiomyocyte transformation rate [51], tumorigenic potential [52], and arrhythmia and rejection [53]. Therefore, reactivation of the cell cycle of cardiomyocytes and stimulation of their proliferation capacity seem to be the most direct approach. Available data and results provide various strategies to trigger this process and generate new cardiomyocytes, such as the direct transdifferentiation mediated by small molecules, transcription factors, and ncRNAs. The modification of m6A has been found to be extremely important for sperm development in existing studies [54]. When the "reader" protein is inactivated, the level of m6A RNA modification mediated by it decreases significantly, leading to a significant imbalance in the posttranscriptional

translation efficiency of related genes that regulate the fate determination of spermatogonial stem cells and sperm formation. It has also been shown that "writer" METTL14 plays a major role in endothelial cell inflammation induced by tumor necrosis factor-α [55]. METTL14 induces endothelial cell inflammation and atherosclerotic plaque by enhancing the m6A modification of FOXO1 and promoting its expression. Meanwhile, the latest studies have shown that m6A can regulate cardiomyocyte renewal [31] and the "eraser" ALKBH5 can regulate the proliferation of cardiomyocytes by demethylating YTHDF1 [56]. The findings of these studies strongly indicate that m6A is important for heart development and can promote the proliferation and differentiation of stem cells in heart disease. In our current study, in addition to explore the regulatory role of m6A modification on gene expression during heart development, a more important purpose is to find a potential therapeutic target for IRI or MI. We thus focused on analyzing and identifying the key genes related to proliferation regulated by m6A modification by comparing heart tissues at different day-ages during development with the potential to stimulate them to arousing myocardium proliferation after IRI and MI injury to achieve the therapeutic purpose. Our results show that, from the peaks and clusters of the three groups of samples, m6A modification tends to be positively correlated with mRNA expression, consistent with some previous observations [57, 58], but differed from other studies [24, 59]. This discrepancy may be due to the differences in animal tissue sources and sample collection, but it still has significant implications. In addition, the specific role of m6A modification in gene expression depends to a large extent on the downstream function of the m6A "readers" [60–62], which have been reported to affect multiple aspects of target RNA metabolism by recognizing different m6A regions, including RNA localization, splicing, transport, translation, and stability [63]. Knocking down or overexpressing key methylases may be a good strategy for studying m6A methylation-mediated cellular responses. Furthermore, the m6A-seq and mRNA-seq data collectively show that there are genes regulated by m6A in a positive or negative manner (Tables 1–4, $\text{Log}_2\text{FC} > 1$, $P < 0.05$). Besides the methylases, we found that there were remarkable changes in Tet2, GATA4, and MEGF6 in our sequencing results, which were associated with proliferation in other tissues such as the lung and colorectum as shown in other studies [64, 65]. We speculate that these genes with specific m6A modification may also be capable of promoting myocardial proliferation and regeneration which deserve further study. By integrating the latest nanotechnology, m6A modification may provide a new direction for treating heart diseases [66, 67].

5. Conclusions

In summary, our research reveals differences in m6A of mRNA of C57BL/6J heart tissue at different developmental stages and shows the distribution and possible function of m6A through statistical analysis and thorough bioinformatics analysis. Our studies have provided a fundamental contribution for further researches aimed at identifying novel therapeutic strategy for heart IRI and MI. However, additional studies are necessary not only to understand the underlying mechanism of m6A in the myocardial regeneration but also for the therapeutic implication for cardiovascular problems.

Abbreviations

BP: Biological process
CC: Cellular component
CDS: Coding sequences
$3'$UTR: $3'$-Untranslated regions
CMs: Cardiac cardiomyocytes
DEGs: Differentially expressed genes
FC: Fold change
FE: Fold enrichment
IRI: Ischemia reperfusion injury
MI: Myocardial infarction
MF: Molecular function
RIN: RNA integrity number.

Data Availability

The data used to support the findings of this study are available from the corresponding author upon request.

Conflicts of Interest

The authors have declared that no competing interest exists.

Authors' Contributions

Yuhui Yang and Siman Shen contributed equally to this work.

Acknowledgments

References

[1] M. Li and J. C. Izpisua Belmonte, "Mending a faltering heart," *Circulation Research*, vol. 118, no. 2, pp. 344–351, 2016.

[2] C. Mummery, D. Ward-van Oostwaard, P. Doevendans et al., "Differentiation of human embryonic stem cells to cardiomyocytes: role of coculture with visceral endoderm-like cells," *Circulation*, vol. 107, no. 21, pp. 2733–2740, 2003.

[3] X. Sun, J. Wu, B. Qiang et al., "Transplanted microvessels improve pluripotent stem cell-derived cardiomyocyte engraftment and cardiac function after infarction in rats," *Science Translational Medicine*, vol. 12, no. 562, 2020.

[4] P. Nigro, B. Bassetti, L. Cavallotti, V. Catto, C. Carbucicchio, and G. Pompilio, "Cell therapy for heart disease after 15 years: unmet expectations," *Pharmacological Research*, vol. 127, pp. 77–91, 2018.

[5] T. Wongtawan, J. E. Taylor, K. A. Lawson, I. Wilmut, and S. Pennings, "Histone H4K20me3 and HP1α are late heterochromatin markers in development, but present in

undifferentiated embryonic stem cells," *Journal of Cell Science*, vol. 124, no. 11, pp. 1878–1890, 2011.

[6] C. E. Nestor, R. Ottaviano, D. Reinhardt et al., "Rapid reprogramming of epigenetic and transcriptional profiles in mammalian culture systems," *Genome Biology*, vol. 16, no. 1, 2015.

[7] M. Ponnusamy, F. Liu, Y. H. Zhang et al., "Long noncoding RNA CPR (cardiomyocyte proliferation regulator) regulates cardiomyocyte proliferation and cardiac repair," *Circulation*, vol. 139, no. 23, pp. 2668–2684, 2019.

[8] M. Xin, Y. Kim, L. B. Sutherland et al., "Hippo pathway effector Yap promotes cardiac regeneration," *Proceedings of the National Academy of Sciences of the United States of America*, vol. 110, no. 34, pp. 13839–13844, 2013.

[9] T. R. Heallen, Z. A. Kadow, J. H. Kim, J. Wang, and J. F. Martin, "Stimulating cardiogenesis as a treatment for heart failure," *Circulation Research*, vol. 124, no. 11, pp. 1647–1657, 2019.

[10] Y. Li, J. Feng, S. Song et al., "gp130 controls cardiomyocyte proliferation and heart regeneration," *Circulation*, vol. 142, no. 10, pp. 967–982, 2020.

[11] K. Kikuchi, "Dedifferentiation, transdifferentiation, and proliferation: mechanisms underlying cardiac muscle regeneration in zebrafish," *Current Pathobiology Reports*, vol. 3, no. 1, pp. 81–88, 2015.

[12] E. R. Porrello, A. I. Mahmoud, E. Simpson et al., "Transient regenerative potential of the neonatal mouse heart," *Science*, vol. 331, no. 6020, pp. 1078–1080, 2011.

[13] E. Lázár, H. A. Sadek, and O. Bergmann, "Cardiomyocyte renewal in the human heart: insights from the fall-out," *European Heart Journal*, vol. 38, no. 30, pp. 2333–2342, 2017.

[14] Y. Fan, Y. Cheng, Y. Li et al., "Phosphoproteomic analysis of neonatal regenerative myocardium revealed important roles of checkpoint kinase 1 via activating mammalian target of rapamycin C1/ribosomal protein S6 kinase b-1 pathway," *Circulation*, vol. 141, no. 19, pp. 1554–1569, 2020.

[15] S. Schwartz, D. A. Bernstein, M. R. Mumbach et al., "Transcriptome-wide mapping reveals widespread dynamic-regulated pseudouridylation of ncRNA and mRNA," *Cell*, vol. 159, no. 1, pp. 148–162, 2014.

[16] D. Dominissini, S. Moshitch-Moshkovitz, S. Schwartz et al., "Topology of the human and mouse m^{6}A RNA methylomes revealed by m^{6}A-seq," *Nature*, vol. 485, no. 7397, pp. 201–206, 2012.

[17] Z. Bodi, A. Bottley, N. Archer, S. T. May, and R. G. Fray, "Yeast m6A methylated mRNAs are enriched on translating ribosomes during meiosis, and under rapamycin treatment," *PLoS One*, vol. 10, no. 7, article e0132090, 2015.

[18] Y. Wan, K. Tang, D. Zhang et al., "Transcriptome-wide high-throughput deep m6A-seq reveals unique differential m6A methylation patterns between three organs in Arabidopsis thaliana," *Genome Biology*, vol. 16, no. 1, 2015.

[19] H. Yue, X. Nie, Z. Yan, and S. Weining, "N6-Methyladenosine regulatory machinery in plants: composition, function and evolution," *Plant Biotechnology Journal*, vol. 17, no. 7, pp. 1194–1208, 2019.

[20] H. B. Li, J. Tong, S. Zhu et al., "m^{6}A mRNA methylation controls T cell homeostasis by targeting the IL-7/STAT5/SOCS pathways," *Nature*, vol. 548, no. 7667, pp. 338–342, 2017.

[21] T. Sun, R. Wu, and L. Ming, "The role of m6A RNA methylation in cancer," *Biomedicine & Pharmacotherapy*, vol. 112, p. 108613, 2019.

[22] Z. Zhang, K. Luo, Z. Zou et al., "Genetic analyses support the contribution of mRNA N^6-methyladenosine (m^{6}A) modification to human disease heritability," *Nature Genetics*, vol. 52, no. 9, pp. 939–949, 2020.

[23] R. Wu, D. Jiang, Y. Wang, and X. Wang, "N (6)-Methyladenosine (m(6)a) methylation in mRNA with a dynamic and reversible epigenetic modification," *Molecular Biotechnology*, vol. 58, no. 7, pp. 450–459, 2016.

[24] X. Wang, Z. Lu, A. Gomez et al., "N^6-methyladenosine-dependent regulation of messenger RNA stability," *Nature*, vol. 505, no. 7481, pp. 117–120, 2014.

[25] P. Mathiyalagan, M. Adamiak, J. Mayourian et al., "FTO-dependent N6-methyladenosine regulates cardiac function during remodeling and repair," *Circulation*, vol. 139, no. 4, pp. 518–532, 2019.

[26] Y. Wang, Y. Li, M. Yue et al., "N^6-methyladenosine RNA modification regulates embryonic neural stem cell self-renewal through histone modifications," *Nature Neuroscience*, vol. 21, no. 2, pp. 195–206, 2018.

[27] F. Xiong, T. Lin, M. Song et al., "Antenatal hypoxia induces epigenetic repression of glucocorticoid receptor and promotes ischemic-sensitive phenotype in the developing heart," *Journal of Molecular and Cellular Cardiology*, vol. 91, pp. 160–171, 2016.

[28] M. Takeda, L. E. Briggs, H. Wakimoto et al., "Slow progressive conduction and contraction defects in loss of Nkx2-5 mice after cardiomyocyte terminal differentiation," *Laboratory Investigation*, vol. 89, no. 9, pp. 983–993, 2009.

[29] P. D. Nguyen, D. E. M. de Bakker, and J. Bakkers, "Cardiac regenerative capacity: an evolutionary afterthought?," *Cellular and Molecular Life Sciences*, vol. 78, no. 12, pp. 5107–5122, 2021.

[30] X. Sun, Q. Han, H. Luo et al., "Profiling analysis of long noncoding RNAs in early postnatal mouse hearts," *Scientific Reports*, vol. 7, no. 1, 2017.

[31] B. Li, Y. Hu, X. Li et al., "Sirt1 antisense long noncoding RNA promotes cardiomyocyte proliferation by enhancing the stability of Sirt1," *Journal of the American Heart Association*, vol. 7, no. 21, article e009700, 2018.

[32] A. Kechin, U. Boyarskikh, A. Kel, and M. Filipenko, "cutPrimers: a new tool for accurate cutting of primers from reads of targeted next generation sequencing," *Journal of Computational Biology*, vol. 24, no. 11, pp. 1138–1143, 2017.

[33] D. Kim, B. Langmead, and S. L. Salzberg, "HISAT: a fast spliced aligner with low memory requirements," *Nature Methods*, vol. 12, no. 4, pp. 357–360, 2015.

[34] Y. Zhang, T. Liu, C. A. Meyer et al., "Model-based analysis of ChIP-Seq (MACS)," *Genome Biology*, vol. 9, no. 9, p. R137, 2008.

[35] L. Shen, N. Y. Shao, X. Liu, I. Maze, J. Feng, and E. J. Nestler, "diffReps: detecting differential chromatin modification sites from ChIP-seq data with biological replicates," *PLoS One*, vol. 8, no. 6, 2013.

[36] M. Ashburner, C. A. Ball, J. A. Blake et al., "Gene ontology: tool for the unification of biology," *Nature Genetics*, vol. 25, no. 1, pp. 25–29, 2000.

[37] D. W. Huang, B. T. Sherman, and R. A. Lempicki, "Bioinformatics enrichment tools: paths toward the comprehensive functional analysis of large gene lists," *Nucleic Acids Research*, vol. 37, no. 1, pp. 1–13, 2009.

[38] K. D. Meyer, Y. Saletore, P. Zumbo, O. Elemento, C. E. Mason, and S. R. Jaffrey, "Comprehensive analysis of mRNA

methylation reveals enrichment in $3'$ UTRs and near stop codons," *Cell*, vol. 149, no. 7, pp. 1635–1646, 2012.

[39] H. Zhang, X. Shi, T. Huang et al., "Dynamic landscape and evolution of m6A methylation in human," *Nucleic Acids Research*, vol. 48, no. 11, pp. 6251–6264, 2020.

[40] K. D. Meyer and S. R. Jaffrey, "The dynamic epitranscriptome: N^6-methyladenosine and gene expression control," *Nature Reviews. Molecular Cell Biology*, vol. 15, no. 5, pp. 313–326, 2014.

[41] Y. Fu, D. Dominissini, G. Rechavi, and C. He, "Gene expression regulation mediated through reversible m6A RNA methylation," *Nature Reviews. Genetics*, vol. 15, no. 5, pp. 293–306, 2014.

[42] W. Wei, X. Ji, X. Guo, and S. Ji, "Regulatory role of N6-methyladenosine (m6A) methylation in RNA processing and human diseases," *Journal of Cellular Biochemistry*, vol. 118, no. 9, pp. 2534–2543, 2017.

[43] J. Lexow, T. Poggioli, P. Sarathchandra, M. P. Santini, and N. Rosenthal, "Cardiac fibrosis in mice expressing an inducible myocardial-specific Cre driver," *Disease Models & Mechanisms*, vol. 6, no. 6, pp. 1470–1476, 2013.

[44] M. Ponnusamy, P. F. Li, and K. Wang, "Understanding cardiomyocyte proliferation: an insight into cell cycle activity," *Cellular and Molecular Life Sciences*, vol. 74, no. 6, pp. 1019–1034, 2017.

[45] K. D. Meyer and S. R. Jaffrey, "Rethinking m⁶A readers, writers, and erasers," *Annual Review of Cell and Developmental Biology*, vol. 33, no. 1, pp. 319–342, 2017.

[46] B. Luo, Z. He, S. Huang et al., "Long non-coding RNA 554 promotes cardiac fibrosis via TGF-β1 pathway in mice following myocardial infarction," *Frontiers in Pharmacology*, vol. 11, p. 585680, 2020.

[47] X. M. Gao, D. A. White, A. M. Dart, and X. J. Du, "Post-infarct cardiac rupture: recent insights on pathogenesis and therapeutic interventions," *Pharmacology & Therapeutics*, vol. 134, no. 2, pp. 156–179, 2012.

[48] M. L. Chang, Y. J. Chiu, J. S. Li, K. P. Cheah, and H. H. Lin, "Analyzing impetus of regenerative cellular therapeutics in myocardial infarction," *Journal of Clinical Medicine*, vol. 9, no. 5, p. 1277, 2020.

[49] M. A. Laflamme and C. E. Murry, "Heart regeneration," *Nature*, vol. 473, no. 7347, pp. 326–335, 2011.

[50] Y. K. Lee, Y. Jiang, X. R. Ran et al., "Recent advances in animal and human pluripotent stem cell modeling of cardiac laminopathy," *Stem Cell Research & Therapy*, vol. 7, no. 1, p. 139, 2016.

[51] S. S. Nunes, J. W. Miklas, J. Liu et al., "Biowire: a platform for maturation of human pluripotent stem cell-derived cardiomyocytes," *Nature Methods*, vol. 10, no. 8, pp. 781–787, 2013.

[52] J. Nussbaum, E. Minami, M. A. Laflamme et al., "Transplantation of undifferentiated murine embryonic stem cells in the heart: teratoma formation and immune response," *The FASEB Journal*, vol. 21, no. 7, pp. 1345–1357, 2007.

[53] Y. M. Zhang, C. Hartzell, M. Narlow, and S. C. Dudley Jr., "Stem cell-derived cardiomyocytes demonstrate arrhythmic potential," *Circulation*, vol. 106, no. 10, pp. 1294–1299, 2002.

[54] Z. Lin, P. J. Hsu, X. Xing et al., "Mettl3-/Mettl14-mediated mRNA N^6-methyladenosine modulates murine spermatogenesis," *Cell Research*, vol. 27, no. 10, pp. 1216–1230, 2017.

[55] D. Jian, Y. Wang, L. Jian et al., "METTL14 aggravates endothelial inflammation and atherosclerosis by increasing FOXO1

N6-methyladeosine modifications," *Theranostics*, vol. 10, no. 20, pp. 8939–8956, 2020.

[56] Z. Han, X. Wang, Z. Xu et al., "ALKBH5 regulates cardiomyocyte proliferation and heart regeneration by demethylating the mRNA of YTHDF1," *Theranostics*, vol. 11, no. 6, pp. 3000–3016, 2021.

[57] G. Z. Luo, A. MacQueen, G. Zheng et al., "Unique features of the m⁶A methylome in *Arabidopsis thaliana*," *Nature Communications*, vol. 5, no. 1, 2014.

[58] Z. Li, H. Weng, R. Su et al., "FTO plays an oncogenic role in acute myeloid leukemia as a N^6-methyladenosine RNA demethylase," *Cancer Cell*, vol. 31, no. 1, pp. 127–141, 2017.

[59] S. Schwartz, M. R. Mumbach, M. Jovanovic et al., "Perturbation of m6A writers reveals two distinct classes of mRNA methylation at internal and $5'$ sites," *Cell Reports*, vol. 8, no. 1, pp. 284–296, 2014.

[60] R. Fang, X. Chen, S. Zhang et al., "EGFR/SRC/ERK-stabilized YTHDF2 promotes cholesterol dysregulation and invasive growth of glioblastoma," *Nature Communications*, vol. 12, no. 1, p. 177, 2021.

[61] H. Huang, H. Weng, W. Sun et al., "Recognition of RNA N^6-methyladenosine by IGF2BP proteins enhances mRNA stability and translation," *Nature Cell Biology*, vol. 20, no. 3, pp. 285–295, 2018.

[62] S. Müller, N. Bley, B. Busch et al., "The oncofetal RNA-binding protein IGF2BP1 is a druggable, post-transcriptional super-enhancer of E2F-driven gene expression in cancer," *Nucleic Acids Research*, vol. 48, no. 15, pp. 8576–8590, 2020.

[63] B. S. Zhao and C. He, "Fate by RNA methylation: m⁶A steers stem cell pluripotency," *Genome Biology*, vol. 16, no. 1, 2015.

[64] A. S. Riching, E. Danis, Y. Zhao et al., "Suppression of canonical TGF-β signaling enables GATA4 to interact with H3K27me3 demethylase JMJD3 to promote cardiomyogenesis," *Journal of Molecular and Cellular Cardiology*, vol. 153, pp. 44–59, 2021.

[65] H. Hu, M. Wang, H. Wang et al., "MEGF6 promotes the epithelial-to-mesenchymal transition via the TGFβ/SMAD signaling pathway in colorectal cancer metastasis," *Cellular Physiology and Biochemistry*, vol. 46, no. 5, pp. 1895–1906, 2018.

[66] M. Mahmoudi, M. Yu, V. Serpooshan et al., "Multiscale technologies for treatment of ischemic cardiomyopathy," *Nature Nanotechnology*, vol. 12, no. 9, pp. 845–855, 2017.

[67] H. Yang, X. Qin, H. Wang et al., "An in vivo miRNA delivery system for restoring infarcted myocardium," *ACS Nano*, vol. 13, no. 9, pp. 9880–9894, 2019.

Research Article

Recombinant High-Mobility Group Box 1 (rHMGB1) Promotes NRF2-Independent Mitochondrial Fusion through CXCR4/PSMB5-Mediated Drp1 Degradation in Endothelial Cells

Shunrong Zhang (iD),[1,2] **Fei Feng** (iD),[2] **Jingting Dai** (iD),[2] **Jia Li** (iD),[2] **Xiangye Bu** (iD),[2] **and Xiaojie Xie** (iD)[1]

[1]*Department of Cardiology, Second Affiliated Hospital, Zhejiang University School of Medicine, Hangzhou, Zhejiang, China*
[2]*Department of Geriatrics, Affiliated Hangzhou First People's Hospital, Zhejiang University School of Medicine, Hangzhou, Zhejiang, China*

Correspondence should be addressed to Xiaojie Xie; xiexj@zju.edu.cn

Mitochondrial dynamics plays an important role in maintaining normal endothelial cell function and in the pathogenesis of cardiovascular disease. It is not identified whether high-mobility group box 1 (HMGB1), a representative damage-associated molecular pattern (DAMP) molecule, could influence mitochondrial dynamics in endothelial cells. The objective of this study is to clarify the effect of HMGB1 on mitochondrial dynamics in endothelial cells and the underlying mechanism. EA.hy926 human endothelial cells were incubated with recombinant HMGB1 (rHMGB1); mitochondrial morphology was observed with a confocal microscope and transmission electron microscope (TEM). The expression of dynamin-related protein 1 (Drp1), Mitofusin 1 (Mfn1), Mitofusin 2 (Mfn2), Optic atrophy 1 (Opa1), phosphatase and tensin homolog- (PTEN-) induced kinase 1 (PINK1), NOD-like receptor 3 (NLRP3), caspase 1, cleaved caspase 1, 20S proteasome subunit beta 5 (PSMB5), and antioxidative master nuclear factor E2-related factor 2 (NRF2) and the concentration of interleukin 1β (IL-1β) were determined. Specific inhibitors C29, TAK-242, FPS-ZM1, AMD3100, and epoxomicin were used to block toll-like receptor 2 (TLR2), toll-like receptor 4 (TLR4), receptor for advanced glycation end products (RAGE), C-X-C-chemokine receptor 4 (CXCR4), and PSMB5, respectively. siRNAs were used to silence the expression of NRF2. rHMGB1 promoted mitochondrial fusion in endothelial cells, while no significant proinflammatory effects were found. The expression of mitochondrial fission protein Drp1 and phosphorylated subtypes p-Drp1-S616 and p-Drp1-S637 were all downregulated; no significant expression changes of PINK1 and Mfn1, Mfn2, and Opa1 were found. Inhibition of CXCR4 but not TLR4, RAGE, or TLR2 reversed rHMGB1-induced Drp1 downregulation and mitochondrial fusion. Interestingly, inhibition of TLR4 with TAK-242 promoted Drp1 downregulation and mitochondrial fusion. rHMGB1 increased the expression of NRF2 and PSMB5; inhibition of PSMB5 but not silencing NRF2 abolished rHMGB1-induced Drp1 downregulation and mitochondrial fusion. These results indicate that rHMGB1 promotes NRF2 independent mitochondrial fusion via CXCR4/PSMB5 pathway-mediated Drp1 proteolysis. rHMGB1 may influence mitochondrial and endothelial function through this effect on mitochondrial dynamics.

1. Introduction

Vascular endothelium, building the inner layer of capillaries and blood vessels, is the largest organ in the body [1]. As a highly active metabolic and endocrine organ [2], the endothelium can produce a variety of different bioactive molecules and plays a crucial role in the regulation of hemostasis, blood flow, maintenance of vascular architecture, control of thrombosis and thrombolysis, mediation of platelet and leukocyte interaction with the vessel wall, and the regulation of vascular tone and growth of blood vessels [3, 4].

Endothelial dysfunction plays an important role in the pathogenesis of many cardiovascular diseases(CVDs), including atherosclerosis [5], hypertension [6], pulmonary

hypertension [7], stroke [8], heart failure [9], and diabetic vascular complications [10]. In fact, one of the earliest detectable changes in the development of atherosclerosis is endothelial cell activation and dysfunction at lesion-prone areas of the arterial vasculature [11]. Endothelial dysfunction is characterized by imbalanced vasodilation and vasoconstriction, elevated reactive oxygen species (ROS), deficiency of nitric oxide (NO) bioavailability, disruption of endothelial barrier permeability [12], and a transformation to proinflammatory phenotype. Proinflammatorily activated endothelium secretes a variety of chemokines, such as intercellular cell adhesion molecule-1 (ICAM-1), vascular cell adhesion molecule-1 (VCAM-1), interleukin 1β (IL-1β), interleukin 8 (IL-8), monocyte chemotactic protein 1 (MCP-1), and granulocyte-monocyte stimulating factor (GM-CSF), promoting monocyte/macrophage transendothelial migration, proliferation of vascular smooth muscle cells (VSMCs), atherosclerotic lesion formation, progression, and rupture [13].

High-mobility group box 1 (HMGB1), also known as high-mobility group protein 1 (HMG-1) and amphoterin, is a highly conserved nonhistone nuclear protein involved in transcription regulation, DNA replication and repair, and nucleosome assembly [14] and is passively released by necrotic tissues or actively secreted by stressed cells. Extracellular HMGB1 acts as a typical damage-associated molecular pattern (DAMP) molecule or alarmin, to promote a variety of cellular responses including inflammation by binding to different receptors, such as toll-like receptors 2 and 4 (TLR2 and TLR4), receptor for advanced glycation end products (RAGE), and C-X-C-chemokine receptor 4 (CXCR4) [15, 16]. Though a research hotspot, the role of HMGB1 in CVDs is very intriguing; both harmful and beneficial effects were reported [14]. As a distinct proinflammatory cytokine, HMGB1 contributed to the pathogenesis of myocardial ischemia-reperfusion injury [17], heart failure [18], and diabetes [19]; however, a series of beneficial effects of HMGB1 in CVDs were also found, such as boosting myocardial regeneration and repair after infarction [20, 21] and protecting against ischemia-reperfusion injury [22]. As for the endothelium, the contradictory effects of HMGB1 were also found; some reported that HMGB1 induced endothelial dysfunction and inflammation [23, 24], inhibited endothelial cell migration [25], and enhanced LDL transcytosis in endothelial cells to promote the pathogenesis of atherosclerosis [26], while others reported that HMGB1 promoted angiogenesis in endothelial cells [27]. Recently, Zhou et al. [28] have reported that endothelial-specific deletion of HMGB1 in mice increased reactive oxygen species (ROS) production and blood pressure and retarded endothelium-dependent relaxation (EDR) and ischemia recovery, demonstrating the crucial role of HMGB1 in maintaining healthy endothelial function.

Mitochondrion is not a static organelle but can dynamically reconstruct its shape by continuous fusion and fission to adapt to the change of homeostasis of cells; this dynamic changing process is called mitochondrial dynamics [29]. Balanced mitochondrial fission-fusion dynamics plays an essential role in mitochondrial quality control, cellular metabolism, homeostasis, and stress responses [30]. Mito-

chondrial dynamics is delicately orchestrated by several fission and fusion mediators; the former includes Mitofusin 1 (Mfn1), Mitofusin 2 (Mfn2), and Optic atrophy 1 (Opa1) [31]; the latter mainly consists of dynamin-related protein 1 (Drp1) and its several adaptors, such as mitochondrial fission 1 protein (Fis1) and mitochondrial dynamics proteins of 49 and 51 kDa (MiD49 and MiD51) [32]. Additionally, the phosphatase and tensin homolog- (PTEN-) induced kinase 1 (PINK1), though primarily a modulator of mitophagy, also plays an important role in regulating mitochondrial dynamics [33]. Disruption of mitochondrial dynamics is associated with a range of human diseases including atherosclerotic cardiovascular disease (ASCVD) [34], heart failure [35], myocardial ischemia-reperfusion (IR) injury [36], and inflammatory diseases [37]. Studies have reported that altered mitochondrial dynamics resulted in endothelial dysfunction [38, 39].

However, whether the aforementioned typical DAMP molecule HMGB1 can influence mitochondrial dynamics in endothelial cells is not clear. In light of the important role of mitochondrial dynamics in maintaining normal mitochondrial and cellular function and in the pathogenesis of CVDs and inflammatory diseases, it is worthful to clarify the impact of HMGB1 on mitochondrial dynamics in endothelial cells. In this study, we detected the influence of recombinant HMGB1 on mitochondrial dynamics and the underlying mechanism in EA.hy926 endothelial cells.

2. Materials and Methods

2.1. Cell Culture. Human endothelial EA.hy926 cells (Cat# 3131C0001000200039; Shanghai cell bank of Chinese Academy of Sciences) were cultured in high-glucose DMEM (REF11965-092, Gibco) with 10% FBS (REF10099-141, Gibco) at 37°C under a humidified 95% air and 5% CO_2 atmosphere. EA.hy926 endothelial cells were transferred and seeded in 6-well plates at a density of 1.5×10^5/well; when cells grew to 80% confluence, human recombinant HMGB1 (rHMGB1, Cat# H4652; Sigma) with different final concentrations (0 μg/ml, 0.1 μg/ml, 0.5 μg/ml, and 1 μg/ml) was added to incubate for 24 hours. For mechanism exploration, cells were preconditioned with specific antagonists for 1 hour prior to incubation with rHMGB1 (1 μg/ml) for 24 hours, respectively. The preconditioned agents were listed as TLR4-specific antagonist TAK-242 (1 μM, Cat# HY-11109; MCE), TLR2-specific antagonist C29 (10 μM, Cat# HY-100461; MCE), RAGE-specific antagonist FPS-ZM1 (1 μM, Cat# HY-19370; MCE), CXCR4-specific antagonist AMD3100 (5 μM, Cat# HY-50912; MCE), and proteasome-selective inhibitor epoxomicin (10 μM, Cat# HY-13821; MCE).

2.2. Cell Transfection. Cells were seeded into 6-well plates (1×10^5 cells/well) to ensure 30-50% confluence in the next day and then transfected with NRF2 siRNAs or vehicles as negative control, respectively. The sequences of NRF2 siRNA duplexes and vehicles were listed in Table S1. Cells were transfected with a matching siRNA-Mate (Cat# G04002; Gene Pharma) for 48 hours to determine the efficiency by

western blot before the following experiments. All the data were quantified independently by two observers that were blinded to the study design.

2.3. *Western Blot.* Cell lysate samples were prepared from cells in RIPA solution (Cat# FD009; Fude) supplemented with protease inhibitor (Cat# FD1001; Fude) and protein phosphatase inhibitor (Cat# FD1002; Fude). Denatured cell lysates were resolved by SDS-PAGE and transferred onto a polyvinylidene fluoride (PVDF) filter membrane. After transfer, membranes were blocked in 5% (wt/vol) nonfat dry milk diluted in TBST. Membranes were incubated with primary antibodies against Mfn1 (1 : 1000, Cat# 14739; CST), Mfn2 (1 : 1000, Cat# 11925; CST), Drp1 (1 : 1000, Cat# 5391; CST), p-Drp1-S616 (1 : 500, Cat# 3455; CST), p-Drp1-S637 (1 : 500, Cat# 4867; CST), Opa1 (1 : 1000, Cat# ab157457; Abcam), PINK1 (1 : 1000, Cat# 6946; CST), NRF2 (1 : 1000, Cat# ab62352; Abcam), NLRP3 (1 : 1000, Cat# ab210491; Abcam), caspase 1 (1 : 1000, Cat# ab207802; Abcam), cleaved caspase 1 (P20) (1 : 1000, Cat# 4199; CST), PSMB5 (1 : 1000, Cat# abs115883; Absin), GAPDH (1 : 3000, Cat# FD0063; Fude), β-actin (1 : 1000, Cat# FD0060; Fude), and β-Tubulin (1 : 1000, Cat# A01030; Abbkine) overnight at 4°C and subsequently incubated with horseradish peroxidase- (HRP-) conjugated secondary antibodies which were detected by enhanced chemiluminescence (Cat# FD802; Fude). Immunoblots were analyzed using ImageJ 5.0 software (NIH; MD).

2.4. *Immunofluorescent Staining.* Cells seeded on 12-well plates were fixed with 4% paraformaldehyde (30 minutes), permeabilized with 0.5% Triton X-100 for 5 minutes, and then blocked with 1% BSA in 0.1% PBS-Tween 20 for 1 hour. The cells were then incubated overnight at 4°C with primary antibodies against CD31 (1 : 300, Cat# ab9498, Abcam) or vWF (1 : 500, Cat# ab154193, Abcam), followed by incubation with secondary antibody Donkey anti-Mouse IgG-Alexa Fluor 488 (1 : 1000, Cat# abs20014, Absin) for CD31 or Donkey anti-Rabbit IgG-Alexa Fluor 594 (1 : 1000, Cat# abs20021, Absin) for vWF. Nuclear DNA was labelled with Hoechst (4 μg/ml, Cat# BL801A, Biosharp). Images were investigated under an inverted fluorescence microscope (Ix71, Olympus; Tokyo).

2.5. *Quantitative RT-PCR Analysis.* Total RNA was reversely transcribed with a cDNA Synthesis kit (Cat# RR037A; Takara Bio), and quantitative PCR (qPCR) was performed to quantify mRNA abundance using a SYBR Green PCR Premix (Cat# RR420A; Takara Bio) on an Applied Biosystem cycler. Data were analyzed using the $\Delta\Delta$Ct method and GAPDH as internal control. Primers used in this study were listed in Table S2.

2.6. *Enzyme-Linked Immunosorbent Assay (ELISA).* Interleukin 1β (IL-1β) concentrations of the supernatant in cell culture were measured with ELISA kits according to the manufacturer's recommendation (Cat# DLB50; R&D).

2.7. *Transmission Electron Microscopy (TEM).* Cells were fixed in 2.5% glutaraldehyde and then postfixed in 1%

osmium tetroxide, dehydrated in ethanol of gradient concentrations, and embedded in Sparr resin for electron microscopy. Sections were double-stained with uranyl acetate and alkaline lead citrate and then examined with a transmission electron microscope (TECNAI 10, Philips; Amsterdam). Ten cells of sections in every group (magnification ×5900) were randomly included to count the mitochondrial numbers of cells and get the average. For comparison of average mitochondrial areas, at least 30 mitochondria of 10 cells for every group were calculated and then analyzed using ImageJ 5.0 software (NIH; MD).

2.8. *Fluorescence Tracing.* Cells plated on glass-bottomed dishes (35 mm) were incubated with MitoTracker Green FM (20 μM, Cat# 40742ES50; Yeasen Biotech) in DMEM with 10% FBS for 20 minutes at 37°C. Fluorescence stained cells were analyzed using confocal laser microscopy with a 63x objective (SP8, Leica; Wetzlar).

2.9. *Statistical Analysis.* Data were shown as the mean ± standard deviation (SD). SPSS version 17.0 was used for statistical analyses. To compare continuous response variables between two groups, unpaired two-tailed Student's t-test was used for normally distributed variables that passed the equal variance test, and a Mann-Whitney U test was performed for variables not passing either normality or equal variance test. $P < 0.05$ was considered statistically significant.

3. Results

3.1. *Exogenous rHMGB1 Incubation Altered Mitochondrial Morphology in EA.hy926 Cells.* EA.hy926 cells are a human vascular endothelial cell line presenting typical characteristics of human primary endothelial cells. To characterize EA.hy926 endothelial cells, we first detected endothelial-specific markers CD31 (cluster of differentiation 31) and vWF (von Willebrand factor) with immunofluorescent staining. As expected, both CD31 and vWF were strongly positive in EA.hy926 cells (Figures S1(a) and S1(b)), demonstrating the endothelial characteristics of EA.hy926 cells.

To investigate the role of HMGB1 in mitochondrial morphology, EA.hy926 cells were incubated with rHMGB1 to investigate the number and morphology of cytosol mitochondrion by TEM and fluorescent tracing, respectively. Compared to the control group, the average numbers of mitochondrion in cytoplasm under TEM were significantly decreased in a dose-dependent manner as incubating with rHMGB1 for 24 hours (Figures 1(a) and 1(b)). In contrast, the average sizes of mitochondrion under TEM were significantly increased in cells incubated with rHMGB1 in comparison to the control group (Figures 1(a) and 1(c)). Meanwhile, profoundly tubulated mitochondria were found under a confocal microscope in rHMGB1-treated cells (Figure 1(d)). Taken together, the results suggested that rHMGB1 might trigger mitochondrial fusion in EA.hy926 cells.

3.2. *Exogenous rHMGB1 Incubation Influenced the Expressions of Mitochondrial Dynamics-Associated Proteins.* To clarify the potential mechanism of mitochondrial fusion induced by rHMGB1, the expressions of profusion (Mfn1, Mfn2,

(a)

(b)

(c)

(d)
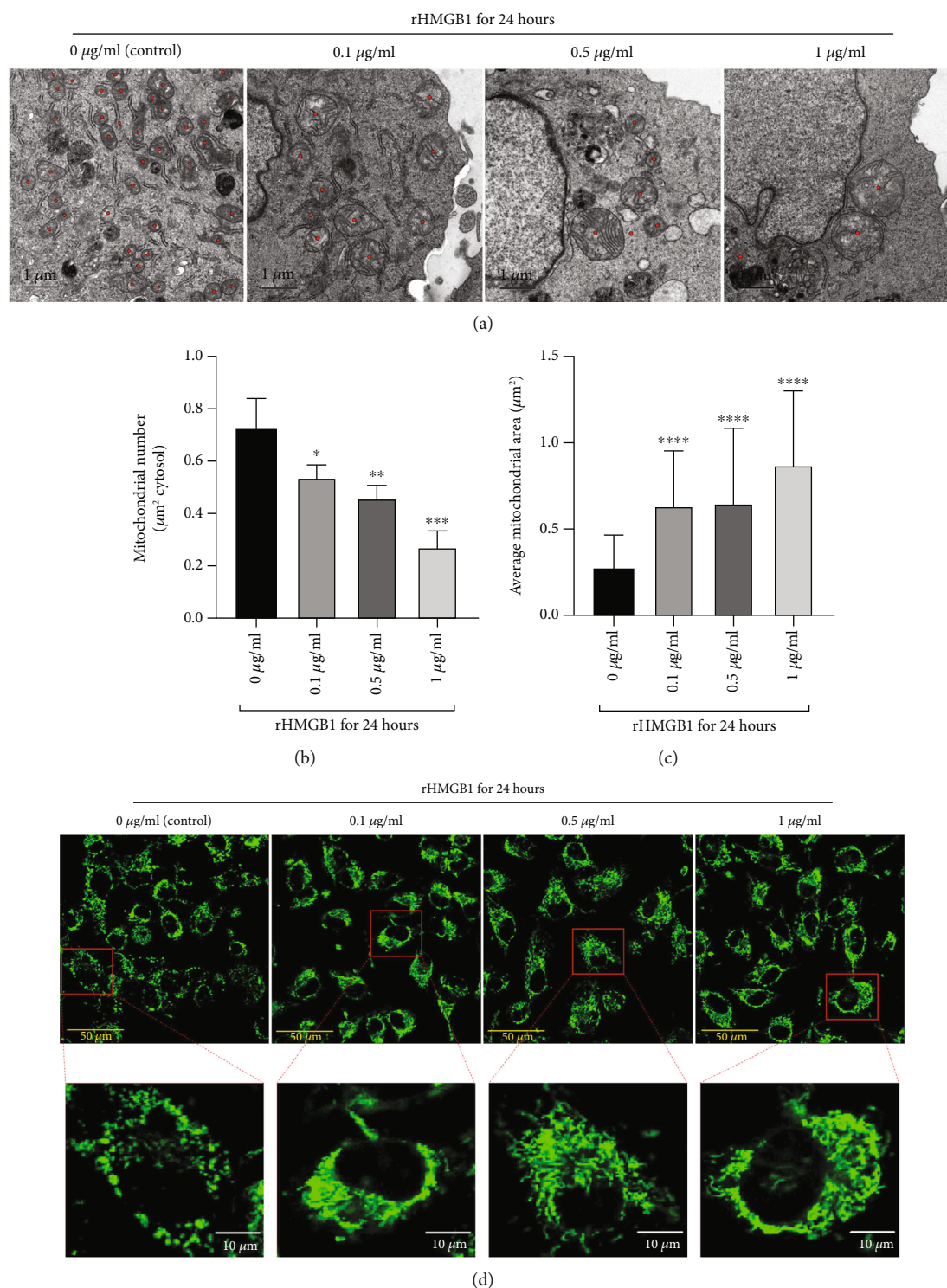
FIGURE 1: rHMGB1 incubation promoted mitochondrial fusion in EA.hy926 endothelial cells. (a) The representative TEM images of mitochondria of EA.hy926 endothelial cells treated with different concentrations (control, 0.1 μg/ml, 0.5 μg/ml, and 1 μg/ml) of rHMGB1. The magnification is 5900. Scale bar: 1 μm. (b) The mitochondrial number changes under TEM in EA.hy926 endothelial cells treated with different concentrations (control, 0.1 μg/ml, 0.5 μg/ml, and 1 μg/ml) of rHMGB1. (c) The average mitochondrial area (μm^2) under TEM of EA.hy926 endothelial cells treated with different concentrations (control, 0.1 μg/ml, 0.5 μg/ml, and 1 μg/ml) of rHMGB1. For comparison of average mitochondrial area, at least 30 mitochondria of 10 cells per group were calculated; for comparison of mitochondrial number, at least 10 cells per group were counted. (d) EA.hy926 endothelial cells were stained with mitochondria-specific fluorescent dye MitoTracker Green FM and imaged under a Leica SP8 confocal microscope. The magnification is 630. Scale bar (original): 50 μm; scale bar (zoom): 10 μm. TEM: transmission electron microscopy. $^{*}P < 0.05$ versus control group; $^{**}P < 0.01$ versus control group; $^{***}P < 0.001$ versus control group; $^{****}P < 0.0001$ versus control group.

and Opa1), profission (Drp1), and mitophagy (PINK1)-associated proteins were determined in EA.hy926 cells, respectively. As a result, there was no significant difference of Mfn1, Mfn2, Opa1, and PINK1 protein expressions between the cells incubated with either rHMGB1 or negative control (Figures 2(a)–2(h)). However, rHMGB1 incubation significantly downregulated the Drp1 protein expression in cells with a dose-dependent manner compared to the negative control ($P < 0.05$, Figures 3(a) and 3(b)). Furthermore, the two phosphorylated subtypes, p-Drp1-S616 and p-Drp1-S637, were also explored. Consistently, compared to the negative control, rHMGB1 incubation for 24 hours at the doses of 0.5 μg/ml and 1 μg/ml significantly downregulated p-Drp1-S616 and p-Drp1-S637 expressions in EA.hy926 cells ($P < 0.05$, Figures 3(c)–3(f)).

Protein expression may be also determined at the gene transcriptional level. To clarify whether rHMGB1 reduces the expression of Drp1 gene at the transcription level, RT-qPCR was performed. As a result, we found that different concentrations (0.1 μg/ml, 0.5 μg/m, and 1 μg/ml) of rHMGB1 incubation for 24 hours had no effect on the mRNA expression level of Drp1 gene in endothelial cells (Figure 3(g)), indicating that rHMGB1 downregulating the expression of Drp1 protein was not at the transcription level, but at the posttranslational level.

3.3. Inhibition of CXCR4 but Not TLR2, TLR4, or RAGE Abolished rHMGB1-Induced Drp1 Downregulation and Mitochondrial Fusion.

HMGB1 acts as a pleiotropic cytokine that plays its biological role through a variety of transmembrane receptors, including TLR2, TLR4, RAGE, and CXCR4. Specific antagonists C29 (for TLR2), TAK-242 (for TLR4), FPS-ZM1 (for RAGE), and AMD3100 (for CXCR4) were preconditioned with cells prior to exogenous rHMGB1 incubation. Cellular Drp1 expressions were significantly downregulated by rHMGB1 incubation, which were not affected by preconditioning with either C29 or FPS-ZM1 (Figures 4(a), 4(c), 4(e), and 4(g)). Interestingly, preconditioning with TAK-242 significantly reduced cellular Drp1 expression whether exogenous rHMGB1 incubation or not (Figures 4(b) and 4(f)). In contrast, preconditioning with AMD3100 significantly reversed the downregulation of Drp1 expression induced by rHMGB1 incubation (Figures 4(d) and 4(h)).

Consistently, preconditioning with C29, TAK-242, or FPS-ZM1 all could not reverse rHMGB1-triggered mitochondrial fusion in endothelial cells, but pretreatment with AMD3100 (also plerixafor octahydrochloride) abolished rHMGB1-triggered mitochondrial fusion (Figures 4(i)–4(l)). Accordingly, TAK-242 preconditioning induced mitochondrial fusion (Figures 4(i)–4(l)), which was in line with the downregulation of Drp1 expression (Figures 4(b) and 4(f)).

Generally, the activation of receptors TLR2, TLR4, or RAGE triggers cellular inflammation. To further demonstrate whether rHMGB1 has no activating effect of TLR2, TLR4, or RAGE or exerts its biological role independent of TLR2, TLR4, or RAGE, we detected the inflammatory phenotype changes of EA.hy926 cells treated with rHMGB1. Cellu-

lar NLRP3, caspase 1, and cleaved caspase 1 expressions were detected by western blot, whereas IL-1β concentration was determined in the culture supernatant by ELISA, respectively. Compared to the negative control, neither the expressions of NLRP3, caspase 1, and cleaved caspase 1 nor IL-1β concentration was altered by rHMGB1 incubation in EA.hy926 cells (Figures S2(a)-S2(c)), indicating that rHMGB1 had no significant proinflammatory effect on EA.hy926 endothelial cells, further supporting the notion that the rHMGB1 we used had no activating effect on receptor TLR2, TLR4, or RAGE.

Taken together, these results suggested that rHMGB1-induced mitochondrial fusion might be mediated by the CXCR4 pathway in EA.hy926 cells.

3.4. Inhibition of PSMB5 Reversed rHMGB1-Induced Decrease of Drp1 Protein Level and Mitochondrial Fusion.

Since the discrepancy of mRNA and protein expression of Drp1 was found in EA.hy926 cells incubated with rHMGB1, 20S proteasome complex subunit β-5 (PSMB5), one of the core components of 20S proteasome critical for Drp1 protein degradation, was further determined. As expected, exogenous rHMGB1 incubation significantly increased PSMB5 expression in EA.hy926 cells with a dose-dependent manner (Figures 5(a) and 5(b)). Furthermore, preconditioning with epoxomicin (5 μM, PSMB5 specific inhibitor) for 1 hour reversed the downregulation of Drp1 expression induced by exogenous rHMGB1 (Figures 5(c) and 5(d)). Expectedly, preconditioning with epoxomicin abolished rHMGB1-induced mitochondrial fusion in EA.hy926 cells as observed by a confocal microscope (Figure 5(e)) and TEM (Figures 5(f)–5(h)). Taken together, these results indicated that rHMGB1 might trigger mitochondrial fusion in endothelial cells through PSMB5-dependent Drp1 proteolysis.

3.5. rHMGB1-Induced Drp1 Decrease and Mitochondrial Fusion Are NRF2 Independent.

Nuclear factor erythroid 2-related factor 2 (NRF2) is the master antioxidant transcription factor regulating the expression of antioxidant proteins to protect against oxidative damage. It is reported that the NRF2 stress response pathway promotes mitochondrial fusion through degradation of the mitochondrial fission protein Drp1 [40]. In our study, we found that rHMGB1 treatment upregulated the expression of NRF2 through the CXCR4 signaling pathway in EA.hy926 cells (Figures 6(a) and 6(d)). This suggested that the activation of NRF2 may be involved in the rHMGB1-induced Drp1 degradation and mitochondrial fusion. We then further silenced the expression of NRF2 with specific siRNAs (Figures 6(b) and 6(e)) to define whether inhibition of NRF2 could block rHMGB1-induced Drp1 decrease and mitochondrial fusion. Unexpectedly, we found that silencing NRF2 expression had no effect on both Drp1 expression level and mitochondrial dynamics (Figures 6(c), 6(f), and 6(i)) and rHMGB1-induced decrease of Drp1 and mitochondrial fusion (Figures 6(g)–6(i)), indicating that rHMGB1-induced Drp1 decrease and mitochondrial fusion was NRF2 independent.

(a)

(b)

(c)

(d)

(e)

(f)
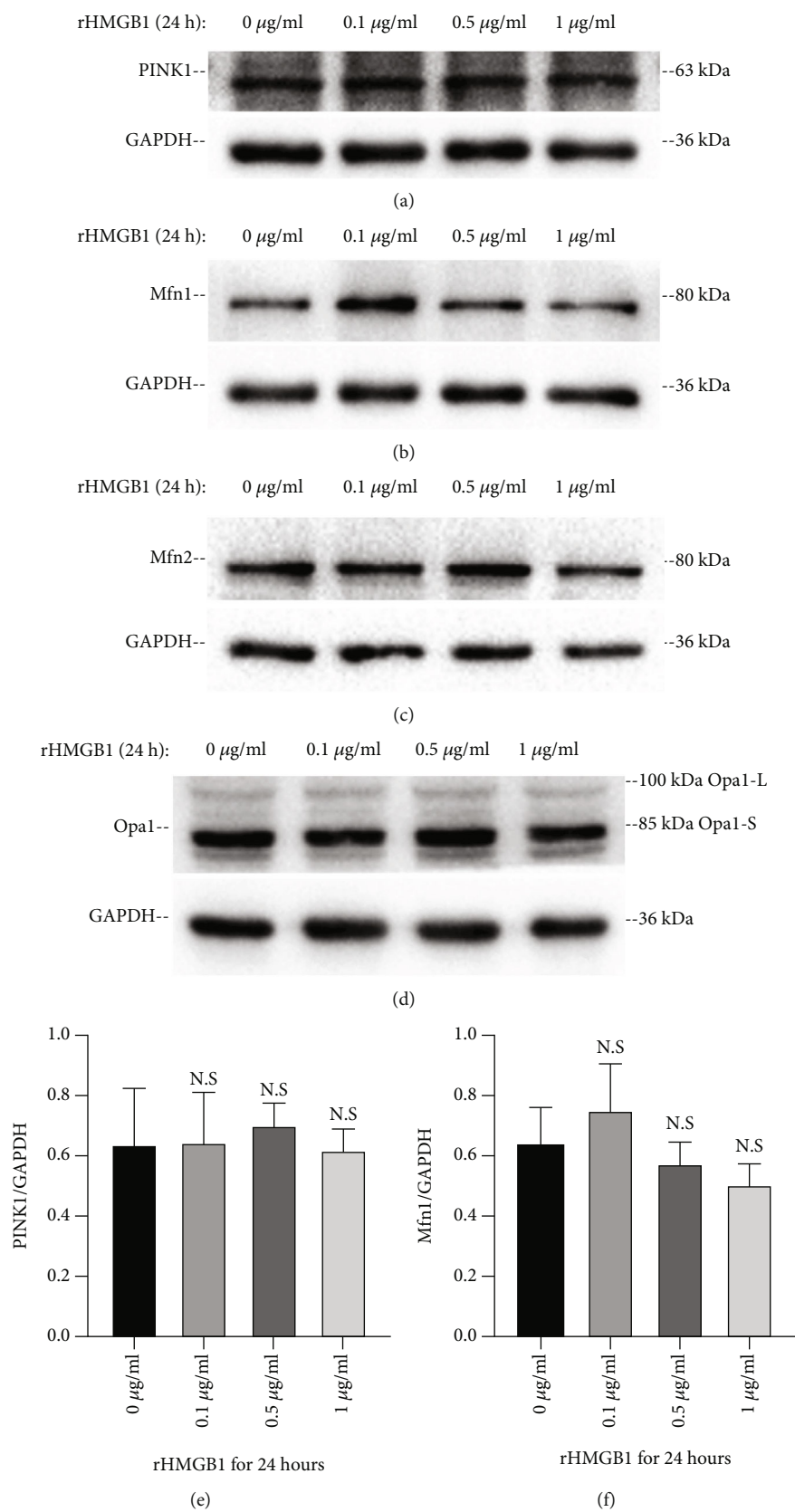
Figure 2: Continued.
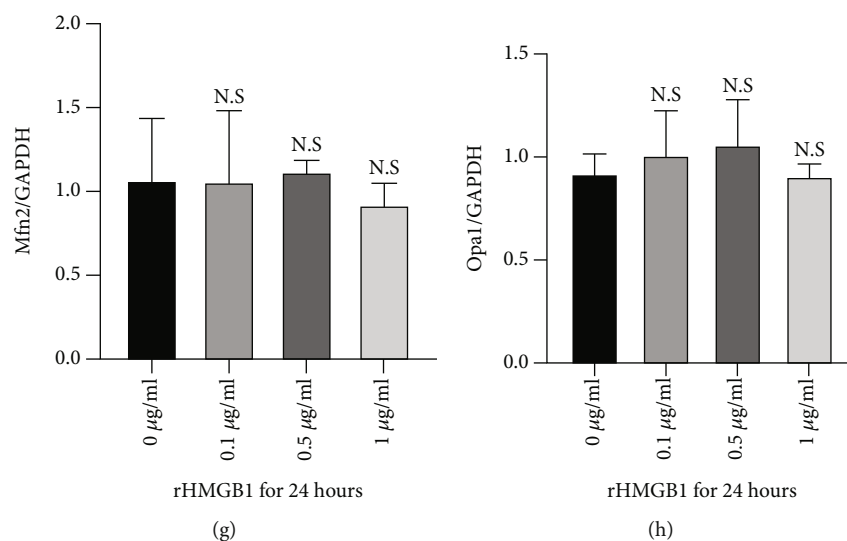
FIGURE 2: rHMGB1 had no significant effect on the protein expression of PINK1, Mfn1, Mfn2, and Opa1. (a–d) Representative immunoblotting bands of PINK1, Mfn1, Mfn2, and Opa1 and the matching internal standard GAPDH. (e–h) The densitometric analysis of relative PINK1, Mfn1, Mfn2, and Opa1 expression referenced to respective matching GAPDH. GAPDH: glyceraldehyde-3-phosphate dehydrogenase. Data were expressed as the mean ± SD.

4. Discussion

HMGB1 is a multifacet protein exerting functions both inside and outside of cells, involved in a large variety of different biological processes such as inflammation, migration, invasion, proliferation, differentiation, and tissue regeneration. As a distinct proinflammatory mediator, extracellular HMGB1 may cause tissue injury and organ dysfunction in the pathogenesis of many different diseases. However, many studies have reported that HMGB plays an important role in tissue repair and regeneration. Meanwhile, the protective role of HMGB1 in cardiovascular pathology was also found. Limana et al. first reported that exogenous HMGB1 protein induced myocardial regeneration after infarction via enhanced cardiac C-kit+ cell proliferation and differentiation [20]. Zhou et al. recently have reported that HMGB1 protected the heart against ischemia-reperfusion injury via PI3K/Akt pathway-mediated upregulation of VEGF expression [22]. Indeed, the protection effect of HMGB1 against IR injury is not restricted in the heart, but systematically, similar protective effects were also found in IR injury of the cerebrum [41], liver [42], and kidney [43].

As aforementioned, emerging roles of HMGB1 in endothelial cells were reported; on the one hand, HMGB1 could induce endothelial dysfunction and inflammation [23, 24], inhibit endothelial cell migration [25], and enhance LDL transcytosis in endothelial cells [26]; on the other hand, HMGB1 promotes angiogenesis in endothelial cells [27] and plays a crucial role in maintaining healthy endothelial function [28].

As a protein of pleiotropic activity, HMGB1 exerts its biological activities depending on different redox forms. Structurally, HMGB1 is composed of three domains: two positively charged proximal DNA-binding domains (A box and B box) and a negatively charged carboxyl terminus. Its molecule contains three cysteine residues critical for its biological activity: two vicinal cysteines in box A (C23 and C45) and a single one in box B (C106). The fully reduced HMGB1 is characterized by all the cysteines in the thiol state and exerts chemotactic activity; the partial oxidated form leads to the formation of an intramolecular disulfide bond between the C23 and C45 and defines the disulphide-HMGB1 acting as a proinflammatory cytokine; the further oxidation of all cysteines to sulfonates characterizes the sulfonyl HMGB1 that has neither chemokine- nor cytokine-like activity [44].

Mitochondria are highly dynamic organelles that constantly undergo fission and fusion. As aforementioned, disruption of mitochondrial dynamics undermines their function and causes a variety of human diseases, including CVDs, neurodegenerative diseases, diabetes, cancer, and inflammatory diseases [34]. The role of mitochondrial dynamics in the pathogenesis of CVDs has aroused extensive attention. Changes in mitochondrial dynamics have been implicated in endothelial dysfunction, vascular smooth cell proliferation, cardiac development and differentiation, cardiomyocyte hypertrophy, myocardial IR injury, cardioprotection, and heart failure [45].

However, as an important cytokine, the effect of HMGB1 on mitochondrial dynamics remains unclear. In consideration of the important role of both HMGB1 and mitochondria dynamics in the pathogenesis of CVDs, this is undoubtedly a topic worthy of researching. As one of the major cell types of the cardiovascular system, endothelial dysfunction is involved in many CVDs, such as coronary artery disease [46], hypertension [47], aneurysm [48], and heart failure [9]. So, in this study, we targeted endothelial cells to explore the influence of HMGB1 on mitochondrial dynamics.

In our study, recombinant HMGB1 from Sigma-Aldrich (Cat# H4652) was used, which is expressed in E. coli as

(a)

(b)

(c)

(d)

(e)

(f)

Figure 3: Continued.

(g)
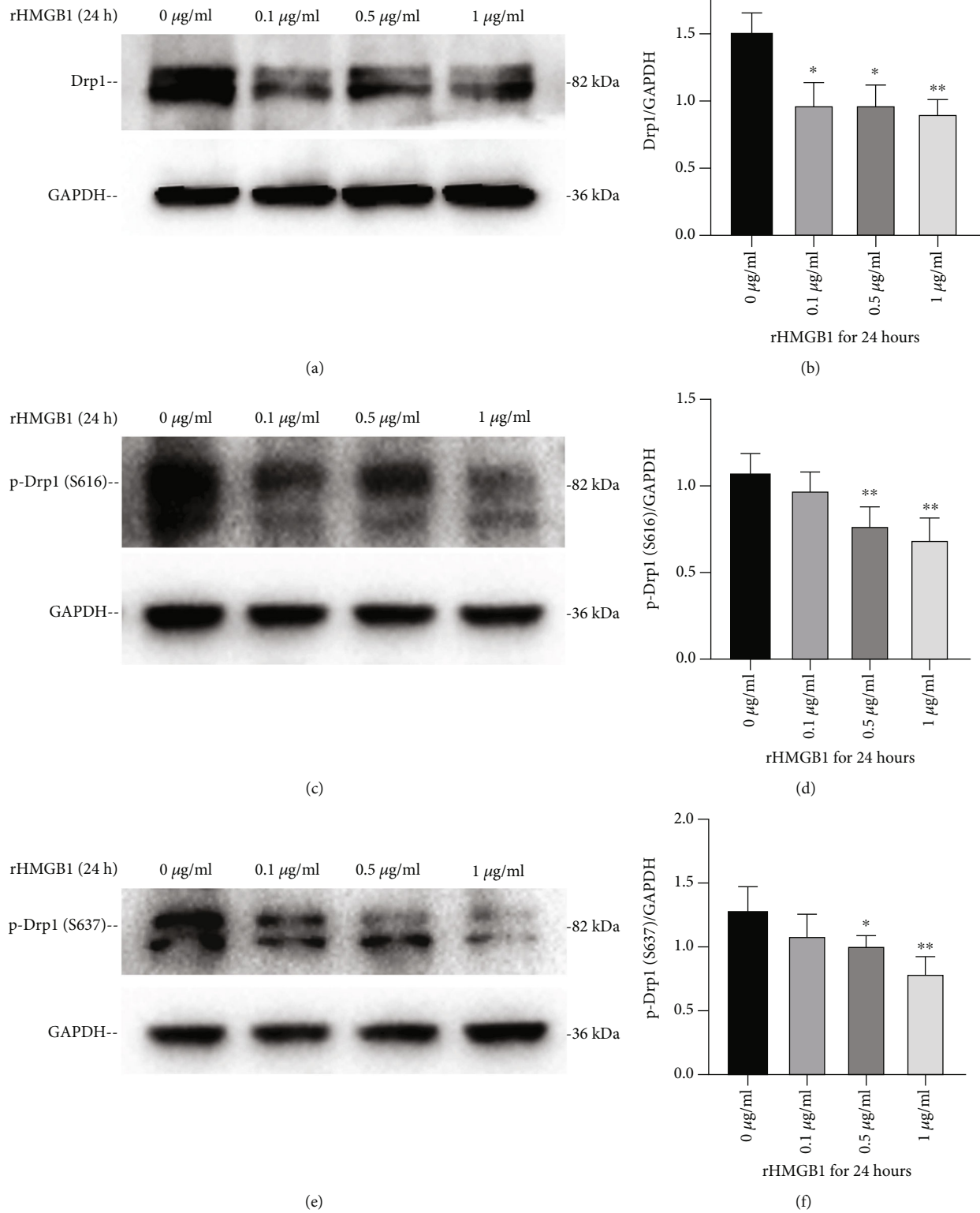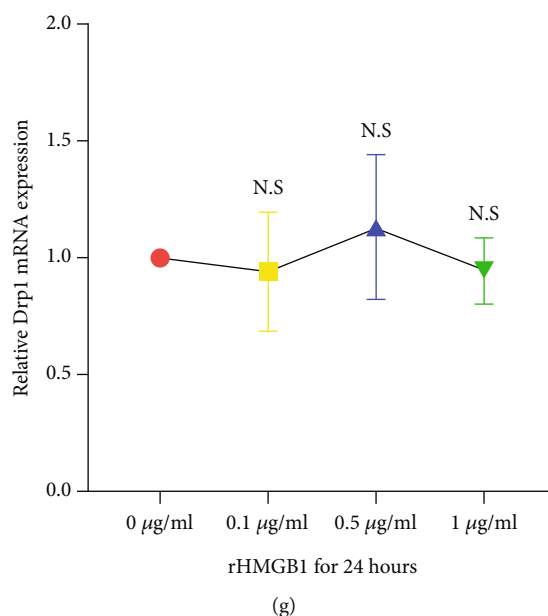
FIGURE 3: Incubation with rHMGB1 reduced the protein expression of Drp1. (a) Representative immunoblotting bands of Drp1 and the matching internal standard GAPDH. (b) The densitometric analysis of relative Drp1 expression referenced to GAPDH. (c) Representative immunoblotting bands of p-Drp1-S616 and the matching internal standard GAPDH. (d) The densitometric analysis of relative p-Drp1-S616 expression referenced to GAPDH. (e) Representative immunoblotting bands of p-Drp1-S637 and the matching internal standard GAPDH. (f) The densitometric analysis of relative p-Drp1-S637 expression referenced to GAPDH. (g) rHMGB1 had no significant effect on the expression of Drp1 mRNA expression. The amount of target mRNAs was normalized to respective internal standard GAPDH mRNA; relative fold was calculated based on the ratio of the normalized values of the cells treated with rHMGB1 to that of controls ($2^{-\Delta\Delta Ct}$). GAPDH: glyceraldehyde-3-phosphate dehydrogenase. Data were expressed as the mean ± SD; $^{*}P < 0.05$ versus control group and $^{**}P < 0.01$ versus control group.

a N-terminal histidine-tagged protein. We found that rHMGB1 treatment induced downregulation of mitochondrial fission protein Drp1 and mitochondrial fusion, indicating as an increase of tubular mitochondria under a confocal microscope, an increase of average mitochondrial area and a decrease of the mitochondrial number under TEM. The expression levels of mitochondrial fusion proteins Mfn1, Mfn2, and Opa1 were not changed significantly, indicating that rHMGB1-induced mitochondrial fusion is caused by a decrease of Drp1. Another mitochondrial dynamics mediator PINK1 expression was also unchanged in endothelial cells treated with rHMGB1.

As for the mechanism of rHMGB1-induced downregulation of Drp1 and mitochondrial fusion, we firstly aimed at the membrane receptors for HMGB1. Extracellular HMGB1 exerts its pleiotropic biological activities by interacting with a variety of different cell surface receptors. To date, more than 10 different HMGB1 receptors have been identified and described, the most studied are focusing on RAGE, TLR2, TLR4, and CXCR4 [49, 50]. The former three receptors have a role of proinflammation [51, 52], while the latter as a chemokine receptor plays an important role in tissue regeneration and cell proliferation [53]. We found that blocking TLR2, TLR4, and RAGE receptors in EA.hy926 cells could not prevent the mitochondrial profusion effects of rHMGB1. However, pretreatment with AMD3100, the CXCR4 receptor antagonist, could completely abrogate the decrease of Drp1 protein expression and mitochondrial fusion triggered by

rHMGB1, indicating that rHMGB1 promotes mitochondrial fusion through the CXCR4 receptor signaling pathway in endothelial cells. Since CXCR4 is a well-defined chemokine receptor, the rHMGB1 used in our study plays a role of chemokine. As aforementioned, fully reduced HMGB1 characterized by all the 3 cysteines in the thiol state exerts chemotactic activity; it is rational to believe that the majority of the rHMGB1 we used were in a fully reduced state. This is also supported by the fact that intracellular HMGB1 is largely in the reduced state due to the strongly negative (reducing) redox potential in cytosol and nucleus [54]. Meanwhile, no proinflammatory effect of rHMGB1 on endothelial cells was found in our study, further demonstrating that the rHMGB1 used was not in a disulphide-HMGB1 state, for the proinflammatory role of HMGB1 relying on oxidation of C23 and C45 within its molecule [55].

Our RT-PCR results showed no significant reduction of the mRNA expression level of Drp1 gene was found in EA.hy926 endothelial cells treated with rHMGB1. We speculated that rHMGB1 induced downregulation of Drp1 protein at the posttranscriptional level. PSMB5 is one of the core components of 20S proteasome, the conserved degradation machinery that is essential for maintaining cellular homeostasis [56, 57]. We found that the PSMB5 protein expression level was also upregulated in cells treated with rHMGB1, and inhibition of PSMB5 activity with epoxomicin (BU-4061T) abolished the induced downregulation of Drp1 and mitochondrial fusion, indicating that rHMGB1 downregulated

(a)

(b)

(c)

(d)

(e)

(f)

(g)

(h)
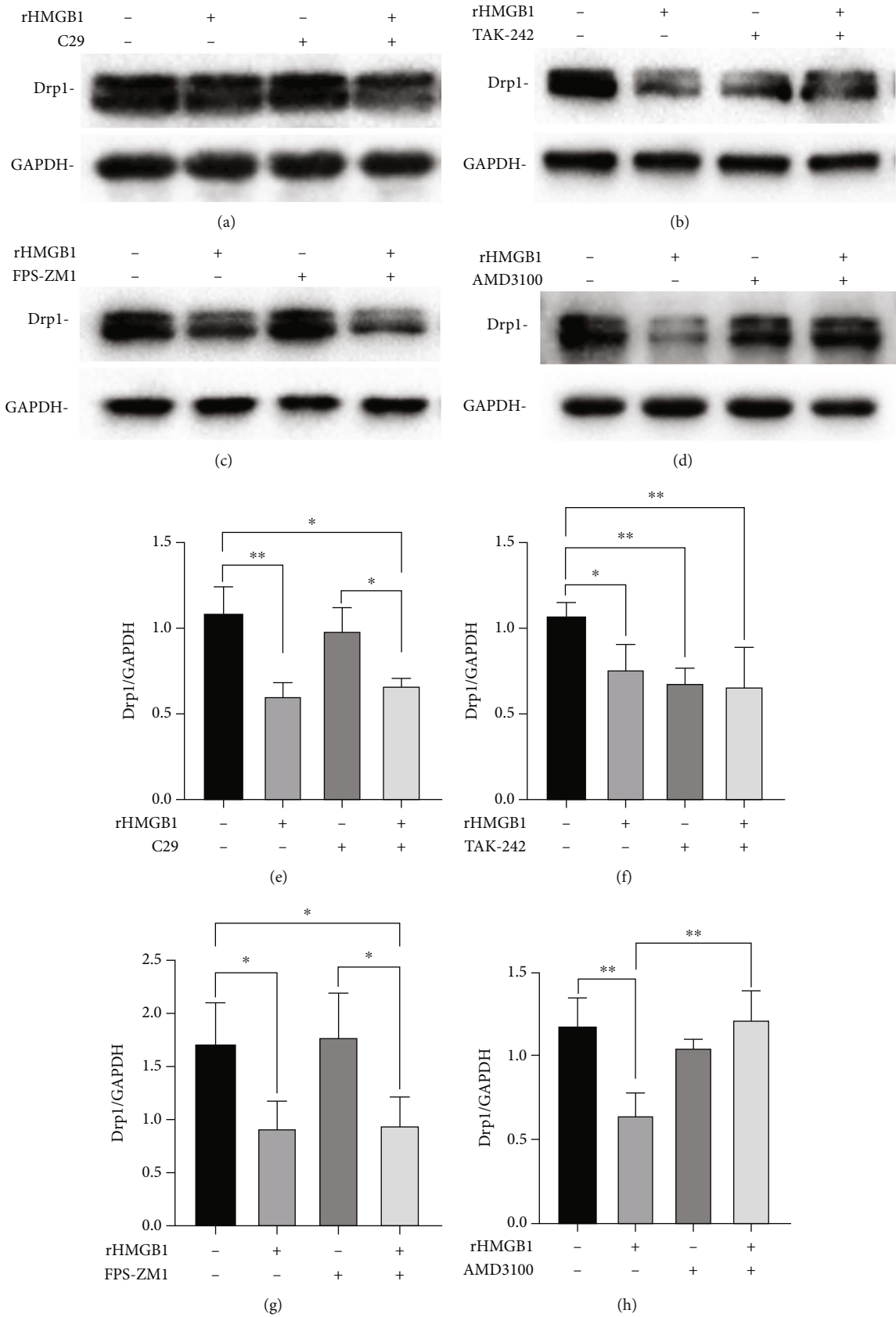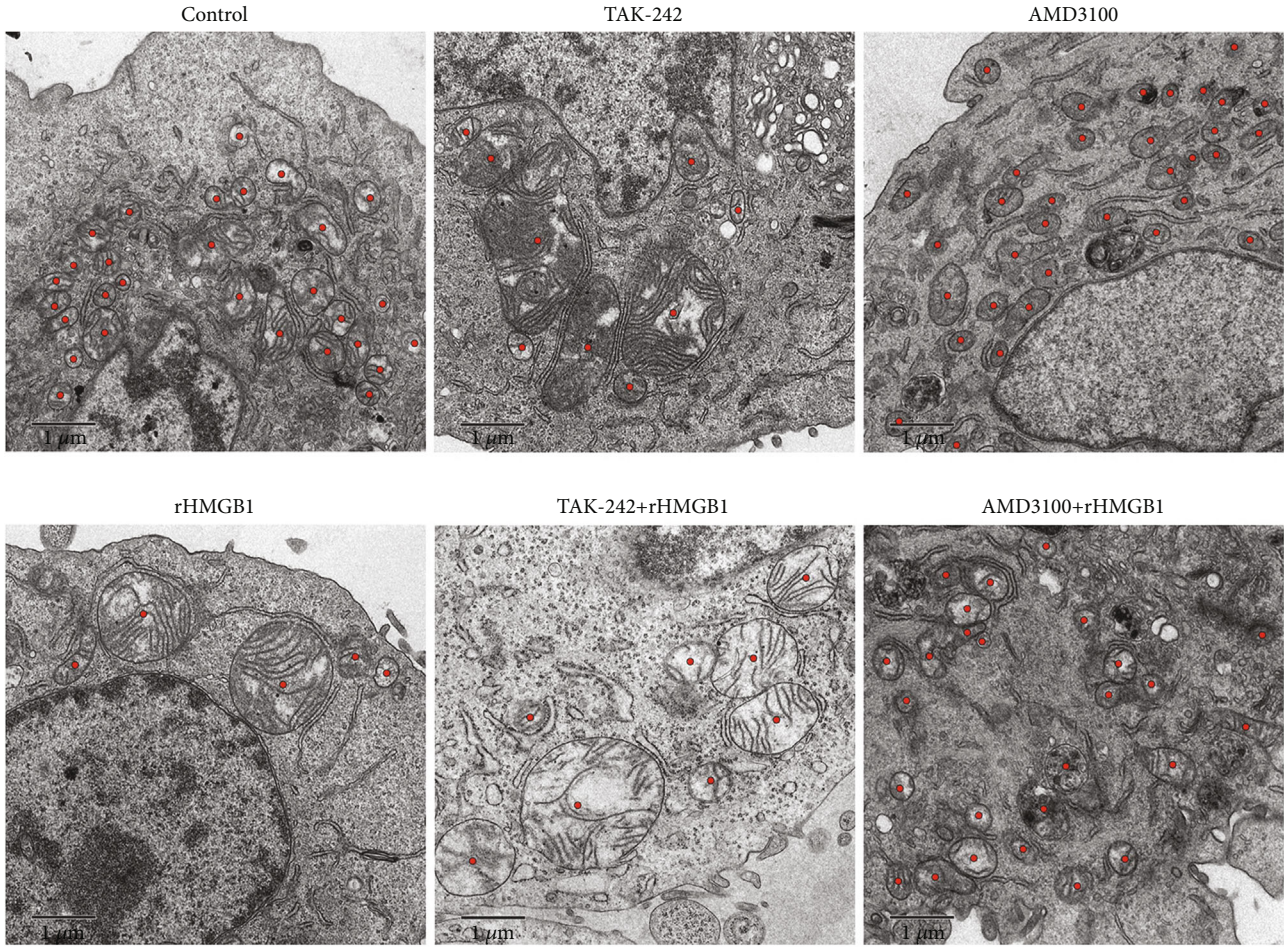
FIGURE 4: Continued.

(i)
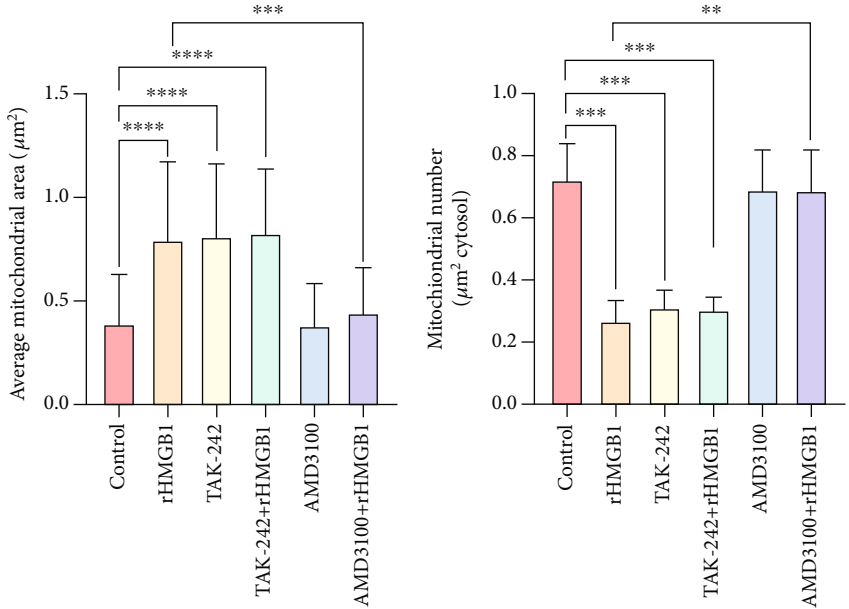
(j)

(k)

Figure 4: Continued.

(l)
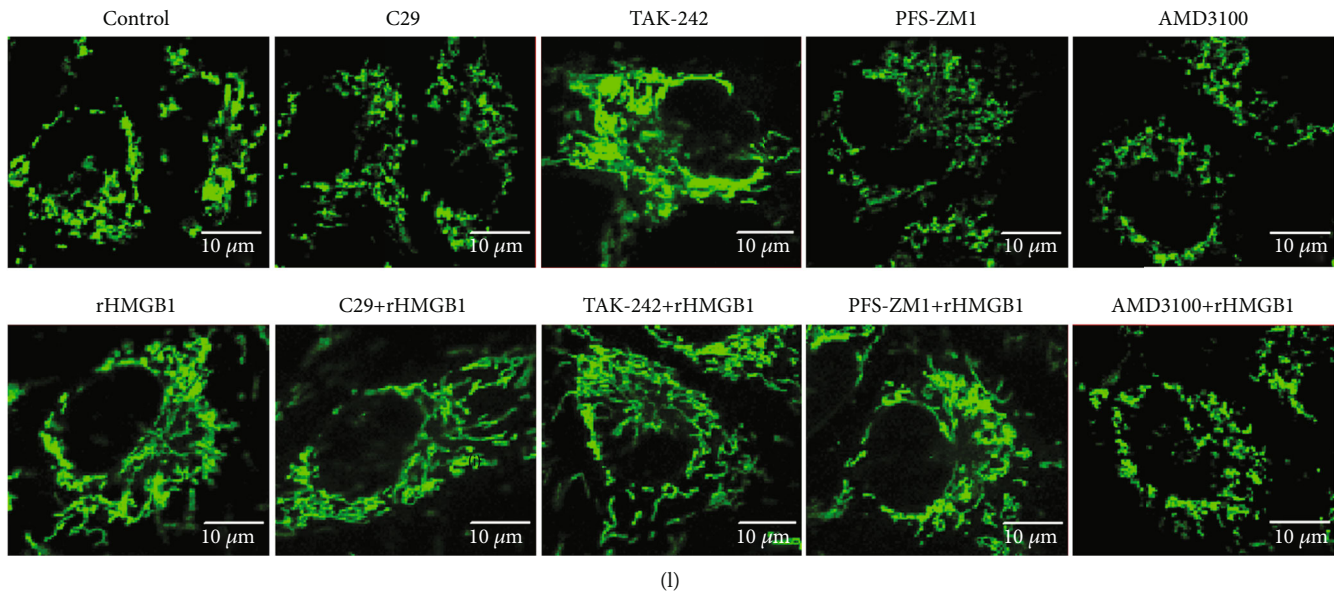
FIGURE 4: Blocking CXCR4 reversed rHMGB1-induced downregulation of Drp1 and mitochondrial fusion. (a–d) Representative immunoblotting bands of Drp1 of cells pretreated with C29, TAK-242, FPS-ZM1, and AMD3100 and the matching internal standard GAPDH. (e–h) The densitometric analysis of relative Drp1 expression of cells pretreated with C29, TAK-242, FPS-ZM1, and AMD3100 referenced to respective matching GAPDH. (i) The representative TEM images of mitochondrial morphology of cells preexposed to TAK-242, AMD3100, and subsequent rHMGB1. (j) The average mitochondrial area (μm^2) changes under TEM of cells preexposed to TAK-242, AMD3100, and subsequent rHMGB1. (k) The mitochondrial number changes under TEM in cells preexposed to TAK-242, AMD3100, and subsequent rHMGB1. (l) Mitochondrial morphology of cells preexposed to C29, TAK-242, FPS-ZM1, AMD3100, and subsequent rHMGB1. Cells were subjected to fluorescent staining with MitoTracker Green FM and observed by a Leica SP8 confocal laser scanning microscope. Scale bar: $10 \mu m$. GAPDH: glyceraldehyde-3-phosphate dehydrogenase; TEM: transmission electron microscopy. Data were expressed as the mean ± SD. For comparison of the average mitochondrial area, at least 30 mitochondria of 10 cells per group were calculated; for comparison of mitochondrial number, at least 10 cells per group were counted. $^*P < 0.05$, $^{**}P < 0.01$, $^{***}P < 0.001$, and $^{****}P < 0.0001$.

the expression of Drp1 by 20S proteasome-dependent degradation.

Several studies have reported that the Keap1-NRF2 anti-oxidation system plays an important role in mediating Drp1 turnover and mitochondrial dynamics. Sabouny et al. first identified that NRF2-modulated increase of proteasome activity promoted the degradation of Drp1 and mitochondrial hyperfusion [40]. Yang et al. has reported that metformin alleviated lead-induced mitochondrial fragmentation dependent on NRF2 activation [58], further supporting the role of NRF2 in promoting mitochondrial fusion. In fact, we did find that treatment with rHMGB1 upregulated the NRF2 protein level in EA.hy926 endothelial cells significantly. In consideration of the reported role of NRF2 in the turnover of Drp1, we silenced the expression of NRF2 successfully. Quite unexpectedly, silencing NRF2 had no significant effect on rHMGB1-induced reduction of Drp1 protein and mitochondrial fusion, indicating that the increase of NRF2 was not directly involved in rHMGB1-induced downregulation of Drp1 and mitochondrial fusion. Contradictory to previous reports, our results were supported by O'Mealey et al. Their study identified that sulforaphane was a NRF2-independent inhibitor of mitochondrial fission [59]. They found that sulforaphane, a potent activator of NRF2 signaling, induced a robust mitochondrial fusion in human retinal pigment epithelial (RPE-1) cells, but the expression of NRF2

was dispensable for sulforaphane-induced mitochondrial fusion. Because knockdown of NRF2 failed to counter this phenotypical change, while NRF2 stabilizing did not induce mitochondrial fusion [59]. This is in line with our results that rHMGB1-induced reduction of Drp1 protein and mitochondrial fusion was independent of NRF2 (Figure 7).

Generally, modest mitochondrial fusion is believed to be beneficial to maintaining a normal mitochondrial and cellular function, whereas mitochondrial fission is detrimental, though excessive mitochondrial fusion may be harmful. For example, many studies have indicated that heart failure and myocardial infarction are related to excessive mitochondrial fission and insufficient mitochondrial fusion [35, 60], while inhibition of Drp1 to promote mitochondrial fusion protects against myocardial ischemia-reperfusion [61, 62]. On the other hand, mitochondrial fission-fusion emerged as a key regulator of cell proliferation and differentiation. Mitochondrial fusion may promote cell proliferation, while mitochondrial fission may inhibit cell proliferation and promote cell cycle exiting to allow entry into differentiation [63, 64]. In the present study, we found that rHMGB1 caused Drp1 degradation and mitochondrial fusion through CXCR4, exerting a role of chemokine. As an important chemokine receptor, the activation of CXCR4 resulted in cell proliferation and tissue regeneration [53]. So, it is reasonable to conclude that rHMGB1-induced CXCR4-dependent mitochondrial fusion
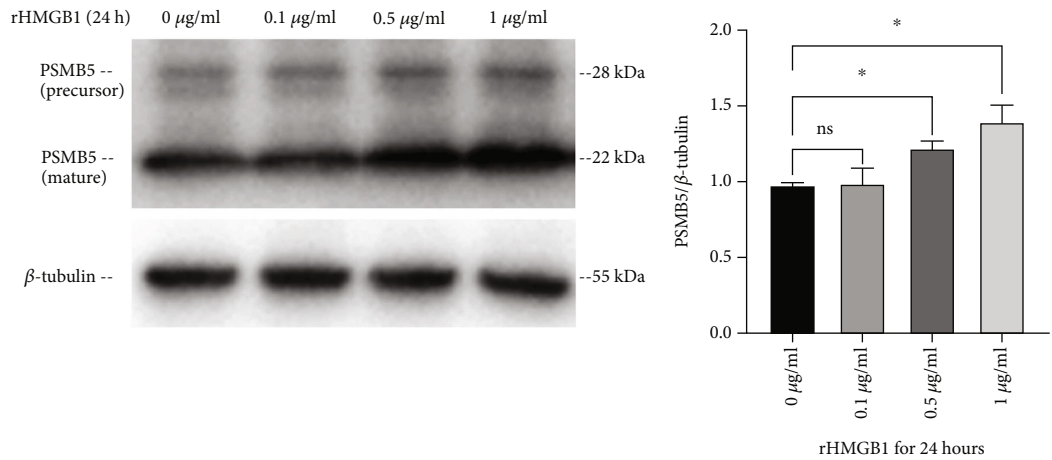
(a)

(b)
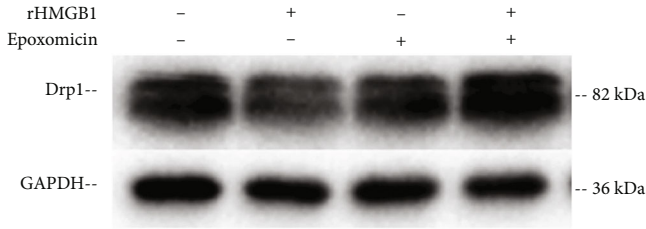
(c)
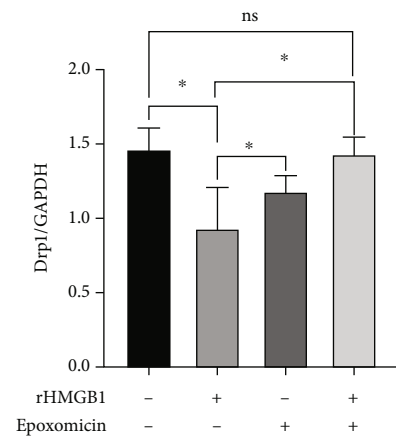
(d)
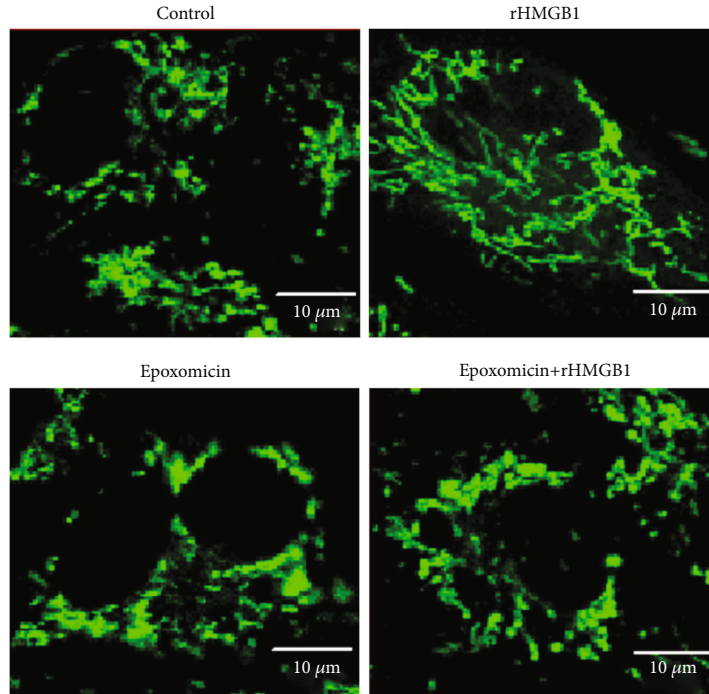
(e)

FIGURE 5: Continued.

(f)

(g)

(h)
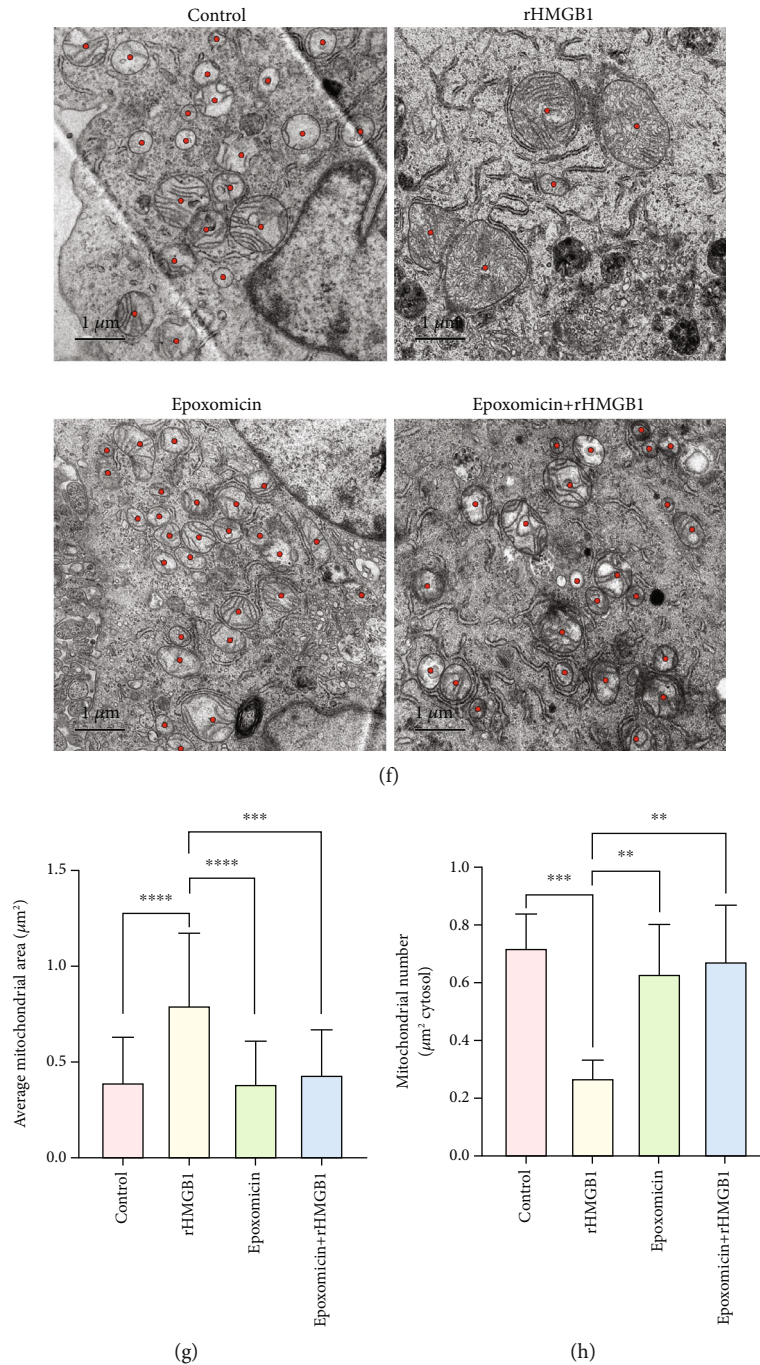
FIGURE 5: Inhibition of PSMB5 abolished rHMGB1-induced decrease in Drp1 protein and mitochondrial fusion. (a) Representative immunoblotting bands of PSMB5 of cells treated with different concentrations of rHMGB1 and the matching internal standard β-Tubulin. (b) The densitometric analysis of relative PSMB5 expression of cells treated with different concentrations of rHMGB1 referenced to matching β-Tubulin. (c) Representative immunoblotting bands of Drp1 of cells preexposed to epoxomicin ($10\,\mu$M) followed by rHMGB1 ($1\,\mu$g/ml) and the matching internal standard GAPDH. (d) The densitometric analysis of relative Drp1 expression of cells preexposed to epoxomicin followed by rHMGB1 referenced to matching GAPDH. (e) Mitochondrial morphology of cells exposed to epoxomicin ($10\,\mu$M) and subsequent rHMGB1 ($1\,\mu$g/ml). Cells were subjected to fluorescent staining with MitoTracker Green FM and observed by a Leica SP8 confocal laser scanning microscope. The magnification is 630. Scale bar: $10\,\mu$m. (f) TEM images of mitochondria of EA.hy926 endothelial cells exposed to epoxomicin ($10\,\mu$M) and subsequent rHMGB1 ($1\,\mu$g/ml). The magnification is 5900. Scale bar: $1\,\mu$m. (g) The average mitochondrial area (μm^2) under TEM changes of EA.hy926 endothelial cells treated with rHMGB1, epoxomicin, or both, compared with the control group. (h) The mitochondrial number changes under TEM in EA.hy926 endothelial cells treated with rHMGB1, epoxomicin, or both, compared with the control group. GAPDH: glyceraldehyde-3-phosphate dehydrogenase; TEM: transmission electron microscopy. Data were expressed as the mean ± SD. For comparison of the average mitochondrial area, at least 30 mitochondria of 10 cells per group were calculated; for comparison of mitochondrial number, at least 10 cells per group were counted. $^*P < 0.05$, $^{**}P < 0.01$, $^{***}P < 0.001$, and $^{****}P < 0.0001$.
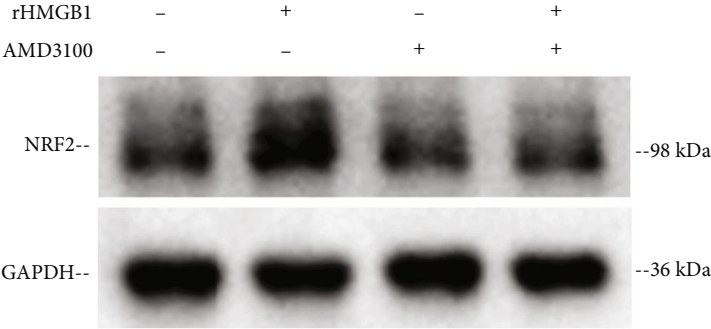
(a)
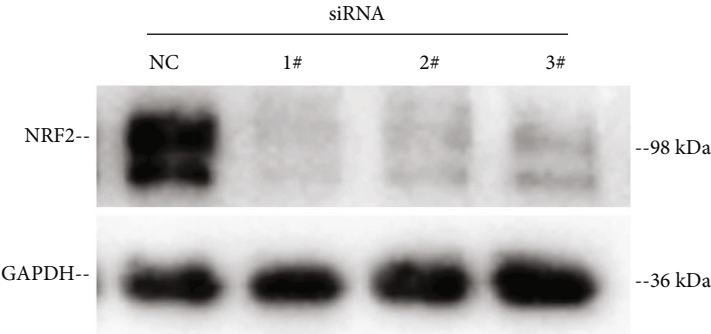
(b)
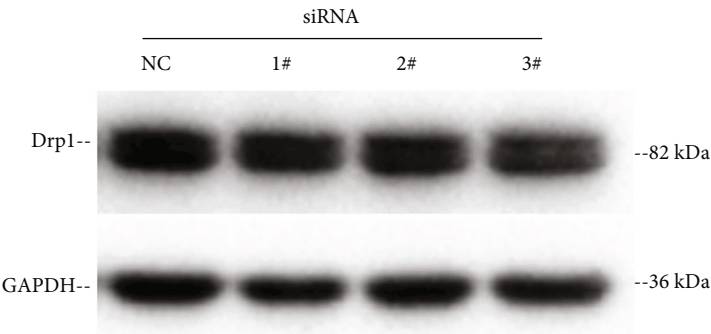
(c)
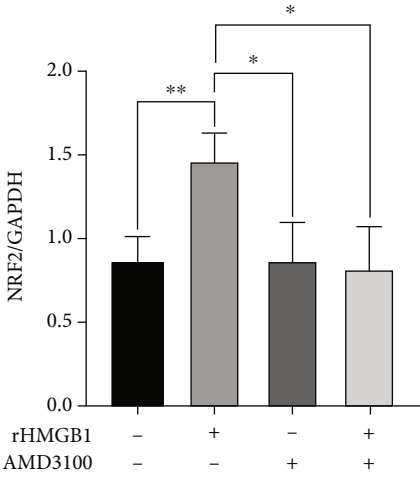
(d)
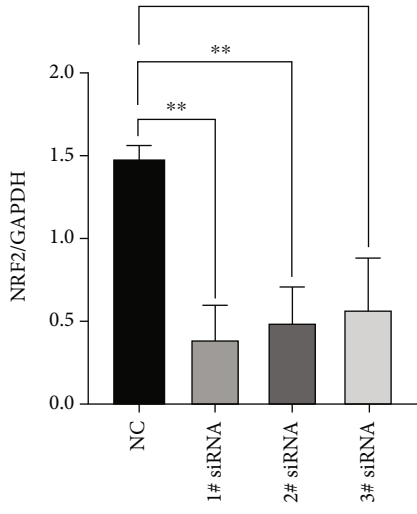
(e)
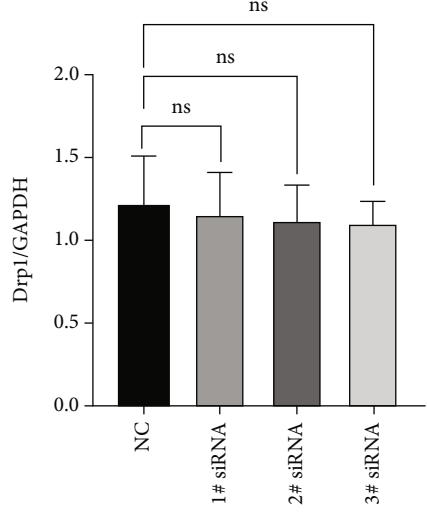
(f)

FIGURE 6: Continued.

(g)

(h)

(i)
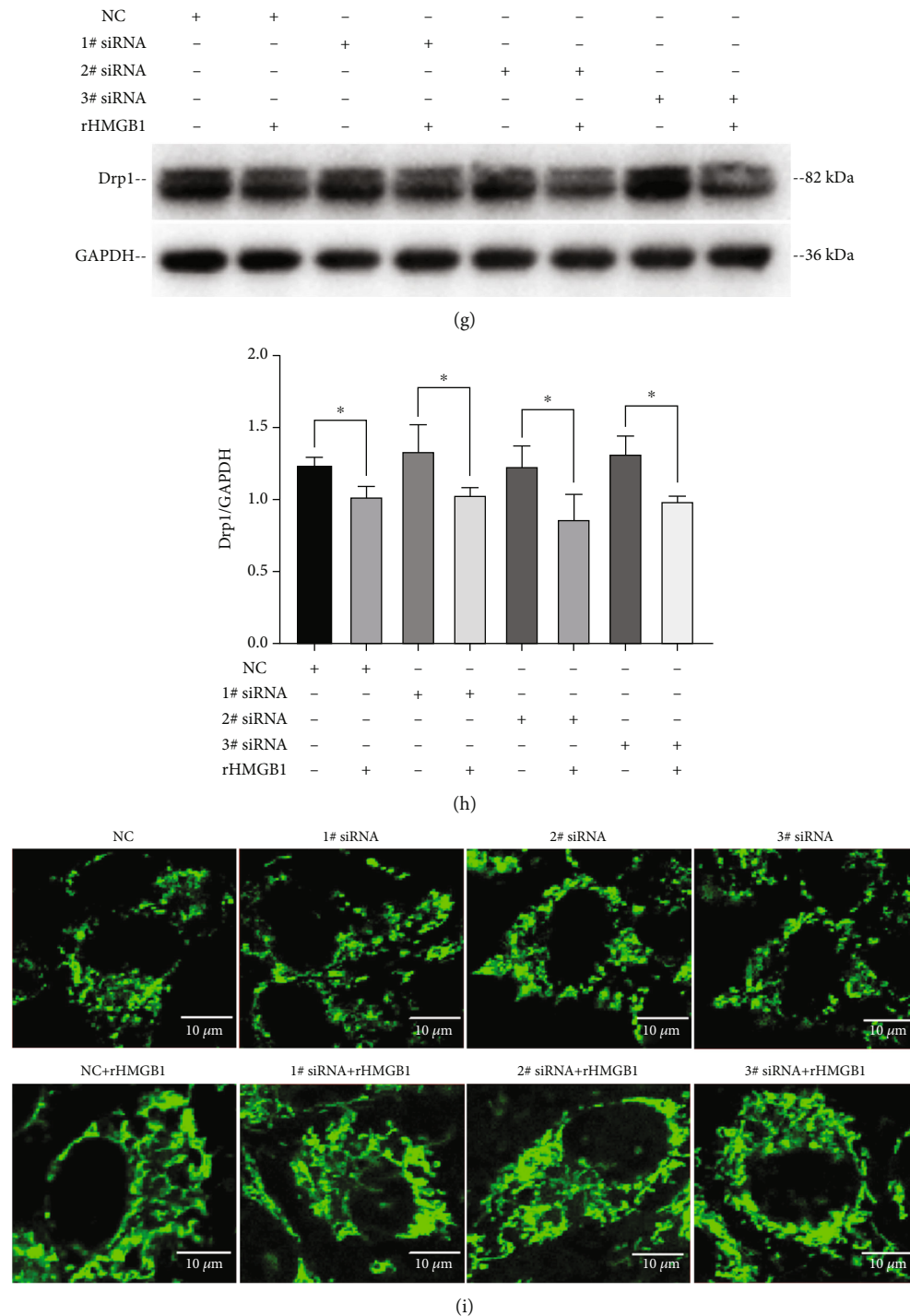
FIGURE 6: rHMGB1 induced downregulation of Drp1 and mitochondrial fusion was NRF2 independent. (a) Immunoblotting result showed that rHMGB1 upregulated the expression of NRF2, and CXCR4 antagonist AMD3100 abolished this effect. (b) Immunoblotting result demonstrated that NRF2 was successfully silenced with specific siRNAs (1# siRNA, 2# siRNA, and 3# siRNA). (c) Immunoblotting result showed that silencing the expression of NRF2 had no significant effect on the expression of Drp1. (d, e) The densitometric analysis of relative NRF2 expression of cells treated with rHMGB1, AMD3100, or siRNAs referenced to matching GAPDH. (f) The densitometric analysis of relative Drp1 expression of cells treated with siRNAs referenced to matching GAPDH. (g) Immunoblotting result showed that silencing the expression of NRF2 had no significant effect on reversing rHMGB1-induced downregulation of Drp1. (h) The densitometric analysis of relative Drp1 expression of cells treated with siRNAs and/or rHMGB1 referenced to matching GAPDH. (i) Confocal result showed that silencing the expression of NRF2 had no significant effect on mitochondrial dynamics or on reversing rHMGB1-induced mitochondrial fusion in EA.hy926 cells. Cells were subjected to fluorescent staining with MitoTracker Green FM and observed by a Leica SP8 confocal laser scanning microscope. Scale bar: 10 μm. GAPDH: glyceraldehyde-3-phosphate dehydrogenase; NC: negative control. Data were expressed as the mean ± SD; $^*P < 0.05$, $^{**}P < 0.01$.
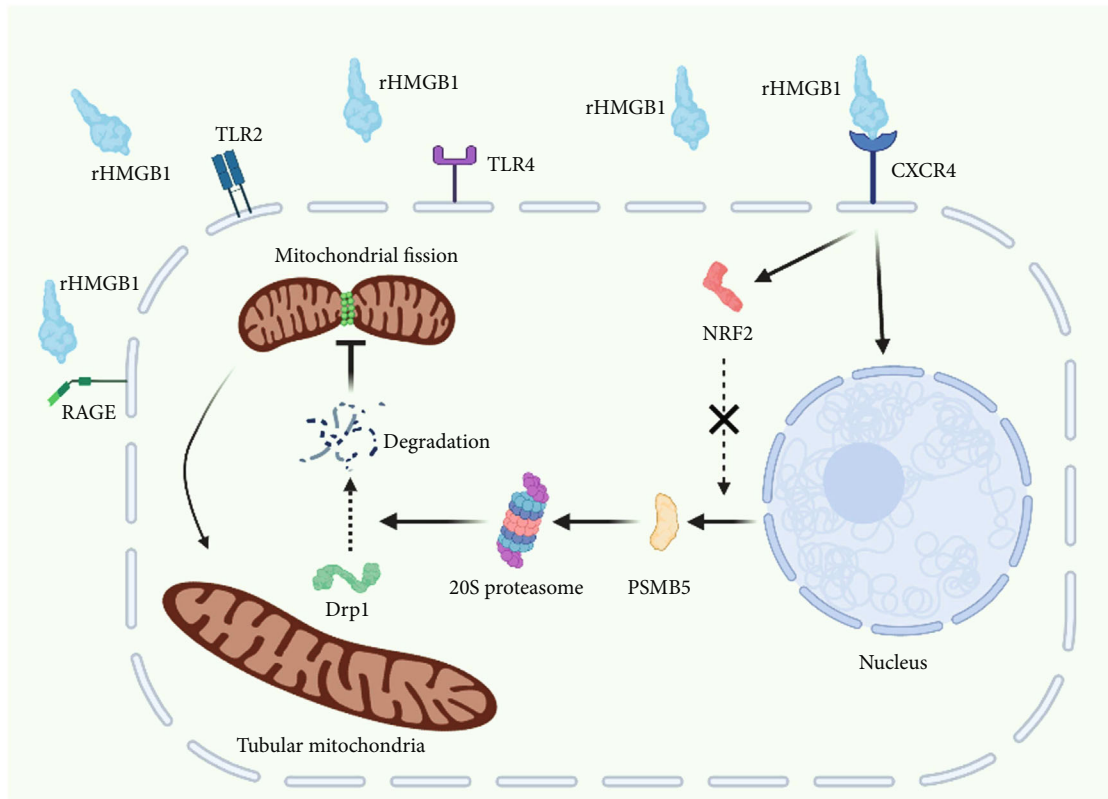
FIGURE 7: Schematic depiction of rHMGB1-induced mitochondrial fusion and the underlying mechanism. rHMGB1 combines and activates the membrane receptor CXCR4, then upregulates the expression of PSMB5 to increase the activity of 20S proteasome, leads to degradation of mitochondrial fission protein Drp1, and results in mitochondrial hyperfusion. rHMGB1: recombinant high-mobility group box 1; CXCR4: C-X-C-chemokine receptor 4; TLR2: toll-like receptor 2; TLR4: toll-like receptor 4; RAGE: receptor for advanced glycation end products; PSMB5: 20S proteasome subunit beta 5; Drp1: dynamin-related protein 1; NRF2: nuclear factor E2-related factor 2.

serves as a key checkpoint in its role of promoting tissue repair and regeneration. Considering the beneficial role of appropriated mitochondrial fusion, our study provided new clues for the mechanism of HMGB1-mediated cytoprotection role.

5. Conclusion

HMGB1 promotes mitochondrial hyperfusion through CXCR4/PSMB5-mediated Drp1 protein degradation in EA.hy926 endothelial cells in a manner of NRF2 independent, without apparent effect on the inflammatory phenotype. In the light of the important role of balanced mitochondrial dynamics in maintaining normal cellular biological function, our study sheds new light on the mechanism of HMGB1-mediated cytoprotective role.

Data Availability

The data used to support the findings of this study are available from the corresponding author upon request.

Conflicts of Interest

The authors declare that there is no conflict of interest regarding the publication of this paper.

Acknowledgments

Supplementary Materials

Supplementary 1. Table S1: The sequences of NRF2 siRNA duplexes and negative control. Table S2: PCR primer sequences for Drp1 and GAPDH genes.

Supplementary 2. Figure S1: CD31 and vWF were strongly positive in EA.hy926 cells detected with immunofluorescent staining. (a) Cells were incubated with CD31 primary

antibody, followed by Alexa Fluor 488 labeled secondary antibody, then counterstained with Hoechst. Clear green fluorescence (mostly located on cytomembrane) indicated the high expression of CD31 in EA.hy926 cells. (b) Cells were incubated with vWF primary antibody, followed by Alexa Fluor 594 labeled secondary antibody, then counterstained with Hoechst. Clear red fluorescence indicated the high expression of vWF in EA.hy926 cells. The magnification is 400. Scale bar: 50 μm. CD31: cluster of differentiation 31; vWF: von Willebrand factor. Figure S2: No significant inflammatory phenotype change was found in EA.hy926 cells treated with rHMGB1. (a) Immunoblotting showed that rHMGB1 had no significant influence on the expression of NLRP3. (b) Immunoblotting showed that rHMGB1 did not increase the expression level of caspase 1 and cleaved caspase 1. (c) ELISA showed that no significant increase of IL-1β concentration was found in the culture supernatant of EA.hy926 cells treated with different concentrations of rHMGB1. Data were expressed as the mean ± SD. GAPDH: glyceraldehyde-3-phosphate dehydrogenase.

References

[1] W. C. Aird, "Endothelium as an organ system," *Critical Care Medicine*, vol. 32, Supplement, pp. S271–S279, 2004.

[2] S. M. Baumgartner-Parzer and W. Waldhäusl, "The endothelium as a metabolic and endocrine organ: its relation with insulin resistance," *Exp Clin Endocrinol Diabetes*, vol. 109, Supplement 2, pp. S166–S179, 2001.

[3] P. Rajendran, T. Rengarajan, J. Thangavel et al., "The vascular endothelium and human diseases," *International Journal of Biological Sciences*, vol. 9, no. 10, pp. 1057–1069, 2013.

[4] X. Pi, L. Xie, and C. Patterson, "Emerging roles of vascular endothelium in metabolic homeostasis," *Circulation Research*, vol. 123, no. 4, pp. 477–494, 2018.

[5] M. A. Gimbrone Jr. and G. Garcia-Cardena, "Endothelial cell dysfunction and the pathobiology of atherosclerosis," *Circulation Research*, vol. 118, no. 4, pp. 620–636, 2016.

[6] D. Konukoglu and H. Uzun, "Endothelial dysfunction and hypertension," *Advances in Experimental Medicine and Biology*, vol. 956, pp. 511–540, 2017.

[7] R. Budhiraja, R. M. Tuder, and P. M. Hassoun, "Endothelial dysfunction in pulmonary hypertension," *Circulation*, vol. 109, no. 2, pp. 159–165, 2004.

[8] A. Tuttolomondo, M. Daidone, and A. Pinto, "Endothelial dysfunction and inflammation in ischemic stroke pathogenesis," *Current Pharmaceutical Design*, vol. 26, no. 34, pp. 4209–4219, 2020.

[9] M. M. Alem, "Endothelial dysfunction in chronic heart failure: assessment, findings, significance, and potential therapeutic targets," *International Journal of Molecular Sciences*, vol. 20, no. 13, p. 3198, 2019.

[10] C. M. Sena, A. M. Pereira, and R. Seiça, "Endothelial dysfunction – a major mediator of diabetic vascular disease," *Biochimica et Biophysica Acta*, vol. 1832, no. 12, pp. 2216–2231, 2013.

[11] L. Hajra, A. I. Evans, M. Chen, S. J. Hyduk, T. Collins, and M. I. Cybulsky, "The Nf-kappa B signal transduction pathway in aortic endothelial cells is primed for activation in regions predisposed to atherosclerotic lesion formation," *Proceedings of the National Academy of Sciences of the United States of America*, vol. 97, no. 16, pp. 9052–9057, 2000.

[12] H. J. Sun, Z. Y. Wu, X. W. Nie, and J. S. Bian, "Role of endothelial dysfunction in cardiovascular diseases: the link between inflammation and hydrogen sulfide," *Frontiers in Pharmacology*, vol. 10, p. 1568, 2020.

[13] S. Sitia, L. Tomasoni, F. Atzeni et al., "From endothelial dysfunction to atherosclerosis," *Autoimmunity Reviews*, vol. 9, no. 12, pp. 830–834, 2010.

[14] A. Raucci, S. di Maggio, F. Scavello, A. D'Ambrosio, M. E. Bianchi, and M. C. Capogrossi, "The Janus face of Hmgb1 in heart disease: a necessary update," *Cellular and Molecular Life Sciences*, vol. 76, no. 2, pp. 211–229, 2019.

[15] A. Tsung, S. Tohme, and T. R. Billiar, "High-mobility group box-1 in sterile inflammation," *Journal of Internal Medicine*, vol. 276, no. 5, pp. 425–443, 2014.

[16] E. Venereau, M. Casalgrandi, M. Schiraldi et al., "Mutually exclusive redox forms of Hmgb1 promote cell recruitment or proinflammatory cytokine release," *The Journal of Experimental Medicine*, vol. 209, no. 9, pp. 1519–1528, 2012.

[17] H. S. Ding, J. Yang, P. Chen et al., "The Hmgb1-Tlr4 axis contributes to myocardial ischemia/reperfusion injury via regulation of cardiomyocyte apoptosis," *Gene*, vol. 527, no. 1, pp. 389–393, 2013.

[18] L. Zhang, M. Liu, H. Jiang et al., "Extracellular high-mobility group box 1 mediates pressure overload-induced cardiac hypertrophy and heart failure," *Journal of Cellular and Molecular Medicine*, vol. 20, no. 3, pp. 459–470, 2016.

[19] F. Biscetti, M. M. Rando, E. Nardella et al., "High mobility group box-1 and diabetes mellitus complications: state of the art and future perspectives," *International Journal of Molecular Sciences*, vol. 20, no. 24, p. 6258, 2019.

[20] F. Limana, A. Germani, A. Zacheo et al., "Exogenous high-mobility group box 1 protein induces myocardial regeneration after infarction via enhanced cardiac C-kit+ cell proliferation and differentiation," *Circulation Research*, vol. 97, no. 8, pp. e73–e83, 2005.

[21] F. Y. Liu, D. Fan, Z. Yang et al., "Tlr9 is essential for Hmgb1-mediated post-myocardial infarction tissue repair through affecting apoptosis, cardiac healing, and angiogenesis," *Cell Death & Disease*, vol. 10, no. 7, p. 480, 2019.

[22] Y. H. Zhou, Q. F. Han, L. Gao et al., "Hmgb1 protects the heart against ischemia-reperfusion injury via Pi3k/Akt pathway-mediated upregulation of Vegf expression," *Frontiers in Physiology*, vol. 10, p. 1595, 2020.

[23] C. Fiuza, M. Bustin, S. Talwar et al., "Inflammation-promoting activity of Hmgb1 on human microvascular endothelial cells," *Blood*, vol. 101, no. 7, pp. 2652–2660, 2003.

[24] Z. Zhu, X. Peng, X. Li et al., "Hmgb1 impairs endothelium-dependent relaxation in diabetes through Tlr4/Enos pathway," *The FASEB Journal*, vol. 34, no. 6, pp. 8641–8652, 2020.

[25] E. M. Bauer, R. Shapiro, T. R. Billiar, and P. M. Bauer, "High mobility group box 1 inhibits human pulmonary artery endothelial cell migration via a toll-like receptor 4- and interferon response factor 3-dependent mechanism(s)*," *The Journal of Biological Chemistry*, vol. 288, no. 2, pp. 1365–1373, 2013.

[26] S. Ghaffari, E. Jang, F. N. Nabi et al., "Endothelial Hmgb1 is a critical regulator of Ldl transcytosis via an Srebp2-Sr-Bi axis," *Arteriosclerosis, Thrombosis, and Vascular Biology*, vol. 41, no. 1, pp. 200–216, 2020.

[27] J. Lan, H. Luo, R. Wu et al., "Internalization of Hmgb1 (high mobility group box 1) promotes angiogenesis in endothelial cells," *Arteriosclerosis, Thrombosis, and Vascular Biology*, vol. 40, no. 12, pp. 2922–2940, 2020.

[28] Q. Zhou, T. Tu, S. Tai, L. Tang, H. Yang, and Z. Zhu, "Endothelial specific deletion of Hmgb1 increases blood pressure and retards ischemia recovery through Enos and Ros pathway in mice," *Redox Biology*, vol. 41, p. 101890, 2021.

[29] S. A. Detmer and D. C. Chan, "Functions and dysfunctions of mitochondrial dynamics," *Nature Reviews. Molecular Cell Biology*, vol. 8, no. 11, pp. 870–879, 2007.

[30] H. Otera and K. Mihara, "Molecular mechanisms and physiologic functions of mitochondrial dynamics," *Journal of Biochemistry*, vol. 149, no. 3, pp. 241–251, 2011.

[31] S. Gao and J. Hu, "Mitochondrial fusion: the machineries in and out," *Trends in Cell Biology*, vol. 31, no. 1, pp. 62–74, 2021.

[32] F. Kraus, K. Roy, T. J. Pucadyil, and M. T. Ryan, "Function and regulation of the divisome for mitochondrial fission," *Nature*, vol. 590, no. 7844, pp. 57–66, 2021.

[33] H. Han, J. Tan, R. Wang et al., "Pink1 phosphorylates Drp1$_{S616}$ to regulate mitophagy-independent mitochondrial dynamics," *EMBO Rep*, vol. 21, no. 8, article e48686, 2020.

[34] S. L. Archer, "Mitochondrial dynamics–mitochondrial fission and fusion in human diseases," *The New England Journal of Medicine*, vol. 369, no. 23, pp. 2236–2251, 2013.

[35] A. A. Knowlton and T. T. Liu, "Mitochondrial dynamics and heart failure," *Comprehensive Physiology*, vol. 6, no. 1, pp. 507–526, 2015.

[36] C. Maneechote, S. Palee, S. Kerdphoo, T. Jaiwongkam, S. C. Chattipakorn, and N. Chattipakorn, "Pharmacological inhibition of mitochondrial fission attenuates cardiac ischemia-reperfusion injury in pre-diabetic rats," *Biochemical Pharmacology*, vol. 182, p. 114295, 2020.

[37] D. C. Chan, "Mitochondrial dynamics and its involvement in disease," *Annual Review of Pathology*, vol. 15, no. 1, pp. 235–259, 2020.

[38] S. M. Shenouda, M. E. Widlansky, K. Chen et al., "Altered mitochondrial dynamics contributes to endothelial dysfunction in diabetes mellitus," *Circulation*, vol. 124, no. 4, pp. 444–453, 2011.

[39] M. J. Tanner, J. Wang, R. Ying et al., "Dynamin-related protein 1 mediates low glucose-induced endothelial dysfunction in human arterioles," *American Journal of Physiology. Heart and Circulatory Physiology*, vol. 312, no. 3, pp. H515–h527, 2017.

[40] R. Sabouny, E. Fraunberger, M. Geoffrion et al., "The Keap1-Nrf2 stress response pathway promotes mitochondrial hyperfusion through degradation of the mitochondrial fission protein Drp1," *Antioxidants & Redox Signaling*, vol. 27, no. 18, pp. 1447–1459, 2017.

[41] C. Wang, X. X. Liu, K. B. Huang et al., "Preconditioning with recombinant high-mobility group box 1 induces ischemic tolerance in a rat model of focal cerebral ischemia–reperfusion," *Journal of Neurochemistry*, vol. 137, no. 4, pp. 576–588, 2016.

[42] K. Izuishi, A. Tsung, G. Jeyabalan et al., "Cutting edge: high-mobility group box 1 preconditioning protects against liver ischemia-reperfusion injury," *Journal of Immunology*, vol. 176, no. 12, pp. 7154–7158, 2006.

[43] H. Wu, R. Steenstra, E. C. de Boer et al., "Preconditioning with recombinant high-mobility group box 1 protein protects the kidney against ischemia-reperfusion injury in mice," *Kidney International*, vol. 85, no. 4, pp. 824–832, 2014.

[44] H. Yang, D. J. Antoine, U. Andersson, and K. J. Tracey, "The many faces of Hmgb1: molecular structure-functional activity in inflammation, apoptosis, and chemotaxis," *Journal of Leukocyte Biology*, vol. 93, no. 6, pp. 865–873, 2013.

[45] S. B. Ong, A. R. Hall, and D. J. Hausenloy, "Mitochondrial dynamics in cardiovascular health and disease," *Antioxidants & Redox Signaling*, vol. 19, no. 4, pp. 400–414, 2013.

[46] Y. Matsuzawa, R. R. Guddeti, T. G. Kwon, L. O. Lerman, and A. Lerman, "Treating coronary disease and the impact of endothelial dysfunction," *Progress in Cardiovascular Diseases*, vol. 57, no. 5, pp. 431–442, 2015.

[47] I. Mordi, N. Mordi, C. Delles, and N. Tzemos, "Endothelial dysfunction in human essential hypertension," *Journal of Hypertension*, vol. 34, no. 8, pp. 1464–1472, 2016.

[48] J. Sun, H. Deng, Z. Zhou, X. Xiong, and L. Gao, "Endothelium as a potential target for treatment of abdominal aortic aneurysm," *Oxidative Medicine and Cellular Longevity*, vol. 2018, Article ID 6306542, 12 pages, 2018.

[49] H. Yang, H. Wang, S. S. Chavan, and U. Andersson, "High mobility group box protein 1 (Hmgb1): the prototypical endogenous danger molecule," *Molecular Medicine*, vol. 21, Supplement 1, pp. S6–s12, 2015.

[50] L. Pellegrini, E. Foglio, E. Pontemezzo, A. Germani, M. A. Russo, and F. Limana, "Hmgb1 and repair: focus on the heart," *Pharmacology & Therapeutics*, vol. 196, pp. 160–182, 2019.

[51] X. Cen, S. Liu, and K. Cheng, "The role of toll-like receptor in inflammation and tumor immunity," *Frontiers in Pharmacology*, vol. 9, p. 878, 2018.

[52] B. I. Hudson and M. E. Lippman, "Targeting rage signaling in inflammatory disease," *Annual Review of Medicine*, vol. 69, no. 1, pp. 349–364, 2018.

[53] M. E. Bianchi and R. Mezzapelle, "The chemokine receptor Cxcr4 in cell proliferation and tissue regeneration," *Frontiers in Immunology*, vol. 11, p. 2109, 2020.

[54] G. Hoppe, K. E. Talcott, S. K. Bhattacharya, J. W. Crabb, and J. E. Sears, "Molecular basis for the redox control of nuclear transport of the structural chromatin protein Hmgb1," *Experimental Cell Research*, vol. 312, no. 18, pp. 3526–3538, 2006.

[55] C. Janko, M. Filipović, L. E. Munoz et al., "Redox modulation of Hmgb1-related signaling," *Antioxidants & Redox Signaling*, vol. 20, no. 7, pp. 1075–1085, 2014.

[56] F. Kumar Deshmukh, D. Yaffe, M. Olshina, G. Ben-Nissan, and M. Sharon, "The contribution of the 20s proteasome to proteostasis," *Biomolecules*, vol. 9, no. 5, p. 190, 2019.

[57] A. L. Goldberg, "Protein degradation and protection against misfolded or damaged proteins," *Nature*, vol. 426, no. 6968, pp. 895–899, 2003.

[58] L. Yang, X. Li, A. Jiang et al., "Metformin alleviates lead-induced mitochondrial fragmentation via Ampk/Nrf2 activation in Sh-Sy5y cells," *Redox Biology*, vol. 36, p. 101626, 2020.

[59] G. B. O'Mealey, W. L. Berry, and S. M. Plafker, "Sulforaphane is a Nrf2-independent inhibitor of mitochondrial fission," *Redox Biology*, vol. 11, pp. 103–110, 2017.

[60] S. B. Ong, S. Subrayan, S. Y. Lim, D. M. Yellon, S. M. Davidson, and D. J. Hausenloy, "Inhibiting mitochondrial fission protects the heart against ischemia/reperfusion injury," *Circulation*, vol. 121, no. 18, pp. 2012–2022, 2010.

[61] M. Ding, Q. Dong, Z. Liu et al., "Inhibition of dynamin-related protein 1 protects against myocardial ischemia-reperfusion

injury in diabetic mice," *Cardiovascular Diabetology*, vol. 16, no. 1, p. 19, 2017.

[62] S. Hernandez-Resendiz, F. Prunier, H. Girao, G. Dorn, D. J. Hausenloy, and EU-CARDIOPROTECTION COST Action (CA16225), "Targeting mitochondrial fusion and fission proteins for cardioprotection," *Journal of Cellular and Molecular Medicine*, vol. 24, no. 12, pp. 6571–6585, 2020.

[63] K. Mitra, "Mitochondrial fission-fusion as an emerging key regulator of cell proliferation and differentiation," *BioEssays*, vol. 35, no. 11, pp. 955–964, 2013.

[64] K. Mitra, R. Rikhy, M. Lilly, and J. Lippincott-Schwartz, "Drp1-dependent mitochondrial fission initiates follicle cell differentiation during Drosophila oogenesis," *The Journal of Cell Biology*, vol. 197, no. 4, pp. 487–497, 2012.

Research Article

Oxidative Stress in Patients before and after On-Pump and Off-Pump Coronary Artery Bypass Grafting: Relationship with Syntax Score

Petar Vukicevic (ID),[1,2] **Aleksandra Klisic** (ID),[3] **Vojislava Neskovic** (ID),[2,4] **Luka Babic** (ID),[1] **Aleksandar Mikic** (ID),[5,6] **Natasa Bogavac-Stanojevic** (ID),[7] **Milos Matkovic** (ID),[6,8] **Vladimir Milićević** (ID),[8] **Nemanja Aleksic** (ID),[6,8] and **Jelena Kotur-Stevuljevic** (ID)[7]

[1]Clinic for Cardiac Surgery, Military Medical Academy, Belgrade, Serbia
[2]University of Defense, Medical Faculty of the Military Medical Academy, Belgrade, Serbia
[3]Primary Health Care Center, University of Montenegro-Faculty of Medicine, Podgorica, Montenegro
[4]Clinic for Anesthesiology and Critical Care, Military Medical Academy, Belgrade, Serbia
[5]Clinic for Cardiac Surgery, UC Clinical Centre, Belgrade, Serbia
[6]University of Belgrade-Faculty of Medicine, Belgrade, Serbia
[7]Department for Medical Biochemistry, University of Belgrade-Faculty of Pharmacy, Belgrade, Serbia
[8]Department for Cardiac Surgery, University Clinical Center of Serbia, Belgrade, Serbia

Correspondence should be addressed to Aleksandra Klisic; aleksandranklisic@gmail.com

Received 25 April 2021; Revised 29 June 2021; Accepted 19 July 2021; Published 2 August 2021

Academic Editor: Ciccarelli Michele

Objective. Coronary artery bypass grafting (CABG) represents the significant source of increased oxidative stress (OS). We aimed to follow the OS status parameters (i.e., ischemia-modified albumin (IMA), malondialdehyde (MDA), superoxide anion, prooxidant-antioxidant balance (PAB), total oxidant status (TOS), total antioxidant status (TAS), and superoxide-dismutase (SOD)) change through the predefined study times in two different surgical procedures, i.e., cardiopulmonary bypass (CPB) and off-pump coronary artery bypass grafting (OPCAB). Additionally, we aimed to investigate those OS status parameters in specific study times according to SYNTAX score (SS), an established angiographic score for evaluating the extensity and severity of coronary artery disease. *Patients and Methods*. A total of 107 patients that were planned to undergo CABG were included (i.e., 47 patients in OPCAB and 60 patients in CPB group). Blood samples were taken at 6 time intervals: before surgery (t1), immediately after intervention (t2), 6 h (t3), 24 h (t4), 48 h (t5), and 96 h after termination of the operation (t6). *Results*. IMA levels were higher in CPB than that in OPCAB baseline and rose in CPB group in t2 point. TOS decreased in both study groups, compared to baseline values, but without statistical significance. Superoxide anion and PAB significantly increased in t3-t6 study times, in both groups. MDA significantly increased only in CPB group in t5 and t6 interval. MDA was significantly higher in CPB group compared to OPCAB in t6 study point. CPB patients had significantly lower TAS compared to OPCAB patients at the beginning and in t2 and t3 study points. They also had significantly lower SOD activities compared to OPCAB, baseline, and in several study points. Moreover, TAS, SOD, and TAS/TOS ratio were significantly lower, whereas PAB and TOS/TAS were significantly higher in patients with high SS compared to corresponding groups. SOD activity, IMA, and TAS level were the best predictors of high SS. *Conclusion*. CPB patients were in more severe ischemia baseline than OPCAB group and IMA rose in CPB patients immediately after the surgery end, but not later. Also, the antioxidant status was significantly lower, whereas the prooxidant status was significantly higher in patients with high SS compared to corresponding groups. SOD activity, IMA, and TAS level were the best predictors of CAD (as determined with SS), showing that SOD and IMA had very good discriminatory capability towards higher SS status.

1. Introduction

It is well known that cardiovascular disease is the leading cause of increased morbidity and mortality worldwide. One of the key surgical procedures that patients with coronary artery disease (CAD) are often subjected to is coronary artery bypass grafting (CABG). However, the cardiopulmonary bypass (CPB) pump increases systemic oxidative stress (OS) and often leads to postoperative complications [1, 2]. This is related to ischemia and harmful effects of extracorporeal circulation (ECC) which induce free radical generation production. Additionally, OS becomes more pronounced during reperfusion followed by the end of the cardioplegic arrest [1–3].

Therefore, attempts have been made to avoid the CPB deleterious effects and ischemia-reperfusion injury and to reduce the postoperative complications [4] questioning if off-pump coronary artery bypass grafting (OPCAB) on the beating heart may lead to diminishing the OS [5] and reduce the rate of morbidity and mortality compared with conventional on-pump CABG (i.e., CPB) [6, 7]. However, these data are inconclusive since other studies report the opposite results [8, 9].

Indeed, we have previously shown that patients who underwent CPB exhibited increased OS (i.e., higher levels of lipid hydroperoxides and advanced oxidation protein products), as compared with patients that underwent OPCAB during the postoperative period [10].

The pathophysiological trait of the relationship between OS and CABG has not been clearly elucidated. Namely, previous studies have evaluated different prooxidant and antioxidant parameters and different study intervals before and after the surgical procedures [1, 10–13], but discordant results were shown.

In an attempt to overcome the knowledge gap between CABG procedure and the changes in redox homeostasis system, we aimed to explore a wide spectrum of OS parameters through the predefined study times caused by the two different surgical procedures, i.e., CPB or OPCAB, which might add contribution to make a proper choice of adequate surgical technique.

In addition, to obtain deeper insight into the relationship between vessel wall lesion complexity and redox status, we evaluated OS status parameters in specific study times according to SYNTAX (synergy between percutaneous coronary intervention with taxus and cardiac surgery) score (SS), an established angiographic score for evaluation the extensity and severity of CAD [14].

2. Patients and Methods

2.1. Patients. The current prospective cohort study was conducted at the Medical Military Academy, Belgrade (Department for Cardiac Surgery), in cooperation with the Faculty of Pharmacy, University of Belgrade (Department for Medical Biochemistry). After approval of the Institutional Ethics Committee (number: 29/II-27), each patient before inclusion in the study provided the written informed consent. Detailed methodology was described elsewhere [10]. In brief, a total of

107 patients were consecutively recruited for CABG. The indications for surgery and patients with stable angina pectoris were selected according to guidelines for CABG Surgery (American College Of Cardiology/American Heart Association Task Force on Practice Guidelines).

The two groups of patients were formed. A total of 47 patients were included in the group where examinees underwent CABG on the beating-heart without using CPB (i.e., off-pump coronary artery bypass grafting-OPCAB), whereas a total of 60 patients encompassed the group undergoing CABG using CPB on the potassium arrested heart (i.e., on-pump coronary artery bypass grafting-CPB).

Patients with metabolic diseases (other than diabetes mellitus), recent myocardial infarction or perioperative myocardial infarction, unstable angina pectoris, heart failure, mediastinal bleeding, massive postoperative and previous stroke or transient ischemic attack, reoperation, chronic renal failure, malignant or autoimmune diseases, acute infections, and use of immunosuppressive drugs and dietary supplements were excluded from this study.

Preoperatively, the SS [14] was calculated for each patient. SS is widely used for prediction events following percutaneous coronary intervention. In line with this, all patients were divided into low (i.e., SS < 22), moderate (i.e., SS between 22 and 30) and high SS subgroup (i.e., SS > 30).

Clinical SYNTAX score (CSS) was also calculated [15]. This score includes age, ejection fraction, and creatinine clearance and should better predict the complexity of patients status than SS alone, which is rather anatomical measure of lesion complexity. By adding CSS calculation, we got better evidence about overall functionality of CAD patients, i.e., some critical functions, like renal function, affected by the main disease.

Two-dimensional transthoracic echocardiography using biplane modified Simpson method was applied as the most commonly used diagnostic procedure to assess left ventricular ejection fraction (LVEF) clinically.

The EuroSCORE II [16] was developed to predict in-hospital mortality after cardiac surgery and includes the following risk factors: dyspnea, angina, extracardiac arteriopathy, poor mobility, previous cardiac surgery, renal dysfunction, active endocarditis, critical preoperative state, LV function or LVEF, urgency of procedure, and recent myocardial infarction.

2.2. Anesthesia. A standardized anesthetic technique was applied to all patients which was induced by (1 mg/kg) sufentanyl (0.5–1 μg/kg) and etomidate (0.1–0.2 mg/kg). General anesthesia was maintained with sufentanyl (0.5–1 μg/kg/h) and sevoflurane (0.6–1.0%).

2.3. Surgical Procedure. A procedure of midline sternotomy and harvesting of left internal mammary artery as a pedicle and saphenous vein grafts was performed and was followed by full exposure of the coronary artery branches for revascularization.

2.3.1. CPB Group. A procedure of ascending aortic cannulation and two-stage venous cannulation in the right atrium

was instituted for CABG using a CPB pump. A low-prime oxygenator with an incorporated cardiotomy reservoir (Sorin Inspire 8, Sorin Group, Mirandola, Italy) and a roller pump (Stockert-S5, Sorin Group, Munich, Germany) were used for CPB circuit.

The perfusion pressure between 50 and 80 mmHg and the nonpulsatile pump flow at 2.2-2.4 L/min/m^2 were maintained during CPB. The protection of miocardium was maintained with 4°C homemade cold potassium cardioplegia. All distal anastomoses of the bypass grafts were done on the arrested heart.

2.3.2. OPCAB Group.

The Octopus® IV Tissue Stabilizer and Starfish™ 2 Heart Positioner (Medtronic, Inc., Minneapolis, MN, USA) was used for the maintenance of mechanical stability of the coronary arteriotomy area.

Soft plastic intraluminally coronary flow-shunt (Medtronic, Clearview®, Medtronic, Inc., Minneapolis, MN, USA) was used for myocardial protection. It was always passed into the coronary arteriotomy to prevent the ischemia of myocardium during placement of distal anastomosis. All of the anastomoses were done on the beating heart.

2.4. Sample Collection and Analyses.

The venipuncture was performed at 6 time intervals: before surgery (t1), immediately after intervention (t2), 6 h (t3), 24 h (t4), 48 h (t5), and 96 h after termination of the operation (t6).

This procedure was the same for OPCAB and CPB group.

The central venous line from the jugular internal vein was used for such purpose. The K$_2$EDTA sample tubes (for plasma) and serum sample tubes were provided. The serum samples were left to clot for 30 minutes and then sera were obtained by centrifugation 3000 rpm for 15 minutes and kept at −80°C, until analysis. The plasma samples were provided after centrifugation of samples in K$_2$EDTA tubes 3000 rpm at room temperature for 15 minutes and kept at −80°C, until analysis.

2.5. Measurement of Oxidative Stress (OS) Status Parameters.

All OS status parameters were determined on an ILAB 650 analyzer (Instrumentation Laboratory, Milan, Italy).

Superoxide anion was measured in plasma following the method of Auclair and Voisin [17], as a rate of nitroblue tetrazolium (NBT) reduction for determination of the rate of superoxide anion generation.

Levels of prooxidant-antioxidant balance (PAB) were determined in serum by the method of Alamdari et al. [18] using $3,3'$, $5,5'$-tetramethylbenzidine as a chromogen.

Malondialdehyde (MDA) levels were measured in serum as a thiobarbituric acid reactive substance [19].

Superoxide-dismutase (SOD) activity was determined in plasma according to method of Misra and Fridovich [20] depending on the capability of the SOD to inhibit autooxidation of adrenalin in alkaline medium.

Ischemia-modified albumin (IMA) was measured in serum by method of Bar-Or et al. [21], and values are reported as absorption units (ABSU).

Total antioxidant status (TAS) and total oxidant status (TOS) were determined in serum with o-dianisidine [22] and an ABTS as a chromogen [23], respectively.

Oxidative stress index (OSI) was calculated as previously described: OSI (arbitrary unit) = TOS (μmol H$_2$O$_2$ equivalent/L)/TAS (μmol Trolox equivalent/L) × 100 [24].

2.6. Statistical Analysis.

A SPSS statistical package (version 18.0 for Windows, SPSS, Chicago, IL, USA) was used for statistical analysis. The sample size for each group (OPCAB and CAB) was calculated by GPower software, and chosen α level and power were 0.05 and 0.80, respectively. We approximated partial eta squared to be small (0.05), so the effect size f was 0.15. In addition, we approximated correlation among repeated measures and nonsphericity correction to be 0.6 and 1, respectively. The calculated sample size was 40 for each group. We increased that number by 15%, considering that nonparametric tests will be used to compare some parameters. The data are presented as mean ± standard deviation (SD), median (interquartile range), or counts and percentages (%). For repeated measured ANOVA, sphericity was tested using Mauchly's test, and Levene's test was used for ANOVA homogeneity of variance checking. ANOVA repeated measures as the nonparametric Friedman test, followed by the Wilcoxon signed-rank test, Kruskal-Wallis nonparametric analysis of variance, followed with the Mann-Whitney U test were used for testing the differences between groups. A chi-square test was used for testing the differences between categorical data. A Spearman's correlation analysis with correlation coefficient (ρ) was applied to examine the relationships between variables. For estimation of clinical and general factors that could influence SS value a logistic regression model of integrated parameters (t1-t6 study times) was applied. We used logistic regression analysis to determine the predicted probabilities of each model formed from redox parameters measured in different time points for further receiver-operating characteristic (ROC) analysis. Accuracy of each logistic model was calculated for discrimination high from low SS patients. In all analyses, a p value <0.05 was regarded to be statistically significant.

3. Results

Regarding SYNTAX Score subgroups, patients did not differ by age, body weight, body mass index (BMI), LVEF, and EuroSCORE-Logistic index. They did not also differ in glucose, creatinine, total proteins, eGFR and hematologic parameters ((white blood cell count (WBC), red blood cell count (RBC), hemoglobin (Hgb), and platelet count (PLT)), therapy usage, and percentage of smokers. Patients with higher SS values had significantly higher extracorporal circulation time (ECC) and aortic cross clamp time (ACC), so as the average bypass number (Table 1).

The several main characteristics of CPB procedure such as aortic cross clamp time (ACC) and extracorporal circulation time (ECC) are significantly higher in patients with higher SS, which implies the more complicated artery lesion condition in patients subjected to this procedure. We have

TABLE 1: General clinical and surgery related parameters according to SYNTAX Score tertile values.

Parameter	Low SS < 22 (15.6 ± 4.8)	Moderate SS 22-32 (27.1 ± 3.2)	High SS > 32 (38.6 ± 6.1)	P
n	34	39	33	/
Age (years)	63.2 ± 9.6	62.2 ± 9.4	67 ± 9.1	ns
Body weight (kg)	81.1 ± 12.7	81.1 ± 10.2	84.4 ± 14.5	ns
BMI (kg/m^2)	27.7 ± 3.1	27.6 ± 3.4	28.8 ± 4.4	ns
sGlucose (mmol/L)	6.40 ± 2.02	6.34 ± 2.12	6.77 ± 2.55	ns
sCreatinine (μmol/L)	85.1 ± 25.8	95.0 ± 58.1	89.5 ± 27.7	ns
sTotal proteins (g/L)	71.2 ± 5.1	71.0 ± 5.4	70.8 ± 4.8	ns
eGFR (mL/min/1.73 m^2)	83.6 ± 21.4	83.0 ± 26.1	79.1 ± 20.1	ns
WBC ($\times 10^9$/L)	7.0 ± 1.8	6.9 ± 1.6	7.1 ± 1.8	ns
RBC ($\times 10^{12}$/L)	4.6 ± 0.5	4.6 ± 0.5	4.6 ± 0.6	ns
Hgb (g/L)	134 ± 14	136 ± 14	135 ± 12	ns
PLT ($\times 10^9$/L)	230 ± 60	233 ± 52	220 ± 69	ns
LVEF (%)	52.0 ± 8.7	50.0 ± 9.9	47.6 ± 10.9	ns
EuroSCORE-logistic	5 (3-8.25)	5 (3-7)	7 (5-10)	ns
Clinical SS	19.1 (13.3-29.1)	33.6 (26.6-43.8)[aaa]	50.4 (43.8-81.2)[aaa,bbb]	<0.001
ECC (min)	0 (0-0)	72 (0-87)[aa]	81 (72.8-114.5)[aaa,bb]	<0.001
ACC (min)	0 (0-0)	29 (0.0-49)[aa]	44 (36-56)[aaa,bb]	<0.001
Bypass number	2.06 ± 0.49	2.33 ± 0.54	2.59 ± 0.64[a]	<0.05
β-Blockers, n (%)	30 (88.2%)	38 (97.4%)	33 (100.0%)	0.055
ACE inhibitors, n (%)	27 (79.4%)	37 (94.9%)	29 (87.9%)	ns
Calcium-antagonists, n (%)	11 (32.4%)	13 (33.3%)	12 (36.4%)	ns
Nitrates, n (%)	29 (85.3%)	34 (87.2%)	32 (97.0%)	ns
Statins, n (%)	22 (64.7%)	30 (76.9%)	24 (72.7%)	ns
Oral antidiabetics, n (%)	8 (23.5%)	5 (12.8%)	8 (24.2%)	ns
Diuretics, n (%)	10 (29.4%)	9 (23.1%)	16 (48.5%)	ns
Smokers, n (%)	23 (67.6%)	30 (76.9%)	22 (66.7%)	ns

BMI: body mass index; LVEF: left ventricular ejection fraction; ECC: extracorporal circulation time; ACC: aortic cross clamp time; P: ANOVA or Kruskall-Wallis nonparametric analysis of variance; Tuckey-Snedecor post hoc test. [a,aa,aaa]: $P < 0.05, 0.01, 0.001$ vs. low SS group; [bb]$P < 0.01$ vs. moderate SS group.

also calculated CSS. With SS increase, we have also found significant CSS increase (Table 1).

The OS status parameters change through the predefined study times according to implemented surgical technique (i.e., CPB or OPCAB) are presented in Figure 1.

TOS decreased in both study groups, compared to baseline values, but this decrease did not reach statistical significance. TOS values were higher in OPCAB compared to CPB group in several study points.

Superoxide anion showed significant increase in t3-t6 study times, in CPB, so as in OPCAB group, with comparable values in both study groups, and the highest values at t6 study point. Similar way of increase has also seen for PAB parameter. MDA significantly increased only in CPB group in t5 and t6 interval. MDA was significantly higher in CPB group compared to OPCAB in t6 study point.

CPB patients had significantly lower TAS compared to OPCAB patients at the beginning and also in t2 and t3 study points. In CPB, we noticed the initial decrease in TAS values, then sharp increase and decrease till the end of the study period. In OPCAB, we found initial increase

in TAS and from the t3 (24 h after the surgery end), significant decrease compared to baseline value. CPB patients had significantly lower SOD activities compared to OPCAB, baseline, and in several study points, when SOD increased in OPCAB patients.

CPB patients had higher IMA baseline than OPCAB group. Initially, IMA rose in CPB, in t2 point, and after that we could not report any significant change in this parameter till the study end.

Parameters in specific study times, which showed significant difference according to SS level (i.e., low, intermediate, and high SS subgroups) are presented at the Table 2.

It is clear that TAS level is significantly lower in patients with high SS level, baseline so as in the first two study times (till 24 h). Also, SOD decrease along with SS increase was obvious, so as TAS/TOS ratio, which is also representative of antioxidative potential. Unexpectedly, TOS was also lower in high SS group of patients. PAB was significantly higher in patients with high SS compared to low and moderate groups. OSI index (TOS/TAS ratio) was also higher in high SS group than in low and moderate groups.
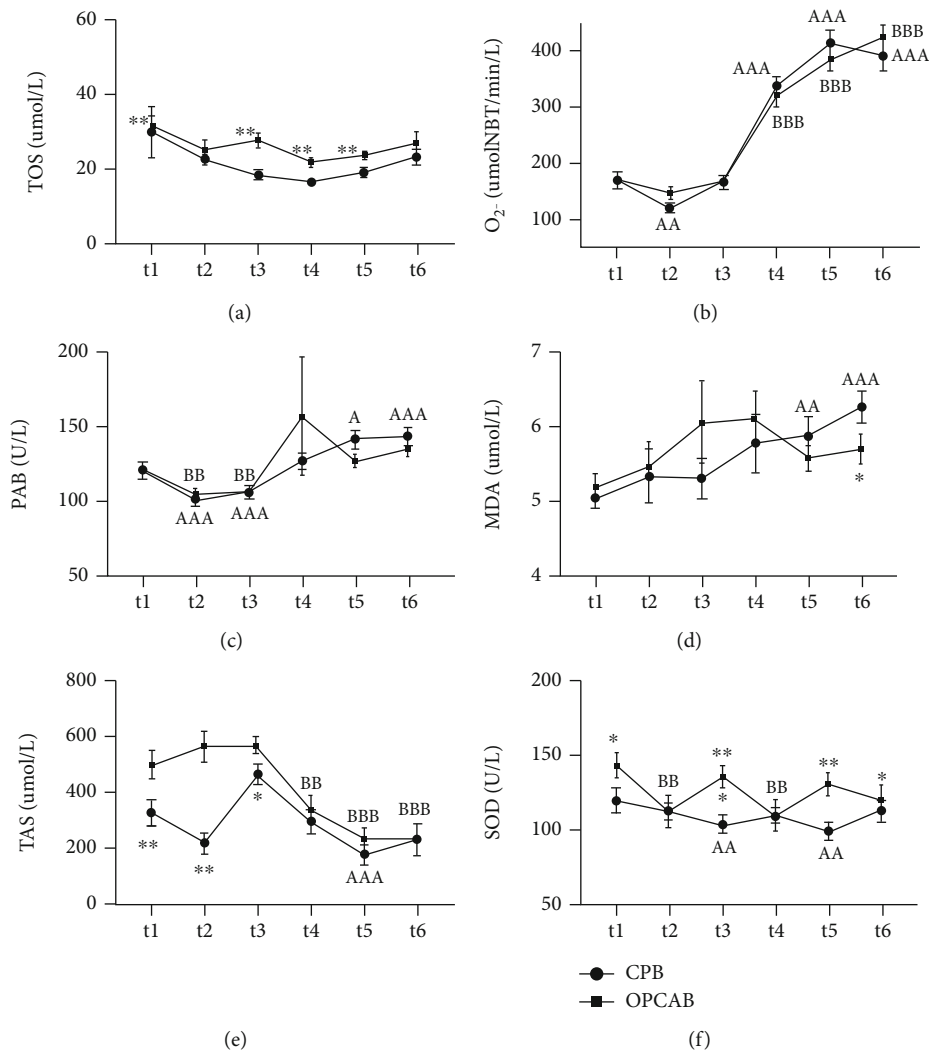
FIGURE 1: Dynamics of oxidative stress parameters' changes in CABG, precisely two surgery types, i.e., CPB and OPCAB before surgery and after the procedure in defined study points. (a) Total oxidative status (sTOS), (b) superoxide anion ($pO_2^{.-}$), (c) prooxidative-antioxidative balance (sPAB), (d) malondyaldehide (sMDA), (e) total antioxidative status (sTAS), and (f) superoxide-dismutase (pSOD). *, **, *** $P < 0.05$; 0.01; 0.001 OPCAB vs. the same time point in CPB group. [a, aa, aaa] $P < 0.05$; 0.01; 0.001 in CPB group (t2-t5) vs. baseline. [b, bb, bbb] $P < 0.05$; 0.01; 0.001 in OPCAB group (t2-t5) vs. baseline. s: serum; p: plasma.

TABLE 2: Oxidative stress status parameters according to SYNTAX Score tertile values in different study times depending on significant change through SS subgroups.

Parameter	Low SS < 22 (15.6 ± 4.8)	Moderate SS 22-32 (27.1 ± 3.2)	High SS > 32 (38.6 ± 6.1)	P
sTAS t1 (μmol/L)	497 (331-564)	393 (157-689)	247 (113-370)[aa]	<0.05
sTAS t2 (μmol/L)	476 (261-653)	238 (206-575)	166 (2.00-290)[aaa,bb]	<0.01
sTAS t3 (μmol/L)	568 (438-638)	617 (434-727)	357 (220-526)[aa,bb]	<0.01
sTOS t3 (μmol/L)	26.4 (20.5-32.7)	18.3 (15.6-22.9)[a]	15.1 (12.5-23.0)[aa,b]	<0.05
sTOS t4 (μmol/L)	20.8 (17.4-24.9)	17.7 (14.3-20.5)	16.7 (10.8-22.6)[a]	<0.05
pSOD t5 (U/L)	144 (120-156)	121 (60-135)[a]	111 (76-122)[aa]	<0.05
sPAB t5 (U/L)	125 (115-145)	118 (107-136)	145 (125-179)[a,b]	<0.05
TAS/TOS t2	20.3 (9.5-28.0)	14.0 (7.8-30.6)	7.3 (0.1-13.7)[aa,bb]	<0.05
OSI index t2	0.05 (0.04-0.11)	0.07 (0.03-0.13)	0.14 (0.07-7.87)[aa,bb]	<0.01

P: Kruskall-Wallis test, [a,aa,aaa] $P < 0.05$; 0.01; 0.001, respectively, vs. low SS group (<22 points), Mann-Whitney U test; [b,bb] $P < 0.05$; 0.01, respectively, vs. moderate SS (22-32 points), Mann-Whitney U test; s: serum; p: plasma.

Correlation analysis of OS status parameters and SS value showed that TAS and TOS parameters had significant negative correlation with SS level for the most study point times.

SOD also showed significant inverse correlation with SS level. PAB 48 h after the surgery showed positive correlation with SS level. Both results are expected having in mind OS parameters nature (Table 3).

Correlation in subgroups according to SS level showed the following: significant negative correlation between IMA and SS in Low SS group, positive TAS correlation in moderate SS group and negative correlation in high SS group, and positive MDA correlation with SS level in high SS group (Table 4).

ROC analysis was performed to find the most significant predictors of SS level (low vs. high SS subgroups). Using logistic regression analysis for integrated OS status parameter models generation, the best SS level predictors were SOD activity, IMA, and TAS level (Figure 2).

Logistic regression analysis showed that SOD and IMA had very good discriminatory capability (AUC = 0.840 and AUC = 0.813, respectively) [25].

Out of 107 CABG patients included in the current study, a total of 3 postoperative complications were noted in the OPCAB group, and 12 in the CPB group and the most prominent ones were leg wound infection, pleural effusion, pulmonary thromboembolism, and shallow sternal wound infection.

4. Discussion

To our knowledge, this is the first study that examined the broad spectrum of OS biomarkers in patients undergoing CABG in relation to different surgery modalities. Several important findings of the current study need to be acknowledged. According to the main aim of this project, we have followed OS status parameters (i.e., IMA, MDA, superoxide anion, PAB, TOS, TAS, and SOD) change through the predefined study times to obtain deeper knowledge into the redox homeostasis before and after CABG intervention. We have also analyzed the difference in OS generation caused by the two different surgical procedures, i.e., CPB or OPCAB and found that CPB patients were in more severe ischemia (as measured with IMA) baseline than OPCAB group. Furthermore, IMA rose in CPB patients immediately after the surgery end and after that no significant change in this parameter was observed.

Following the change of OS status parameters before and after the surgical intervention in CPB and OPCAB group, we have observed the decrease (but without statistical significance) in TOS in both study groups, compared to the levels before the operation. We have shown that TOS levels, as a measure of peroxide generation [23], were lower in CPB compared to OPCAB group in several study points. It seems that dynamics of this parameter change was not compatible with our study times. Precisely, peroxides generation is probably the fast process, and this kind of reactive species are subjected to rapid decomposition, during the surgical procedure, i.e., the times which we did not include in this study.

TABLE 3: Spearman's nonparametric correlation between SYNTAX Score value and OS status parameters.

OSS parameter	SYNTAX score
sTAS, μmol/L t1	-0.318*
sTAS, μmol/L t2	-0.417***
sTAS, μmol/L t3	-0.249*
sTAS, μmol/L t6	-0.259*
sTOS, μmol/L t1	-0.259*
sTOS, μmol/L t3	-0.418**
sTOS, μmol/L t4	-0.331**
sTOS, μmol/L t5	-0.298*
sTOS, μmol/L t6	-0.247*
pSOD, U/L t3	-0.310*
pSOD, U/L t5	-0.368**
sPAB, U/L t5	0.256*

Data were shown with (ρ)-Spearman's correlation coefficient. *,**$P < 0.05$, 0.01, respectively, are only for the significant correlation between SS and OS status parameters in different study times; s: serum; p: plasma.

TABLE 4: Spearman's nonparametric correlation in SYNTAX Score subgroups (SS < 22, SS 22-32, SS > 32).

Parameter, study time	Low SS < 22	Moderate SS (22-32)	High SS > 32
sIMA, ABSU t4	-0.460*	/	/
sIMA, ABSU t5	-0.455*	/	/
sTAS, μmol/L t3	/	0.474*	/
sTAS, μmol/L t4	/	/	-0.526*
sMDA, μmol/L t1	/	/	0.551*

Data were shown with (ρ)-Spearman's correlation coefficient. *$P < 0.05$ for the significant correlation between SS and OS status parameters in SS level subgroups. s: serum.

After the initial decrease, superoxide anion showed significant increase in other study times in both, OPCAB and CPB group, exhibiting the highest levels at the end of the observed period. Similar way of increase was also seen for PAB. MDA significantly increased only in CPB group towards the end of the observed period. MDA is a marker of late peroxidation phase [19], and we have shown that it was significantly higher in CPB group compared to OPCAB in 96th h after the surgery completion.

CPB patients had significantly lower TAS levels compared to OPCAB patients at the beginning and also 6 h after intervention. CPB patients had significantly lower SOD activities compared to OPCAB, baseline, and in several study points, when SOD increased in OPCAB patients. SOD dynamics was interesting and could be analyzed with the changes of other oxidative status factors, primarily with superoxide anion dynamics, which is a substrate for SOD enzymatic activity [20].

Luyten et al. [26] found an increase in SOD activity, which returned to the baseline values 24 h after the surgical
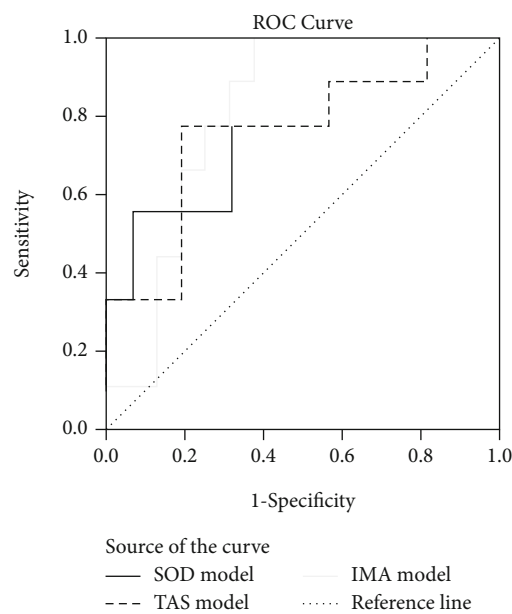
Figure 2: ROC analysis of different OSS parameters as SYNTAX Score value predictors. AUC (SE): area under the curve (standard error); 95th CI (confidence interval); P: significance. Logistic regression models of integrated parameters (t1-t6 study times) are presented.

Figure 3: Ischemia-modified albumin (sIMA) concentration in CABG subjects and according the two surgery types (CPB and OPCAB) before surgery (t1) and after the procedure (t2-t6). *, **, $P < 0.05$; 0.01 OPCAB vs. the same time point in CPB group; s: serum.

procedure. At the same time in the mentioned study, the authors reported huge increase of the total antioxidant capacity of 60%. In our current study, antioxidants (enzymatic and nonenzymatic) showed also initial increase and then decrease till the study end (96 h).

In our previous study, we have recorded higher levels of lipid hydroperoxides and advanced oxidation protein products in the CPB, as compared with OPCAB group during the postoperative period, showing that OS was higher in the CPB group which could be attributed to more harmful conditions of the CPB patients or their diminished ability to respond to the OS threat [10].

By measuring IMA, we aimed to follow up changes in ischemic condition in CAD patients. Initially, IMA has increased after the surgery in our group of patients, but earlier in CPB compared to OPCAB patients (Figure 3). Kanko et al. [13] also found significantly increased IMA values in a group of CPB patients. Taking into account that IMA is a marker of the early myocardial ischemia, we assumed that IMA measurement is worthwhile in cardiovascular bypass surgery settings. Thus, IMA measurement could contribute to the earlier treatment and better follow-up of the CABG patients. According to Bar-Or et al. [21], a value of 0.400 ABSU represents the cut-off point which delineates ischemic condition. It was obvious that our patients' values were far above 0.400 ABSU in the whole course of the observed period, suggesting that examined CAD patients were in chronic ischemia state, which was more pronounced in CPB compared to OPCAB patients. Ischemia may lead to increased production of reactive oxygen species and consequent modification of albumin. These processes result in an increased IMA formation, which was shown to be a reliable
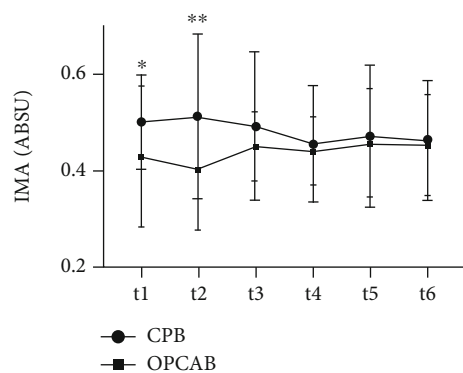
marker in detection of the early stages of ischemia, before the occurrence of necrosis [13].

In order to get better insight into the relationship between vessel wall lesion complexity and redox status, we have divided study patients at low, moderate, and high SS subgroups and compared OS status parameters in specific study times. Namely, it was previously shown that patients with SS above 22 (boundary between low and moderate atherosclerotic lesion) according to the results of Syntax score study [14] should be subjected exclusively to CABG surgery in order to avoid adverse cardiovascular events and need for revascularization. The several main characteristics of CPB procedure, such as aortic cross clamp time (ACC) and extracorporal circulation time (ECC), were significantly higher in patients with higher SS, which implies the more complicated artery lesion condition in patients subjected to this procedure. With SS increase, we have also found significant CSS increase, which suggests general worsening of patients' systemic condition as a consequence of advanced atherosclerosis (Table 1).

Additionally, we revealed that the antioxidative potential (i.e., TAS, SOD, and TAS/TOS ratio) was significantly lower, whereas parameters that show OS balance (i.e., PAB and OSI index) were significantly higher in patients with high SS compared to low and intermediate SS group. Unexpectedly, TOS was also lower in high SS group of patients, and this finding should be subjected to further analysis.

Thereafter, ROC analysis was performed to find the most significant predictors of SS level (low vs. high SS subgroups). Using logistic regression analysis for OS status parameter generation, the best SS level predictors were SOD activity, IMA, and TAS level. SOD and IMA showed very good discriminatory capability towards higher SS status.

Antioxidant capacity has previously been recorded as a predictive marker in determining postoperative complications [12].

The CPB technique is a main reason for ischemia-reperfusion which causes the release of superoxide anion, primarily by the xanthine oxidase (XO) system [27].

Products of purine bases (hypoxanthine and xanthine) accumulate in ischemic tissues, and XO was suggested to be a key source of reactive oxygen species (ROS) during ischemia/reperfusion. With the onset of ischemic state, the accumulation of hypoxanthine produced via the catabolism of ATP, and a consequent conversion of xanthine dehydrogenase (XDH) to XO occurs, which is the key source of ROS [28]. Along with the reperfusion process, it is assumed that oxygen and accumulated hypoxanthine react with XO leading to increased production of superoxide anion [27].

In addition, treatments with allopurinol and SOD were shown to be efficient in attenuating the response of vascular permeability induced by ischemia/reperfusion process, thus suggesting that XO-derived superoxide, a substrate for SOD enzymatic activity [20], was involved in the endothelial dysfunction [27].

Despite the fact that we have included a wide spectrum of parameters of redox homeostasis in this study, we should mention its several drawbacks. The limitation of the current study lies in the fact that it included a relatively small number of patients, and all measurements of oxidative stress parameters were performed once. However, this is the standard procedure for determination of oxidative stress parameters because all methods are validated, the calibration was performed, and the reliability of results and the quality control are maintained by measuring normal and abnormal control material before analyses.

We were also limited for determination of lipid metabolism parameters which may affect the results of the study [29, 30]. Moreover, we were not able to exclude type 2 diabetes, smoking, and medications other than immunosuppressive drugs and dietary supplements, which all might affect the results of the study. In addition, a control group of healthy subjects could have been useful to compare the baseline oxidative stress status parameters with the study group. Also, this is a single-center study. Therefore, new multicenter studies with larger sample size and with control group included would be of benefit to better evaluate the role of oxidative stress in the mentioned pathology and to validate our results.

5. Conclusion

The results of the current study revealed that patients with high SS exhibited pronounced redox imbalance reflected by increased prooxidant species, while reduced antioxidant elements compared to patients with low and intermediate SS. Additionally, two redox status opposite features, both with protein nature, i.e., one important enzymatic antioxidant (SOD) and the other product of oxidative stress burden (IMA), could predict CAD severity and complexity, determined as SS values. This study adds information about more severe ischemic condition of CPB patient baseline compared with OPCAB group, and also, we got insight into severe ischemia development in the CPB patients after the surgery. Importantly, this ischemia did not persist in subsequent study points, which is encouraging having in mind worse condition of these patients compared to OPCAB ones.

Taking all these into account, further investigation of redox status parameters would be of great importance in different cardiac surgery modalities which might enable to reduce the deleterious effects of these procedures, by inclusion of some preoperative and/or postoperative antioxidants as supportive therapy.

Data Availability

The data will be available upon reasonable request (contact person: aleksandranklisic@gmail.com).

Conflicts of Interest

All authors declare no conflicts of interest.

Acknowledgments

References

[1] A. C. Hatemi, K. Çeviker, A. Tongut, İ. Özgöl, M. Mert, and A. Kaya, "Oxidant status following cardiac surgery with phosphorylcholine-coated extracorporeal circulation systems," *Oxidative Medicine and Cellular Longevity*, vol. 2016, Article ID 3932092, 10 pages, 2016.

[2] M. Zakkar, G. Guida, M. S. Suleiman, and G. D. Angelini, "Cardiopulmonary bypass and oxidative stress," *Oxidative Medicine and Cellular Longevity*, vol. 2015, Article ID 189863, 8 pages, 2015.

[3] S. G. Raja and G. A. Berg, "Impact of off-pump coronary artery bypass surgery on systemic inflammation: current best available evidence," *Journal of Cardiac Surgery*, vol. 22, no. 5, pp. 445–455, 2007.

[4] J. C. Cleveland Jr., A. L. Shroyer, A. Y. Chen, E. Peterson, and F. L. Grover, "Off-pump coronary artery bypass grafting decreases risk-adjusted mortality and morbidity," *The Annals of Thoracic Surgery*, vol. 72, no. 4, pp. 1282–1289, 2001.

[5] P. Menasché, "The systemic factor: the comparative roles of cardiopulmonary bypass and off- pump surgery in the genesis of patient injury during and following cardiac surgery," *The Annals of Thoracic Surgery*, vol. 72, no. 6, pp. S2260–S2265, 2001.

[6] A. Marui, H. Okabayashi, T. Komiya et al., "Benefits of off-pump coronary artery bypass grafting in high-risk patients," *Circulation*, vol. 126, 11_supplement_1, pp. S151–S157, 2012.

[7] Z. S. Meharwal, Y. K. Mishra, V. Kohli, R. Bapna, S. Singh, and N. Trehan, "Off-pump multivessel coronary artery surgery in high-risk patients," *The Annals of Thoracic Surgery*, vol. 74, no. 4, pp. 1353–1357, 2002.

[8] M. Kowalewski, M. Jasiński, J. Staromłyński et al., "On-pump vs. off-pump coronary artery bypass surgery in atrial fibrillation. Analysis from the polish national registry of cardiac surgery procedures (KROK)," *PLoS ONE*, vol. 15, no. 4, p. e0231950, 2020.

[9] A. R. Lamy, P. J. Devereaux, and S. Yusuf, "Five-year outcomes after off-pump or on-pump coronary-artery bypass grafting," *The New England Journal of Medicine*, vol. 376, no. 9, pp. 894-895, 2017.

[10] P. Vukicevic, A. Klisic, J. Kotur-Stevuljevic et al., "Paraoxonase 1 low activity and SYNTAX score may predict postoperative complications after coronary artery surgery," *European Review for Medical and Pharmacological Sciences*, vol. 25, pp. 1511–1521, 2021.

[11] M. Thielmann, S. Pasa, T. Holst et al., "Heart-Type Fatty Acid Binding Protein and Ischemia-Modified Albumin for Detection of Myocardial Infarction After Coronary Artery Bypass Graft Surgery," *The Annals of Thoracic Surgery*, vol. 104, no. 1, pp. 130–137, 2017.

[12] S. Vogt, A. Sattler, A. S. Sirat et al., "Different Profile of Antioxidative Capacity Results in Pulmonary Dysfunction and Amplified Inflammatory Response After CABG Surgery," *The Journal of Surgical Research*, vol. 139, no. 1, pp. 136–142, 2007.

[13] M. Kanko, S. Yavuz, C. Duman, T. Hosten, E. Oner, and T. Berki, "Ischemia-modified albumin use as a prognostic factor in coronary bypass surgery," *Journal of Cardiothoracic Surgery*, vol. 7, no. 1, 2012.

[14] P. W. Serruys, Y. Onuma, S. Garg et al., "Assessment of the SYNTAX score in the Syntax study," *EuroIntervention*, vol. 5, no. 1, pp. 50–56, 2009.

[15] S. Garg, G. Sarno, H. M. Garcia-Garcia et al., "A new tool for the risk stratification of patients with complex coronary artery Disease," *Circulation. Cardiovascular Interventions*, vol. 3, no. 4, pp. 317–326, 2010.

[16] S. A. Nashef, F. Roques, L. D. Sharples et al., "EuroSCORE II," *European Journal of Cardio-Thoracic Surgery*, vol. 41, no. 4, pp. 734–745, 2012.

[17] C. Auclar and E. Voisin, "Nitroblue tetrazolium reduction," in *CRC Handbook of Methods for Oxygen Radical Research*, R. A. Greenworld, Ed., pp. 123–132, CRC Press, Boca Raton, Fla, 1985.

[18] D. H. Alamdari, K. Paletas, T. Pegiou, M. Sarigianni, C. Befani, and G. Koliakos, "A novel assay for the evaluation of the prooxidant-antioxidant balance, before and after antioxidant vitamin administration in type II diabetes patients," *Clinical Biochemistry*, vol. 40, no. 3-4, pp. 248–254, 2007.

[19] M. J. Girotti, N. Khan, and B. A. Mc Lellan, "Early Measurement of Systemic Lipid Peroxidation Products in the Plasma of Major Blunt Trauma Patients," *The Journal of Trauma: Injury, Infection, and Critical Care*, vol. 31, no. 1, pp. 32–35, 1991.

[20] H. P. Misra and I. Fridovich, "The Role of Superoxide Anion in the Autoxidation of Epinephrine and a Simple Assay for Superoxide Dismutase," *The Journal of Biological Chemistry*, vol. 247, no. 10, pp. 3170–3175, 1972.

[21] D. Bar–Or, E. Lau, and J. V. Winkler, "A novel assay for cobalt-albumin binding and its potential as a marker for myocardial ischemia–a preliminary report[1]," *The Journal of Emergency Medicine*, vol. 19, no. 4, pp. 311–315, 2000.

[22] O. Erel, "A novel automated direct measurement method for total antioxidant capacity using a new generation, more stable ABTS radical cation," *Clinical Biochemistry*, vol. 37, no. 4, pp. 277–285, 2004.

[23] O. Erel, "A new automated colorimetric method for measuring total oxidant status," *Clinical Biochemistry*, vol. 38, no. 12, pp. 1103–1111, 2005.

[24] A. Klisic, N. Kavaric, S. Vujcic, V. Spasojevic-Kalimanovska, J. Kotur-Stevuljevic, and A. Ninic, "Total oxidant status and oxidative stress index as indicators of increased Reynolds Risk Score in postmenopausal women," *European Review for Medical and Pharmacological Sciences*, vol. 24, no. 19, pp. 10126–10133, 2020.

[25] A. M. Šimundić, "Measures of diagnostic accuracy: basic definitions," *EJIFCC.*, vol. 19, no. 4, pp. 203–211, 2009.

[26] C. R. Luyten, F. J. van Overveld, L. A. De Backer et al., "Antioxidant defence during cardiopulmonary bypass surgery," *European Journal of Cardio-Thoracic Surgery*, vol. 27, no. 4, pp. 611–616, 2005.

[27] D. N. Granger and P. R. Kvietys, "Reperfusion injury and reactive oxygen species: the evolution of a concept," *Redox Biology*, vol. 6, pp. 524–551, 2015.

[28] A. Klisic, G. Kocic, N. Kavaric, M. Jovanovic, V. Stanisic, and A. Ninic, "Body mass index is independently associated with xanthine oxidase activity in overweight/obese population," *Eating and Weight Disorders - Studies on Anorexia, Bulimia and Obesity*, vol. 25, no. 1, pp. 9–15, 2020.

[29] A. Klisic, N. Kavaric, S. Vujcic, V. Spasojevic-Kalimanovska, J. Kotur-Stevuljevic, and A. Ninic, "Factorial analysis of the cardiometabolic risk influence on redox status components in adult population," *Oxidative Medicine and Cellular Longevity*, vol. 2021, Article ID 6661940, 9 pages, 2021.

[30] A. Klisic, N. Kavaric, V. Stanisic et al., "Endocan and a novel score for dyslipidemia, oxidative stress and inflammation (DOI score) are independently correlated with glycated hemoglobin (HbA1c) in patients with prediabetes and type 2 diabetes," *Archives of Medical Science*, vol. 16, no. 1, pp. 42–50, 2020.

Research Article

Inhibition of Fatty Acid Metabolism Increases EPA and DHA Levels and Protects against Myocardial Ischaemia-Reperfusion Injury in Zucker Rats

Janis Kuka [iD],[1] **Marina Makrecka-Kuka,**[1] **Karlis Vilks,**[1,2] **Stanislava Korzh,**[1] **Helena Cirule,**[1] **Eduards Sevostjanovs,**[1] **Solveiga Grinberga** [iD],[1] **Maija Dambrova** [iD],[1,3] **and Edgars Liepinsh**[1]

[1]*Latvian Institute of Organic Synthesis, Laboratory of Pharmaceutical Pharmacology, Riga, Latvia*
[2]*University of Latvia, Faculty of Biology, Riga, Latvia*
[3]*Riga Stradins University, Faculty of Pharmacy, Riga, Latvia*

Correspondence should be addressed to Janis Kuka; janis.kuka@farm.osi.lv

Long-chain ω-3 polyunsaturated fatty acids (PUFAs) are known to induce cardiometabolic benefits, but the metabolic pathways of their biosynthesis ensuring sufficient bioavailability require further investigation. Here, we show that a pharmacological decrease in overall fatty acid utilization promotes an increase in the levels of PUFAs and attenuates cardiometabolic disturbances in a Zucker rat metabolic syndrome model. Metabolome analysis showed that inhibition of fatty acid utilization by methyl-GBB increased the concentration of PUFAs but not the total fatty acid levels in plasma. Insulin sensitivity was improved, and the plasma insulin concentration was decreased. Overall, pharmacological modulation of fatty acid handling preserved cardiac glucose and pyruvate oxidation, protected mitochondrial functionality by decreasing long-chain acylcarnitine levels, and decreased myocardial infarct size twofold. Our work shows that partial pharmacological inhibition of fatty acid oxidation is a novel approach to selectively increase the levels of PUFAs and modulate lipid handling to prevent cardiometabolic disturbances.

1. Introduction

The combination of interrelated metabolic risk factors such as obesity, dysglycaemia, dyslipidaemia, and insulin resistance creates the basis of metabolic syndrome [1, 2] and promotes the development of cardiovascular diseases and type 2 diabetes mellitus. Metabolic syndrome, when compared to obesity, is related to a higher incidence of major coronary events, including fatal and nonfatal myocardial infarctions [3] and is also associated with increased 20-year mortality in patients [4]. While obesity can be effectively treated by lifestyle and dietary adjustments [5] and/or bariatric surgery [6], a much broader strategy including drug therapy is required to tackle metabolic syndrome [2]. To ensure better translation of novel cardiometabolic therapies to the clinical setting, multiple cardiovascular risk factors and comorbidities should be taken into account when evaluating compounds in a preclinical setting [7–9].

Multiple studies have found an association between the consumption of fish containing omega-3 polyunsaturated fatty acids (PUFAs) and improved cardiovascular outcomes [10]. In contrast, a recent meta-analysis of 23 randomized, double-blind, placebo-controlled trials in cardiovascular patients did not show a protective effect of an additional intake of eicosapentaenoic acid (EPA) and docosahexaenoic acid (DHA) on total mortality and cardiovascular mortality, particularly in the presence of statins [11]. Of interest for the treatment of complications of metabolic syndrome could be finding in a rat model that treatment with ω-3 PUFAs decreases the severity of postresuscitation myocardial dysfunction, lipid peroxidation, and systemic inflammation in the early phase of recovery following cardiac arrest [12]. Likewise, transgenic fat-1 mice with constantly elevated levels of endogenous ω-3 PUFAs have preserved cardiac contractile function and less inflammation and oxidative stress when challenged with LPS than wild type animals [13]. In

insulin-resistant states, an increased reliance of cardiomyocytes on the oxidation of free fatty acids is present and associated with both a lower yield of ATP per oxygen molecule and likely decreased energetic efficiency [14]. It should be noted that complete oxidation of PUFAs is more than 2 times faster than the oxidation of saturated fatty acids [15]. Thus, one can assume that dietary PUFAs are less likely to accumulate to reach the levels/ratios required to induce beneficial effects. In turn, as PUFAs are the preferred substrate [16] for mitochondrial fatty acid metabolism, inhibition of overall fatty acid oxidation could lead to a comparably higher increase in the levels of PUFAs but not saturated fatty acids. Interestingly, plasma lipid parameters are normalized, and the levels of several short- to medium-chain acylcarnitines are significantly decreased by up to 30% after treatment with PUFAs [17]. Altogether, we hypothesized that long-term pharmacological inhibition of carnitine palmitoyltransferase I- (CPT I-) dependent mitochondrial fatty acid metabolism increases the levels of PUFAs and could induce anti-infarction activity in a Zucker rat metabolic syndrome model.

The aim of the present study was to test whether treatment with the carnitine/acylcarnitine-lowering compound methyl-GBB (4-[ethyl(dimethyl)ammonio]butanoate) can decrease overall fatty acid oxidation, thus increasing PUFA availability; and could these alterations in lipid metabolism reduce ischaemia-reperfusion (I/R)-induced cardiac damage in Zucker rats with metabolic syndrome? Zucker rats were used as a representative preclinical model of continuous nutritional overload, physical inactivity, and abdominal obesity, which over time lead to the development of metabolic syndrome [18, 19].

2. Materials and Methods

2.1. Animals and Treatment. Zucker fa/fa male rats ($n = 36$) and age-matched (5-7-week-old, ~140 g at the time of purchase) Zucker lean male rats ($n = 18$) were obtained from Charles River, and 18 C57BL/6JOlaHsd inbred mice (4-6 weeks old, ~18 g at the time of purchase) were obtained from Envigo. Animals were housed for one week prior to treatment under standard conditions (21-23°C, 12-h light/dark cycle, relative humidity 45-65%) with unlimited access to food R70 diet from Lantmännen and water. The experimental procedures were performed in accordance with the guidelines of the European Community and local laws and policies (Directive 2010/63/EU), and all of the procedures were approved by the Food and Veterinary Service, Riga, Latvia. All experiments were performed in a blinded manner. Studies involving animals are reported in accordance with the ARRIVE guidelines [20, 21].

By limiting the availability of long-chain acylcarnitines (LCAC), methyl-GBB (5–20 mg/kg) significantly decreases infarct size (IS) ex vivo by approximately 50% in normoglycaemic animals [22, 23]. In the present study, a dose of 10 mg/kg was chosen based on previous data regarding methyl-GBB cardiac tissue levels, the effects on carnitine/acylcarnitine levels, cardioprotection in normoglycaemic animals, and data from models with impaired energy metabolism. Although ex vivo methyl-GBB, even at a dose of 5 mg/kg, induces a maximal decrease in IS [23], in previous studies using high-fat diet-fed ApoE$^{-/-}$ knockout mice, methyl-GBB at a dose of 10 mg/kg was required to significantly decrease atherosclerotic lesions and dyslipidaemia [24], two major factors contributing to metabolic syndrome.

Data from previous experiments where I/R damage was determined in methyl-GBB-treated animals were subjected to statistical power analysis, and calculations indicated that $n = 10$ for the infarction study would produce significant results with power > 0.9. Animals were randomly separated into two experimental groups and given daily oral doses of water (Zucker fa/fa control group, $n = 10$) or 10 mg/kg methyl-GBB (Zucker fa/fa methyl-GBB group, $n = 10$) for 12 weeks (18 weeks old at the time of infarction study). Zucker lean rats ($n = 10$) were used as a nonhyperlipidaemic control. To assess mitochondrial levels of acylcarnitines, changes in glucose utilization, molecular pathway upregulation, and mitochondrial functionality, additional experiments were performed in animals treated as described above. Animals were separated randomly into two experimental groups and given daily oral doses of water (Zucker fa/fa control group, $n = 8$) or 10 mg/kg methyl-GBB (Zucker fa/fa methyl-GBB group, $n = 8$). Zucker lean rats ($n = 8$) were used as a nonhyperlipidaemic control. Additional experiments to determine plasma EPA, DHA, and free fatty acid (FFA) concentrations were performed in normoglycaemic C57BL/6 mice. Mice were separated randomly into two experimental groups and given daily oral doses of water (mouse control group, $n = 9$) or 5 mg/kg methyl-GBB (mouse methyl-GBB group, $n = 9$) for 4 weeks. For all experiments, nonfasting or postovernight-fasting blood samples were collected from tail veins; samples were centrifuged, and the plasma was stored at -80°C for future analysis.

2.2. Isolated Rat Heart Infarction Study. The infarction was performed according to the Langendorff technique as described previously [25, 26], with some modifications. Animals were anaesthetized with sodium pentobarbital (70 mg/kg), and after the loss of nociceptive reflexes, hearts were immediately excised, thus, sacrificing animals. Hearts were retrogradely perfused with Krebs-Henseleit (KH) buffer solution supplemented with 10 mM glucose (Fresenius Kabi), 0.3 mM sodium palmitate (TCI Europe) bound to 0.5% bovine serum albumin (BSA) (Europa Bioproducts Ltd.), 2 mM lactate (Fischer Scientific), 0.2 mM pyruvate (Acros Organics), and 3 ng/ml insulin aspart (Novo Nordisk) at a constant perfusion pressure of 70 mmHg. After an adaptation period of 20 min, the left anterior descending coronary artery (LAD) was subsequently occluded for 30 min followed by 120 min of reperfusion. IS was determined as described previously [26]. Heart functional parameters, coronary flow, left ventricle developed pressure (LVDP), heart rate, and cardiac workload were registered using the PowerLab system from ADInstruments. Briefly, at the end of reperfusion, the LAD was reoccluded, and the heart was perfused with 0.1% methylene blue dissolved in KH buffer solution to delineate

risk and no-risk areas. Afterwards, the ventricles of the heart were transversely cut into 2 mm thick slices and photographed. Computerized planimetric analysis of the stained left-ventricle slice photographs was performed using Image-Pro Plus v6.3 software to determine the area at risk (AR) and the area of necrosis (AN), and each area was expressed as a percentage of the slice area. The obtained values were then used to calculate the IS as a percentage of the risk area, based on the formula IS = AN/AR × 100%.

2.3. Determination of Glucose Oxidation in Isolated Hearts.

The rate of radiolabelled glucose oxidation was measured in additional sets of rat hearts according to a method previously described [22, 23] with the following modifications. Glucose oxidation measurement was performed according to the Langendorff perfusion technique. The hearts were perfused retrogradely (constant perfusion pressure, 70 mmHg) with KH buffer solution supplemented with 10 mM glucose, 0.3 mM sodium palmitate bound to 0.5% bovine serum albumin (BSA), 2 mM lactate, 0.2 mM pyruvate, and 3 ng/ml insulin. After a 10 min adaptation time, the perfusate was switched to the oxygenated radiolabelled KH buffer solution, and perfusion was continued for 10 min at a constant pressure. The glucose oxidation rate was determined by measuring the $^{14}CO_2$ released from the metabolism of [U-^{14}C]glucose (specific activity, 300 mCi/mmol).

2.4. Mitochondrial Energy Metabolism.

The mitochondrial energy metabolism was determined in the permeabilized cardiac fibres prepared as described previously [25, 27] with some modifications. The bundles of fibres were permeabilized using 50 μg/ml saponin (Acros Organics) and 0.5 mg/ml collagenase (Sigma-Aldrich) at 4°C in 1 ml of buffer A (20 mM imidazole, 20 mM taurine (all Acros Organics), 0.5 mM dithiothreitol (Tocris Bioscience), 7.1 mM $MgCl_2$ (Penta Chemicals), 50 mM MES, 5 mM ATP, 15 mM phosphocreatine, 2.6 mM CaK_2EGTA, and 7.4 mM K_2EGTA (all Sigma-Aldrich), pH 7.0 at 0°C). After a 15 min incubation, the fibres were washed for 15 min in 2 ml of buffer B (20 mM imidazole, 0.5 mM dithiothreitol, 20 mM taurine, 1.6 mM $MgCl_2$, 100 mM MES, 3 mM KH_2PO_4 (Enola Ltd.), 2.9 mM CaK_2EGTA, 7 mM K_2EGTA, pH 7.1 at 37°C).

High-resolution fluorespirometry was performed using Oxygraph-2 k (O2k; OROBOROS INSTRUMENTS). All experiments were performed at 37°C in MiR05 medium (110 mM sucrose (Enola Ltd.), 60 mM K-lactobionate (Sigma-Aldrich), 0.5 mM EGTA (Sigma-Aldrich), 3 mM $MgCl_2$, 20 mM taurine, 10 mM KH_2PO_4, 20 mM HEPES (Acros Organics), pH 7.1 at 30°C, and 0.1% essential fatty acid free BSA). The medium was reoxygenated when the oxygen concentration dropped to 80 μM. Palmitoyl-CoA (10 μM) (Larodan AB), carnitine (500 μM for Zucker lean rats and Zucker fa/fa control rats and 20 μM for methyl-GBB-treated rats), and malate (0.5 mM) (Acros Organics) were used to measure CPT I-linked fatty acid oxidation (FAO) dependent on the LEAK state. ADP (Sigma-Aldrich) was added to a concentration of 5 mM to determine oxidative phosphorylation-dependent respiration (OXPHOS state).

The FA oxidation-dependent OXPHOS coupling efficiency was calculated as follows:

$$1 - \frac{\text{Resp.rate LEAK state}}{\text{Resp.rate OXPHOS state}}. \tag{1}$$

Then, pyruvate (5 mM) was added to determine the pyruvate and FA metabolism interaction. The pyruvate-dependent flux control factor was calculated as

$$1 - \frac{\text{Resp.rate before the addition of pyruvate (PCoA OXPHOS)}}{\text{Resp.rate after the addition of pyruvate (PCoA + pyruvate OXPHOS)}}. \tag{2}$$

2.5. Determination of Reactive Oxygen Species (ROS) Production.

H_2O_2 flux (ROS flux) in cardiac fibres was measured simultaneously with respirometry using an O2k-Fluorometer and the H_2O_2-sensitive probe Ampliflu™ Red (AmR) (Sigma-Aldrich) as described previously [27, 28] with some modifications. First, 10 μM AmR, 1 U/ml horseradish peroxidase (HRP), and 5 U/ml superoxide dismutase (SOD) (all Sigma-Aldrich) were added to the chamber, and H_2O_2 detection was performed based on the conversion of AmR to fluorescent resorufin. Calibrations were performed by adding 0.1 μM H_2O_2 stepwise. The H_2O_2 flux was corrected to take into account the background (AmR slope before sample addition). The respiration protocol was similar to that described above, with the exception that after the assessment of FAO and pyruvate-linked respiration, succinate (10 mM, complex II (CII) substrate) (Sigma-Aldrich) was then added to reconstitute convergent FAO-CI-II-linked respiration. Then, an inhibitor of adenine nucleotide translocator, carboxyatractyloside (Catr) (Sigma-Aldrich), was added to determine the LEAK$_{Catr}$ respiration. Titration with an uncoupler, carbonyl cyanide m-chlorophenyl hydrazine (0.5 μM steps to maximum oxygen consumption) (Sigma-Aldrich), was performed to determine the H_2O_2 production rate at the electron transfer system capacity state.

2.6. mRNA Isolation and qPCR Analysis.

Total RNA from the heart tissues was isolated using TRI reagent (Sigma-Aldrich), and first-strand cDNA synthesis was carried out using a High Capacity cDNA Reverse Transcription Kit (Applied Biosystems™) following the manufacturer's instructions. qPCR analysis of gene expression was performed by mixing SYBR® Green Master Mix (Applied Biosystems™) with synthesized cDNA and forward and reverse primers specific for carnitine palmitoyltransferase IA (CPT IA) and IB (CPT IB), long-chain fatty acid CoA synthetase (ACSL), pyruvate dehydrogenase lipoamide kinase isozyme 4 (PDK4), acyl-CoA oxidase 1 (ACOX), and valosin-containing protein (VCP) and running the reactions on a Bio-Molecular Systems MIC qPCR Cycler according to manufacturer's protocol using following conditions: 95°C for 10 minutes, (95°C for 15 seconds, 60°C for 60 seconds) (60 cycles), 95°C for 60 seconds, followed by melt curve analysis 72-95°C, 0.3°C/sec to ensure amplicon specificity. The relative expression levels for each gene were calculated with the $\Delta\Delta C_t$ method and normalized

to the expression of VCP. The primer sequences used for the qPCR analysis are available upon request.

2.7. Western Blot Analysis of Tissue Lysates. Heart muscle tissues were homogenized with an Omni Bead Ruptor 24 homogenizer (Omni International) at a ratio of $1:10$ (w/v) at 4°C in a buffer containing 100 mM Tris-HCl (Acros Organics), pH 7.4, 10 mM EDTA (Sigma-Aldrich), 5 mM $MgCl_2$, 1 mM glycerol 3-phosphate, 1 mM NaF (all from Fluka), 500 μM Na_3VO_4 (Sigma-Aldrich), 1 mM DTT (Tocris Bioscience), phosphatase inhibitor cocktail I 1:100 (Alfa Aesar), protease inhibitors (10 μM leupeptin, 1 μM pepstatin (both from Tocris Bioscience), 1 μM aprotinin, and 100 μM AEBSF (both from Sigma-Aldrich)). Total protein was detected using the Lowry method. SDS-PAGE and Western blotting were performed as described previously with some modifications [29]. Briefly, 20 μg of total protein was loaded into Bolt™ 4-12% Bis-Tris Plus Gels (Thermo Scientific). After transfer, the polyvinylidene fluoride membranes (Thermo Scientific) were blocked with 5% BSA (Sigma-Aldrich) in Tris-buffered saline (TBS) for 1 h at room temperature and then incubated overnight at 4°C with primary antibodies. After washing with TBS, the blots were incubated for 1 h at room temperature with secondary peroxidase-coupled goat anti-rabbit IgG (lot: 26, #7074 Cell Signaling Technology) and then washed again with TBS. The blots were developed using chemiluminescence reagents (Millipore) and an Azure c400 Imaging System. The Western blot images were analysed using AzureSpot2.0 software. The phosphorylation levels of Akt at Ser473 on the membranes were detected with a phospho-Akt Ser473 (lot: 23, #4060 Cell Signaling Technology) antibody, and the obtained data were normalized to the total Akt level (lot: 20, #4691 Cell Signaling Technology).

2.8. Determination of Biochemical Measures. The plasma insulin concentrations were determined using a Sensitive Rat Insulin RIA Kit. Blood glucose was measured using a MediSense Optium glucometer from Abbott Diabetes Care. The concentration of FFAs was determined using a kit from Wako in plasma, and lactate was determined using a kit from Roche Diagnostics. Triglycerides, total cholesterol, aspartate aminotransferase (ASAT), and alanine aminotransferase (ALAT) in plasma were determined using kits from Instrumentation Laboratory. HOMA-IR was calculated according to the formula

$$\frac{\text{fasting insulin} \, (\mu U/L) \, x \, \text{fasting glucose}}{22.5}. \tag{3}$$

2.9. Measurement of Carnitine, Methyl-GBB, Acylcarnitines, and Poly-Unsaturated Fatty Acids by UPLC/MS/MS and Metabolomics. The determination of carnitine and methyl-GBB in heart tissues and plasma samples was performed by ultraperformance liquid chromatography-tandem mass spectrometry (UPLC/MS/MS) using the positive ion electrospray mode [23]. Mitochondria samples were prepared as previously described [30], and acylcarnitines were analysed by the UPLC MS/MS method [29]. PUFAs were measured

as follows: 200 μl of acetonitrile–methanol mixture (3 : 1, v/v) were added to 40 μl of plasma samples or calibration sample solution. The samples were thoroughly mixed and centrifuged for 10 min at 10000 rpm, and the supernatants were subjected to UPLC/MS/MS analysis. The analysis was performed on Acquity UPLC system coupled with Xevo TQ-S microtriple-quadrupole mass spectrometer (Waters Corp.). The separation of analytes was carried out on an Acquity UPLC BEH C18 column (2.1×50 mm, 1.7 μm, Waters Corp.) operated at 30°C under a gradient elution from 40 to 98% acetonitrile in 0.1% FA. Flow rate was 0.4 ml/min, and injection volume was 1 μl. The mass spectrometer was operated using an electrospray ionization source in negative ion mode. The multiple reaction monitoring (MRM) mode was employed for quantitative determination of target compounds. The main ionization settings were optimized as follows: capillary voltage of 2.0 kV; source and desolvation temperatures of 140 and 600°C, respectively; desolvation gas (nitrogen) flow of 800 L/h. Cone voltage (V) and collision energy (eV) values were specified for each compound: 20 and 15 for EPA; 20 and 12 for DHA, respectively. Quantitative analysis was performed under MRM mode by calculating the peak areas. Precursor to product ion transitions m/z $301.29 \rightarrow 203.31$ and $301.29 \rightarrow 257.45$ for EPA and m/z $327.30 \rightarrow 229.35$ and $327.30 \rightarrow 283.35$ for DHA were monitored. Data acquisition and processing were performed using the MassLynx V4.1 and QuanLynx V4.1 software (Waters Corp.). The samples were kept at 10°C in the autosampler. The calibrators were run in triplicate and the samples in duplicate. Concentrations of EPA, DHA, and FFAs (C12-C20) were measured in mice plasma samples by Biocrates Life Sciences AG (Innsbruck, Austria) as a part of their metabolomics analysis service by using Biocrates MxP Quant 500 Kit.

2.10. Statistical Analysis. The data are presented as the mean ± S.E.M. (standard error of the mean). Based on a normality test (D'Agostino & Pearson omnibus normality test (Shapiro-Wilk normality test if $N = 7$ or lower)) of the data, statistically significant differences in the mean values were evaluated using one-way ANOVA or the Kruskal-Wallis test. If ANOVA indicated $P < 0.05$, Tukey's test was performed, and the differences were considered significant when $P < 0.05$. If the Kruskal-Wallis test indicated $P < 0.05$, Dunn's multiple comparison test was performed, and the differences were considered significant when $P < 0.05$. The data were analysed using GraphPad Prism statistical software (GraphPad Inc., USA). For IS determination, 1 heart could not be analysed in the methyl-GBB-treated rat group, and 3 hearts could not be analysed in the Zucker lean rat group due to isolated heart perfusion system tubing failure. To determine functional heart parameters, LCAC levels, and metabolic patterns, an additional experiment was performed; 1 sample could not be analysed in the Zucker fa/fa rat control group, as the animal died suddenly of natural causes, and the data represent the mean values of $N = 7$ for this group. The data and statistical analyses comply with the recommendations for experimental design and analysis in pharmacology [31].

2.11. Materials. Methyl-GBB (a phosphate salt) was obtained from JSC Grindeks (Riga, Latvia). An insulin RIA kit was purchased from Millipore (USA) and [U-^{14}C]glucose was purchased from Biotrend Chemikalien GmbH (Germany).

3. Results

3.1. Plasma Concentrations of EPA, DHA, and Lipid Species. First, data on EPA and DHA plasma concentrations were obtained from normoglycaemic mice treated with methyl-GBB for 4 weeks at a dose of 5 mg/kg. EPA and DHA plasma concentrations in methyl-GBB-treated mice were significantly increased 3.4- and 1.9-fold in plasma from fasted mice, respectively, and 2.5- and 2.3-fold in plasma from fed mice, respectively (Supplementary Figure 1). Moreover, the concentration of FFAs (sum of C12-C20) was 1.3-fold increased only in fasted mouse plasma after treatment with methyl-GBB (Supplementary Figure 2). Next, in Zucker rats, plasma concentrations of EPA and DHA were measured after 12 weeks of treatment with methyl-GBB at a dose of 10 mg/kg. No significant difference was observed between EPA levels in the Zucker lean and Zucker fa/fa rat control groups, although there was a tendency for higher EPA concentrations in the Zucker fa/fa control group. Methyl-GBB treatment resulted in a significant 6.3- and 2.3-fold increase in the plasma EPA concentration compared to the Zucker lean rat and Zucker fa/fa rat control groups (Figure 1(a)). DHA levels were similar in the Zucker lean and Zucker fa/fa control groups. Treatment with methyl-GBB increased the DHA concentration 2.1-fold, but the effect was not statistically significant (Figure 1(b)). The carnitine levels in the Zucker lean and Zucker fa/fa rat hearts were similar, while in the methyl-GBB-treated rat hearts, the carnitine level was significantly decreased by 95% (Figure 1(c)). The LCAC content was determined in isolated cardiac mitochondria. Interestingly, the LCAC content in isolated cardiac mitochondria after I/R was 52% lower in the Zucker fa/fa control rat group than in the Zucker lean rat group; however, this effect was not statistically significant. Treatment with methyl-GBB significantly decreased the heart mitochondrial content of LCAC 25-fold compared to the Zucker fa/fa control group (Figure 1(d)).

In the fed state, the concentration of FFAs in plasma was significantly higher in the Zucker fa/fa control and methyl-GBB-treated Zucker fa/fa rats than in the Zucker lean rats (Figure 1(e)). Similarly, the concentrations of triglycerides and total cholesterol in plasma were significantly higher in the fed Zucker fa/fa control and methyl-GBB-treated Zucker fa/fa rats than in the Zucker lean rats (Table 1). Methyl-GBB treatment had no significant effect on the ASAT and ALAT levels when compared to the Zucker fa/fa rat control group. While methyl-GBB treatment significantly increased the PUFA content by up to 2.3-fold (Figures 1(a) and 1(b)), only a nonsignificant tendency to increase the total FFA concentration by 30% in the methyl-GBB-treated group was observed when compared to the Zucker fa/fa control group (Figure 1(e)). Zucker fa/fa rats gained significantly more weight than Zucker lean rats, and methyl-GBB had no effect on weight gain or on the organ-to-body weight ratio. Overall, while treatment with methyl-GBB significantly increased plasma concentrations of PUFAs, it had no effect on other lipid species.

3.2. Isolated Rat Heart Infarction and Haemodynamic Parameters and Mitochondrial Function after Ischaemic Damage. A heart infarction study was performed after 12 weeks of treatment with methyl-GBB at a dose of 10 mg/kg. Treatment with methyl-GBB significantly decreased the myocardial IS by 51% (Figure 2(b)) compared to the Zucker fa/fa rat control group. The IS in the methyl-GBB-treated group was also significantly lower (46%) than that of the Zucker lean rat group. There was no statistically significant difference between the area at risk (AR) values in the Zucker fa/fa rat control group and in the methyl-GBB-treated Zucker fa/fa groups. The AR value in the Zucker fa/fa control group was significantly larger by 36% than that in the Zucker lean rat group (Figure 2(a)). As in previous studies in healthy animals, methyl-GBB treatment had no significant effect on normoxic heart functional parameters in Zucker fa/fa rats when compared to the Zucker fa/fa control group (Figures 2(c)–2(g)). Coronary flow during LAD occlusion was decreased by 40% in the Zucker lean rat group and by 43% and 45% in the Zucker fa/fa control and methyl-GBB-treated groups, respectively (Figure 2(c)). During reperfusion, recovery of coronary flow was significantly better in the methyl-GBB-treated group than in the Zucker fa/fa control group. During reperfusion, LVDP (Figure 2(d)) was significantly higher in methyl-GBB-treated rat hearts than in Zucker lean and Zucker fa/fa rat hearts, and a tendency to preserve cardiac workload (Figure 2(g)) was observed in methyl-GBB-treated Zucker rat hearts. Methyl-GBB treatment had no effect on heart rate when compared to the Zucker fa/fa control group (Figure 2(e)). Heart contractility at the end of reperfusion was significantly higher by 67 and 64% in the methyl-GBB-treated group than in the Zucker lean rat and Zucker fa/fa control groups, respectively (Figure 2(f)).

To evaluate the effects of methyl-GBB treatment on mitochondrial functionality after ischaemic damage, permeabilized cardiac fibres were compared from both nonrisk (NR) and AR regions of the heart. In the presence of carnitine concentrations that mimic the tissue carnitine content, methyl-GBB decreased the CPT I-dependent OXPHOS coupling efficiency with palmitoyl-coenzyme A (PCoA) in normoxic cardiac fibres and after reperfusion, indicating an overall decrease in FAO (Figure 2(h)). Interestingly, in the Zucker fa/fa control group after reperfusion, no increase in the PCoA-dependent OXPHOS coupling efficiency was observed when risk and normoxic nonrisk areas were compared. In contrast, fatty acid metabolism during reperfusion was increased by 34% in cardiac fibres from AR regions from methyl-GBB-treated rat hearts compared to normoxic NR areas from these hearts. In addition, methyl-GBB significantly increased pyruvate metabolism in both normoxic and reperfused tissues (Figure 2(h)). I/R tended to increase mitochondrial reactive oxygen species (ROS) production in the OXPHOS state and significantly increased ROS production
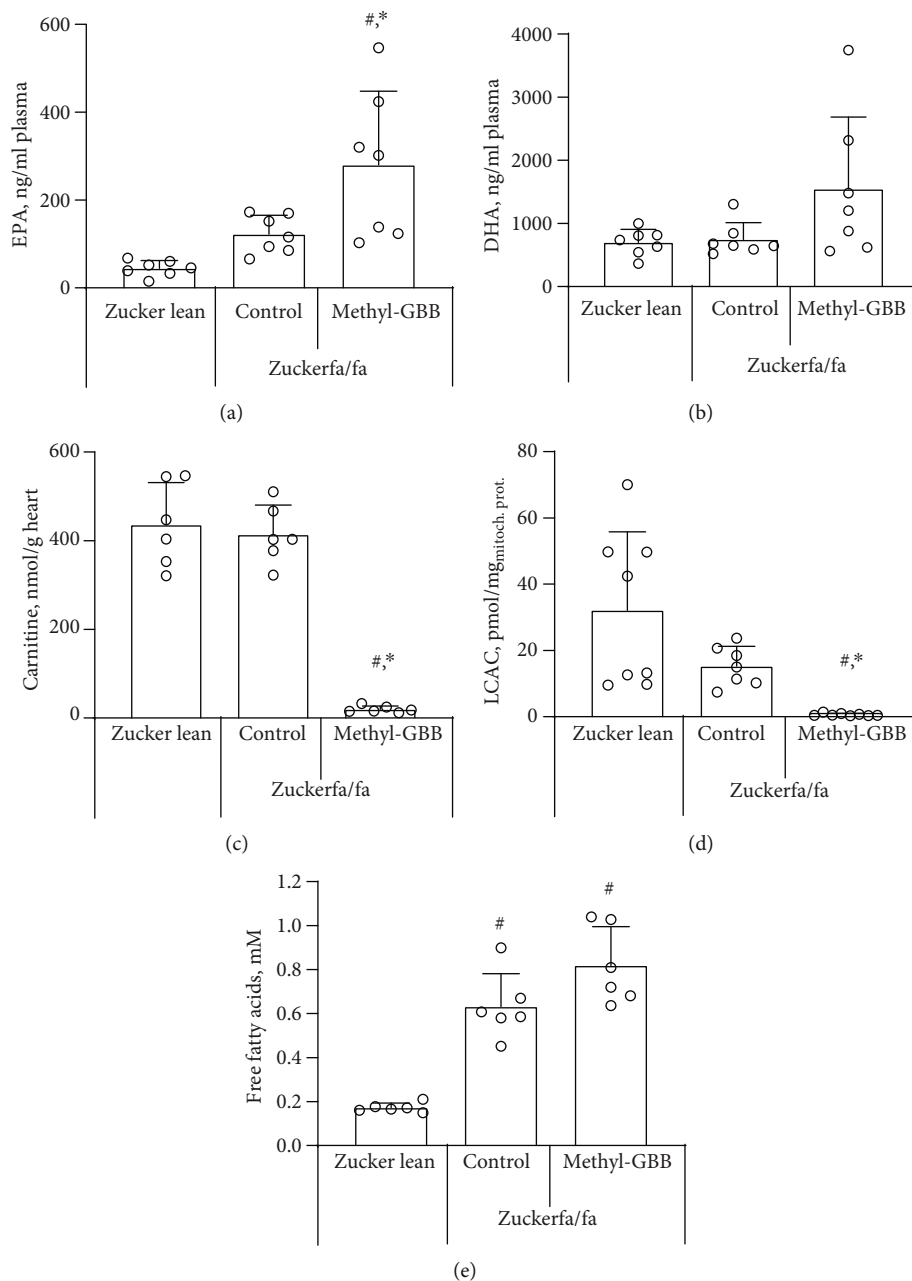
FIGURE 1: The effect of methyl-GBB administration on plasma EPA (a) and DHA (b) concentrations, cardiac tissue carnitine content (c), mitochondrial LCAC content (d), and plasma free fatty acid concentration (e) after 12 weeks of treatment. Each value was calculated as the mean ± S.E.M. of 7 rats for (a) and (b), 6 rats for (c) and (e), and 8(7) rats for (d). *Significantly different from the Zucker fa/fa control group; #significantly different from the Zucker lean rat group (ANOVA followed by Tukey's test; $P < 0.05$).

in the LEAK$_{Catr}$ state compared to normoxic conditions. Methyl-GBB treatment prevented an increase in ROS production, particularly in the LEAK$_{Catr}$ state (Figure 2(i)). Together, treatment with methyl-GBB optimizes energy metabolism and preserves mitochondrial functionality.

3.3. Insulin Sensitivity and Energy Metabolism Regulation. The glucose concentration was similar in fed Zucker lean and Zucker fa/fa rat blood (Figure 3(a)). In the fasted state, the blood glucose concentration in Zucker fa/fa rats was significantly higher (26%) than that of fasted Zucker lean rats

(Figure 3(a)). In addition, insulin concentrations were significantly 22- and 13-fold higher in Zucker fa/fa rat plasma than in Zucker lean rats in the fasted and fed states, respectively. Treatment with methyl-GBB significantly decreased plasma insulin concentrations by 42% and 40% in the fasted and fed states, respectively (Figure 3(b)). The homeostasis model assessment of insulin resistance (HOMA-IR) value for healthy Zucker lean rats was 1.38, while it was 30.5-fold higher in the Zucker fa/fa control group. Treatment with methyl-GBB significantly decreased the HOMA-IR value in Zucker fa/fa rats by 1.8-fold compared to the Zucker fa/fa

TABLE 1: The effects of methyl-GBB administration on triglyceride, total cholesterol, ASAT and ALAT concentrations in fed rat plasma, and weight gain after 12 weeks of treatment.

	Zucker lean	Zucker fa/fa	
		Control	Methyl-GBB 10 mg/kg
Triglycerides, mM	0.18 ± 0.02	1.55 ± 0.23[#]	1.56 ± 0.52[#]
Total cholesterol, mg/100 ml	48 ± 4	108 ± 3[#]	113 ± 7[#]
ASAT, U/l	47.6 ± 1.5	48.7 ± 3.5	45.9 ± 1.3
ALAT, U/l	23.5 ± 1.7	39.8 ± 3.0[#]	38.7 ± 2.1[#]
Body weight gain, g	$+241 \pm 10$	$+414 \pm 10$[#]	$+390 \pm 14$[#]
Heart to body weight, mg/g	3.70 ± 0.23	2.97 ± 0.09[#]	2.97 ± 0.10[#]
Liver to body weight, mg/g	34.4 ± 0.6	36.4 ± 1.1	35.4 ± 0.7
Kidney to body weight, mg/g	5.82 ± 0.07	4.61 ± 0.08	4.47 ± 0.08

Each value was calculated as the mean ± S.E.M. of 6 rats for triglyceride and total cholesterol concentrations, 8 rats for ASAT and ALAT levels, and 10 rats for body weight gain. [#]Significantly different from the Zucker lean group (ANOVA followed by Tukey's test; $P < 0.05$).

control group (Figure 3(c)). The lactate plasma concentration was determined in the fed state and was significantly higher (2.5-fold) in the Zucker fa/fa rat control group than in the Zucker lean rats; however, treatment with methyl-GBB significantly decreased the plasma lactate level by 48%, indicating more complete glucose metabolism (Figure 3(d)).

Because methyl-GBB treatment was found to improve insulin sensitivity in Zucker fa/fa rats, the glucose oxidation rate was measured in isolated perfused normoxic rat hearts. Glucose utilization was significantly impaired in Zucker fa/fa control rat hearts, with a 2.7-fold decrease compared to that in Zucker lean rat hearts. Treatment with methyl-GBB increased glucose utilization close to the level observed in the Zucker lean rat group (Figure 3(e)). Mitochondrial fatty acid and pyruvate metabolism were evaluated in cardiac fibres from nonischaemic areas of the heart. Methyl-GBB treatment significantly decreased the CPT I-dependent oxidative phosphorylation- (OXPHOS-) coupled mitochondrial metabolism of long-chain PCoA by 40% compared to that of the Zucker fa/fa control group (Figure 3(f)). In addition, OXPHOS-coupled pyruvate metabolism was significantly facilitated in methyl-GBB-treated Zucker rats compared to Zucker lean rats (Figure 3(f)).

We measured the protein phosphorylation levels of phosphorylated Akt (P-Akt) and standardized them to the total Akt level. The P-Akt level was significantly lower in the Zucker fa/fa control group than in the Zucker lean group. The P-Akt level in methyl-GBB-treated rat hearts was close to that in Zucker lean rat hearts (Figure 3(g)). The effects of methyl-GBB on the expression of PPARα/PGC1α target genes related to fatty acid and glucose metabolism were determined in cardiac tissues. Treatment with methyl-GBB significantly increased the expression of CPT IB, ACOX, and ACSL up to 1.9-fold when compared to both Zucker lean and Zucker fa/fa control rats (Figure 3(h)). Moreover, the expression of the PDK4 gene was significantly upregulated 2.5-fold in methyl-GBB-treated rat hearts, indicating activation of the PPARα/PGC1α pathway (Figure 3(h)). Together, treatment with methyl-GBB improves insulin sensing, decreases fatty acid levels, and, in turn, increases glucose metabolism.

4. Discussion

The present study shows that the cardioprotective drug methyl-GBB can decrease I/R damage, diminish energy metabolism dysfunction in mitochondria, and reduce glucose-lactate metabolism disturbances in Zucker rats with metabolic syndrome. The data for the first time show that a significant decrease in fatty acid oxidation in mitochondria by methyl-GBB treatment results in increased plasma availability of PUFAs. Moreover, an increase in PUFA availability was also observed in normoglycaemic mice treated with methyl-GBB, indicating that a pharmacological decrease in fatty acid metabolism is a viable option to further increase PUFA availability.

Treatment with methyl-GBB increases plasma concentrations of PUFAs, particularly that of EPA, and decreases the levels of acylcarnitines. Previous studies have shown that long-term treatment with PUFAs provides cardioprotection in rats in vivo [32]. While CD36-mediated transport is pivotal for FA oxidation to support myocardial contractile function [33], lipotoxicity, in turn, is a well-known paradigm based on cardiac imbalance between reduced utilization of FAs and noninterrupted FA delivery [34]. Thus, ongoing CPT I-dependent metabolism of FAs and subsequent accumulation of saturated LCAC is known to impair mitochondrial functionality, which further damages the myocardium after I/R [35, 36]. In a recent study, we demonstrated that the accumulation of LCAC in mitochondria during ischaemia inhibits ATP synthesis, enhances ROS production, and induces I/R damage [30]. Here, we show that pharmacologically limited fatty acid oxidation in methyl-GBB-treated Zucker fa/fa rats decreases the LCAC content in cardiac mitochondria and elevates PUFA levels. These changes are accompanied by the prevention of I/R-induced increases in ROS production. As a result, a marked 51% decrease in IS is achieved even in obese Zucker rats with metabolic syndrome and severely impaired energy metabolism.

LCAC accumulation induces insulin resistance by inhibiting the Akt-mediated signalling pathway [29]. Recently, we showed that methyl-GBB, by decreasing LCAC tissue levels, improves insulin sensitivity and glucose tolerance test

(a)

(b)

(c)

(d)

(e)

(f)

(g)

(h)

FIGURE 2: Continued.

(i)
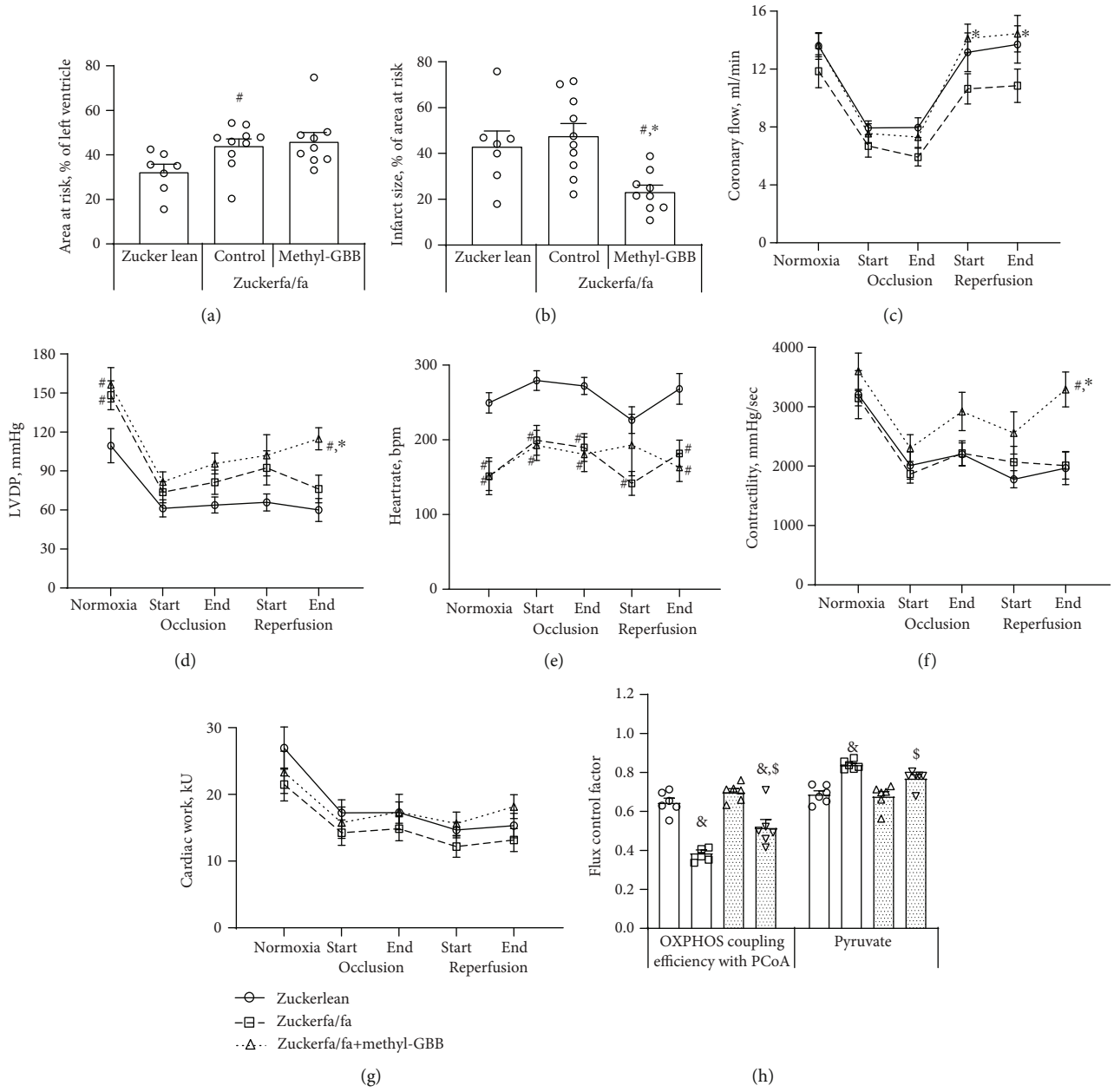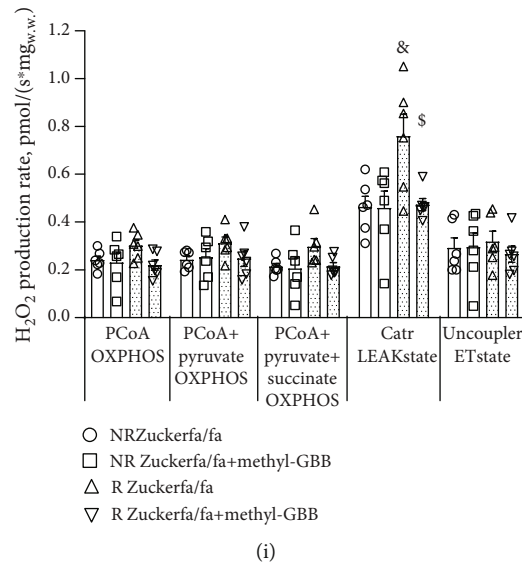
Figure 2: The effect of methyl-GBB administration on myocardial infarct size (a, b) and heart functional parameters (c–g) in Langendorff-perfused isolated hearts and the flux control factor (h) and mitochondrial ROS production (i) in permeabilized cardiac fibres from normoxic nonrisk (NR) and reperfused area at risk (R) regions of the heart after 12 weeks of treatment. Each value was calculated as the mean ± S.E.M. of 7 hearts in the Zucker lean group, 9 hearts in the methyl-GBB-treated group, and 10 hearts in the Zucker fa/fa control group for (a) and (b) and 8(7) hearts for (c–g), and 6 hearts for (h) and (i). *Significantly different from the Zucker fa/fa control group; #significantly different from the Zucker lean rat (Kruskal-Wallis test followed by Dunn's multiple comparison test; $P < 0.05$ for (a), ANOVA followed by Tukey's test; $P < 0.05$ for (b), two-way ANOVA followed by Tukey's test; $P < 0.05$ for (c–g)). $Significantly different from the respective Zucker fa/fa control (NR or R) group. &Significantly different from the respective normoxic (NR) group (ANOVA followed by Tukey's test; $P < 0.05$).

responses [37]. Moreover, the levels of PUFAs have a strong positive correlation with insulin sensitivity [38], and improvement in insulin sensitivity after treatment with EPA was shown to result in functional improvements in glucose and fatty acid uptake and cardiomyocyte shortening [39]. In the present study, Akt phosphorylation was preserved, insulin sensitivity was significantly improved, and glucose and pyruvate metabolism was facilitated. Akt phosphorylation is another parameter that could be increased not only due to the decrease in LCAC availability but also due to the increase in PUFA availability [40]. Overall, pharmacological limitation of fatty acid oxidation improves insulin sensitivity in Zucker rats.

In insulin-resistant tissues, the accumulation of lipids and their metabolites inhibits the metabolism of pyruvate [41, 42]; this leads to a situation where glycolysis is not coupled to oxidative phosphorylation. As a result, the lactate concentration in plasma is increased to the level typical of the lactate threshold induced by excessive physical activities. In this state, pyruvate oxidation in the mitochondria is significantly decreased, followed by the formation of lactate and elevated lactate plasma concentrations [37, 43–45]. In morbidly obese Zucker rats, the lactate plasma concentration is increased almost 3-fold, while methyl-GBB treatment significantly improves pyruvate metabolism in mitochondria and decreases the lactate concentration almost to the control level. Recently, we confirmed that the effects related to insulin sensitization and the facilitation of pyruvate and lactate oxidation depend mostly on a decrease in the LCAC content in muscles [29, 41], while the current study for the first time confirms that these effects also apply to cardiac tissues from

animals with metabolic syndrome. Overall, facilitation of glucose metabolism by the activation of pyruvate metabolism in mitochondria could also be partially responsible for the anti-infarction effect of methyl-GBB.

Current findings further indicate that treatment with methyl-GBB prevents an I/R-induced increase in mitochondrial ROS production under conditions of limited oxidative phosphorylation. Since it has been shown that the accumulation of LCAC in ischaemic cardiac mitochondria promotes ROS production due to the inhibition of oxidative phosphorylation [30, 46], the observed prevention of oxidative stress in ischaemic hearts by methyl-GBB treatment is more likely associated with the prevention of LCAC accumulation during ischaemia. Moreover, activation of mitochondrial respiration and FA oxidation decreases lipotoxicity [47], and it has been suggested that stimulation of fatty acid oxidation during reperfusion could be beneficial against I/R-induced oxidative stress [48]. Treatment with methyl-GBB increases mitochondrial fatty acid oxidation after ischaemia, thus ensuring effective utilization of accumulated fatty acid intermediates and subsequent reduction of oxidative stress. Overall, these results indicate that a pharmacological decrease in the LCAC content in cardiac mitochondria attenuates ROS production under conditions of limited oxidative phosphorylation after I/R and protects against myocardial damage.

Previously, it was shown that methyl-GBB limits I/R damage in animals with intact glucose metabolism [22, 23], while the present findings extend the cardioprotective effect to conditions with markedly impaired cardiac glucose metabolism, such as metabolic syndrome. The current results provide additional proof that the cardioprotective effect of

(a)

(b)

(c)

(d)

(e)

(f)

(g)

(h)
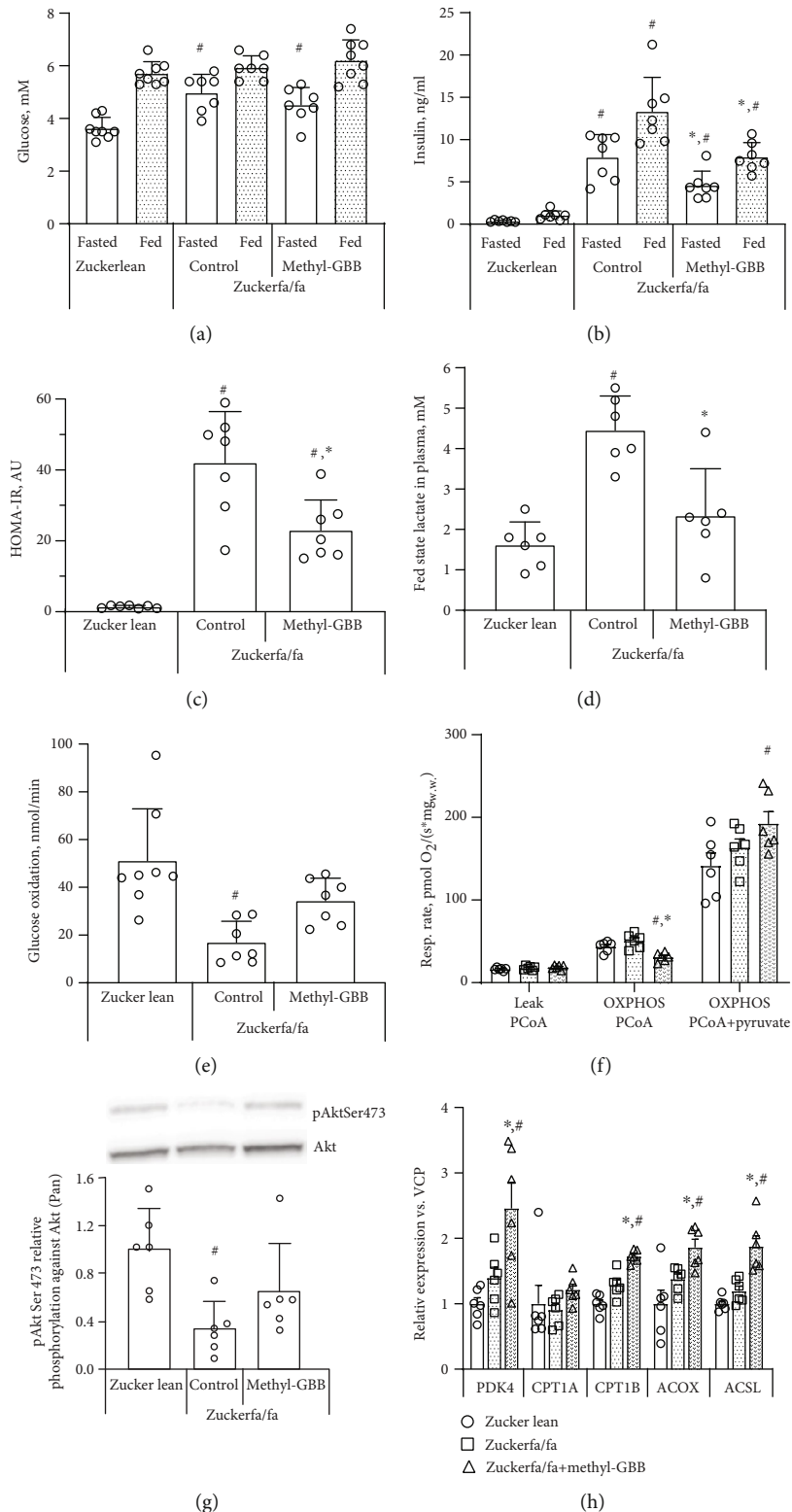
FIGURE 3: The effects of methyl-GBB administration on blood glucose (a), insulin (b), HOMA-IR (c), plasma lactate (d) concentrations, glucose oxidation in isolated Langendorff-perfused rat hearts (e), and pyruvate and CPT I-dependent fatty acid metabolism in cardiac fibres (f) under normoxic conditions, Akt phosphorylation (g), and the expression of genes related to fatty acid and glucose metabolism (h) after 12 weeks of treatment. Representative Western blots for Akt phosphorylation are presented in (g). Each value was calculated as the mean ± S.E.M. of 6 rats for (d) and (f–h) and of 7-8 rats for (a–c) and (e). *Significantly different from the Zucker fa/fa control group (ANOVA followed by Tukey's test/Kruskal-Wallis followed by Dunn's test; $P < 0.05$). #Significantly different from the Zucker lean group (ANOVA followed by Tukey's test/Kruskal-Wallis followed by Dunn's test; $P < 0.05$).

methyl-GBB is related to changes in fatty acid handling. Thus, EPA and DHA each can protect the heart against myocardial infarction damage [40], and treatment with methyl-GBB increases the availability of the aforementioned PUFAs. In addition, earlier observations by Harmancey and colleagues [49] indicate that the improved utilization of long-chain fatty acids during reperfusion leads to better recovery in insulin-resistant hearts. While treatment with methyl-GBB decreases CPT I-dependent long-chain fatty acid conversion to LCAC and overall fatty acid metabolism, a significant increase in fatty acid mitochondrial utilization in areas at risk compared to that in normoxic areas from the same heart was observed in methyl-GBB-treated hearts after reperfusion but not in control Zucker fa/fa rat hearts. Changes in the fatty acid metabolism pattern are accompanied by improved cardiac functionality in methyl-GBB-treated Langendorff-perfused isolated Zucker fa/fa rat hearts during reperfusion. This effect was not observed before in normoglycaemic animals [22, 23]. Significant increases in the expression of several PPARα/PGC1α target genes involved in fatty acid oxidation might at least partially be the result of increased PUFA levels [50, 51] and could be responsible for increased fatty acid oxidation recovery in reperfused tissues.

5. Conclusions

The current study highlights the potential benefits of pharmacologically increasing PUFAs and decreasing LCAC levels by methyl-GBB to improve insulin sensitivity and mitochondrial functionality as well as the cardioprotective effect of methyl-GBB in treating metabolic syndrome. Presented here is a strategy to accumulate PUFAs and to facilitate overall fatty acid metabolism during reperfusion to decrease LCAC availability. This leads to the protection of the myocardium against damage induced by ischaemia under complex metabolic conditions and raises expectations for the successful translation of such a strategy to clinical settings.

Data Availability

The datasets analysed during the current study are available from the corresponding author on reasonable request.

Ethical Approval

The experimental procedures involving animals were performed in accordance with the guidelines of the European Community (Directive 2010/63/EU) and local laws and policies, and all of the procedures were approved by Food and Veterinary Service, Riga, Latvia. Studies involving animals are reported in accordance with the ARRIVE guidelines.

Consent

Consent is not necessary.

Conflicts of Interest

JK, MMK, HC, SG, MD, and EL are listed as inventors in several international patent applications regarding the use of methyl-GBB for the treatment of cardiovascular and cardiometabolic diseases. None of the authors currently own any of these patents.

Authors' Contributions

JK, MD, and EL participated in the research design; JK, MMK, KV, SK, HC, ES, and SG performed the experiments; JK, MMK, HC, SG, and EL analysed the data; JK, MD, EL, and MMK participated in writing the manuscript; all authors reviewed and approved the finalized version of the manuscript.

Acknowledgments

Supplementary Materials

Supplementary Figure 1: the effect of methyl-GBB administration on mouse plasma EPA (A) and DHA (B) concentrations after 4 weeks of treatment at a dose of 5 mg/kg. Each value was calculated as the mean ± S.E.M. of 9 mice. *Significantly different from the respective fed or fasted control group (ANOVA followed by Tukey's test; $P < 0.05$). Supplementary Figure 2: the effect of methyl-GBB administration on mouse plasma FFA concentration (sum of C12-C20 FAs) after 4 weeks of treatment at a dose of 5 mg/kg. Each value was calculated as the mean ± S.E.M. of 9 mice. *Significantly different from the respective fasted control group; # (ANOVA followed by Tukey's test; $P < 0.05$). (Supplementary Materials)

References

[1] K. G. Alberti, R. H. Eckel, S. M. Grundy et al., "Harmonizing the Metabolic Syndrome," Circulation, vol. 120, no. 16, pp. 1640–1645, 2009.

[2] S. M. Grundy, J. I. Cleeman, S. R. Daniels et al., "Diagnosis and Management of the Metabolic Syndrome," Circulation, vol. 112, no. 17, pp. 2735–2752, 2005.

[3] C. J. Girman, T. Rhodes, M. Mercuri et al., "The metabolic syndrome and risk of major coronary events in the Scandinavian Simvastatin Survival Study (4S) and the Air Force/Texas Coronary Atherosclerosis Prevention Study (AFCAPS/TexCAPS)," The American Journal of Cardiology, vol. 93, no. 2, pp. 136–141, 2004.

[4] A. Younis, A. Younis, B. Tzur et al., "Metabolic syndrome is independently associated with increased 20-year mortality in

patients with stable coronary artery disease," *Cardiovascular Diabetology*, vol. 15, no. 1, 2016.

[5] T. A. Wadden, S. Volger, D. B. Sarwer et al., "A two-year randomized trial of obesity treatment in primary care practice," *The New England Journal of Medicine*, vol. 365, no. 21, pp. 1969–1979, 2011.

[6] V. L. Gloy, M. Briel, D. L. Bhatt et al., "Bariatric surgery versus non-surgical treatment for obesity: a systematic review and meta-analysis of randomised controlled trials," *BMJ*, vol. 347, 2013.

[7] I. Andreadou, A. Daiber, G. F. Baxter et al., "Influence of cardiometabolic comorbidities on myocardial function, infarction, and cardioprotection: role of cardiac redox signaling," *Free Radical Biology & Medicine*, vol. 166, pp. 33–52, 2021.

[8] G. Heusch, "Critical issues for the translation of cardioprotection," *Circulation Research*, vol. 120, no. 9, pp. 1477–1486, 2017.

[9] X. Rossello and D. M. Yellon, "Cardioprotection: the disconnect between bench and bedside," *Circulation*, vol. 134, no. 8, pp. 574-575, 2016.

[10] A. Jayedi, M. S. Zargar, and S. Shab-Bidar, "Fish consumption and risk of myocardial infarction: a systematic review and dose-response meta-analysis suggests a regional difference," *Nutrition Research*, vol. 62, pp. 1–12, 2019.

[11] A. Sethi, A. Bajaj, S. Khosla, and R. R. Arora, "Statin use mitigate the benefit of omega-3 fatty acids supplementation-a meta-regression of randomized trials," *American Journal of Therapeutics*, vol. 23, no. 3, pp. e737–e748, 2016.

[12] C. Cheng, H. Li, L. Liang et al., "Effects of ω-3 PUFA and ascorbic acid combination on post-resuscitation myocardial function," *Biomedicine & Pharmacotherapy*, vol. 133, article 110970, 2021.

[13] S. Mao, H. Ma, P. Chen, Y. Liang, M. Zhang, and A. Hinek, "Fat-1 transgenic mice rich in endogenous omega-3 fatty acids are protected from lipopolysaccharide-induced cardiac dysfunction," *ESC Heart Failure*, vol. 8, no. 3, pp. 1966–1978, 2021.

[14] A. Juszczyk, K. Jankowska, B. Zawislak, A. Surdacki, and B. Chyrchel, "Depressed cardiac mechanical energetic efficiency: a contributor to cardiovascular risk in common metabolic diseases-from mechanisms to clinical applications," *Journal of Clinical Medicine*, vol. 9, no. 9, p. 2681, 2020.

[15] J. P. DeLany, M. M. Windhauser, C. M. Champagne, and G. A. Bray, "Differential oxidation of individual dietary fatty acids in humans," *The American Journal of Clinical Nutrition*, vol. 72, no. 4, pp. 905–911, 2000.

[16] M. B. Schulze, A. M. Minihane, R. N. M. Saleh, and U. Riserus, "Intake and metabolism of omega-3 and omega-6 polyunsaturated fatty acids: nutritional implications for cardiometabolic diseases," *The Lancet Diabetes and Endocrinology*, vol. 8, no. 11, pp. 915–930, 2020.

[17] R. K. Berge, M. S. Ramsvik, P. Bohov et al., "Krill oil reduces plasma triacylglycerol level and improves related lipoprotein particle concentration, fatty acid composition and redox status in healthy young adults - a pilot study," *Lipids in Health and Disease*, vol. 14, no. 1, 2015.

[18] C. Nilsson, K. Raun, F. F. Yan, M. O. Larsen, and M. Tang-Christensen, "Laboratory animals as surrogate models of human obesity," *Acta Pharmacologica Sinica*, vol. 33, no. 2, pp. 173–181, 2012.

[19] S. K. Wong, K. Y. Chin, F. H. Suhaimi, A. Fairus, and S. Ima-Nirwana, "Animal models of metabolic syndrome: a review," *Nutrition & Metabolism*, vol. 13, no. 1, 2016.

[20] C. Kilkenny, W. Browne, I. C. Cuthill, M. Emerson, D. G. Altman, and NC3Rs Reporting Guidelines Working Group, "Animal research: reporting in vivo experiments: the ARRIVE guidelines," *British Journal of Pharmacology*, vol. 160, no. 7, pp. 1577–1579, 2010.

[21] J. C. McGrath, G. B. Drummond, E. M. McLachlan, C. Kilkenny, and C. L. Wainwright, "Guidelines for reporting experiments involving animals: the ARRIVE guidelines," *British Journal of Pharmacology*, vol. 160, no. 7, pp. 1573–1576, 2010.

[22] J. Kuka, M. Makrecka-Kuka, H. Cirule et al., "Decrease in long-chain acylcarnitine tissue content determines the duration of and correlates with the cardioprotective effect of methyl-GBB," *Basic & Clinical Pharmacology & Toxicology*, vol. 121, no. 2, pp. 106–112, 2017.

[23] E. Liepinsh, M. Makrecka-Kuka, J. Kuka et al., "Inhibition of L-carnitine biosynthesis and transport by methyl-γ-butyrobetaine decreases fatty acid oxidation and protects against myocardial infarction," *British Journal of Pharmacology*, vol. 172, no. 5, pp. 1319–1332, 2015.

[24] R. Vilskersts, J. Kuka, E. Liepinsh et al., "Methyl-γ-butyrobetaine decreases levels of acylcarnitines and attenuates the development of atherosclerosis," *Vascular Pharmacology*, vol. 72, pp. 101–107, 2015.

[25] J. Kuka, R. Vilskersts, H. Cirule et al., "The cardioprotective effect of mildronate is diminished after co-treatment with L-carnitine," *Journal of Cardiovascular Pharmacology and Therapeutics*, vol. 17, no. 2, pp. 215–222, 2012.

[26] E. Liepinsh, J. Kuka, and M. Dambrova, "Troubleshooting digital macro photography for image acquisition and the analysis of biological samples," *Journal of Pharmacological and Toxicological Methods*, vol. 67, no. 2, pp. 98–106, 2013.

[27] M. Makrecka-Kuka, S. Korzh, K. Vilks et al., "Mitochondrial function in the kidney and heart, but not the brain, is mainly altered in an experimental model of endotoxaemia," *Shock*, vol. 52, no. 6, pp. e153–e162, 2019.

[28] M. Makrecka-Kuka, G. Krumschnabel, and E. Gnaiger, "High-resolution respirometry for simultaneous measurement of oxygen and hydrogen peroxide fluxes in permeabilized cells, tissue homogenate and isolated mitochondria," *Biomolecules*, vol. 5, no. 3, pp. 1319–1338, 2015.

[29] E. Liepinsh, M. Makrecka-Kuka, E. Makarova et al., "Acute and long-term administration of palmitoylcarnitine induces muscle-specific insulin resistance in mice," *BioFactors*, vol. 43, no. 5, pp. 718–730, 2017.

[30] E. Liepinsh, M. Makrecka-Kuka, K. Volska et al., "Long-chain acylcarnitines determine ischaemia/reperfusion-induced damage in heart mitochondria," *The Biochemical Journal*, vol. 473, no. 9, pp. 1191–1202, 2016.

[31] M. J. Curtis, R. A. Bond, D. Spina et al., "Experimental design and analysis and their reporting: new guidance for publication in BJP," *British Journal of Pharmacology*, vol. 172, no. 14, pp. 3461–3471, 2015.

[32] B. Q. Zhu, R. E. Sievers, Y. P. Sun, N. Morse-Fisher, W. W. Parmley, and C. L. Wolfe, "Is the reduction of myocardial infarct size by dietary fish oil the result of altered platelet function?," *American Heart Journal*, vol. 127, no. 4, pp. 744–755, 1994.

[33] J. F. C. Glatz, F. Wang, M. Nabben, and J. Luiken, "CD36 as a target for metabolic modulation therapy in cardiac disease," *Expert Opinion on Therapeutic Targets*, pp. 1–8, 2021.

[34] M. De Rosa, J. Gambardella, J. Shu, and G. Santulli, "Dietary fat is a key determinant in balancing mitochondrial dynamics in heart failure: a novel mechanism underlying the obesity paradox," *Cardiovascular Research*, vol. 114, no. 7, pp. 925–927, 2018.

[35] M. Makrecka-Kuka, E. Liepinsh, A. J. Murray et al., "Altered mitochondrial metabolism in the insulin-resistant heart," *Acta Physiologica*, vol. 228, no. 3, article e13430, 2020.

[36] C. J. Zuurbier, L. Bertrand, C. R. Beauloye et al., "Cardiac metabolism as a driver and therapeutic target of myocardial infarction," *Journal of Cellular and Molecular Medicine*, vol. 24, no. 11, pp. 5937–5954, 2020.

[37] E. Liepinsh, M. Makrecka-Kuka, E. Makarova et al., "Decreased acylcarnitine content improves insulin sensitivity in experimental mice models of insulin resistance," *Pharmacological Research*, vol. 113, no. Part B, pp. 788–795, 2016.

[38] J. P. Huang, M. L. Cheng, C. Y. Hung et al., "Docosapentaenoic acid and docosahexaenoic acid are positively associated with insulin sensitivity in rats fed high-fat and high-fructose diets," *Journal of Diabetes*, vol. 9, no. 10, pp. 936–946, 2017.

[39] V. Franekova, Y. Angin, N. T. Hoebers et al., "Marine omega-3 fatty acids prevent myocardial insulin resistance and metabolic remodeling as induced experimentally by high insulin exposure," *American Journal of Physiology. Cell Physiology*, vol. 308, no. 4, pp. C297–C307, 2015.

[40] N. Madingou, K. Gilbert, L. Tomaro et al., "Comparison of the effects of EPA and DHA alone or in combination in a murine model of myocardial infarction," *Prostaglandins, Leukotrienes, and Essential Fatty Acids*, vol. 111, pp. 11–16, 2016.

[41] M. Makrecka, J. Kuka, K. Volska et al., "Long-chain acylcarnitine content determines the pattern of energy metabolism in cardiac mitochondria," *Molecular and Cellular Biochemistry*, vol. 395, no. 1-2, pp. 1–10, 2014.

[42] D. M. Muoio and P. D. Neufer, "Lipid-induced mitochondrial stress and insulin action in muscle," *Cell Metabolism*, vol. 15, no. 5, pp. 595–605, 2012.

[43] S. Daneshyar, R. Gharakhanlou, R. Nikooie, and Y. Forutan, "The effect of high-fat diet and streptozotocin-induced diabetes and endurance training on plasma levels of calcitonin gene-related peptide and lactate in rats," *Canadian Journal of Diabetes*, vol. 38, no. 6, pp. 461–465, 2014.

[44] K. E. Kim, Y. Jung, S. Min et al., "Caloric restriction of db/db mice reverts hepatic steatosis and body weight with divergent hepatic metabolism," *Scientific Reports*, vol. 6, no. 1, article 30111, 2016.

[45] E. Liepinsh, E. Skapare, B. Svalbe, M. Makrecka, H. Cirule, and M. Dambrova, "Anti-diabetic effects of mildronate alone or in combination with metformin in obese Zucker rats," *European Journal of Pharmacology*, vol. 658, no. 2-3, pp. 277–283, 2011.

[46] H. Tominaga, H. Katoh, K. Odagiri et al., "Different effects of palmitoyl-L-carnitine and palmitoyl-CoA on mitochondrial function in rat ventricular myocytes," *American Journal of Physiology. Heart and Circulatory Physiology*, vol. 295, no. 1, pp. H105–H112, 2008.

[47] S. R. Lee, J. H. Heo, S. L. Jo et al., "Progesterone receptor membrane component 1 reduces cardiac steatosis and lipotoxicity via activation of fatty acid oxidation and mitochondrial respiration," *Scientific Reports*, vol. 11, no. 1, 2021.

[48] M. Dambrova, C. J. Zuurbier, V. Borutaite, E. Liepinsh, and M. Makrecka-Kuka, "Energy substrate metabolism and mitochondrial oxidative stress in cardiac ischemia/reperfusion injury," *Free Radical Biology & Medicine*, vol. 165, pp. 24–37, 2021.

[49] R. Harmancey, H. G. Vasquez, P. H. Guthrie, and H. Taegtmeyer, "Decreased long-chain fatty acid oxidation impairs postischemic recovery of the insulin-resistant rat heart," *The FASEB Journal*, vol. 27, no. 10, pp. 3966–3978, 2013.

[50] G. Krey, O. Braissant, F. L'Horset et al., "Fatty acids, eicosanoids, and hypolipidemic agents identified as ligands of peroxisome proliferator-activated receptors by coactivator-dependent receptor ligand assay," *Molecular Endocrinology*, vol. 11, no. 6, pp. 779–791, 1997.

[51] N. Shimojo, S. Jesmin, S. Sakai et al., "Fish oil constituent eicosapentaenoic acid inhibits endothelin-induced cardiomyocyte hypertrophy via PPAR-α," *Life Sciences*, vol. 118, no. 2, pp. 173–178, 2014.

Review Article

Circular RNA Expression: Its Potential Regulation and Function in Abdominal Aortic Aneurysms

Yanshuo Han [iD],[1] **Hao Zhang,**[1] **Ce Bian,**[2] **Chen Chen** [iD],[3] **Simei Tu,**[1] **Jiahui Guo,**[1] **Yihao Wu,**[1]
Dittmar Böckler [iD],[4] **and Jian Zhang** [iD][5]

[1]*School of Life and Pharmaceutical Science, Dalian University of Technology, Dalian, China*
[2]*Department of Cardiovascular Surgery, The General Hospital of the PLA Rocket Force, Beijing Normal University, Beijing, China*
[3]*School of Biomedical Sciences, The University of Queensland, Brisbane, Australia*
[4]*Department of Vascular and Endovascular Surgery, University of Heidelberg, Heidelberg, Germany*
[5]*Department of Vascular Surgery, The First Hospital, China Medical University, Shenyang, China*

Correspondence should be addressed to Yanshuo Han; yanshuohan@dlut.edu.cn,
Dittmar Böckler; dittmar.boeckler@med.uni-heidelberg.de, and Jian Zhang; jianzhang@cmu.edu.cn

Abdominal aortic aneurysms (AAAs) have posed a great threat to human life, and the necessity of its monitoring and treatment is decided by symptomatology and/or the aneurysm size. Accumulating evidence suggests that circular RNAs (circRNAs) contribute a part to the pathogenesis of AAAs. circRNAs are novel single-stranded RNAs with a closed loop structure and high stability, having become the candidate biomarkers for numerous kinds of human disorders. Besides, circRNAs act as molecular "sponge" in organisms, capable of regulating the transcription level. Here, we characterize that the molecular mechanisms underlying the role of circRNAs in AAA development were further elucidated. In the present work, studies on the biosynthesis, bibliometrics, and mechanisms of action of circRNAs were aims comprehensively reviewed, the role of circRNAs in the AAA pathogenic mechanism was illustrated, and their potential in diagnosing AAAs was examined. Moreover, the current evidence about the effects of circRNAs on AAA development through modulating endothelial cells (ECs), macrophages, and vascular smooth muscle cells (VSMCs) was summarized. Through thorough investigation, the molecular mechanisms underlying the role of circRNAs in AAA development were further elucidated. The results demonstrated that circRNAs had the application potential in the diagnosis and prevention of AAAs in clinical practice. The study of circRNA regulatory pathways would be of great assistance to the etiologic research of AAAs.

1. Introduction

Abdominal aortic aneurysms (AAAs) frequently induce cardiovascular death among the elderly male population within various European and Asian countries [1–3]. AAAs are featured by permanent expansion and weakening of a localized abdominal aorta [4–6]. There are symptomatic, asymptomatic, and ruptured AAAs clinically [7]. As estimated by a UK study, 1.5% of its population has an AAA greater than 30 mm in size [8]. Besides, a USA multicenter aneurysm screening study has suggested that 4.6% of its population

aged 65-74 suffers from an AAA [9]. In Sweden, the incidence of the AAA among male population aged above 65 is reported to be 1.8% [10]. Because of the lack of effective surgical methods and unpredictability of the disease, continuous enlargement of the aortic wall will lead to the wall rupture and serious bleeding, resulting in a death rate as high as 80% [11]. A majority of AAA cases are progressive and asymptomatic, which are usually discovered accidentally by the diagnostic imaging of other diseases. The survival of AAA patients after diagnosis has improved, but its morbidity and mortality rates show an ascending trend [3]. Generally,

the AAA-related mortality cannot be affected by AAA screening, but may be lowered by other factors like smoking less [12].

Conventionally, AAAs are mostly treated with elective retroperitoneal or open transperitoneal surgery [13], but now, the endovascular repair (EVAR) is recommended as a better alternative to open surgical repair [14–16]. Currently, no curative treatment is available for restricting AAA development and preventing AAA rupture [17], and the only strategy is to continuously monitor the aneurysm size before surgery [18].

The pathogenic mechanism of AAAs is complicated and involves multiple factors. Previous studies suggest that AAAs are associated with the weakened defective adventitial/medial arterial layers, like fibroblasts and smooth muscle cells (SMCs) [19–22]. Recently, research on human tissue and animal models indicates that the AAA occurrence arises from the dynamic vascular remodelling [23, 24]. Additionally, the critical pathological features of AAAs are oxidative stress (OS), vascular inflammation, aortic wall thinning due to the loss of vascular smooth muscle cells (VSMCs), and aortic extracellular matrix (ECM) decomposition [22, 24].

Due to strong gene expression regulation effects, epigenetic alterations, such as histone modification, DNA methylation, and noncoding RNA (ncRNA) modification [25–27], have been increasingly acknowledged as an importance contributor to AAA development. It has been proven that epigenetic modifications take place in the early embryogenesis and primordial cell development processes, but it is of great significance to explore the effects of these alterations in "later life." In such, "later life" epigenetic modifications caused by the dietary intervention were analyzed [28]. Generally, ncRNAs can be divided into small ncRNAs and long ncRNAs (lncRNAs) according to the arbitrary threshold size of 200 nucleotides (nt). Among small ncRNAs, microRNAs (miRNAs) with a length of about 22 nt have been extensively investigated. By contrast, there is less studies on the functions of lncRNAs with a length of over 200 nt. Although ncRNAs have been demonstrated to regulate the interactions and activities of fibroblasts, vascular inflammatory cells, endothelial cells (ECs), and SMCs, the key factors resulting in AAA occurrence remain unidentified. According to a new eukaryotic gene expression feature discovered in 2012, circRNAs are ubiquitously expressed in genes previously considered to express linear ncRNAs or messenger RNAs (mRNAs) only. circRNAs are RNA molecules with a circular and covalently closed structure, which usually consist of exon sequences and can be spliced at the typical splice sites.

In particular, many articles have demonstrated the important roles of ncRNAs in cardiovascular diseases (CVDs), such as aortic dissection and AAAs. Meanwhile, circRNAs are also considered to exhibit certain effects on some CVDs, but their expression levels and roles in AAAs still remain unclarified.

In the present work, the roles of circRNAs in the occurrence and development of AAAs were illustrated, and their significance in treating AAAs was discussed. In addition, the regulation effect of circRNAs and their corresponding target genes on AAAs and the underlying mechanisms were

also investigated. The ncRNAs that were previously recognized to be involved in several processes leading in AAAs were highlighted. The in-depth investigation on such circRNAs will shed lights on the prevention and treatment of AAAs, and these circRNAs may be used as candidate prognostic biomarkers and therapeutic targets for the prediction of the AAA incidence and the evaluation of patient prognosis.

2. Genetic Causes of AAA Pathogenesis

2.1. Mendelian Causes. A Mendelian factor that causes AAAs often refers to single-gene mutations [29]. Marfan syndrome can also induce AAAs, which is often accompanied by a family history. Marfan syndrome arises mainly from FBN1 gene mutation [30], accounting for an autosomal dominant genetic disorder. The TGFβR1, TGFβR2, and TGFβR3 gene mutations promote the production of matrix metalloproteinases (MMPs) and eventually lead to medial degradation [31]. Other syndromes can provoke the occurrence of aortic root aneurysms. In addition, some diseases derived from single-gene mutations affect ECM components of the aortic wall. The Ehlers Danlos syndrome, for instance, originates from COL3A1 gene mutation [32]. AAAs may be detected in cases who develop autosomal recessive disorders, such as pseudoxanthoma elasticum and homocystinuria, which stem from ABCC6 and CBS gene mutations, respectively [29].

2.2. Non-Mendelian Causes. There are various non-Mendelian factors leading to AAAs, including the ECM, endothelial cell (EC) specification, SMCs differentiation, inflammation, and cell adhesion.

2.2.1. ECM. The ECM is a complex network of macromolecular substances that supports and connects tissue as well as mediates tissue generation and cell physiological activities. The proteins of the Matrix Metalloproteinases (MMP) family can regulate the ECM turnover, which is related to the formation of genes that encode MMP and ECM components in AAAs. Besides, upregulated MMP-2 and MMP-9 levels can be detected within human AAA tissue [33, 34]. Moreover, the single-nucleotide polymorphisms (SNPs) rs3025058 in MMP-3 and rs2252070 in MMP-13 are suggested to lead to a higher AAA risk [35]. Inhibiting the ablation of MMP-3 can promote aneurysm formation. Additionally, the G allele of rs2252070 also contributes to a higher AAA risk [36].

2.2.2. SMC Differentiation. AAAs are related to rs1795061 localized at around 40 kb upstream of the SMYD2 transcription start site [37]. SMYD proteins belong to the lysine methyltransferases, and they play a vital part in the regulation of cardiac and skeletal morphogenesis [38]. According to a recent report, SMYD2 is possibly associated with the pathogenic mechanism of AAAs [39]. Importantly, Toghill et al. evaluated DNA methylation within VSMCs collected from AAA patients using targeted bisulphite next-generation sequencing (NGS) for the first time. They found evident DNA hypomethylation within the promoter region of SYMD2 gene among AAA cases and a close association between the average methylation degree of CpGs and gene

expression levels [40]. Typically, methylation of the SMYD2 promoter region may be related to AAA development, rather than its progression [40].

2.2.3. EC Specification. In the study of Jones et al., the SNP rs2836411, an AAA risk variation localized at 21q22.2 in the intrinsic region of ERG gene, was detected [37]. ERG can encode one transcription factor (TF) existing in ECs and hematopoietic cells (HPCs) under normal conditions. ERG plays a part in the vascular development mediated by the vascular endothelial growth factor (VEGF)/mitogen-activated protein kinase (MAPK) and also regulates new vessel formation [41]. The minor (T) allele of rs2836411 correlates with a greater risk of AAAs in several populations [42].

2.2.4. Inflammation. CD4+T cells are found to accumulate on the aneurysm wall, and AAA-related SNPs are detected in some human genes encoding such critical inflammatory components. AAA patients show an increased circulating IL-6 level. IL-6 is secreted by the aneurysm, and its expression level is related to the aneurysm surface area. Angiotensin II can affect AAAs by acting on the IL-6 signaling pathway in mice.

3. Epigenetic Regulation of AAAs

Epigenetic modifications are induced by developmental or environmental factors. They do not change the genetic code but can regulate the tissue- or context-specific expression of information encoded in DNA [43, 44]. Traditional views hold that epigenetic markers are stable, which may be transmitted to progeny, and control the steady differentiation of different types of cells with significantly diverse gene expression profiles [45]. On the whole, epigenetic alterations are divided into 3 major types: (1) DNA methylation, (2) histone modifications, and (3) ncRNAs. Of them, ncRNAs will not bring about heritable alterations, but they are usually deemed as epigenetic mechanisms due to their vital regulating functions in the genome nonprotein-coding regions. A small number of studies have revealed the important role of the above-mentioned three categories of epigenetic modifications in AAA occurrence [25–27, 40, 46, 47].

3.1. DNA Methylation in AAAs. DNA methylation, one of the potent epigenetic mechanisms, is crucial in preserving the DNA structure, deactivating the X chromosome and maintaining chromosome stability. Besides, DNA methylation also modulates components (retrotransposons and transposons) and regulates gene levels [48]. It is claimed that some key processes contributing to AAA occurrence may be affected by DNA methylation. Generally speaking, DNA methylation is catalyzed by the DNA methyltransferases (DNMTs), including DNMT1 (maintenance enzymes) and DNMT3 (de novo enzymes). Researchers are focusing on DNA methylation in T lymphocyte, and the analysis of different types of vascular cells, such as ECs, SMCs, and adventitial cells, may provide more targets specific to aneurysms [47]. Increasing evidence suggests that T cell dysfunction, especially the reduced suppression of CD4+ CD25+ regulatory T cells, induces AAA occurrence [46]. Apart from DNA hypomethylation, DNA hypermethylation in certain

gene promoter regions also contributes to AAA occurrence. This opinion is addressed in a recent article, which evaluates the global methylation level in AAA patient-derived peripheral blood mononuclear cells (PBMCs) and compares it with that in PBMCs from normal subjects [40]. The study conducted by Skorvanova et al. revealed no association of AAA development with DNA methylation of gelatinases and their tissue inhibitors (e.g., MMP2, TIMP2, TIMP1, and MMP9) [49].

3.2. Histone Acetylation in AAAs. Gene activation and inactivation depend on specific signatures of histone modifications in critical enhancer or promoter gene regions. Such modifications are harbored in histone deacetylases, histone acetylases, together with methyltransferases [50]. The findings of our work show that the abnormal epigenetic modifications in AAAs are the changed expression of lysine [K] histone acetyltransferases (KATs) and related histone acetylation. The above results shed novel lights on the pathogenic mechanism of AAAs [26]. As suggested in another study, the levels of some histone deacetylases (HDACs) in AAA mice and ApoE$^{-/-}$AAA mice infused with Angiotensin (Ang) II are higher than those in normal controls [51]. As a class III HDAC, Sirtuin 1 (SIRT1) is also studied for its role in AAA occurrence and the mechanisms underlying vascular inflammation and aging. The result suggests that SIRT1 in VSMCs provides a new therapeutic target for preventing AAA occurrence [52].

3.3. ncRNAs in AAAs. It has been established that over 97% of the genome can encode the noncoding transcripts, most of which can be processed into short ncRNAs (such as miRNAs) and lncRNAs. There are various factors leading to AAAs, and the pathology and pathogenic mechanisms of AAAs at the molecular level remain largely unclear. Therefore, it will become a novel research direction to investigate the AAA etiology at the epigenetic level. Studies have shown that ncRNAs take part in the AAA genesis. Many ncRNAs are differentially expressed in AAA patients and regulate gene expression at transcriptional and posttranscriptional levels. The regulatory pathways of some ncRNAs have also been confirmed, which is conducive to the study of other molecular mechanisms [27, 53–56].

3.3.1. miRNAs in AAAs. MiRNAs are short (21-23-nt-long) RNA molecules existing in eukaryotes, capable of regulating the expression of other genes [57]. They are ncRNAs and control posttranscriptional expression by specifically binding with mRNAs [58]. In general, negative regulation is mainly achieved by the degradation of mRNAs or inhibition of mRNAs expression. MiRNAs can be regulated by a variety of approaches. A miRNA may possess several target genes, while several miRNAs may modulate the same target gene. MiRNAs adjust target gene expression of one or more genes through forming complicated regulatory networks [59, 60]. MiRNAs are closely associated with the AAA pathogenic mechanism [61]. In AAA patients, miRNAs affect the pathogenesis of AAAs by forming networks to regulate the ECM turnover, MMP family, different inflammatory components, and vascular smooth muscle development [62–65].

The most typical type of miRNAs is miRNA-29 family members, which promote the AAA formation by regulating fibrosis and the ECM. miRNA-29 inhibits the expression of several ECM proteins and antiapoptotic factors in SMCs, thereby boosting the aneurysm generation [66, 67]. Studies have confirmed that AAAs with overexpressed miRNA-29b are more prone to rupture. Reducing the miRNA-29b levels can lower the probability of AAA rupture. Upregulation of miRNA-21 can be detected in AAA patients and mouse models. Overexpressed miRNA-21 can downregulate the phosphatase and tensin homolog (PTEN) levels, thereby inhibiting the viability of SMCs and maintaining vessel wall stability in mouse models with elastin degradation-induced aneurysms [68]. Moreover, Wang et al. have observed that the anti-miRNA-21 drug-eluting stent successfully prevents in-stent myointimal hyperplasia in a humanized rat model, further highlighting the complex roles of miRNA-21 in various vascular pathologies [69]. Furthermore, a decline in miRNA-33 leads to attenuated p38 and JNK (c-Jun N-terminal kinase) signals as a result of increased ABCA1 expression, the inhibition effect of $CaCl_2$ and Ang II-induced aneurysm formation in mice [70]. In conclusion, the expression level of miRNAs is tightly bound to the AAA development. Therefore, it is of great significance to study the pathogenesis of AAAs.

3.3.2. lncRNAs in AAAs. lncRNAs are a type of ncRNAs longer than 200 nt without the protein encoding function, and they are involved in regulating numerous processes [71]. In recent years, many research groups have been devoted to the study of lncRNAs and their pathological function [72]. However, a lot of efforts and in-depth exploration are still required in this field. lncRNAs serve as a gene domain and TF scaffold, guiding the transcription complex of activators and inhibitors to the regulatory region to regulate transcription [73, 74]. One lncRNA associated with the AAA is H19. The H19 level in AAA samples is higher than that in normal controls, and inhibiting the expression of H19 arrests the growth of AAAs [53]. H19 seems to affect the pathogenesis of AAAs through inflammation [55]. Another study has shown that PVT1, an lncRNA, is upregulated in AAA patients. Overexpression of PVT1 promotes apoptosis of VSMCs and degradation of the ECM [75], and PVT1 knockout in vitro notably reduces the incidence of AAAs. It further confirms that PVT1 promotes the formation of AAAs. lncRNAs can also affect AAAs via acting on the development and differentiation of SMCs. The representative example is lnc-Ang362, which enhances the proliferation of VSMCs [76]. Moreover, relevant studies have proven that SMILR can regulate the migration and proliferation of VSMCs, and SMILR knockout restrains the proliferation of SMCs [77], indicating that lncRNAs also play an important part in AAA occurrence and progression. Decreased plasma levels of SMILR have been observed in TAA cases [78].

3.3.3. circRNAs in AAAs. Like lncRNAs, circRNA transcripts have been a recent addition to the functionally relevant ncRNAs in our genomic landscape. They have long been disregarded since their discovery in the 1990s due in part to a limitation in their detection method, but the emerging novel bioinformatics and deep RNA sequencing approaches provide the foundation for circRNA research [79]. Recent studies suggest that there are many endogenous circRNAs in mammalian cells, and some of them show high abundances and evolutionary conservation. circRNAs initially have been shown to mediate miRNA functions (e.g., via sponging) and control important events in transcription (e.g., RNA folding and endonuclease protection) [80]. At present, circRNAs are proven to be stable, endogenous and functional ncRNAs abundant in mammalian cells [81]. They may be generated through directly ligating the $3'$ and $5'$ ends of linear RNAs by means of back-splicing [82]. The downstream $5'$ splice site (donor) will bind to the upstream $3'$ site (acceptor) or serve as the intermediate during RNA processing (Figure 1). Not every circRNA possesses many miRNA binding sites, so it remains controversial whether miRNAs are suppressed by circRNAs.

3.3.4. Bibliometrics of ncRNAs in AAAs. Firstly, we explored the relationship between publication volume and time in Figure 2(a), the abscissa is the time series, and the ordinate is publication volume. The purple dot represents the annual publication volume for publication of circRNAs, corresponding to the right ordinate axis. Meanwhile, the red block represents the annual publication volume of "ncRNAs and AAAs," corresponding to the left ordinate axis. Moreover, green triangle represents the annual publication volume of "circRNAs and AAAs" and also corresponds to left ordinate axis. From 2009 to 2020, the number of papers published on "ncRNAs and AAAs" has increased year by year. There are large quantities of papers on circRNAs, up to more than 2000 papers, but few about the relationship between "circRNAs and AAAs," but they are generally close. The past few years have witnessed an ascending trend (Figure 2(a)).

Then, we also explored the relationship between publication volume and time for ncRNA in Figure 2(b). The cyan dot represents the annual publication volume of circRNAs corresponding to the right ordinate axis, the blue block represents the annual publication volume of miRNAs corresponding to the left ordinate axis, and the orange triangle represents the annual publication volume of lncRNAs corresponding to left ordinate axis. From 2000 to 2020, there are great many papers published on ncRNAs (circRNAs, lncRNAs, and miRNAs) annually, and the total number is still climbing. The miRNA publications account for the largest part of the total number of published papers, up to more than 15000 publications, while circRNA publications take up the smallest share (Figure 2(b)). The above data imply that the relationship between "circRNAs and AAAs" may become a research hotspot and the international research direction in the future.

Keyword analysis is relatively essential to the research of the entire paper. It can help us to figure out the research direction. Figure 3(a) is the tag view of keywords, which reflects the timing of keywords and the relationship network diagram of cluster analysis. The size of the dot indicates the frequency of occurrence, and the colour of the dot represents the cluster and the time of occurrence. The curve describes the interrelationship. The disease formation, target, and
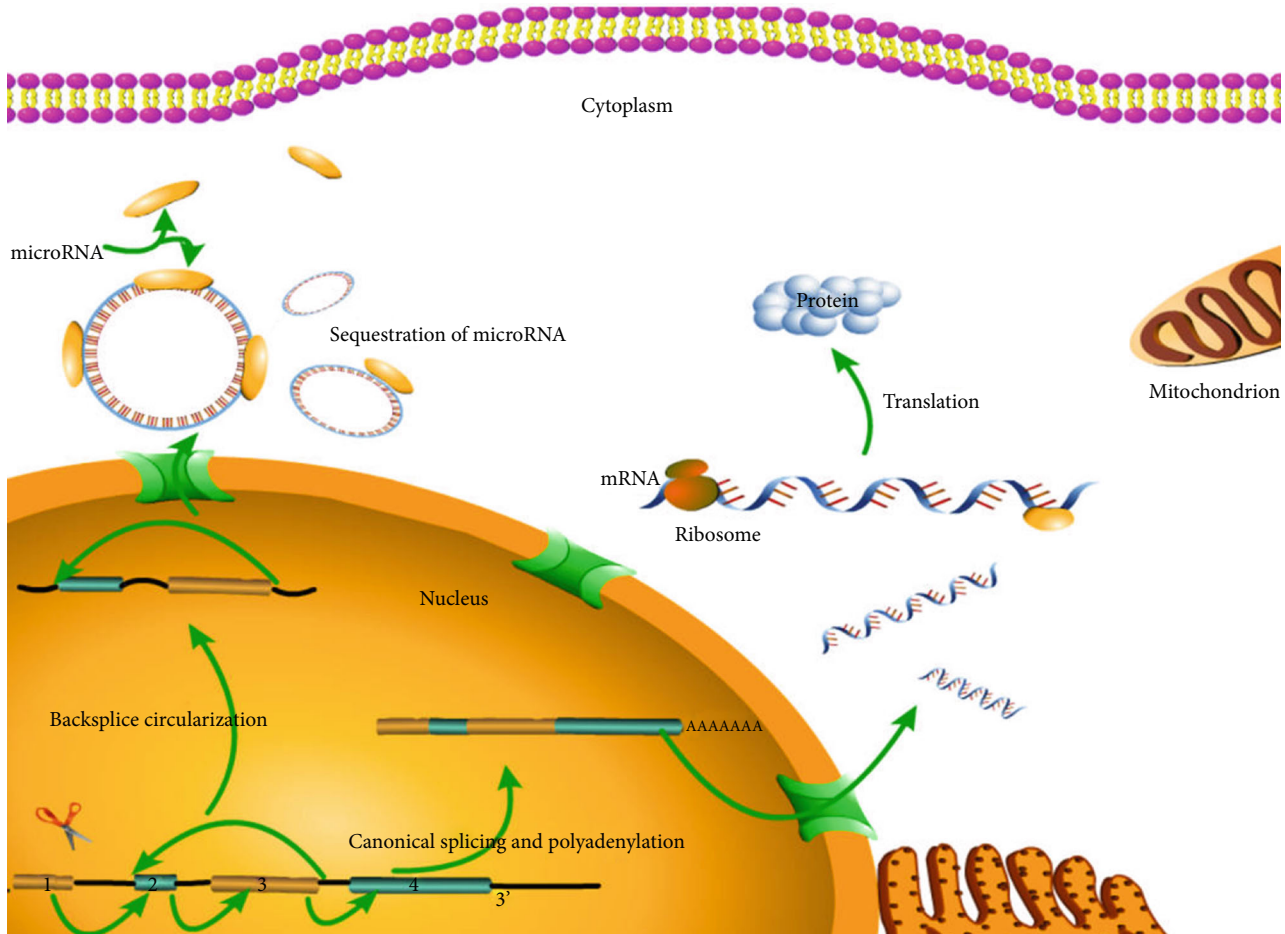
FIGURE 1: Formation and mechanism of RNA in cells. The formation process and mode of action of circRNAs and mRNAs in cells.

regulation mode can be roughly acquired through cluster analysis. It can be seen from the time sequence that lncRNAs, AAAs, and circRNAs are newly emerging keywords in recent years. Figure 3(b) is a timeline view of analyzing keywords from 1996 to 2020.

The classification method is to name the index terms in the search keywords. We can get ten clusters with an order from #0 to #10. The smaller the number # is, the more keywords the cluster contains. Each cluster is composed of multiple closely related words. The largest cluster is "aortic aneurysm" (#0), followed by "abdominal aortic aneurysm formation" (#1). A module clustering value (Q value) greater than >3 generally means a significant clustering structure. In the figure, modularity $Q = 0.684$. Figure 4(a) is a network diagram obtained based on the number of papers published and cooperative relationships in each country, showing the interconnection between countries. The heat map in Figure 4(b) presents the number of national papers published on the world map.

4. Verified circRNAs in AAAs

Data on circRNAs in aneurysms are scarce, but abnormal expression of circRNAs in aneurysms has been observed in emerging studies. However, the functional role(s) of these circRNAs in AAA development in animal models and their therapeutic potential are yet to be elucidated.

4.1. circRNA Microarray Profiling of Human AAAs. Zhou et al. from China observed differential expression of circRNAs in AAA samples and controls, so they subsequently conducted high-throughput sequencing to determine the circRNA expression patterns in four pairs of aortic samples, including four consecutive AAA cases undergoing open surgery and four brain-dead heart-beating organ samples [83]. Finally, a total of 411 differentially expressed circRNAs were detected in AAA samples, including 145 upregulated circRNAs and 266 downregulated circRNAs. Six abnormally expressed circRNAs, namely, hsa_circ_0070382 (AFF1), hsa_circ_0060063 (UQCC1), hsa_circ_0028198 (ANAPC7), hsa_circ_0027446 (HMGA2), hsa_circ_0002168 (TMEM189), and hsa_circ_0005360 (LDLR), were then screened out for RT-PCR analysis. Among the six circRNAs, 2 were upregulated, and 4 were downregulated. According to a population-based genome-wide association study, LDLR is the parental gene of hsa_circ_0005360, and its variant is related to AAAs [84]. Additionally, LDLR-deficient mice infused with Ang II infusion are extensively used as AAA animal models [85–87]. Given the alternative transcription of hsa_circ_0005360 in the LDLR exons, hsa_circ_0005360 possibly plays a vital
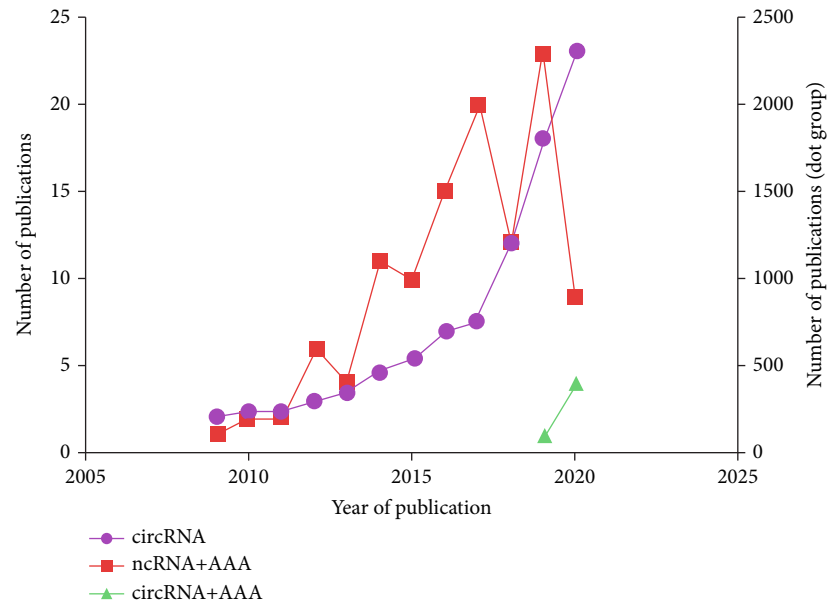
(a)
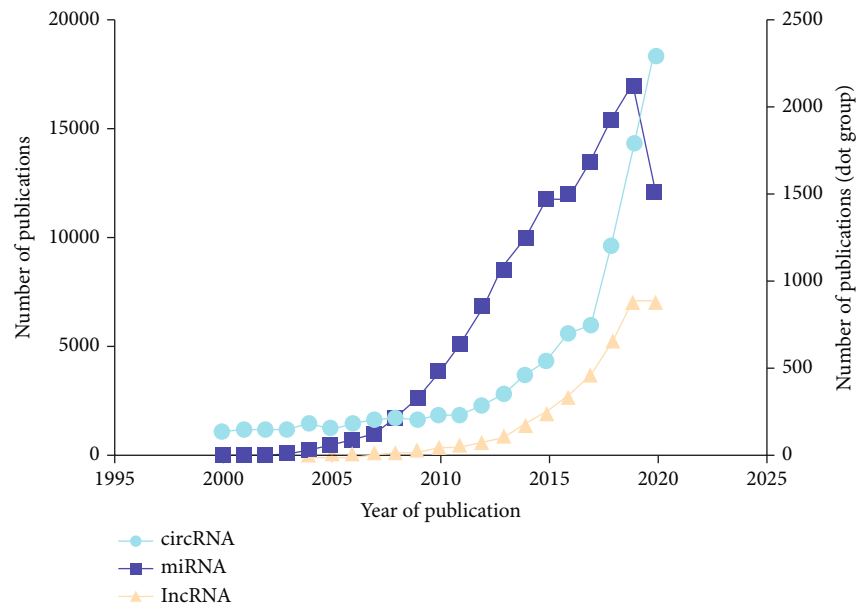
(b)

Figure 2: Statistics of AAA and ncRNA papers published. (a) The relationship between "circRNA, ncRNA, and abdominal aortic aneurysm" and "published volume and year of publication" (b) The relationship between the number of "circRNA, miRNA, mRNA" and "the year of publication".

part in the pathogenic mechanism of AAAs. In the meantime, the interaction networks of circRNAs/miRNAs were also predicted by computational analysis (Table 1).

As indicated in the interaction networks of circRNAs/miRNAs, hsa_circ_0002168 and hsa_circ_0005360 contain one binding site for miR-15a and miR-181b, respectively. It is evident that overexpressed miR-181b in AAA patients downregulates elastin and the MMP-3 tissue inhibitor, thereby promoting AAA development [88]. As for miR-15a, it negatively regulates CDKN2B expression and thereby promotes VSMC apoptosis, possibly resulting in AAA path-

ogenesis [89]. Nonetheless, the hsa_circ_0002168/miR-15a and hsa_circ_0005360/miR-181b axes should be further validated in AAAs by more studies (Figure 5).

4.2. circRNA Microarray Profiling of Mouse AAAs Induced by Ang II. Wang et al. collected two samples from each of the AAA and control groups and analyzed the circRNA expression profiles. The AAA samples of C57BL/6J male mice were treated with Ang II and 3,4-benzopyrene (BAP), and the circRNA expression in these AAA samples was compared with that in the control group [90]. The qRT-PCR results showed

(a)

(b)
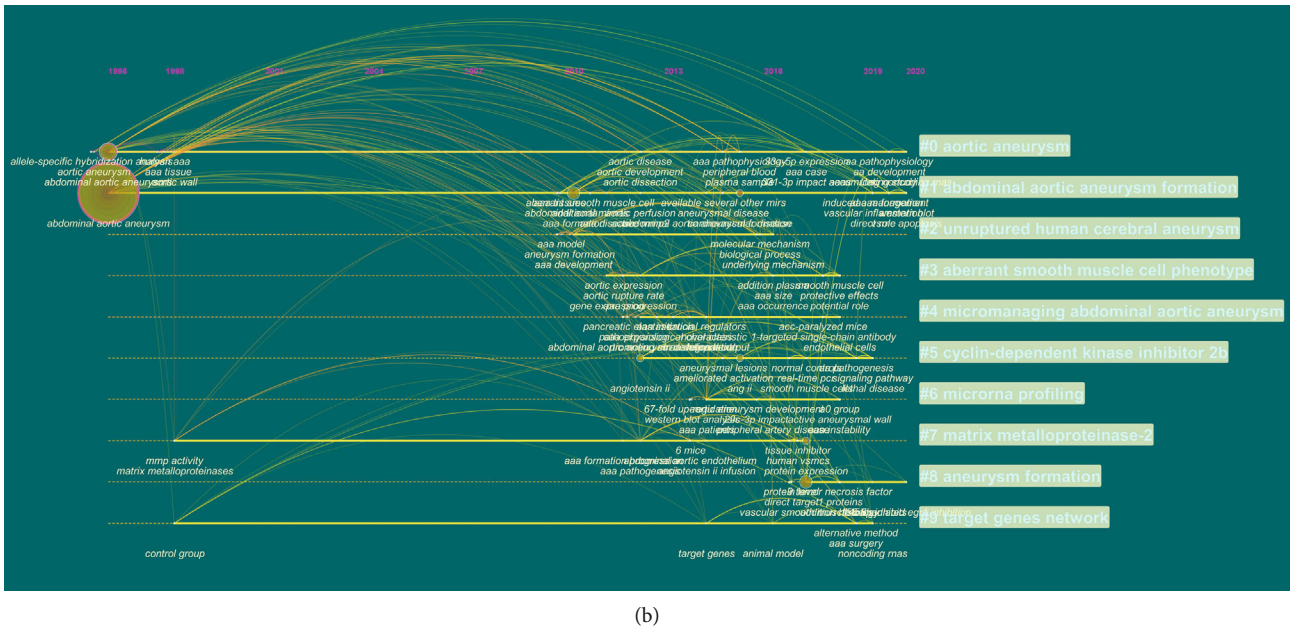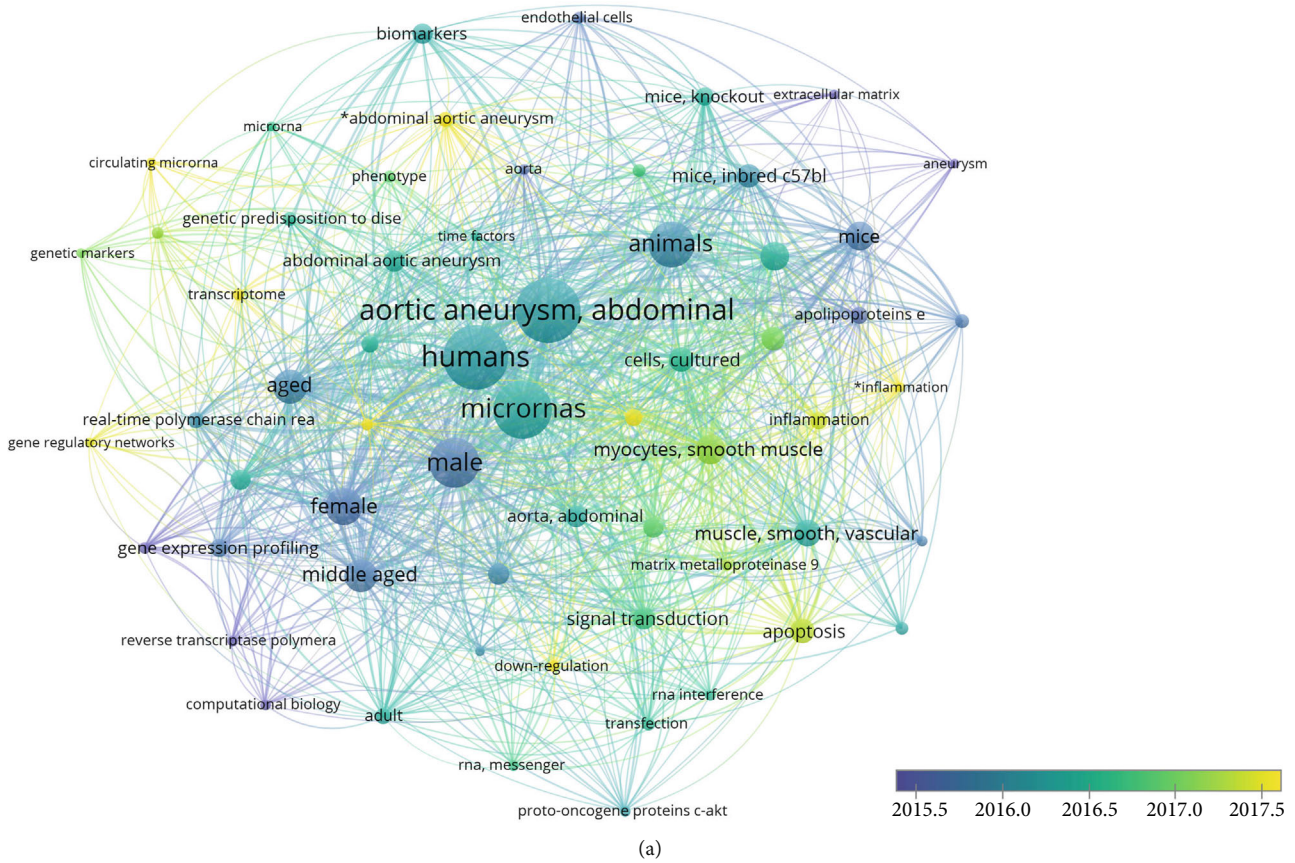
FIGURE 3: Bibliometric analysis of keywords. Keyword cluster analysis, visual analysis based on the year when the keyword appears, so as to make (a) network drawing and (b) timeline graph production.

that 271 circRNAs showed upregulation while 142 circRNAs were downregulated (Table 1). After predicting the related regulatory pathway, the authors mapped the downregulated mRNAs into 7 pathways, including apoptosis. It should be noted that apoptosis is well-received as a critical biological process of VSMCs in AAAs, and VSMC apoptosis can also

be detected in AAAs induced by Bap/Ang II. In line with the above results, Wang et al. examined the competitive endogenous RNA (ceRNA) mechanism related to certain apoptotic circRNAs. For instance, two miRNAs (mmu-let-7a-2-3p and mmu-miR-199a-3p) of differentially expressed mmu_circRNA_001265 and their response elements were
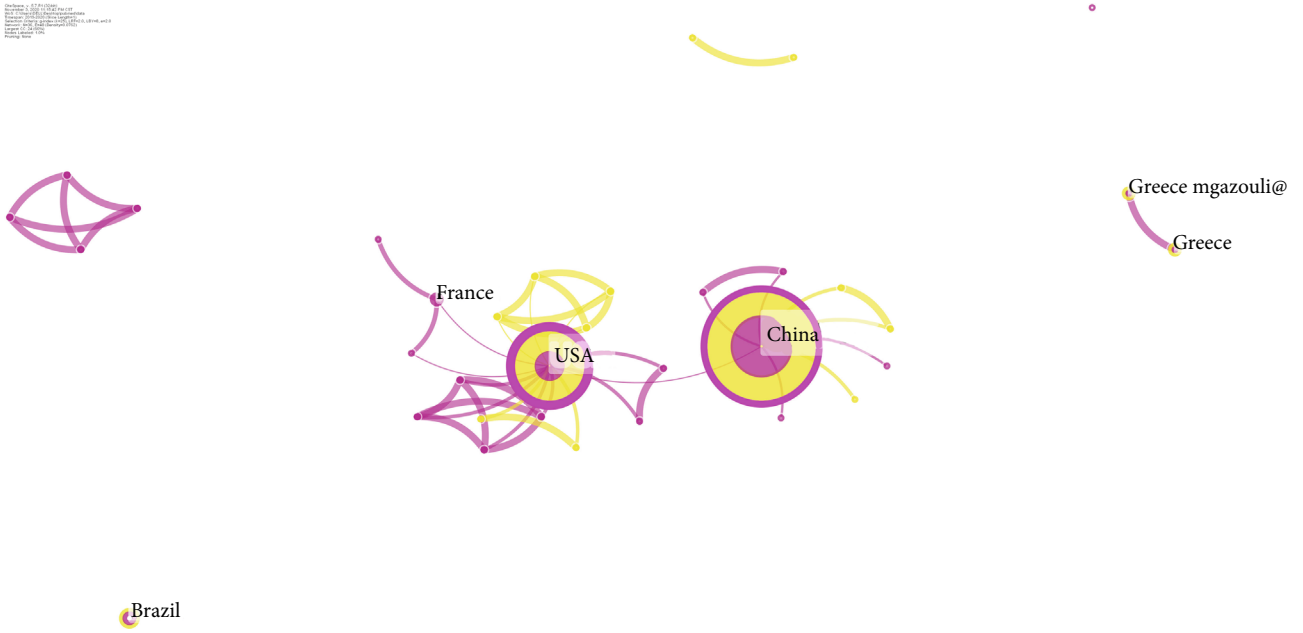
(a)
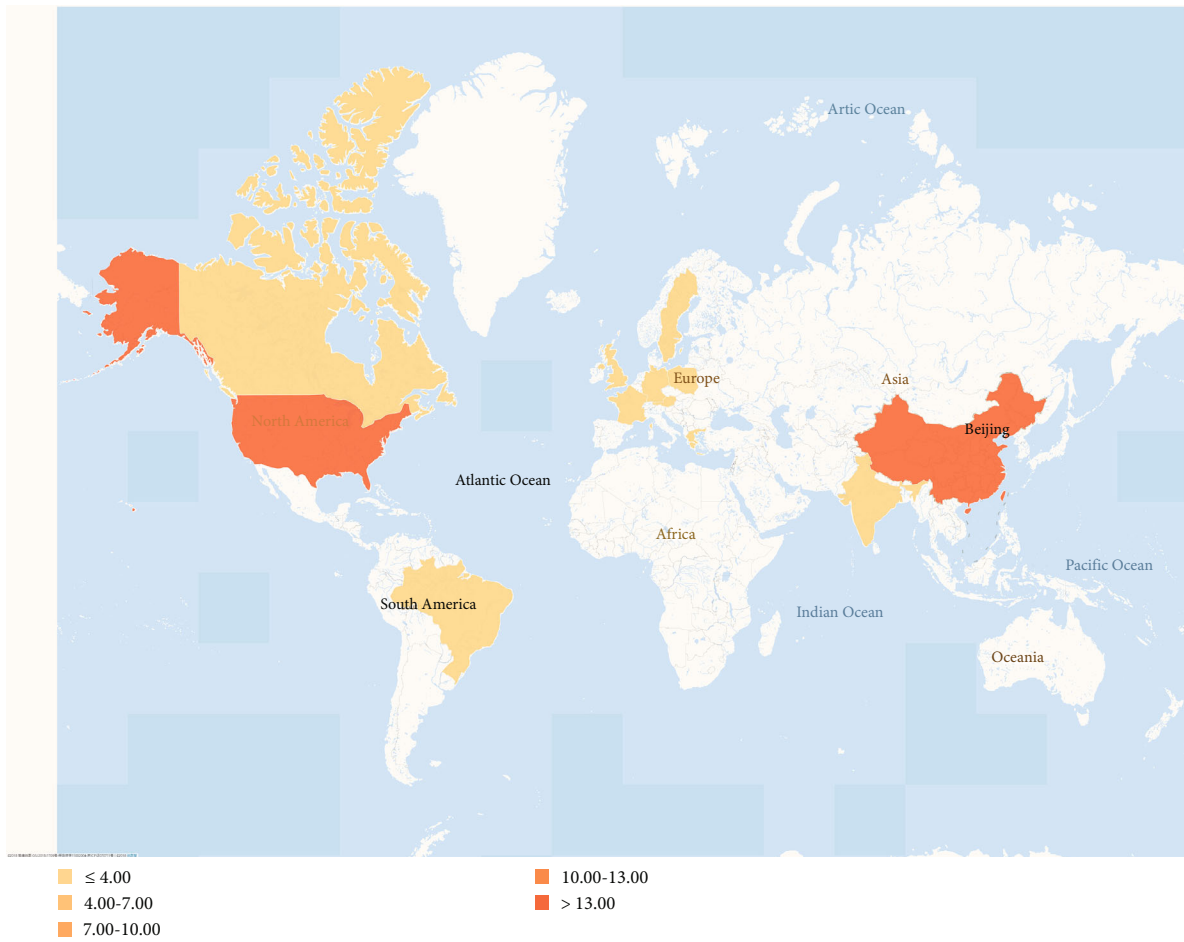
(b)

FIGURE 4: The analysis of total country output based on ncRNA research. (a) Network map of countries/regions engaged in ncRNA research (b) World map of total country output engaged in ncRNA research.

Table 1: Verified circRNAs in AAAs.

	circRNA	Gene symbol	Regulation	Pathway	Cell type	Function	Ref
Homo sapiens	hsa_circ_0002168	TMEM189	Down	hsa-miR-298, hsa-miR-503b-5p, hsa-miR-296b-3p, hsa-miR-612, hsa-miR-15a-3p, hsa-miR-15a, hsa-miR-670-3p	circRNA microarray analysis of AAA tissue and healthy aorta tissue	N/A	83
	hsa_circ_0005360	LDLR	Down	hsa-miR-181b, hsa-miR-671-5p, hsa-miR-616-3p, hsa-miR-135b-3p, hsa-miR-186-5p	circRNA microarray analysis of AAA tissue and healthy aorta tissue	N/A	83
	hsa_circ_0060063	UQCC1	Up	hsa-miR-223-3p, hsa-miR-541-5p, hsa-miR-145b-3p, hsa-miR-137	circRNA microarray analysis of AAA tissue and healthy aorta tissue	N/A	83
	hsa_circ_0070382	AFF1	Up	hsa-miR-432-3p, hsa-miR-890, hsa-miR-135b-3p, hsa-miR-24-3p, hsa-miR-6882-3p, hsa-miR-129-5p	circRNA microarray analysis of AAA tissue and healthy aorta tissue	N/A	83
	hsa_circ_0027446	HMGA2	Up	hsa-miR-331-3p, hsa-miR-1236-3p, hsa-miR-3925-3p, hsa-miR-493-3p	circRNA microarray analysis of AAA tissue and healthy aorta tissue	N/A	83
	hsa_circ_0028198	ANAPC7	Up	hsa-miR-153-5p, hsa-miR-7-5p, hsa-miR-205-3p	circRNA microarray analysis of AAA tissue and healthy aorta tissue	Expression of ASPH and PDE3B may be regulated by hsa_circ_0028198,	83
	hsa_circ_CCDC66	CCDC66	Up	*hsa-miR-342-3p	SMC	VSMC growth and apoptosis	91
	hsa_circ_CBFB	CBFB	Up	*hsa-miR-28-5p/GRIA4/LYPD3 axis	VSMC	VSMC apoptosis and growth	92
	hsa_circ_CDR1as	CDR1as	Down	*hsa-miRNA-7/CKAP4 axis	AAA and VSMC	VSMC apoptosis and growth	94
	has_circ_000595	N/A	Up	*hsa-miRNA-19a			95

Table 1: Continued.

circRNA	Gene symbol	Regulation	Pathway	Cell type	Function	Ref
mmu_circ_29892	Pros1	Up	mmu-miR-212-5p mmu-miR-7033-3p	circRNA microarray analysis of Ang II-induced in mice	N/A	90
mmu_circ_45403	Wdr44	Up	mmu-miR-23b-3p mmu-miR-6947-3p mmu-miR-541-5p mmu-miR-7235-3p mmu-miR-141-5p	circRNA microarray analysis of Ang II-induced in mice	N/A	90
mmu_circ_40388	Kdm3a	Up	mmu-miR-7026-3p mmu-miR-301a-5p mmu-miR-92a-2-5p mmu-miR-6922-3p mmu-miR-3078-3p	circRNA microarray analysis of Ang II-induced in mice	N/A	90
Mus musculus mmu_circ_27294	Ccdc66	Up	mmu-let-7c-1-3p mmu-miR-500-5p mmu-miR-19b-2-5p mmu-miR-7092-3p mmu-miR-6946-3p	circRNA microarray analysis of Ang II-induced in mice	N/A	90
mmu_circ_001265	Chordc1	Down	mmu-miR-7094b-2-5p mmu-miR-7578 mmu-miR-26a-2-3p mmu-miR-107-5p mmu-miR-103-1-5p	circRNA microarray analysis of Ang II-induced in mice	N/A	90
mmu_circ_018331	Hivep1	Down	mmu-miR-103-2-5p mmu-let-7a-2-3p mmu-miR-199b-3p mmu-miR-149-5p mmu-miR-204-5p	circRNA microarray analysis of Ang II-induced in mice	N/A	90
mmu_circ_40599	Frmd4b	Down	mmu-miR-30b-3p mmu-miR-7679-5p mmu-miR-5620-5p mmu-miR-337-3p mmu-miR-320-5p mmu-miR-7079-5p mmu-miR-215-3p mmu-miR-7021-3p	circRNA microarray analysis of Ang II-induced in mice	N/A	90
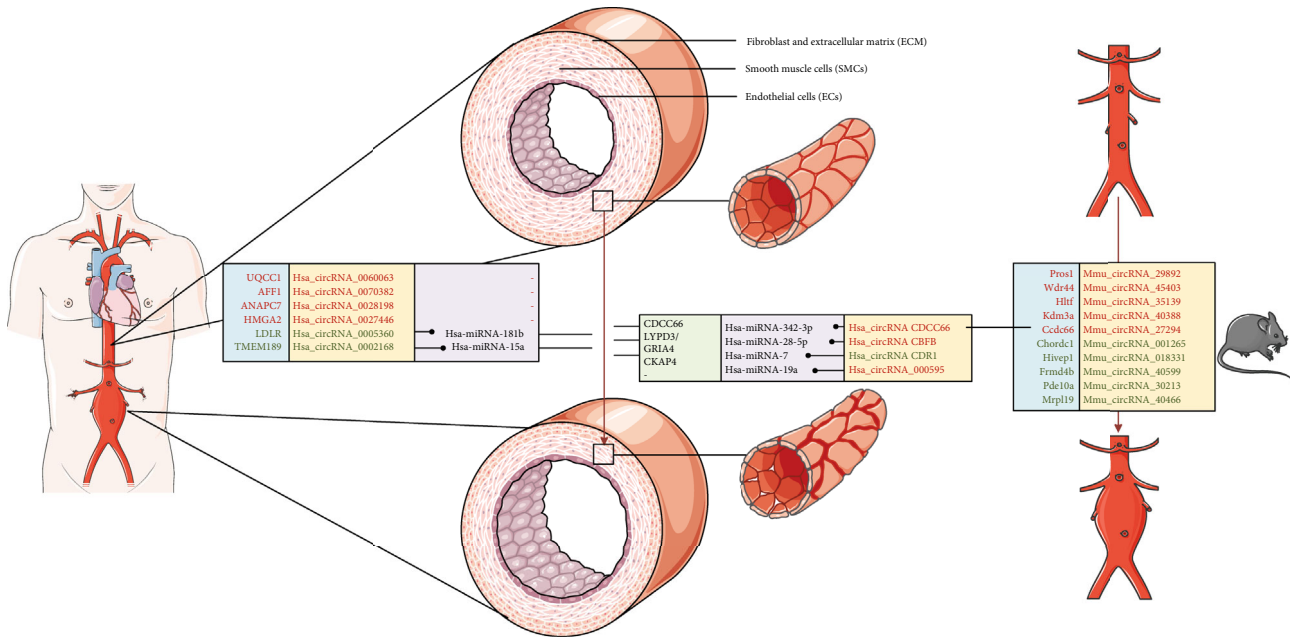
FIGURE 5: Several circRNA mediated signaling pathways in AAA. In human and mouse abdominal aortic aneurysms, the plan view of the abdominal aorta and several circRNA mediated signal pathways.

predicted. Another study suggests that lncRNA H19 causes aneurysms partially through endogenously competing with let-7a miRNA for inducing transcription of the target gene (IL-6) [55].

4.3. Examples of Several circRNA-Guided Signaling Pathways in AAAs

4.3.1. circRNA CCDC66. To prove the role of circRNA CCDC66 in the pathogenesis of AAAs and identify its corresponding pathway, Yang et al. carried out a study and found that circCCDC66 played a role in the proliferation of VSMCs [91]. Through further investigation, they discovered that circCCDC66 promoted the expression of CCDC66, and CCDC66 suppression had the same effect as circCCDC66 deletion on the development and apoptosis of VSMCs. Moreover, the RNA pull-down test results suggested that the content of circCCDC66 and CCDC66 was the highest in the miR-342-3p group, indicating that circCCDC66 influenced CCDC66 through miR-342-3p. Taken together, it is concluded that overexpression of CCDC66 causes AAAs through the circCCDC66/miR-342-3p/CCDC66 pathway (Figure 5).

4.3.2. circRNA CBFB. Findings of this study reveal that miR-28-5p, circCBFB, GRIA4, and LYPD3 are involved in AAAs. circCBFB serves as the miR-28-5p sponge, capable of regulating the proliferation and apoptosis of VSMCs in a LYPD3/GRIA4-dependent manner [92]. With regard to the relationship between circCBFB and AAAs, it is established previously that the expression of miR-28-5p increases in AAAs. As reported by Yue et al., miR-28-5p promotes VSMC apoptosis and suppresses their proliferation, thereby contributing to AAA occurrence [92]. Moreover, bioinformatic

analysis verifies LYPD3 and GRIA4 as the potential miR-28-5p target genes. The mechanical experiments of this study suggest that miR-28-5p targets GRIA4 and LYPD3 and restrains their expression in VSMCs. Additionally, functional analysis proves that GRIA4 and LYPD3 deficiency promotes the apoptosis of VSMCs. More innovative strategies are required to identify the role of the circCBFB molecule in AAAs. Based on the above analysis, it can be concluded that circCBFB induces cell apoptosis and AAA formation through the circCBFB/miR-28-5p/GRIA4/LYPD3 pathway (Figure 5).

4.3.3. circRNA CDR1. There are over 70 miR-7 binding sites in the cerebellar degeneration-related protein 1 antisense RNA (CDR1as), and these sites regulate the effect of CDR1as on the target gene expression [93]. According to recent research, the expression levels of CDR1as and CKAP4 (the estimated miR-7 target) are lower in AAA cases than those in normal controls [94]. Zhao et al. suggested that the CDR1as/miR-7/CKAP4 axis plays a role in VSMCs of AAA cases and that CDR1as upregulation may curb the expression of miR-7. What is more, CDR1as upregulation enhances the CKAP4 level, promotes VSMC proliferation, and suppresses VSMC apoptosis, thereby resulting in VSMC remodeling along with AAA progression. Such novel mechanism offers insights into AAA treatment approaches (Figure 5).

4.3.4. Hsa_circ_000595. Through screening circRNAs in tissue specimens from AAA patients, Zheng et al. observed increased expression of hsa-circ-000595 in diseased specimens [95]. A similar pattern was found in hypoxic aortic SMCs, and the knockdown of hsa-circ-000595 reduced SMC apoptosis. Besides, they also found that miR-19a might serve as a potential downstream target of hsa-circ-000595. Hsa-circ-000595 on the chromosome 14 can modulate the
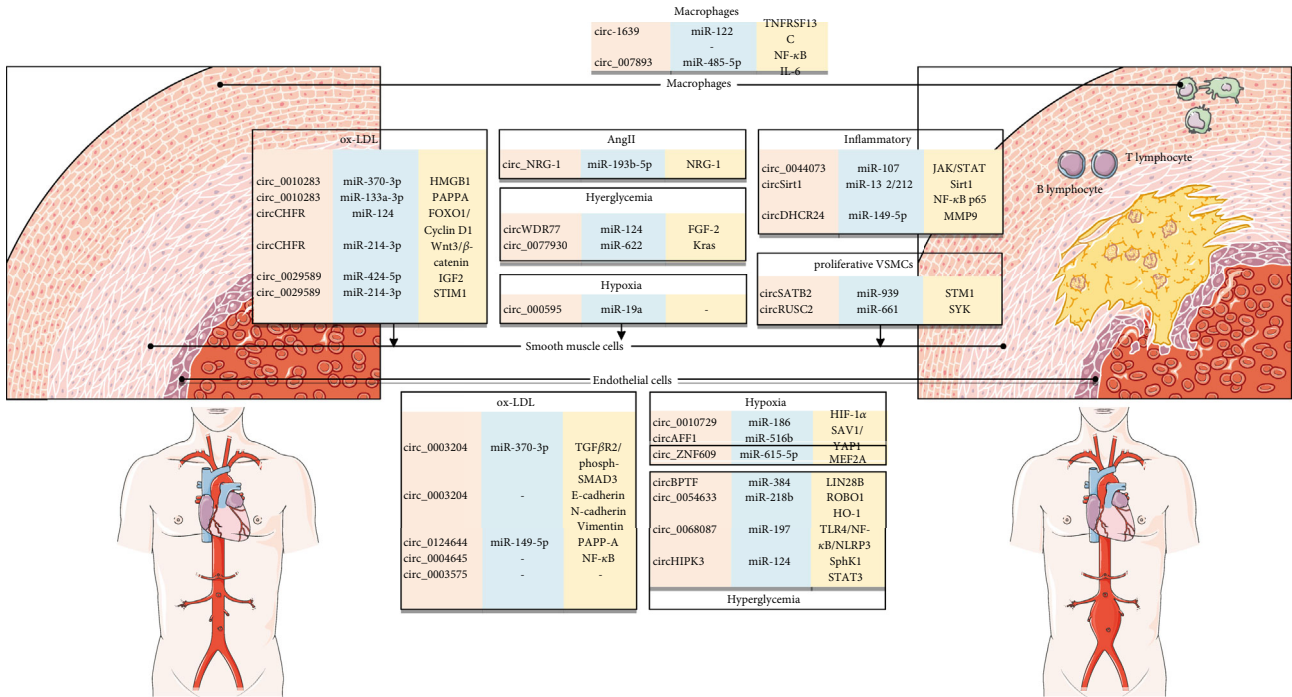
FIGURE 6: Potential ncRNA in a variety of cells in AAA tissue. Examples of several ncRNAs that may lead to the formation of AAA in macrophages, smooth muscle cells, and endothelial cells include circRNAs, miRNAs, and mRNAs.

miR-19a activity and acts on AAAs through suppressing cell apoptosis [95].

5. Potential circRNAs in AAAs

At present, the pathogenic mechanism of AAAs is mainly explored through studying aortic tissue from AAA patients undergoing open surgery. Several subtypes of vascular cells (including SMCs, ECs, and adventitial cells) are involved in AAA genesis [20] (Figure 6).

Disordered ECs may induce adventitia and media inflammation [96]. The chronic inflammatory reaction induced by T cells [97] triggers MMP- and macrophage-mediated proteolytic remodeling, finally weakening the ECM structure. Such process is related to elastic fiber loss, collagen fiber structural alterations, and new vessel formation (angiogenesis). Generally speaking, inflammation is a vital contributor to aneurysm occurrence and development. Infiltrating leukocytes and macrophages are the main proteinase sources. The transformation of VSMCs from the contractile/-differentiated phenotype to the synthetic/dedifferentiated phenotype correlates with AAA occurrence [98]. VSMCs constitute the principal part of the aortic wall. They proliferate and dedifferentiate to trigger different signaling cascades, which in turn stimulate proliferation, dedifferentiation, apoptosis, and migration of VSMCs.

However, these physiological characteristics facilitate the formation of vulnerable atherosclerotic plaques in the aneurysmal wall, which illustrates that AS is a vital risk factor for AAAs [99]. Age, smoking, and the genetic background are common and the most potent factors leading to these two disorders [100]. Therefore, these processes are at least partly regulated by circRNAs. We aim to speculate the potential relationship of circRNAs with ECs and SMCs in AAAs.

5.1. circRNAs and ECs in AAAs. Numerous pathophysiological stimuli can result in EC disorders in AAAs, including hypoxia [101], advanced glycation end products (AGEs) [102], reactive oxygen species (ROS) [103], oxidized low-density lipoproteins (ox-LDLs) [104], and proinflammatory cytokines [105] (Table 2).

A study has revealed the potential role of hypoxia-mediated new vessel formation in the pathogenic mechanism of AAAs [106]. Dang et al. examined the expression patterns of circRNAs in hypoxia-stressed human umbilical vein endothelial cells (HUVECs) and detected the notable upregulation of hsa_circ_0010729. They also found that hsa_circ_0010729 deletion inhibited cell migration and proliferation, but promoted cell apoptosis through targeting the miR-186/HIF-1α axis [107]. Recent evidence suggests that the hypoxia-induced circAFF1 can lead to disordered vascular ECs through triggering SAV1/YAP1. From the mechanical perspective, the circAFF1/miR-516b/SAV1/YAP1 axis partially contributes to vascular endothelium dysfunction, and it may be used as an indicator of hypoxia injury-induced vascular diseases [108]. Furthermore, significantly upregulated cZNF609 was observed by Liu et al. in HUVECs exposed to hypoxia and HG environments. As claimed by some researchers, the silencing of cZNF609 prevents EC apoptosis but stimulates tube formation and migration of ECs, demonstrating that cZNF609 can promote the apoptosis of stress-challenged ECs. Mechanically, cZNF609 acts as a ceRNA, which upregulates the expression of myocyte enhancer factor 2A (MEF2A) through separating and suppressing miR-615-

TABLE 2: CircRNAs causing EC disorder in AAAs.

circRNA	Cell type	Inducing factor	Expression	Pathway	Function	Ref
circ_0003204	HAEC	ox-LDL	Up	miR-370-3p/TGFβR2/ phosph-SMAD3	Inhibited viability, migration, proliferation, and tube formation	121
circ_0124644	HUVECs	ox-LDL	Up	miR-149-5p/PAPP-A	Inhibited apoptosis	123
circ_0003645	HUVECs	ox-LDL	Up	NF-κB	Promoted inflammatory response and promoted the production of adhesion molecules	124
hsa_circ_0003575	HUVECs	ox-LDL	Down	—	Promoted apoptosis, inhibited proliferation and angiogenesis	116
circ_0003204	HUVECs	ox-LDL	Down	—	Inhibited the proliferation, migration, and invasion, promoted apoptosis	122
circHIPK3	HUVECs+HAECs	HG	Down	miR-124S/phK1 and STAT3	Inhibited apoptosis	116
circ-0054633	HUVECs	HG	Up	miR-218/roundabout1 miR-218/heme oxygenase-1	Promoted proliferation and migration, inhibited apoptosis	115
hsa_circ_0068087	HUVECs	HG	Up	mi-197/TLR4/ NF-κB/NLRP3	Promoted inflammation and dysfunction	114
circBPTF	HUVEC	HG	Up	miR-384/LIN28B	Promoted apoptosis, the release of proinflammatory cytokines and oxidative stress	113
hsa_circ_0010729	HUVECs	Hypoxic	Up	miR-186/HIF-1α	Promoted proliferation and migration; inhibited apoptosis	107
circAFF1	HUV-EC-C and HBEC-5i	Hypoxic	Up	miR-516b/SAV1/YAP1	Inhibited the proliferation, tube formation, and migration of vascular endothelial cells	108
circ-ZNF609	HUVECs	Hypoxic+HG	Up	miR-615-5p/MEF2A	Promoted apoptosis, inhibited migration and tube formation	109

5p [109]. According to the above research results, circRNAs regulate EC phenotypes in the hypoxic environment.

High glucose (HG) affects the formation and development of AAAs [110, 111] through enhancing ROS generation [112] and AGE synthesis. In HG-stimulated EC models, circRNAs regulate the phenotypes of ECs. circBPTF is under tight regulation within the HG-challenged HUVECs, and circBPTF deletion prevents the HG-mediated OS and inflammatory injuries through regulating the miR-384/LIN28B axis [113]. In addition, the expression of hsa_circ_0068087 also increases within the HG-challenged HUVECs, and hsa_circ_0068087 deletion attenuates the inflammation and angiogenic disorder in HG-challenged HUVECs through pathways like pyrin domain-containing protein 3 (NLRP3) inflammasome, LRR, and toll-like receptor 4 (TLR4)/NF-κB/NOD as the miR-197 sponge [114]. Previous evidence demonstrates that the expression of hsa_circ_0054633 increases in HG-challenged HUVECs. Downregulating the hsa_circ_0054633 expression blocks HUVEC proliferation, angiogenesis, and migration, but boosts HUVEC apoptosis via the heme oxygenase-1 (HO-1) and miRNA-218/round-about-1 (ROBO1) axes [115]. In addition, the HG-induced circHIPK3 downregulation enables miR-124 to accumulate in human aortic endothelial cells (HAECs) and HUVECs. From the mechanical perspective, circHIPK3 silencing enhances the HG-mediated apoptosis via the miR-124/sphingosine kinase 1 (SphK1)/signal transducer and activator of transcription 3 (STAT3) axis [116].

OxLDLs affect the O2•- concentration in several ways. Increasing the O2•- concentration causes the NOS to dephosphorize to produce O2• [117, 118], inhibits dismutase activities, and curbs O2•- reduction to H_2O_2. OxLDLs promote inflammatory cell infiltration into the aortic wall through enhancing the activities of MMP2 [119], chemokines, and adhesion particles [120]. Research has found circ_0003204 is mostly located in the cytoplasm of HAECs, and its expression increases in ox-LDL-challenged HAECs. Overexpressed circ_0003204 restrains the proliferation, tube formation, and migration of ox-LDL-challenged HAECs. Mechanically, circ_0003204 acts as the miR-370 sponge, which increases the protein levels of transforming growth factor (TGF) βR2 and the corresponding downstream phosph-SMAD3 [121]. A recent study focusing on circ_0003204 underlines the vital role of hsa_circ_0003204 in HUVEC proliferation and new vessel formation. Besides, hsa_circ_0003204 deletion evidently downregulates the expression of E-cadherin and upregulates the expression of vimentin and N-cadherin in oxLDL-challenged HUVECs [122]. Wang et al. have noticed that circ_0124644 alleviates the endothelial injuries in ox-LDL-challenged HUVECs through the miR-149-5p/PAPP-A axis [123]. It is also shown that circ_0003645 deletion mitigates the apoptosis and inflammation in oxLDL-challenged ECs [124].

5.2. circRNAs and SMCs in AAAs. VSMC phenotypic transformation within AAAs is ascribed to pathophysiological

TABLE 3: CircRNAs causing VSMC disorder in AAAs.

circRNA	Cell type	Inducing factor	Expression	Pathway	Function	Ref
circ_0010283	VSMCs	ox-LDL	Up	miR-370-3p/HMGB1	Promoted VSMC viability and migration, and proliferating cell nuclear antigen	125
	HVSMCs	ox-LDL	Up	miR-133a-3p/PAPPA	Promoted VSMC proliferation, migration and invasion	126
circCHFR	VSMCs	ox-LDL	Up	miR-370/FOXO1/Cyclin D1	Promoted proliferation and migration ability of VSMCs	127
	VSMCs	ox-LDL	Up	miR-214-3p/Wnt3/β-catenin	Promoted cell growth, migration, and inflammation	128
circ_0029589	VSMCs	ox-LDL	Up	miR-424-5p/IGF2	Promoted proliferation, migration, and invasion	129
	VSMCs	ox-LDL	Up	miR-214-3p and STIM1	Promoted proliferation, migration, and invasion	130
circNRG-1	MASMCs	Ang II	Down	miR-193b-5p/NRG-1	Promoted apoptosis	131
circWDR77	VSMCs	HG	Up	miR-124/FGF-2	Promoted migration and proliferation	
circ_0077930	HUVEC-Exos>VSMCs	HG	—	miR-622-Kras	Induce cellular senescence in VSMCs	132
circ_0044073	HUVEC	LPS	Down	miR-107/JAK/STAT	Promoted the proliferation and invasion	133
	HUVSMCs		Up			
circ-Sirt1	VSMCs	TNF-α	Down	miR-132/212/SIRT1	Inhibited inflammation	134
circDHCR24	HA-VSMC	PDGF-BB	Up	miR-149-5p/MMP9	Promoted proliferation, migration, and phenotypic switch	135
circ-SATB2	Proliferative VSMCs	N/A	Up	miR-939/STM1	Promoted migration, proliferation; inhibited apoptosis	136
circ-RUSC2	Proliferative VSMCs	N/A	Up	miR-661/SYK	Promoted migration, proliferation; inhibited apoptosis	137
circACTA2	HASMCs	N/A	Up	NRG-1/circACTA2/miR-548f-5p	Promoted contraction	

incentives as diverse as ox-LDLs, Ang II, proinflammatory factors, and hyperglycemia (Table 3).

The circ_0010283 level in ox LDL-challenged VSMCs is remarkably higher than that in control VSMCs. The circ_0010283 target is miR-370-3p, which targets HMGB1. As a result, circ_0010283 modulates the level of HMGB1 through miR-370-3p [125]. The high serum expression of circ_0010283 in AS cases and human VSMCs treated with ox-LDLs is confirmed by Feng et al., who report that circ_0010283 modulates the PAPPA level through regulating miR-133a-3p [126]. Similarly, the abnormal expression of circCHFR is also detected in ox-LDL-treated VSMCs. In addition, the circCHFR/miR-370/FOXO1/Cyclin D1 axis is found to play a key role in SMCs, which increases our knowledge of circRNAs in SMCs [127]. As revealed by a study, circCHFR is upregulated in serum of atherosclerosis patients and ox-LDL-stimulated VSMCs. circCHFR controls cell growth, migration, and inflammation via regulating the expression of Wnt3 as a ceRNA of miR-214 in ox-LDL-treated VSMCs [128]. In the study of Yu et al., increased circ_0029589 levels and decreased miR-424-5p levels in ox-LDL-challenged VSMCs demonstrate that circ_0029589 regulates VSMC proliferation and migration possibly via miR-424-5p/IGF2 [129]. Correspondingly, circ_0029589 deletion

suppresses the proliferation, invasion, and migration of ox-LDL-challenged VSMCs through modulating STIM1 and miR-214-3p [130].

Ang II has been suggested to enhance VSMC proliferation in the process of vascular remodeling and play a vital part in AAA formation. According to circRNA microarray analysis, mmu-circRNA-42742 is conspicuously downregulated in Ang II-treated mouse aortic smooth muscle cells (MASMCs). The parental gene of mmu-circRNA-42742 is NRG-1, which modulates vascular remodeling via the ErbB signal transduction pathway. Besides, the circNRG-1/miR-193b-5p/NRG-1 axis can be potentially used as the Ang II target for inhibiting VSMC apoptosis and facilitating vascular remodeling [131].

The analysis of circRNA expression in the HG-induced VSMCs shows that circWDR77 is upregulated. The predicted results are miR-124 and fibroblast growth factor 2 (FGF-2), whose interaction is verified by the RNA pull-down experiment and luciferase reporter gene assay. More importantly, Wang et al. found that exosomes from HG-induced HUVECs caused VSMC senescence via the circRNA-0077930/miR622/Kras ceRNA axis, while exosomes with circRNA-0077930 depletion had no implications for VSMC senescence [132].

Furthermore, Zheng et al. noticed the upregulation of hsa_circ_000595 in the hypoxia-induced human aortic smooth muscle cells (HASMCs). They concluded that hsa_circ_000595 silencing acted as the miR-19a sponge to suppress cell apoptosis [95].

AAAs are a type of chronic inflammatory disorders, so the in vitro AS model can be constructed by inflammatory stimulation. circRNA-0044073 is upregulated in the LPS-treated human umbilical vein smooth muscle cells (HUVSMCs) but downregulated in LPS-treated HUVECs. Further exploration indicates that circRNA-0044073 overexpression evidently promotes HUVSMC and HUVEC proliferation and invasion through the miR-107/Janus kinase (JAK)/STAT signal transduction pathway [133]. As demonstrated by Kong et al., the circ-Sirt1 expression level is distinctly downregulated in TNF-α-treated VSMCs, and circ-Sirt1 overexpression impedes the NF-κB p65 nuclear translocation and lowers the levels of adhesion molecules and proinflammatory cytokines (particularly VCAM-1, MCP-1, and ICAM-1) [134]. Moreover, they have also discovered that circ-Sirt1 prevents the transcription and acetylation of NF-κB p65 induced by TNF-α through reversing the inhibition effect of miR-132/212 on SIRT1. The study results of Kong et al. suggest that circ-Sirt1 may mitigate the NF-κB p65-induced inflammation via direct and indirect approaches. After treating the human aortic vascular smooth muscle cells (HA-VSMCs) with PDGF-BB, Peng et al. found that circDHCR24 deletion served as the miR-149-5p sponge and diminished the cell proliferation [135].

Additionally, the levels of circ_RUSC2 and circ_SATB2 decrease within the proliferating VSMCs. It is disclosed by Mao et al. that circ-SATB2 promotes STIM1, which can be explained by the role of miR-939 in proliferative VSMCs. Mechanically, circ-SATB2 overexpression inhibits the expression of contractile VSMC marker SM22a, while miR-939 promotes its expression, indicating an association between circ-SATB2 and VSMC phenotypic differentiation [136]. circ_RUSC2 is reported to enhance the proliferation, migration, and phenotypic regulation of VSMCs, but suppress their apoptosis through the miR-661/spleen-associated tyrosine kinase (SYK) signal transduction pathway [137].

5.3. circRNAs and Macrophages in AAAs.
CircRNAs are proven to be essential for the modulation of macrophages. Studies have shown that in LPS-induced macrophages Raw264.7, circ_1639 promotes the proinflammatory response in Raw264.7 cells. The study of Lu et al. demonstrates that circ_1639 expression is tremendously upregulated in LPS-treated Raw264.7 cells. The level of p-P65 increases in circ_1639 mock-transfected cells, but declines in cells transfected with circ_1639 inhibitor plasmid. Therefore, circ_1639 regulates inflammatory response through the NF-κB signaling pathway. When Raw264.7 cells are transfected with the circ_1639 mimic, the level of miR-122 gene is significantly reduced, while the expression of its target gene TNFRSF13C increases. Hence, it can be concluded that in Raw264.7 cells, circ_1639 affects the inflammatory response through the miR-122/TNFRSF13C regulatory axis [138].

In Raw264.7 macrophages stimulated by the calcitonin gene-related peptide (CGRP), increased expression of mmu_circRNA_007893 and decreased expression of miR-485-5p are detected. The coimmunoprecipitation reaction further confirms the interaction among mmu_circRNA_007893, miR-485-5p, and IL-6. In Raw264.7 cells, the mmu_circRNA_007893/miR-485-5p/IL-6 regulatory pathway regulates the inflammatory response by controlling the expression of the cytokine IL-6 and ultimately affects the cell function [139].

The above results indicate that the function of macrophages can be affected by the expression level of the circRNA regulatory axis, such as the proinflammatory cytokines (e.g., TNF-α and IL-6) and anti-inflammatory cytokines. There is a lot of evidence that circRNAs play a vital role in macrophages, and it will assist with further research on the diseases caused by macrophages and circRNAs.

5.4. circRNAs in Aortic Dissection Tissue and Intracranial Aneurysms

5.4.1. circRNAs in Aortic Dissection Tissue.
In a previous study, a targeted circRNA array was applied to exploring differentially expressed circRNAs in tissue specimens from thoracic aortic dissection (TAA) patients undergoing surgery [140]. As observed from the qRT-PCR assays, the expression levels of hsa_circRNA_102771, hsa_circRNA_002271, hsa_circRNA_101238, hsa_circRNA_104349, hsa_circRNA_104634, COL6A3, and COL1A1 increase, while the expression of hsa_circRNA_005525, hsa_circRNA_102683, hsa_circRNA_103458, and FLNA is downregulated. Meanwhile, circRNA_101238 is found to not only be deregulated with the disease but also potentially affect miR-320a expression and MMP9 levels. Moreover, the expression of both hsa_circRNA_104634 interacting with hsa-miR-145-3p and hsa_circRNA_104349 interacting with hsa-miR-26a-3p is upregulated, which promotes the apoptosis or phenotypic transformation of SMCs [141]. According to another study, hsa_circRNA_104033 and hsa_circRNA_102683 can suppress hsa-miR-195-3p and hsa-miR-29b-1-5p levels, respectively, thereby aggravating aortic wall apoptosis and ECM degradation and promoting collagen remodeling [142]. Thus, those differentially expressed circRNAs discovered possibly contribute to TAD occurrence through several biological processes [140].

Through carrying out RNA-Seq on the affected ascending aortic samples from patients with acute Stanford type A aortic dissection (AAAD), Tian et al. have identified 506 evidently differentially expressed circRNAs [143]. Besides, the levels of ten circRNAs with the most significant differential expression are either increased or decreased by 2-5 folds. Specifically, circUBA2, circARHGAP26, circIQGAP1, circCHSY1, circMED13, circMBNL1, circMYH10, and circRAB7A are upregulated, while circFAM120B and circCEP70 are downregulated. Moreover, the analysis results of the circRNA-miRNA-mRNA network disclose the regulatory effect of circMARK3 on the expression of Fgr, which is a kind of tyrosine-protein kinase. The findings of Tian et al. demonstrate the clinical significance of the circMARK3-

miR-1273-Fgr interaction and that the combined use of circRNAs and additional biomarkers can improve the diagnostic accuracy.

5.4.2. circRNAs in Peripheral Blood of Intracranial Aneurysms.

One recent effort identifies the hsa_circ_0021001 in peripheral blood of patients with intracranial aneurysms, but its potential contribution to aneurysmal expansion is not expounded [144]. Hsa_circ_0021001 has an area under the receiver operating characteristic ROC curve (AUC) of 0.87, demonstrating its effectiveness in IA diagnosis.

In a study, the circRNA sequencing on IA patients recognizes two novel circRNAs in the peripheral blood samples from IA cases, and their expression in peripheral blood of normal subjects are also analyzed. The results suggest that hsa_circ_0008433 and hsa_circ_0072309 are new and critical circRNAs associated with IAs. This study may provide novel prognostic biomarkers and therapeutic targets for IAs [145].

5.4.3. Hsa_circRNA_0020397 in Intracranial Aneurysm Tissue.

Wang et al. acquired arterial wall tissue samples from the aneurysm site in 12 cases and discovered that circRNA_0020397 was downregulated in IAs. The decreased circRNA_0020397 expression possibly suppressed the proliferation of VSMCs through upregulating miR-138 levels and downregulating KDR levels [146].

6. Summary and Perspectives

AAAs are one of the major causes leading to cardiovascular death among the senile male population, and their etiology is complex, including apoptosis of SMCs and inflammatory reaction. It is of urgent need to develop new pharmacological approaches or gene therapy strategies for delaying aneurysm development or lowering the risk of acute rupture. Over the last few decades, ncRNAs are increasingly identified as critical regulators for AAA occurrence and development. Hence, it is necessary to identify abnormally expressed ncRNAs and validate them in relevant human AAA tissue and animal models, so as to better explore the pathophysiological mechanisms related to AAA genesis and development.

Different from traditional linear RNAs, circRNAs are a novel class of RNAs with a closed loop structure that can be detected in the eukaryotic genome. Besides, they show higher stability and greater resistance to RNase degradation, so they are widely used as biomarkers. However, there is no evidence that peripheral blood circRNAs are effective biomarkers for the diagnosis of AAAs, and further investigation is required to confirm the relationship between circulating circRNAs and AAAs.

It is reported that circRNAs function as the molecular "sponge," capable of regulating transcription and posttranscriptional gene expression by binding to and blocking microRNA regulatory factors. The regulatory pathway of circRNAs is circRNA-miRNA-mRNA. A circRNA specifically binds to an miRNA and inhibits its expression, thereby regulating the expression level of the template RNA.

In this paper, the relationship between circRNAs and AAAs is briefly described. It is proved that several circRNAs affect the formation of AAAs by regulating the proliferation and apoptosis of VSMCs. Meanwhile, the changes of aneurysmal wall cells (e.g., immune cells and ECs) in the AAA development process can be well analyzed based on the circRNAs extracted from these cells. When the differential expression of these circRNAs is verified, the molecular mechanisms of circRNAs in regulating AAA occurrence are investigated both in vitro and in vivo. Meanwhile, the mechanism of action is further elaborated.

Because of the above-mentioned characteristics, circRNAs have been listed as a biomarker and therapeutic target for AAAs. The expression and regulation of circRNAs will directly affect the development of AAAs.

Data Availability

No data were used to support this study.

Conflicts of Interest

The authors declare that there is no conflict of interest regarding the publication of this paper.

Authors' Contributions

All authors read and approved the final manuscript.

Acknowledgments

References

[1] W. S. Aronow, "Peripheral arterial disease and abdominal aortic aneurysm in elderly people," *Minerva Medica*, vol. 102, no. 6, pp. 483–500, 2011.

[2] US Preventive Services Task Force, D. K. Owens, K. W. Davidson et al., "Screening for abdominal aortic aneurysm: US Preventive Services Task Force recommendation statement," *JAMA*, vol. 322, no. 22, pp. 2211–2218, 2019.

[3] J. S. Lindholt, "Abdominal aortic aneurysms," *Danish Medical Bulletin*, vol. 57, no. 12, p. B4219, 2010.

[4] F. A. Hellenthal, W. A. Buurman, W. K. Wodzig, and G. W. Schurink, "Biomarkers of AAA progression. Part 1: extracellular matrix degeneration," *Nature Reviews. Cardiology*, vol. 6, no. 7, pp. 464–474, 2009.

[5] F. A. Hellenthal, W. A. Buurman, W. K. Wodzig, and G. W. Schurink, "Biomarkers of abdominal aortic aneurysm

progression. Part 2: inflammation," *Nature Reviews. Cardiology*, vol. 6, no. 8, pp. 543–552, 2009.

[6] R. W. Thompson, P. J. Geraghty, and J. K. Lee, "Abdominal aortic aneurysms: basic mechanisms and clinical implications," *Current Problems in Surgery*, vol. 39, no. 2, pp. 110–230, 2002.

[7] F. L. Moll, J. T. Powell, G. Fraedrich et al., "Management of abdominal aortic aneurysms clinical practice guidelines of the European society for vascular surgery," *European Journal of Vascular and Endovascular Surgery*, vol. 41, Suppl 1, pp. S1–S58, 2011.

[8] A. Conway, A. H. Malkawi, R. J. Hinchliffe et al., "First-year results of a national abdominal aortic aneurysm screening programme in a single centre," *The British Journal of Surgery*, vol. 99, no. 1, pp. 73–77, 2012.

[9] H. A. Ashton, M. J. Buxton, N. E. Day et al., "The Multicentre Aneurysm Screening Study (MASS) into the effect of abdominal aortic aneurysm screening on mortality in men: a randomised controlled trial," *Lancet*, vol. 360, no. 9345, pp. 1531–1539, 2002.

[10] M. Zarrouk, J. Holst, M. Malina et al., "The importance of socioeconomic factors for compliance and outcome at screening for abdominal aortic aneurysm in 65-year-old men," *Journal of Vascular Surgery*, vol. 58, no. 1, pp. 50–55, 2013.

[11] M. Gawenda and J. Brunkwall, "Ruptured abdominal aortic aneurysm: the state of play," *Deutsches Ärzteblatt International*, vol. 109, no. 43, pp. 727–732, 2012.

[12] M. Johansson, P. H. Zahl, V. Siersma, K. J. Jørgensen, B. Marklund, and J. Brodersen, "Benefits and harms of screening men for abdominal aortic aneurysm in Sweden: a registry-based cohort study," *Lancet*, vol. 391, no. 10138, pp. 2441–2447, 2018.

[13] H. H. Eckstein, T. Bruckner, P. Heider et al., "The relationship between volume and outcome following elective open repair of abdominal aortic aneurysms (AAA) in 131 German hospitals," *European Journal of Vascular and Endovascular Surgery*, vol. 34, no. 3, pp. 260–266, 2007.

[14] R. M. Greenhalgh and E. V. The, "Comparison of endovascular aneurysm repair with open repair in patients with abdominal aortic aneurysm (EVAR trial 1), 30-day operative mortality results: randomised controlled trial," *Lancet*, vol. 364, no. 9437, pp. 843–848, 2004.

[15] Y. Han, S. Zhang, J. Zhang, C. Ji, and H. H. Eckstein, "Outcomes of endovascular abdominal aortic aneurysm repair in octogenarians: meta-analysis and systematic review," *European Journal of Vascular and Endovascular Surgery*, vol. 54, no. 4, pp. 454–463, 2017.

[16] M. Trenner, B. Haller, M. Storck, B. Reutersberg, M. A. Kallmayer, and H. H. Eckstein, "Trends in patient safety of intact abdominal aortic aneurysm repair: German registry data on 36,594 procedures," *European Journal of Vascular and Endovascular Surgery*, vol. 53, no. 5, pp. 641–647, 2017.

[17] J. Golledge, "Abdominal aortic aneurysm: update on pathogenesis and medical treatments," *Nature Reviews. Cardiology*, vol. 16, no. 4, pp. 225–242, 2019.

[18] Y. D. Wang, Z. J. Liu, J. Ren, and M. X. Xiang, "Pharmacological therapy of abdominal aortic aneurysm: an update," *Current Vascular Pharmacology*, vol. 16, no. 2, pp. 114–124, 2018.

[19] A. Giraud, L. Zeboudj, M. Vandestienne et al., "Gingival fibroblasts protect against experimental abdominal aortic aneurysm development and rupture through tissue inhibitor of metalloproteinase-1 production," *Cardiovascular Research*, vol. 113, no. 11, pp. 1364–1375, 2017.

[20] K. Riches, E. Clark, R. J. Helliwell et al., "Progressive development of aberrant smooth muscle cell phenotype in abdominal aortic aneurysm disease," *Journal of Vascular Research*, vol. 55, no. 1, pp. 35–46, 2018.

[21] H. Lu, J. Sun, W. Liang et al., "Cyclodextrin prevents abdominal aortic aneurysm via activation of vascular smooth muscle cell TFEB," *Circulation*, vol. 142, no. 5, pp. 483–498, 2020.

[22] N. Bogunovic, J. P. Meekel, D. Micha, J. D. Blankensteijn, P. L. Hordijk, and K. K. Yeung, "Impaired smooth muscle cell contractility as a novel concept of abdominal aortic aneurysm pathophysiology," *Scientific Reports*, vol. 9, no. 1, p. 6837, 2019.

[23] G. M. Longo, S. J. Buda, N. Fiotta et al., "MMP-12 has a role in abdominal aortic aneurysms in mice," *Surgery*, vol. 137, no. 4, pp. 457–462, 2005.

[24] W. W. Lu, L. X. Jia, X. Q. Ni et al., "Intermedin1-53 attenuates abdominal aortic aneurysm by inhibiting oxidative stress," *Arteriosclerosis, Thrombosis, and Vascular Biology*, vol. 36, no. 11, pp. 2176–2190, 2016.

[25] E. J. Ryer, K. E. Ronning, R. Erdman et al., "The potential role of DNA methylation in abdominal aortic aneurysms," *International Journal of Molecular Sciences*, vol. 16, no. 5, pp. 11259–11275, 2015.

[26] Y. Han, F. Tanios, C. Reeps et al., "Histone acetylation and histone acetyltransferases show significant alterations in human abdominal aortic aneurysm," *Clinical Epigenetics*, vol. 8, no. 1, p. 3, 2016.

[27] L. Maegdefessel, J. M. Spin, U. Raaz et al., "miR-24 limits aortic vascular inflammation and murine abdominal aneurysm development," *Nature Communications*, vol. 5, no. 1, p. 5214, 2014.

[28] K. S. Bishop and L. R. Ferguson, "The interaction between epigenetics, nutrition and the development of cancer," *Nutrients*, vol. 7, no. 2, pp. 922–947, 2015.

[29] A. O. Caglayan and M. Dundar, "Inherited diseases and syndromes leading to aortic aneurysms and dissections," *European Journal of Cardio-Thoracic Surgery*, vol. 35, no. 6, pp. 931–940, 2009.

[30] L. Y. Sakai, D. R. Keene, M. Renard, and J. De Backer, "FBN1: the disease-causing gene for Marfan syndrome and other genetic disorders," *Gene*, vol. 591, no. 1, pp. 279–291, 2016.

[31] K. Benke, B. Agg, B. Szilveszter et al., "The role of transforming growth factor-beta in Marfan syndrome," *Cardiology journal*, vol. 20, no. 3, pp. 227–234, 2013.

[32] M. Frank, J. Albuisson, B. Ranque et al., "The type of variants at the COL3A1 gene associates with the phenotype and severity of vascular Ehlers-Danlos syndrome," *European Journal of Human Genetics*, vol. 23, no. 12, pp. 1657–1664, 2015.

[33] T. Freestone, R. J. Turner, A. Coady, D. J. Higman, R. M. Greenhalgh, and J. T. Powell, "Inflammation and matrix metalloproteinases in the enlarging abdominal aortic aneurysm," *Arteriosclerosis, Thrombosis, and Vascular Biology*, vol. 15, no. 8, pp. 1145–1151, 1995.

[34] V. Davis, R. Persidskaia, L. Baca-Regen et al., "Matrix metalloproteinase-2 production and its binding to the matrix are increased in abdominal aortic aneurysms," *Arteriosclerosis, Thrombosis, and Vascular Biology*, vol. 18, no. 10, pp. 1625–1633, 1998.

[35] C. Saracini, P. Bolli, E. Sticchi et al., "Polymorphisms of genes involved in extracellular matrix remodeling and abdominal aortic aneurysm," *Journal of Vascular Surgery*, vol. 55, no. 1, pp. 171–179, 2012, e2.

[36] G. Makrygiannis, E. Mourmoura, K. Spanos et al., "Risk factor assessment in a Greek cohort of patients with large abdominal aortic aneurysms," *Angiology*, vol. 70, no. 1, pp. 35–40, 2019.

[37] G. T. Jones, G. Tromp, H. Kuivaniemi et al., "Meta-analysis of genome-wide association studies for abdominal aortic aneurysm identifies four new disease-specific risk loci," *Circulation Research*, vol. 120, no. 2, pp. 341–353, 2017.

[38] M. Abu-Farha, S. Lanouette, F. Elisma et al., "Proteomic analyses of the SMYD family interactomes identify HSP90 as a novel target for SMYD2," *Journal of Molecular Cell Biology*, vol. 3, no. 5, pp. 301–308, 2011.

[39] W. Tang, A. Saratzis, J. Pattee et al., "Replication of newly identified genetic associations between abdominal aortic aneurysm and SMYD2, LINC00540, PCIF1/MMP9/ZNF335, and ERG," *European Journal of Vascular and Endovascular Surgery*, vol. 59, no. 1, pp. 92–97, 2020.

[40] B. J. Toghill, A. Saratzis, P. J. Freeman, N. Sylvius, and M. J. Bown, "SMYD2 promoter DNA methylation is associated with abdominal aortic aneurysm (AAA) and SMYD2 expression in vascular smooth muscle cells," *Clinical Epigenetics*, vol. 10, p. 29, 2018.

[41] J. D. Wythe, L. T. Dang, W. P. Devine et al., "ETS factors regulate Vegf-dependent arterial specification," *Developmental Cell*, vol. 26, no. 1, pp. 45–58, 2013.

[42] J. Marsman, G. Gimenez, R. C. Day, J. A. Horsfield, and G. T. Jones, "A non-coding genetic variant associated with abdominal aortic aneurysm alters erg gene regulation," *Human Molecular Genetics*, vol. 29, no. 4, pp. 554–565, 2020.

[43] A. Brunet and S. L. Berger, "Epigenetics of aging and aging-related disease," *The Journals of Gerontology. Series A, Biological Sciences and Medical Sciences*, vol. 69, Suppl 1, pp. S17–S20, 2014.

[44] P. van der Harst, L. J. de Windt, and J. C. Chambers, "Translational perspective on epigenetics in cardiovascular disease," *Journal of the American College of Cardiology*, vol. 70, no. 5, pp. 590–606, 2017.

[45] G. Natoli, "Maintaining cell identity through global control of genomic organization," *Immunity*, vol. 33, no. 1, pp. 12–24, 2010.

[46] Q. Xia, J. Zhang, Y. Han et al., "Epigenetic regulation of regulatory T cells in patients with abdominal aortic aneurysm," *FEBS Open Bio*, vol. 9, no. 6, pp. 1137–1143, 2019.

[47] H. Jiang, Q. Xia, S. Xin et al., "Abnormal epigenetic modifications in peripheral T cells from patients with abdominal aortic aneurysm are correlated with disease development," *Journal of Vascular Research*, vol. 52, no. 6, pp. 404–413, 2016.

[48] L. D. Moore, T. Le, and G. Fan, "DNA methylation and its basic function," *Neuropsychopharmacology*, vol. 38, no. 1, pp. 23–38, 2013.

[49] M. Skorvanova, T. Matakova, M. Skerenova et al., "Methylation of MMP2, TIMP2, MMP9 and TIMP1 in abdominal aortic aneurysm," *Bratislavské Lekárske Listy*, vol. 121, no. 10, pp. 717–721, 2020.

[50] T. F. Whayne, "Epigenetics in the development, modification, and prevention of cardiovascular disease," *Molecular Biology Reports*, vol. 42, no. 4, pp. 765–776, 2015.

[51] M. Galán, S. Varona, M. Orriols et al., "Induction of histone deacetylases (HDACs) in human abdominal aortic aneurysm: therapeutic potential of HDAC inhibitors," *Disease Models & Mechanisms*, vol. 9, no. 5, pp. 541–552, 2016.

[52] H. Z. Chen, F. Wang, P. Gao et al., "Age-associated sirtuin 1 reduction in vascular smooth muscle links vascular senescence and inflammation to abdominal aortic aneurysm," *Circulation Research*, vol. 119, no. 10, pp. 1076–1088, 2016.

[53] D. Y. Li, A. Busch, H. Jin et al., "H19 induces abdominal aortic aneurysm development and progression," *Circulation*, vol. 138, no. 15, pp. 1551–1568, 2018.

[54] X. He, S. Wang, M. Li et al., "Long noncoding RNA GAS5 induces abdominal aortic aneurysm formation by promoting smooth muscle apoptosis," *Theranostics*, vol. 9, no. 19, pp. 5558–5576, 2019.

[55] Y. Sun, L. Zhong, X. He et al., "LncRNA H19 promotes vascular inflammation and abdominal aortic aneurysm formation by functioning as a competing endogenous RNA," *Journal of Molecular and Cellular Cardiology*, vol. 131, pp. 66–81, 2019.

[56] S. Kumar, R. A. Boon, L. Maegdefessel, S. Dimmeler, and H. Jo, "Role of noncoding RNAs in the pathogenesis of abdominal aortic aneurysm," *Circulation Research*, vol. 124, no. 4, pp. 619–630, 2019.

[57] D. P. Bartel, "MicroRNAs: target recognition and regulatory functions," *Cell*, vol. 136, no. 2, pp. 215–233, 2009.

[58] K. Saliminejad, H. R. Khorram Khorshid, S. Soleymani Fard, and S. H. Ghaffari, "An overview of microRNAs: biology, functions, therapeutics, and analysis methods," *Journal of Cellular Physiology*, vol. 234, no. 5, pp. 5451–5465, 2019.

[59] T. X. Lu and M. E. Rothenberg, "MicroRNA," *The Journal of Allergy and Clinical Immunology*, vol. 141, no. 4, pp. 1202–1207, 2018.

[60] C. Schulte, M. Karakas, and T. Zeller, "MicroRNAs in cardiovascular disease - clinical application," *Clinical Chemistry and Laboratory Medicine*, vol. 55, no. 5, pp. 687–704, 2017.

[61] R. A. Boon and S. Dimmeler, "MicroRNAs and aneurysm formation," *Trends in Cardiovascular Medicine*, vol. 21, no. 6, pp. 172–177, 2011.

[62] A. Liu, Y. Liu, B. Li, M. Yang, Y. Liu, and J. Su, "Role of miR-223-3p in pulmonary arterial hypertension via targeting ITGB3 in the ECM pathway," *Cell Proliferation*, vol. 52, no. 2, article e12550, 2019.

[63] L. Shi, C. Yu, X. Tian et al., "Effect of microRNA-133a-3p/matrix metalloproteinase-9 axis on the growth of atherosclerotic vascular smooth muscle cells," *Experimental and Therapeutic Medicine*, vol. 18, no. 6, pp. 4356–4362, 2019.

[64] T. Nakao, T. Horie, O. Baba et al., "Genetic ablation of microRNA-33 attenuates inflammation and abdominal aortic aneurysm formation via several anti-inflammatory pathways," *Arteriosclerosis, Thrombosis, and Vascular Biology*, vol. 37, no. 11, pp. 2161–2170, 2017.

[65] Y. Sun, Y. U. Xiao, H. Sun et al., "miR-27a regulates vascular remodeling by targeting endothelial cells' apoptosis and interaction with vascular smooth muscle cells in aortic dissection," *Theranostics*, vol. 9, no. 25, pp. 7961–7975, 2019.

[66] L. Maegdefessel, J. Azuma, R. Toh et al., "Inhibition of microRNA-29b reduces murine abdominal aortic aneurysm development," *The Journal of Clinical Investigation*, vol. 122, no. 2, pp. 497–506, 2012.

[67] D. R. Merk, J. T. Chin, B. A. Dake et al., "miR-29b participates in early aneurysm development in Marfan syndrome," *Circulation Research*, vol. 110, no. 2, pp. 312–324, 2012.

[68] L. Maegdefessel, J. Azuma, R. Toh et al., "MicroRNA-21 blocks abdominal aortic aneurysm development and nicotine-augmented expansion," *Science translational medicine*, vol. 4, no. 122, article 122ra22, 2012.

[69] D. Wang, T. Deuse, M. Stubbendorff et al., "Local microRNA modulation using a novel anti-miR-21-eluting stent effectively prevents experimental in-stent restenosis," *Arteriosclerosis, Thrombosis, and Vascular Biology*, vol. 35, no. 9, pp. 1945–1953, 2015.

[70] L. Zhao, J. Huang, Y. Zhu et al., "miR-33-5p knockdown attenuates abdominal aortic aneurysm progression via promoting target adenosine triphosphate-binding cassette transporter A1 expression and activating the PI3K/Akt signaling pathway," *Perfusion*, vol. 35, no. 1, pp. 57–65, 2020.

[71] R. A. Boon, N. Jaé, L. Holdt, and S. Dimmeler, "Long noncoding RNAs: from clinical genetics to therapeutic targets?," *Journal of the American College of Cardiology*, vol. 67, no. 10, pp. 1214–1226, 2016.

[72] N. Romero-Barrios, M. F. Legascue, M. Benhamed, F. Ariel, and M. Crespi, "Splicing regulation by long noncoding RNAs," *Nucleic Acids Research*, vol. 46, no. 5, pp. 2169–2184, 2018.

[73] G. St Laurent, C. Wahlestedt, and P. Kapranov, "The landscape of long noncoding RNA classification," *Trends in Genetics*, vol. 31, no. 5, pp. 239–251, 2015.

[74] L. Ma, V. B. Bajic, and Z. Zhang, "On the classification of long non-coding RNAs," *RNA Biology*, vol. 10, no. 6, pp. 925–933, 2013.

[75] Z. Zhang, G. Zou, X. Chen et al., "Knockdown of lncRNA PVT1 inhibits vascular smooth muscle cell apoptosis and extracellular matrix disruption in a murine abdominal aortic aneurysm model," *Molecules and Cells*, vol. 42, no. 3, pp. 218–227, 2019.

[76] A. Leung, C. Trac, W. Jin et al., "Novel long noncoding RNAs are regulated by angiotensin II in vascular smooth muscle cells," *Circulation Research*, vol. 113, no. 3, pp. 266–278, 2013.

[77] A. D. Mahmoud, M. D. Ballantyne, V. Miscianinov et al., "The human-specific and smooth muscle cell-enriched LncRNA SMILR promotes proliferation by regulating mitotic CENPF mRNA and drives cell-cycle progression which can be targeted to limit vascular remodeling," *Circulation Research*, vol. 125, no. 5, pp. 535–551, 2019.

[78] V. Patamsytė, G. Žukovas, D. Gečys et al., "Long noncoding RNAs CARMN, LUCAT1, SMILR, and MALAT1 in thoracic aortic aneurysm: validation of biomarkers in clinical samples," *Disease Markers*, vol. 2020, Article ID 8521899, 6 pages, 2020.

[79] W. R. Jeck and N. E. Sharpless, "Detecting and characterizing circular RNAs," *Nature Biotechnology*, vol. 32, no. 5, pp. 453–461, 2014.

[80] T. B. Hansen, T. I. Jensen, B. H. Clausen et al., "Natural RNA circles function as efficient microRNA sponges," *Nature*, vol. 495, no. 7441, pp. 384–388, 2013.

[81] L. L. Chen, "The biogenesis and emerging roles of circular RNAs," *Nature Reviews. Molecular Cell Biology*, vol. 17, no. 4, pp. 205–211, 2016.

[82] W. L. Tan, B. T. Lim, C. G. Anene-Nzelu et al., "A landscape of circular RNA expression in the human heart," *Cardiovascular Research*, vol. 113, no. 3, pp. 298–309, 2017.

[83] M. Zhou, Z. Shi, L. Cai et al., "Circular RNA expression profile and its potential regulative role in human abdominal aortic aneurysm," *BMC Cardiovascular Disorders*, vol. 20, no. 1, p. 70, 2020.

[84] D. T. Bradley, A. E. Hughes, S. A. Badger et al., "A variant in LDLR is associated with abdominal aortic aneurysm," *Circulation. Cardiovascular Genetics*, vol. 6, no. 5, pp. 498–504, 2013.

[85] D. Harris, Y. Liang, C. Chen, S. Li, O. Patel, and Z. Qin, "Bone marrow from blotchy mice is dispensable to regulate blood copper and aortic pathologies but required for inflammatory mediator production in LDLR-deficient mice during chronic angiotensin II infusion," *Annals of Vascular Surgery*, vol. 29, no. 2, pp. 328–340, 2015.

[86] H. Qing, K. L. Jones, E. B. Heywood, H. Lu, A. Daugherty, and D. Bruemmer, "Deletion of the NR4A nuclear receptor NOR1 in hematopoietic stem cells reduces inflammation but not abdominal aortic aneurysm formation," *BMC Cardiovascular Disorders*, vol. 17, no. 1, p. 271, 2017.

[87] Y. Alsiraj, S. E. Thatcher, R. Charnigo et al., "Female mice with an XY sex chromosome complement develop severe angiotensin II-induced abdominal aortic aneurysms," *Circulation*, vol. 135, no. 4, pp. 379–391, 2017.

[88] K. Di Gregoli, N. N. Mohamad Anuar, R. Bianco et al., "MicroRNA-181b controls atherosclerosis and aneurysms through regulation of TIMP-3 and elastin," *Circulation Research*, vol. 120, no. 1, pp. 49–65, 2017.

[89] P. Gao, J. Si, B. Yang, and J. Yu, "Upregulation of microRNA-15a contributes to pathogenesis of abdominal aortic aneurysm (AAA) by modulating the expression of cyclin-dependent kinase inhibitor 2B (CDKN2B)," *Medical Science Monitor*, vol. 23, pp. 881–888, 2017.

[90] J. Wang, H. Sun, Y. Zhou et al., "Circular RNA microarray expression profile in 3,4-benzopyrene/angiotensin II-induced abdominal aortic aneurysm in mice," *Journal of Cellular Biochemistry*, vol. 120, no. 6, pp. 10484–10494, 2019.

[91] R. Yang, Z. Wang, G. Meng, and L. Hua, "Circular RNA CCDC66 facilitates abdominal aortic aneurysm through the overexpression of CCDC66," *Cell Biochemistry and Function*, vol. 38, no. 7, pp. 830–838, 2020.

[92] J. Yue, T. Zhu, J. Yang et al., "CircCBFB-mediated miR-28-5p facilitates abdominal aortic aneurysm via LYPD3 and GRIA4," *Life Sciences*, vol. 253, p. 117533, 2020.

[93] S. Memczak, M. Jens, A. Elefsinioti et al., "Circular RNAs are a large class of animal RNAs with regulatory potency," *Nature*, vol. 495, no. 7441, pp. 333–338, 2013.

[94] F. Zhao, T. Chen, and N. Jiang, "CDR1as/miR-7/CKAP4 axis contributes to the pathogenesis of abdominal aortic aneurysm by regulating the proliferation and apoptosis of primary vascular smooth muscle cells," *Experimental and Therapeutic Medicine*, vol. 19, no. 6, pp. 3760–3766, 2020.

[95] C. Zheng, H. Niu, M. Li et al., "Cyclic RNA hsa-circ-000595 regulates apoptosis of aortic smooth muscle cells," *Molecular Medicine Reports*, vol. 12, no. 5, pp. 6656–6662, 2015.

[96] J. Zhou, Y. S. Li, and S. Chien, "Shear stress-initiated signaling and its regulation of endothelial function," *Arteriosclerosis, Thrombosis, and Vascular Biology*, vol. 34, no. 10, pp. 2191–2198, 2014.

[97] I. Hinterseher, R. Erdman, L. A. Donoso et al., "Role of complement cascade in abdominal aortic aneurysms," *Arteriosclerosis, Thrombosis, and Vascular Biology*, vol. 31, no. 7, pp. 1653–1660, 2011.

[98] M. R. Alexander and G. K. Owens, "Epigenetic control of smooth muscle cell differentiation and phenotypic switching in vascular development and disease," *Annual Review of Physiology*, vol. 74, pp. 13–40, 2012.

[99] A. Palazzuoli, M. Gallotta, G. Guerrieri et al., "Prevalence of risk factors, coronary and systemic atherosclerosis in abdominal aortic aneurysm: comparison with high cardiovascular risk population," *Vascular Health and Risk Management*, vol. 4, no. 4, pp. 877–883, 2008.

[100] B. J. Toghill, A. Saratzis, and M. J. Bown, "Abdominal aortic aneurysm–an independent disease to atherosclerosis?," *Cardiovascular Pathology*, vol. 27, pp. 71–75, 2017.

[101] S. H. Tsai, P. H. Huang, Y. J. Hsu et al., "Inhibition of hypoxia inducible factor-1alpha attenuates abdominal aortic aneurysm progression through the down-regulation of matrix metalloproteinases," *Scientific Reports*, vol. 6, p. 28612, 2016.

[102] W. Hauzer, W. Witkiewicz, and J. Gnus, "Calprotectin and receptor for advanced glycation end products as a potential biomarker in abdominal aortic aneurysm," *Journal of Clinical Medicine*, vol. 9, no. 4, 2020.

[103] T. I. Emeto, J. V. Moxon, M. Au, and J. Golledge, "Oxidative stress and abdominal aortic aneurysm: potential treatment targets," *Clinical Science (London, England)*, vol. 130, no. 5, pp. 301–315, 2016.

[104] Ł. Gutowski, K. Gutowska, M. Pioruńska-Stolzmann, P. Formanowicz, and D. Formanowicz, "Systems approach to study associations between OxLDL and abdominal aortic aneurysms," *International Journal of Molecular Sciences*, vol. 20, no. 16, 2019.

[105] R. Batra, M. K. Suh, J. S. Carson et al., "IL-1beta (interleukin-1beta) and TNF-alpha (tumor necrosis factor-alpha) impact abdominal aortic aneurysm formation by differential effects on macrophage polarization," *Arteriosclerosis, Thrombosis, and Vascular Biology*, vol. 38, no. 2, pp. 457–463, 2018.

[106] T. Blassova, Z. Tonar, P. Tomasek et al., "Inflammatory cell infiltrates, hypoxia, vascularization, pentraxin 3 and osteoprotegerin in abdominal aortic aneurysms - a quantitative histological study," *PLoS One*, vol. 14, no. 11, article e0224818, 2019.

[107] R. Y. Dang, F. L. Liu, and Y. Li, "Circular RNA hsa_circ_0010729 regulates vascular endothelial cell proliferation and apoptosis by targeting the miR-186/HIF-1alpha axis," *Biochemical and Biophysical Research Communications*, vol. 490, no. 2, pp. 104–110, 2017.

[108] H. G. Wang, H. Yan, C. Wang et al., "circAFF1 aggravates vascular endothelial cell dysfunction mediated by miR-516b/SAV1/YAP1 axis," *Frontiers in Physiology*, vol. 11, p. 899, 2020.

[109] C. Liu, M. D. Yao, C. P. Li et al., "Silencing of circular RNA-ZNF609 ameliorates vascular endothelial dysfunction," *Theranostics*, vol. 7, no. 11, pp. 2863–2877, 2017.

[110] F. Zhang, K. C. Kent, D. Yamanouchi et al., "Anti-receptor for advanced glycation end products therapies as novel treatment for abdominal aortic aneurysm," *Annals of Surgery*, vol. 250, no. 3, pp. 416–423, 2009.

[111] K. Prasad, "AGE-RAGE stress play a role in aortic aneurysm: a comprehensive review and novel potential therapeutic target," *Reviews in Cardiovascular Medicine*, vol. 20, no. 4, pp. 201–208, 2019.

[112] J. Sun, Y. Pu, P. Wang et al., "TRPV1-mediated UCP2 upregulation ameliorates hyperglycemia-induced endothelial dysfunction," *Cardiovascular Diabetology*, vol. 12, no. 1, p. 69, 2013.

[113] W. Zhang and Y. Sui, "CircBPTF knockdown ameliorates high glucose-induced inflammatory injuries and oxidative stress by targeting the miR-384/LIN28B axis in human umbilical vein endothelial cells," *Molecular and Cellular Biochemistry*, vol. 471, no. 1-2, pp. 101–111, 2020.

[114] J. Cheng, Q. Liu, N. Hu et al., "Downregulation of hsa_circ_0068087 ameliorates TLR4/NF-κB/NLRP3 inflammasome-mediated inflammation and endothelial cell dysfunction in high glucose conditioned by sponging miR-197," *Gene*, vol. 709, pp. 1–7, 2019.

[115] L. Pan, W. Lian, X. Zhang et al., "Human circular RNA-0054633 regulates high glucose-induced vascular endothelial cell dysfunction through the microRNA-218/roundabout 1 and microRNA-218/heme oxygenase-1 axes," *International Journal of Molecular Medicine*, vol. 42, no. 1, pp. 597–606, 2018.

[116] Y. Cao, G. Yuan, Y. Zhang, and R. Lu, "High glucose-induced circHIPK3 downregulation mediates endothelial cell injury," *Biochemical and Biophysical Research Communications*, vol. 507, no. 1-4, pp. 362–368, 2018.

[117] J. R. Hickok, D. Vasudevan, K. Jablonski, and D. D. Thomas, "Oxygen dependence of nitric oxide-mediated signaling," *Redox Biology*, vol. 1, pp. 203–209, 2013.

[118] U. Simonsen, R. Rodriguez-Rodriguez, T. Dalsgaard, N. H. Buus, and E. Stankevicius, "Novel approaches to improving endothelium-dependent nitric oxide-mediated vasodilatation," *Pharmacological Reports*, vol. 61, no. 1, pp. 105–115, 2009.

[119] H. X. Li, F. J. Kong, S. Z. Bai et al., "Involvement of calcium-sensing receptor in oxLDL-induced MMP-2 production in vascular smooth muscle cells via PI3K/Akt pathway," *Molecular and Cellular Biochemistry*, vol. 362, no. 1-2, pp. 115–122, 2012.

[120] F. Chang, S. Flavahan, and N. A. Flavahan, "Superoxide inhibition restores endothelium-dependent dilatation in aging arteries by enhancing impaired adherens junctions," *American Journal of Physiology. Heart and Circulatory Physiology*, vol. 314, no. 4, pp. H805–H811, 2018.

[121] S. Zhang, G. Song, J. Yuan et al., "Circular RNA circ_0003204 inhibits proliferation, migration and tube formation of endothelial cell in atherosclerosis via miR-370-3p/TGFbetaR2/-phosph-SMAD3 axis," *Journal of Biomedical Science*, vol. 27, no. 1, p. 11, 2020.

[122] H. Liu, X. Ma, Z. Mao, M. Shen, J. Zhu, and F. Chen, "Circular RNA has_circ_0003204 inhibits oxLDL-induced vascular endothelial cell proliferation and angiogenesis," *Cellular Signalling*, vol. 70, p. 109595, 2020.

[123] G. Wang, Y. Li, Z. Liu et al., "Circular RNA circ_0124644 exacerbates the ox-LDL-induced endothelial injury in human vascular endothelial cells through regulating PAPP-A by acting as a sponge of miR-149-5p," *Molecular and Cellular Biochemistry*, vol. 471, no. 1-2, pp. 51–61, 2020.

[124] M. Qin, W. Wang, H. Zhou, X. Wang, F. Wang, and H. Wang, "Circular RNA circ_0003645 silencing alleviates inflammation and apoptosis via the NF-kappaB pathway in endothelial cells induced by oxLDL," *Gene*, vol. 755, p. 144900, 2020.

[125] P. Ding, Y. Ding, Y. Tian, and X. Lei, "Circular RNA circ_0010283 regulates the viability and migration of oxidized low-density lipoprotein-induced vascular smooth muscle

cells via an miR-370-3p/HMGB1 axis in atherosclerosis," *International Journal of Molecular Medicine*, vol. 46, no. 4, pp. 1399–1408, 2020.

[126] Z. Feng, Y. Zhu, J. Zhang, W. Yang, Z. Chen, and B. Li, "Hsa-circ_0010283 regulates oxidized low-density lipoprotein-induced proliferation and migration of vascular smooth muscle cells by targeting the miR-133a-3p/pregnancy-associated plasma protein A axis," *Circulation Journal*, vol. 84, no. 12, pp. 2259–2269, 2020.

[127] L. Yang, F. Yang, H. Zhao, M. Wang, and Y. Zhang, "Circular RNA circCHFR facilitates the proliferation and migration of vascular smooth muscle via miR-370/FOXO1/Cyclin D1 pathway," *Molecular Therapy-Nucleic Acids*, vol. 16, pp. 434–441, 2019.

[128] J. B. Zhuang, T. Li, X. M. Hu et al., "Circ_CHFR expedites cell growth, migration and inflammation in ox-LDL-treated human vascular smooth muscle cells via the miR-214-3p/Wnt3/beta-catenin pathway," *European Review for Medical and Pharmacological Sciences*, vol. 24, no. 6, pp. 3282–3292, 2020.

[129] H. Yu, L. Zhao, Y. Zhao, J. Fei, and W. Zhang, "Circular RNA circ_0029589 regulates proliferation, migration, invasion, and apoptosis in ox-LDL-stimulated VSMCs by regulating miR-424-5p/IGF2 axis," *Vascular Pharmacology*, vol. 135, p. 106782, 2020.

[130] Z. Huang, P. Li, L. Wu et al., "Hsa_circ_0029589 knockdown inhibits the proliferation, migration and invasion of vascular smooth muscle cells via regulating miR-214-3p and STIM1," *Life Sciences*, vol. 259, p. 118251, 2020.

[131] Y. Sun, S. Zhang, M. Yue, Y. Li, J. Bi, and H. Liu, "Angiotensin II inhibits apoptosis of mouse aortic smooth muscle cells through regulating the circNRG-1/miR-193b-5p/NRG-1 axis," *Cell Death & Disease*, vol. 10, no. 5, p. 362, 2019.

[132] S. Wang, J. Zhan, X. Lin, Y. Wang, Y. Wang, and Y. Liu, "CircRNA-0077930 from hyperglycaemia-stimulated vascular endothelial cell exosomes regulates senescence in vascular smooth muscle cells," *Cell Biochemistry and Function*, vol. 38, no. 8, pp. 1056–1068, 2020.

[133] L. Shen, Y. Hu, J. Lou et al., "CircRNA-0044073 is upregulated in atherosclerosis and increases the proliferation and invasion of cells by targeting miR-107," *Molecular Medicine Reports*, vol. 19, no. 5, pp. 3923–3932, 2019.

[134] P. Kong, Y. Yu, L. Wang et al., "circ-Sirt1 controls NF-kappaB activation via sequence-specific interaction and enhancement of SIRT1 expression by binding to miR-132/212 in vascular smooth muscle cells," *Nucleic Acids Research*, vol. 47, no. 7, pp. 3580–3593, 2019.

[135] W. Peng, T. Li, S. Pi, L. Huang, and Y. Liu, "Suppression of circular RNA circDHCR24 alleviates aortic smooth muscle cell proliferation and migration by targeting miR-149-5p/MMP9 axis," *Biochemical and Biophysical Research Communications*, vol. 529, no. 3, pp. 753–759, 2020.

[136] Y. Y. Mao, J. Q. Wang, X. X. Guo, Y. Bi, and C. X. Wang, "Circ-SATB2 upregulates STIM1 expression and regulates vascular smooth muscle cell proliferation and differentiation through miR-939," *Biochemical and Biophysical Research Communications*, vol. 505, no. 1, pp. 119–125, 2018.

[137] J. Sun, Z. Zhang, and S. Yang, "Circ_RUSC2 upregulates the expression of miR-661 target gene SYK and regulates the function of vascular smooth muscle cells," *Biochemistry and Cell Biology*, vol. 97, no. 6, pp. 709–714, 2019.

[138] X. Lu, Y. Liu, W. Xuan et al., "Circ_1639 induces cells inflammation responses by sponging miR-122 and regulating TNFRSF13C expression in alcoholic liver disease," *Toxicology Letters*, vol. 314, pp. 89–97, 2019.

[139] T. Deng, L. Yang, Z. Zheng et al., "Calcitonin generelated peptide induces IL6 expression in RAW264.7 macrophages mediated by mmu_circRNA_007893," *Molecular Medicine Reports*, vol. 16, no. 6, pp. 9367–9374, 2017.

[140] M. Zou, C. Huang, X. Li et al., "Circular RNA expression profile and potential function of hsa_circRNA_101238 in human thoracic aortic dissection," *Oncotarget*, vol. 8, no. 47, pp. 81825–81837, 2017.

[141] N. J. Leeper, A. Raiesdana, Y. Kojima et al., "MicroRNA-26a is a novel regulator of vascular smooth muscle cell function," *Journal of Cellular Physiology*, vol. 226, no. 4, pp. 1035–1043, 2011.

[142] L. M. Holdt, A. Stahringer, K. Sass et al., "Circular non-coding RNA ANRIL modulates ribosomal RNA maturation and atherosclerosis in humans," *Nature Communications*, vol. 7, p. 12429, 2016.

[143] C. Tian, X. Tang, X. Zhu et al., "Expression profiles of circRNAs and the potential diagnostic value of serum circ-MARK3 in human acute Stanford type A aortic dissection," *PLoS One*, vol. 14, no. 6, article e0219013, 2019.

[144] L. Teng, Y. U. Chen, H. Chen et al., "Circular RNA hsa_circ_0021001 in peripheral blood: a potential novel biomarker in the screening of intracranial aneurysm," *Oncotarget*, vol. 8, no. 63, pp. 107125–107133, 2017.

[145] Q. Huang, Q. Y. Huang, Y. Sun, and S. Y. Wu, "High-throughput data reveals novel circular RNAs via competitive endogenous RNA networks associated with human intracranial aneurysms," *Medical Science Monitor*, vol. 25, pp. 4819–4830, 2019.

[146] Y. Wang, Y. Wang, Y. Li et al., "Decreased expression of circ_0020397 in intracranial aneurysms may be contributing to decreased vascular smooth muscle cell proliferation via increased expression of miR-138 and subsequent decreased KDR expression," *Cell Adhesion & Migration*, vol. 13, no. 1, pp. 220–228, 2019.

Research Article

Resveratrol Prevents Right Ventricle Dysfunction, Calcium Mishandling, and Energetic Failure via SIRT3 Stimulation in Pulmonary Arterial Hypertension

Judith Bernal-Ramírez [ID],[1] Christian Silva-Platas [ID],[1] Carlos Jerjes-Sánchez [ID],[1,2] Martín R. Ramos-González [ID],[1] Eduardo Vázquez-Garza [ID],[1] Héctor Chapoy-Villanueva [ID],[1] Alicia Ramírez-Rivera,[3] Ángel Zarain-Herzberg [ID],[4] Noemi García [ID],[1,2,5] and Gerardo García-Rivas [ID][1,2,5]

[1]Tecnológico de Monterrey, Escuela de Medicina y Ciencias de la Salud, Cátedra de Cardiología. N. L, Monterrey, Mexico
[2]Tecnológico de Monterrey, Centro de Investigación Biomédica, Hospital Zambrano Hellion, San Pedro Garza García, Mexico
[3]Unidad de Investigación Clínica en Medicina, Monterrey, Mexico
[4]Facultad de Medicina, Universidad Nacional Autónoma de México, Departamento de Bioquímica, Ciudad de México, Mexico
[5]Tecnológico de Monterrey, Centro de Medicina Funcional, Hospital Zambrano Hellion, San Pedro Garza García, Mexico

Correspondence should be addressed to Gerardo García-Rivas; gdejesus@itesm.mx

Pulmonary arterial hypertension (PAH) is characterized by pulmonary vessel remodeling; however, its severity and impact on survival depend on right ventricular (RV) failure. Resveratrol (RES), a polyphenol found in red wine, exhibits cardioprotective effects on RV dysfunction in PAH. However, most literature has focused on RES protective effect on lung vasculature; recent finding indicates that RES has a cardioprotective effect independent of pulmonary arterial pressure on RV dysfunction, although the underlying mechanism in RV has not been determined. Therefore, this study is aimed at evaluating sirtuin-3 (SIRT3) modulation by RES in RV using a monocrotaline- (MC-) induced PAH rat model. Myocyte function was evaluated by confocal microscopy as cell contractility, calcium signaling, and mitochondrial membrane potential ($\Delta\Psi m$); cell energetics was assessed by high-resolution respirometry, and western blot and immunoprecipitation evaluated posttranslational modifications. PAH significantly affects mitochondrial function in RV; PAH is prone to mitochondrial permeability transition pore (mPTP) opening, thus decreasing the mitochondrial membrane potential. The compromised cellular energetics affects cardiomyocyte function by decreasing sarco-endoplasmic reticulum Ca^{2+}-ATPase (SERCA) activity and delaying myofilament unbinding, disrupting cell relaxation. RES partially protects mitochondrial integrity by deacetylating cyclophilin-D, a critical component of the mPTP, increasing SIRT3 expression and activity and preventing mPTP opening. The preserved energetic capability rescues cell relaxation by maintaining SERCA activity. Avoiding Ca^{2+} transient and cell contractility mismatch by preserving mitochondrial function describes, for the first time, impairment in excitation-contraction-energetics coupling in RV failure. These results highlight the importance of mitochondrial energetics and mPTP in PAH.

1. Introduction

Pulmonary arterial hypertension (PAH) is a complex disease resulted from the interplay of several biological and environmental processes leading to pulmonary vasculature remodeling, therefore pulmonary hypertension [1]. Consequently, the low-pressure, thin-walled, crescent-shaped RV has to overcome structural changes to accomplish its function and pump against such an increased afterload [2]. Therefore, RV hypertrophy is a necessary adaptation to preserve RV-pulmonary arterial coupling by decreasing RV wall tension and increasing RV cardiomyocyte force-generating capacity

[2]. Consequently, in early stages, it emerges as an adaptive remodeling, while at end stage of the disease, it becomes a maladaptive remodeling [2]. Despite the publication of 41 randomized clinical trials in the past 25 years and the regulatory approval of multiple drugs delivered by four administration routes [3], there is no drug focused on improving RV performance and/or reducing inflammation [4]. Despite currently available therapies PAH patients remain significant morbidity and mortality [1]. A polyphenol from the stilbene family, 3,5,4′-trihydroxystilbene resveratrol (RES), has drawn researchers' attention by its cardioprotective activity in other cardiovascular diseases [5]. Although RES acts as a pleiotropic agent in several conditions, it has an intrinsic antioxidant capacity, as well as an ability to regulate membrane receptors, kinases, and other enzymes [6–8]. In PAH models, RES improves lung functioning through its antiproliferative [9], antioxidant [10], and anti-inflammatory properties [11]. More precisely, RES activates sirtuins, a relevant group of deacetylases that participate in the regulation of numerous cellular processes [12]. In the heart, sirtuin activation has been linked to the prevention of hypertrophy [13] and energetic dysfunction [14, 15].

Previously, we found the prevention of RV hypertrophy and cardiac fibrosis by RES in PAH, accompanied by a decrease in the RV acetylation profile [16]. However, the connection between these two mechanisms remains unclear. Progression to RV failure has been linked to mitochondrial dysfunction [17, 18], as PAH generates a disruption in the mitochondrial structure [17], decreasing its oxidative capability [19] and diminishing ATP production [17, 20]. The compromised cardiac energetics impairs RV contractility by reducing creatine kinase expression [21], a key component in transferring energy to myofilaments. Thus, protecting mitochondrial function with cyclosporine A (CsA), which blocks mPTP opening by interacting with cyclophilin D (CypD), prevents mitochondrial disruption in PAH and preserves RV function [22]. CypD hyperacetylation is an essential trigger of mPTP opening [23], and its contribution to mitochondrial dysfunction and heart failure has been established in animal models [24] and humans [15]. Notably, CypD acetylation is regulated by SIRT3 [23, 24], a sirtuin stimulated by RES [12], which is associated with the loss-of-function polymorphism found in PAH patients [25].

The search for additional therapeutic options for more effective PAH management has led to the development and approval of new drugs [26]; however, the available treatments focus on exclusively in managing pulmonary alterations [27]. Gaining a basic understanding of RV alterations through dysfunction, RV failure, and mechanisms that delay these changes may be helpful in developing new therapeutic strategies to improve PAH prognosis. Therefore, the aim of this study is to evaluate the extent of SIRT3 activation in the cardioprotection conferred by RES in the RV of a MC-induced PAH model.

2. Materials and Methods

2.1. Reagents. All reagents were purchased from Sigma-Aldrich (St. Louis, MO, USA), unless otherwise stated.

2.2. Murine Model of Pulmonary Arterial Hypertension. PAH was induced in male Sprague–Dawley rats (Bioinvert, Edo. de México, MX) weighing >300 g by a single MC (PHL8925) dose (60 mg/kg, subcutaneous) diluted in dimethylsulfoxide (DMSO, 472301), as previously reported [16]. The control group was treated with equivalent volume of DMSO. Animals were kept at 25°C with 12 h light/dark cycle. Water and food were given ad libitum. A group of MC-injected animals was treated with RES dissolved in water (20 mg/kg/day, intra gastric) during day 1 to 42 after MC injection (PAH-RES) [16]. The other groups were given equivalent volume of water (intragastric). All animals were observed for general appearance and respiratory symptomatology. A group of control animals treated with RES during 42 days (20 mg/kg/day, intragastric) was evaluated.

2.3. Histologic Preparations. As reported previously [16], after injection of sodium heparin (1000 U/kg), animals were anesthetized with 5% sevoflurane and the heart and lungs were removed to be fixed in 4% (wt/vol) paraformaldehyde in PBS at room temperature for more than 2 hours. Afterwards, tissues were embedded in paraffin and stained with hematoxylin/eosin (H&E) and Masson's trichrome. An Imager Z1 Zeiss microscope with an AxioCam HRm was used, and images were processed with the AxioVision software. Micrograph from the whole Masson's trichrome stained slides was taken at 2.5x; then, the image was decomposed in more than 7 fields at 5x. Fibrotic index was assessed by quantification of blue and red pixels, using ImageJ (http://imagej.nih.gov/ij/, NIH, Bethesda, MD, USA); a blue%/red% ratio was made. Two blinded analysts performed the analysis, and three different fields were analyzed. H&E micrograph from the papillary muscles was used to quantify cardiomyocyte area at 10x. An object carrier with a capacity for 7 slides was used to analyze all slides with their respective batches. Arterioles with smooth muscular medial layer proliferation were quantified in seven random fields of lung H&E micrograph, to analyze its diameter, and the occlusion vessel of 100 μm was selected. Occlusion was obtained by averaging more than seven measurements of the medial layer thickness.

2.4. Cardiomyocyte Isolation. Ventricular myocytes were isolated modifying a previous report [28]. Briefly after, animals were heparinized (1000 U/kg, intraperitoneal) and anesthetized with sevoflurane (1.5%-3%/1 L/min, inhaled). Hearts were excised and mounted on a Langendorff apparatus to be perfused with Tyrode solution (Ty) (mM: 128 NaCl, 0.4 NaH$_2$PO$_4$, 6 glucose, 5.4 KCl, 0.5 MgCl-6H$_2$O, 5 creatinine, 5 taurine and 25 HEPES, pH 7.4) at 37°C for 5 min and digested by collagenase type II (0.1% in Ty) (Worthington Biochemical, Lakewood, NJ). Subsequently, RV was dissected and cells were mechanically disaggregated. Cardiomyocytes were rinsed with 0.1% albumin in Ty solution at increasing Ca^{2+} concentrations (0.25, 0.5, and 1 mM). All the confocal measurements were acquired using a Leica TCS SP5 confocal microscope equipped with a D-apochromatic 63X, 1.2 NA, oil objective (Leica Microsystems, Wetzlar, Germany). Only rod-shaped cells with visible striations were selected for the

study. All records were analyzed using ImageJ (http://imagej .nih.gov/ij/, NIH, Bethesda, MD, USA).

2.5. Cell Shortening and Ca^{2+} Handling in Intact Cardiomyocytes.

Cell shortening was evaluated in 0.5 Hz paced Ca^{2+} transient records, where the scanned line was longer than the cell length, following a previous report [29]. Briefly, a rectangular region comprising both cellular edges was selected and a threshold was set to distinguish the intracellular from the extracellular space, converting the image into binary. The cell border of the resulting binary image was compared to the border on the original record to ensure a close fit. Cell shortening parameters evaluated were time to peak shortening from fully cell rest length and time to 50% of relaxation from maximal shortening. ImageJ software (http://imagej.nih.gov/ij/, NIH, Bethesda, MD, USA) was used to process images. Intracellular Ca^{2+} signaling was measured as previously reported [28, 30]. Recently isolated cardiomyocytes were incubated with $10\,\mu M$ Fluo-4 AM (F14201, Life Technologies, USA) (in Ty, 1 mM Ca^{2+}) for 45 min at 25°C. Later, cells were washed with fluorophore-free solution, plated on laminin- (L2020) covered glass coverslips, and mounted in a superfusion chamber. Line scan images were recorded by the cell longitudinal axis (400 Hz, 1 μm section thickness) by confocal microscopy under 0.5 Hz field stimulation (MYP100 MyoPacer Field Stimulator; Ion-Optix, Milton, MA, USA). Fluorophore excitation was 488 nm, and emission window was 500-600 nm. β-Adrenergic stimulation was assessed after 10 min of 100 nM isoproterenol (16504) (ISO in Ty, 1 mM Ca^{2+}) perfusion at 1 Hz stimulation. Fluorescence data is shown as $\Delta F/F_0$, where F_0 is the average fluorescence intensity before field stimulation. To evaluate spark characteristics in freshly isolated myocytes, the longitudinal cell axis with 100 nm pixel size records was taken at 1 Hz pace. Analysis was performed using ImageJ software (http://imagej.nih.gov/ij/, NIH, Bethesda, MD, USA) with the SparkMaster plugin [31].

2.6. Mitochondrial Membrane Potential in Intact Cardiomyocytes.

Freshly isolated cardiomyocyte cells were incubated with 300 nM tetramethylrhodamine ethyl ester perchlorate (TMRE) (T669, Thermo Fisher Scientific, USA) for 30 min at 25°C (in Ty, 1 mM Ca^{2+}) [32]. After washing with a fluorophore-free and Ca^{2+}-free solution, 2D images (1024×1024 pixels, 400 Hz, 1 μm section thickness) were taken using 543 nm excitation and 555-700 nm emission window. Results were normalized to the CTRL group as a percentage. The degree of mitochondrion polarization was then expressed as TMRE intensity per cell. As a negative control, cells were perfused with $0.8\,\mu M$ cyanide m-chlorophenyl hydrazone (CCCP) (C2759) during 10 min (data not shown).

2.7. Mitochondrial Isolation.

Heart mitochondrial fractions were obtained according to the method described previously [33]. Briefly, the heart was isolated and placed in an ice-cold buffer (SHE), containing (mM) the following: 250 sucrose, 10 HEPES and 1 EGTA, and pH 7.3. After, only RV tissue was digested for 10 min using 0.12 mg of protease in cold SHE buffer and centrifuged at 800 x g. The homogenates were

centrifuged at 10000 x g for 10 min, and then the resulting pellet was suspended in SH buffer containing (mM) the following: 250 sucrose, 10 HEPES, pH 7.3, and free EGTA. Isolated mitochondria were suspended (0.6 mg/ml) in respiration buffer containing (in mM) the following: 125 KCl, 3 KH_2PO_4, 10 HEPES, and pH 7.3.

2.8. Mitochondrial Function from RV in the PAH Model.

For the respiratory studies, 0.1 mg/ml mitochondria in respiratory medium (140 mM K^+-gluconate, 5 mM KH_2PO_4, 2 μg/ml rotenone, 10 mM succinate, 10 mM HEPES pH 7.2) was evaluated during the respiratory states of no-phosphorylation (state 4), phosphorylation (state 3, ADP added), and maximal respiratory activity (uncoupled with FCCP). Oxygen consumption was recorded using high-resolution respirometry (Oroboros Instrument, Innsbruck, Austria) [32].

2.9. Ca^{2+} Retention Capacity (CRC).

mPTP opening sensitivity was evaluated in isolated mitochondrial by CRC. Mitochondria were incubated in a medium containing $0.3\,\mu M$ Calcium Green-5N (C3739, Life Technologies, Carlsbad, CA, US), 10 mM succinate plus rotenone (10 μg/ml), 200 μM ADP, and 0.25 μg Oligomycin A. After 5-minute incubation, 10 μM of Ca^{2+} pulses was added every 3 min and fluorescence was recorded at 488 nm excitation and 500-600 nm emission. After enough Ca^{2+} loading, a massive release of mitochondrial Ca^{2+} indicates mPTP opening. The amount of $CaCl_2$ necessary to trigger this enormous Ca^{2+} release was used as an indicator of the susceptibility to mPTP opening due to Ca^{2+} overload [32].

2.10. Protein Extraction.

50 mg heart tissue was macerated using a Polytron PT1200 E (Kinematica AG, Switzerland) with 500 μl of buffer SHE added with 1 mM phenylmethylsulfonyl fluoride (PMSF, P7626) and 1 mM dithiothreitol (DTT, D0632). Afterwards, the homogenate was centrifuged at 2000 rpm during 10 min at 4°C. Protein was quantified in the supernatant by the Lowry method using bovine serum albumin as standard.

2.11. Western Blot.

Protein were resolved on SDS-PAGE gel and transferred onto a PVDF membrane, which was incubated with primary antibody. The membrane was washed three times for 10 min with PBS-0.5% Tween 20 and subsequently probed with an HPR-conjugated secondary for 2 hours at 25°C. After washing three times with PBS-0.5% Tween 20 for 10 min, the blots were developed with SuperSignal West Dura Extended Duration Substrate (TG268239, Thermo Fisher Scientific, Waltham, MA, US) and quantified by using a BioSpectrum 415 Image Acquisition System (UVP, Upland, CA, USA). Protein acetylation used 30 μg of isolated mitochondria in a 15% SDS-PAGE gel; to SIRT3 expression, 15 μg of isolated mitochondria was used in a 12% SDS-PAGE gel; electrophoresis and transfer conditions were 105 V, 25°C, 2.5 h, and 300 mA, 4°C, 2 h, respectively, to both. SERCA2, phospholamban (PLB), and D-glyceraldehyde-3-phosphate dehydrogenase (GAPDH) were quantified in the same blot. 40 μg of tissue homogenate was loaded in 12% SDS-PAGE gel. Electrophoresis and

transfer conditions were 85 V, 25°C, 2 h, and 350 mA, 25°C, 1.5 h, respectively. Primary antibodies used were as follows: anti-Acetylated-Lysine (9441S, Cell Signaling, Danvers, MA, US) (1 : 1000); anti-SIRT3 (D22A3, Cell Signaling, Danvers, MA, US) (1 : 2000); anti-SERCA (sc-8094, Santa Cruz Biotechnology, MA, US) (1 : 10000); and anti-PLB (sc-21923, Santa Cruz Biotechnology, MA, US) (1 : 1000). Anti-COX4 (4D11-B3-E8, Cell Signaling, Danvers, MA, US) (1 : 2000) [25] and anti-GAPDH (sc-25778, Santa Cruz Biotechnology, MA, US) (1 : 10000) antibodies were used as a loading control.

2.12. Real-Time Polymerase Chain Reaction (PCR) Analysis. Total RNA from right ventricles was extracted using TRIzol Reagent (15596026, Invitrogen, Carlsbad, CA, USA). Sample purity was confirmed measuring a 260/280 nm absorbance ratio using a Take3 multivolume plate in a Synergy HT microplate reader (BioTek Instruments, Winooski, USA). SensiFAST cDNA Synthesis Kit (BIO-65053, Bioline, London, UK) was used to reverse-transcribe cDNA from 1 μg of total RNA. qPCR reaction was performed using the SensiFAST SYBR Lo-ROX Kit (BIO-94020, Bioline, London, UK) in a Quant-Studio 3 RT PCR System (Thermo Fisher Scientific, Waltham, TX, USA). Data was analyzed by $2-\Delta\Delta Ct$ method to estimate mRNA expression from each gene [15, 34]. T4 Oligo (Mexico) synthesized primers. Primer sequences are detailed in Supplementary Table 1.

2.13. Oxidative Stress Markers. Free thiol groups were evaluated in 200 μg of isolated mitochondria incubated with 5,5-dithio-bis-(2-nitrobenzoic acid) (DNTB, 300 μM) (D8130), during 10 min at 25°C in darkness. After 10 min centrifugation at 10000 rpm, the supernatant was measured at 412 nm. Protein carbonyl content was assessed in homogenized tissue following assay kit (ab126287, Abcam, UK) instructions. Membrane lipid peroxidation was analyzed by measuring the generation of thiobarbituric acid-reactive substances (TBARS) as previously reported [35]. DNA oxidation was analyzed by ELISA assay according to the kit manufacturer's instructions (ab101245, Abcam, UK). The concentration of 8-hydroxy-20-deoxyguanosine (8-OHdG) was measured using a standard curve and expressed in nanograms per micrograms of DNA [36]. Enzyme activities were evaluated in a homogenized heart tissue. Catalase activity was measured by O_2 production assessed by an electrode type Clark [36]. Briefly, 50 μg protein was added to phosphate buffer (KH_2PO_4 50 mM, pH 7.8), and the addition of 5 mM H_2O_2 (quantified at 240 nm with an extinction coefficient of $43.6\,M^{-1} \times cm^{-1}$) started the reaction. Data were expressed as units per milligram of protein (U/mg). Aconitase activity was measured by monitoring *cis*-aconitate synthesis from citrate at 30°C on 240 nm. 150 μg protein was added to 1 ml of medium (100 mM KH_2PO_4, 0.01% Triton X-100, 0.6 mM $MnCl_2$, 0.2 mM NADP, and 1 mM citrate, pH 7.2). Enzyme activity is expressed as $nmol \times min^{-1} \times mg^{-1}$, using *cis*-aconitate extinction coefficient (E240 nm = $3.6\,mM^{-1} \times cm^{-1}$). Superoxide dismutase activity was measured as previously reported [36]. Briefly, 50 μg protein was added to phosphate buffer (50 mM KH_2PO_4, 1 mM EDTA, 10 mM xanthine,

50 μM nitro-blue tetrazolium chloride (NBT), 1 U catalase, 1.5 U Xantina oxidase, pH 7.8). Oxidation of NBT by superoxide anion was measured at 560 nm. To measure Mn-SOD, 3 mM KCN was added. One activity unit was defined as 50% oxidation of NBT. Results were expressed as units per milligram of protein (U/mg).

2.14. Immunoprecipitation. As described before [15], isolated mitochondria from right ventricles (1 mg) were solubilized in buffer containing (in mM) the following: 150 NaCl, 1 EGTA, Igepal 1%, 20 Tris-HCl, pH 7.2, and protease inhibitor cocktail (Roche). Afterwards, they were clarified of endogenous IgG and incubated with 2 μg of mouse anti-CypD (ab110324, Abcam, UK), or the isotype IgG as control, 1 hour at 4°C in a rotator. The immunoprecipitation complexes were captured by adding 50% activated slurry of Protein G Sepharose beads (GE) to the solubilized protein and incubated overnight at 4°C in a rotator. Beads were centrifuged and washed thrice. Complexes were eluted in SDS-loading buffer prior to electrophoretic separation and subsequent western blot analysis.

2.15. Statistics. Data is presented as the mean ± SEM. Statistical analysis and graphs were performed using GraphPad Prism software (V.5.01; La Jolla, CA, USA). Data were analyzed by one-way ANOVA or two-tailed Student's *t*-test;to compare the groups, Dunn's post hoc test was performed when appropriate. Statistical significance was set at $p < 0.05$.

2.16. Study Approval. All procedures performed in animals were supervised and approved by the Internal Committee for Care and Handling of Laboratory Animals of the School of Medicine of the Tecnológico de Monterrey (Protocols no. 2017-006 and 2019-019) and were performed following the Mexican National Laboratory Animal Health Guidelines (NOM 062-ZOO 1999).

3. Results

3.1. RES Preserves Right Ventricular Function with a Limited Effect on Lung Vasculature. The PAH model requires 28–42 days to develop phenotypic changes in the lungs and heart [37]. Previously, it has been shown that heart alterations caused by MC target the RV and RES treatment improve RV function with a limited protective effect on pulmonary architecture [16]. In addition, rats treated only with RES showed no differences compared to the control animals (without MC) for lung morphological parameters such avessel lumen diameter, number of muscular arteries, luminal occlusion, and RV histological characteristics (Supplemental Figure 1).

3.2. RES Prevents Contractility Alterations and Improves Ca^{2+} Handling. RV myocyte function was evaluated by characterizing cell contraction and Ca^{2+} dynamics to assess alterations in excitation-contraction coupling (ECC). Cell shortening was less efficient in the PAH group since time to peak shortening (Figure 1(b)) and half relaxation (Figure 1(c)) were 82% and 41% slower, respectively. RES treatment accelerated the time to peak shortening by 22% in PAH (Figure 1(b)) and

(a)

(b)

(c)

(d)

(e)

(f)

(g)

(h)
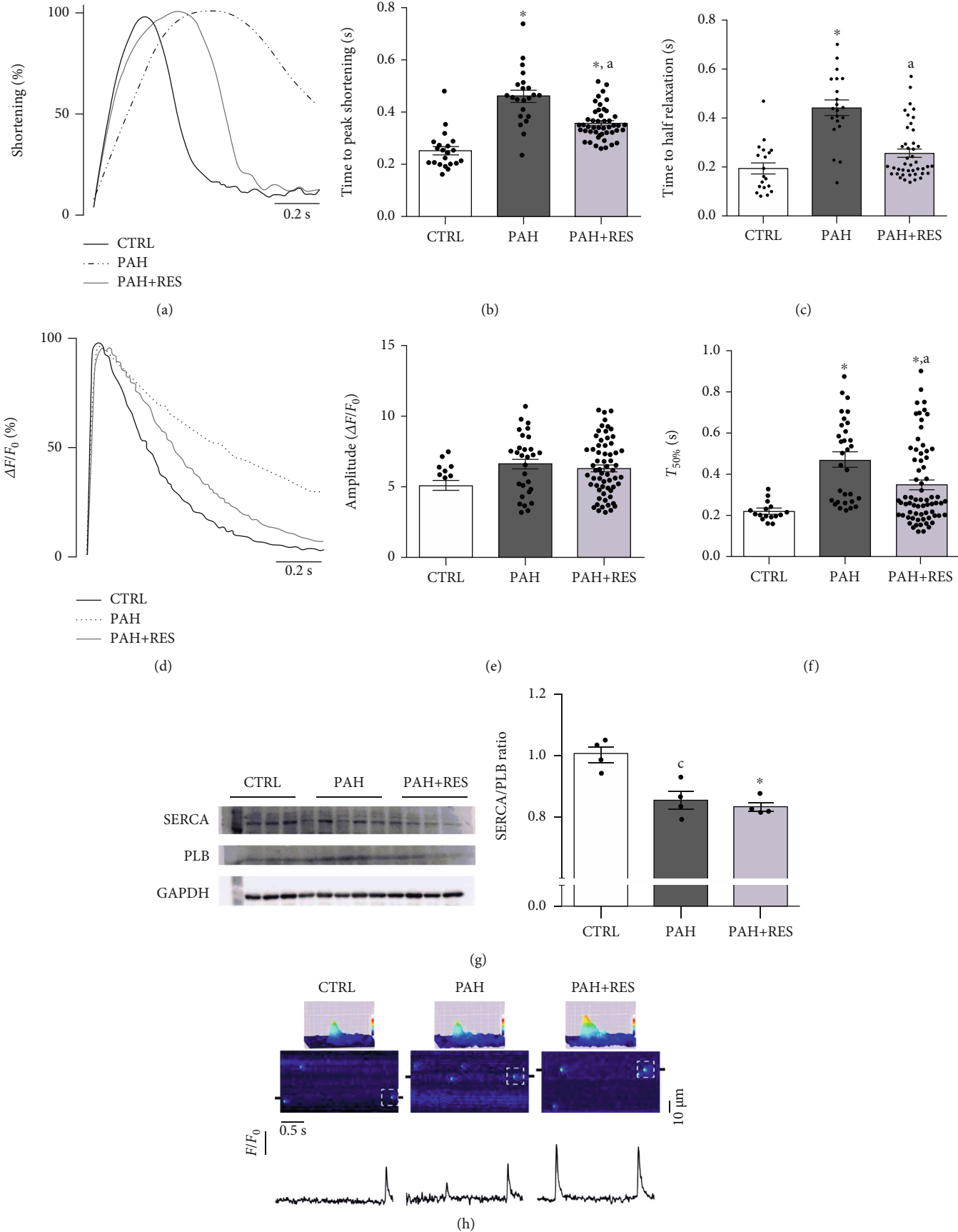
FIGURE 1: Continued.
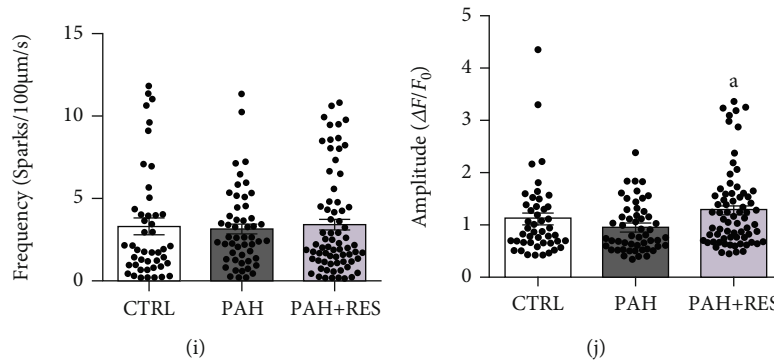
Figure 1: Characterization of cell contraction and Ca^{2+} dynamics in isolated RV myocytes. (a) Representative profile of cellular shortening. Average of time to peak shortening (b) (CTRL: $n = 20$ cells; PAH: $n = 21$ cells; PAH+RES: $n = 45$) and time to 50% relaxation (c) (CTRL: $n = 18$ cells; PAH: $n = 17$ cells; PAH+RES: $n = 16$). (d) Representative florescence profile of Ca^{2+} transient. Pooled data from Ca^{2+} transient amplitude (e) and $T_{50\%}$ (f) (CTRL: $n = 16$ cells; PAH: $n = 53$ cells; PAH+RES: $n = 69$ cells). (g) Representative images and pooled data of western blot to the SERCA2/PLB ratio; GAPDH was used as a loading control ($n = 4$). (h) Representative line scan images of treated groups; surface plots from selected sparks (doted square) are above; shown below are line profiles from $2\,\mu m$ regions of the selected spark (black marks in line scan images). Pooled data of Ca^{2+} spark frequency (i) and amplitude (j) (CTRL: $n = 46$ cells, 3 animals; PAH: $n = 55$ cells, 3 animals; PAH+RES: $n = 71$ cells, 5 animals). CTRL (solid black line), pulmonary arterial hypertension (PAH, dotted line), and PAH treated with resveratrol (PAH+RES, solid gray line). CTRL: control; PAH: pulmonary arterial hypertension; PAH+RES: PAH treated with resveratrol. All data are presented as the mean ± SEM. $^*p < 0.05$ vs. CTRL; $^ap < 0.05$ vs. PAH, calculated by 1-way ANOVA; $^cp < 0.05$ vs. CTRL, calculated by a 2-tailed t-test.

maintained the CTRL group time to half relaxation (Figure 1(c)), indicating that RES treatment improved cell relaxation in PAH.

Since intracellular Ca^{2+} dynamics orchestrates cell contractility, transient parameters were characterized. Transient amplitude (Figure 1(e)) did not change between groups. However, in transient decay, the PAH group showed a 1.2-fold slower $T_{50\%}$ than CTRL, while RES reduced this effect by 26% (Figure 1(f)); however, no significant differences were shown in the SERCA2/PLB ratio between the PAH and PAH+RES groups (Figure 1(g)), indicating that the improved $T_{50\%}$ might have been due to increased SERCA activity rather than changes in its expression. Gene expression of other Ca^{2+} extrusion mechanisms, Na/Ca^{2+} exchanger (NCX) and mitochondria calcium uniplex (MCU), did not change between groups (NCX: CTRL $= 1 \pm 0.11$, PAH $= 1.03 \pm 0.15$, PAH+RES $= 0.86 \pm 0.12$; MCU: CTRL $= 0.88 \pm 0.13$, PAH $= 0.88 \pm 0.13$, PAH+RES $= 0.96 \pm 0.15$ mRNA/HPRT).

Ca^{2+} spark frequency (Figure 1(i)) and amplitude (Figure 1(j)) were measured as an indicative of RyR activity. No changes were observed between PAH and CTRL groups; thus, RyR activity was not affected. However, the PAH-RES group had a higher spark amplitude than the PAH group (PAH:$0.96 \pm 0.06\Delta F/F_0$, RES+PAH:$1.3 \pm 0.09\Delta F/F_0$, $p < 0.05$), suggesting a higher SR Ca^{2+} content.

RV myocytes were challenged after isoprenaline (ISO, 100 nM) perfusion to induce the β-adrenergic response (β-AR), a highly energy-dependent state (Supplemental. Fig. 2). All groups were capable to increase Ca^{2+} transient amplitude and to reduce $T_{50\%}$. However, cell contraction failed to comply in the PAH group, while RES-treated PAH prevented this Ca^{2+} transient and cell contractility mismatch.

3.3. RES Prevents Cellular Energetics Failure. Since β-AR emphasizes the disruption of excitation-contraction-

energetic coupling (ECEC) in PAH, mitochondrial function was evaluated in isolated myocytes and mitochondria from the RV tissue. PAH compromises ATP production by altering mitochondrial functioning, as $\Delta\Psi m$ decreased by 47% in PAH myocytes ($p < 0.001$), while in RES-treated PAH, the control level was sustained ($95.4 \pm 11.6\%$) (Figure 2(b)). RV mitochondria from the PAH group also showed a 26% reduction in respiratory activity during state 3 of respiration (Figure 2(c)) with no change in basal respiratory activity in state 4 (Figure 2(d)), thus decreasing respiratory control ratio (CTRL: 2.1 ± 0.19; PAH: 1.5 ± 0.15) (Figure 2(e)). In the PAH-RES group, mitochondria maintained the respiratory control ratio (2 ± 0.04) (Figure 2(e)) by preserving the phosphorylation response (CTRL: 36.93 ± 3.24 nmol O_2/min•mg; PAH+RES: 33.89 ± 0.69 nmol O_2/min•mg) (Figure 2(c)). Isolated mitochondria from the PAH group also showed increased mPTP, demonstrated by an 81% decrease in Ca^{2+} retention capacity (CRC), while RES treatment produced a 2.5-fold decrease in mitochondrial fragility in the PAH-RES group (Figure 2(f)). The enhanced permeability was a consequence of mPTP opening since the effect is inhibited by CsA, a potent inhibitor of the mPTP (mean ± SEM: CTRL $= 216.7 \pm 33.33$ nmol Ca^{2+}/mg, PAH $= 186.1 \pm 45.24$ nmol Ca^{2+}/mg, PAH+RES $= 186.7 \pm 54.52$ nmol Ca^{2+}/mg; $p = 0.3831$; n: 7, 6, and 5 mitochondrial preparations, respectively).

The involvement of oxidative stress in mitochondria permeability transitioning was also evaluated. As shown in Figure 3(b), there was an increase in membrane peroxidation concomitant with 48% decrease in aconitase activity in the PAH group indicating an increased oxidant environment within the mitochondria. However, other antioxidant enzymes and oxidation in protein or DNA did not change in the PAH group (Figure 3). RES treatment maintained the same level of aconitase activity as CTRL (97%;

(a)

(b)

(c)

(d)

(e)

(f)
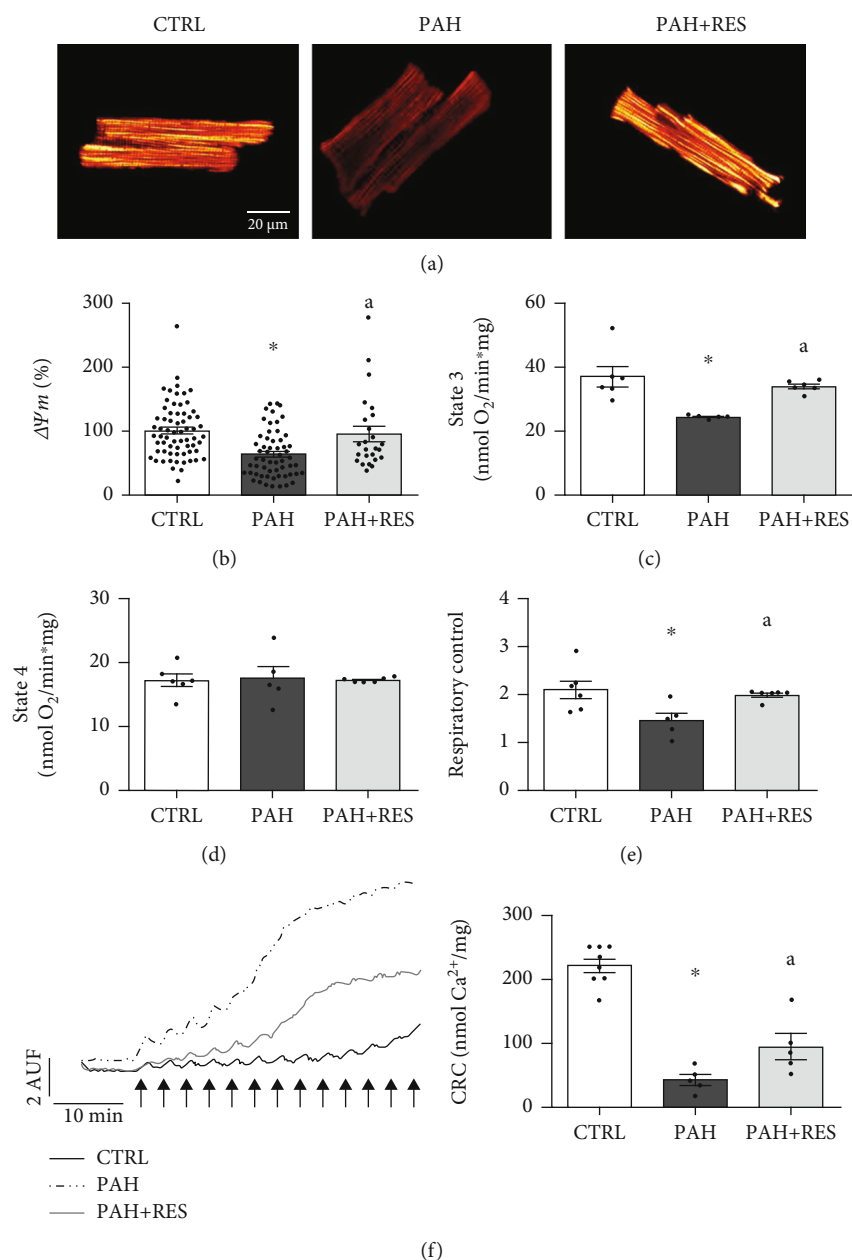
FIGURE 2: Characterization of mitochondrial function from RV. Representative images (a) and pooled data (b) from $\Delta\Psi m$ in isolated RV myocytes (CTRL: $n = 66$ cells and 3 animals; PAH: $n = 59$ cells and 3 animals; PAH+RES: $n = 25$ cells and 2 animals). Mitochondrial respiratory states (c, d) and respiratory control ratio (e) of isolated mitochondria preparations (CTRL: $n = 6$, PAH: $n = 5$, PAH+RES: $n = 6$). (f) CRC from isolated mitochondria, in left image each arrow represents a 10 nmol $CaCl_2$ bolus (CTRL: $n = 8$, PAH: $n = 5$, PAH+RES: $n = 4$; [a]$p < 0.05$ vs. PAH, calculated by a 2-tailed t-test). CTRL: control; PAH: pulmonary arterial hypertension; PAH+RES: PAH treated with resveratrol. All data are presented as the mean ± SEM. [*]$p < 0.05$ vs. CTRL; [a]$p < 0.05$ vs. PAH, calculated by 1-way ANOVA.

Figure 3(e)) and increased mitochondrial superoxide dismutase (SOD) by 36% compared to the PAH group (Figure 3(g)), which is a direct target of SIRT3.

3.4. RES Decreases the Acetylation of CypD. To evaluate the extent of sirtuin activation by RES, the mitochondrial protein acetylation profile, SIRT3 expression, and acetylation of CypD were assessed. In Figure 4(a), the protein acetylation profiles of isolated mitochondria show a 59% increase in acetylated proteins in the PAH group, including a threefold

increase in CypD acetylation (Figure 4(c)). Protein acetylation was decreased by 13% in the PAH-RES group ($p = 0.5303$ vs. PAH); however, SIRT3 was 96% overexpressed (Figure 4(b)). Importantly, CypD was a critical component of mitochondria permeability transitioning, as shown by the significant decrease of 51% ($p = 0.0581$, vs. PAH) in acetylation in the PAH-RES group (Figure 4(c)), indicating the importance of SIRT3 in reducing mitochondrial permeability transitioning. There were no significant between-group differences in SIRT1 gene expression (CTRL = 0.89 ±
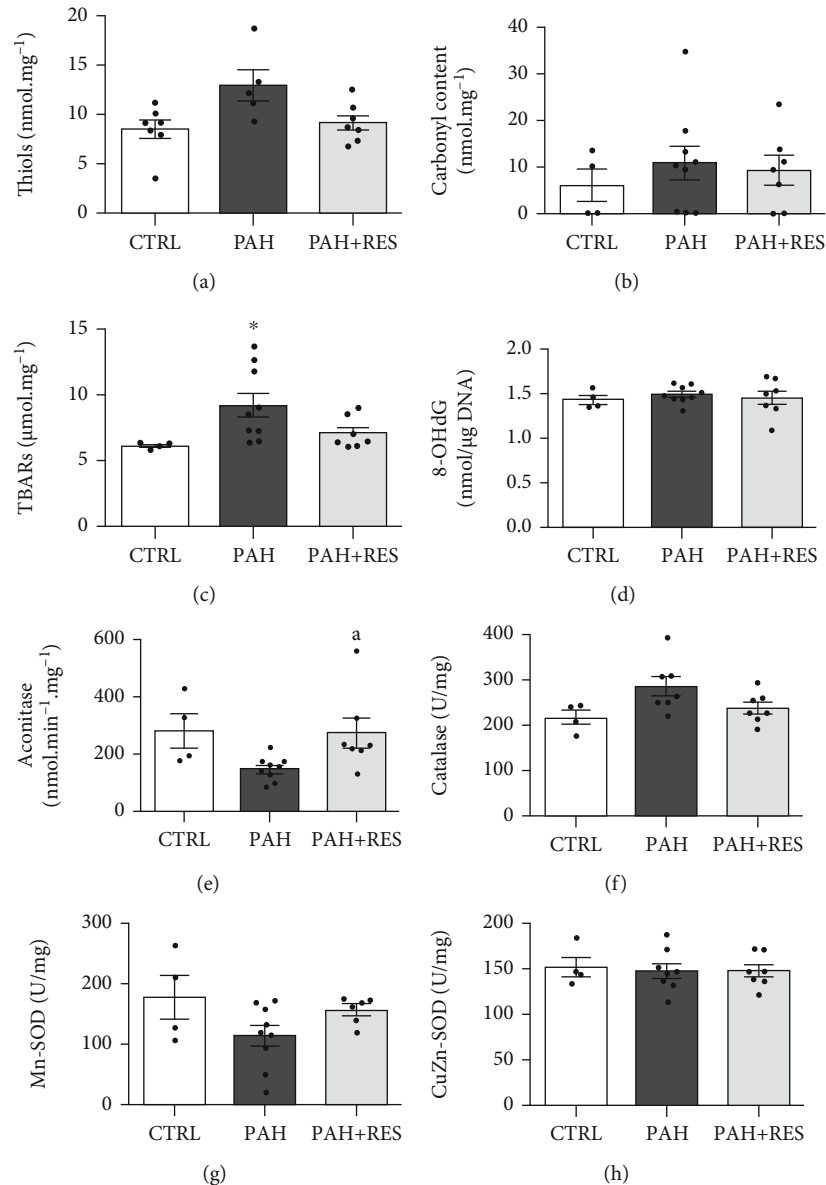
FIGURE 3: Oxidative stress markers in RV. Pooled data from free thiol groups in isolated mitochondria (a). Average of protein carbonylation (b), TBARS (c), and 8-OHdG/total DNA ratio in RV tissue (d). Enzymatic activity of aconitase (e), catalase (f), manganese superoxide dismutase (Mn-SOD) (g), and copper-zinc superoxide dismutase (CuZn-SOD) (h). Control (CTRL: $n = 4$-7); pulmonary arterial hypertension (PAH, $n = 5$-9); PAH treated with resveratrol (PAH+RES, $n = 6$-7). All data are presented as the mean ± SEM. $^{*}p < 0.05$ vs. CTRL; $^{a}p < 0.05$ vs. PAH, calculated by 1-way ANOVA.

0.08; PAH = 0.96 ± 0.12; PAH+RES = 0.82 ± 0.09 mRNA/ HPRT), while SIRT5 decreased in both the PAH and PAH+ RES groups (CTRL = 0.92 ± 0.11; PAH = 0.43 ± 0.08; PAH+ RES = 0.45 ± 0.071 mRNA/HPRT).

4. Discussion

The cardiovascular protective actions of RES in PAH have been reported in RV function [16, 38]; however, the mechanisms involved have not been fully described. According to our results, PAH causes an energetic dysfunction in the RV myocyte by promoting the opening of the mPTP due to CypD hyperacetylation. The decreased energy supply

impairs the highly energy-demanding processes involved in myocyte functions, such as cellular relaxation, by hampering SERCA activity and delaying myofibrils' unbinding. Treating this model with RES stimulates and overexpresses SIRT3, which prevents mPTP opening by acting directly on CypD deacetylation. Preserving cellular energetics also preserves myocyte contraction and relaxation.

4.1. RES Improves Cell Relaxation and SERCA Activity.
Intracellular Ca^{2+} oscillations orchestrate cell contraction-relaxation cycle during Ca^{2+} transient, since cytosolic Ca^{2+} interacts with troponin C allowing actin-myosin interaction.

(a)

(b)

(c)
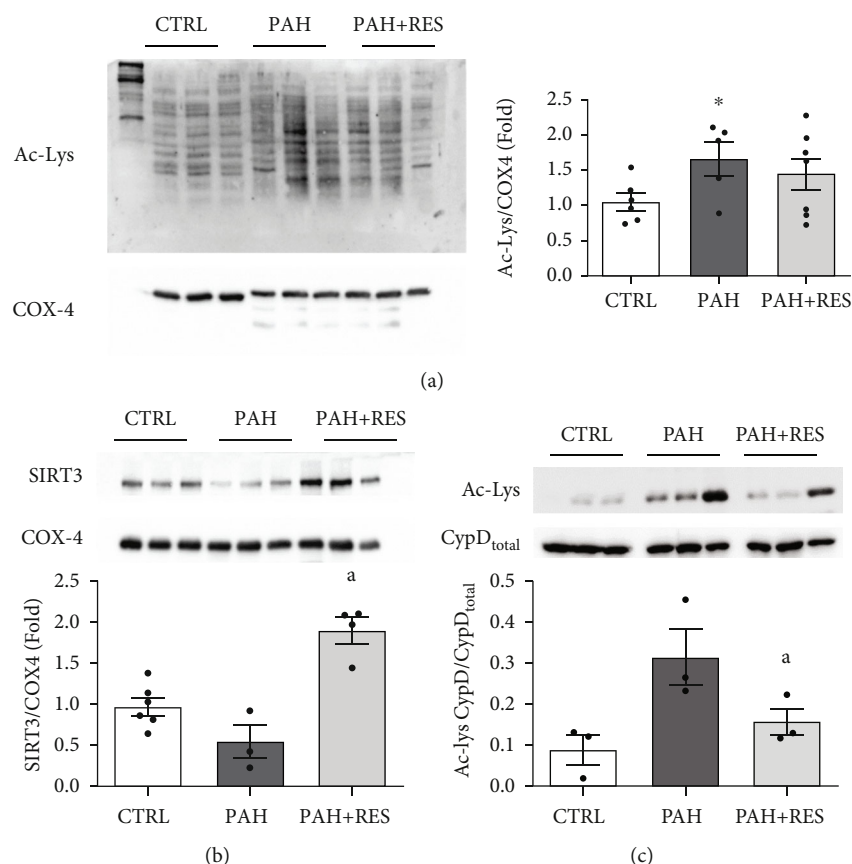
Figure 4: Protein acetylation and SIRT3 expression in RV. Representative image and pooled data of western blot to acetylated lysine (Ac-Lys) profile from isolated mitochondria (a) (CTRL: $n = 5$, PAH: $n = 4$, PAH+RES: $n = 6$). $^*p < 0.05$ vs. CTRL unpaired 2-tailed t-test. (b) Representative images and pooled data of western blot from isolated mitochondria against SIRT3; cytochrome c oxidase subunit 4 (COX-4) was used as a loading control (CTRL: $n = 6$, PAH: $n = 3$, PAH+RES: $n = 4$). (c) Immunoprecipitation (IP) of cyclophilin D (CypD) followed by immunoblot analysis against Ac-Lys; acetylation signal was normalized to total CypD (CTRL: $n = 3$, PAH: $n = 3$, PAH+RES: $n = 3$). Control (CTRL); pulmonary arterial hypertension (PAH); PAH treated with resveratrol (PAH+RES). All data are presented as the mean ± SEM. $^*p < 0.05$ vs. CTRL, $^ap < 0.05$ vs. PAH, calculated by 1-way ANOVA.

RV myocyte functioning was evaluated using confocal microscopy by assessing intracellular Ca^{2+} signaling and cell shortening. Characterization of the cellular contraction-relaxation cycle showed that PAH has a negative impact on the overall contraction-relaxation dynamic. Regardless, no alterations in SR Ca^{2+} release synchronicity during Ca^{2+} transient; it takes longer to accomplish maximal shortening. Treating PAH with RES decreased time to maximal shortening possibly by increased myofilament Ca^{2+} sensitivity [39, 40]; however, it does not fully normalize this parameter. Interestingly, relaxation dynamics showed the most significant changes. PAH considerably prolongs cell relaxation, while PAH under RES treatment keeps the relaxation rate similar to the CTRL group, a finding that has not been previously reported.

Accordingly, major alteration in intracellular Ca^{2+} transient caused by PAH was a decreased SERCA activity caused by a decreased SERCA/PLB ratio. However, both increased [41] and decreased [42] SERCA activities have been reported, as well as no change in SERCA and PLB expression [41]. Although RES treatment did not change the SERCA/PLB

ratio, it did increase intracellular Ca^{2+} removal, thus SERCA activity.

This behavior was replicated after stimulating the β-AR, a highly energy-demanding condition [43, 44]. PAH showed the highest transient amplitude but the lowest cell shortening, while RES preserved the proportionality of Ca^{2+} released and cell contraction.

This effect might be related to a mismatch in the ECEC since it has been documented that creatine kinase (CK) expression is diminished in failing RV caused by PAH due to a decreased ATP supply [21, 45, 46]. Failing to meet the energetic demand, myofilament cross-bridge cycling is inhibited in finding shorter sarcomere lengths [21], compromising myocyte function. In this regard, the preservation of ATP production by RES preserves CK activity and an efficient ATP supply to SERCA, displaying improved cell contraction and relaxation.

Additionally, PAH did not modify Ca^{2+} spark frequency, indicating intact RyR activity [47], unlike previous reports [41, 42]. RES treatment also showed no changes in spark frequency and amplitude.

4.2. RES Preserves Mitochondrial Functioning and Integrity.
Since major alterations caused by PAH reside among highly
energy-dependent mechanisms, cell excitation and contrac-
tion must be tightly linked to the energy supply to ensure
the proper functioning of the myocyte as a whole in an
ECEC process. Since mitochondrial dysfunction has been
identified as one of the mechanisms underlying heart fail-
ure [18, 19, 22, 46], mitochondrial activity was evaluated
in this model. In isolated myocytes, PAH compromises
ATP production by decreasing $\Delta\Psi m$; the electrochemical
force needed for ATP production, decreasing the oxidative
phosphorylation rate (state 3). Decreased phosphorylation
response have been reported in RV by PAH [48–50].
The cardioprotective effects of RES on mitochondria have
been described in several models [51–53]. Similarly, RES
treatment preserved $\Delta\Psi m$ and respiratory chain activity
in PAH. Even though the results obtained by mitochon-
drial respiration and fragility are evident when stimulating
complex II, these same aspects have yet to be evaluated
under NADH-dependent respiration.

Mitochondrial function preservation by RES in PAH
could be related to decrease mitochondrial fragility. The loss
of mitochondrial integrity by mPTP formation has been
described as a main contributor to ventricular dysfunction
in the right and left ventricles [22, 54, 55]. Most importantly,
preventing mPTP opening using CsA has been shown to
reduce RV dysfunction in PAH [22]. Mitochondrial Ca^{2+}
overload in PAH, complemented by an increased oxidative
environment within the mitochondria, makes them more
prone to permeability transition [54, 56]; however, unlike
other reports [57], no critical signs of proteins being modified
by oxidative stress were observed, indicating that the antiox-
idant system is capable of managing oxidative stress caused
by PAH in this model.

Although evident impairment in $\Delta\Psi m$ was found in this
study, outright evidence from reduced cellular bioenergetics
in this PAH model would directly measure ATP levels and
evaluate the phosphocreatine system. However, it is well
established that the ATP phosphorylation is particularly
sensitive to decreases of mitochondrial membrane potential;
for every 14 mV decrease in proton-motive force (equivalent
to $\Delta\Psi m$), the ATP/ADP ratio decreases by 10-fold [58]. Also,
the mitochondrial membrane potential has been described as
a crucial factor to generate rotational torque by the F_0 nano-
motor [59, 60]. Thus, a decrease in this electrochemical force
may impede ATP production. In this regard, the integrity of
$\Delta\Psi m$ in PAH+RES RV myocytes suggests a capable, ener-
getic system to sustain the cardiac ECC.

*4.3. RES Promotes the Deacetylation of CypD by SIRT3
Overexpression.* One of the mechanisms through which RES
bestows its protective effects is the activation of deacetylases.
In pulmonary arterial smooth muscle cells (PASMC), the
protective effect of RES has been linked to expression and
activity modulation of the cytosolic deacetylase SIRT1
[61, 62]. Similarly, an increase in acetylated proteins was
found in PAH RV myocytes [16, 38], and the cardiac pro-
tection of RES through SIRT1 activation has been reported
in different conditions [38, 63–65]. Since PAH's effect is

on mitochondrial function and activity, the expression of
SIRT3 and mitochondrial acetylome were evaluated to
determine the extent of its involvement.

The mitochondrial deacetylase SIRT3, which regulates
mitochondrial function [66–69], is modulated by RES [12],
and the rs11246020 polymorphism, associated with a ~30%
loss of function, has been found to be overrepresented in
patients with idiopathic PAH [25]. PAH showed an increase
in the protein acetylation profile from mitochondria, similar
to reports in PASMC [25]. RES treatment increased SIRT3
expression almost 3.5-fold; however, the acetylation profile
did not decrease significantly from PAH levels. Regardless
of this discrepancy, an important direct target of SIRT3,
cyclophilin D (CypD), decreased by almost half its hyperace-
tylation, diminishing the mitochondria's proneness to mPTP
opening [15, 23], thus preserving the cellular energetic state
(Figure 5).

Furthermore, SIRT3 activity has been linked to the
prevention of myocardial dysfunction. Treatment with
honokiol, a potent SIRT3 activator, prevents and reverses
ventricular hypertrophy [70] and preserves mitochondrial
integrity and energetic capability [70, 71]. The mecha-
nisms involved still need to be elucidated; however, it
has been found that SIRT3 prevents mitochondrial Ca^{2+}
overload by regulating mitochondrial Ca^{2+} uptake, regulat-
ing the expression of mitochondrial Ca^{2+} uniporter and its
main regulator MICU1. These data are relevant because it
was established that MCU and the MICU1 promoter are
regulated by SIRT3-dependent histone acetylation [72].
However, no change in MCU gene expression was found
in this model.

While SIRT3 activity has been identified as being
involved in cardiovascular protection [73–77], it is not the
only mechanism through which RES acts as a cardioprotec-
tive agent. Other sirtuins and enzymes, such as SIRT1,
SIRT5, and AMPK [5, 6, 78], contribute to modulating the
activation or repression of a wide range of cellular compo-
nents [5, 6, 78]. Furthermore, PAH pathogenesis is not
caused by a single modification; according to the widely
accepted "multiple-hit" hypothesis: inflammation, genetic
determinants, and environmental factors are needed to
develop the disease [79, 80].

Another important mechanism involved in modulating
mitochondrial functioning that we did not explore thor-
oughly in this study is mitochondrial dynamics. The deacety-
lation of OPA1 by SIRT3 has been described as a regulator of
mitochondrial dynamics and plays a role in maintaining a
competent mitochondrial population in the heart when it is
under pathological stress [81]. While previous reports did
not find changes in the gene expression of proteins involved
in mitochondrial dynamics and biogenesis in PAH [82], it
has been reported that RES promotes mitochondrial fission
[83]. This phenomenon is needed to preserve mitochondrial
function [84] and may be involved in $\Delta\Psi m$ preservation by
RES in this model. However, the implications of mitochon-
drial dynamics in the progression of RV failure still need to
be addressed; this phenomenon could be an interesting area
of research in the future to elucidate new therapeutic targets
in PAH.
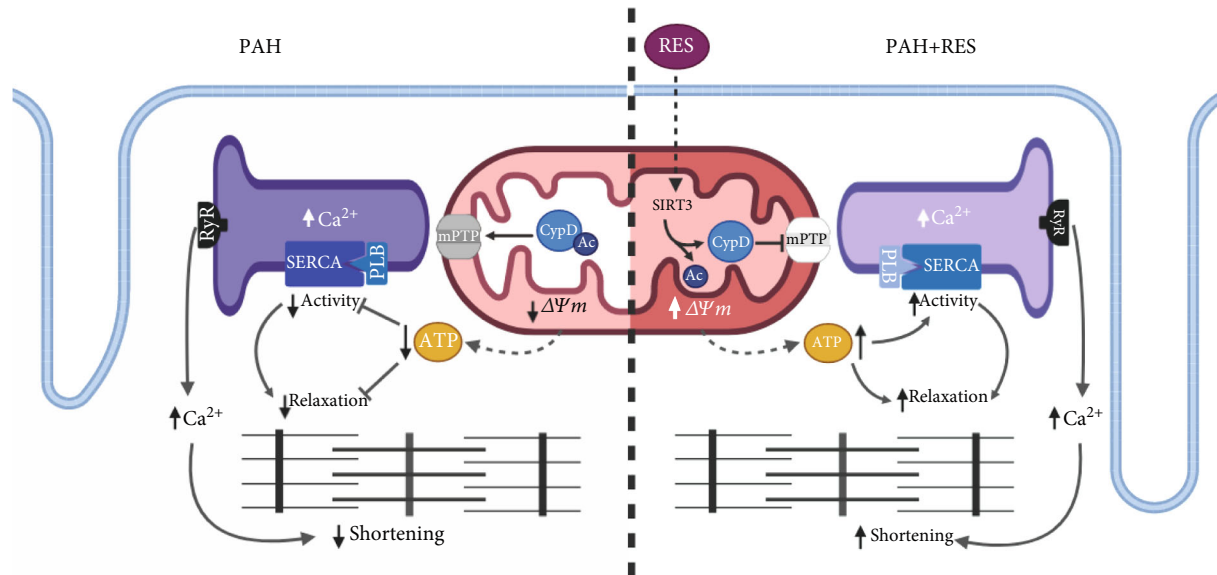
FIGURE 5: Proposed mechanism of RES cardioprotection. Resveratrol stimulates SIRT3 activation and expression, which deacetylates CypD preventing mPTP formation and preserving $\Delta\Psi m$, thus increasing ATP synthesis. The preserved mitochondrial function promotes a high-energy demand process to occur, such as cellular relaxation and SERCA activity, preventing excitation-contraction-energetic coupling mismatch. RES: resveratrol; LTCC: L-type Ca^{2+} channel; RyR: ryanodine receptor; SERCA2: sarco-endoplasmic reticulum Ca^{2+}-ATPase; PLB: phospholamban; mPTP: mitochondrial permeability and transition pore; CypD: cyclophilin D; Ac: acetyl-group; SIRT3: sirtuin 3; $\Delta\Psi m$: mitochondrial membrane potential. Created with http://BioRender.com.

Although we found a strong relationship between preservation of mitochondrial function and CypD acetylation via SIRT3, loss and gain of function experiments can assess its definitive role in this model. The availability of deficient-SIRT3 mice faces the challenge of PHA model development, since it has been reported that mouse PAH models may not develop pulmonary hypertension, RV hypertrophy, and RV failure regardless pulmonary artery remodeling; besides, some of the models show spontaneous reverse of pulmonary hypertension once the inductor is not present [85, 86].

4.4. Clinical Implications. This study suggests that mitochondrial protection and cellular energetic preservation could be possible therapeutic targets to improve the PAH phenotype. The currently approved PAH medications decrease vascular remodeling by restoring the balance between vasoactive and vasodilator mediators [87]. However, researchers have begun to focus on mitochondrial disorders to develop new strategies. Molecules that prevent and reverse mitochondrial bioenergetic abnormalities in PASMC are being explored due to their ability to promote apoptosis, thus decreasing pulmonary vascular remodeling [88–91] and, in RV fibroblasts, reducing cardiac fibrosis in PAH [92]. Unfortunately, cardioprotective effects on RV muscle cells have not been explored. Although RES' usefulness in treating cardiovascular diseases has been observed as an overall beneficial effect in diverse clinical trials, further research is needed to ensure sustained effectiveness in patients since its major disadvantage is its poor bioavailability [93]. No published studies have evaluated RES use in PAH patients. Finally, ECEC disruption is a phenomenon found in the right and left heart failure. Describing the underlying mechanism and identifying shared targets may be useful to recognize therapeutic strategies that can help to improve heart failure prognosis and care.

5. Conclusions

The present work assessed the alterations in RV myocytes caused by PAH and RES' protection. For the first time, we showed that the development of PAH causes a mismatch in the ECEC: compromised mitochondrial functioning and altered ATP synthesis resulted in deficient cell relaxation and disrupted cell contraction. RES protects mitochondria integrity by decreasing CypD hyperacetylation and increasing SIRT3 expression and activity, preventing mPTP opening, and preserving the $\Delta\Psi m$. Maintaining cellular energetics preserves ECEC, ensuring the proper functioning of the myocyte as a whole. Understanding the mechanisms involved in the protection that RES confers on the RV in PAH could facilitate the development of new adjuvant therapies that improve the daily lives of PAH patients.

Data Availability

The data used to support the findings of this study are available from the corresponding author upon request.

Disclosure

This work was submitted in partial fulfilment of the requirements for the PhD degree (JBR) for the Doctorate in Biotechnology, Tecnológico de Monterrey.

Conflicts of Interest

The authors declare that there is no conflict of interest regarding the publication of this paper.

Acknowledgments

Supplementary Materials

Supplemental Table 1: qPCR primer sequences hypoxanthine phosphoribosyltransferase 1 (HPRT), Na^+/Ca^{2+} exchanger (NCX), sirtuin 1 (Sirt1), sirtuin 5 (Sirt5), and mitochondria calcium uniplex (MCU). HPRT was used as a housekeeping gene. Supplementary Figure 1: heart and lung structural comparison between control animals and RES-treated control animals. Pooled data of muscularized arteries (A), luminal diameter (B), and occlusion (C) in the lung tissue (H&E, 10x). Bar graph depicting the myocyte area (D) in RV. Data was normalized to CTRL mean values. All data are presented as the mean ± SEM. $^*p < 0.05$ vs. CTRL calculated by a t-test followed by the Mann–Whitney test. Supplementary Figure 2: characterization of RV myocytes Ca^{2+} transient in isolated RV myocytes. (A) Representative line scan images of Ca^{2+} transient before (baseline) and after β-adrenergic stimulation with 100 nM isoproterenol (ISO). Pooled data of Ca^{2+} transient amplitude (B), time to 50% decay ($T_{50\%}$, C), and time to peak (D) (CTRL:$n = 115.48$cells and 4 animals; PAH:$n = 51.36$cells and 3-4 animals; PAH+RES:$n = 68.37$ cells and 4 animals; baseline and ISO, respectively). (E) Percentage of maximal shortening before and after β-adrenergic stimulation (CTRL:$n = 40.8$cells and 1-4 animals; PAH:$n = 26.35$cells and 3-4 animals; PAH+RES:$n = 54.36$cells and 4 animals; baseline and ISO, respectively). Records were taken under 1 Hz pace. CTRL: control; PAH: pulmonary arterial hypertension; PAH+RES: PAH treated with resveratrol. All data are presented as the mean ± SEM, unless otherwise stated. $^*p < 0.05$ vs. respective CTRL, $^ap < 0.05$ vs. respective PAH, and $^bp < 0.05$ vs. respective basal, calculated by 1-way ANOVA. (Supplementary Materials)

References

[1] A. Hemnes, A. M. K. Rothman, A. J. Swift, and L. S. Zisman, "Role of biomarkers in evaluation, treatment and clinical studies of pulmonary arterial hypertension," *Pulmonary Circulation*, vol. 10, no. 4, 2020.

[2] F. S. de Man, M. L. Handoko, and A. Vonk-Noordegraaf, "The unknown pathophysiological relevance of right ventricular hypertrophy in pulmonary arterial hypertension," *European Respiratory Journal*, vol. 53, no. 4, 2019.

[3] N. Galiè, R. N. Channick, R. P. Frantz et al., "Risk stratification and medical therapy of pulmonary arterial hypertension," *European Respiratory Journal*, vol. 53, no. 1, p. 1801889, 2019.

[4] A. Huertas, L. Tu, M. Humbert, and C. Guignabert, "Chronic inflammation within the vascular wall in pulmonary arterial hypertension: more than a spectator," *Cardiovascular Research*, vol. 116, no. 5, pp. 885–893, 2020.

[5] S. Bradamante, L. Barenghi, and A. Villa, "Cardiovascular Protective Effects of Resveratrol," *Cardiovascular drug reviews*, vol. 22, no. 3, pp. 169–188, 2004.

[6] S. S. Kulkarni and C. Cantó, "The molecular targets of resveratrol," *Biochimica et Biophysica Acta (BBA) - Molecular Basis of Disease*, vol. 1852, no. 6, pp. 1114–1123, 2015.

[7] A. Sanches-Silva, L. Testai, S. F. Nabavi et al., "Therapeutic potential of polyphenols in cardiovascular diseases: regulation of mTOR signaling pathway," *Pharmacological Research*, vol. 152, p. 104626, 2020.

[8] D. Bonnefont-Rousselot, "Resveratrol and cardiovascular diseases," *Nutrients*, vol. 8, no. 5, p. 250, 2016.

[9] A. Csiszar, N. Labinskyy, S. Olson et al., "Resveratrol prevents monocrotaline-induced pulmonary hypertension in rats," *Hypertension*, vol. 54, no. 3, pp. 668–675, 2009.

[10] R. K. Vella, C. Pullen, F. R. Coulson, and A. S. Fenning, "Resveratrol prevents cardiovascular complications in the SHR/STZ rat by reductions in oxidative stress and inflammation," *BioMed Research International*, vol. 2015, Article ID 918123, 8 pages, 2015.

[11] M. M. Poulsen, K. Fjeldborg, M. J. Ornstrup, T. N. Kjær, M. K. Nøhr, and S. B. Pedersen, "Resveratrol and inflammation: challenges in translating pre-clinical findings to improved patient outcomes," *Biochimica et Biophysica Acta (BBA) - Molecular Basis of Disease*, vol. 1852, no. 6, pp. 1124–1136, 2015.

[12] N. Treviño-Saldaña and G. García-Rivas, "Regulation of sirtuin-mediated protein deacetylation by cardioprotective phytochemicals," *Oxidative Medicine and Cellular Longevity*, vol. 2017, Article ID 1750306, 16 pages, 2017.

[13] N. R. Sundaresan, M. Gupta, G. Kim, S. B. Rajamohan, A. Isbatan, and M. P. Gupta, "Sirt3 blocks the cardiac hypertrophic response by augmenting Foxo3a-dependent antioxidant defense mechanisms in mice," *The Journal of Clinical Investigation*, vol. 119, no. 9, pp. 2758–2771, 2009.

[14] M. Kerr, J. J. Miller, D. Thapa et al., "Rescue of myocardial energetic dysfunction in diabetes through the correction of mitochondrial hyperacetylation by honokiol," *JCI insight*, vol. 5, no. 17, 2020.

[15] E. C. Castillo, J. A. Morales, H. Chapoy-Villanueva et al., "Mitochondrial hyperacetylation in the failing hearts of obese patients mediated partly by a reduction in SIRT3: the involvement of the mitochondrial permeability transition pore," *Cellular Physiology and Biochemistry*, vol. 53, no. 3, pp. 465–479, 2019.

[16] E. Vázquez-Garza, J. Bernal-Ramírez, C. Jerjes-Sánchez et al., "Resveratrol prevents right ventricle remodeling and dysfunction in monocrotaline-induced pulmonary arterial hypertension with a limited improvement in the lung vasculature," *Oxidative Medicine and Cellular Longevity*, vol. 2020, Article ID 1841527, 13 pages, 2020.

[17] N. V. Shults, S. S. Kanovka, J. E. Ten Eyck, V. Rybka, and Y. J. Suzuki, "Ultrastructural changes of the right ventricular myocytes in pulmonary arterial hypertension," *Journal of the*

American Heart Association, vol. 8, no. 5, article e011227, 2019.

[18] F. Potus, C. Hindmarch, K. Dunham-Snary, J. Stafford, and S. Archer, "Transcriptomic signature of right ventricular failure in experimental pulmonary arterial hypertension: deep sequencing demonstrates mitochondrial, fibrotic, inflammatory and angiogenic abnormalities," *International Journal of Molecular Sciences*, vol. 19, no. 9, 2018.

[19] L. Piao, Y.-H. Fang, V. J. J. Cadete et al., "The inhibition of pyruvate dehydrogenase kinase improves impaired cardiac function and electrical remodeling in two models of right ventricular hypertrophy: resuscitating the hibernating right ventricle," *Journal of Molecular Medicine (Berlin, Germany)*, vol. 88, no. 1, pp. 47–60, 2010.

[20] L. Piao, G. Marsboom, and S. L. Archer, "Mitochondrial metabolic adaptation in right ventricular hypertrophy and failure," *Journal of Molecular Medicine (Berlin, Germany)*, vol. 88, no. 10, pp. 1011–1020, 2010.

[21] E. D. Fowler, D. Benoist, M. J. Drinkhill et al., "Decreased creatine kinase is linked to diastolic dysfunction in rats with right heart failure induced by pulmonary artery hypertension," *Journal of Molecular and Cellular Cardiology*, vol. 86, pp. 1–8, 2015.

[22] D. S. Lee and Y. W. Jung, "Protective effect of right ventricular mitochondrial damage by cyclosporine A in monocrotaline-induced pulmonary hypertension," *Korean Circulation Journal*, vol. 48, no. 12, pp. 1135–1144, 2018.

[23] A. V. Hafner, J. Dai, A. P. Gomes et al., "Regulation of the mPTP by SIRT3-mediated deacetylation of Cyp D at lysine 166 suppresses age-related cardiac hypertrophy," *Aging*, vol. 2, no. 12, pp. 914–923, 2010.

[24] T. Bochaton, C. Crola-Da-Silva, B. Pillot et al., "Inhibition of myocardial reperfusion injury by ischemic postconditioning requires sirtuin 3-mediated deacetylation of cyclophilin D," *Journal of Molecular and Cellular Cardiology*, vol. 84, pp. 61–69, 2015.

[25] R. Paulin, P. Dromparis, G. Sutendra et al., "Sirtuin 3 deficiency is associated with inhibited mitochondrial function and pulmonary arterial hypertension in rodents and humans," *Cell Metabolism*, vol. 20, no. 5, pp. 827–839, 2014.

[26] J. R. Klinger, C. G. Elliott, D. J. Levine et al., "Therapy for pulmonary arterial hypertension in adults: update of the CHEST guideline and expert panel report," *Chest*, vol. 155, no. 3, pp. 565–586, 2019.

[27] D. Santos-Ribeiro, P. Mendes-Ferreira, C. Maia-Rocha, R. Adão, A. F. Leite-Moreira, and C. Brás-Silva, "Hypertension arterielle pulmonaire : connaissances de base pour les cliniciens," *Archives of Cardiovascular Diseases*, vol. 109, no. 10, pp. 550–561, 2016.

[28] C. E. Guerrero-Beltrán, J. Bernal-Ramírez, O. Lozano et al., "Silica nanoparticles induce cardiotoxicity interfering with energetic status and Ca^{2+} handling in adult rat cardiomyocytes," *American Journal of Physiology-Heart and Circulatory Physiology*, vol. 312, no. 4, pp. H645–H661, 2017.

[29] P. Pérez-Treviño, J. Sepúlveda-Leal, and J. Altamirano, "Simultaneous assessment of calcium handling and contractility dynamics in isolated ventricular myocytes of a rat model of post-acute isoproterenol- induced cardiomyopathy," *Cell Calcium*, vol. 86, p. 102138, 2020.

[30] E. Fernández-Sada, C. Silva-Platas, C. A. Villegas et al., "Cardiac responses to β-adrenoceptor stimulation is partly dependent on mitochondrial calcium uniporter activity," *British Journal of Pharmacology*, vol. 171, no. 18, pp. 4207–4221, 2014.

[31] E. Picht, A. V. Zima, L. A. Blatter, and D. M. Bers, "SparkMaster: automated calcium spark analysis with ImageJ," *American Journal of Physiology. Cell Physiology*, vol. 293, no. 3, pp. C1073–C1081, 2007.

[32] C. Silva-Platas, C. E. Guerrero-Beltrán, M. Carrancá et al., "Antineoplastic copper coordinated complexes (Casiopeinas) uncouple oxidative phosphorylation and induce mitochondrial permeability transition in cardiac mitochondria and cardiomyocytes," *Journal of Bioenergetics and Biomembranes*, vol. 48, no. 1, pp. 43–54, 2016.

[33] G. de Jesús García-Rivas, A. Guerrero-Hernández, G. Guerrero-Serna, J. S. Rodríguez-Zavala, and C. Zazueta, "Inhibition of the mitochondrial calcium uniporter by the oxo-bridged dinuclear ruthenium amine complex (Ru360) prevents from irreversible injury in postischemic rat heart," *The FEBS Journal*, vol. 272, no. 13, pp. 3477–3488, 2005.

[34] H. Chapoy-Villanueva, C. Silva-Platas, A. K. Gutiérrez-Rodríguez et al., "Changes in the stoichiometry of uniplex decrease mitochondrial calcium overload and contribute to tolerance of cardiac ischemia/reperfusion injury in hypothyroidism," *Thyroid*, vol. 29, no. 12, pp. 1755–1764, 2019.

[35] N. García, J. J. García, F. Correa, and E. Chávez, "The permeability transition pore as a pathway for the release of mitochondrial DNA," *Life Sciences*, vol. 76, no. 24, pp. 2873–2880, 2005.

[36] J. E. Vela-Guajardo, P. Pérez-Treviño, I. Rivera-Álvarez, F. A. González-Mondellini, J. Altamirano, and N. García, "The 8-oxo-deoxyguanosine glycosylase increases its migration to mitochondria in compensated cardiac hypertrophy," *Journal of the American Society of Hypertension*, vol. 11, no. 10, pp. 660–672, 2017.

[37] R. Nogueira-Ferreira, R. Vitorino, R. Ferreira, and T. Henriques-Coelho, "Exploring the monocrotaline animal model for the study of pulmonary arterial hypertension: a network approach," *Pulmonary Pharmacology & Therapeutics*, vol. 35, pp. 8–16, 2015.

[38] P. Chelladurai, O. Boucherat, K. Stenmark et al., "Targeting histone acetylation in pulmonary hypertension and right ventricular hypertrophy," *British Journal of Pharmacology*, vol. 178, no. 1, pp. 54–71, 2021.

[39] R. Liew, M. A. Stagg, K. T. MacLeod, and P. Collins, "The red wine polyphenol, resveratrol, exerts acute direct actions on guinea- pig ventricular myocytes," *European Journal of Pharmacology*, vol. 519, no. 1-2, pp. 1–8, 2005.

[40] S. E. Pineda-Sanabria, I. M. Robertson, and B. D. Sykes, "Structure of trans-resveratrol in complex with the cardiac regulatory protein troponin C," *Biochemistry*, vol. 50, no. 8, pp. 1309–1320, 2011.

[41] J. Sabourin, A. Boet, C. Rucker-Martin et al., "Ca^{2+} handling remodeling and STIM1L/Orai1/TRPC1/TRPC4 upregulation in monocrotaline-induced right ventricular hypertrophy," *Journal of Molecular and Cellular Cardiology*, vol. 118, pp. 208–224, 2018.

[42] D. Benoist, R. Stones, M. J. Drinkhill et al., "Cardiac arrhythmia mechanisms in rats with heart failure induced by pulmonary hypertension," *American Journal of Physiology-Heart and Circulatory Physiology*, vol. 302, no. 11, pp. H2381–H2395, 2012.

[43] Y. Fu, R. E. Westenbroek, T. Scheuer, and W. A. Catterall, "Phosphorylation sites required for regulation of cardiac

calcium channels in the fight-or-flight response," *Proceedings of the National Academy of Sciences of the United States of America*, vol. 110, no. 48, pp. 19621–19626, 2013.

[44] A. E. Messer and S. B. Marston, "Investigating the role of uncoupling of troponin I phosphorylation from changes in myofibrillar Ca^{2+}-sensitivity in the pathogenesis of cardiomyopathy," *Frontiers in Physiology*, vol. 5, p. 315, 2014.

[45] E. D. Fowler, M. J. Drinkhill, R. Stones, and E. White, "Diastolic dysfunction in pulmonary artery hypertension: Creatine kinase and the potential therapeutic benefit of beta-blockers," *Clinical and Experimental Pharmacology and Physiology*, vol. 45, no. 4, pp. 384–389, 2018.

[46] E. D. Fowler, D. Hauton, J. Boyle, S. Egginton, D. S. Steele, and E. White, "Energy metabolism in the failing right ventricle : limitations of oxygen delivery and the creatine kinase system," *International Journal of Molecular Sciences*, vol. 20, no. 8, 2019.

[47] A. Kushnir, B. Wajsberg, and A. R. Marks, "Ryanodine receptor dysfunction in human disorders," *Biochimica et Biophysica Acta (BBA) - Molecular Cell Researchs*, vol. 1865, no. 11, pp. 1687–1697, 2018.

[48] K. A. Cottrill and S. Y. Chan, "Metabolic dysfunction in pulmonary hypertension: the expanding relevance of the Warburg effect," *European Journal of Clinical Investigation*, vol. 43, no. 8, pp. 855–865, 2013.

[49] J. Gomez-Arroyo, S. Mizuno, K. Szczepanek et al., "Metabolic gene remodeling and mitochondrial dysfunction in failing right ventricular hypertrophy secondary to pulmonary arterial hypertension," *Circulation. Heart Failure*, vol. 6, no. 1, pp. 136–144, 2013.

[50] A. Vonk-Noordegraaf, F. Haddad, K. M. Chin et al., "Right heart adaptation to pulmonary arterial hypertension: physiology and pathobiology," *Journal of the American College of Cardiology*, vol. 62, no. 25, pp. D22–D33, 2013.

[51] L. C. Thuc, Y. Teshima, N. Takahashi et al., "Inhibition of Na(+)-H(+) exchange as a mechanism of rapid cardioprotection by resveratrol," *British Journal of Pharmacology*, vol. 166, no. 6, pp. 1745–1755, 2012.

[52] M. M. Sung, S. K. Das, J. Levasseur et al., "Resveratrol treatment of mice with pressure-overload-induced heart failure improves diastolic function and cardiac energy metabolism," *Circulation. Heart Failure*, vol. 8, no. 1, pp. 128–137, 2015.

[53] T. Li, L. Chen, Y. Yu, B. Yang, P. Li, and X.-Q. Tan, "Resveratrol alleviates hypoxia/reoxygenation injury-induced mitochondrial oxidative stress in cardiomyocytes," *Molecular Medicine Reports*, vol. 19, no. 4, pp. 2774–2780, 2019.

[54] A. Riojas-Hernández, J. Bernal-Ramírez, D. Rodríguez-Mier et al., "Enhanced oxidative stress sensitizes the mitochondrial permeability transition pore to opening in heart from Zucker Fa/fa rats with type 2 diabetes," *Life Sciences*, vol. 141, pp. 32–43, 2015.

[55] F. Ahmad, A. P. Singh, D. Tomar et al., "Cardiomyocyte-GSK-3α promotes mPTP opening and heart failure in mice with chronic pressure overload," *Journal of Molecular and Cellular Cardiology*, vol. 130, pp. 65–75, 2019.

[56] R. Endlicher, Z. Drahota, and Z. Červinková, "In vitro and in vivo activation of mitochondrial membrane permeability transition pore using triiodothyronine," *Physiological Research*, vol. 65, no. 2, pp. 321–331, 2016.

[57] N. L. Jernigan, J. S. Naik, L. Weise-Cross et al., "Contribution of reactive oxygen species to the pathogenesis of pulmonary

[58] D. G. Nicholls, "Mitochondrial membrane potential and aging," *Aging Cell*, vol. 3, no. 1, pp. 35–40, 2004.

[59] P. Dimroth, G. Kaim, and U. Matthey, "Crucial role of the membrane potential for ATP synthesis by F (1) F (o) ATP synthases," *The Journal of Experimental Biology*, vol. 203, no. 1, pp. 51–59, 2000.

[60] D. Stock, C. Gibbons, I. Arechaga, A. G. Leslie, and J. E. Walker, "The rotary mechanism of ATP synthase," *Current Opinion in Structural Biology*, vol. 10, no. 6, pp. 672–679, 2000.

[61] S. Zhou, M.-T. Li, Y.-Y. Jia et al., "Regulation of Cell Cycle Regulators by SIRT1 Contributes to Resveratrol- Mediated Prevention of Pulmonary Arterial Hypertension," *BioMed Research International*, vol. 2015, Article ID 762349, 14 pages, 2015.

[62] L. Yu, Y. Tu, X. Jia et al., "Resveratrol protects against pulmonary arterial hypertension in rats via activation of silent information regulator 1," *Cellular Physiology and Biochemistry*, vol. 42, no. 1, pp. 55–67, 2017.

[63] S. Ma, J. Feng, R. Zhang et al., "SIRT1 activation by resveratrol alleviates cardiac dysfunction via mitochondrial regulation in diabetic cardiomyopathy mice," *Oxidative Medicine and Cellular Longevity*, vol. 2017, Article ID 4602715, 15 pages, 2017.

[64] N. Fourny, C. Lan, E. Seree, M. Bernard, and M. Desrois, "Protective effect of resveratrol against ischemia-reperfusion injury via enhanced high energy compounds and eNOS-SIRT1 expression in type 2 diabetic female rat heart," *Nutrients*, vol. 11, no. 1, 2019.

[65] Z.-H. Liu, Y. Zhang, X. Wang et al., "SIRT1 activation attenuates cardiac fibrosis by endothelial-to-mesenchymal transition," *Biomedicine & Pharmacotherapy*, vol. 118, p. 109227, 2019.

[66] D. B. Lombard, F. W. Alt, H.-L. Cheng et al., "Mammalian Sir 2 homolog SIRT3 regulates global mitochondrial lysine acetylation," *Molecular and Cellular Biology*, vol. 27, no. 24, pp. 8807–8814, 2007.

[67] S. Zhao, W. Xu, W. Jiang et al., "Regulation of cellular metabolism by protein lysine acetylation," *Science*, vol. 327, no. 5968, pp. 1000–1004, 2010.

[68] L. W. S. Finley, W. Haas, V. Desquiret-Dumas et al., "Succinate dehydrogenase is a direct target of sirtuin 3 deacetylase activity," *PLoS One*, vol. 6, no. 8, article e23295, 2011.

[69] M. D. Hirschey, T. Shimazu, E. Jing et al., "SIRT3 deficiency and mitochondrial protein hyperacetylation accelerate the development of the metabolic syndrome," *Molecular Cell*, vol. 44, no. 2, pp. 177–190, 2011.

[70] V. B. Pillai, S. Samant, N. R. Sundaresan et al., "Honokiol blocks and reverses cardiac hypertrophy in mice by activating mitochondrial Sirt3," *Nature Communications*, vol. 6, no. 1, 2015.

[71] V. B. Pillai, A. Kanwal, Y. H. Fang et al., "Honokiol, an activator of Sirtuin-3 (SIRT3) preserves mitochondria and protects the heart from doxorubicin-induced cardiomyopathy in mice," *Oncotarget*, vol. 8, no. 21, pp. 34082–34098, 2017.

[72] P. Gao, Y. Jiang, H. Wu et al., "Inhibition of mitochondrial calcium overload by SIRT3 prevents obesity-or age-related whitening of brown adipose tissue," *Diabetes*, vol. 69, no. 2, pp. 165–180, 2020.

[73] A. Benigni, P. Cassis, S. Conti et al., "Sirt3deficiency shortens life span and impairs cardiac mitochondrial function rescued

byOpa1gene transfer," *Antioxidants & Redox Signaling*, vol. 31, no. 17, pp. 1255–1271, 2019.

[74] S. Wang, Z. Zhao, Y. Fan et al., "Mst1 inhibits Sirt3 expression and contributes to diabetic cardiomyopathy through inhibiting Parkin-dependent mitophagy," *Biochimica et Biophysica Acta - Molecular Basis of Disease*, vol. 1865, no. 7, pp. 1905–1914, 2019.

[75] A. E. Dikalova, A. Pandey, L. Xiao et al., "Mitochondrial deacetylase Sirt 3 reduces vascular dysfunction and hypertension while Sirt 3 depletion in essential hypertension is linked to vascular inflammation and oxidative stress," *Circulation Research*, vol. 126, no. 4, pp. 439–452, 2020.

[76] X. Palomer, M. S. Román-Azcona, J. Pizarro-Delgado et al., "SIRT3-mediated inhibition of FOS through histone H3 deacetylation prevents cardiac fibrosis and inflammation," *Signal Transduction and Targeted Therapy*, vol. 5, no. 1, p. 14, 2020.

[77] Z. Zhu, H. Li, W. Chen, Y. Cui, A. Huang, and X. Qi, "Perindopril improves cardiac function by enhancing the expression of SIRT3 and PGC-1α in a rat model of isoproterenol-induced cardiomyopathy," *Frontiers in Pharmacology*, vol. 11, p. 94, 2020.

[78] A. McCalley, S. Kaja, A. J. Payne, and P. Koulen, "Resveratrol and calcium signaling: molecular mechanisms and clinical relevance," *Molecules*, vol. 19, no. 6, pp. 7327–7340, 2014.

[79] R. Souza, C. Jardim, and M. Humbert, "Idiopathic pulmonary arterial hypertension," *Seminars in Respiratory and Critical Care Medicine*, vol. 34, no. 5, pp. 560–567, 2013.

[80] R. Paulin and E. D. Michelakis, "The metabolic theory of pulmonary arterial hypertension," *Circulation Research*, vol. 115, no. 1, pp. 148–164, 2014.

[81] S. A. Samant, H. J. Zhang, Z. Hong et al., "SIRT3 deacetylates and activates OPA1 to regulate mitochondrial dynamics during stress," *Molecular and Cellular Biology*, vol. 34, no. 5, pp. 807–819, 2014.

[82] D. R. Bruns, R. D. Brown, K. R. Stenmark, P. M. Buttrick, and L. A. Walker, "Mitochondrial integrity in a neonatal bovine model of right ventricular dysfunction," *American Journal of Physiology. Lung Cellular and Molecular Physiology*, vol. 308, no. 2, pp. L158–L167, 2015.

[83] X. Ren, L. Chen, J. Xie et al., "Resveratrol ameliorates mitochondrial elongation via Drp1/Parkin/PINK1 signaling in senescent-like cardiomyocytes," *Oxidative Medicine and Cellular Longevity*, vol. 2017, Article ID 4175353, 20 pages, 2017.

[84] S. Pickles, P. Vigie, and R. J. Youle, "Mitophagy and quality control mechanisms in mitochondrial maintenance," *Current Biology*, vol. 28, no. 4, pp. R170–R185, 2018.

[85] J. Gomez-Arroyo, S. J. Saleem, S. Mizuno et al., "A brief overview of mouse models of pulmonary arterial hypertension: problems and prospects," *American Journal of Physiology. Lung Cellular and Molecular Physiology*, vol. 302, no. 10, pp. L977–L991, 2012.

[86] B. L. Carman, D. N. Predescu, R. Machado, and S. A. Predescu, "Plexiform arteriopathy in rodent models of pulmonary arterial hypertension," *The American Journal of Pathology*, vol. 189, no. 6, pp. 1133–1144, 2019.

[87] M. Bisserier, N. Pradhan, and L. Hadri, "Current and emerging therapeutic approaches to pulmonary hypertension," *Reviews in Cardiovascular Medicine*, vol. 21, no. 2, pp. 163–179, 2020.

[88] B. Li, Y. Zhu, Q. Sun et al., "Reversal of the Warburg effect with DCA in PDGF-treated human PASMC is potentiated by pyruvate dehydrogenase kinase-1 inhibition mediated through blocking Akt/GSK-3β signalling," *International Journal of Molecular Medicine*, vol. 42, no. 3, pp. 1391–1400, 2018.

[89] M. S. McMurtry, S. Bonnet, X. Wu et al., "Dichloroacetate prevents and reverses pulmonary hypertension by inducing pulmonary artery smooth muscle cell apoptosis," *Circulation Research*, vol. 95, no. 8, pp. 830–840, 2004.

[90] E. D. Michelakis, V. Gurtu, L. Webster et al., "Inhibition of pyruvate dehydrogenase kinase improves pulmonary arterial hypertension in genetically susceptible patients," *Science Translational Medicine*, vol. 9, no. 413, 2017.

[91] R. Kurosawa, K. Satoh, N. Kikuchi et al., "Identification of celastramycin as a novel therapeutic agent for pulmonary arterial hypertension," *Circulation Research*, vol. 125, no. 3, pp. 309–327, 2019.

[92] L. Tian, D. Wu, A. Dasgupta et al., "Epigenetic metabolic reprogramming of right ventricular fibroblasts in pulmonary arterial hypertension: a pyruvate dehydrogenase kinase-dependent shift in mitochondrial metabolism promotes right ventricular fibrosis," *Circulation Research*, vol. 126, no. 12, pp. 1723–1745, 2020.

[93] A. Y. Berman, R. A. Motechin, M. Y. Wiesenfeld, and M. K. Holz, "The therapeutic potential of resveratrol: a review of clinical trials," *NPJ Precision Oncology*, vol. 1, no. 1, 2017.

Research Article

RIPK3-Mediated Necroptosis in Diabetic Cardiomyopathy Requires CaMKII Activation

Yun Chen [ID],[1,2] **Xinshuai Li** [ID],[1] **Yuyun Hua** [ID],[1] **Yue Ding** [ID],[1] **Guoliang Meng** [ID],[1,2] **and Wei Zhang** [ID][1,2]

[1]*Department of Pharmacology, School of Pharmacy, Nantong University, Key Laboratory of Inflammation and Molecular Drug Target of Jiangsu Province, Nantong, 226001 Jiangsu, China*
[2]*School of Medicine, Nantong University, Nantong, China*

Correspondence should be addressed to Guoliang Meng; mengguoliang@ntu.edu.cn and Wei Zhang; zhangw@ntu.edu.cn

Activation of Ca^{2+}/calmodulin-dependent protein kinase (CaMKII) has been proved to play a vital role in cardiovascular diseases. Receptor-interaction protein kinase 3- (RIPK3-) mediated necroptosis has crucially participated in cardiac dysfunction. The study is aimed at investigating the effect as well as the mechanism of CaMKII activation and necroptosis on diabetic cardiomyopathy (DCM). Wild-type (WT) and the RIPK3 gene knockout (RIPK3$^{-/-}$) mice were intraperitoneally injected with 60 mg/kg/d streptozotocin (STZ) for 5 consecutive days. After 12 w of feeding, 100 μL recombinant adenovirus solution carrying inhibitor 1 of protein phosphatase 1 (I1PP1) gene was injected into the caudal vein of mice. Echocardiography, myocardial injury, CaMKII activity, necroptosis, RIPK1 expression, mixed lineage kinase domain-like protein (MLKL) phosphorylation, and mitochondrial ultrastructure were measured. The results showed that cardiac dysfunction, CaMKII activation, and necroptosis were aggravated in streptozotocin- (STZ-) stimulated mice, as well as in (Lepr) KO/KO (db/db) mice. RIPK3 deficiency alleviated cardiac dysfunction, CaMKII activation, and necroptosis in DCM. Furthermore, I1PP1 overexpression reversed cardiac dysfunction, myocardial injury and necroptosis augment, and CaMKII activity enhancement in WT mice with DCM but not in RIPK3$^{-/-}$ mice with DCM. The present study demonstrated that CaMKII activation and necroptosis augment in DCM via a RIPK3-dependent manner, which may provide therapeutic strategies for DCM.

1. Introduction

Diabetes mellitus (DM) is an independent risk factor of diabetic cardiomyopathy (DCM), in the deficiency of coronary artery diseases, hypertension, and other cardiovascular risk factors. DCM is characterized by a series of structural and functional abnormalities, including myocardial stiffness, contractility impairment, myocardial fibrosis, and hypertrophy [1, 2]. Special attention must be paid to DCM due to its concealed onset, rapid evolution but poor treatment efficacy. Possible pathophysiological factors of DCM involve hyperglycemia, hyperlipidemia, insulin resistance, oxidative stress, endoplasmic reticulum stress, cardiomyocyte death, and mitochondrial dysfunction [3, 4]. However, the exact mechanism is still obscure. Investigation to find out potential

preventative and therapeutic strategies is an urgent problem to be solved.

Recent advances have revealed a new necrotic type of regulated cell death, necroptosis, which is morphologically distinct from apoptosis and necrosis [5]. Necroptosis is characterized by cell enlargement, organelle swelling, and plasma membrane rupture, followed by cell disintegration and intracellular component release without obvious changes in nuclear chromatin [6]. Receptor-interaction protein kinase 3 (RIPK3) plays the core role in the necroptotic signaling pathway. RIPK3, along with receptor-interacting protein 1 (RIP1) and mixed lineage kinase domain-like protein (MLKL), executes necroptosis [7, 8]. Besides, Zhang et al. identified Ca^{2+}/calmodulin-dependent protein kinase (CaMKII) as a novel substrate of RIPK3 mediating ischemia- and

oxidative stress-induced myocardial necroptosis [9]. Emerging evidences have corroborated the vital role of necroptosis in cardiovascular diseases. However, contribution of necroptosis in DCM remains insufficient.

CaMKII is a serine/threonine kinase which has various functions including regulation of key proteins involved in Ca^{2+} handling, intercellular coupling, cell death, inflammation, and mitochondrial function [10–13]. CaMKII can be activated by binding to calcium-bound calmodulin (Ca^{2+}/-CaM), autophosphorylation, oxidation, S-nitrosylation, and O-GlcNAcylation [14–16]. Activation of CaMKII mediates physiological or pathological responses and remodeling under cardiac stresses. It has been well established that CaMKII plays a prominent role in myocardial hypertrophy, pressure overload-induced cardiac hypertrophy and fibrosis, ischemia/reperfusion (I/R) injury, heart failure (HF), postmyocardial infarction (MI) remodeling, and ventricular arrhythmias [15, 17–21]. Recently, some studies have revealed the potential contribution of CaMKII in DCM [10]. Therefore, identification of the mechanism of CaMKII is beneficial to aid in providing a novel pharmacologic target for DCM.

CaMKII has four isoforms: α, β, γ, and δ, among which CaMKIIδ is prominent in the heart. CaMKIIδ expresses three variants CaMKIIδA, CaMKIIδB, and CaMKIIδC after alternative splicing of its exon 14, 15, or 16 by splicing factors. Alternative splicing of CaMKIIδ is strictly regulated. Once it is disordered, the expression of three variants imbalances to lead to cardiomyocyte dysfunction and ultimately heart diseases [22].

Protein phosphatase 1 (PP1) is a serine/threonine phosphatase mainly present in the heart and plays a vital role in regulating the phosphorylation of splicing factors to eventually mediate CaMKIIδ alternative splicing [14]. PP1 also regulates CaMKII dephosphorylation. It has been shown that PP1 expression was elevated in the heart of heart failure patients [23]. However, the clinical application value of PP1 has not been found. Inhibitor 1 of protein phosphatase 1 (I1PP1) binds to PP1 and subsequently inhibits its activity. I1PP1 transgenic mice demonstrated minor hypertrophy after transverse aortic constriction (TAC). Our previous studies have demonstrated that CaMKII regulation by I1PP1 alleviates necroptosis in high glucose-induced cardiomyocyte injury [24].

In the present study, we investigated the role of necroptosis in the development of DCM and the molecular mechanism underlying necroptosis. We also try to demonstrate the contribution of I1PP1 on the regulation of CaMKIIδ alternative splicing and CaMKII activity to ameliorate necroptosis in the myocardium of streptozotocin- (STZ-) induced wild-type and RIPK3$^{-/-}$ diabetic mice and db/db mice.

2. Materials and Methods

2.1. Animals.
Male 8-week C57BL/6 mice (wild type, WT) were provided by the Experimental Animal Center of Nantong University (Nantong, China). RIPK3 knockout (RIPK3$^{-/-}$) mice with C57BL/6 background were donated by the Institute of Molecular Medicine, Peking University (Beijing, China).

Male 12-week (Lepr) KO/KO mice (db/db) and (Lepr) WT/WT mice purchased from GemPharmatech Limited Company (Nanjing, China) were fed in separate cages. All the procedures were in accordance with both the recommendations of the Guidelines for the Care and Use of Laboratory Animals published by the National Institutes of Health and the Instructional Animal Care and Use Committee of Nantong University (approval no. NTU-20161225).

2.2. Establishment of Mouse Diabetic Models.
After adaptive feeding for a week, mice were injected with 60 mg/kg/d STZ (Sigma, USA), dissolved in 0.1 mol/L citrate buffer for 5 consecutive days after a 12-hour overnight fast [25]. Mice in the control group were injected with the same amount of citrate buffer. Mice with fasting blood glucose (FBG) level above 16.7 mmol/L were considered as the diabetic mice. Mice were randomly divided into different groups: WT group (WT), WT mice with DCM group (WT-DCM), RIPK3 KO group (RIPK3$^{-/-}$), and RIPK3 KO mice with DCM group (RIPK3$^{-/-}$-DCM).

2.3. Measurement of the Glycosylated Hemoglobin (HbA1c).
12 weeks after STZ injection, blood samples were collected and heparinized. The level of HbA1c was measured using the Glycosylated Hemoglobin A1c Assay Kit according to the manufacturer's instructions (Jiancheng Bioengineering Institute, Nanjing, China).

2.4. Measurement of Triglyceride (TG).
Blood samples were obtained and centrifuged at 1000 g for 10 min. The supernatant was collected, and serum TG content was measured with the Triglyceride Assay Kit (Jiancheng Bioengineering Institute, Nanjing, China). Absorbance was recorded at the wavelength of 510 nm.

2.5. Echocardiography.
12 weeks after STZ injection, the mice were anesthetized with 1.5% isoflurane and examined by 2-D guided M-mode echocardiography (Visual Sonic Vevo 2100, Toronto, ON, Canada) to assess cardiac configuration and function. Ejection fraction (EF) was calculated with the percentage of the difference between end-diastolic volume (EDV) and end-systolic volume (ESV) to EDV, whereas fractional shortening (FS) was calculated with the percentage of the difference between end-diastolic diameter (EDD) and end-systolic diameter (ESD) to EDD. In addition, the ratio of early (E) to late (A) diastolic velocity ratio (E/A) was calculated. All indexes were obtained from three consecutive beats.

2.6. I1PP1 Adenovirus Injection.
Recombinant adenovirus solution carrying I1PP1 gene (100 μL) was injected into the caudal vein of mice as previously mentioned. Mice in the control group were injected with recombinant adenovirus solution carrying GFP gene (100 μL) from the caudal vein. The efficiency and effect of I1PP1 adenovirus injection were assessed by western blot for further study.

2.7. Hematoxylin-Eosin (HE) Staining.
The left ventricles were fixed with 4% paraformaldehyde overnight, embedded

in paraffin, and then cut into sections at $5 \mu m$ thickness. The sections were stained with hematoxylin and eosin successively and dehydrated with ethanol. Then, sections were observed and photographed under an optical microscope.

2.8. Observation of Myocardial Ultrastructure. Hearts were cut into pieces of 1mm^3 and fixed with 4% glutaraldehyde for 2 h at 4°C and 1% osmium tetroxide for 2 h at room temperature successively. The samples were dehydrated, infiltrated, embedded with Epon812, and cut into ultrathin sections of 60-80 nm and then stained with uranyl acetate and lead citrate. Myocardial ultrastructure was examined with a transmission electron microscope (TEM) (HT7700, HITACHI, Japan), and the number of mitochondria was counted.

2.9. Cardiac Troponin I (cTnI) Measurement. 12 weeks after STZ injection, the myocardium was cut up, homogenated, and centrifuged at 2000 rpm for 20 min. The supernatants were collected and incubated with mouse Cardiac Troponin I ELISA Kit (Jiancheng Bioengineering Institute, Nanjing, China). Absorbance was recorded at the wavelength of 450 nm.

2.10. TdT-Mediated dUTP Nick End Labeling (TUNEL) Staining. The left ventricles were fixed with 4% paraformaldehyde overnight, embedded in paraffin, and then cut into sections at $5 \mu m$ thickness. After staining with TUNEL (Beyotime, Shanghai, China) at 37°C for 60 min, the sections were rinsed 3 times with PBS and then observed and photographed under an optical microscope and quantified using Image J analysis software.

2.11. Real-Time Polymerase Chain Reaction. The total RNA of the myocardium was extracted from the myocardium using a Trizol separation reagent. The cDNA was then synthesized by the Prime Script™ RT Master Mix Kit (Takara, Kyoto, Japan) before quantitative real-time PCR were performed using the SYBR Green Fast qPCR mix (Takara) with the ABI StepOne PCR System (ABI, Carlsbad, CA, USA). All primers used were the following: atrial natriuretic peptide- (ANP-) F 5′-GAGAAGATGCCGGTAGAAGA-3′, ANP-R 5′-AAGCAC TGCCGTCTCTCAGA-3′; brain natriuretic peptide (BNP-F), 5′-CTGCTGGAGCTGATAAGAGA-3′, BNP-R 5′-TGCC CAAAGCAGCTTGAGAT-3′; CaMKIIδA-F 5′-CGAGAA ATTTTTCAGCAGCC-3′, CaMKIIδA-R 5′-ACAGTAGTT TGGGGCTCCAG-3′; CaMKIIδB-F 5′-CGAGAAATTTT TCAGCAGCC-3′, CaMKIIδB-R 5′-GCTCTCAGTTGACT CCATCATC-3′; CaMKIIδC-F 5′-CGAGAAATTTTTCAGC AGCC-3, CaMKIIδC-R 5′-CTCAGTTGACTCCTTTACC CC-3′; 18S-F 5′-AGTCCCTGCCCTTTGTACACA-3′, 18S-R 5′-CGATCCGAGGGCCTCACTA-3′. Experimental cycle threshold values were normalized to 18S, a housekeeping gene, and relative mRNA expression was calculated versus a control sample.

2.12. Western Blot. The same amount of protein sample extraction from the myocardium was separated with sodium dodecyl sulfate-polyacrylamide gel electrophoresis (SDS-PAGE) and transferred to polyvinylidene difluoride (PVDF) membrane (Millipore, Massachusetts, USA). The membrane was blocked with 5% skim milk dissolved in TBST for 1 h at room temperature and then incubated with primary at 4°C overnight. The primary antibodies used were listed as follows: anti-I1PP1 (1 : 1000) and anti-PP1 (1 : 1000) (Santa Cruz Biotechnology, Santa Cruz, CA, USA); anti-ox-CaMKII (1 : 1000) (Millipore, Kenilworth, NJ, USA); anti-CaMKII (1 : 1000) (Abcam, Cambridge, UK); anti-caspase 3, anti-cleaved caspase 3, anti-MLKL, anti-p-MLKL, and anti-RIPK1 (1 : 1000, Cell Signaling Technology, Danvers, MA, USA); anti-p-CaMKII (1 : 1000, Thermo Fisher Scientific, Rockford, IL, USA); anti-GAPDH (1 : 5000, Sigma-Aldrich, St. Louis, MO, USA). Horseradish peroxidase- (HRP-) conjugated secondary antibodies were incubated for 1.5 h at room temperature. Protein bands were visualized with enhanced chemiluminescence (ECL) (Thermo Fisher Scientific Inc., Rockford, IL, USA). The target protein expression level was normalized to the level of GAPDH.

2.13. Statistical Analysis. All data were presented as standard error of the mean (S.E.M.). Statistical analysis was performed by the unpaired Student t test on comparisons between two groups and by the one-way ANOVA test and followed by the Bonferroni post hoc test on comparisons among multiple groups. $P < 0.05$ was considered statistically significant.

3. Results

3.1. Cardiac Dysfunction, CaMKIIδ Activity, and Necroptosis Are Augmented in DCM. FPG, HbA1c, serum TG, and myocardial hypertrophic gene expression were increased significantly in mice with DCM, which suggested that STZ injection produced diabetes mellitus (Figure S1). Mice with FBG more than 16.7 mmol/L were confirmed as diabetic mice and used for further experiments. Compared to the mice in the control group, mice with DCM suffered diastolic and systolic dysfunctions, elucidated by decreased EF, FS, and E/A (Figures 1(a)–1(c)). It suggested that DCM was successfully established in the present study. HE staining displayed hypertrophy, distortion, and irregular arrangement of myocardial cells in the hearts of mice with DCM (Figure 1(d)). The cTnI level was detected to evaluate myocardial injury. The cTnI level was significantly higher in the DCM group than that in the control group (Figure 1(e)). Disorder of CaMKIIδ alternative splicing is prone to promote cardiomyocyte dysfunction and ultimately heart diseases [24, 26]. Since no specific antibodies of CaMKIIδ variants were available, CaMKIIδA, CaMKIIδB, and CaMKIIδC mRNA expressions were measured by quantitative real-time PCR. There was a significant decrease of CaMKIIδA and CaMKIIδB but an increase of CaMKIIδC in diabetic mice, indicating disorder of CaMKIIδ alternative splicing in mice with DCM (Figure 1(f)). Moreover, oxidation and phosphorylation of CaMKII also increased in the DCM group (Figures 1(g) and 1(h)). Various studies have confirmed that RIPK3 was involved in necroptosis. Our study verified that RIPK3 was significantly increased in the hearts of DCM mice (Figure 1(i)). As apoptosis is a critical manifestation of necroptosis, TUNEL staining and cleaved-caspase 3

(a)

(b)

(c)

(d)

(e)

(f)

Figure 1: Continued.

(g)

(h)

(i)

(j)
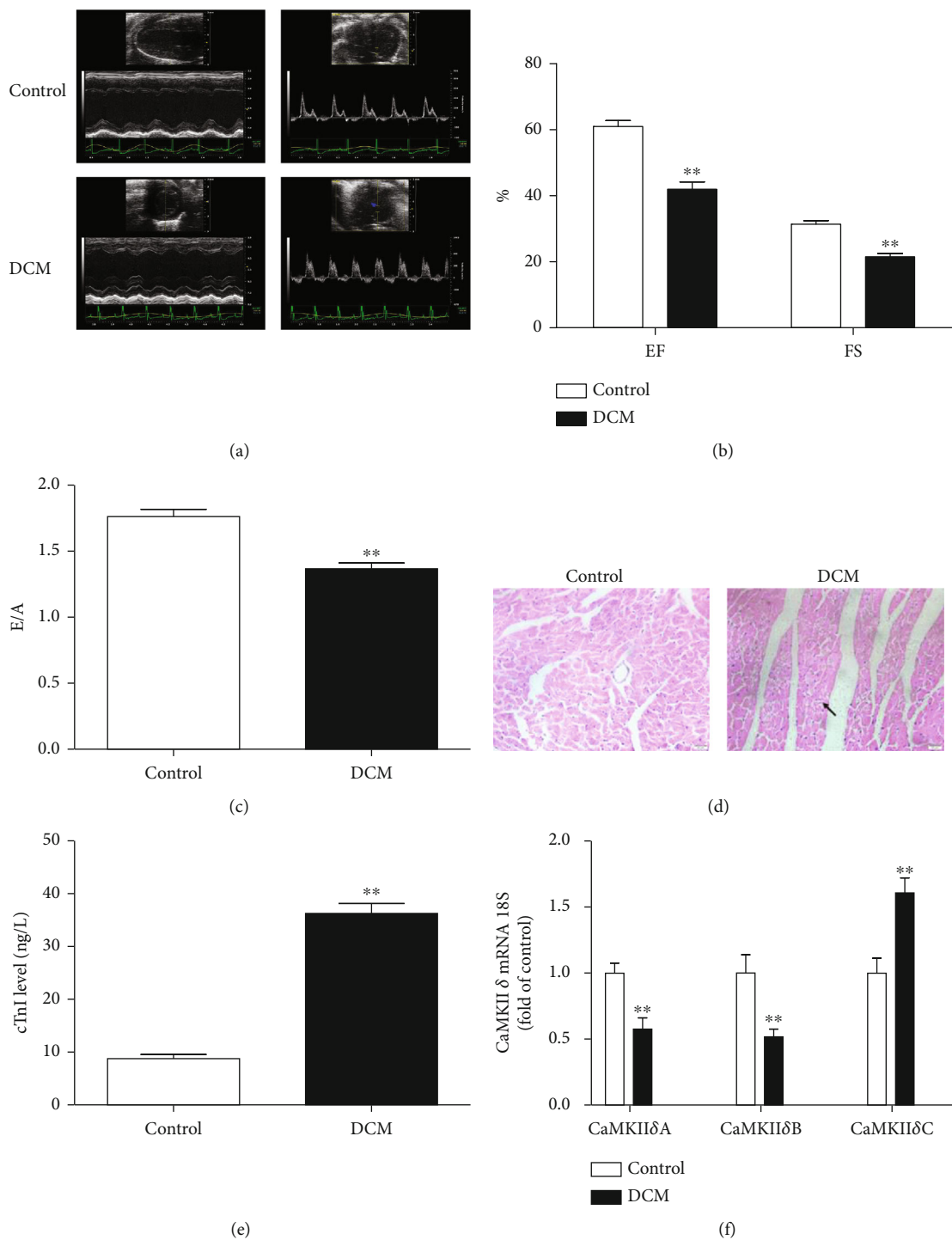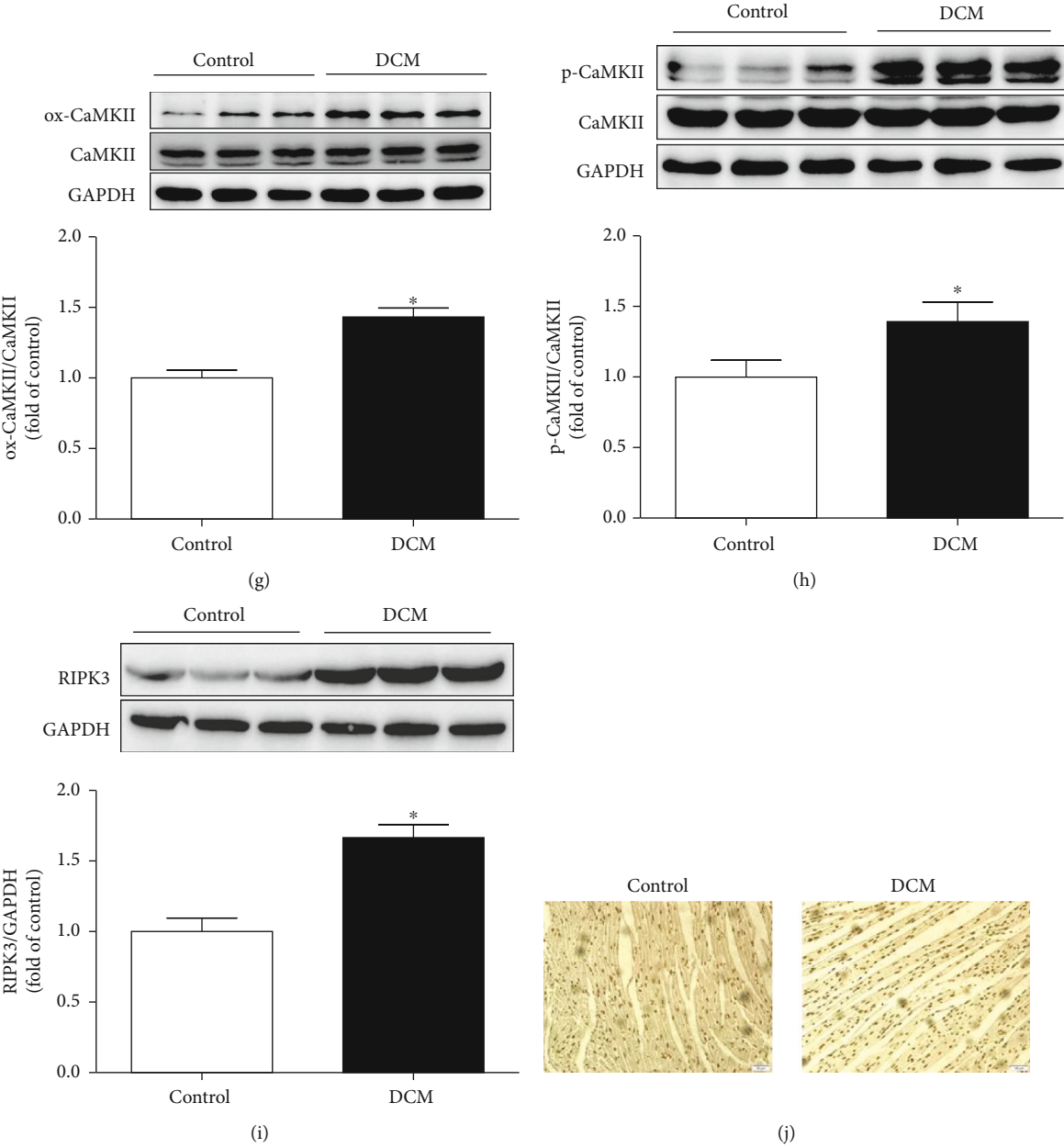
FIGURE 1: Continued.
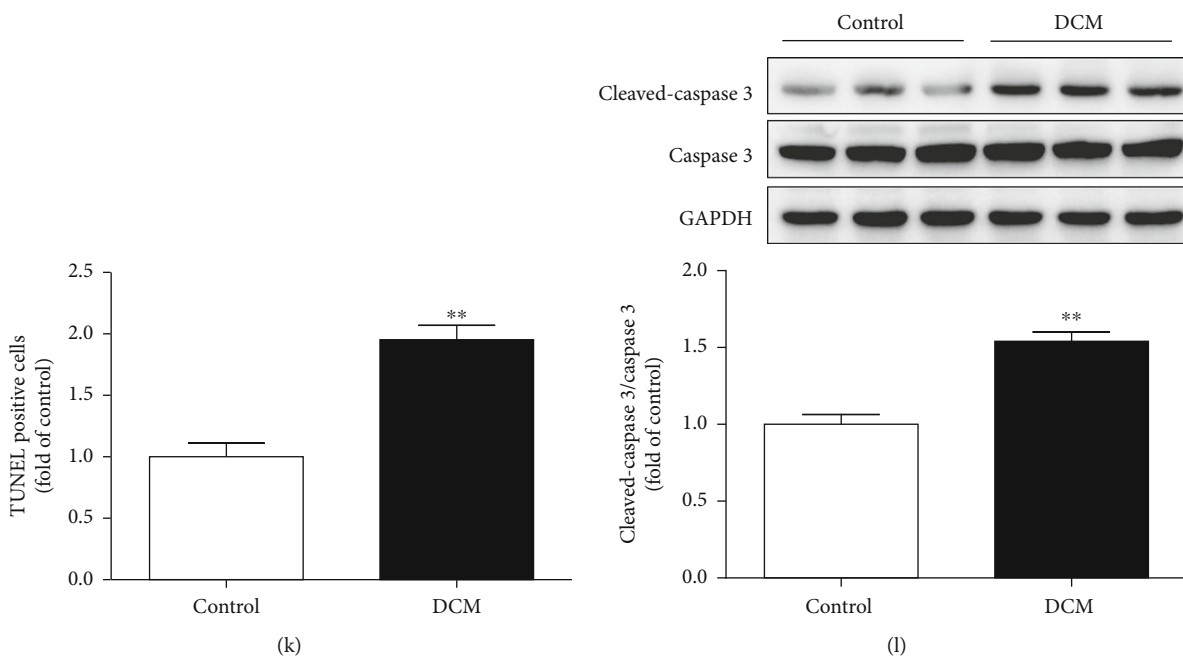
Figure 1: Cardiac dysfunction, CaMKIIδ activity, and necroptosis are augmented in DCM. Male C57BL/6 mice were injected with 60 mg/kg/d STZ for 5 consecutive days after a 12-hour overnight fast. Mice in the control group were injected with the same amount of citrate buffer. (a–c) Cardiac function was assessed by echocardiography, and EF, FS, and E/A were calculated. (d) Myocardium injury was measured by HE staining. Bar = 20 μm. (e) cTnI was detected. (f) The mRNA levels of CaMKIIδA, CaMKIIδB, and CaMKIIδC of the myocardium were detected by quantitative real-time PCR. 18S was serviced as a housekeeping mRNA. (g–h) Expression of CaMKII oxidation (ox-CaMKII), CaMKII phosphorylation (p-CaMKII), and total CaMKII was quantified by western blot. GAPDH was used as a loading control. (i) RIPK3 protein expression was quantified by western blot. GAPDH was used as a loading control. (j, k) Cell apoptosis of myocardium was detected with TUNEL staining and quantified with Image J analysis software. Bar = 50 μm. (l) Cleaved-caspase 3 and caspase 3 protein expression were quantified by western blot. GAPDH was used as a loading control. $^*P < 0.05$ and $^{**}P < 0.01$, significantly from control, $n = 6$.

expression indicated that the necroptotic cardiomyocytes in mice with DCM were significantly more than that in the control mice (Figures 1(j)–1(l)). All these data suggested that cardiac dysfunction, CaMKIIδ activity, and necroptosis were augmented in DCM.

In accordance, both systolic and diastolic cardiac functions of db/db mice were significantly impaired as compared to WT mice (Figures 2(a)–2(c)), CaMKIIδ variant expression disordered and RIPK3 expression was increased in the myocardium of db/db mice (Figures 2(d) and 2(e)).

3.2. RIPK3 Deficiency Alleviates Cardiac Dysfunction, CaMKIIδ Alternative Splicing Disorder, and Necroptosis in DCM.

To further investigate the contribution of RIPK3 in the development of DCM, RIPK3-KO (RIPK3$^{-/-}$) mice were used in our study. In diabetic mice, RIPK3 deficiency significantly enhanced EF, FS, and E/A, suggesting both systolic and diastolic functions were improved (Figures 3(a)–3(c)). Notably, RIPK3$^{-/-}$ hearts were resistant to myocardial injury in DCM, as evidenced by improved structure of myocardium and reduced cTnI level (Figures 3(d) and 3(e)). Disorder of CaMKIIδ alternative splicing was alleviated in RIPK3 deficiency mice with DCM (Figure 3(f)). TUNEL staining and western blot assay revealed that necroptosis was attenuated in RIPK3

deficiency mice with DCM (Figures 3(g)–3(k)). These data suggested that the impairment of cardiac dysfunction and the augment of necroptosis were attenuated in mice with DCM if RIPK3 was deficient.

3.3. RIPK3 Deficiency Decreases RIPK1 Expression, MLKL Phosphorylation, and CaMKII Activity and Improves Myocardial Mitochondrial Ultrastructure in Mice with DCM.

Besides RIPK3, previous studies have demonstrated that RIPK1 also participated in the process of necroptosis, and phosphorylation of MLKL was an essential effector molecule of necroptosis [27]. In the present study, RIPK1 expression and MLKL phosphorylation were markedly elevated in the myocardium of mice with DCM, which were significantly decreased in RIPK3$^{-/-}$ mice with DCM (Figures 4(a) and 4(b)). A recent study identified CaMKII as one of the substrates of RIPK3 in cardiac ischemic disease [8]. Our results revealed that RIPK3 deficiency attenuated CaMKII oxidation and phosphorylation in the myocardium of mice with DCM (Figures 4(c) and 4(d)). TEM analysis of myocardial mitochondrial ultrastructure showed irregular and swelled mitochondria and fractured mitochondrial cristae in the left ventricular myocardium of mice with DCM. However, the abnormalities of mitochondria with DCM were improved in RIPK3$^{-/-}$ mice (Figure 4(e)).
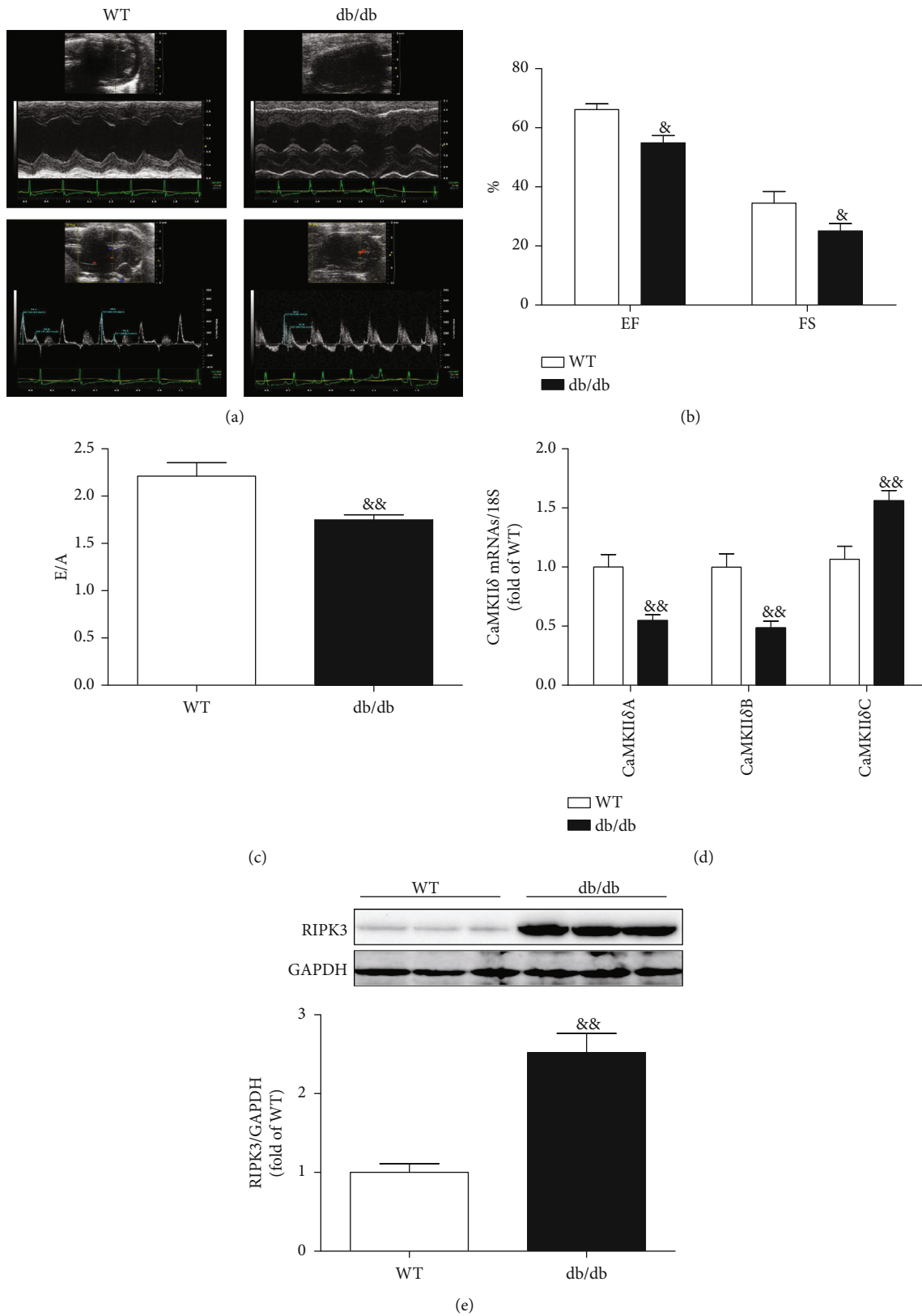
FIGURE 2: Cardiac dysfunction, CaMKIIδ activity, and RIPK3 expression are augmented in db/db mice. (a–c) In db/db and its wild-type mice, cardiac function was assessed by echocardiography and EF, FS, and E/A were calculated. (d) In db/db and its wild-type mice, the mRNA levels of CaMKIIδA, CaMKIIδB, and CaMKIIδC of the myocardium were detected by quantitative real-time PCR. 18S was serviced as a housekeeping mRNA. (e) In db/db and its wild-type mice, RIPK3 protein expression was quantified by western blot. GAPDH was used as a loading control. $^{\&}P < 0.05$ and $^{\&\&}P < 0.01$, significantly from WT. $n = 6$.

(a)

(b)

(c)

(d)

(e)
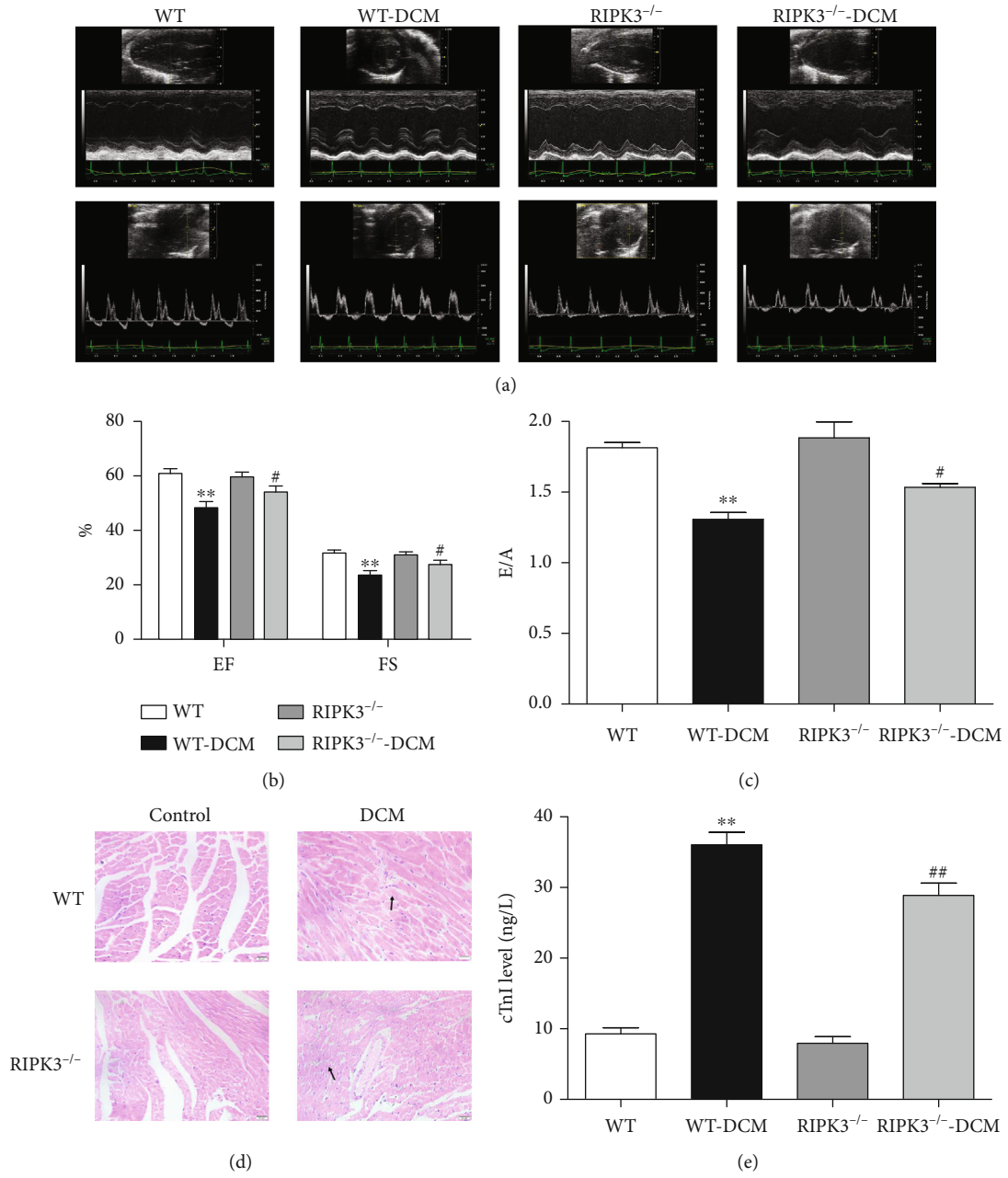
FIGURE 3: Continued.

(f)

(g)

(h)

(i)

(j)

(k)
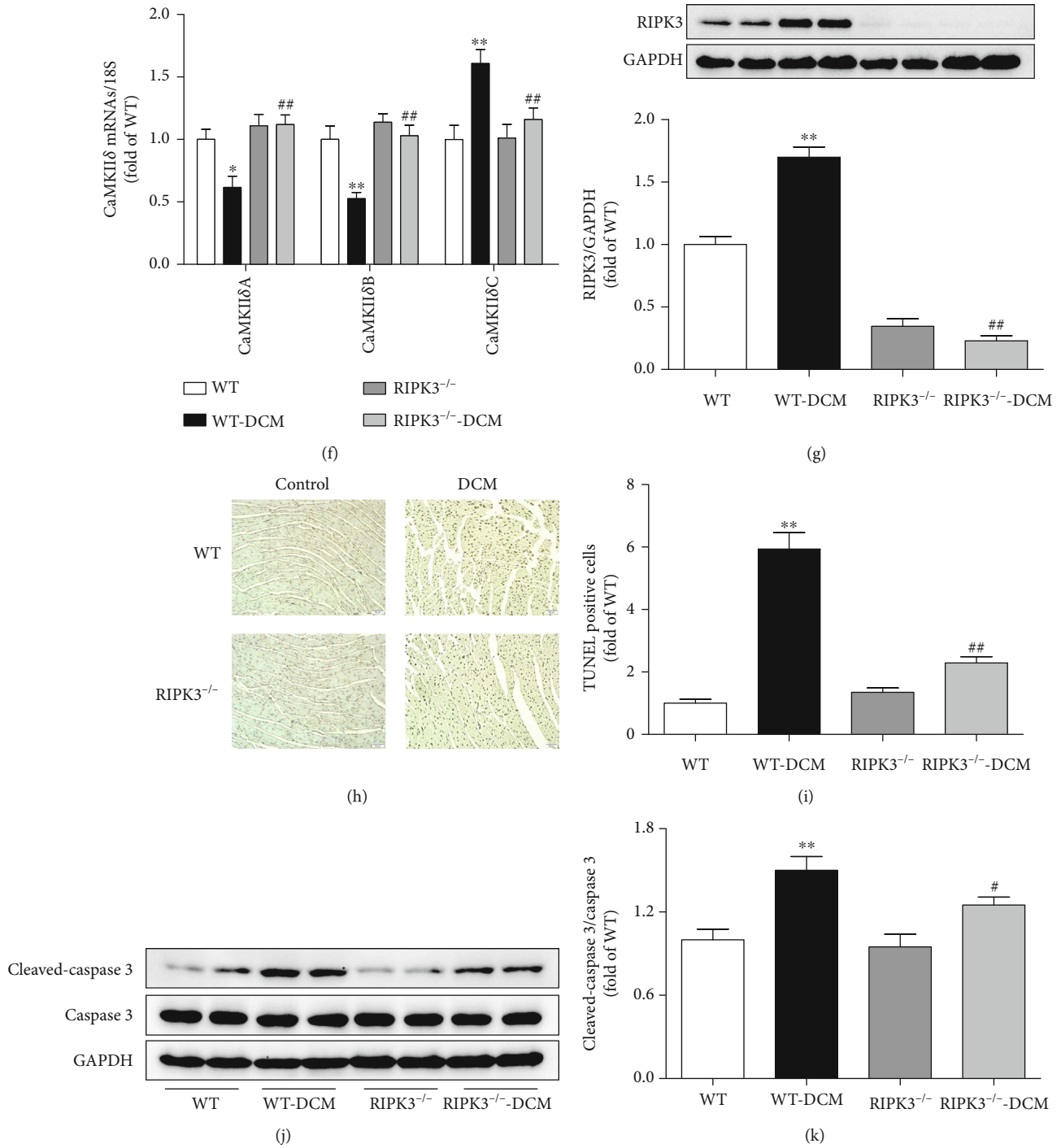
FIGURE 3: RIPK3 deficiency alleviates cardiac dysfunction, CaMKIIδ alternative splicing disorder, and necroptosis in DCM. Male C57BL/6 mice and RIPK3 knockout mice (RIPK3$^{-/-}$) were injected with 60 mg/kg/d STZ for 5 consecutive days after a 12-hour overnight fast. WT and RIPK3$^{-/-}$ mice in the control group were injected with the same amount of citrate buffer. (a–c) Cardiac function was assessed by echocardiography, and EF, FS, and E/A were calculated. (d) Myocardium injury was measured by HE staining. Bar = 20 μm. (e) cTnI was detected. (f) The mRNA levels of CaMKIIδA, CaMKIIδB, and CaMKIIδC of the myocardium were detected by quantitative real-time PCR. 18S was serviced as a housekeeping mRNA. (g) RIPK3 expression was quantified by western blot. GAPDH was used as a loading control. (h, i) Cell apoptosis of the myocardium was detected with TUNEL staining. (j, k) Cleaved-caspase 3 and caspase 3 protein expression were quantified by western blot. GAPDH was used as a loading control. $^{**}P < 0.01$ and $^{*}P < 0.05$ significantly from WT; $^{##}P < 0.01$ and #$P < 0.05$ significantly from WT-DCM. $n = 6$.

(a)

(b)

(c)

(d)

Figure 4: Continued.

(e)
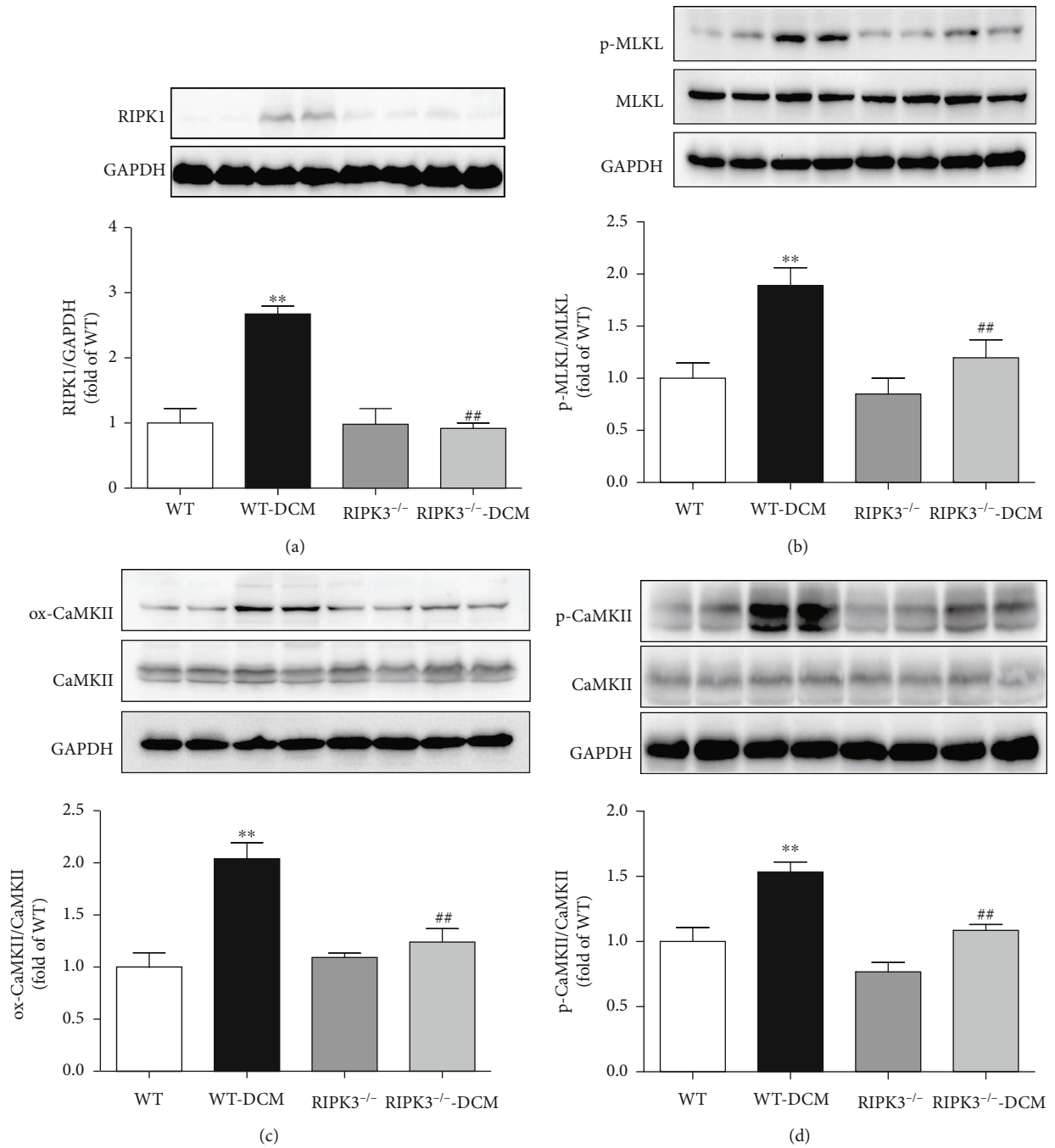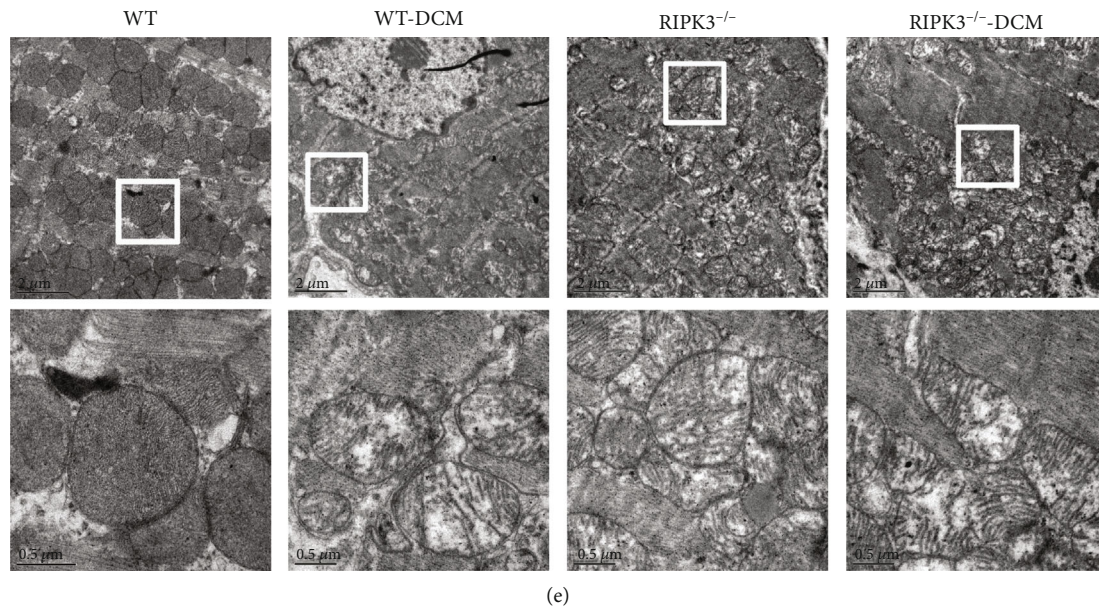
FIGURE 4: RIPK3 deficiency decreases RIPK1 expression, MLKL phosphorylation, and CaMKII activity and improves myocardial mitochondrial ultrastructure in DCM. (a) RIPK1 expression in cardiomyocytes was quantified by western blot. GAPDH was used as a loading control. (b) MLKL phosphorylation (p-MLKL) and total MLKL were quantified by western blot. GAPDH was used as a loading control. (c, d) Expression of CaMKII oxidation (ox-CaMKII), CaMKII phosphorylation (p-CaMKII), and total CaMKII was quantified by western blot. GAPDH was used as a loading control. (e) Myocardial mitochondrial ultrastructure was examined with a transmission electron microscope. Scale bars: $2\,\mu$m (upper) and $0.5\,\mu$m (lower), respectively. $^{**}P < 0.01$, significantly from WT; $^{##}P < 0.01$ and $#P < 0.05$, significantly from WT-DCM. $n = 6$.

3.4. I1PP1 Overexpression Reverses Cardiac Dysfunction, Myocardial Injury, and Necroptosis Augment in Mice with DCM. To further evaluate the relative contribution of CaMKIIδ variant disorder in DCM, the recombinant adenovirus carrying the I1PP1 gene was directly injected into the caudal vein of mice to regulate CaMKIIδ alternative splicing. Two weeks after injection, western blot assay showed that I1PP1 was overexpressed and significantly inhibited PP1 expression in the myocardium of mice (Figure S2). EF, FS, and E/A were improved after I1PP1 overexpression in WT mice with DCM but not in RIPK3$^{-/-}$ mice with DCM. Moreover, cardiac function of RIPK3$^{-/-}$ mice with DCM was further improved as compared to WT mice with DCM after I1PP1 overexpression (Figures 5(a)–5(e)). Similarly, I1PP1 overexpression reduced cTnI level, improved myocardial structure, and alleviated necroptosis augment in WT mice with DCM but not in RIPK3$^{-/-}$ mice with DCM. In addition, lower cTnI level, better myocardial structure, and weaker necroptosis augment were detected in RIPK3$^{-/-}$ mice with DCM as compared to WT mice with DCM after I1PP1 overexpression (Figures 5(f)–5(j)). All the above data suggested CaMKII was possible downstream of RIPK3 during necroptosis in DCM.

The effects of I1PP1 overexpression were also detected in db/db mice. Results showed that EF, FS, and E/A were significantly elevated in db/db mice after I1PP1 overexpression (Figure 6), indicating CaMKII regulation was beneficial to improve cardiac function of db/db mice.

3.5. I1PP1 Overexpression Inhibits Oxidation and Phosphorylation of CaMKII and Improves Myocardial Mitochondrial Ultrastructure in Mice with DCM. Further studies were done to investigate the mechanism of I1PP1 overexpression on necroptosis in DCM mice. Oxidation and phosphorylation of CaMKII were inhibited after I1PP1 overexpression in WT mice with DCM but not in RIPK3$^{-/-}$ mice with DCM. Lower CaMKII oxidation and phosphorylation were measured in RIPK3$^{-/-}$ mice with DCM as compared to WT mice with DCM after I1PP1 overexpression (Figures 7(a) and 7(b)). I1PP overexpression improved mitochondrial ultrastructure in WT mice with DCM but not in RIPK3$^{-/-}$ mice with DCM. Better mitochondrial ultrastructure was observed in RIPK3$^{-/-}$ mice with DCM as compared to WT mice with DCM after I1PP1 overexpression (Figure 7(c)).

4. Discussion

Accumulated evidence has shown that diabetes results in structural and functional impairment of the hearts. DCM features glucotoxicity, lipotoxicity, and hypertrophy. The results showed increased FBG, HbA1c, serum TG, ANP, and BNP expression in mice with DCM. However, there are still no specific strategies for prevention and treatment of DCM [28]. Necroptosis, a form of regulated necrosis, has been contributable to cardiovascular diseases, such as myocardial infarction, atherosclerosis, and abdominal aortic aneurysm [29]. Our study verified that necroptosis was augmented in mice with DCM. Given RIPK3 is a critical

(a)

(b)

(c)

(d)
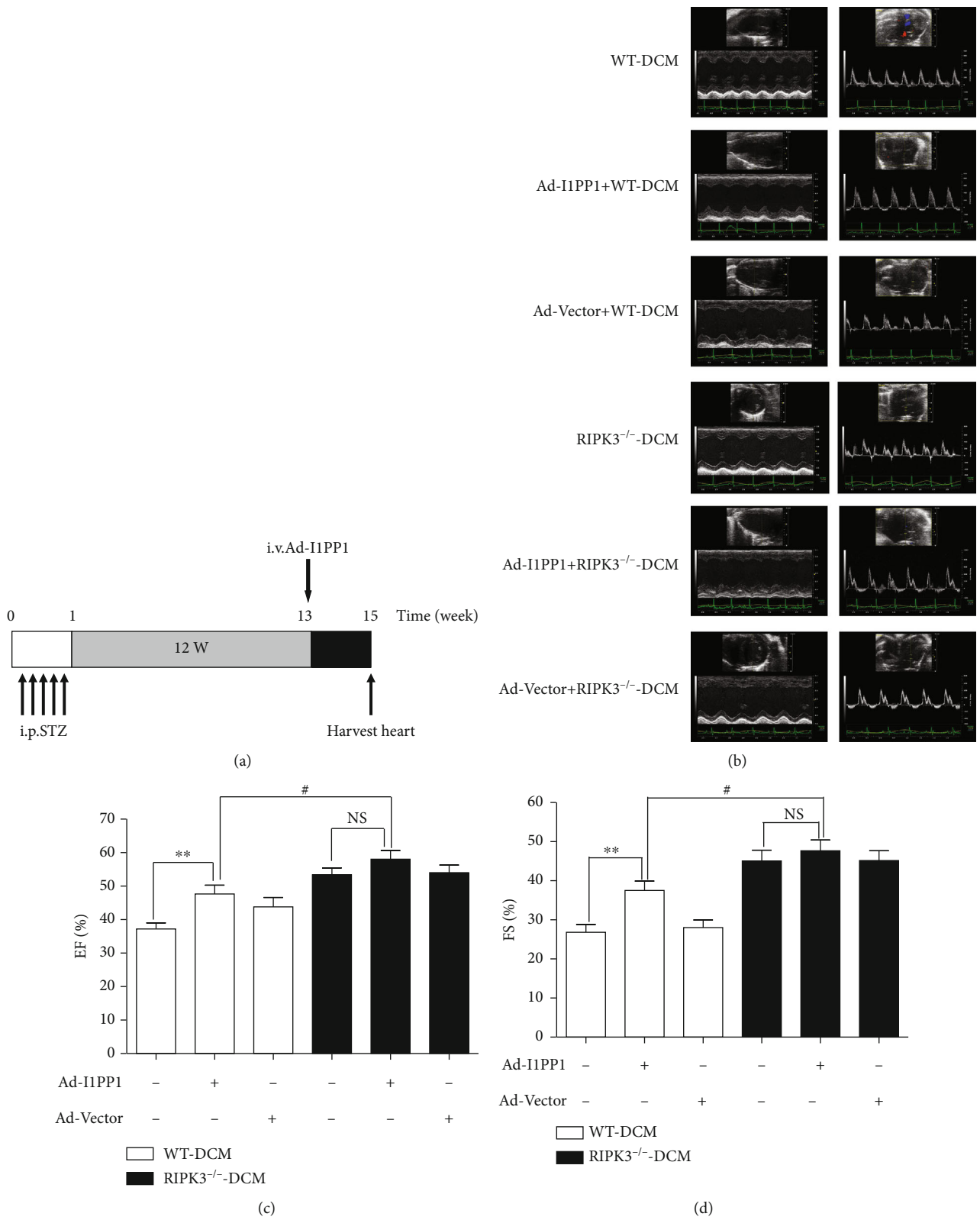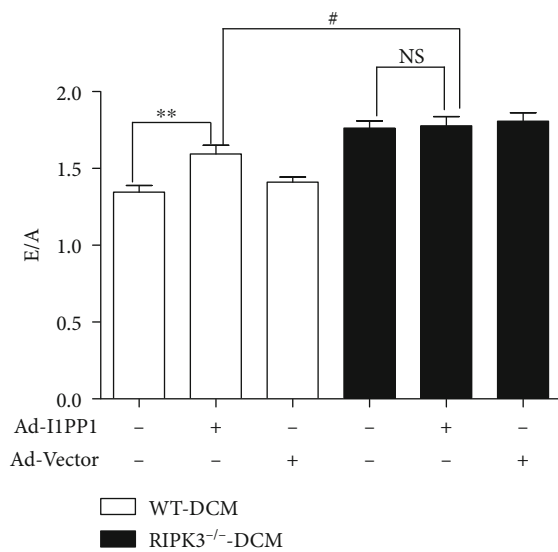
FIGURE 5: Continued.

(e)
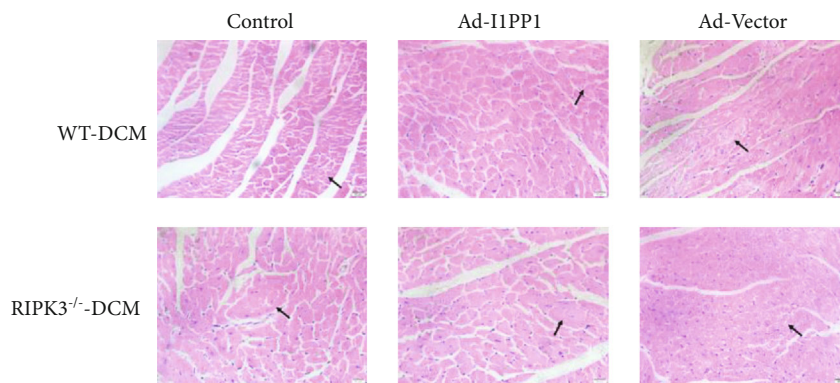
(f)
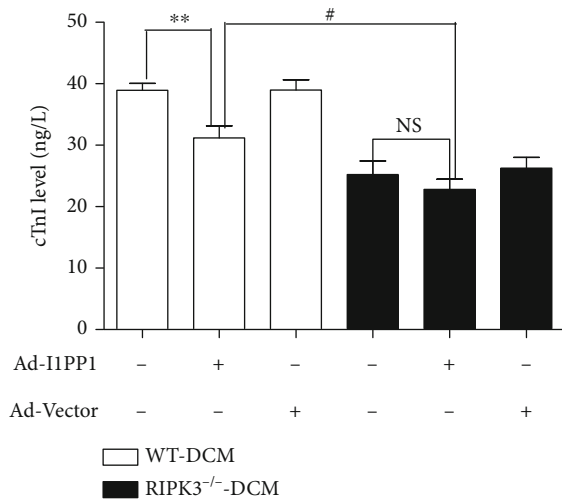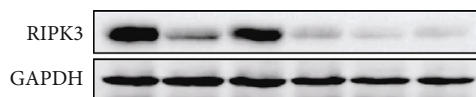
(g)
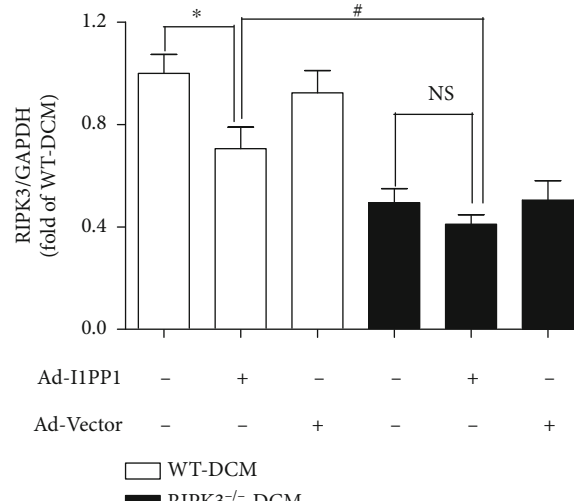
(h)

FIGURE 5: Continued.

(i)

(j)
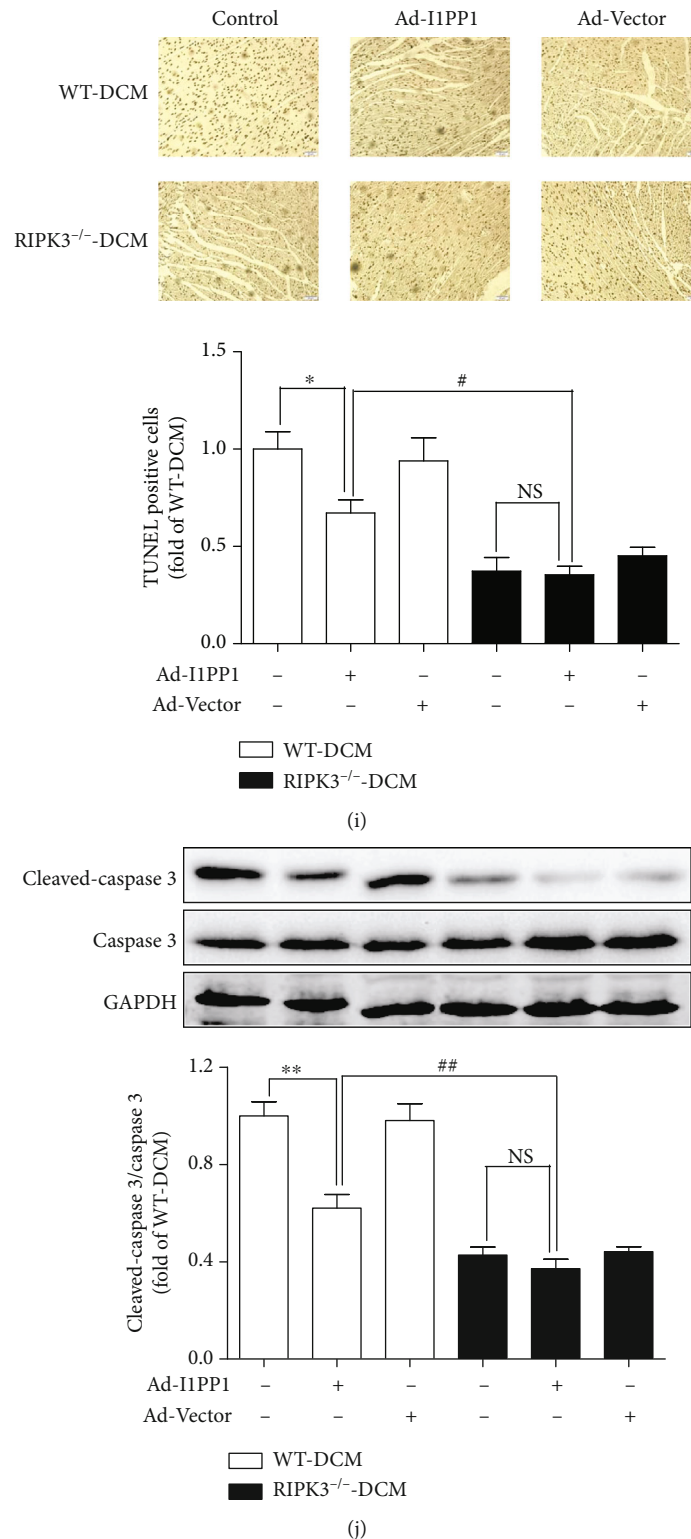
FIGURE 5: I1PP1 overexpression reverses cardiac dysfunction, myocardial injury, and necroptosis augment in mice with DCM. 100 μL recombinant adenovirus solution carrying I1PP1 gene or vector was injected into the caudal vein of mice 12 weeks after STZ injection or injected into the caudal vein of db/db mice or its WT mice. (a) The timeline of animal treatment was summarized. (b–e) Cardiac function was assessed by echocardiography, and EF, FS, and E/A were calculated. (f) Myocardium injury was measured by HE staining. Bar = 20 μm. (g) cTnI was detected. (h) RIPK3 expression was quantified by western blot. GAPDH was used as a loading control. (i) Cell apoptosis of the myocardium was detected with TUNEL staining. (j) Cleaved-caspase 3 and caspase 3 protein expression were quantified by western blot. GAPDH was used as a loading control. $^{**}P < 0.01$ and $^{*}P < 0.05$; $^{\#\#}P < 0.01$ and $\#P < 0.05$; NS: no significance, $n = 6$.

(a)

(b)

(c)
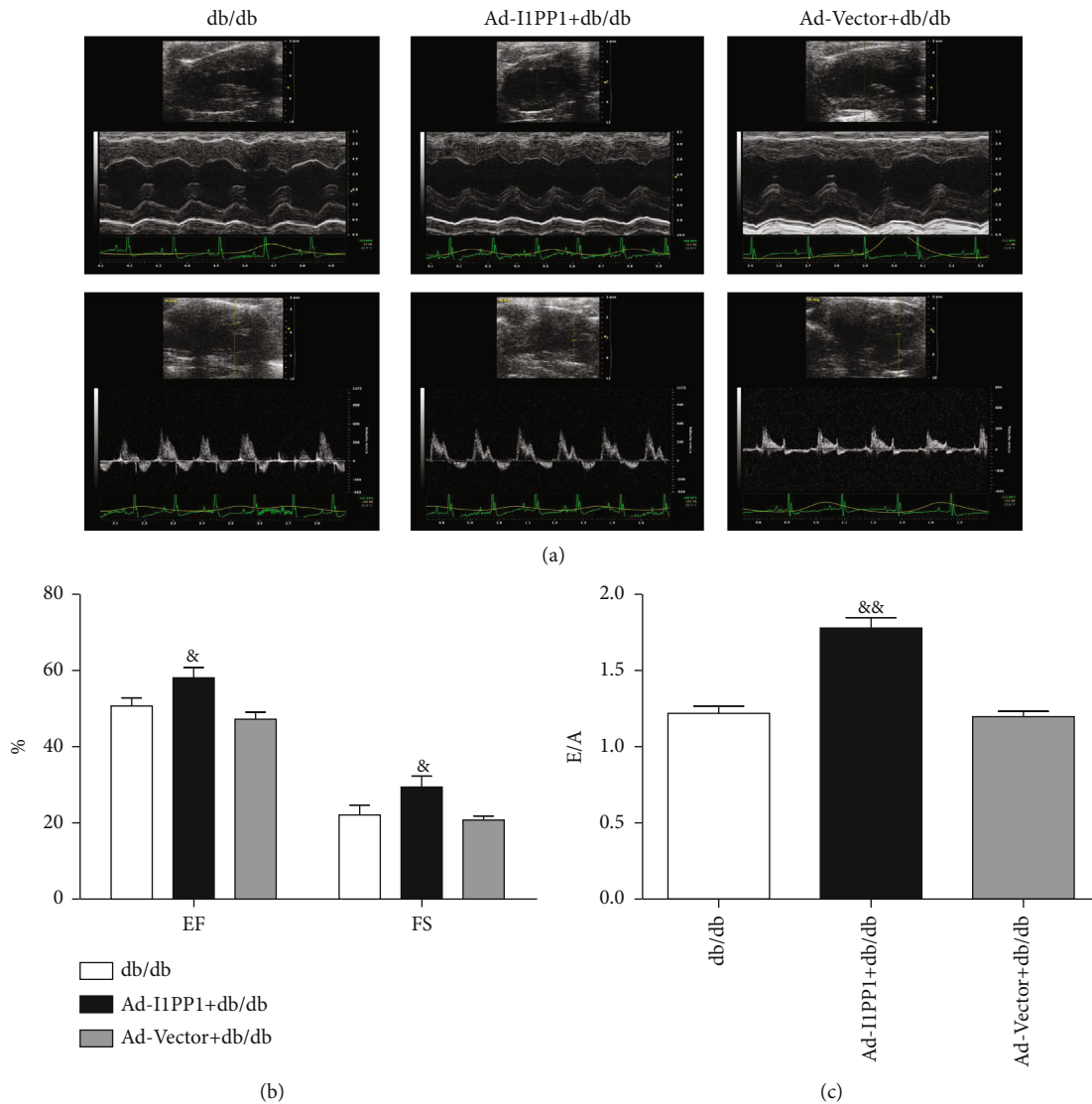
Figure 6: I1PP1 overexpression reverses cardiac dysfunction of db/db mice. (a–c) In db/db and its WT mice, cardiac function was assessed by echocardiography and EF, FS, and E/A were calculated. $^{\&\&}P < 0.01$ and $^{\&}P < 0.05$ significantly from db/db. $n = 6$.

molecule for necroptosis in large amount types of cells, the differences between WT mice and RIPK3$^{-/-}$ mice during DCM were further investigated. Furthermore, RIPK3$^{-/-}$ alleviated cardiac dysfunction, myocardial injury, and necroptosis in diabetic mice.

RIPK1, one common partner of RIPK3, interacts with RIPK3 via a shared RIP homotypic interaction motif domain to form a complex called "necrosome" [30, 31]. Necrostatin-1 (Nec-1), an inhibitor of RIPK1, exerts a protective effect against necroptosis during multiple diseases [32]. MLKL, a recently acknowledged substrate of RIPK3, oligomerizes and translocates to the plasma membrane after being phosphorylated by RIPK3, finally leading to necroptotic cell death. A previous study demonstrated that MLKL deficiency protected against necroptosis in cells including tumor cells, macrophages, and fibroblasts [33–35]. Our results revealed that both RIPK1 expression and MLKL phosphorylation were significantly upregulated in the myocardium of mice with DCM. Moreover, RIPK3$^{-/-}$ mice with DCM showed

decreased RIPK1 expression and MLKL phosphorylation. Anyhow, the detailed pathway of RIPK3-evoked myocardial necroptosis was unknown.

CaMKII is a pleiotropic signal that regulates gene expression, contractility, metabolism, Ca^{2+} cycling, and cell survival of cardiomyocytes [36, 37]. CaMKII is inactivated under basal conditions. Sustained activation of CaMKII promotes cardiomyocyte death under conditions of oxidative stress, hyperglycemia, and ischemic and hypoxic injury [38–40]. Zhang et al. reported that RIPK3 contributed to myocardial necroptosis by oxidizing and phosphorylating CaMKII after ischemia-reperfusion injury or doxorubicin challenge [9]. Our previous study demonstrated CaMKII an alternative substrate of RIPK3 in high glucose-induced cardiomyocyte necroptosis [24]. Our present study found significant enhancement of phosphorylation and oxidation of CaMKII both in DCM mice and in AGE-stimulated cardiomyocytes, which were markedly reversed in RIPK3$^{-/-}$ mice. Moreover, no matter I1PP1 is overexpressed or not, cardiac function

(a)

(b)

(c)
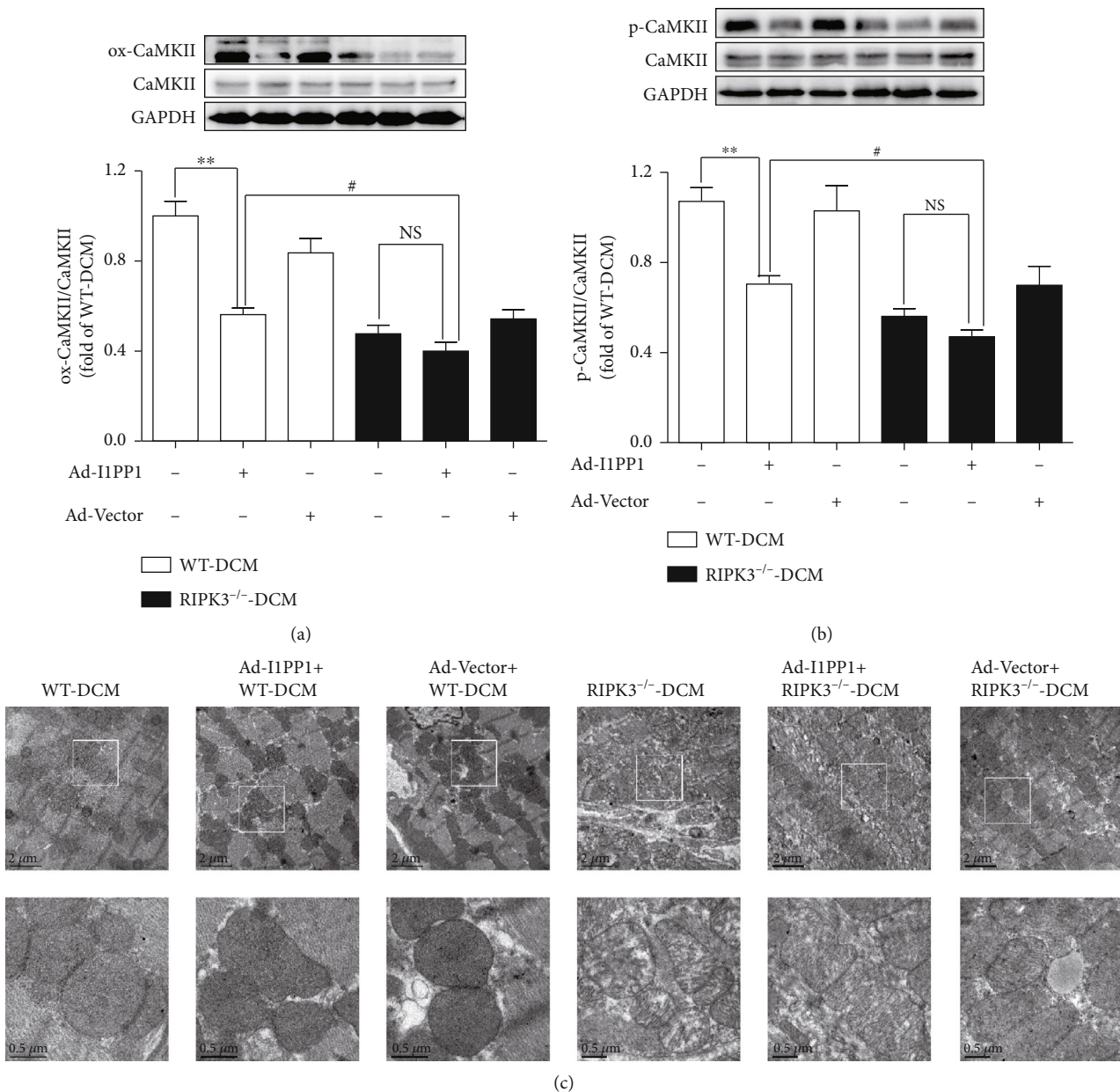
Figure 7: I1PP1 overexpression inhibits oxidation and phosphorylation of CaMKII and improves myocardial mitochondrial ultrastructure in DCM mice. (a, b) Expression of CaMKII oxidation (ox-CaMKII), CaMKII phosphorylation (p-CaMKII), and total CaMKII was quantified by western blot. GAPDH was used as a loading control. (c) Myocardial mitochondrial ultrastructure was examined with a transmission electron microscope. Scale bars: 2 μm (upper) and 0.5 μm (lower), respectively. **$P < 0.01$ and #$P < 0.05$; NS: no significance. $n = 6$.

was improved and necroptosis was suppressed in RIPK3$^{-/-}$ mice. Taken together, the CaMKII signal pathway was possible downstream or substrate of RIPK3 in DCM.

Various studies have confirmed mitochondrial dysfunction as a key underlying mechanism of necroptosis. Mitochondria are a major source of energy and ROS generation, and mitochondrial dysfunction leads to ROS overproduction as well as cell death [41]. RIPK3 increased mitochondrial localization of NADPH oxidase-4 (NOX4) but inhibited mitochondrial complex I and –III and finally promoted kidney tubular injury [42]. Besides, knockdown of RIPK3 reversed the reduced adenosine triphosphate (ATP) production and attenuated the mitochondrial permeability transi-

tion pore (mPTP) opening of cardiomyocytes induced by hypoxia-reoxygenation (HR) injury [43]. Our present study found that RIPK3 deficiency improved the ultrastructure of mitochondria in the myocardium of diabetic mice. These results highlighted that mitochondrial injury is possibly responsible for RIPK3-induced necroptosis in DCM.

PP1 is a serine/threonine protein phosphatase that dephosphorylates diverse cellular substrates, acting as a key regulator of some cellular processes [44]. I1PP1 is the first recognized endogenous inhibitor of PP1 and greatly low expressed in cardiomyocytes under basal conditions. Early studies have been reported overexpression of I1PP1 in engineered heart tissue, and rat cardiac myocytes improved
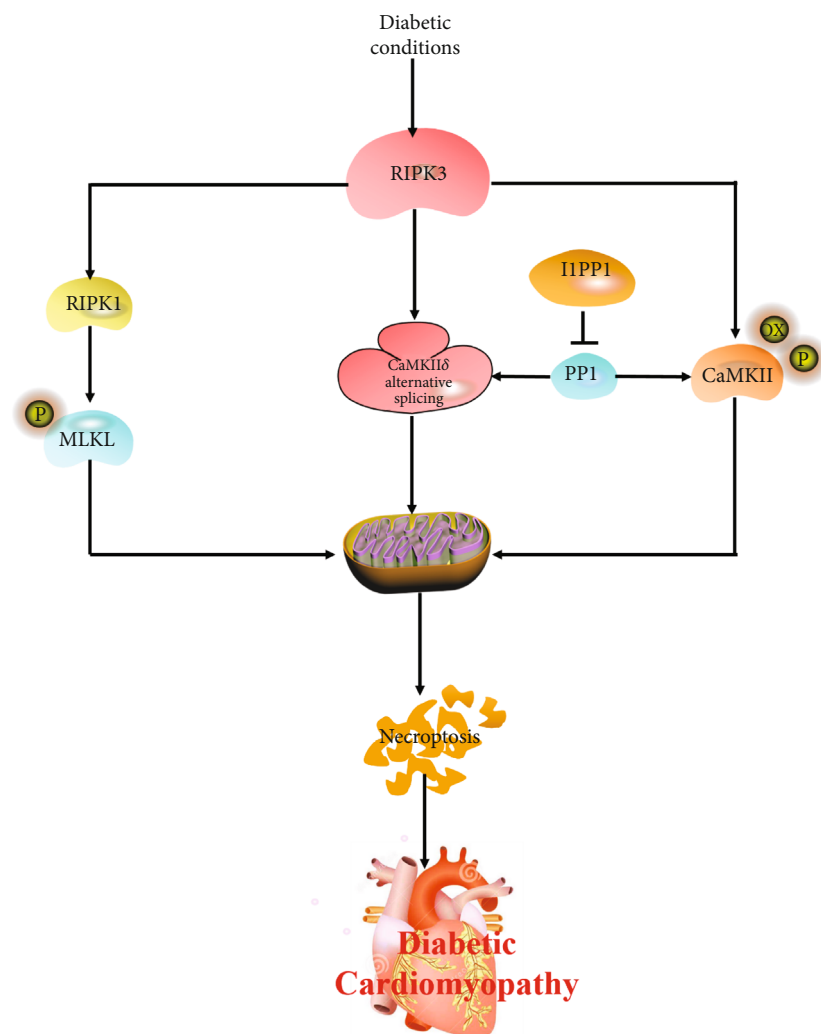
FIGURE 8: Increased RIPK3 activates RIPK1 expression, MLKL phosphorylation, CaMKIIδ alternative splicing disorder, oxidation, and phosphorylation of CaMKII under diabetic conditions. I1PP1 overexpression corrects CaMKIIδ alternative splicing, inhibits CaMKII activation, and attenuates necroptosis in DCM. Taken together, CaMKII activation and necroptosis augment in diabetic cardiomyopathy via RIPK3-dependent manner.

contractile function [45]. Our previous studies also uncovered the role of I1PP1 overexpression in protecting against myocardial ischemia-reperfusion injury through CaMKII regulation and necroptosis alleviating in high glucose-induced cardiomyocyte injury [24, 46]. Our present study corroborated the important role of overexpression of I1PP1 in inhibiting necroptosis to alleviate diabetic cardiomyopathy by regulating CaMKIIδ alternative splicing and CaMKII activity. However, the protective effect of I1PP1 overexpression on DCM was less stronger than that of RIPK3 deficiency. Moreover, I1PP1 overexpression showed no cardioprotective effects in diabetic mice without the RIPK3 gene, indicating that CaMKII might be served as the substrate to mediate necroptosis in the development of DCM.

In conclusion, our study proved there was serious necroptosis in DCM. RIPK3 deficiency alleviated myocardial injury, improved cardiac function, suppressed CaMKII activation, and attenuated necroptosis in mice with DCM mice.

Taken together, CaMKII activation and necroptosis augment in diabetic cardiomyopathy via a RIPK3-dependent manner (Figure 8). These findings will be a benefit to the understanding of the pathology of diabetic cardiomyopathy and provide novel therapeutic strategies for diabetic cardiomyopathy.

Data Availability

The data used to support the findings of this study are available from the corresponding authors upon request.

Disclosure

The manuscript has been presented as preprint according to the following link: https://authorea.com/doi/full/10.22541/au.158465453.30390557.

Conflicts of Interest

The authors declare that there is no conflict of interest regarding the publication of this paper.

Authors' Contributions

Yun Chen and Xinshuai Li contributed equally to this work.

Supplementary Materials

Figure S1: glucose concentration, HbA1c level, TG level, ANP, and BNP gene expression increased after STZ injection. (A) Fast blood glucose was measured periodically from the control and diabetic mice in different time after STZ injection. (B) HbA1c level was detected 12 weeks after STZ injection. (C) Serum TG level was measured 12 weeks after STZ injection. (D) Myocardial ANP mRNA and BNP mRNA were quantified by real-time PCR 12 weeks after STZ injection. 18S gene was used as a housekeeping gene. $^{**}P < 0.01$ significantly different from control. $n = 6$. Figure S2: I1PP1 is overexpressed by caudal vein injection of recombinant adenovirus carrying the I1PP1 genes in mice. 100 μL recombinant adenovirus solution carrying I1PP1 gene (1×10^{11} PFU/mL) or vector was injected into the caudal vein of mice 8 weeks after STZ injection. I1PP1 and PP1 expression were quantified by western blot. GAPDH was used as a loading control. $^{**}P < 0.01$ significantly different from WT-DCM without injection of recombinant adenovirus solution carrying I1PP1 gene; $^{##}P < 0.01$ and $^{#}P < 0.05$ significantly different from Ad-Vector+RIPK3$^{-/-}$-DCM without injection of recombinant adenovirus solution carrying I1PP1 gene. $n = 6$. (Supplementary Materials)

References

[1] B. Parim, V. V. Sathibabu Uddandrao, and G. Saravanan, "Diabetic cardiomyopathy: molecular mechanisms, detrimental effects of conventional treatment, and beneficial effects of natural therapy," *Heart Failure Reviews*, vol. 24, no. 2, pp. 279–299, 2019.

[2] H. Cai, S. Chen, J. Liu, and Y. He, "An attempt to reverse cardiac lipotoxicity by aerobic interval training in a high-fat diet- and streptozotocin-induced type 2 diabetes rat model," *Diabetology & Metabolic Syndrome*, vol. 11, p. 43, 2019.

[3] H. Cao, T. Chen, and Y. Shi, "Glycation of human serum albumin in diabetes: impacts on the structure and function," *Current Medicinal Chemistry*, vol. 22, no. 1, pp. 4–13, 2015.

[4] G. Jia, M. A. Hill, and J. R. Sowers, "Diabetic cardiomyopathy: an update of mechanisms contributing to this clinical entity," *Circulation Research*, vol. 122, no. 4, pp. 624–638, 2018.

[5] X. Yu, Y. Ruan, X. Huang et al., "Dexrazoxane ameliorates doxorubicin-induced cardiotoxicity by inhibiting both apoptosis and necroptosis in cardiomyocytes," *Biochemical and Biophysical Research Communications*, vol. 523, no. 1, pp. 140–146, 2020.

[6] D. Tang, R. Kang, T. Vanden Berghe, P. Vandenabeele, and G. Kroemer, "The molecular machinery of regulated cell death," *Cell Research*, vol. 29, no. 5, pp. 347–364, 2019.

[7] R. K. S. Malireddi, S. Kesavardhana, and T. D. Kanneganti, "ZBP1 and TAK1: master regulators of NLRP3 inflammasome/pyroptosis, apoptosis, and necroptosis (PAN-optosis)," *Frontiers in Cellular and Infection Microbiology*, vol. 9, p. 406, 2019.

[8] A. Shrestha, I. Mehdizadeh Gohari, and B. A. McClane, "RIP1, RIP3, and MLKL contribute to cell death caused by Clostridium perfringens enterotoxin," *mBio*, vol. 10, no. 6, p. e02985, 2019.

[9] T. Zhang, Y. Zhang, M. Cui et al., "CaMKII is a RIP3 substrate mediating ischemia- and oxidative stress-induced myocardial necroptosis," *Nature Medicine*, vol. 22, no. 2, pp. 175–182, 2016.

[10] B. Hegyi, D. M. Bers, and J. Bossuyt, "CaMKII signaling in heart diseases: emerging role in diabetic cardiomyopathy," *Journal of Molecular and Cellular Cardiology*, vol. 127, pp. 246–259, 2019.

[11] A. G. Nickel, M. Kohlhaas, E. Bertero et al., "CaMKII does not control mitochondrial Ca(2+) uptake in cardiac myocytes," *The Journal of Physiology*, vol. 598, no. 7, pp. 1361–1376, 2020.

[12] N. E. Chalmers, J. Yonchek, K. E. Steklac et al., "Calcium/calmodulin-dependent kinase (CaMKII) inhibition protects against Purkinje cell damage following CA/CPR in mice," *Molecular Neurobiology*, vol. 57, no. 1, pp. 150–158, 2020.

[13] H. Takanari, V. J. A. Bourgonje, M. S. C. Fontes et al., "Calmodulin/CaMKII inhibition improves intercellular communication and impulse propagation in the heart and is antiarrhythmic under conditions when fibrosis is absent," *Cardiovascular Research*, vol. 111, no. 4, pp. 410–421, 2016.

[14] N. Shioda and K. Fukunaga, "Physiological and pathological roles of CaMKII-PP1 signaling in the brain," *International Journal of Molecular Sciences*, vol. 19, no. 1, p. 20, 2017.

[15] L.-H. Kong, F.-M. Xiong, X.-L. Su, N. Sun, J.-J. Zhou, and J. Yu, "CaMKII mediates myocardial ischemia/reperfusion injury induced contracture in isolated rat heart," *Molecular Medicine Reports*, vol. 44, no. 2, 2019.

[16] B. M. Wood, M. Simon, S. Galice et al., "Cardiac CaMKII activation promotes rapid translocation to its extra-dyadic targets," *Journal of Molecular and Cellular Cardiology*, vol. 125, pp. 18–28, 2018.

[17] R. Kamada, H. Yokoshiki, H. Mitsuyama et al., "Arrhythmogenic beta-adrenergic signaling in cardiac hypertrophy: the role of small-conductance calcium-activated potassium channels via activation of CaMKII," *European Journal of Pharmacology*, vol. 844, pp. 110–117, 2019.

[18] Z. Wang, Y. Xu, M. Wang et al., "TRPA1 inhibition ameliorates pressure overload-induced cardiac hypertrophy and fibrosis in mice," *EBioMedicine*, vol. 36, pp. 54–62, 2018.

[19] Q. He, J. Cheng, and Y. Wang, "Chronic CaMKII inhibition reverses cardiac function and cardiac reserve in HF mice," *Life Sciences*, vol. 219, pp. 122–128, 2019.

[20] H. W. Lee, M. Ahmad, J. J. Weldrick, H.-W. Wang, P. G. Burgon, and F. H. H. Leenen, "Effects of exercise training and TrkB blockade on cardiac function and BDNF-TrkB signaling postmyocardial infarction in rats," *American Journal of Physiology-Heart and Circulatory Physiology*, vol. 315, no. 6, pp. H1821–H1834, 2018.

[21] L. Jiang, L. Li, Y. Ruan et al., "Ibrutinib promotes atrial fibrillation by inducing structural remodeling and calcium dysregulation in the atrium," *Heart Rhythm*, vol. 16, no. 9, pp. 1374–1382, 2019.

[22] J. Yao, X. Qin, J. Zhu, and H. Sheng, "Dyrk1A-ASF-CaMKII-delta signaling is involved in valsartan inhibition of cardiac hypertrophy in renovascular hypertensive rats," *Cardiology*, vol. 133, no. 3, pp. 198–204, 2016.

[23] D. R. Zakhary, C. S. Moravec, R. W. Stewart, and M. Bond, "Protein kinase A (PKA)-dependent troponin-I phosphorylation and PKA regulatory subunits are decreased in human dilated cardiomyopathy," *Circulation*, vol. 99, no. 4, pp. 505–510, 1999.

[24] L. Sun, Y. Chen, H. Luo, M. Xu, G. Meng, and W. Zhang, "Ca(2+)/calmodulin-dependent protein kinase II regulation by inhibitor 1 of protein phosphatase 1 alleviates necroptosis in high glucose-induced cardiomyocytes injury," *Biochemical Pharmacology*, vol. 163, pp. 194–205, 2019.

[25] J. Wang, H. Liu, N. Li, Q. Zhang, and H. Zhang, "The protective effect of fucoidan in rats with streptozotocin-induced diabetic nephropathy," *Marine Drugs*, vol. 12, no. 6, pp. 3292–3306, 2014.

[26] H. Luo, S. Song, Y. Chen et al., "Inhibitor 1 of protein phosphatase 1 regulates Ca(2+)/calmodulin-dependent protein kinase II to alleviate oxidative stress in hypoxia-reoxygenation injury of cardiomyocytes," *Oxidative Medicine and Cellular Longevity*, vol. 2019, Article ID 2193019, 2019.

[27] J. Chen, R. Kos, J. Garssen, and F. Redegeld, "Molecular insights into the mechanism of necroptosis: the necrosome as a potential therapeutic target," *Cells*, vol. 8, no. 12, p. 1486, 2019.

[28] J. Luo, D. Yan, S. Li et al., "Allopurinol reduces oxidative stress and activates Nrf2/p62 to attenuate diabetic cardiomyopathy in rats," *Journal of Cellular and Molecular Medicine*, vol. 24, no. 2, pp. 1760–1773, 2019.

[29] K. Gupta, N. Phan, Q. Wang, and B. Liu, "Necroptosis in cardiovascular disease - a new therapeutic target," *Journal of Molecular and Cellular Cardiology*, vol. 118, pp. 26–35, 2018.

[30] J. Yan, K. Xiong, L.-M. Guo et al., "RIP3/MLKL-mediated neuronal necroptosis induced by methamphetamine at 39 degrees C," *Neural Regeneration Research*, vol. 15, no. 5, pp. 865–874, 2020.

[31] S. B. Lee, J. J. Kim, S.-A. Han et al., "The AMPK-Parkin axis negatively regulates necroptosis and tumorigenesis by inhibiting the necrosome," *Nature Cell Biology*, vol. 21, no. 8, pp. 940–951, 2019.

[32] K. Abe, T. Yano, M. Tanno et al., "mTORC1 inhibition attenuates necroptosis through RIP1 inhibition-mediated TFEB activation," *Biochimica et Biophysica Acta (BBA) - Molecular Basis of Disease*, vol. 1865, no. 12, article 165552, 2019.

[33] D. Pajuelo, N. Gonzalez-Juarbe, U. Tak, J. Sun, C. J. Orihuela, and M. Niederweis, "NAD(+) depletion triggers macrophage necroptosis, a cell death pathway exploited by Mycobacterium tuberculosis," *Cell Reports*, vol. 24, no. 2, pp. 429–440, 2018.

[34] H. Fan, H.-B. Tang, L.-Q. Shan et al., "Quercetin prevents necroptosis of oligodendrocytes by inhibiting macrophages/-microglia polarization to M1 phenotype after spinal cord injury in rats," *Journal of Neuroinflammation*, vol. 16, no. 1, p. 206, 2019.

[35] Z. Cai and Z. G. Liu, "Detection of MLKL oligomerization during programmed necrosis," *Methods in Molecular Biology*, vol. 1857, pp. 85–92, 2018.

[36] J. Nie, N. Ta, L. Liu, G. Shi, T. Kang, and Z. Zheng, "Activation of CaMKII via ER-stress mediates coxsackievirus B3-induced cardiomyocyte apoptosis," *Cell Biology International*, vol. 44, no. 2, pp. 488–498, 2020.

[37] S. Neef, A. Steffens, P. Pellicena et al., "Improvement of cardiomyocyte function by a novel pyrimidine-based CaMKII-inhibitor," *Journal of Molecular and Cellular Cardiology*, vol. 115, pp. 73–81, 2018.

[38] L. Daniels, J. R. Bell, L. M. D. Delbridge, F. J. McDonald, R. R. Lamberts, and J. R. Erickson, "The role of CaMKII in diabetic heart dysfunction," *Heart Failure Reviews*, vol. 20, no. 5, pp. 589–600, 2015.

[39] D. Zheng, Z. Li, X. Wei et al., "Role of miR-148a in mitigating hepatic ischemia-reperfusion injury by repressing the TLR4 signaling pathway via targeting CaMKIIalpha in vivo and in vitro," *Cellular Physiology and Biochemistry*, vol. 49, no. 5, pp. 2060–2072, 2018.

[40] J. Hu, Y. Zhang, X. Jiang et al., "ROS-mediated activation and mitochondrial translocation of CaMKII contributes to Drp1-dependent mitochondrial fission and apoptosis in triple-negative breast cancer cells by isorhamnetin and chloroquine," *Journal of Experimental & Clinical Cancer Research*, vol. 38, no. 1, p. 225, 2019.

[41] P. G. Santamaría, A. Floristán, B. Fontanals-Cirera et al., "Lysyl oxidase-like 3 is required for melanoma cell survival by maintaining genomic stability," *Cell Death & Differentiation*, vol. 25, no. 5, pp. 935–950, 2018.

[42] A. Sureshbabu, E. Patino, K. C. Ma et al., "RIPK3 promotes sepsis-induced acute kidney injury via mitochondrial dysfunction," *JCI Insight*, vol. 3, no. 11, 2018.

[43] X. Song and T. Li, "Ripk3 mediates cardiomyocyte necrosis through targeting mitochondria and the JNK-Bnip3 pathway under hypoxia-reoxygenation injury," *Journal of Receptors and Signal Transduction*, vol. 39, no. 4, pp. 331–340, 2019.

[44] Y. Zhu, Y. Gao, X. Sun et al., "Discovery of novel serine/threonine protein phosphatase 1 inhibitors from traditional Chinese medicine through virtual screening and biological assays," *Journal of Biomolecular Structure and Dynamics*, vol. 38, no. 18, pp. 5464–5473, 2019.

[45] A. El-Armouche, T. Rau, O. Zolk et al., "Evidence for protein phosphatase inhibitor-1 playing an amplifier role in beta-adrenergic signaling in cardiac myocytes," *The FASEB Journal*, vol. 17, no. 3, pp. 437–439, 2003.

[46] J. Yu, Y. Chen, M. Xu et al., "Ca2+/calmodulin-dependent protein kinase II regulation by inhibitor 1 of protein phosphatase 1 protects against myocardial ischemia-reperfusion injury," *Journal of Cardiovascular Pharmacology and Therapeutics*, vol. 24, no. 5, pp. 460–473, 2019.

Research Article

Kirenol Inhibits B[a]P-Induced Oxidative Stress and Apoptosis in Endothelial Cells via Modulation of the Nrf2 Signaling Pathway

Peramaiyan Rajendran [ID],[1] **Abdullah M. Alzahrani** [ID],[1] **Emad A. Ahmed** [ID],[1,2] **and Vishnu Priya Veeraraghavan** [ID][3]

[1]*College of Science, Department of Biological Sciences, King Faisal University, Al Ahsa, 31982., Saudi Arabia*
[2]*Department of Molecular Physiology, Zoology Department, Faculty of Science, Assiut University, Egypt*
[3]*Department of Biochemistry, Saveetha Dental College, Saveetha Institute of Medical and Technical Sciences, Saveetha University, Chennai 600 077, India*

Correspondence should be addressed to Peramaiyan Rajendran; prajendran@kfu.edu.sa

Atherosclerosis is a persistent inflammatory disorder specified by the dysfunction of the arteries, the world's leading cause of cardiovascular diseases. We sought to determine the effectiveness of KRL in B[a]P-induced oxidative stress and programmed cell death in endothelial cells. Western blotting, real-time PCR, DCFH2-DA, and TUNEL staining were performed to detect pPI3K, pAKT, Nrf2, HO-1, NQO-1, Bcl2, Bax, and caspase-3 on the HUVECs. Through the pretreatment of KRL, a drastic enhancement was observed in the cell viability of HUVECs, whereas DNA damage and generation of reactive oxygen species induced by B[a]P was suppressed. KRL's potential use as an antioxidant was observed to have a direct correlation with an antioxidant gene's augmented expression and the nuclear translocation activation of Nrf2, even during the event when B[a]P was found to be absent. In addition, this study proved that the signaling cascades of PI3K/AKT mediated Nrf2 translocation. Activation of suppressed nuclear Nrf2 and reduced antioxidant genes across cells interacting with an LY294002 confirmed this phenomenon. In addition, knockdown of Nrf2 by Nrf2-siRNA transfection abolished the protective effects of KRL on HUVECs cells against oxidative damage. Finally, the expression of apoptotic proteins also supported the hypothesis that KRL may inhibit endothelial dysfunction. This study showed that KRL potentially prevents B[a]P-induced redox imbalance in the vascular endothelium by inducing the Nrf2 signaling via the PI3K/AKT pathway.

1. Introduction

As pervasive environmental carcinogens, heterocyclic aromatic hydrocarbons cause genetic damage and endowed with a strongly bioaccumulation attribute. As a PAH (polyaromatic hydrocarbon), benzo[a]pyrene (B[a]P) finds itself in first class of carcinogens issued by the International Agency for Research on Cancer. Exposure to toxic B[a]P mainly takes place because of the existing food chain and cigarettes. As per previous studies, 9.20 ng/day is the maximum exposure of people to this PAH [1]. Meanwhile, its sustained exposure can lead to metastasis as well as angiogenesis in many organs of the human body, such as the stomach, liver, skin, lungs, and colorectal organs [2, 3]. According to a vast body of scholarly research, one of the strongest causes of vascular inflammation is oxidative stress [4]. Previous literature in animal models clearly illustrated that direct exposure to B[a]P can cause including cancers and pulmonary, neurodegenerative, and cardiovascular diseases [2, 5–7]. Atherosclerosis is thought, at least in part, to be an inflammatory mechanism caused by free radicals [8, 9]. In addition to this, B[a]P was shown to stimulate formation of ROS and promote the progression of atherosclerosis [10, 11]. Mechanisms that are redox-sensitive are used to monitor various

inflammatory genes and related transcription factors. B[a]P is known to cause atherosclerotic lesions when it comes to animal models [12, 13].

Nrf2 can easily get liberated from "Kelch-like ECH-associated protein 1" (KEAP1) and transport from the cytosol to the nucleus when confronted with oxidative stress, activating antioxidative gene expression including heme oxygenase-1 (HO-1). The phospholipid, namely, phosphatidylinositol 3-kinase (PI3K) super family, belongs to the DNA-dependent protein kinase catalytic subunit (DNA-PKcs). From the previous literature, we can understand that DNA-PKcs and the PI3K/protein kinase B (AKT) signaling pathway have been involved in HO-1 induction with response to PAH-induced oxidative stress [14–16]. AKT's reversible oxidation is its planned mechanism. For this reason, regulating signaling of Nrf2 mediated by PI3/AKT, to control DNA damage induced by ROS, could possibly be helpful in developing new drugs against vascular damages induced by B[a]P. In order to reduce toxicity induced by B[a]P as well as to treat atherosclerosis, natural products serve as important resources to atherosclerosis therapy [17–19]. In this context, kirenol (KRL) is sourced from *Herba Siegesbeckia*, which has historically utilized in China for the treatment of rheumatoid arthritis. KRL exhibits anti-inflammatory and antirheumatic properties [20]. In addition to demonstrating that this compound can lower the pathology of inflammation in model rats, other literature suggests that it can also inhibit TNF-α and IL-1β production in adjuvant arthritis model animal serum [21–23]. Wu et al. also demonstrated that KRL offers potent cardioprotective effects [24]. Here, we hypothesized that KRL can activate Nrf2 possibly because of the phenolic compounds' antioxidant action against vascular toxicity induced by B[a]P.

2. Materials and Methods

2.1. Reagents. All reagents (standard) were derived from Sigma-Aldrich unless mentioned otherwise. This study used the following antibodies: antibodies against pAKT, AKT, pPI3K, PI3K, BCL2, BAX, HO-1, NQO-1, pNrf2, actin, and lamin B1 derived from Invitrogen, Waltham, MA-based Thermo Fisher Scientific, Inc., LY294002 (L9908). Meanwhile, caspase-3 (anti-cleaved) (ab32042) antibody was purchased from Abcam (Branford, CT, USA). Lipofectamine 2000 (11668027) and Nrf2 siRNA were procured from Thermo Fisher Scientific, Inc.

2.2. Cell Culture. Derived from Shanghai Institute of Cell Biology, the culturing of HUVECs (passage 15) in DMEM was done with heat-inactivated FBS, 100 U/ml penicillin, and 100 U/ml streptomycin. The maintenance of cells was done in 100 mm dishes in CO_2 humidified atmosphere with 37°C incubation.

2.3. Cell Culture Treatment. To examine the protective effect of KRL against oxidative stress, HUVECs cells were treated with 25 μmol of KRL for 2 h before B[a]P (5 μmol); cell lysate was collected for analysis after 24 h.

2.4. Intracellular ROS Assay. The HUVECs cells' seeding was undertaken in the eight-well chamber (LabTech). This chamber comprised 10% DMEM by FBS, with a confluence growth of 80%. After the treatment, the mechanism of dichlorofluorescin diacetate (DCFH2-DA) was utilized for washing cells with PBS. In addition, intracellular ROS was measured by a Leica D6000 fluorescence microscope.

2.5. Measurement of Nitric Oxide Production. Cells were grown on 35 mm diameter cell culture dishes and then incubated for 6 h with the test compounds or DMSO as a solvent control (0.1%) in Dulbecco's modified Eagle's medium (Invitrogen, Carlsbad, CA, USA). Nitric oxide production was estimated by determination of nitrites/nitrates in the cell culture medium using the Griess reaction. Detection involved the enzymatic conversion of nitrates to nitrites by nitrate reductase (Sigma-Aldrich), followed by colorimetric detection of nitrites as a colored azo dye product. The absorbance was measured at 546 nm using the SPECTRA Rainbow (Tecan, Austria) microplate reader.

2.6. Preparation of Cytosolic and Nuclear Extracts. The resuspending of cell pellets was done in buffer I for preparing cytosolic extracts in a period of five minutes. Buffer I consisted of 5 mM KCl, 0.5 mM $MgCl_2$, 25 mM HEPES pH 7.9, and 1 mM dithiothreitol. The suspension was then bolstered with buffer II with the same specifications. Thereafter, the suspension was added by NP40, which, in turn, was supplemented by phosphatase/protease inhibitors. The incubation of resultant samples was done for 15 min. These lysates were centrifuged at 2500 rpm for 5 min. For getting rid of residual nuclei, these lysates were centrifuged at the same temperature after which the transferring of supernatants was done to Eppendorf tubes. The rotation of lysates was done at a temperature of 4°C for a period of 1 hour before it was centrifuged at the same temperature for 10 min [25].

2.7. Nrf2-siRNA Transient Transfection. During the transfection, the plating of cells was done in six-well plates for reaching a confluency of 40–60%. After that, 500 μl of culture medium (Opti-MEM) was utilized, whereas the cells were transfected by the RNAiMAX transfection reagent. A combination of siRNA100 pM, an Opti-MEM (500 μl), and RNAiMAX reagent was used in a different tube. After transfecting siRNA using Lipofectamine RNAiMax, the instructions of KRL manufacturers were complied with. The incubation of siRNA/RNAiMAX blend was done for a period of 25 min. Subsequently, this solution was added with the cells in the aforementioned plates, following which the solution was finally incubated for a period of 6 hours. This was followed by a culturing of cells at normal temperature after substituting the medium of transfection using a standardised growth medium.

2.8. Western Blotting. Following the treatment, the scraping of cells was done before being rinsed inside cold PBS. After that, the preparation of nuclear, total, and cytoplasmic extract was undertaken. In all the samples, Bio-Rad protein assay helped ascertain the concentration of protein and bovine serum albumin (BSA) in order to be used as the
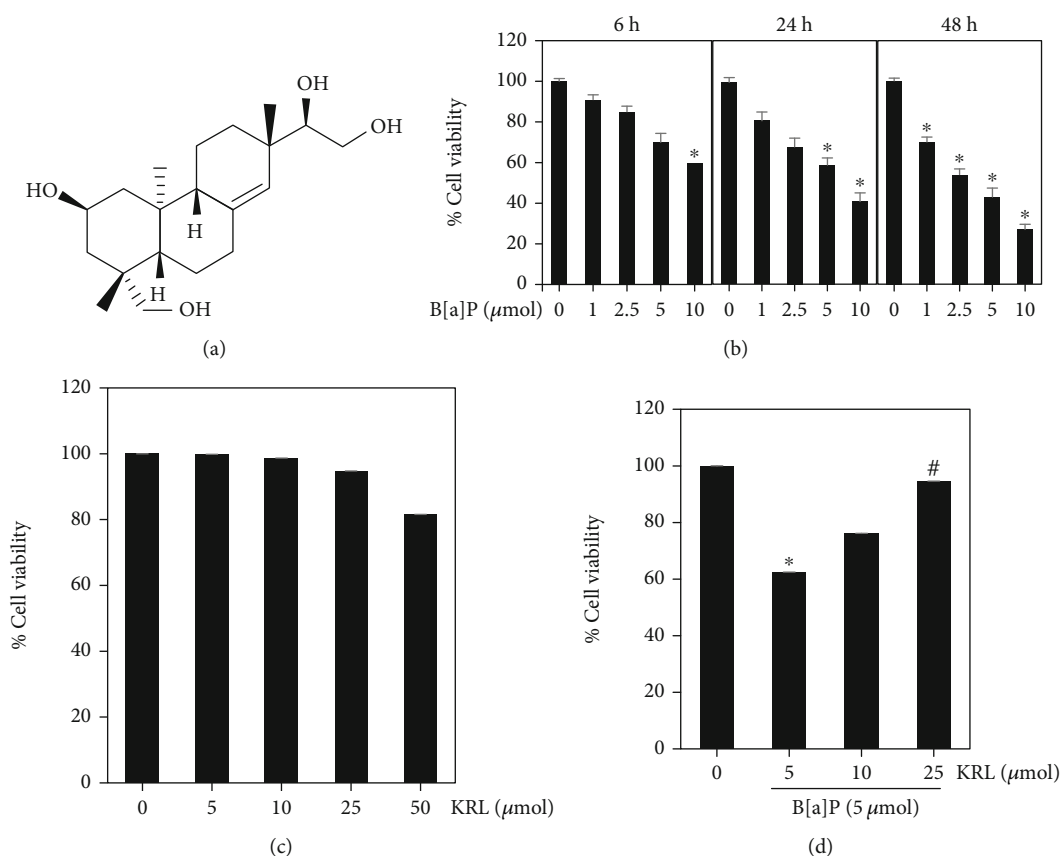
Figure 1: Impact of B[a]P and KRL on cell viability. (a) Chemical structure of KRL. (b) HUVECs cells were added to the different dosages of B[a]P for 6, 24, and 48 hours in various concentrations after which cell viability was determined using MTT assay. (c) Cytotoxic effect of KRL on HUVECs cells. The exposure of cells was made to varying KRL concentrations for 24 hours. (d) KRL safeguards the cytotoxic effect of B[a]P, as analyzed by MTT assay. Data is shown as the mean ± SD of triplicate values ($n = 3$), whereas $*p < 0.05$ signifies a major difference as compared to the control group. On the other hand, $\#p < 0.05$ denotes significant variations when compared to B[a]P alone as well as KRL with the B[a]P treatment groups.

standard of reference. On the other hand, equal quantities (50 μg) of protein were resolved using SDS-PAGE (8-15%) before being moved across to nitrocellulose membranes. On the other hand, the membranes were blocked for half an hour at room temperature using 5% skimmed milk, prior to being incubated for a couple of hours using primary antibodies. Subsequently, anti-rabbit secondary antibody or goat anti-mouse (horseradish peroxidase-conjugated) incubated the membranes for the same duration. The membranes were developed with an improved chemiluminescence substrate. Meanwhile, the samples were examined using an LI-COR chemiluminescence imaging system. Finally, the graphs pertaining to the intensities of the densitometric band were made using Image Studio™ Lite software. Normalisation of the untreated control band's intensity was fixed at 1.

2.9. TUNEL Assay. The cells were incubated with KRL and/or B[a]P for 24 h at given doses, and TUNEL assay was studied as described previously [26].

2.10. Real-Time Polymerase Chain Reaction (RT-PCR). The treatment of HUVECs cells was done using B[a]P and/or KRL (0, 5, 10, and 25 μmol) for 24 hours. After extracting total RNA with a TRIzol reagent, RNA was turned into cDNA through the use of Taq polymerase as well as super-script reverse transcriptase via reverse chain reaction of transcription polymerase. The relative expressions of Nrf2 (5′-CATCCAGTCAGAAACCAGTGG-3′ and 5′-GCAGTC ATCAAAGTACAAAGCAT-3′), HO-1 (5′-CTTCTTCAC CTTCCCCAACA-3′ and 5′-ATTGCCTGGATGTGCT TTTC-3′), and NQO-1 (5′-GGGATCCACGGGGACA TGAATG-3′ and 5′-ATTTGAATTCGGGCGTCTGCTG-3′) were analyzed by using RT-PCR. The combination of SYBR Green system and ViiA-7 Applied Biosystem was used to perform RT-qPCR. All genes' mRNA expression was converted into β-actin. The calculation of fold change across various groups was done by making use of Ct value through $2^{-\Delta\Delta Ct}$ (Δ^{Ct} = Ct [target gene] − Ct[β − actin]).

2.11. Statistical Analysis. For this purpose, GraphPad Prism software version 6.0 was utilized; on the other hand, three groups were compared using one-way ANOVA. All findings

(a)

(b)

(c)
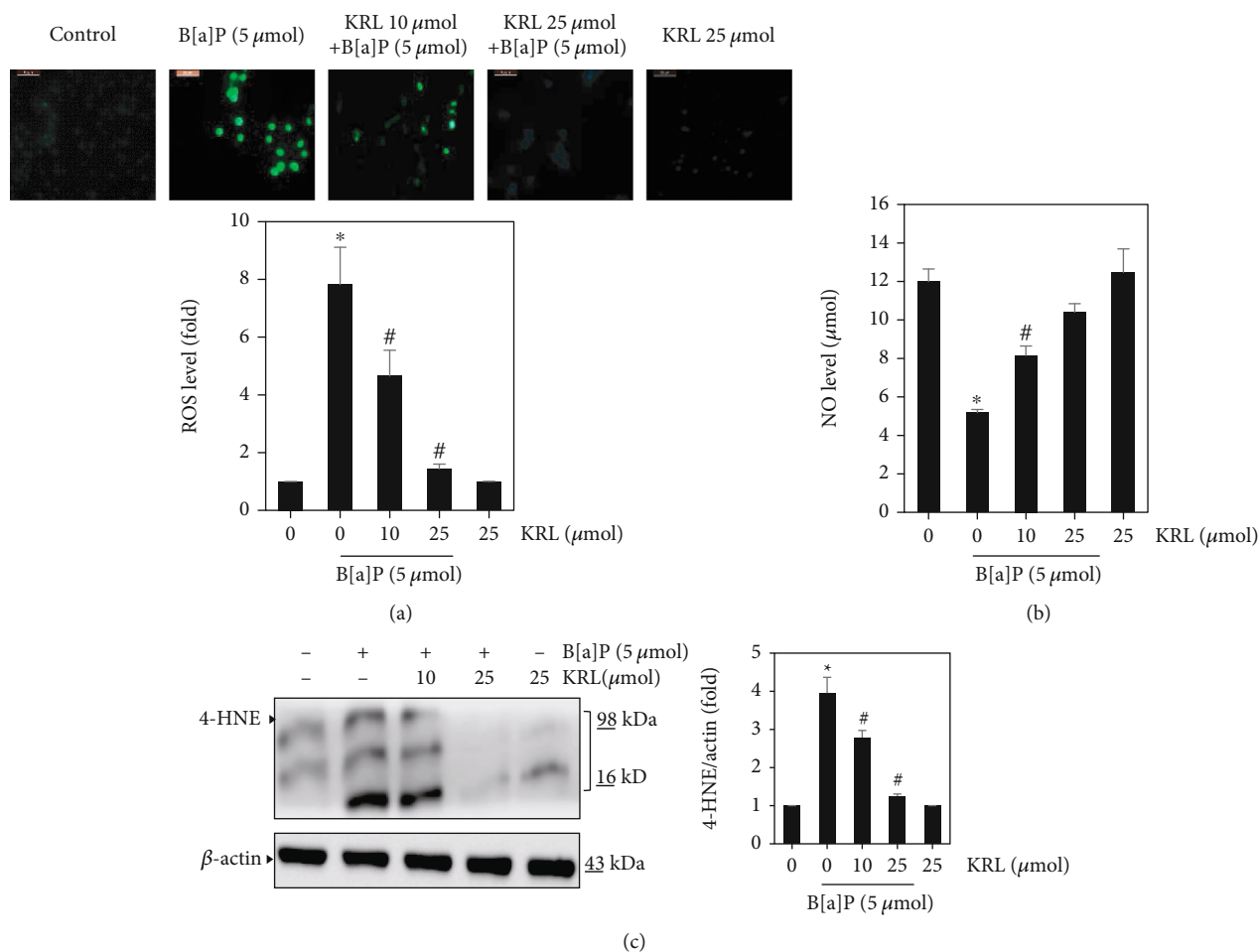
Figure 2: KRL inhibits ROS formation. HUVECs cells confluent at 80% were incubated with B[a]P (5 μmol) and/or KRL 10 and 25 μmol for 60 minutes. (a) DCFH2-DA was made use for the purpose of measuring generation of intracellular ROS. After reacting with ROS, DCFH2-DA metabolized into DCF, which, in turn, was proportionate to ROS's generation. (b) KRL effect on NO production in B[a]P-induced oxidative stress. (c) KRL on oxidative marker 4-HNE protein activation. Data was represented as the mean ± SD of triplicate values ($n = 3$), and $^{*}p < 0.05$ represents a significant discrepancy when compared to the control group. On the other hand, $^{#}p < 0.05$ signifies major differences compared to the B[a]P alone and KRL with the B[a]P treatment groups.

were expressed in the form of mean ± SD, and $p < 0.05$ was deemed statistically important.

3. Results

3.1. KRL Inhibits B[a]P-Induced Cytotoxicity. The HUVECs' cell viability was evaluated by using the B[a]P effects for ascertaining KRL's cytotoxic potentiality. The incubation of cells was done for 6 hours, 24 hours, and 48 hours using B[a]P (Figure 1(b)). B[a]P cytotoxicity testing showed significant toxicity to HUVEC cells at different dose and times. KRL cytotoxicity testing showed that concentrations as high as 25 μmol KRL were not significantly toxic to HUVECs cells (Figure 1(c)). Having said that, as illustrated in Figure 1(d), significant protection (dose-dependent) against cell death induced by B[a]P was seen with cells' preincubation using B[a]P (5 μmol) and KRL (5, 10, and 25 μmol).

3.2. B[a]P Induced Vascular Endothelial Cells ROS Inhibition by KRL. Next, we used the method of DCFH2-DA fluorescent staining for ascertaining whether or not KRL could inhibit B[a]P-induced ROS generation in HUVECs cells. Figure 1(b) shows that in the context of induced cell death, ROS are the primary source of cellular death. The excessive generation of ROS has a close relationship with vascular dysfunction and cell death [4, 27]. Subsequently, we used the method of DCFH2-DA fluorescent staining for determining the curtailment ability of ROS generation induced by B[a]P. Figure 2(a) shows a radical growth in intracellular ROS generation after B[a]P-related stimulation for one hour. The amount of free radicals generation was directly correlated to enhanced intensity of dichlorodihydrofluorescein (DCF). Nevertheless, the excessive ROS was significantly suppressed owing to KRL treatment, as Figure 2 shows. Inhibition and/or scavenging of free radicals was observed, which shows that KRL exhibits an oxidative stress induced by B[a]P as far as HUVECs endothelial cells are concerned. The improvement of endothelial dysfunction in HUVECs treated with KRL was associated with increased NO levels and was also upregulated (Figure 2(b)).
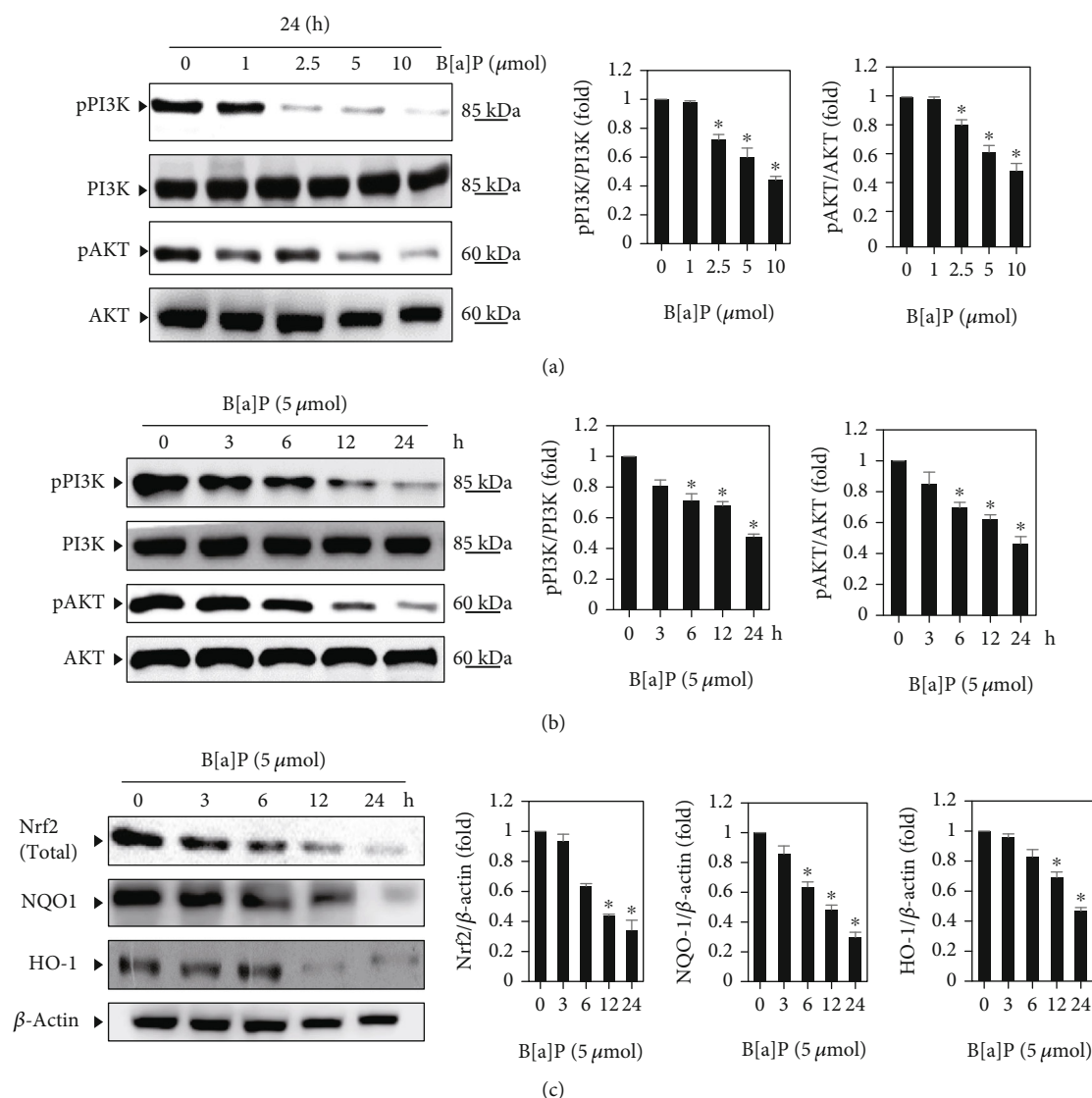
FIGURE 3: B[a]P inhibits the PI3/AKT-mediated Nrf2 signaling. (a) Cells were incubated with different concentrations of B[a]P for 24 hours, with equal amounts of whole cell lysate being exposed to SDS-PAGE. Membranes probed with anti-pPI3K and anti-pAKT antibodies and PI3K and AKT levels were deemed internal control. (b) HUVECs cells were treated with B[a]P (5 μmol) for 0, 3, 6, 12, and 24 hours, and the membranes were probed with anti-pPI3K and anti-pAKT antibodies. In addition, PI3K and AKT levels were also regarded as internal control. (c) The treatment of cells with B[a]P (5 μmol) for different indicated periods. After preparing extracts of total protein, western blot assessments were undertaken and analyzed Nrf2, Ho-1, and NQO-1 activations. Data is shown as the mean ± SD of triplicate values ($n = 3$), whereas $^*p < 0.05$ denotes a major discrepancy when compared to the control group; on the other hand, $^\#p < 0.05$ represents noteworthy difference when compared to the B[a]P alone and KRL with the B[a]P treatment groups.

3.3. KRL Regulated 4-HNE Activation.

ROS and by products and oxidative stress can induce various types of protein modifications such as aldehydic adducts (4-HNE and MDA). Consequently, in our study, we performed an analysis using western blot to determine whether KRL could inhibit the oxidative markers including 4-HNE. It was found that the B[a]P treatment of H9c2 cells markedly increased the accumulation of these oxidative markers. Subsequently, KRL treatment prevented this accumulation completely (Figure 2(c)). This finding demonstrates the probable effects of KRL in suppressing the elevated levels of 4-HNE.

3.4. B[a]P Downregulates Phosphorylation of PI3/AKT and Nrf2 Expression.

According to several studies, ROS help activate apoptosis via pathways of PI3/AKT [28–30]. Oxidative stress is known to downregulate PI3/AKT phosphorylation and leads the inactivation of various transcription factors such as Nrf2. In order to clarify whether or not B[a]P has an impact on PI3/AKT phosphorylation expression, HUVECs were subjected to dose and time periods induced by B[a]P (Figures 3(a) and 3(b)). Through western blotting, HUVECs' exposure to B[a]P for indicated time/dose periods revealed a significant decline in the phosphorylation of

(a)

(b)
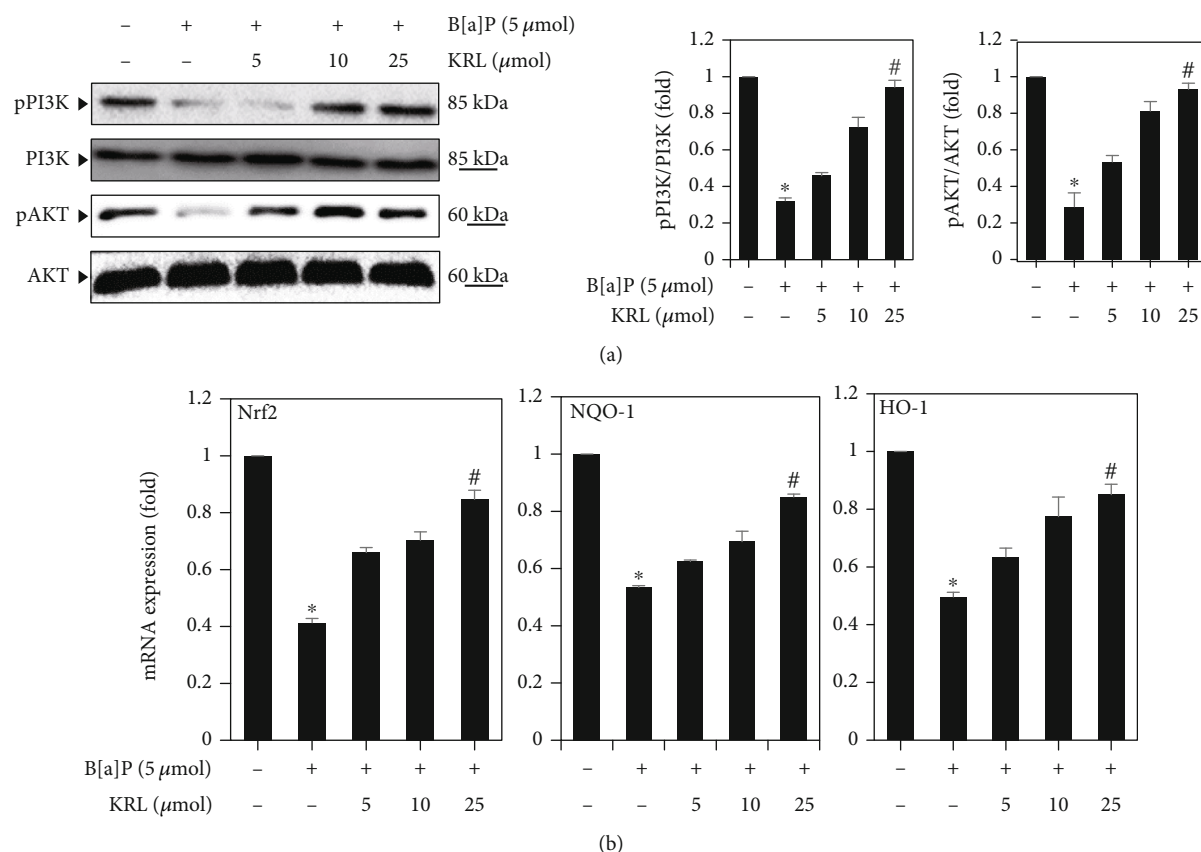
Figure 4: KRL activates the PI3/AKT signaling. (a) HUVECs cells were treated with B[a]P (5 μmol) and/or KRL (5, 10, and 25 μmol) for 24 hours. The findings of western blotting reveal the impacts of KRL on anti-pPI3K and anti-pAKT. The expression's relative ratios shown in the results of western blotting are presented below each of the results in the form of values that are relative to PI3K and AKT expression. (b) Nrf2, NQO-1, and HO-1 expression was assessed by RT-PCR. Data is represented as the mean $\pm$ SD of triplicate values ($n = 3$), and $^*p < 0.05$ represents major variations as compared to the control. $^\#p < 0.05$ meanwhile signifies noteworthy discrepancies in comparison to the B[a]P alone and KRL with the B[a]P treatment groups.

PI3/AKT expression. Similarly, the expression of Nfr2 antibodies (HO-1 and NQO-1) was significantly reduced by HUVECs cells treated by B[a]P (Figure 3(c)). These results clearly show that B[a]P could play a role in inhibiting the PI3/AKT signaling which selectively targets HUVECs cells.

3.5. KRL Upregulates PI3/AKT Phosphorylation. Next, we sought to know if KRL induces PI3/AKT in HUVECs cells treated with B[a]P. For this reason, western blot was undertaken. The HUVECs were put into KRL (0, 5, 10, and 25 μmol) and/or B[a]P incubation for 24 hours as per the findings of western blotting.

HUVECs exposure to KRL (0-25 μmol) in evaluating pPI3 and pAKT expression showed that KRL enhanced the p-PI3K as well as p-AKT expression in a dose-dependent manner. However, the expression of PI3K and AKT remained almost unaltered. Therefore, the level of pPI3K and pAKT cells was significantly increased after KRL treatment. Along the same lines, KRL (0-25 μmol) pretreatment and/or B[a]P (5 μmol) via RT-PCR evaluation revealed high levels of mRNA concerning NQO-1, HO-1 and Nrf2, HO-1 (Figure 4(b)). At the same time, their expression was significantly higher in 25 μmol KRL in comparison to others.

3.6. KRL Upregulates Nrf2 Signaling Proteins. In order to carry out further investigation of the protective mechanisms implicated via the impacts of KRL on cells treated with B[a]P, western blotting was carried out to examine protein expression levels of Kaep-1 and Nrf2 signaling proteins. We observed a reduced expression of Nrf2 and its target genes HO-1 in the B[a]P (5 μmol) exposed to HUVECs cells, which was markedly reversed by KRL (10 and 25 μmol), thereby upregulating the expression of Nrf2 and HO-1 in the cells (Figure 5).

3.7. KRL Upregulates Nrf2 Activation through the PI3/AKT Pathways. Based on above results, we undertook an examination of the manner in which KRL had an impact on oxidative stress induced by B[a]P when a PI3K/AKT inhibitor was found to be present. For ascertaining whether the pathway's activation by KRL played an important role in ensuring HUVECs cells' survival rate by modulating the expression of HO-1, we examined the kind of impact of LY294002 had on the protein expression of the aforementioned protein signals. Figure 6(a) shows that B[a]P and/or KRL enhanced the levels of protein expression in comparison to the group that was treated with B[a]P alone, although LY294002 had largely
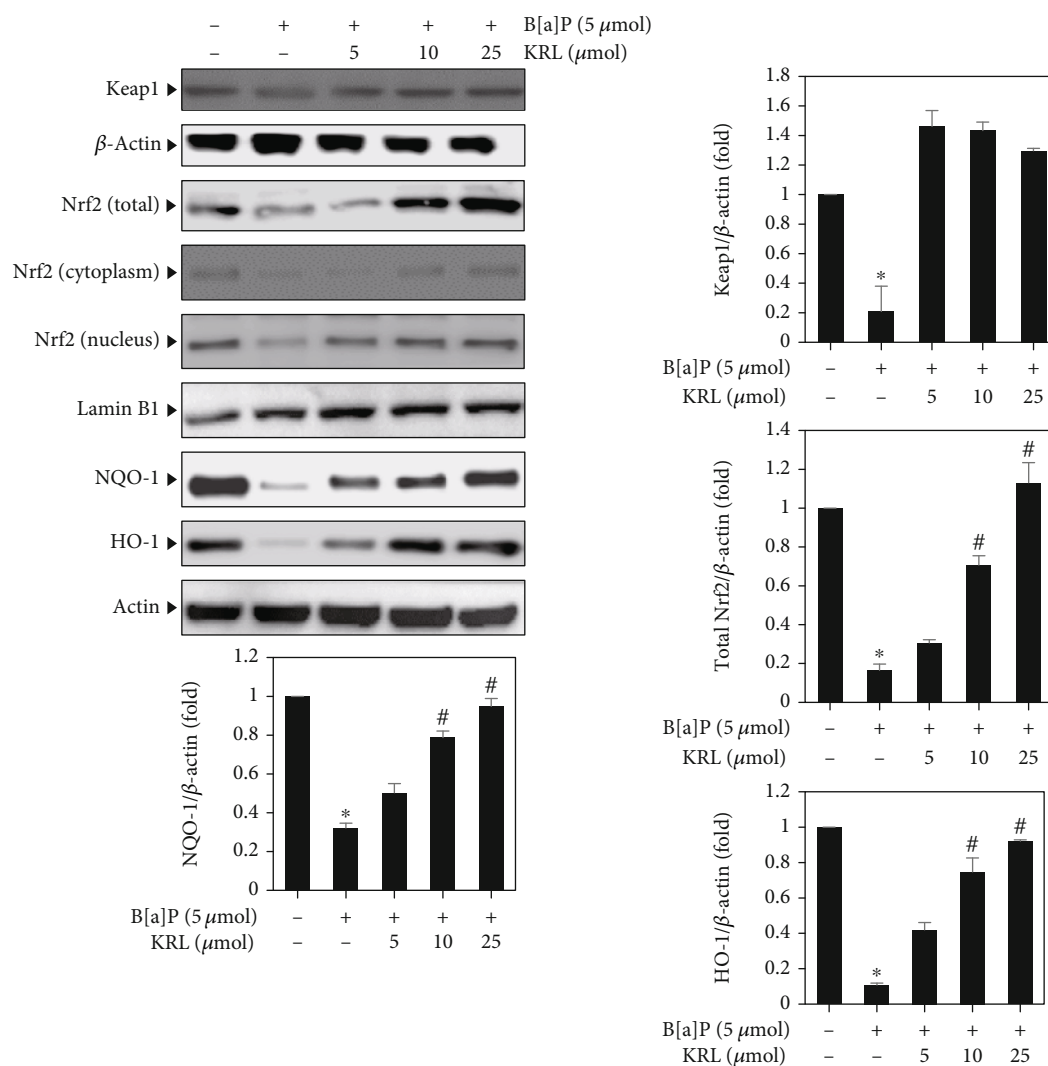
FIGURE 5: KRL upregulates the Nrf2 signaling pathways. HUVECs cell was treated with B[a]P (5 μmol) and/or KRL (5, 10, and 25 μmol) for 24 hours; western blotting method was used to examine what kind of impact of dose concentration had on the expressions of total, cytoplasm, and nuclear Nrf2, NQO-1, and HO-1 and antioxidant genes. In the form of internal control, β-actin and lamin B1 were used. Data is represented as the mean ± SD of triplicate values ($n = 3$), and $^*p < 0.05$ denotes noteworthy variations in comparison to the control. $^\#p < 0.05$ represents remarkable discrepancies when compared with the B[a]P alone and KRL with the B[a]P treatment groups.

negated this finding. LY294002 also abolished the rise in the KRL-induced levels of protein expression of all three protein signals. In addition, immunofluorescence staining showed that both B[a]P and KRL stimulated Nrf2 nuclear transloca-tion in HUVECs cells (Figure 6(b)). However, we observed that pretreatment with KRL induced more Nrf2 nuclear translocation compared with the B[a]P treatment group.

3.8. Nrf2 Knockdown Attenuated the Protective Effect of KRL on HUVECs Cells under Oxidative Stress. To determine the importance of regulating Nrf2, we developed a model of Nrf2 knockdown using siRNA transfection. To further eluci-date the role of Nrf2 in the cytoprotective effects of KRL against oxidative stress, we transfected HUVECs cells with a Nrf2 siRNA for 24 h, then pretreated with 25 μmol KRL followed by the treatment of 5 μmol B[a]P. As shown in Figures 7(a) and 7(b), after the transfection with si-Nrf2 in KRL and the B[a]P treatment group, we observed markedly

decreased protein expression level of Nrf2, HO-1, and NQO-1 compared with the KRL with B[a]P transfected with the scrambled group.

3.9. KRL Inhibits B[a]P-Induced Apoptosis HUVECs. The B[a]P-induced cell apoptosis was examined using TUNEL assay. Figure 8(a) shows that B[a]P (5 μmol) induces the TUNEL-positive nuclei in HUVECs cells. However, KRL pretreatment (25 μmol) significantly reduced B[a]P-induced cell apoptosis. Therefore, KRL pretreatment safeguards HUVECs cells from oxidative stress induced by B[a]P while also preventing cell apoptosis.

3.10. KRL Downregulates Caspase-3 and Upregulates Bcl2 Expression. Caspase-3 plays an important role in determining apoptotic events, which includes chromatin DNA fragmenta-tion, condensation, and apoptotic bodies' generation [31]. For this reason, our hypothesis was that the activation of

(a)

(b)
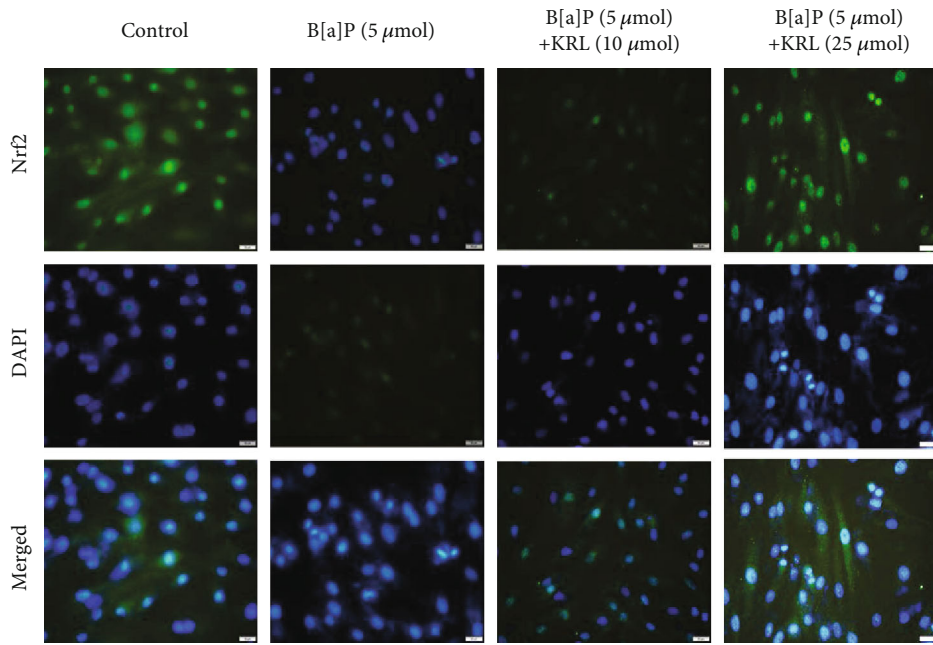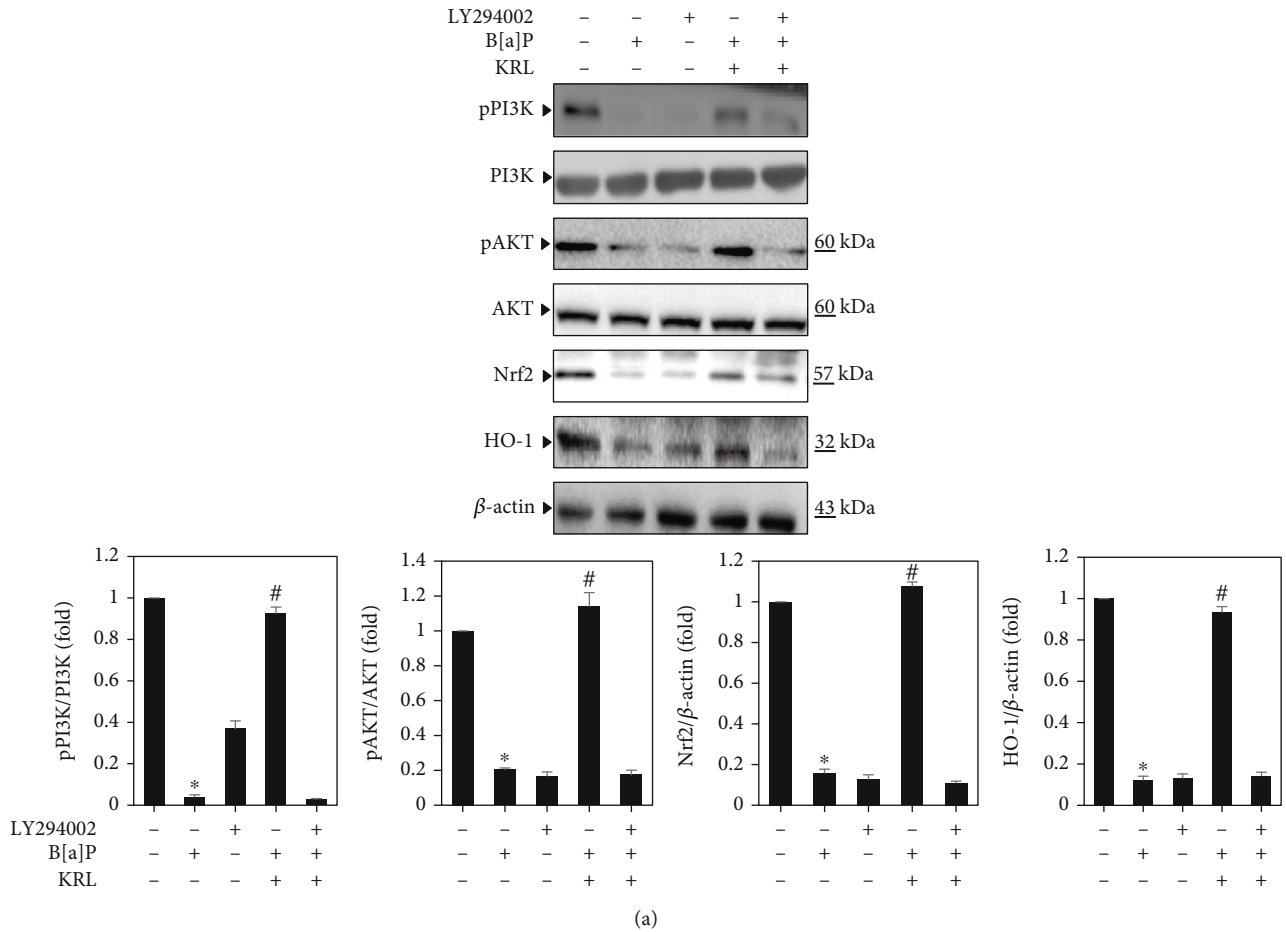
FIGURE 6: KRL can be seen to trigger the PI3/AKT pathway in B[a]P-induced HUVECs cells. (a) Cells were pretreated using a PI3K/AKT inhibitor for 2 hours. This was followed by KRL (25 μmol) and/or B[a]P (5 μmol) for 24 hours. Western blotting detected the pPI3K, pAKT, Nrf2, and HO-1 levels by anti-PI3K, anti-pAKT, anti-Nrf2, and anti-HO-1. (b) Nrf2 translocations. Data was represented as the mean ± SD of triplicate values ($n = 3$), whereas $*p < 0.05$ represents noteworthy discrepancies in comparison to the control. $#p < 0.05$ represents major variations when compared to the B[a]P alone and KRL with the B[a]P treatment groups.

(a)

(b)
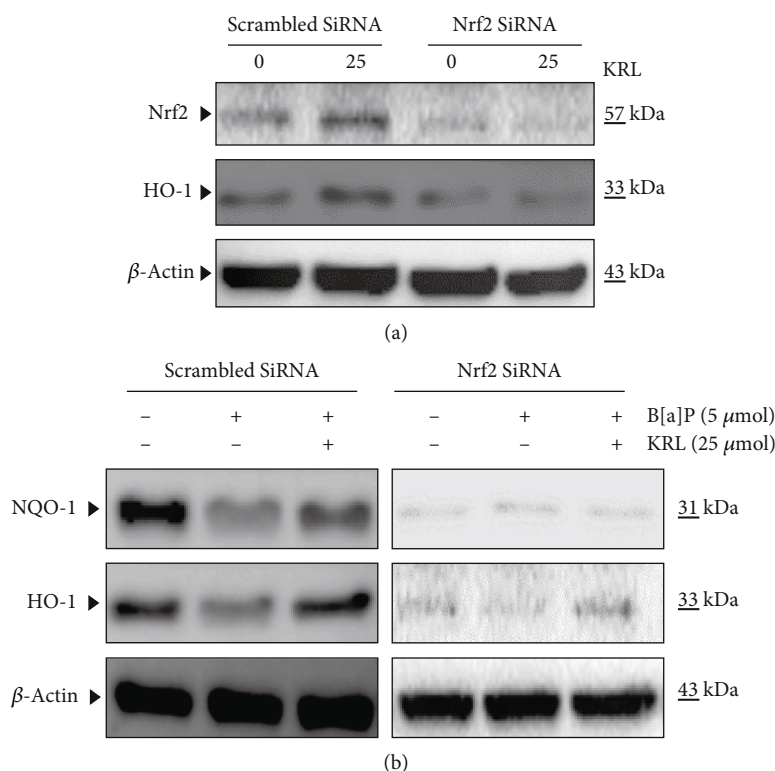
FIGURE 7: Role of Nrf2 in KRL-induced HO-1 and NQO-1 expression in endothelial cells. (a) HUVECs cells were transfected transiently with siRNA-Nrf2 and treated with 25 μmol KRL. Protein was isolated and analyzed for the measurement of Nrf2 protein by western blot analysis. (b) Western blot analysis to determine the levels of NQO-1 and HO-1.

caspase-3 mediates apoptosis and B[a]P-induced DNA damage. Figure 8(b) shows that exposure of B[a]P led to an increase in the activation of caspase-3 in endothelial cells significantly, while KRL majorly curtailed the activation of caspase-3. According to our findings, the B[a]P significantly enhanced Bax expression while reducing the expression of Bcl-2 expression. On the contrary, the Bcl-2 protein level was upregulated with KRL pretreatment, while it could not downregulate the Bax expression (B[a]P-induced). Thus, it can be inferred that caspase-3's activation and the Bcl-2/Bax ratio's dysregulation mediate KRL's protective impact against apoptosis induced by B[a]P within endothelial cells.

4. Discussion

According to numerous studies both *in vitro* and *in vivo*, oxidative stress makes changes in homeostasis, which impairs functionality of vascular endothelia [32–34]. B[a]P, which is a major environmental carcinogen, causes DNA damage by promoting oxidative stress. This study entailed the demonstration of a significant cytoprotective effect of KRL against oxidative stress induced by B[a]P within endothelial cells. It is a known fact that the mitochondria denote a prominent source of oxygen intermediates, whereas ROS' production during the consumption of oxygen causes biological structures' oxidative damage [35]. B[a]P-triggered vascular challenge has been associated with oxidative damage. For this reason, we undertook the measurement of oxidative stress, and our study data pointed out that the treatment using

B[a]P alone radically increased the levels of ROS levels when it comes to endothelial cells. Nevertheless, this impact was dose dependently and majorly inhibited owing to KRL pretreatment, which was consistent with prior studies indicating that several extracts of plants suppress formation of ROS by activating Nrf2 cascades [36].

When it comes to the regulation of the Nrf2 signaling, the signaling pathway of PI3K/AKT plays a key role [37]. For this reason, we explored the possibility of the PI3K/AKT-mediated Nrf2 signaling induced by KRL. According to our findings, the phosphorylation levels of AKT protein were notably lower in B[a]P alone-treated cells, whereas these effects significantly elevated in KRL treatment. On the other hand, significant alterations were not observed in the overall levels of AKT protein, thus implying that increasing phosphorylation of AKT protein could be a contributing factor to the Nrf2 signaling induced by KRL. We used a distinct PI3K/AKT inhibitor to treat HUVECs along with KRL for identifying the role played by the aforementioned pathway. As per our findings, when KRL was present, the PI3K/AKT signaling pathway significantly blocked the signaling.

Nrf2 enhances the responses (intracellular) to oxidative challenges [38]. Several studies have reported its beneficial impacts on many vascular ailments [39, 40]. Typically, Nrf2 can be easily degraded via the pathway of ubiquitin-proteasome. However, after it is exposed to an inducer or stressor, Nrf2 gets segregated from Keap1, moves on to the nucleus, before being sequestered with antioxidant and cytoprotective enzymes' antioxidant response facets for

(a)

(b)
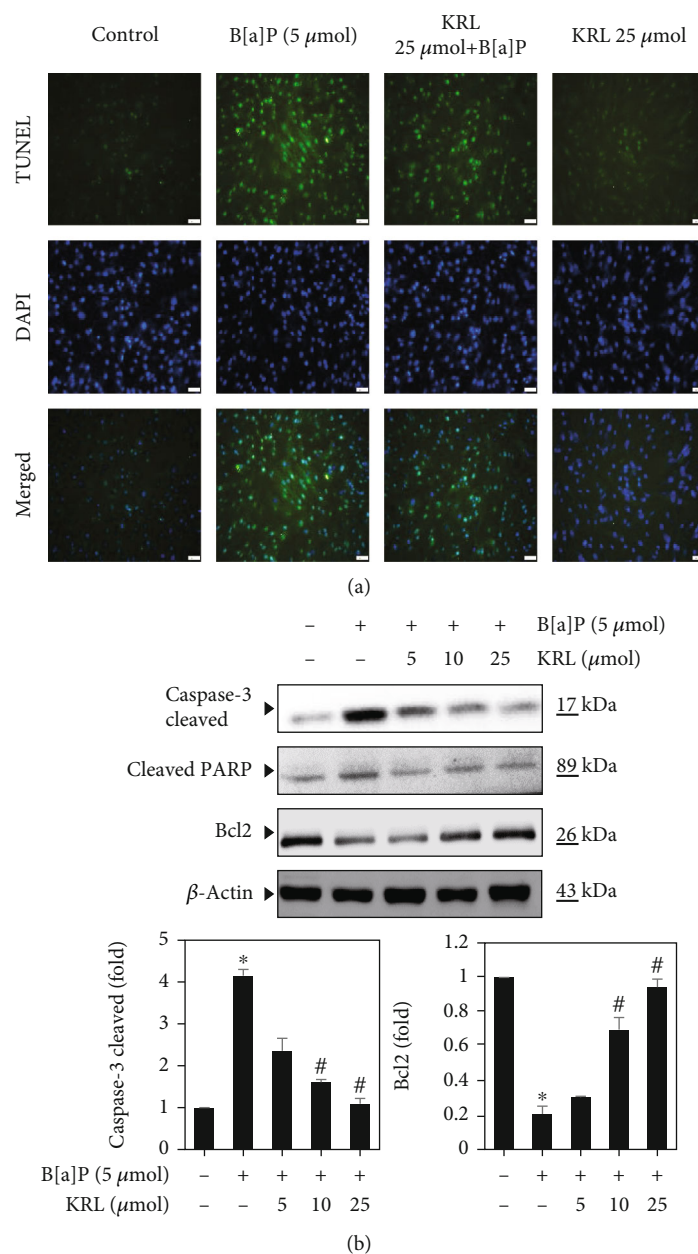
Figure 8: KRL suppresses DNA damage and apoptosis induced by B[a]P in HUVECs cells. (a) The pretreatment of cells was done using B[a]P (5 μmol) or KRL (5, 10, and 25 μmol) for a period of 24 hours and studied the TUNEL assay. (b) Cells were exposed to KRL and/or B[a]P for 24 h, and western blot was executed. Data was represented as the mean ± SD of triplicate values ($n = 3$), and $^*p < 0.05$ represents noteworthy differences in comparison to control. $^{\#}p < 0.05$ represents major variations in comparison to B[a]P alone and KRL with the B[a]P treatment groups.

promoting the expression of genes [41]. According to this study, the expression of Nrf2 enhanced significantly with a corresponding rise in the duration/concentration of the treatment involving KRL. Moreover, this treatment also significantly elevated HO-1's expression. It is noteworthy that HO-1 facilitates heme's decomposition to biliverdin, iron and iron, carbon monoxide. Importantly, the products created as a result of this enzymatic reaction play a key role in cytoprotective as well as antioxidant processes via the elimination of ROS for suppressing cellular death/damage [42, 43]. Findings of this study indicated that induction of HO-1 and Nrf2 mediated by KRL could lead to the curtailment of ROS by lowering the levels of oxidative stress within HUVECs cells. At the same time, this study entailed the use of NAC, which is a popular ROS scavenger, for treating HUVECs in the form of positive control. In turn, this significantly lowered overproduction of ROS induced by B[a]P; the extent of which was similar to that of treatment using KRL.

Apoptosis is predicated on the balance between anti and proapoptotic proteins. In this context, Bcl-2 family proteins

regulate apoptosis in the capacity of inhibitors (Bcl-2) or inducers (Bax). The exposure of HUVECs to B[a]P in this study for 24 hours was denoted by a higher rise of Bax/Bcl-2 ratio, thus indicating apoptosis induction. Enhanced apoptosis disrupts function of endothelial cell and atherosclerosis's progression, and possibly increases the instability associated with atherosclerotic plaques. Moreover, this study also revealed that KRL decreased the aforementioned ratio to possibly attenuate the endothelial cell's apoptotic death induced by B[a]P. Consistent with our results, another study had revealed that male sperm cells' death was caused by B[a]P exposure, more particularly by getting the Bax/Bcl-2 signaling activated. Another observation of that study was that this phenomenon is linked to abnormal stress (mediated by ROS) and inflammation [44]. In addition to getting the Bax/Bcl-2 ratio's dysregulation attenuated, the extracts of KRL are also likely to prevent myocardial cells' apoptotic death among animals that have reached an advanced age [45]. KRL's cytoprotective impact is linked to enhanced activity of antioxidants and lower oxidative stress. Therefore, inference of these findings is that KRL possibly prevents apoptosis (B[a]P-induced) via enhanced status of antioxidants.

5. Conclusion

In conclusions, this is the first study demonstrating that pretreatment with KRL could alleviate B[a]P-induced oxidative stress in human umbilical vein endothelial cells by improving the antioxidant capacity and activating the Nrf2 signaling via the PI3/AKT pathway.

Data Availability

The data that support the findings of this study are available from the corresponding author upon reasonable request.

Conflicts of Interest

There is no financial conflict of interest in this research work.

Acknowledgments

References

[1] S.-C. Jee, M. Kim, K. S. Kim, H.-S. Kim, and J.-S. Sung, "Protective effects of myricetin on benzo [a] pyrene-induced 8-hydroxy-2′-deoxyguanosine and BPDE-DNA adduct," *Antioxidants*, vol. 9, no. 5, p. 446, 2020.

[2] P. Rajendran, G. Ekambaram, and D. Sakthisekaran, "Effect of mangiferin on benzo (a) pyrene induced lung carcinogenesis in experimental Swiss albino mice," *Natural Product Research*, vol. 22, no. 8, pp. 672–680, 2008.

[3] T. Rengarajan, P. Rajendran, N. Nandakumar, B. Lokeshkumar, P. Rajendran, and I. Nishigaki, "Exposure to polycyclic aromatic hydrocarbons with special focus on can-

cer," *Asian Pacific Journal of Tropical Biomedicine*, vol. 5, no. 3, pp. 182–189, 2015.

[4] P. Rajendran, T. Rengarajan, J. Thangavel et al., "The vascular endothelium and human diseases," *International Journal of Biological Sciences*, vol. 9, no. 10, pp. 1057–1069, 2013.

[5] X. Kong, Q. Liu, M. Zheng, J. Liu, C. Zhang, and H. Wang, "Structural characterization of Ginkgo biloba L. leaves cyclopeptides and anti-inflammatory potency evaluation in human umbilical vein endothelial cells," *Phytochemistry Letters*, vol. 39, pp. 12–18, 2020.

[6] W. Li, J. Hu, O. Adebali et al., "Human genome-wide repair map of DNA damage caused by the cigarette smoke carcinogen benzo [a] pyrene," *Proceedings of the National Academy of Sciences*, vol. 114, pp. 201706021–201706757, 2017.

[7] P. Rajendran, G. Ekambaram, and D. Sakthisekaran, "Protective role of mangiferin against benzo (a) pyrene induced lung carcinogenesis in experimental animals," *Biological and Pharmaceutical Bulletin*, vol. 31, no. 6, pp. 1053–1058, 2008.

[8] I. Tabas and Y. Wang, "Emerging roles of mitochondria ROS in atherosclerotic lesions: causation or association?," *Journal of Atherosclerosis and Thrombosis*, vol. 21, no. 5, pp. 381–390, 2014.

[9] X. Wu, H. Zhang, W. Qi et al., "Nicotine promotes atherosclerosis via ROS-NLRP3-mediated endothelial cell pyroptosis," *Cell Death & Disease*, vol. 9, no. 2, pp. 1–12, 2018.

[10] N. C. Chandra, "Atherosclerosis and carcinoma: two facets of dysfunctional cholesterol homeostasis," *Journal of Biochemical and Molecular Toxicology*, vol. 34, no. 12, article e22595, 2020.

[11] K. Zhu, Q. Meng, Z. Zhang et al., "Aryl hydrocarbon receptor pathway: role, regulation and intervention in atherosclerosis therapy (review)," *Molecular Medicine Reports*, vol. 20, no. 6, pp. 4763–4773, 2019.

[12] D. M. Curfs, E. Lutgens, M. J. Gijbels, M. M. Kockx, M. J. Daemen, and F. J. van Schooten, "Chronic exposure to the carcinogenic compound benzo [a] pyrene induces larger and phenotypically different atherosclerotic plaques in ApoE-knockout mice," *The American Journal of Pathology*, vol. 164, no. 1, pp. 101–108, 2004.

[13] K. Ji, C. Xing, F. Jiang et al., "Benzo [a] pyrene induces oxidative stress and endothelial progenitor cell dysfunction via the activation of the NF-κB pathway," *International Journal of Molecular Medicine*, vol. 31, no. 4, pp. 922–930, 2013.

[14] P. Rajendran, R. B. Ammar, F. J. Al-Saeedi et al., "Kaempferol inhibits zearalenone-induced oxidative stress and apoptosis via the PI3K/Akt-mediated Nrf2 signaling pathway: in vitro and in vivo studies," *International Journal of Molecular Sciences*, vol. 22, no. 1, p. 217, 2021.

[15] A. R. Timme-Laragy, L. A. Van Tiem, E. A. Linney, and R. T. Di Giulio, "Antioxidant responses and NRF2 in synergistic developmental toxicity of PAHs in zebrafish," *Toxicological Sciences*, vol. 109, no. 2, pp. 217–227, 2009.

[16] S. Wittkopp, N. Staimer, T. Tjoa et al., "Nrf2-related gene expression and exposure to traffic-related air pollution in elderly subjects with cardiovascular disease: an exploratory panel study," *Journal of Exposure Science & Environmental Epidemiology*, vol. 26, no. 2, pp. 141–149, 2016.

[17] X. Ding, L. Zheng, B. Yang, X. Wang, and Y. Ying, "Luteolin attenuates atherosclerosis via modulating signal transducer and activator of transcription 3-mediated inflammatory response," *Drug Design, Development and Therapy*, vol. -Volume 13, pp. 3899–3911, 2019.

[18] W.-J. Fu, T. Lei, Z. Yin et al., "Anti-atherosclerosis and cardio-protective effects of the Angong Niuhuang pill on a high fat and vitamin D3 induced rodent model of atherosclerosis," *Journal of Ethnopharmacology*, vol. 195, pp. 118–126, 2017.

[19] Q. Zhou, X. Han, R. Li et al., "Anti-atherosclerosis of oligomeric proanthocyanidins from Rhodiola rosea on rat model via hypolipemic, antioxidant, anti-inflammatory activities together with regulation of endothelial function," *Phytomedicine*, vol. 51, pp. 171–180, 2018.

[20] Q. Yu, J. Wu, Q. Li et al., "Kirenol inhibit the function and inflammation of fibro-blast-like synoviocytes in rheumatoid arthritis in vitro and in vivo," *Frontiers in Immunology*, vol. 10, p. 1304, 2019.

[21] Y. Lu, J. Xiao, Z.-W. Wu et al., "Kirenol exerts a potent anti-arthritic effect in collagen-induced arthritis by modifying the T cells balance," *Phytomedicine*, vol. 19, no. 10, pp. 882–889, 2012.

[22] J. Wu, Y. Qu, J.-x. Deng et al., "Molecular docking studies of kirenol a traditional Chinese medicinal compound against rheumatoid arthritis cytokine drug targets (TNF-?, IL-1 and IL-6)," *Biomedical Research*, vol. 28, no. 5, pp. 1992–1995, 2017.

[23] J. Xiao, R. Yang, L. Yang, X. Fan, W. Liu, and W. Deng, "Kirenol attenuates experimental autoimmune encephalomyelitis by inhibiting differentiation of Th1 and th17 cells and inducing apoptosis of effector T cells," *Scientific Reports*, vol. 5, no. 1, p. 9022, 2015.

[24] B. Wu, X. Y. Huang, L. Li et al., "Attenuation of diabetic cardiomyopathy by relying on kirenol to suppress inflammation in a diabetic rat model," *Journal of Cellular and Molecular Medicine*, vol. 23, no. 11, pp. 7651–7663, 2019.

[25] F. Zheng, C. Yue, G. Li et al., "Nuclear AURKA acquires kinase-independent transactivating function to enhance breast cancer stem cell phenotype," *Nature Communications*, vol. 7, no. 1, pp. 1–17, 2016.

[26] Y.-P. Chen, K. Sivalingam, M. A. Shibu et al., "Protective effect of fisetin against angiotensin II-induced apoptosis by activation of IGF-IR-PI3K-Akt signaling in H9c2 cells and spontaneous hypertension rats," *Phytomedicine*, vol. 57, pp. 1–8, 2019.

[27] W. Yang, G. Zhang, F. Jiang et al., "BPDE and B[_a_]P induce mitochondrial compromise by ROS-mediated suppression of the SIRT1/TERT/PGC-1α pathway in spermatogenic cells both in vitro and in vivo," *Toxicology and Applied Pharmacology*, vol. 376, pp. 17–37, 2019.

[28] B. Rubin, J. Manso, H. Monticelli et al., "Crude extract ofOriganum vulgareL. induced cell death and suppressed MAPK and PI3/Akt signaling pathways in SW13 and H295R cell lines," *Natural Product Research*, vol. 33, no. 11, pp. 1646–1649, 2019.

[29] M.-H. Tsai, J.-F. Liu, Y.-C. Chiang et al., "Artocarpin, an isoprenyl flavonoid, induces p53-dependent or independent apoptosis via ROS-mediated MAPKs and Akt activation in non-small cell lung cancer cells," *Oncotarget*, vol. 8, no. 17, pp. 28342–28358, 2017.

[30] Q. Zhang, D. Maddock, J. Chen et al., "Cytokine-induced p38 activation feedback regulates the prolonged activation of AKT cell survival pathway initiated by reactive oxygen species in response to UV irradiation in human keratinocytes," *International Journal of Oncology*, vol. 19, no. 5, pp. 1057–1061, 2001.

[31] Y.-C. Hseu, C.-W. Chou, K. S. Kumar et al., "Ellagic acid protects human keratinocyte (HaCaT) cells against UVA-induced oxidative stress and apoptosis through the upregulation of the HO-1 and Nrf-2 antioxidant genes," *Food and Chemical Toxicology*, vol. 50, no. 5, pp. 1245–1255, 2012.

[32] P. Bhatia and N. Singh, "Tadalafil ameliorates memory deficits, oxidative stress, endothelial dysfunction and neuropathological changes in rat model of hyperhomocysteinemia induced vascular dementia," *International Journal of Neuroscience*, pp. 1–13, 2020.

[33] P. Scicchitano, F. Cortese, M. Gesualdo et al., "The role of endothelial dysfunction and oxidative stress in cerebrovascular diseases," *Free Radical Research*, vol. 53, no. 6, pp. 579–595, 2019.

[34] M. H. Talukder, W. M. Johnson, S. Varadharaj et al., "Chronic cigarette smoking causes hypertension, increased oxidative stress, impaired NO bioavailability, endothelial dysfunction, and cardiac remodeling in mice," *American Journal of Physiology. Heart and Circulatory Physiology*, vol. 300, no. 1, pp. H388–H396, 2011.

[35] Y. Li, X. Zou, K. Cao et al., "Curcumin analog 1, 5-bis (2-trifluoromethylphenyl)-1, 4-pentadien-3-one exhibits enhanced ability on Nrf2 activation and protection against acrolein-induced ARPE-19 cell toxicity," *Toxicology and Applied Pharmacology*, vol. 272, no. 3, pp. 726–735, 2013.

[36] Y. Yang, W. Duan, Z. Liang et al., "Curcumin attenuates endothelial cell oxidative stress injury through Notch signaling inhibition," *Cellular Signalling*, vol. 25, no. 3, pp. 615–629, 2013.

[37] M. A. Shibu, C. H. Kuo, B.-C. Chen et al., "Oolong tea prevents cardiomyocyte loss against hypoxia by attenuating p-JNK mediated hypertrophy and enhancing P-IGF1R, p-akt, and p-Badser136 activity and by fortifying NRF2 antioxidation system," *Environmental Toxicology*, vol. 33, no. 2, pp. 220–233, 2018.

[38] Y.-C. Hseu, H.-W. Lo, M. Korivi, Y.-C. Tsai, M.-J. Tang, and H.-L. Yang, "Dermato-protective properties of ergothioneine through induction of Nrf2/ARE-mediated antioxidant genes in UVA-irradiated human keratinocytes," *Free Radical Biology and Medicine*, vol. 86, pp. 102–117, 2015.

[39] B. K. Ooi, B. H. Goh, and W. H. Yap, "Oxidative stress in cardiovascular diseases: involvement of Nrf2 antioxidant redox signaling in macrophage foam cells formation," *International Journal of Molecular Sciences*, vol. 18, no. 11, p. 2336, 2017.

[40] A. Yadav, A. Sunkaria, N. Singhal, and R. Sandhir, "Resveratrol loaded solid lipid nanoparticles attenuate mitochondrial oxidative stress in vascular dementia by activating Nrf2/HO-1 pathway," *Neurochemistry International*, vol. 112, pp. 239–254, 2018.

[41] X. N. Li, L. Y. Ma, H. Ji, Y. H. Qin, S. S. Jin, and L. X. Xu, "Resveratrol protects against oxidative stress by activating the Keap-1/Nrf2 antioxidant defense system in obese-asthmatic rats," *Experimental and Therapeutic Medicine*, vol. 16, no. 6, pp. 4339–4348, 2018.

[42] M. J. Alcaraz and M. L. Ferrándiz, "Relevance of Nrf2 and heme oxygenase-1 in articular diseases," *Free Radical Biology and Medicine*, vol. 157, pp. 83–93, 2020.

[43] A. Loboda, M. Damulewicz, E. Pyza, A. Jozkowicz, and J. Dulak, "Role of Nrf2/HO-1 system in development, oxidative stress response and diseases: an evolutionarily conserved mechanism," *Cellular and Molecular Life Sciences*, vol. 73, no. 17, pp. 3221–3247, 2016.

[44] B. Banerjee, S. Chakraborty, D. Ghosh, S. Raha, P. C. Sen, and K. Jana, "Benzo (a) pyrene induced p53 mediated male germ cell apoptosis: synergistic protective effects of curcumin and resveratrol," *Frontiers in Pharmacology*, vol. 7, p. 245, 2016.

[45] S.-Y. Ke, D.-H. Liu, L. Wu et al., "Ginsenoside Rb1 ameliorates age-related myocardial dysfunction by regulating the NF-κB signaling pathway," *The American Journal of Chinese Medicine*, vol. 48, no. 6, pp. 1369–1383, 2020.

Research Article

Plasma Small Extracellular Vesicle-Carried miRNA-501-5p Promotes Vascular Smooth Muscle Cell Phenotypic Modulation-Mediated In-Stent Restenosis

Xiao-Fei Gao,[1,2] Zhi-Mei Wang,[1] Ai-Qun Chen,[1] Feng Wang,[1] Shuai Luo,[1] Yue Gu,[1] Xiang-Quan Kong,[1] Guang-Feng Zuo,[1] Xiao-Min Jiang,[1] Guan-Wen Ding,[3] Yan Chen,[4] Zhen Ge,[1] Jun-Jie Zhang ⓘ,[1,2] and Shao-Liang Chen ⓘ[1,2]

[1]*Department of Cardiology, Nanjing First Hospital, Nanjing Medical University, Nanjing, China*
[2]*Department of Cardiology, Nanjing Heart Centre, Nanjing, China*
[3]*Nanjing Foreign Language School, Nanjing, China*
[4]*Department of Neurology, Affiliated Drum Tower Hospital of Nanjing University, Medical School, Nanjing, China*

Correspondence should be addressed to Jun-Jie Zhang; jameszll@163.com and Shao-Liang Chen; chmengx@126.com

Vascular smooth muscle cell (VSMC) phenotypic modulation plays an important role in the occurrence and development of in-stent restenosis (ISR), the underlying mechanism of which remains a key issue needing to be urgently addressed. This study is designed to investigate the role of plasma small extracellular vesicles (sEV) in VSMC phenotypic modulation. sEV were isolated from the plasma of patients with ISR (ISR-sEV) or not (Ctl-sEV) 1 year after coronary stent implantation using differential ultracentrifugation. Plasma sEV in ISR patients are elevated markedly and decrease the expression of VSMC contractile markers α-SMA and calponin and increase VSMC proliferation. miRNA sequencing and qRT-PCR validation identified that miRNA-501-5p was the highest expressed miRNA in the plasma ISR-sEV compared with Ctl-sEV. Then, we found that sEV-carried miRNA-501-5p level was significantly higher in ISR patients, and the level of plasma sEV-carried miRNA-501-5p linearly correlated with the degree of restenosis ($R^2 = 0.62$). Moreover, miRNA-501-5p inhibition significantly increased the expression of VSMC contractile markers α-SMA and calponin and suppressed VSMC proliferation and migration; in vivo inhibition of miRNA-501-5p could also blunt carotid artery balloon injury induced VSMC phenotypic modulation in rats. Mechanically, miRNA-501-5p promoted plasma sEV-induced VSMC proliferation by targeting Smad3. Notably, endothelial cells might be the major origins of miRNA-501-5p. Collectively, these findings showed that plasma sEV-carried miRNA-501-5p promotes VSMC phenotypic modulation-mediated ISR through targeting Smad3.

1. Introduction

Percutaneous coronary intervention with stent implantation has been an extremely important treatment for patients with coronary artery disease, but it is also blamed for 5%-10% risk of in-stent restenosis (ISR) [1–3], despite drug-eluting stents (DES) are widely used nowadays. The currently accepted causes of ISR are excessive vascular smooth muscle cells (VSMC) hyperplasia and extracellular matrix (ECM) deposition. Responding to vessel injury and local environmental alternations after stent implantation, contractile (also called

mature or differentiated) VSMC for hemodynamic regulation can be switched to a synthetic/dedifferentiated phenotype to increase proliferation, migration, and ECM synthesis for tissue reparation or abnormal vessel narrowing [4, 5]. This process of VSMC phenotypic modulation has been studied for decades, but we still do not fully understand the mechanisms well enough to be able to prevent or treat ISR successfully.

miRNAs, a class of short single-stranded RNAs, have been demonstrated to play an important role in VSMC phenotypic modulation, such as miR-143/145 cluster [6] and

miR-22 [7] driving VSMC towards the contractile phenotype. Other miRNAs, such as miR-21 [8] and miR-221/222 [9], could drive VSMC towards the synthetic phenotype. Notably, these miRNAs are mainly transported to target cells through small extracellular vesicles (sEV), which can protect the internal miRNAs from being degraded in the circulation and participate in cell-to-cell communication [10–12]. However, there is still a lack of definitive evidence regarding the effects of circulating sEV-carried miRNA in ISR patients. Accordingly, the present study is designed to address the functional effects and underlying mechanisms of plasma sEV-carried miRNA in VSMC phenotypic modulation-mediated ISR.

2. Methods

2.1. Experimental Animals. Male Sprague-Dawley rats (8 weeks) were obtained from Animal Core Facility of Nanjing Medical University (Nanjing, China). All animal protocols and procedures were performed according to the Guide for the Care and Use of Laboratory Animal published by the US National Institutes of Health (2011) and approved by the Experimental Animal Care and Use Committee of Nanjing Medical University. Rats were housed in a temperature-controlled room with a 12 h light/dark cycle and free access to water and food.

2.2. Rat Carotid Artery Balloon Injury Model. The method of rat carotid artery balloon injury (CABI) model has been reported previously [13]. Briefly, 8-week rats were anesthetized with pentobarbital sodium (60 mg/kg, i.p.) and subjected to insertion of Fogarty balloon catheter (2F, Edwards Lifesciences) into the right external carotid artery between the common carotid artery bifurcation and the distal ligation site. In the sham group, the right carotid artery was exposed but not subjected to the insertion of Fogarty balloon. At 28 days after procedure, the rats were sacrificed with an overdose of pentobarbital sodium (200 mg/kg, iv), and their venous blood and carotid arteries were subsequently collected for further study.

2.3. Patients. The method and results of ULTIMATE trial have been reported previously [14, 15]. This trial was performed in accordance with Declaration of Helsinki and International conference, and the protocol was approved by the ethics committee of each participating center. All participants have signed written informed consent. Two groups of subjects from ULTIMATE trial were enrolled in this study, including 20 patients with ISR and 20 patients without ISR after DES implantation. ISR patients are defined as those who had an angiographic minimal lumen diameter (MLD) stenosis ≥ 50% of a stented segment or within 5 mm of a stent edge [1]. Moreover, late lumen loss, reflecting the degree of restenosis, is defined as the difference between poststenting MLD minus MLD at the time of angiographic follow-up. All analyses were performed by two investigators who were blinded to the group information.

2.4. Plasma Small sEV Isolation. Venous blood samples were drawn from rats and patients into EDTA-containing vacutainers (BD biosciences, USA). The plasma was obtained by centrifuging at $1600 \times g$ for 20 minutes at 4°C and subsequently stored at -80°C for further experiments. Plasma sEV were purified using differential ultracentrifugation according to the guideline [16]. Briefly, plasma was centrifuged at $10,000 \times g$ for 30 minutes at 4°C to remove cells and debris, then twice at $100,000 \times g$ for 1 hour at 4°C with a SW-41 rotor (Beckman Coulter, USA). The pellets were washed with phosphate buffered saline (PBS) and centrifuged again at $100,000 \times g$ for 1 hour at 4°C to purify the sEV. The isolated plasma sEV were collected and resuspended in 1x PBS for subsequent analysis.

2.5. Plasma sEV Identification. After isolation, the morphology of plasma sEV was assessed by transmission electron microscope (TEM, FEI Tecnai G2 spirit). Briefly, $20 \mu L$ of sEV suspension was placed on a carbon-coated 200-mesh copper grid for 5 minutes at room temperature and stained with 2% phosphotungstic acid for one minute. Then, the samples were dried for 10 minutes and visualized with TEM at 80 kV. The concentration and size of plasma sEV were analyzed by nanoparticle tracking analysis (NTA) using ZetaView particle tracker (Particle Metrix, Germany). Moreover, protein markers of sEV, such as CD63 (1:1000, ab68418, Abcam) and TSG101 (1:1000, ab125011, Abcam), were identified by western blots (WB).

2.6. Cell Culture. Primary human aortic smooth muscle cells (HASMC) were obtained from American Type Culture Collection (ATCC, PCS-100-012). HASMCs were cultured in Smooth Muscle Cell Growth Basal Medium (ScienCell, 1101) with 2% fetal bovine serum (FBS) at 37°C with 95% humid air and 5% CO_2. After growing to 70%-80% confluence, cells were washed with PBS and then maintained in Smooth Muscle Cell Growth Basal Medium with 10% exosome-depleted FBS (Gibco, USA) and subsequently incubated with plasma sEV for 24 hours.

2.7. sEV Labeling and Uptake. Plasma sEV were labeled with PKH26 Red Fluorescent Cell Linker Kit (Sigma-Aldrich, USA) in accordance with the manufacturer's protocol. Briefly, $100 \mu L$ of sEV was added to $150 \mu L$ of Diluent C, which were incubated with PKH26 dye ($1 \mu L$) Diluent C ($250 \mu L$) solution for 4 minutes at room temperature. To terminate the labeling reaction, $500 \mu L$ of 1% Bull Serum Albumin (BSA) was added. The labeled sEV were isolated using differential ultracentrifugation as described above to eliminate the excess dye and resuspended in $100 \mu L$ of 1x PBS, which were subsequently incubated with HASMC on 24-well plates at 37°C for 6 hours. Then, the images were visualized by confocal microscopy (ZEISS, German).

2.8. Concentration of Plasma sEV. BCA Protein Assay Kit (Thermo Scientific, USA) was used to measure the protein concentration in plasma sEV according to the manufacturer's instructions, which has been considered as an index of the number of sEV. The final concentration of plasma sEV was $30 \mu g/mL$ in the cell growth medium in vitro, while $20 \mu g$ sEV in $100 \mu L$ PBS were intravenously injected weekly in vivo.

2.9. miRNA Microarray Assay. miRNA microarray was performed by a commercial service (Shanghai OE Biotech Co., Ltd, China). Briefly, total RNAs were extracted from sEV isolated from 2 mL of plasma from ISR patients and control patients. The extracted RNA was labeled and hybridized to an Agilent Human miRNA Microarray Kit (Release 21.0, 8 × 60K), and this microarray contains 2570 probes for mature miRNA. Then, differentially expressed miRNAs between these two groups were screened out using cluster analysis.

2.10. Western Blots. Smooth muscle cells and plasma sEV were lysed using RIPA buffer, proteinase inhibitor, and phosphatase inhibitor. Proteins from cultured cells or plasma sEV were quantified with BCA protein assay kits (Beyotime, China). Equal amounts (60 μg) of protein were separated by 10% SDS-PAGE and transferred to PVDF membranes (Millipore, USA), which were then blocked with 5% BSA and incubated overnight at 4°C with individual primary antibodies, followed by incubation with the corresponding secondary antibodies for 2 hours at room temperature. Primary antibodies against CD63 (ab68418), TSG101 (ab125011), α-SMA (ab7817), calponin (ab46794), and Samd3 (ab40854) were purchased from Abcam (Cambridge, UK). Primary antibodies against Smad2 (5339), Smad4 (46535), and GAPDH (5174) were acquired from Cell Signaling Technology (Massachusetts, USA). Bands were analyzed by the ImageJ software, and all analyses were performed by two investigators who were blinded to the group information.

2.11. Quantitative Real-Time-PCR (qRT-PCR). Total RNA was extracted using Trizol reagent (Invitrogen) from sEV, HASMC, and carotid artery according to the standard protocol. For sEV-carried miRNA quantification, cel-miR-39 (5 fmol/μL) was added to the isolated RNAs as an exogenous control. For RNA detection in cells and tissues, U6 was set as an endogenous control. The primer sequences for the real-time PCR (RT-PCR) assays were listed in Supplemental Table 1.

2.12. Luciferase Reporter Assays. For reporter assays, 293T cells were cotransfected with pmiR-RB-Report™ h-Smad3-WT/-MUT and micrON™ has-miR-501-5p mimic/negative control using Lipofectamine-3000 (Invitrogen) according to the manufacturer's instructions. Firefly and Renilla luciferase activities were analyzed after 48 h using the dual luciferase assay system (Promega, USA) following the manufacturer's instructions.

2.13. Cell Transfection of miRNA-501-5p Mimic and Inhibitor. HASMC in 6-well plates were transfected with miR-501-5p mimic (50 nmol/L), miR-501-5p inhibitor (100 nmol/L), or their negative controls (GenePharma, China) using Lipofectamine RNAiMAX (Invitrogen) following the manufacturers' instructions. In the inhibitor experiments, HASMC were transfected with miR-501-5p inhibitor or negative control first, and plasma sEV were added 24 hours later.

2.14. miRNA Antagomir Injection. Rats were intravenously injected with antagomir (100 nmol) and negative controls (GenePharma, China) in 200 μL of saline buffer twice a week after the CABI procedure of rats.

2.15. Cell Proliferation and Migration Assay. HASMC proliferation was assessed using MTT and EdU assay (Thermo Scientific, USA). Cell migration was measured using Wound Healing and Transwell assay with 8 μm pore size inserts (Corning). Every experiment was repeated three times independently by investigators who did not know the group allocation according to the manufacturers' instructions.

2.16. Statistical Analysis. The Shapiro-Wilk normality test was used to assess the distribution of continuous variables. All continuous variables were expressed as mean ± standard error of mean (SEM) and compared using the Student's t-test (two groups) or one-way ANOVA followed by Bonferroni's post hoc test (three or more groups). All statistical tests were two-tailed, and a p value <0.05 was considered statistically significant. All analyses were performed using the GraphPad Prism 8.0.

3. Results

3.1. The Association between Plasma sEV and ISR. Study flowchart was summarized in Supplemental Figure 1. sEV were isolated from the plasma of patients with ISR (ISR-sEV) or not (Ctl-sEV) 1 year after coronary stent implantation using differential ultracentrifugation. TEM images showed rounded particles of both ISR-sEV and Ctl-sEV (Figure 1(a)), and NTA revealed a similar size distribution (118.80 ± 1.96 vs. 113.20 ± 1.02 nm) but a higher plasma concentration (9.27 ± 0.15 vs. 5.40 ± 0.06, $\times 10^{11}$ particles/mL) of ISR-sEV compared with Ctl-sEV (Figure 1(b)). WB analysis confirmed the presence of sEV marker proteins (Figure 1(c)). We then constructed rat carotid artery stenosis by CABI model, and HE staining showed significant VSMC proliferation 28 days after balloon injury (Figure 1(d)). sEV were purified from the plasma of rats with carotid stenosis (RS-sEV) or sham procedure (Sham-sEV). TEM images revealed rounded particles of both RS-sEV and Sham-sEV (Figure 1(e)), and NTA showed a similar size distribution (134.00 ± 1.21 vs. 133.70 ± 1.92 nm, Supplemental Figure 2(a)) but a higher plasma concentration (3.03 ± 0.03 vs 2.37 ± 0.09, $\times 10^{9}$ particles/mL) of RS-sEV than those of Sham-sEV (Figure 1(f)). WB analysis confirmed the presence of sEV marker proteins (Supplemental Figure 2(b)). Taken together, these data showed a relative higher level of plasma sEV in ISR patients and rat carotid artery stenosis.

3.2. Plasma sEV Promoting VSMC Phenotypic Modulation. We incubated HASMC with PKH26-labeled plasma sEV, and confocal images found that sEV were internalized by HASMC after a 6-hour incubation (Figure 2(a) and Supplemental Figure 3). Notably, preincubation with ISR-sEV, but not Ctl-sEV, for 24 hours could decrease the expression of HASMC contractile markers α-SMA and calponin (Figures 2(b) and 2(c)), and increase HASMC proliferation (Figures 2(d) and 2(e)) and migration (Figures 2(f) and 2(g)). Meanwhile, in vivo study showed the reduced mRNA

(a)

(b)

(c)

(d)

(e)

Figure 1: Continued.

(f)
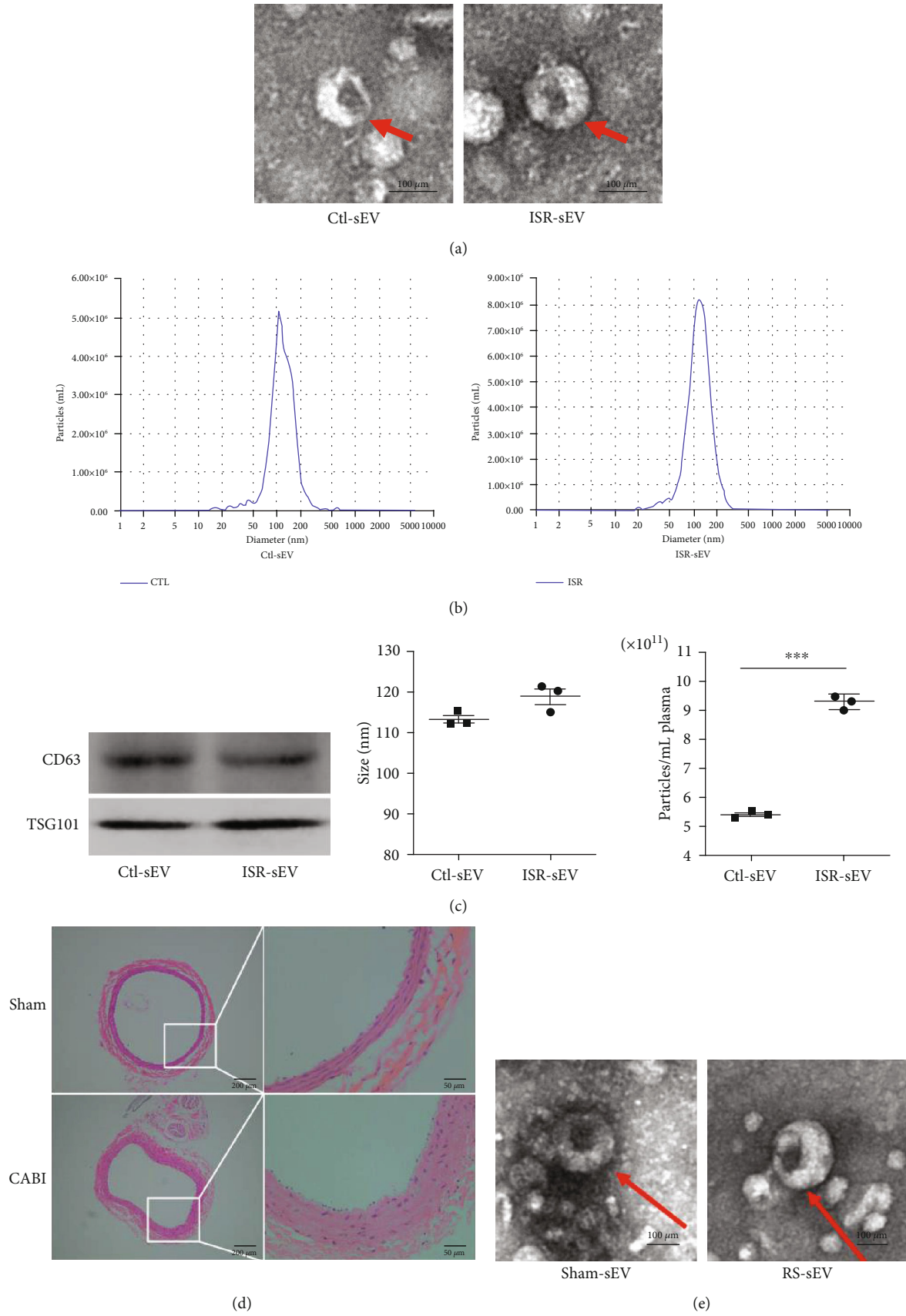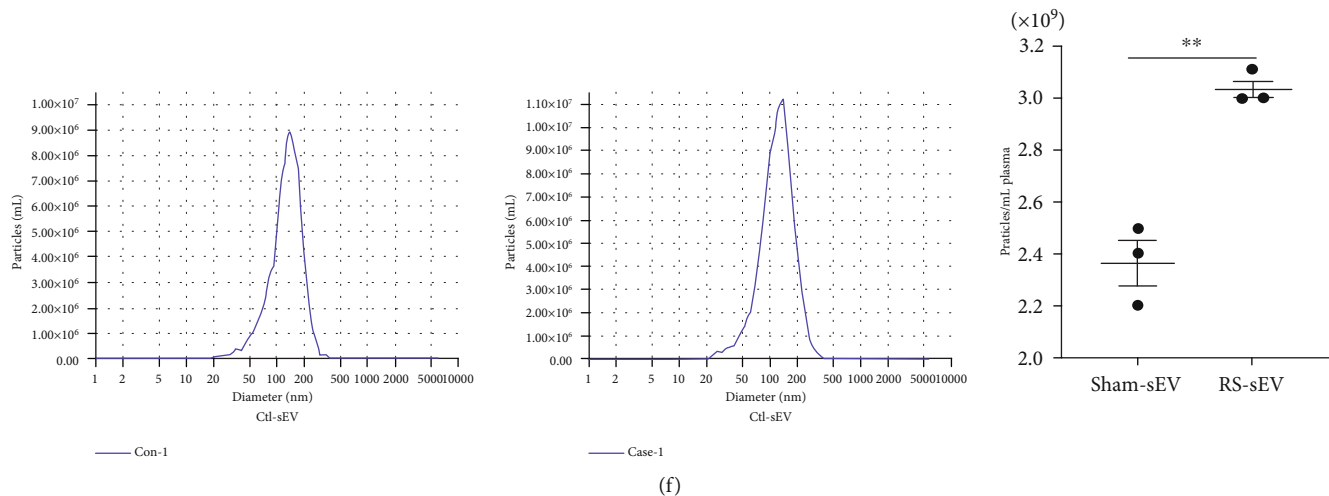
FIGURE 1: Characterization and function of plasma sEV from patients and rats. The isolated small extracellular vesicles (sEV) from patients with in-stent restenosis (ISR) or not (control) were used for the characterization. (a) Representative transmission electron microscopic (TEM) images of sEV. (b) Representative results of nanoparticle tracking analysis (NTA) demonstrating the particle distribution of sEV ($n = 3$). (c) Representative western blots identifying the biomarkers of sEV including CD63 and TSG101 in the same amount of plasma sEV. (d) Representative hematoxylin-eosin stained images of carotid arteries from rat carotid artery balloon injury (CABI) model or sham group ($n = 6$). (e) Representative TEM images of sEV from rats. (f) NTA showing the concentration of sEV ($n = 3$). Values are mean ± SEM. **P < 0.01 and ***P < 0.001. Ctl-sEV: sEV purified from the plasma of patients without ISR after stent implantation; ISR-sEV: sEV purified from the plasma of patients with ISR after stent implantation; Sham-sEV: sEV purified from the plasma of rats with sham procedure; CABI-sEV: sEV purified from the plasma of rats with carrotid artery stenosis after balloon injury.

level of contractile markers (α-SMA and calponin) in rat carotid artery stenosis compared with the sham group (Figure 2(h)). In addition, we found that CABI rats treated with RS-sEV could further decrease the expression of α-SMA and calponin compared with Sham-sEV treatment (Figure 2(i)). Collectively, these results demonstrated that plasma sEV from ISR patients could promote VSMC phenotypic modulation.

3.3. Plasma sEV-Carried miRNA-501-5p and ISR.
We performed Agilent human miRNA microarray assay comparing the differential miRNAs between plasma ISR-sEV and Ctl-sEV to explore the possibility of miRNA resulting in ISR-sEV induced VSMC phenotypic modulation. A total of 15 differential miRNAs (fold change ≥ 2.0; $P < 0.05$) of 2570 miRNAs were detected (Figure 3(a)), and 13 upregulated miRNAs of them were further validated by qRT-PCR. qRT-PCR analysis found that miRNA-501-5p was the highest expressed miRNA in plasma ISR-sEV (Figure 3(b)). To further investigate the relationship of plasma sEV-carried miRNA-501-5p and ISR, 20 patients with ISR and 20 patients without ISR 1 year after stent implantation were enrolled, and the baseline clinical characteristics of them are summarized in Supplemental Table 2. Plasma sEV were purified from these 40 patients using differential ultracentrifugation, and we found that sEV-carried miRNA-501-5p level was significantly higher in ISR patients than that in control patients (Figure 3(c)). Furthermore, the level of plasma sEV-carried miRNA-501-5p linearly correlated with late lumen loss (an indicator of the degree of restenosis, $R^2 =$

0.62, Figure 3(d)). These results suggested that plasma sEV-carried miRNA-501-5p was definitely associated with ISR.

3.4. sEV-Carried miRNA-501-5p Promoting VSMC Phenotypic Modulation.
To evaluate the functional effects of miRNA-501-5p, transfection with miRNA-501-5p mimic for 24 hours could decrease the expression of HASMC contractile markers α-SMA and calponin (Figures 4(a) and 4(b)) and increase HASMC proliferation (Figures 4(c) and 4(d)) and migration (Figures 4(e) and 4(f)). In addition, downregulation of miRNA-501-5p significantly attenuated ISR-sEV-induced HASMC proliferation and migration (Figures 4(g)–4(j) and Supplemental Figure 4-5). To better understand the function of plasma sEV-carried miRNA-501-5p in vivo, we performed qRT-PCR analysis of miRNA-501-5p and its precursor in carotid artery of rats with CABI or RS-sEV treatment. The level of miRNA-501-5p was markedly increased in both CABI rats and RS-sEV-treated rats, but the significant change of pre-miRNA-501-5p level was not found (Figures 5(a) and 5(b)), which indicated that plasma sEV delivered miRNA-501-5p to carotid artery. Furthermore, plasma RS-sEV-treated rats exhibited VSMC proliferation (Figures 5(c) and 5(d) and Supplemental Figure 6) and elevated the media thickness of carotid artery (Figures 5(e) and 5(f)). More importantly, antagomir-501-5p injection could increase the contractile markers α-SMA and calponin (Supplemental Figure 7), reverse the VSMC proliferation (Figures 5(c) and 5(d)), and decrease media thickness as well as the ratio of media thickness/lumen diameter in CABI rats by blocking the miRNA-501-5p (Figures 5(e) and 5(f)). Taken together,

(a)

(b)

(c)

(d)

Figure 2: Continued.

(e)

(f)

(g)

FIGURE 2: Continued.

(h)

(i)
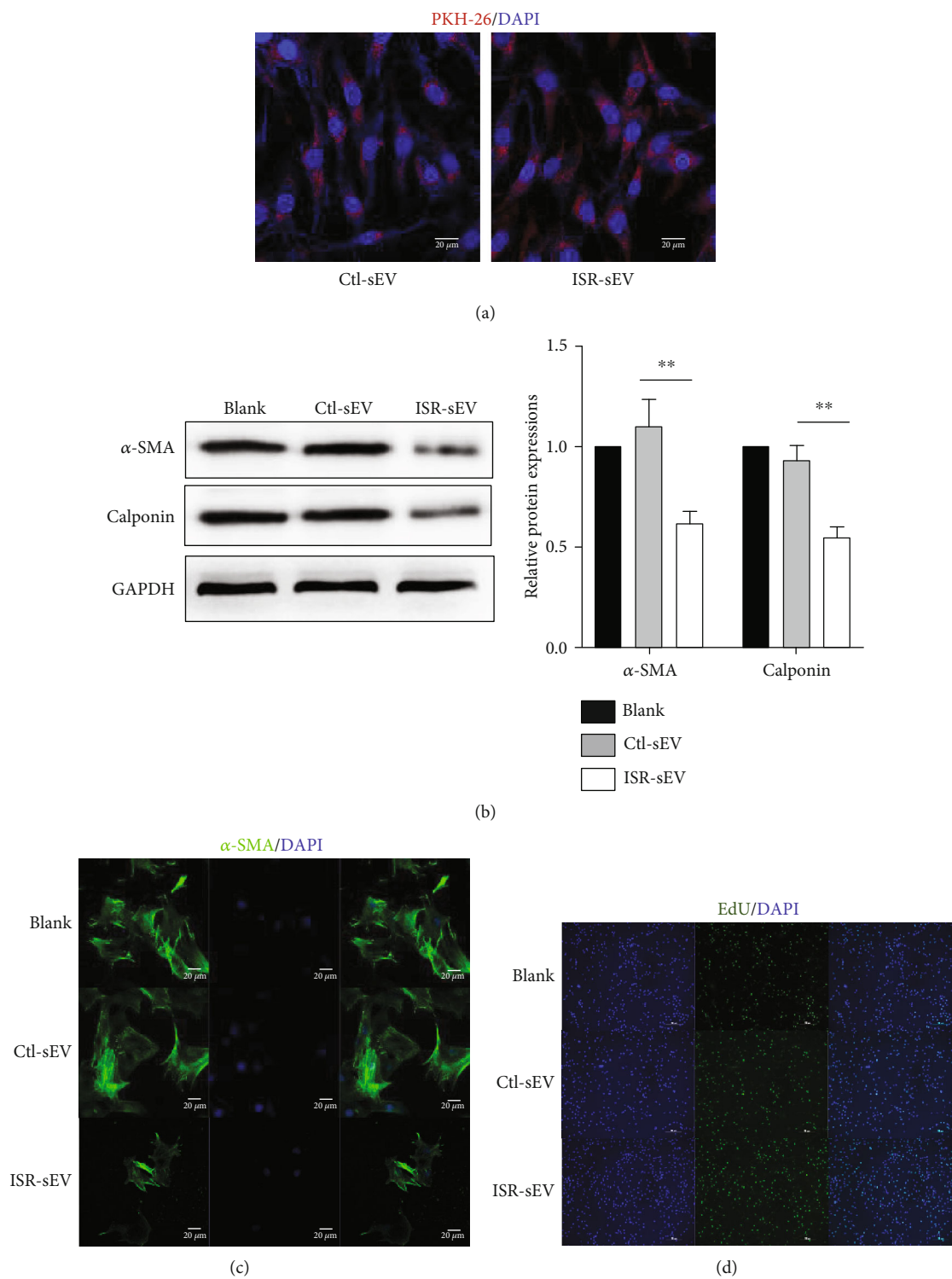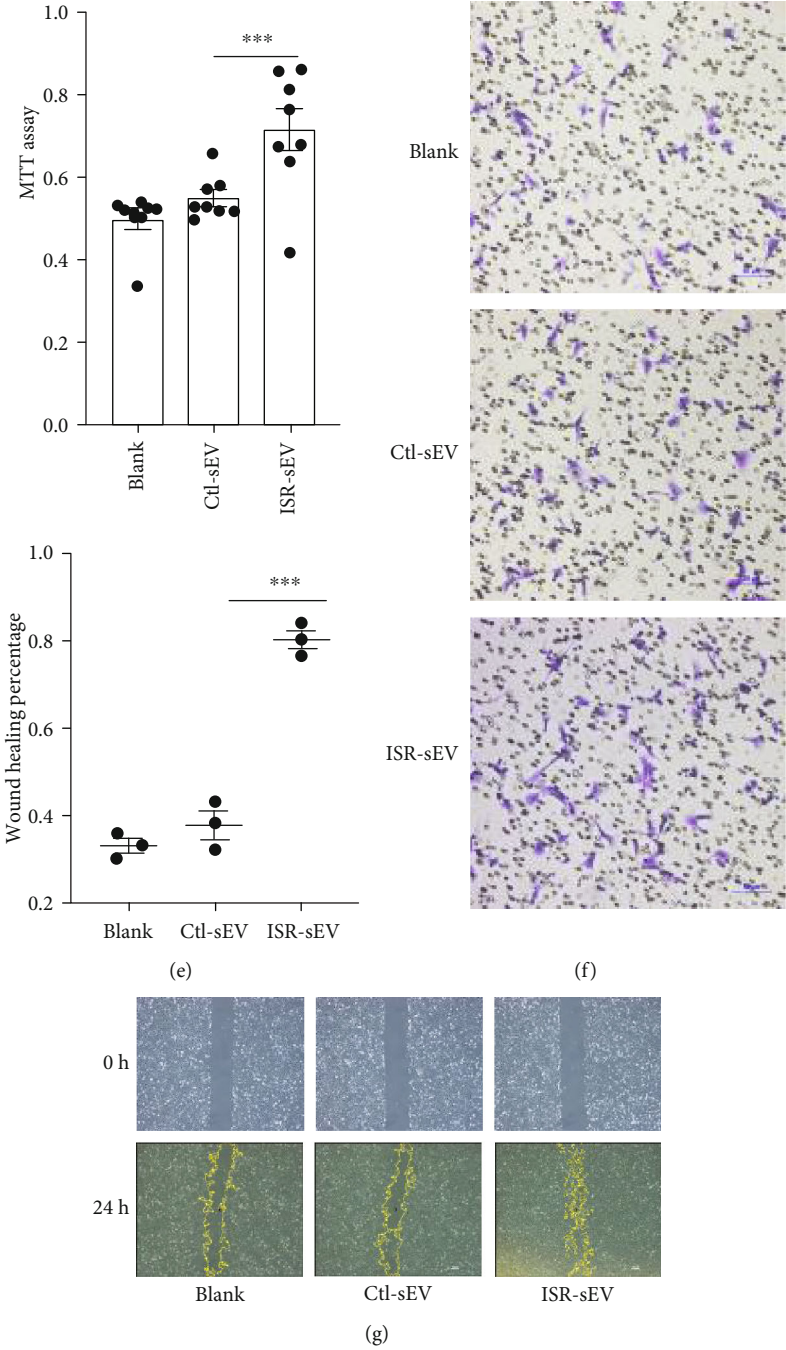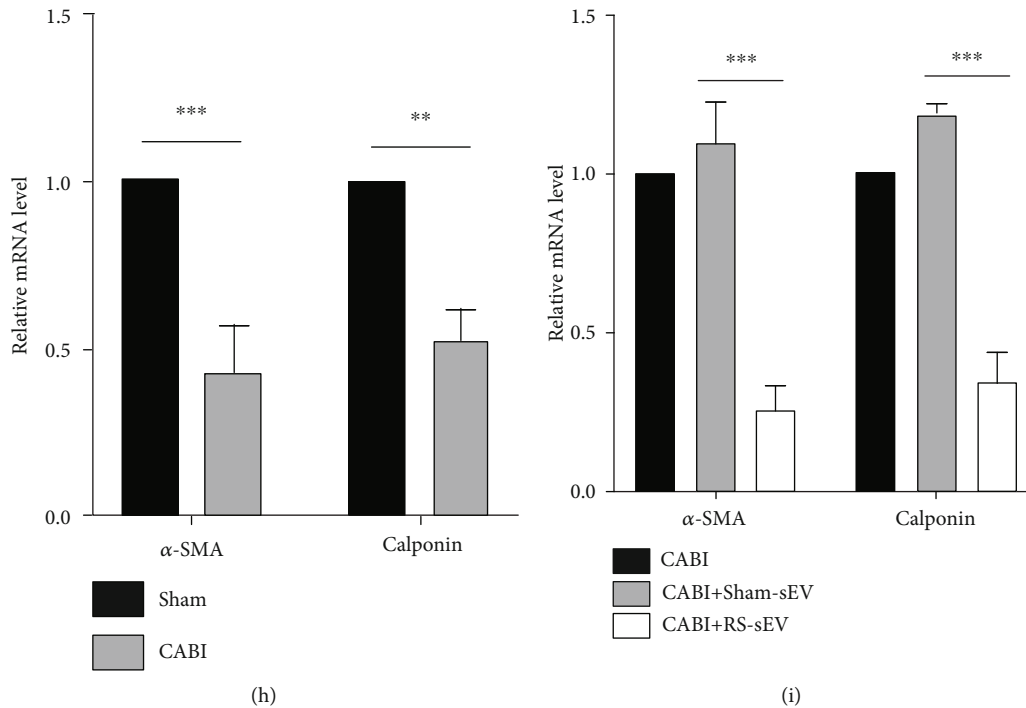
FIGURE 2: The effect of plasma sEV from patients on vascular smooth muscle cells proliferation and migration. (a) Primary human aortic smooth muscle cells (HASMC) were cultured in the presence of PKH26-labeled sEV. Representative confocal images showing the red sEV and the blue nuclei (DAPI) of HASMC. (b) Representative blots and quantified data showing the expression of vascular smooth muscle cell- (VSMC-) specific contractile marker (α-SMA and calponin) in HASMC treated with plasma sEV. (c) Representative confocal images showing immunofluorescent staining for VSMC-specific contractile marker (α-SMA, green) to determine VSMC identity. Nuclei were stained with DAPI (blue). The VSMC proliferation was evaluated with Edu-positive cells (d) and MTT assay (e) in HASMC treated with plasma sEV. The VSMC migration was measured using Transwell (f) and wound healing assay (g) in HASMC treated with plasma sEV. (h) The reduced mRNA expression of VSMC-specific contractile markers (α-SMA and calponin) in CABI group ($n = 6$). Data are normalized to U6. (i) The further reduced mRNA expression of VSMC-specific contractile marker (α-SMA and calponin) in CABI rats treated with sEV ($n = 6$). Values are mean ± SEM. $^{**}P < 0.01$ and $^{***}P < 0.001$.

these results demonstrated that miRNA-501-5p played a crucial role in plasma sEV induced VSMC phenotypic modulation.

3.5. Target Gene of miRNA-501-5p in VSMC.
By using three online databases, including Targetscan, miRwalk, and miRDB, combining with genes involving in VSMC phenotypic modulation reported by previous articles [17–20], we finally focused on Smad3 as a potential target gene of miRNA-501-5p (Figure 6(a)). GO and KEGG analyses of miRNA-501-5p were also conducted (Supplemental Figure 8-9). Next, luciferase reporter assays were performed with plasmids containing wild-type or mutant Smad3 3′ UTR with miRNA-501-5p binding sites (Figure 6(b)). The result showed that miRNA-501-5p could decrease luciferase activity of Smad3 wild-type 3′UTR constructs but had no effect of Smad3 mutated forms (Figure 6(c)). Furthermore, preincubation with miRNA-501-5p mimic markedly inhibited the expression of Smad3 in HASMC (Figure 6(d)). In vivo studies showed decreased mRNA levels of Smad3 in CABI rats (Supplemental Figure 10) and RS-sEV-treated rats (Figure 6(e)) but an elevated level of Smad3 when blocking miRNA-501-5p (Figure 6(f)). Collectively, these results demonstrated that miRNA-501-

5p promoted VSMC phenotypic modulation by targeting Smad3.

3.6. The Potential Origin of Plasma sEV-Carried miRNA-501-5p.
To investigate the potential origins of elevated plasma ISR-sEV-carried miRNA-501-5p, we evaluated the level of miRNA-501-5p and its precursor in the aorta, heart, liver, lung, adipose, and kidney of rats with CABI or not. Both miRNA-501-5p and its precursor markedly elevated only in the aorta and adipose of rats with carotid artery stenosis (Figures 7(a) and 7(b)). Next, the removal of aortic endothelial cells significantly decreased the expression of miRNA-501-5p and its precursor, indicating that endothelial cells might be the major origin of miRNA-501-5p in the aorta (Figure 7(c)). Therefore, we propose that DES implantation increases the production of miRNA-501-5p in multiple tissues, especially in endothelial cells. miRNA-501-5p, cargoed in sEV, is delivered to the VSMC by plasma sEV and promotes VSMC proliferation and migration by targeting Smad3 (Figure 7(d)).

4. Discussion

This study for the first-time reports that plasma sEV-carried miRNA-501-5p promotes VSMC phenotypic modulation-
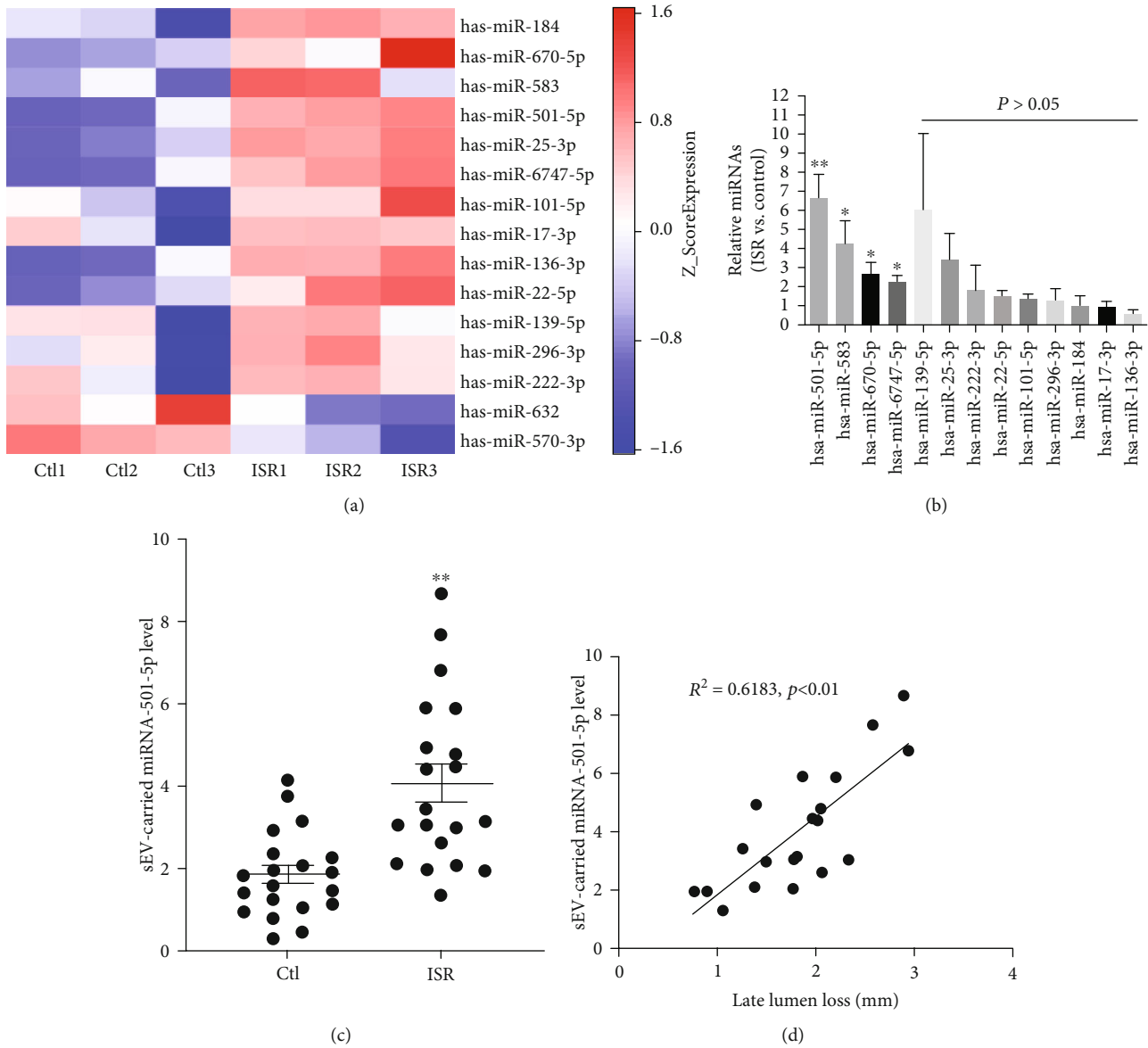
FIGURE 3: miRNA microarray assay and the relationship of miRNA-501-5p and in-stent restenosis. (a) miRNA microarray assays were performed in plasma sEV purified from patients with in-stent restenosis (ISR) or not ($n = 3$). (b) qRT-PCR analysis of the 13 upregulated miRNAs in ISR-sEV and Ctl-sEV ($n = 3$). Data are normalized to cel-miRNA-39. (c) qRT-PCR analysis of plasma sEV-carried miRNA-501-5p level in patients with ISR or not ($n = 20$). Data are normalized to cel-miRNA-39. (d) The relationship between plasma sEV-carried miRNA-501-5p level and late lumen loss (reflecting the degree of restenosis) ($n = 20$). Data are normalized to cel-miRNA-39. $^*P < 0.05$ and $^{**}P < 0.01$.

mediated ISR through targeting Smad3. There are several major findings in the present study. First, the concentration of plasma sEV in ISR patients was higher compared with non-ISR patients. Second, plasma sEV-carried miRNA-501-5p was identified to enhance VSMC proliferation and migration by targeting Smad3, and the level of plasma sEV-carried miRNA-501-5p linearly correlated with the degree of restenosis. Third, vascular endothelial cells might be the major primary origin of plasma sEV miRNA-501-5p. These findings exhibit a novel mechanism of VSMC-mediated ISR by plasma sEV-carried miRNA-501-5p.

In this study, we investigated the mechanism of VSMC phenotypic modulation-mediated ISR. In the DES era, ISR

still remains a therapeutic challenge in spite of the improvements of stent design, novel coating drugs, and polymers. The current opinion [1] is that the underlying mechanisms of ISR are quite complex, at least including mechanical and biologic factors. VSMC is the major cell type in the artery, and fully differentiated/contractile VSMC can maintain the arterial function of contraction/dilation and control normal blood pressure. Differentiated VSMC could switch to a dedifferentiated phenotype to gain the function of proliferation, migration, and ECM synthesis for tissue reparation in response to vessel injury. Imbalanced VSMC switching leads to the excessive VSMC hyperplasia and ECM deposition and ultimately results in artery stenosis. In our study, rats with
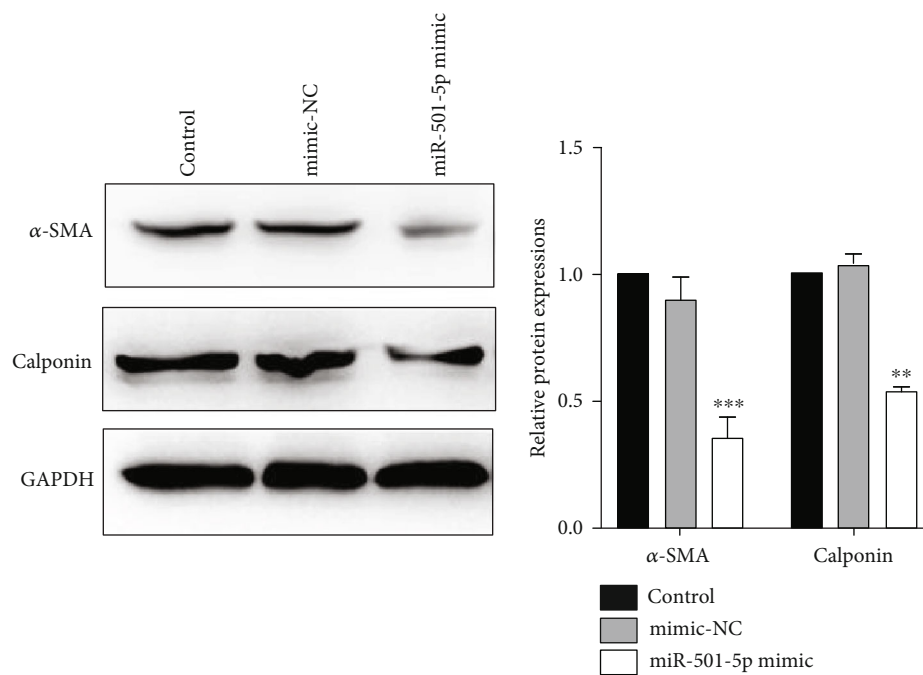
(a)
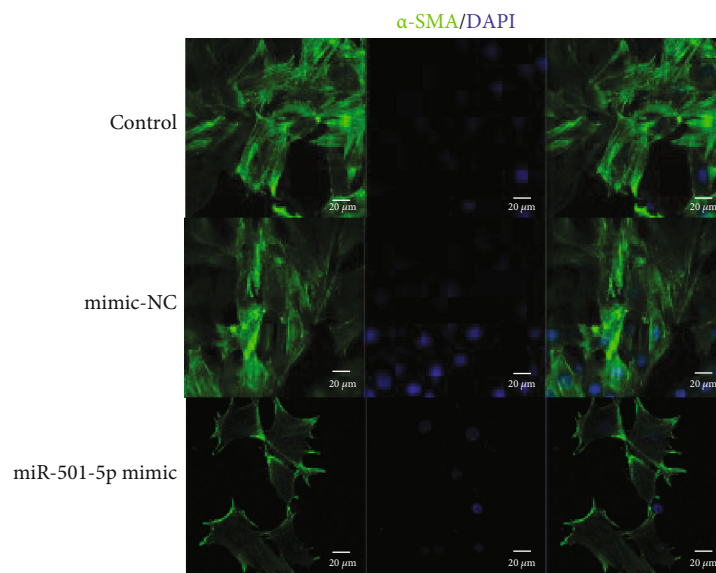
(b)

FIGURE 4: Continued.

(c)

(d)

(e)
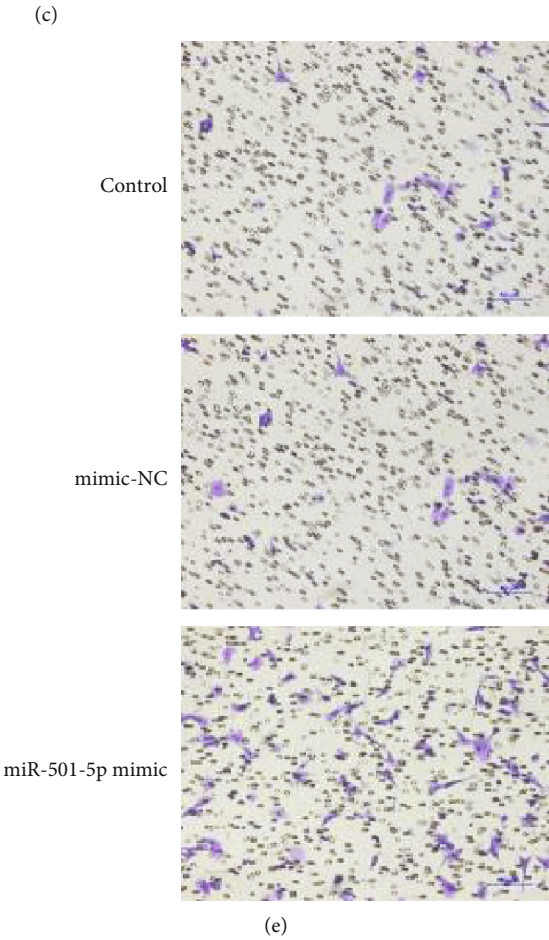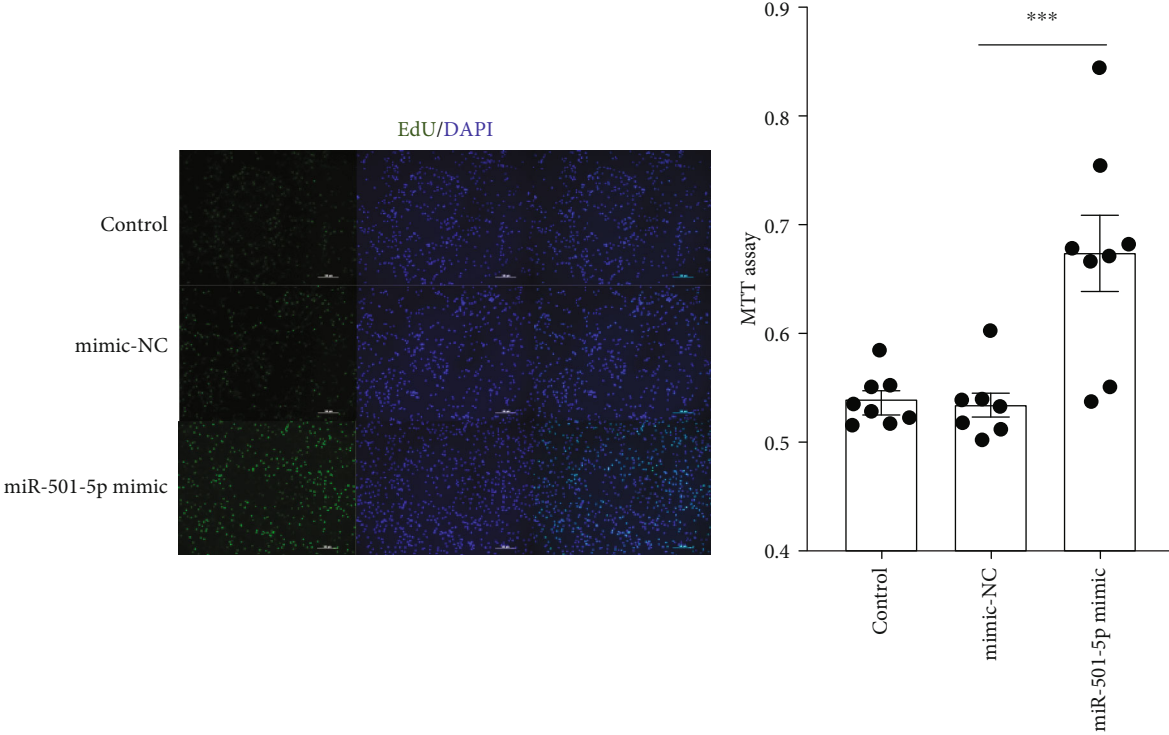
FIGURE 4: Continued.

(f)

(g)

(h)

Figure 4: Continued.

(i)

(j)
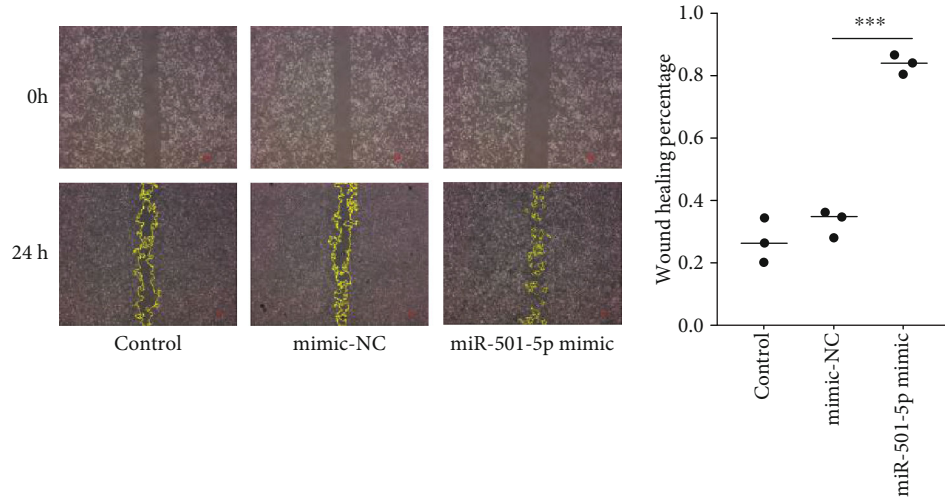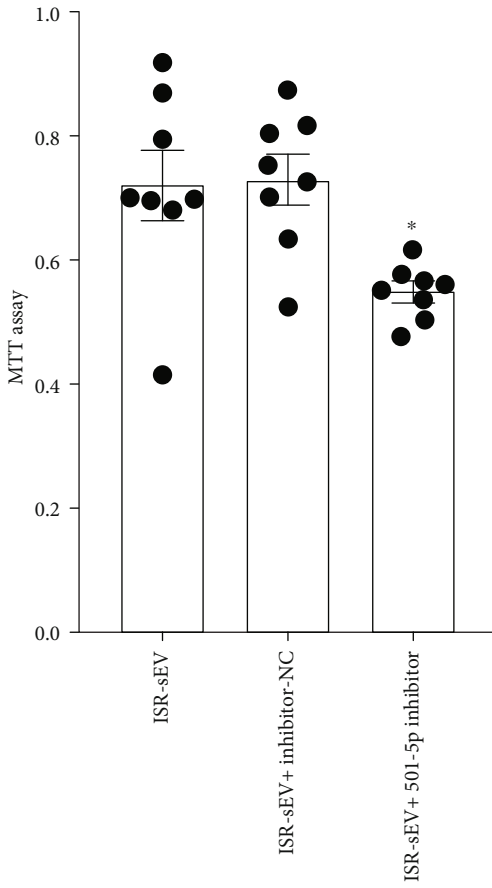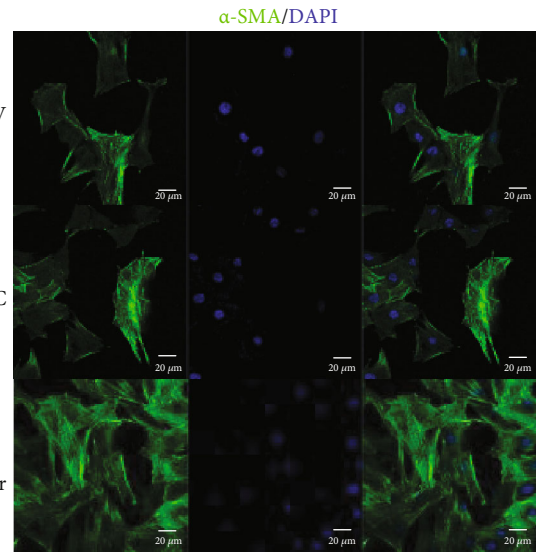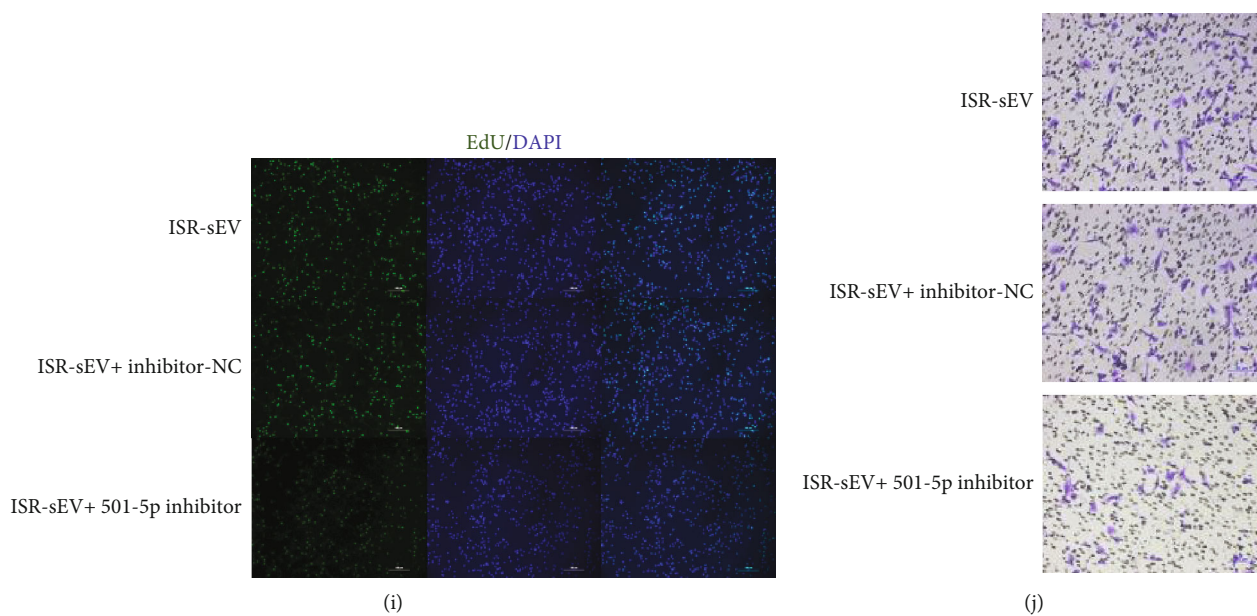
FIGURE 4: The effect of miRNA-501-5p on smooth muscle cell proliferation and migration. (a) Representative blots and quantified data showing the expression of vascular smooth muscle cell- (VSMC-) specific contractile marker (α-SMA and calponin) in primary human aortic smooth muscle cells (HASMC) transfected with miRNA-501-5p mimic. (b) Representative confocal images showing immunofluorescent staining for VSMC-specific contractile marker (α-SMA, green) to determine VSMC identity. Nuclei were stained with DAPI (blue). The VSMC proliferation was evaluated with Edu-positive cells (c) and MTT assay (d) in HASMC transfected with miRNA-501-5p mimic. The VSMC migration was measured using Transwell (e) and wound healing assay (f) in HASMC transfected with miRNA-501-5p mimic. Effects of miRNA-501-5p inhibitor on MTT assay (g), immunofluorescent staining of α-SMA (h), Edu assay (i), and transwell assay (j), in HASMC treated with plasma sEV, then transfected with miRNA-501-5p inhibitor or not. $n = 8$ per group in (d) and (g); $n = 3$ per group in other groups. NC: negative control. Values are mean ± SEM. $^{*}P < 0.05$, $^{**}P < 0.01$, and $^{***}P < 0.001$.

(a)

(b)

FIGURE 5: Continued.

(c)

(d)

(e)

(f)
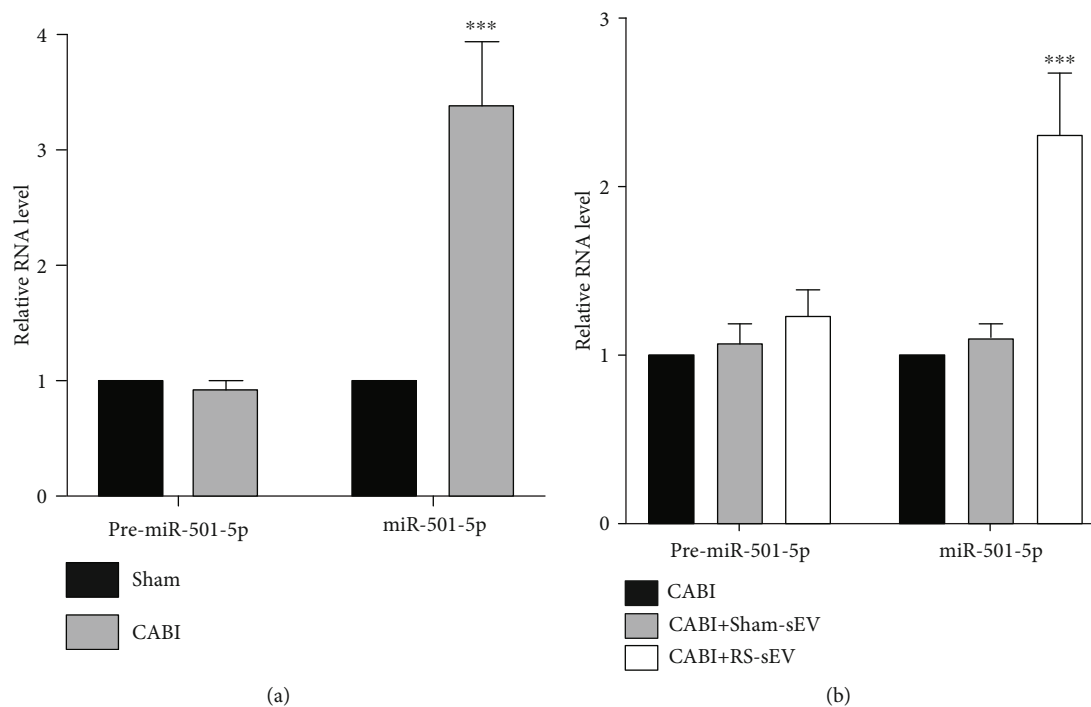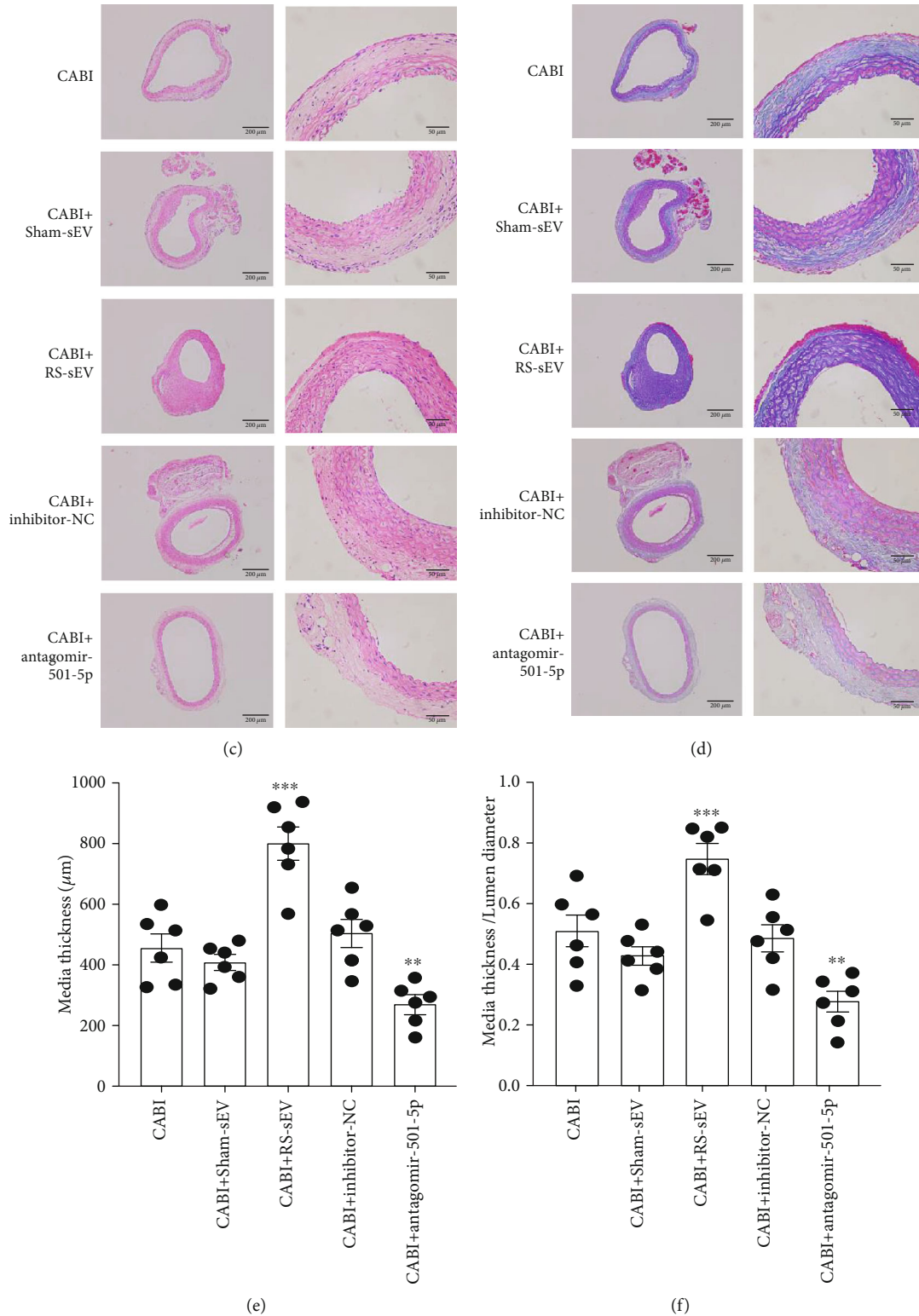
FIGURE 5: Plasma sEV-carried miRNA-501-5p promotes rat carotid artery stenosis. (a) qRT-PCR analysis of pre-miRNA-501-5p and miRNA-501-5p in carotid artery from rats with carotid artery balloon injury (CABI) or sham procedure. Data are normalized to U6. (b) qRT-PCR analysis of pre-miRNA-501-5p and miRNA-501-5p in carotid artery from CABI rats treated with plasma sEV. Data are normalized to U6. (c) Representative hematoxylin-eosin stained images of carotid arteries from CABI rats treated with plasma sEV or antagomir-501-5p. (d) Representative Masson stained images of carotid arteries from CABI rats treated with plasma sEV or antagomir-501-5p. (e and f) Quantitative analysis for media thickness and the ratio of media thickness and lumen diameter. $n = 6$ for each group. Values are mean ± SEM. $^{**}P < 0.01$ and $^{***}P < 0.001$.

(a)

Target site 2378-2385

5'UTR   3'UTR

Smad3 Wt-3'UTR   5' … GUUUUGUGUUUUUCC<u>AAAGGAU</u>A …

                    | | | | | | |

miR-501-5p   3'   AGAGUGGGUCCCUGUUUCCUAA

Smad3 Wt-3'UTR   5' … GUUUUGUGUUUUUCC<u>TTTCCTA</u>A …

(b)

(c)

Figure 6: Continued.

(d)

(e)

(f)
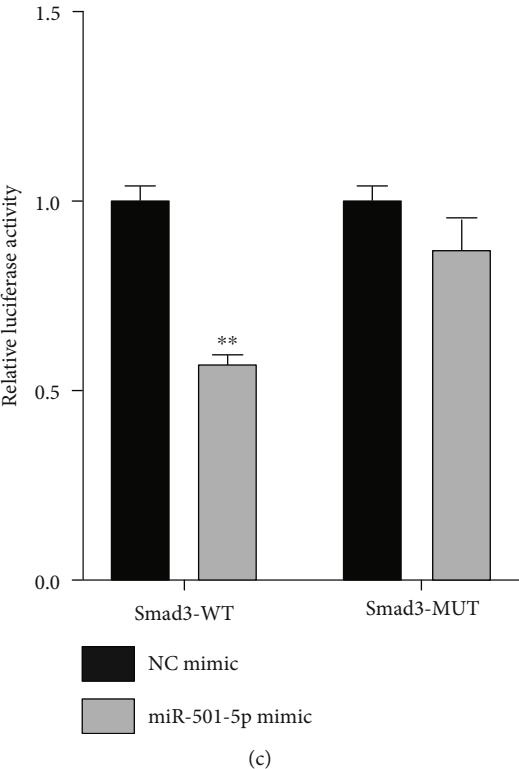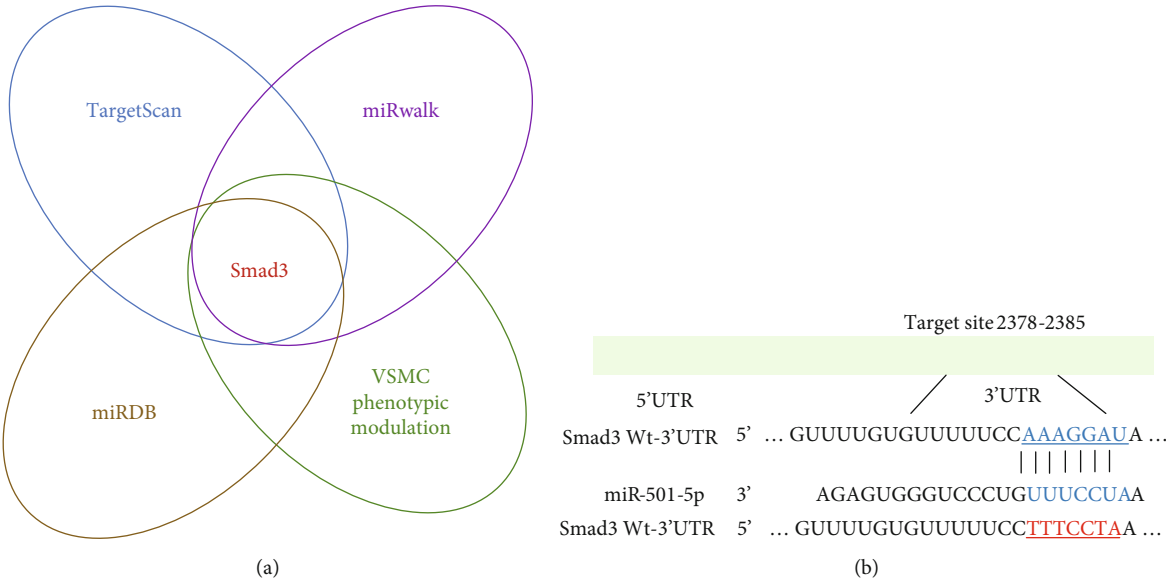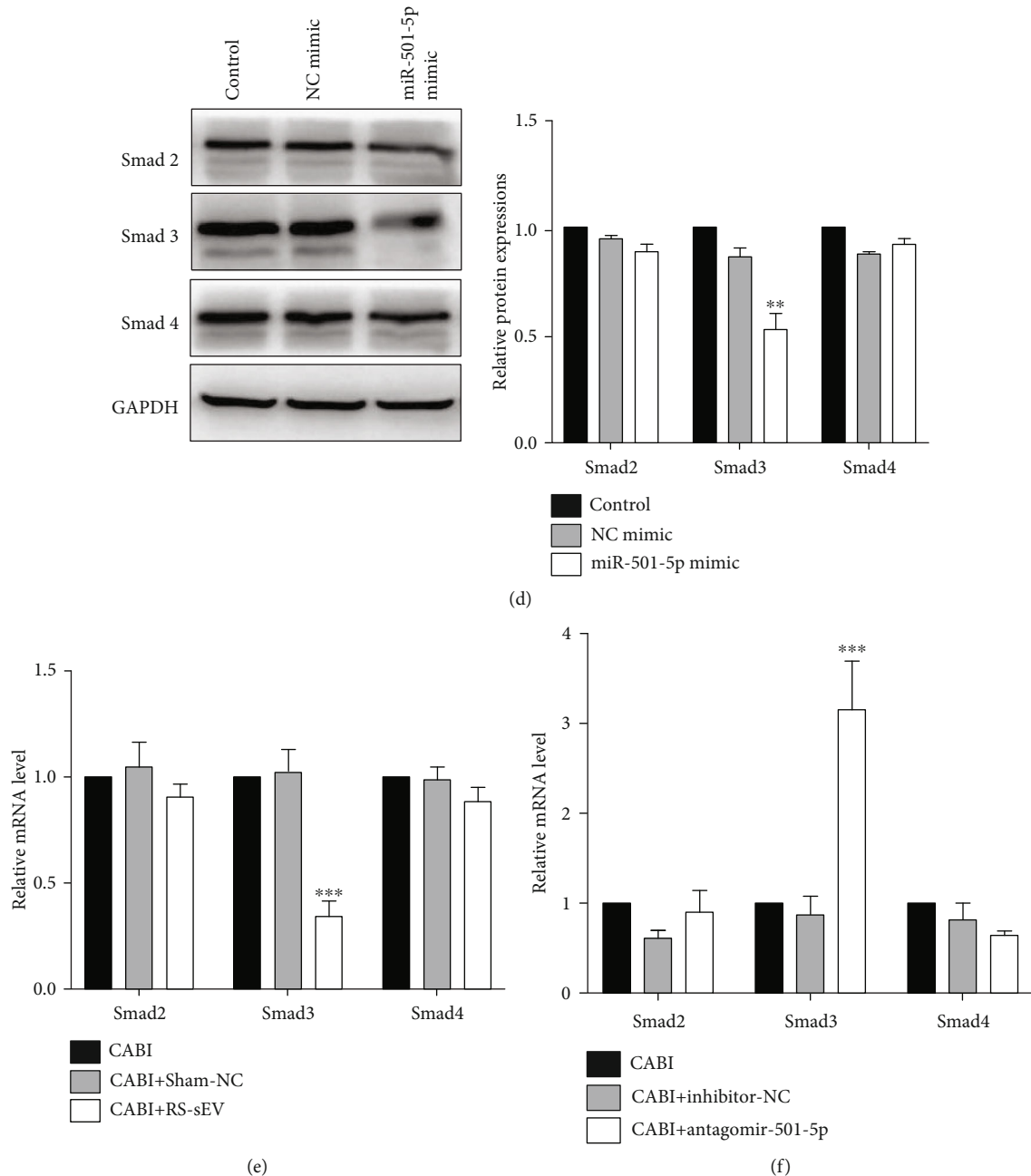
FIGURE 6: Smad3 is target gene of plasma sEV-carried miRNA-501-5p in smooth muscle cells. (a) Screening scheme for putative target gene of miRNA-501-5p. (b) Schematic of miRNA-501-5p putative target sites in the $3'$URT of Smad3 and the sequences of mutant UTRs. (c) Dual luciferase reporter assay of 293T cells cotransfected with miRNA-501-5p mimic or negative control (NC) ($n = 3$). (d) Representative blots and quantified data showing protein expressions of Smad2, Smad3, and Smad4 in human aortic smooth muscle cells (HASMC) transfected with miRNA-501-5p mimic or NC ($n = 3$). (e) qRT-PCR analysis of Smad2, Smad3, and Smad4 in carotid artery from rats with carotid artery balloon injury (CABI) undergoing sEV injection ($n = 6$). Data are normalized to U6. (f) qRT-PCR analysis of Smad2, Smad3, and Smad4 in carotid artery from rats with carotid artery balloon injury (CABI) undergoing antagomir-501-5p injection ($n = 6$). Data are normalized to U6. Values are mean ± SEM. $^{**}P < 0.01$ and $^{***}P < 0.001$.

carotid artery stenosis after balloon injury exhibited decreased expression of contractile markers α-SMA and calponin and increased VSMC proliferation compared with rats in the sham group. Our results, in line with previous articles [4, 5, 21], confirmed that VSMC phenotypic modulation plays a crucial role in restenosis.

sEV, small endogenous membrane vesicles released from various cell types, are of great interest because of their extensive participation in cell-to-cell communication [10, 12]. The mean size of most sEV in our study was 110-130 nm, indicating that the sEV are very likely to be exosomes. Several previous studies [4–6, 10, 22] have reported the association of sEV

(a)

(b)

(c)
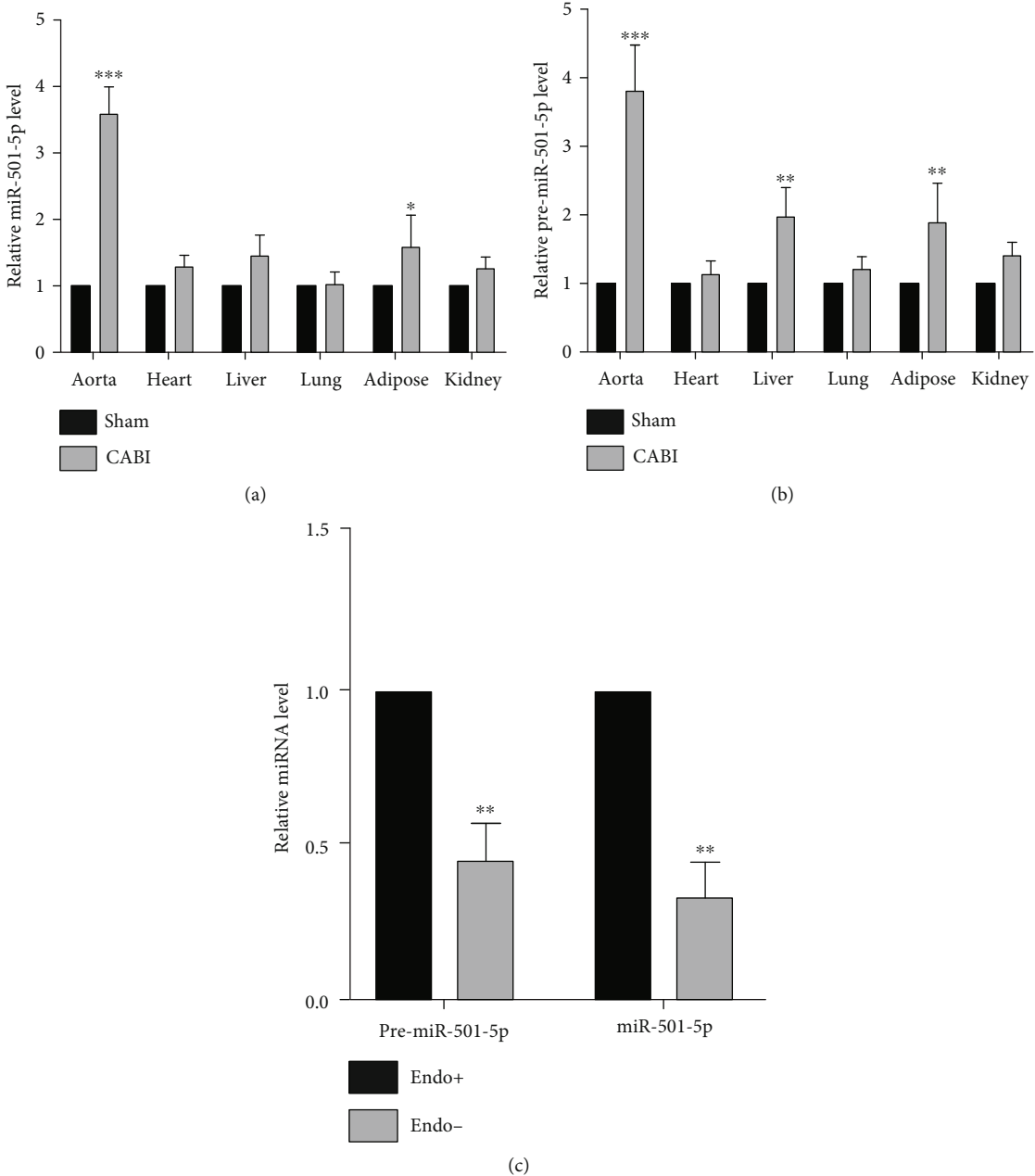
FIGURE 7: Continued.

(d)
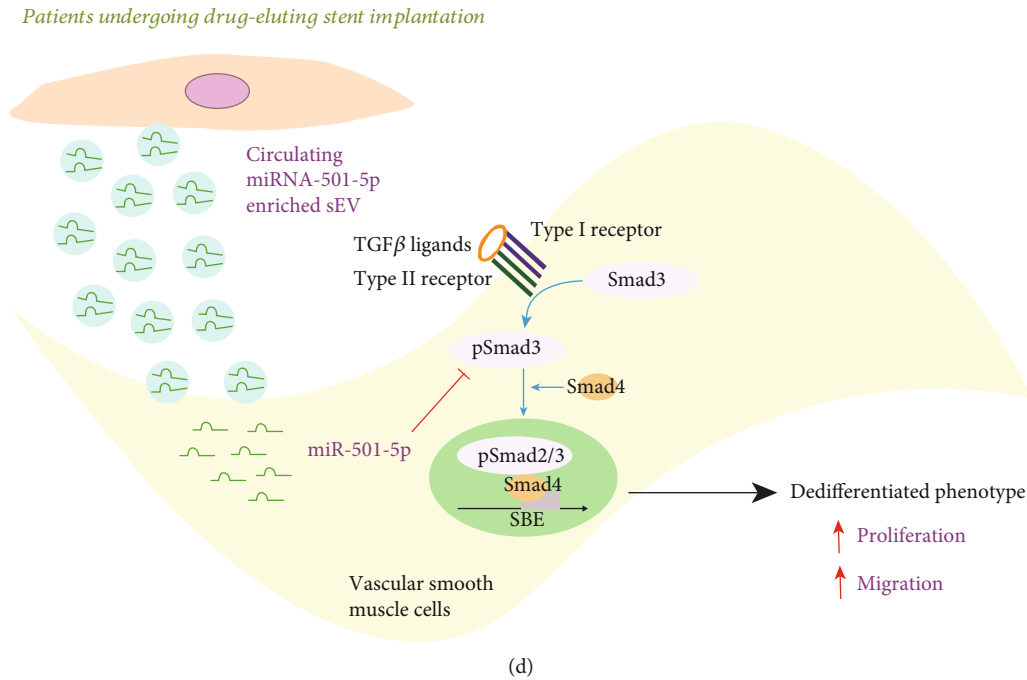
FIGURE 7: The potential origin of miRNA-501-5p and the proposed schematic. qRT-PCR analysis of miRNA-501-5p (a) and pre-miRNA-501-5p (b) in tissues from rats with carotid artery balloon injury (CABI) or not. Data are normalized to U6 ($n = 6$). (c) qRT-PCR analysis showing that the expressions of miRNA-501-5p and pre-miRNA-501-5p are significantly higher in rat aorta with endothelium (endo+) than that without endothelium (endo-). Data are normalized to U6 ($n = 6$). (d) Drug-eluting stent implantation increases the production of miRNA-501-5p in multiple tissues, especially in endothelial cells. miRNA-501-5p, cargoed in sEV, is delivered to the vascular smooth muscle cells (VSMC) by plasma sEV and promotes VSMC proliferation and migration by targeting Smad3. Values are mean ± SEM. $^*P < 0.05$, $^{**}P < 0.01$, and $^{***}P < 0.001$.

and VSMC phenotypic modulation at the level of cell and animal experiment, but evidence from patient level still remains insufficient. In our study, we purified plasma sEV directly from ISR patients and found that the concentration of plasma sEV in ISR patients was higher than that in non-ISR patients. More importantly, these plasma sEV could be internalized by VSMC and decrease the expression of VSMC contractile markers α-SMA and calponin and increase VSMC proliferation and migration.

sEV harbor proteins, miRNAs, and mRNAs and deliver these signals to receptor cells through systemic circulation. In fact, miRNAs, as a class of epigenetic factors, have been reported to drive VSMC toward the differentiated/contractile phenotype, including miRNA 1 [23], miRNA-124 [24], miRNA-143/145 [6], and miRNA-663 [25]. In response of vascular injury, several miRNAs, such as miRNA-206 [26], miRNA-221 [9], and miRNA-222 [27], could switch VSMC toward the dedifferentiated/synthetic phenotype to tissue reparation. With new-generation sequencing and qRT-PCR validation in plasma sEV from patients, we found that miRNA-501-5p was markedly elevated in ISR patients or CABI rats. miRNA-501-5p is a relative novel miRNA and has been reported to promote cell proliferation and migration in the development of cancer [28–30]. Similarly, in our study, plasma sEV-carried miRNA-501-5p decreased the expression of VSMC contractile markers α-SMA and calponin, increased VSMC proliferation and migration, and exhibited profound function of promoting VSMC phenotypic

modulation both in vivo and in vitro. More importantly, the level of plasma sEV-carried miRNA-501-5p linearly correlated with the degree of restenosis, which provides a possibility for potential clinical application.

Further bioinformatic analysis and validation experiments showed that Smad3 is target of miRNA-501-5p in VSMC. It is well established that Smad3 plays a crucial role in maintaining the differentiated/contractile phenotype of VSMC [17, 20], and loss of Smad3 can increase VSMC proliferation and reduce expression of VSMC contractile markers [18, 19]. Consistent with these studies, our data found that miRNA-501-5p markedly reduced the expression of α-SMA and calponin and promoted VSMC proliferation and migration in vitro by inhibiting Smad3 expression. Meanwhile, in vivo study with suppressing miRNA-501-5p showed the increased expression of Smad3 and VSMC contractile markers and the decreased VSMC proliferation in carotid artery.

Furthermore, we investigated the potential origins of increased plasma sEV-carried miRNA-501-5p. We found that both miRNA-501-5p and its precursor pre-miRNA-501-5p significantly elevated in the aorta and adipose. Notably, the removal of aortic endothelium could markedly reduce the expression of miRNA-501-5p and its precursor, elucidating that endothelial cells might be the major origin of miRNA-501-5p. Our data, in line with previous study [31], indicated that endothelial cells are the important origin of plasma sEV-carried miRNAs.

There are several limitations in the present study. First, we found plasma sEV-carried miRNA-501-5p promoted VSMC phenotypic modulation-mediated ISR by targeting Smad3, but we could not rule out a possibility of other miR-NAs and other targets of miRNA-501-5p. Second, although CABI rat is a widely used in vivo model for studying VSMC phenotype, this model cannot simulate the situation of ISR after stent implantation completely. Third, our study found endothelial cells might be the major origins of the increased plasma sEV-carried miRNAs, but other tissues could not be totally excluded because of the lack of further validation.

5. Conclusion

Plasma sEV in ISR patients are elevated and play a crucial role in VSMC phenotypic modulation. miRNA-501-5p was identified in plasma sEV to enhance VSMC proliferation and migration by targeting Smad3. Vascular endothelial cells might be the major origin of plasma sEV miRNA-501-5p. Collectively, these findings showed that plasma sEV-carried miRNA-501-5p promotes VSMC phenotypic modulation-mediated ISR through targeting Smad3.

Data Availability

The data used to support the results of this study are included within the article.

Conflicts of Interest

The authors declare that no conflict of interest exists.

Authors' Contributions

Shao-Liang Chen and Jun-Jie Zhang designed the study, interpreted the data, and revised the manuscript critically. Xiao-Fei Gao, Zhi-Mei Wang, and Ai-Qun Chen conducted the majority of the experiments, performed the statistical analysis, and wrote the manuscript. Feng Wang, Shuai Luo, Yue Gu, Xiang-Quan Kong, Guang-Feng Zuo, Xiao-Min Jiang, and Zhen Ge conducted parts of the experiments. Guan-Wen Ding and Yan Chen revised the manuscript. All the authors approved the submission. Xiao-Fei Gao, Zhi-Mei Wang, and Ai-Qun Chen contributed equally to this work.

Supplementary Materials

Supplemental Figure 1: study flowchart. Supplemental Table 1: the primer sequences for RT-PCR assays. Supplemental Table 2: clinical characteristics of enrolled patients. Supplemental Figure 2: identification of plasma small extracellular vesicles (sEV). Supplemental Figure 3: PKH26-labeled sEV internalized by human aortic smooth muscle cells (HASMC). Supplemental Figure 4: miRNA-501-5p inhibition and vascular smooth muscle cells (VSMC) contractile markers. Supplemental Figure 5: miRNA-501-5p inhibition suppressing VSMC migration. Supplemental Figure 6: plasma sEV-carried miRNA-501-5p and VSMC proliferation. Supplemental Figure 7: miRNA-501-5p inhibition and VSMC contractile markers of rats. Supplemental Figure 8: GO analyses of miRNA-501-5p. Supplemental Figure 9: KEGG analysis of miRNA-501-5p. Supplemental Figure 10: α-SMA and Smad3 expression in carotid artery of rats. (*Supplementary Materials*)

References

[1] E. Shlofmitz, M. Iantorno, and R. Waksman, "Restenosis of drug-eluting stents," *Circulation: Cardiovascular Interventions*, vol. 12, no. 8, p. e007023, 2019.

[2] X.-F. Gao, S. Lu, Z. Ge et al., "Relationship between high platelet reactivity on clopidogrel and long-term clinical outcomes after drug-eluting stents implantation (PAINT-DES): a prospective, propensity score-matched cohort study," *BMC Cardiovascular Disorders*, vol. 18, no. 1, p. 103, 2018.

[3] X.-F. Gao, J. Kan, Y.-J. Zhang et al., "Comparison of one-year clinical outcomes between intravascular ultrasound-guided versus angiography-guided implantation of drug-eluting stents for left main lesions: a single-center analysis of a 1,016-patient cohort," *Patient Preference and Adherence*, vol. 8, pp. 1299–1309, 2014.

[4] A. Frismantiene, M. Philippova, P. Erne, and T. J. Resink, "Smooth muscle cell-driven vascular diseases and molecular mechanisms of VSMC plasticity," *Cellular Signalling*, vol. 52, pp. 48–64, 2018.

[5] S. Allahverdian, C. Chaabane, K. Boukais, G. A. Francis, and M. L. Bochaton-Piallat, "Smooth muscle cell fate and plasticity in atherosclerosis," *Cardiovascular Research*, vol. 114, no. 4, pp. 540–550, 2018.

[6] E. Hergenreider, S. Heydt, K. Tréguer et al., "Atheroprotective communication between endothelial cells and smooth muscle cells through miRNAs," *Nature Cell Biology*, vol. 14, no. 3, pp. 249–256, 2012.

[7] F. Yang, Q. Chen, S. He et al., "miR-22 is a novel mediator of vascular smooth muscle cell phenotypic modulation and neointima formation," *Circulation*, vol. 137, no. 17, pp. 1824–1841, 2018.

[8] R. Ji, Y. Cheng, J. Yue et al., "MicroRNA expression signature and antisense-mediated depletion reveal an essential role of MicroRNA in vascular neointimal lesion formation," *Circulation Research*, vol. 100, no. 11, pp. 1579–1588, 2007.

[9] X. Liu, Y. Cheng, S. Zhang, Y. Lin, J. Yang, and C. Zhang, "A necessary role of miR-221 and miR-222 in vascular smooth muscle cell proliferation and neointimal hyperplasia," *Circulation Research*, vol. 104, no. 4, pp. 476–487, 2009.

[10] X. F. Gao, Z. M. Wang, F. Wang, Y. Gu, J. J. Zhang, and S. L. Chen, "Exosomes in coronary artery disease," *International Journal of Biological Sciences*, vol. 15, no. 11, pp. 2461–2470, 2019.

[11] D. M. Pegtel and S. J. Gould, "Exosomes," *Annual Review of Biochemistry*, vol. 88, no. 1, pp. 487–514, 2019.

[12] R. Kalluri and L. B. VS, "The biology, function, and biomedical applications of exosomes," *Science*, vol. 367, no. 6478, p. - eaau6977, 2020.

[13] D. A. Tulis, "Rat carotid artery balloon injury model," *Methods in Molecular Medicine*, vol. 139, pp. 1–30, 2007.

[14] J. Zhang, X. Gao, J. Kan et al., "Intravascular Ultrasound Versus Angiography-Guided Drug-Eluting Stent Implantation: The ULTIMATE Trial," *Journal of the American College of Cardiology*, vol. 72, no. 24, pp. 3126–3137, 2018.

[15] J. Zhang, X. Gao, Z. Ge et al., "Impact of intravascular ultrasound-guided drug-eluting stent implantation on patients with chronic kidney disease: results from ULTIMATE trial," *Catheterization and Cardiovascular Interventions*, vol. 93, no. 7, pp. 1184–1193, 2019.

[16] C. Théry, K. W. Witwer, E. Aikawa et al., "Minimal information for studies of extracellular vesicles 2018 (MISEV2018): a position statement of the International Society for Extracellular Vesicles and update of the MISEV2014 guidelines," *Journal of Extracellular Vesicles*, vol. 7, no. 1, 2018.

[17] F. Yao, P. Yu, Y. Li et al., "Histone variant H2A.Z is required for the maintenance of smooth muscle cell identity as revealed by single-cell transcriptomics," *Circulation*, vol. 138, no. 20, pp. 2274–2288, 2018.

[18] D. Zabini, E. Granton, Y. Hu et al., "Loss of SMAD3 promotes vascular remodeling in pulmonary arterial hypertension via MRTF disinhibition," *American Journal of Respiratory and Critical Care Medicine*, vol. 197, no. 2, pp. 244–260, 2018.

[19] D. Wong, A. W. Turner, and C. L. Miller, "Genetic insights into smooth muscle cell contributions to coronary artery disease," *Arteriosclerosis, Thrombosis, and Vascular Biology*, vol. 39, no. 6, pp. 1006–1017, 2019.

[20] D. Iyer, Q. Zhao, R. Wirka et al., "Coronary artery disease genes SMAD3 and TCF21 promote opposing interactive genetic programs that regulate smooth muscle cell differentiation and disease risk," *PLoS Genet*, vol. 14, no. 10, p. e1007681, 2018.

[21] E. L. Low, A. H. Baker, and A. C. Bradshaw, "TGFβ, smooth muscle cells and coronary artery disease: a review," *Cellular Signalling*, vol. 53, pp. 90–101, 2019.

[22] C. M. Boulanger, X. Loyer, P. E. Rautou, and N. Amabile, "Extracellular vesicles in coronary artery disease," *Nature Reviews. Cardiology*, vol. 14, no. 5, pp. 259–272, 2017.

[23] J. Chen, H. Yin, Y. Jiang et al., "Induction of microRNA-1 by myocardin in smooth muscle cells inhibits cell proliferation," *Arteriosclerosis, Thrombosis, and Vascular Biology*, vol. 31, no. 2, pp. 368–375, 2011.

[24] Y. Tang, S. Yu, Y. Liu, J. Zhang, L. Han, and Z. Xu, "MicroRNA-124 controls human vascular smooth muscle cell phenotypic switch via Sp1," *American Journal of Physiology. Heart and Circulatory Physiology*, vol. 313, no. 3, pp. H641–H649, 2017.

[25] P. Li, N. Zhu, B. Yi et al., "MicroRNA-663 regulates human vascular smooth muscle cell phenotypic switch and vascular neointimal formation," *Circulation Research*, vol. 113, no. 10, pp. 1117–1127, 2013.

[26] H. Sun, S. Cai, M. Zhang et al., "MicroRNA-206 regulates vascular smooth muscle cell phenotypic switch and vascular neo-

intimal formation," *Cell Biology International*, vol. 41, no. 7, pp. 739–748, 2017.

[27] Z. Wang, H. Zhu, H. Shi et al., "Exosomes derived from M1 macrophages aggravate neointimal hyperplasia following carotid artery injuries in mice through miR-222/CDKN1B/CDKN1C pathway," *Cell Death & Disease*, vol. 10, no. 6, p. 422, 2019.

[28] X. Ma, J. Feng, M. Lu et al., "microRNA-501-5p promotes cell proliferation and migration in gastric cancer by downregulating LPAR1," *Journal of Cellular Biochemistry*, vol. 121, no. 2, pp. 1911–1922, 2020.

[29] R. Pan, W. Cai, J. Sun, C. Yu, P. Li, and M. Zheng, "Inhibition of KHSRP sensitizes colorectal cancer to 5-fluoruracil through miR-501-5p-mediated ERRFI1 mRNA degradation," *Journal of Cellular Physiology*, vol. 235, no. 2, pp. 1576–1587, 2020.

[30] D. Fan, B. Ren, X. Yang, J. Liu, and Z. Zhang, "Upregulation of miR-501-5p activates the wnt/β-catenin signaling pathway and enhances stem cell-like phenotype in gastric cancer," *Journal of Experimental & Clinical Cancer Research*, vol. 35, no. 1, p. 177, 2016.

[31] Z. Hou, X. Qin, Y. Hu et al., "Longterm exercise-derived exosomal miR-342-5p," *Circulation Research*, vol. 124, no. 9, pp. 1386–1400, 2019.

Research Article

ALKBH5 Exacerbates Aortic Dissection by Promoting Inflammatory Response and Apoptosis of Aortic Smooth Muscle Cells via Regulating lnc-TMPO-AS1/EZH2/IRAK4 Signals in an m6A Modification Manner

Peng Wang [ID],[1,2,3] **Min Zhang,**[1,2] **Zhiwei Wang** [ID],[1,2] **Qi Wu,**[1,2,3] **Feng Shi,**[1,2,3] **and Shun Yuan**[1,2,3]

[1]*Department of Cardiovascular Surgery, Renmin Hospital of Wuhan University, 238# Jiefang Road, Wuhan,*
 430000 Hubei Province, China
[2]*Cardiovascular Surgery Laboratory, Renmin Hospital of Wuhan University, 9# Zhangzhidong Road, Wuhan,*
 430000 Hubei Province, China
[3]*Central Laboratory, Renmin Hospital of Wuhan University, 9# Zhangzhidong Road, Wuhan, 430000 Hubei Province, China*

Correspondence should be addressed to Zhiwei Wang; wangzhiwei@whu.edu.cn

Recently, mounting evidence indicates that N6-methyladenosine (m6A) modification functions as a pivotal posttranscriptional modification that regulates noncoding RNA biogenesis to influence the progression of multiple diseases. However, whether m6A modification is involved in aortic dissection (AD) development has never been reported. Meanwhile, numerous studies have shown that AngII-induced inflammatory damage and excessive apoptosis of human aortic smooth muscle cells (HASMCs) are the crucial pathological features of AD development. Therefore, in this study, we intended to explore whether m6A modification can regulate AD progression by influencing the damage effects of AngII on HASMCs and elucidate the underlying mechanisms. Firstly, we screened and confirmed the high expression of alkylation repair homolog protein 5 (ALKBH5), a key m6A demethylase, in aortic tissues from AD patients, indicating that m6A modification may indeed be involved in AD progression. Subsequently, we demonstrated that ALKBH5 can exacerbate the AngII-induced HASMC inflammatory injury as well as apoptosis and shorten the survival time of AngII-infused mice. Mechanistically, we revealed that lncRNA TMPO-AS1 is a downstream target for ALKBH5 to affect AD progression in vitro and vivo. Meanwhile, we confirmed that ALKBH5-mediated m6A demethylation downregulates lnc-TMPO-AS1 by decreasing the stability of its nascent. Further, we demonstrated that lnc-TMPO-AS1 exhibits its functions in HASMCs, at least partly, through downregulating IRAK4 at the epigenetic level by combining with EZH2. Finally, the direct positive correlation between ALKBH5 and IRAK4 in terms of the expression level and biological function was confirmed, which further enforced the preciseness and correctness of our findings. In conclusion, our study demonstrated that ALKBH5 aggravates AD by promoting inflammatory response and apoptosis of HASMCs via regulating lnc-TMPO-AS1/EZH2/IRAK4 signals in an m6A modification manner and may provide a novel molecular basis for subsequent researchers to searching for novel therapeutic approaches to improve the health of patients fighting AD and other cardiovascular diseases.

1. Introduction

Aortic dissection (AD) is a life-threatening cardiovascular emergency due to a tear in the aorta intima or bleeding within the aortic wall, leading to the separation of the differ-

ent layers of the aortic wall [1, 2]. One of the first prerequisites to explore new therapeutic strategies for AD is to elucidate the potential molecular mechanisms involved.

Numerous studies have shown that inflammatory damage and excessive apoptosis of human aortic smooth muscle

cells (HASMCs) are the crucial pathological features of AD development [3–5]. Meanwhile, our previous study has demonstrated that treating ASMCs with a certain concentration of angiotensin II (AngII) can simulate the status of cellular injury during the development of AD in the physiological state [6]. Therefore, in the present study, we intended to identify some signaling molecules that could regulate AD progression by influencing the damage effects of AngII on HASMCs and clarify their mechanisms of action.

The dysfunction of HASMCs is a complex biological process caused by epigenetic abnormalities and/or abnormal genetic variations. Epigenetic abnormalities mainly occur at the following levels: histone modification [7], DNA [8], and RNA [9]. In RNA levels, over 100 types of RNA modifications have been identified, among which N6-methyladenosine (m6A) RNA methylation is the most common modification in eukaryotes [10–12]. Moreover, m6A modification is demonstrated by many studies to be a dynamic and reversible process, constructed primarily by a methyltransferase complex called m6A "writers," including methyltransferase like 3 (METTL3), vir-like methyltransferase (VIRMA), coupled with WT1-associated protein (WTAP) and removed by demethylases called m6A "erasers," including alkylation repair homolog protein 5 (ALKBH5) and fat mass and obesity-associated protein (FTO) [13, 14].

Recently, increasing evidence also revealed that m6A modification functions as a pivotal posttranscriptional modification that regulates mRNA and noncoding RNA biogenesis to influence the progression of multiple diseases; for instance, Lin et al. demonstrated that METTL3 could facilitate lung cancer development by promoting translation initiation of many oncogenes through m6A modification [15]. Lan et al. reported that VIRMA could contribute to liver cancer progression by causing the separation of the RNA-binding protein HuR and the degradation of GATA3 pre-mRNA in an m6A modification manner [16]. Zhang et al. found that ALKBH5 could promote invasion and metastasis of gastric cancer via decreasing methylation of the lncRNA NEAT1 [17]. However, whether m6A modification is involved and whether it acts by regulating noncoding RNAs in the development of AD has never been reported.

In the present study, we confirmed that ALKBH5 was highly expressed in AD tissues as well as HASMCs treated with AngII and could exacerbate AngII-induced HASMC inflammation and apoptosis in vitro. Moreover, overexpressing ALKBH5 increased the incidence of AD in AngII-infused mice and shorten their survival time. Mechanistically, ALKBH5-mediated m6A demethylation induced the downregulation of long noncoding RNA (lncRNA) TMPO-AS1 by reducing the stability of nascent lnc-TMPO-AS1, which subsequently enhanced the expression of IRAK4 by decreasing binding to EZH2 at the epigenetic level. Collectively, our findings provided a novel insight into the role of m6A modification in the onset and progression of AD.

2. Materials and Methods

2.1. Clinical Samples. Aortic media samples ($n = 40$) were obtained from acute thoracic AD patients who underwent

emergency aortic replacement surgery from May 2016 to November 2019. Patients enrolled in our study were confirmed to have no connective tissue diseases, such as Marfan syndrome and Ehlers-Danlos syndrome, or a family history of aortic diseases. Meanwhile, normal aorta tissues ($n = 40$) were collected from heart donors declared brain dead. Both the informed written consent of all participants and the approval of the Clinical Research Ethics Committees of Renmin Hospital of Wuhan University for the collection and usage of clinical specimens were obtained. The baseline characteristics of the AD patients and aortic donors are presented in Supplementary Table 1.

2.2. Cell Culture and Liposome Transfection. HASMCs were purchased from ATCC (PCS-100-012™) and incubated in DMEM (HyClone, UT) containing 10% fetal bovine serum (FBS; Invitrogen) and 1% penicillin/streptomycin (Sigma). The external conditions for cell culture were as follows: 37°C, humidified atmosphere containing 5% CO_2. As previously reported, we established the cell model simulating the damaged state of HASMCs during AD in the present study by treating HASMCs with $0.1\,\mu M$ AngII for 12 h [18].

To obtain stable cell lines, we purchased multiple lentivirus, including ALKBH5 overexpression lentivirus (termed as LV-ALKBH5), a negative control (termed as LV-NC), ALKBH5 knockdown lentivirus (termed as sh-ALKBH5), or scramble control (termed as sh-NC) from GeneChem (Shanghai, China). Lentiviruses were separately transfected into HASMCs when cell confluence attained 60%. Stable cell clones were selected using puromycin ($4\,\mu g/ml$) for 1 week.

For the overexpression of specific genes, we obtained overexpression plasmids, pcDNA3.1-TMPO-AS1, pcDNA3.1-EZH2, and pcDNA3.1-IRAK4, from GeneChem Co., Ltd. (Shanghai, China). Meanwhile, we commissioned RiboBio Co., Ltd. to synthesize small interfering RNA (siRNA) to specifically target sequences in TMPO-AS1 (si-TMPO-AS1), EZH2 (si-EZH2), and IRAK4 (si-IRAK4). The pcDNA3.1 empty vector (pcDNA-NC) or si-scr-RNA (si-NC) was their respective negative control. HASMCs were randomly transiently transfected with one of the plasmids or siRNAs using Lipofectamine 3000 (Invitrogen, USA).

2.3. AngII Infusion AD Model and Adenovirus Vector Transfection. The animal experiments were approved by the Ethical Committee of the Renmin Hospital of Wuhan University and performed following the Current Guidelines for the Care and Use of Laboratory Animals published by the National Institutes of Health. Male C57BL/6N mice were purchased from the Guangdong Medical Laboratory Animal Center (Foshan, China). All mice were in a pathogen-free environment with proper temperature (22°C) as well as humidity (60–65%) and given a normal chow diet and water.

The angiotensin II (AngII) infusion mouse AD model was constructed as described in a previous study [19]. Concretely, osmotic minipumps (ALZET, USA) containing AngII ($1\,\mu g/kg/min$, Enzo Life Sciences, USA) were implanted in eight-week-old male C57BL/6N mice. All mice were monitored daily to record their survival time and death reasons. The experimental endpoint was mouse death from

aortic rupture or treatment time up to 28 days. Whether they died within 28 days or were euthanized on the 28th day, the aortas were collected to confirm the formation of AD.

To interfere with ALKBH5 level in vivo, adeno-associated virus 9 (AAV9) that can transfect the aorta tissue was used in the present study. 1×10^{12} viral genome particles carrying different plasmids and interfering RNAs in $100\,\mu$l of saline were randomly injected through the tail vein of C57BL/6N mice.

2.4. RNA Extraction and qRT-PCR Analyses. Total RNA was extracted from tissues and cells via using TRIzol Reagent (Invitrogen, USA). Then, samples with OD value greater than 1.9 were reverse transcribed to cDNA by utilizing the Super-Script III Reverse Transcriptase kit (Invitrogen). Quantitative real-time PCR (qRT-PCR) was performed on the Applied Biosystems™ 7500 Real-Time PCR System using Fast SYBR Green Master Mix Kit (Applied Biosystems, USA). The relative expression level mRNA was evaluated using the $2^{-\Delta\Delta Ct}$ method and normalized to their corresponding internal control, U6 snRNA, or β-actin. All primers were designed and synthesized by RiboBio Co. (Guangzhou, China).

2.5. Western Blot. Tissue specimens or cells were lysed by RIPA lysis buffer containing 1% protease inhibitors (Sigma, USA). The protein extractions were quantified by BCA Protein Assay Kit (Beyotime, China). Equivalent protein samples ($25\,\mu$g) were electrophoretically separated on 10% SDS-PAGE and then transferred to polyvinylidene difluoride membrane (PVDF). After being blocked in 5% skim milk, PVDFs were incubated with monoclonal primary antibodies, including anti-ALKBH5 (ab69325; Abcam), anti-EZH2 (#5246; Cell Signaling Technology), anti-IRAK4 (ab32511; Abcam), anti- pNFκB (ab32536; Abcam), and anti-GAPDH (ab9485; Abcam) at 4°C overnight. Next, the membranes were incubated with a peroxidase-conjugated secondary antibody. The western blot bands were visualized by Pierce™ ECL (Thermo Fisher Scientific Inc., USA) and analyzed using ImageJ software [20].

2.6. Enzyme-Linked Immunosorbent Assay (ELISA). The levels of inflammatory factors (IL-1β, IL-6, IL-17A, and TNF-α) in the culture medium supernatants of HASMCs treated or untreated with AngII were measured by ELISA kits (R&D, MN, USA). The OD value at 450 nm wavelength was detected by Infinite F50® microplate reader (Tecan, CH).

2.7. TUNEL Assay. HASMCs were fixed in paraformaldehyde for 15 min and stained by In Situ Cell Death Detection Kit (TMR red) (Roche, Switzerland). Six visual fields were randomly chosen from each group to calculate the positive TUNEL-stained cells which were visualized with a fluorescence microscope (BX63, Olympus, Japan).

2.8. Flow Cytometry. Each group of HASMCs was collected, resuspended, and double-stained with Annexin V-FITC (556547, BD), coupled with propidium iodide (PI; Solarbio, China) at room temperature for 10 min in darkness. Subsequently, cell apoptosis was analyzed within 1 h using the

FACScan flow cytometer installed with Cell Quest software (BD Biosciences, USA).

2.9. Microarray Analysis. To obtain the lncRNA expression profiling in aorta tissues for further hierarchical clustering analysis, a microarray analysis was performed on Human lncRNA Array v4.0 (8×60 K, Arraystar, USA) and its results were analyzed by using R software with related packages.

2.10. RNA m6A Dot Blots. The poly(A)$^+$ RNAs (100 and 250 ng, respectively) were denatured by heating at 65°C for 5 min and spotted onto a nylon membrane (Sigma, USA) with a Bio-Dot apparatus (Bio-Rad, USA). The membranes were ultraviolet (UV) crosslinked, blocked, incubated with m6A antibody (1:20091000, Synaptic Systems, #202003) overnight at 4°C, and then incubated with HRP-conjugated anti-mouse IgG (1 : 5000, Proteintech, USA). After extensive washing, membranes were visualized by the chemiluminescence system (Bio-Rad, USA). The membrane stained with 0.02% methylene blue (MB) in 0.3 M sodium acetate (pH 5.2) was used to ensure consistency between groups.

2.11. Chromatin Immunoprecipitation (ChIP) Assay. ChIP assay was performed according to the manufacturer's manual (Millipore, USA) as described previously [13]. The specific antibodies for H3 trimethyl-Lys-27 or EZH2 were purchased from Millipore.

2.12. RNA Immunoprecipitation (RIP) Assay. RIP assay was conducted using Magna RIP™ RNA-Binding Protein Immunoprecipitation Kit (Millipore, USA). After HASMCs were lysed and centrifuged, the supernatant was incubated with magnetic beads conjugated with antibodies against Argonaute-2 (anti-Ago2), m6A (anti-m6A), or anti-Immunoglobulin G (anti-IgG) at 4°C overnight. The precipitated RNAs were eluted, purified, and then examined by qRT-PCR.

2.13. Subcellular Fractionation Analysis. Cytoplasmic and Nuclear RNA Purification Kit (Cat. 21000; Norgen, Canada) was utilized for subcellular isolation of RNAs in HASMCs. The fractions of cytoplasmic and nuclear were detected by qRT-PCR, with GAPDH and U6 serving as their internal references, respectively.

2.14. Immunofluorescence and Fluorescence In Situ Hybridization (FISH). HASMCs were fixed in PBS containing 4% paraformaldehyde for 10 min at room temperature and permeabilized in PBS containing 0.1% Triton-X as well as 1% BSA at room temperature for 30 min. DNA staining was conducted with DAPI. EZH2 (Bioss) was detected with an anti-EZH2 antibody for approximately 16 h (37°C). Specific FISH probes to lncRNA TMPO-AS1 were designed and synthesized by RiboBio Co. (Guangzhou, China). The hybridization was performed in HASMCs as previously reported [12]. Imaging was performed on a confocal laser scanning microscope (Leica Microsystems, Mannheim, Germany).

2.15. mRNA Stability Detection. To detect the influence of ALKBH5 on the half-life of lnc-TMPO-AS1, we treated HASMCs with $5\,\mu$g/ml actinomycin D (Act-D) (#A9415, Sigma, USA). After incubation at the indicated times, the

total RNA of cells was extracted for qRT-PCR. The mRNA half-life of lnc-TMPO-AS1 was calculated using ln2/slope, with GAPDH being used for normalization.

2.16. HE Staining. Resected aorta samples from the normal and AD mice were fixed in 4% formaldehyde overnight, dehydrated, paraffin-embedded, and cut into 4 μm thick sections. The tissue sections were stained with hematoxylin and eosin (HE). Then, the samples were placed under a microscope and photographed at 100x and 400x fields of view as previously described [21].

2.17. Statistical Analysis. All statistical analyses were performed by using SPSS 24.0 (IBM Co., USA) and GraphPad Prism 8.0 (GraphPad Software, USA). Two-tailed Student's *t*-test and Pearson's correlation coefficient analysis were, respectively, adopted to analyze differences between groups or the correlations between ALKBH5, lncRNA, TMPO-AS1, EZH2, and IRAK4. Kaplan-Meier curve with the log-rank test was used to compare the survival time. A two-sided P value < 0.05 was considered statistically significant. Each experiment was performed in triplicate, and all data are presented as mean ± standard error of the mean (SEM).

3. Results

3.1. ALKBH5 Is Upregulated in AD Tissues and HASMCs Treated with AngII. In recent years, more and more evidence confirmed that m6A methylation modification acts a crucial role in various biological processes. However, hardly any studies have been conducted in AD [1, 2]. In the present study, to determine whether m6A modification participates in AD progress, the expression levels of multiple key genes involved in m6A modification, as enumerated in Section 1, were measured in 40 pairs of AD and normal arterial tissues. Higher levels of ALKBH5 and lower levels of KIAA1429 were confirmed in AD tissues compared with normal arterial tissues (Figure 1(a)). The results of western blot also revealed the low expression of KIAA1429 and the high expression of ALKBH5 in aortic tissues from AD patients compared with donors (Figure 1(b); Supplementary Fig. 1). The same results emerged when we detected their expression level in 20 pairs of normal and diseased aorta samples from the normal and AngII-induced AD mice by qRT-PCR and western blot (Figures 1(c) and 1(d); Supplementary Fig. 2). Moreover, we also detected ALKBH5 and KIAA1429 levels in HASMCs untreated and treated with AngII; as described in Section 2, the results consistent with the trends measured in tissues appearing (Figures 1(e) and 1(f)). Given the more drastic changes in the mRNA expression level of ALKBH5, we chose it as the research object of this study. Taken together, the aberrant expression of ALKBH5 in AD tissues derived from humans and mice and HASMCs treated with AngII was verified, suggesting that m6A modification might be indeed involved in the development of AD.

3.2. ALKBH5 Exacerbates AngII-Induced Inflammatory Response and Apoptosis of HASMCs and Increases the Incidence of AD in AngII-Infused Mice. To investigate the biological function of m6A modification in HASMCs, we overexpressed or knocked down ALKBH5, a vital m6A demethylase exhibiting a negative correlation with m6A levels, via transfection with LV-ALKBH5 and sh-ALKBH5 in HASMCs, respectively. The interference effects of transfection were detected by qRT-PCR and western blot (Figures 2(a) and 2(b)). Subsequently, we first measured the levels of proinflammatory mediators in the supernatant of the cell culture medium using ELISA. The results showed that the secretion of inflammatory cytokines, including IL-1β, IL-6, IL-17A, and TNF-α, were greatly elevated in the AngII-treated groups. Meanwhile, the overexpression of ALKBH5 evidently enhanced the promoting effect of AngII on their secretion (Figures 2(c)–2(f)). On the contrary, we also found that ALKBH5 knockdown could suppress the expression of the genes corresponding to the aforesaid inflammatory factors in HASMCs by using qRT-PCR (Figures 2(g)–2(j)). Furthermore, nuclear factor kappa B (NFκB) is a key regulator of immune development, immune responses, and inflammation. Its activation leads to the activation of associated inflammatory pathways, and the level of phosphorylation of NFκB (pNFκB) in cells can reflect the level at which it is activated [22]. Herein, we investigated the influence of ALKBH5 on the levels of pNFκB. The result showed that the expression of pNFκB was upregulated in the AngII-treated group and ALKBH5 significantly enhanced the promoting effect of AngII on it (Figure 2(k); Supplementary Fig. 3). Next, we performed TUNEL assay and observed that AngII could induce apoptosis of HASMCs. Moreover, this effect was significantly enhanced when ALKBH5 was overexpressed and weakened when it is silenced (Figure 2(l); Supplementary Fig. 4).

To further examine whether ALKBH5 affects AD progression in vivo, after 28 days of AngII infusion, we observed the incidence of AD and the survival time of mice in multiple groups that received different AAV9 injections. The results revealed that AngII could significantly increase the incidence of AD, and this impact was significantly enhanced by the overexpression of ALKBH5 and reduced by its knockdown (Figure 2(m)). Consistent with the above trends, mice in the AngII+LV-ALKBH5 group and AngII+sh-ALKBH5 group had the shortest and longest lifespans, respectively (Figure 2(n)). In this study, we confirmed whether the mice had AD through gross observation and HE staining of histological observation of their aortic tissue. Gross observations showed that the aorta of AD mice was significantly congested and thickened, and histological observations confirmed the destruction of aortic tissue and the formation of AD (Figures 2(o) and 2(p)). Collectively, our findings revealed that ALKBH5 can exacerbate AngII-induced inflammatory response and apoptosis of HASMCs, as well as the progression of AD in vivo.

3.3. lncRNA TMPO-AS1 Is a Downstream Target of ALKBH5. Two previous studies have confirmed that METTL3, a key methylase upregulating m6A levels, can affect cellular function by regulating specific downstream lncRNA in cancer [3, 4]. We herein identified whether ALKBH5 also functions in HASMCs via modulating its target lncRNAs. Firstly, through using lncRNA microarrays, we obtained lncRNA
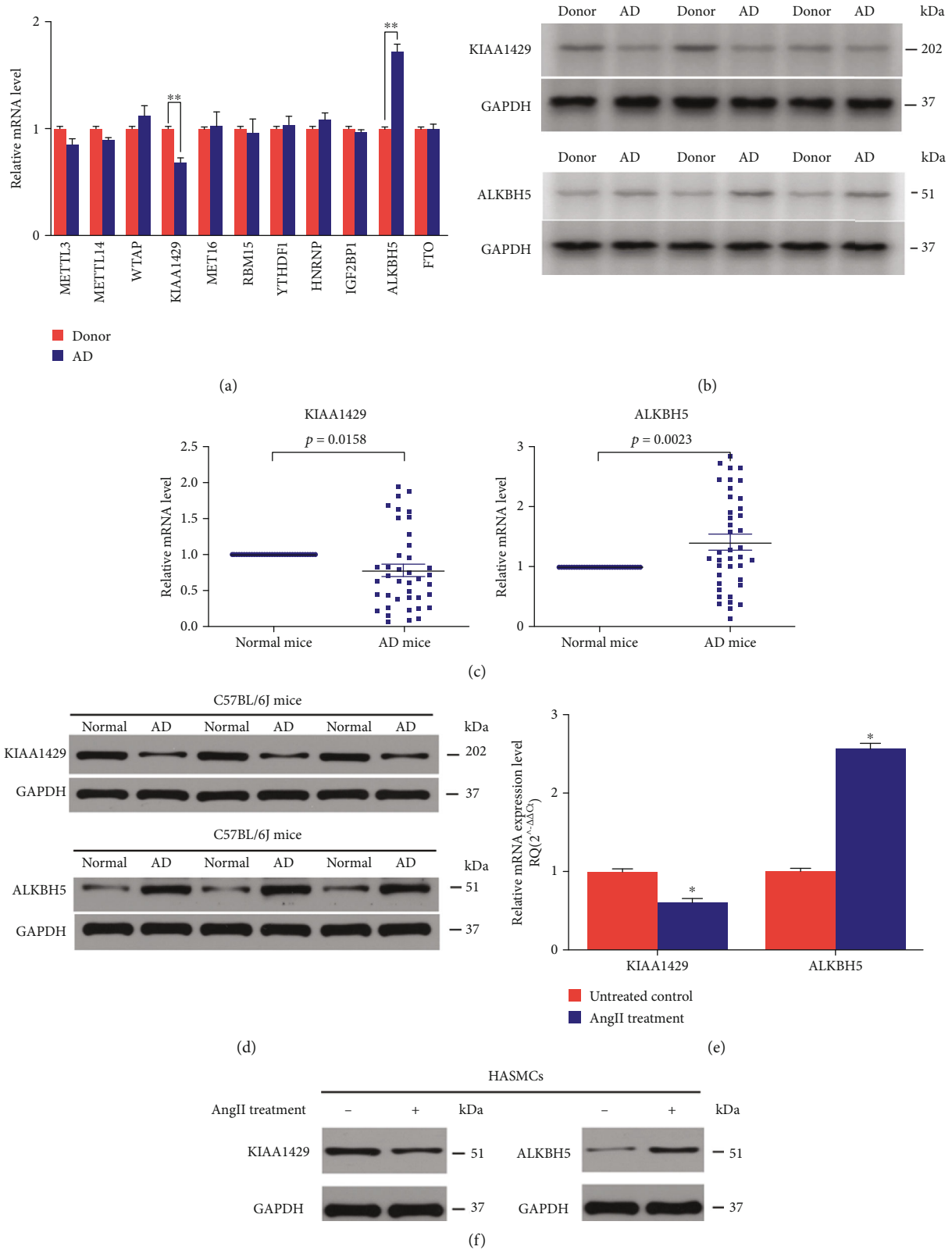
FIGURE 1: ALKBH5 is upregulated in AD tissues and HASMCs treated with AngII. (a) The expression levels of multiple key genes related to m6A modification were measured in 40 pairs of the AD and normal arterial tissues. (b) The results of western blot also revealed the low expression of KIAA1429 and the high expression of ALKBH5 in aortic tissues from AD patients. (c, d) The results of western blot also revealed the low expression of KIAA1429 and the high expression of ALKBH5 in aortic tissues from AD mice compared with normal mice. (e, f) The results of western blot also revealed the low expression of KIAA1429 and the high expression of ALKBH5 in HASMCs treated with AngII. Data represented the mean ± SEM from three independent experiments, $^{*}P < 0.05$, $^{**}P < 0.01$.

(a)

(b)

(c)

(d)

(e)

(f)

Figure 2: Continued.

(g)

(h)

(i)

(j)

(k)

FIGURE 2: Continued.

(l)

(m)

(n)

(o)

(p)
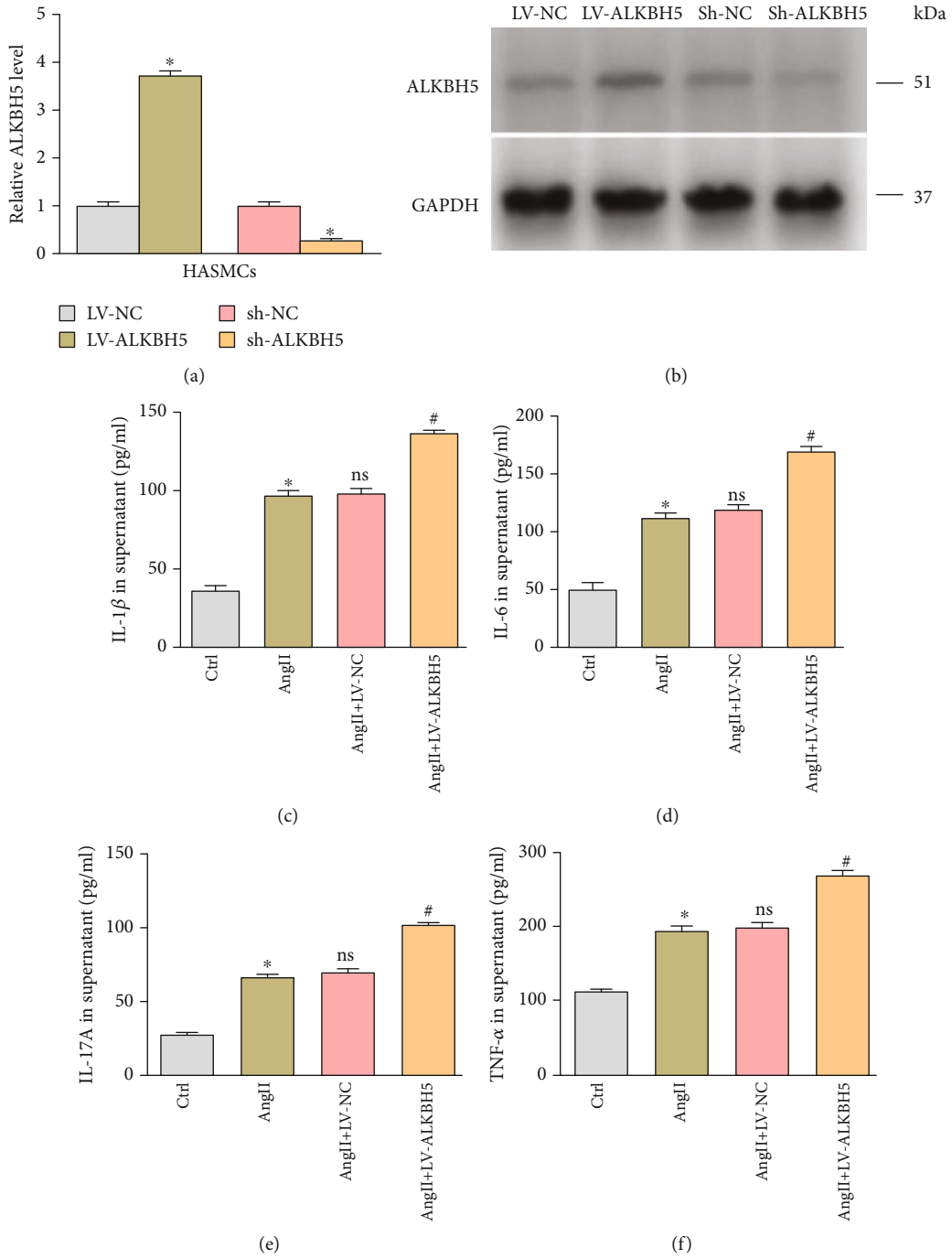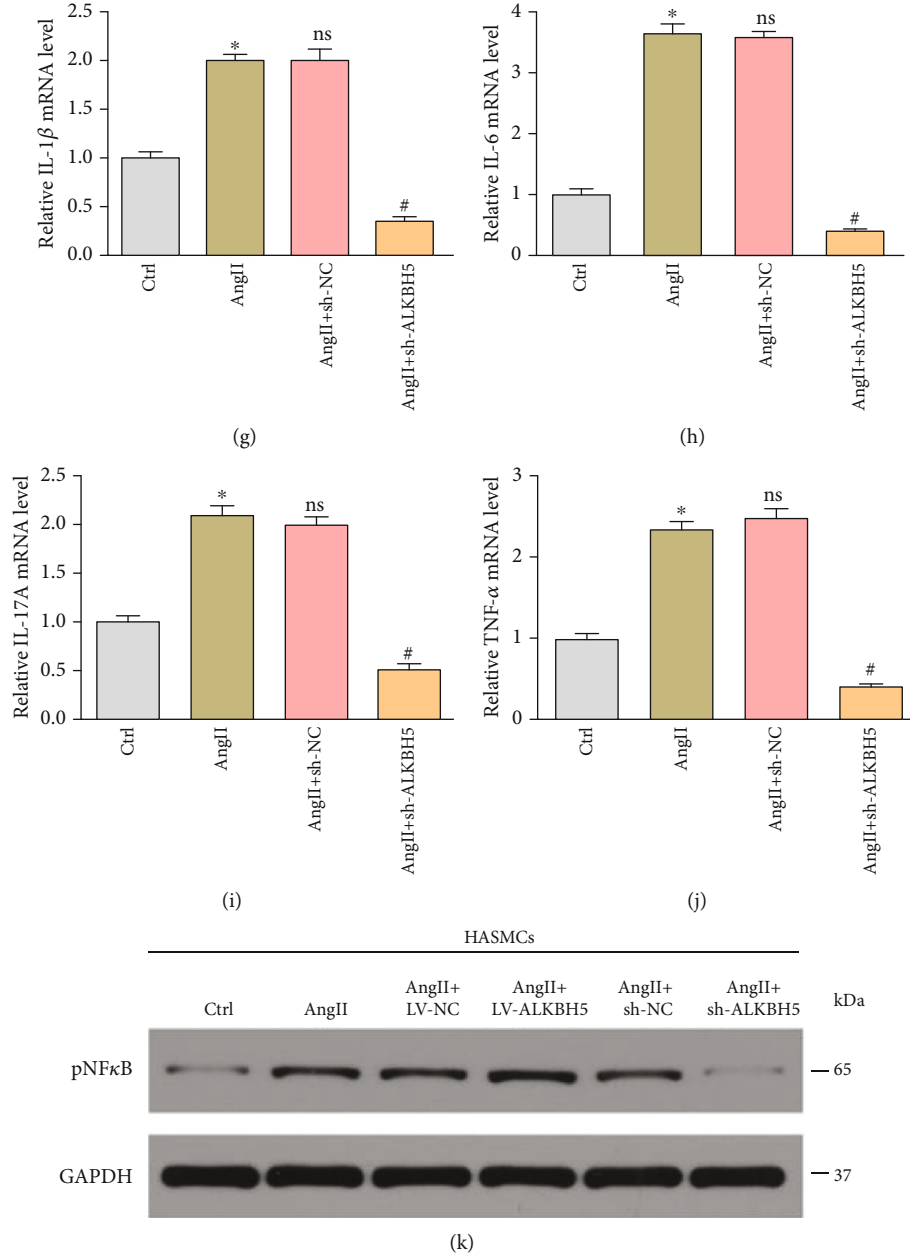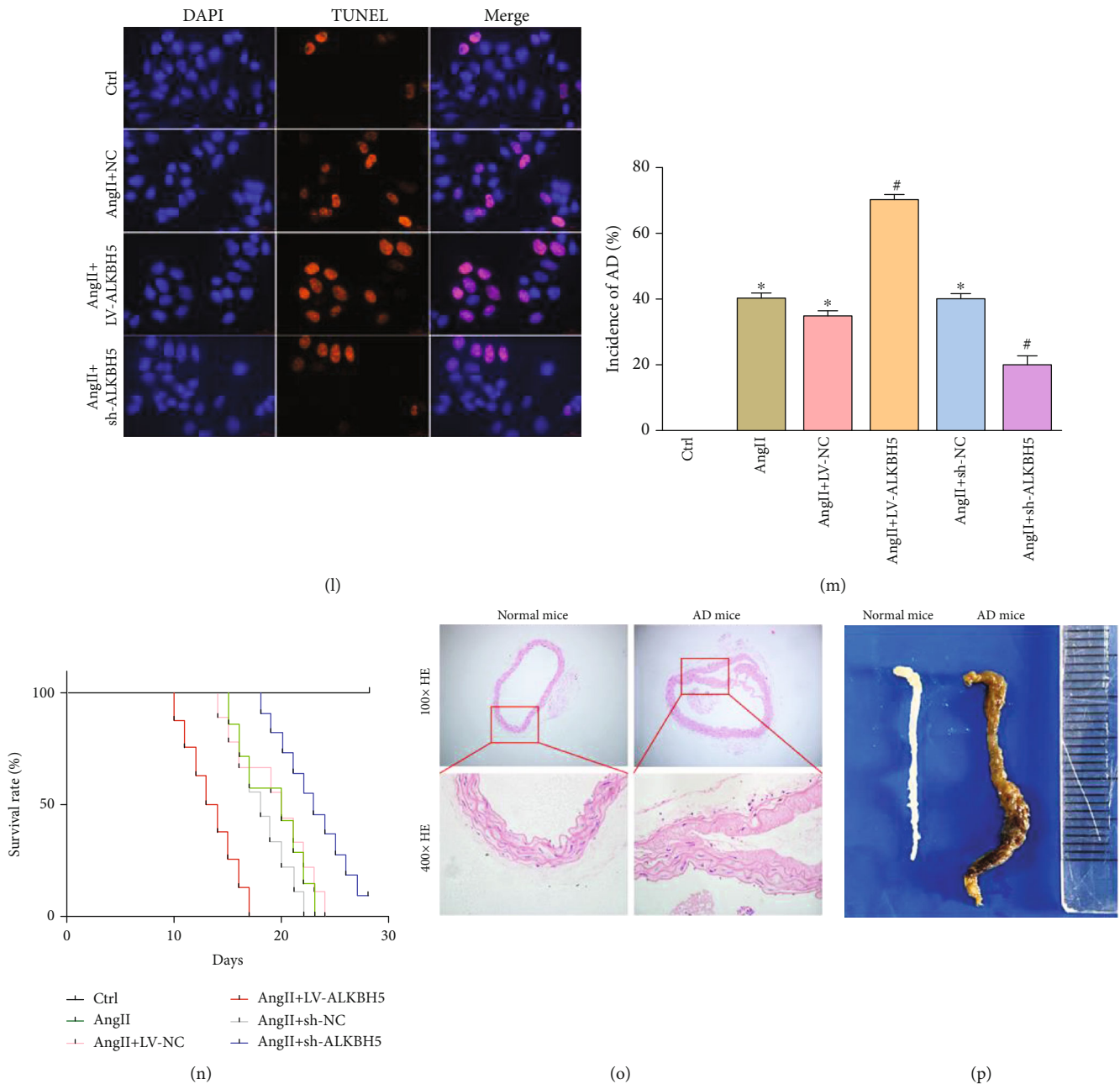
Figure 2: ALKBH5 exacerbates AngII-induced inflammatory response and apoptosis of HASMCs and increases the incidence of AD in AngII-infused mice. (a, b) The interference effects of LV-ALKBH5 and sh-ALKBH5 on ALKBH5 expression in HASMCs were detected by qRT-PCR and western blot. (c–f) The overexpression of ALKBH5 evidently enhanced the promoting effect of AngII on the secretion of inflammatory cytokines in HASMCs. (g–j) ALKBH5 knockdown could suppress the expression of the genes corresponding to the aforesaid inflammatory factors in HASMCs. (k) The expression of pNFκB was upregulated in the AngII-treated group and ALKBH5 significantly enhanced the promoting effect of AngII on it. (l) AngII could induce HASMC apoptosis, and this effect was significantly enhanced when ALKBH5 was overexpressed and weakened when it is silenced. (m) AngII could significantly increase the incidence of AD, and this impact was significantly enhanced by the overexpression of ALKBH5 and reduced by its knockdown. (n) Mice in the AngII+LV-ALKBH5 group and AngII+sh-ALKBH5 group had the shortest and longest lifespans, respectively. (o, p) Gross observations showed that the aorta of AD mice was significantly congested and thickened, and histological observations confirmed the destruction of aortic tissue and the formation of AD. Data represented the mean ± SEM from three independent experiments, $^*P < 0.05$ versus the Ctrl group; $^#P < 0.05$ versus the AngII+ LV-NC/sh-NC group; $^{ns}P > 0.05$ versus the AngII group.

expression profiles in aorta tissues from AD patients or donors and observed that 508 lncRNAs in AD specimens showed distinct fold changes, among which 282 were down-regulated and 226 upregulated (fold change < 0.5 or >1.8, $P < 0.05$). In combination with the bioinformatics analysis and literature review, from the above differentially expressed lncRNAs, 40 candidate lncRNAs that may be involved in AD progression were selected for hierarchical clustering

(a)

(b)

(c)

(d)

FIGURE 3: Continued.

(e)

(f)

Figure 3: Continued.

(g)

(h)

(i)

(j)

FIGURE 3: Continued.

(k)

(l)
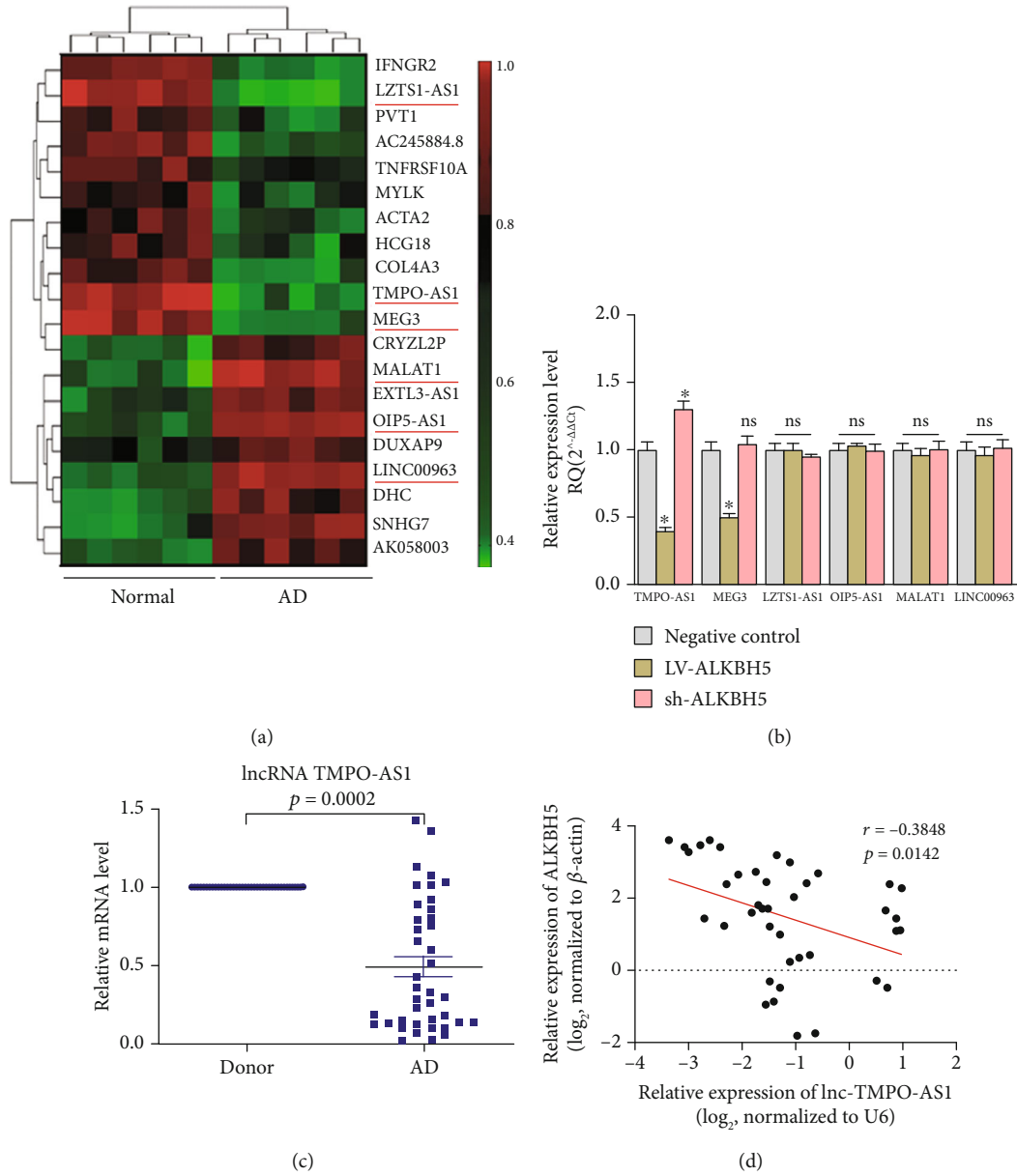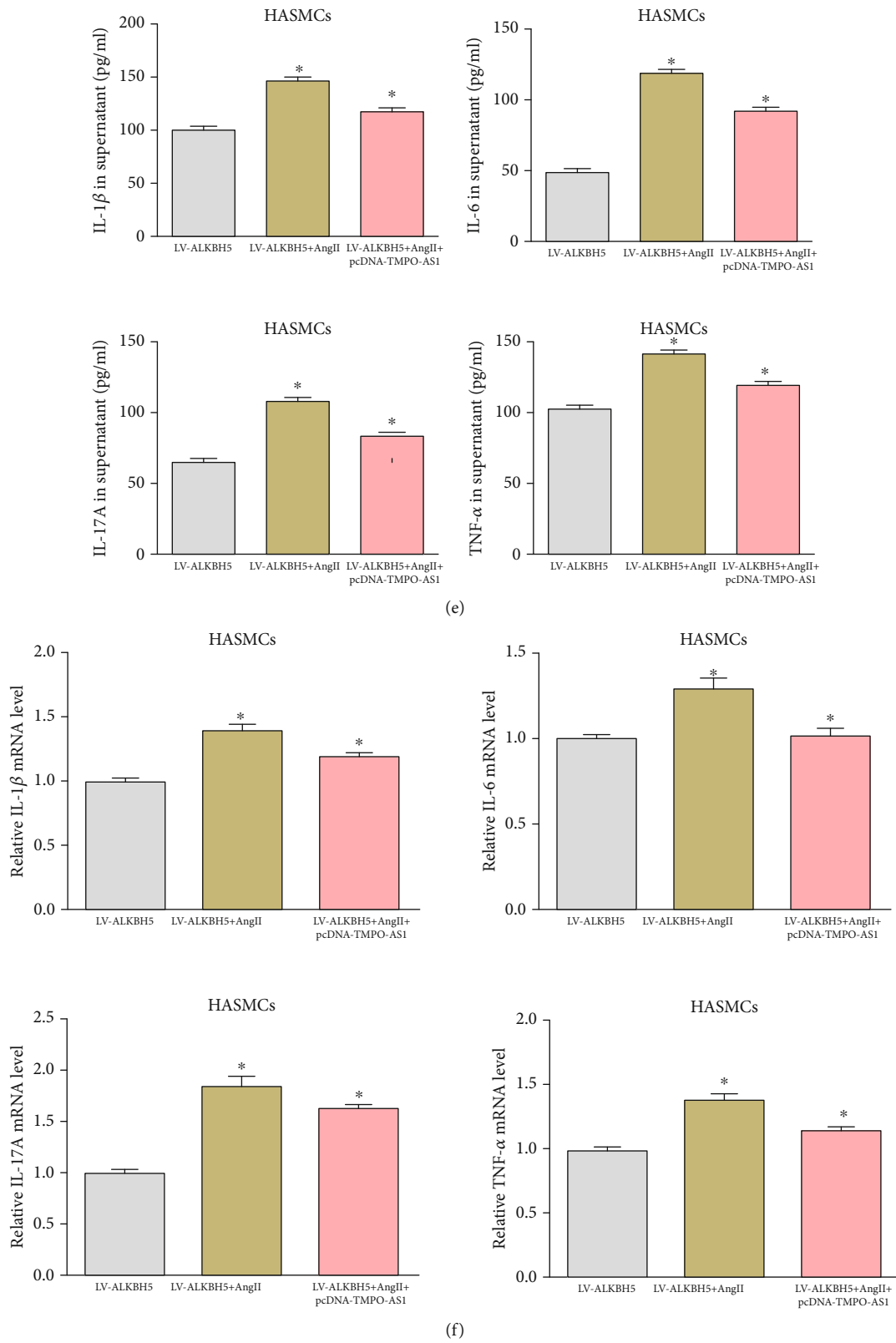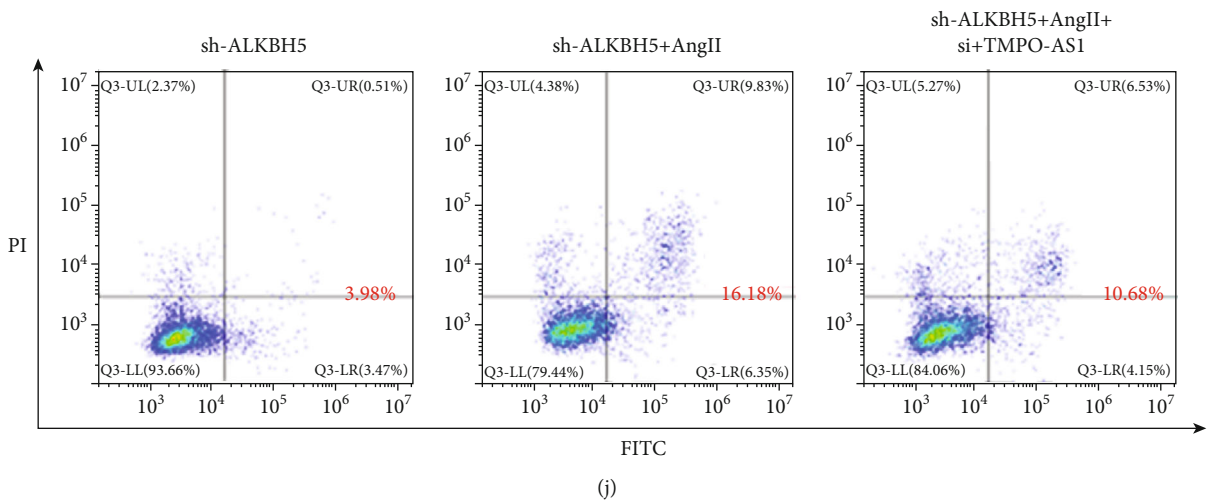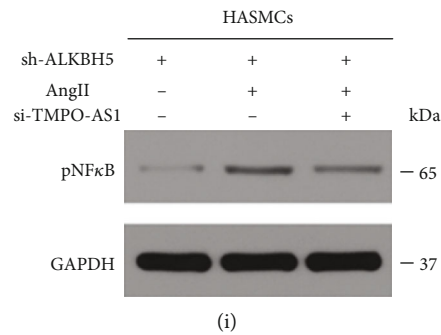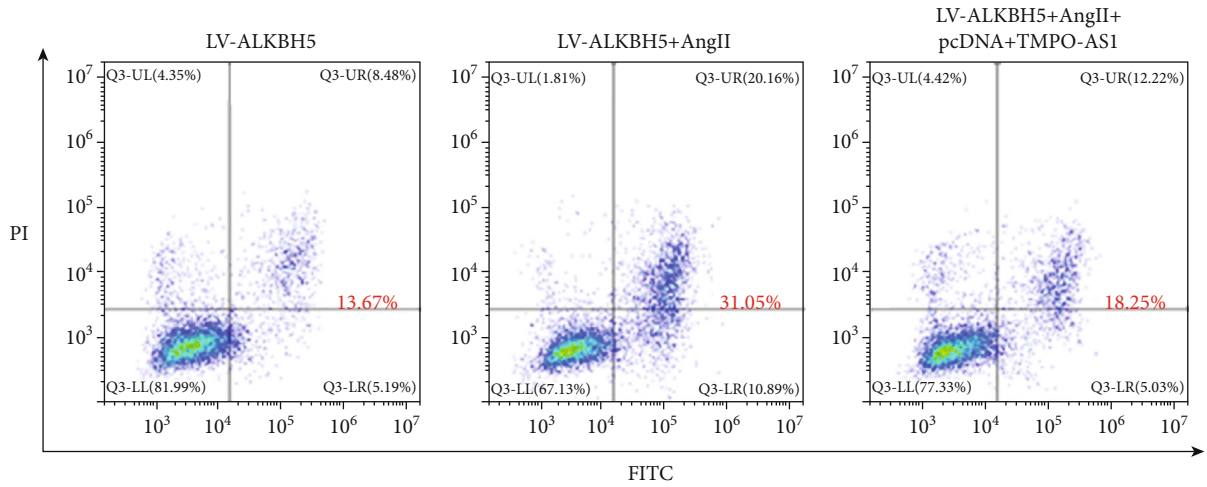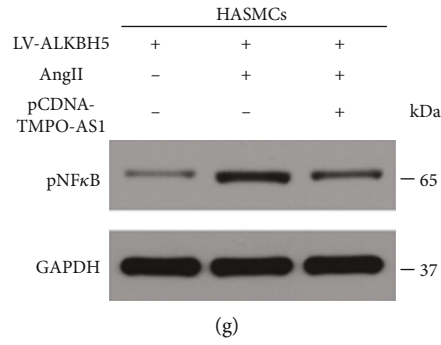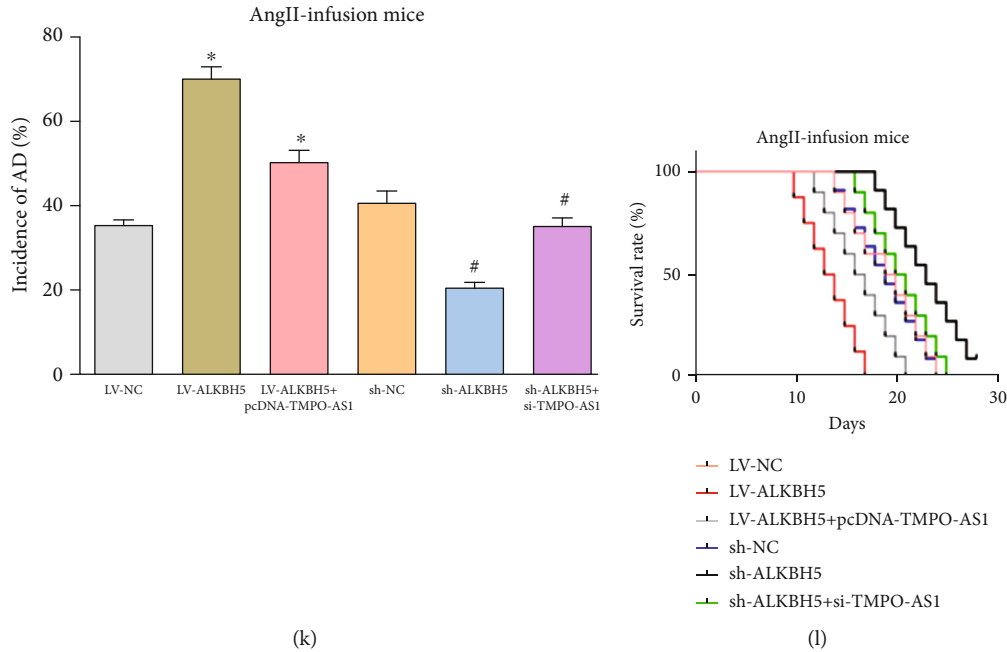
Figure 3: lncRNA TMPO-AS1 is a downstream target of ALKBH5. (a) 40 candidate lncRNAs that may be involved in AD progression were selected for hierarchical clustering analysis. (b) Only the expression of lnc-TMPO-AS1 was altered when ALKBH5 was either overexpressed or silenced. (c, d) The low expression of lnc-TMPO-AS1 in clinical samples and the significantly negative correlation between it and ALKBH5 were confirmed by qRT-PCR and Pearson's correlation coefficient analysis, respectively ($r = -0.438$, $P = 0.043$). (e–h) lnc-TMPO-AS1 upregulation could partly weaken the promoting effect of ALKBH5 overexpression on AngII-induced inflammatory response and apoptosis of HASMCs. (i, j) Downregulation of lnc-TMPO-AS1 could partly reverse the impact of ALKBH5 knockdown on the apoptosis of HASMCs induced by AngII. (k) lnc-TMPO-AS1 upregulation could partly reduce the stimulating effect of ALKBH5 overexpression on the incidence of AD in AngII-infused mice, while its knockdown could partly counteract the impact of ALKBH5 knockdown on this index. (l) lnc-TMPO-AS1 could prolong the survival time of mice and partly counteract the effect of ALKBH5. Data represented the mean ± SEM from three independent experiments, $^*P < 0.05$; ns represents no statistical difference between groups.

analysis (Figure 3(a)). Next, we chose several of these lncRNAs with the most significant changes and determined the variations in their expression levels when ALKBH5 was overexpressed or silenced in cells. The results showed that lncRNA TMPO-AS1 and MEG3 were remarkably downregulated after ALKBH5 overexpression. However, when ALKBH5 was silenced, only the expression of lncRNA TMPO-AS1 was markedly enhanced (Figure 3(b)). Based on this, we chose lnc-TMPO-AS1 for the following study. At the tissue level, its low expression in clinical samples and the significantly negative correlation between it and ALKBH5 were confirmed by qRT-PCR and Pearson's correlation coefficient analysis, respectively (Figures 3(c) and 3(d); $r = -0.438$, $P = 0.043$).

To explore the biological function of lnc-TMPO-AS1 in AD progression as a downstream target of ALKBH5, we first upregulated lnc-TMPO-AS1 in stable ALKBH5-overpressing HASMCs (Supplementary Fig. 5A) and observed that its upregulation could partly weaken the promoting effect of ALKBH5 overexpression on AngII-induced inflammatory response and apoptosis of HASMCs (Figures 3(e)–3(h); Supplementary Fig. 6A). Consistently, when we silenced lnc-TMPO-AS1 in stable ALKBH5-deleting HASMCs (Supplementary Fig. 5B), we found that the downregulation of lnc-TMPO-AS1 could partly reverse the impact of

ALKBH5 knockdown on the inflammatory response and apoptosis of HASMCs induced by AngII (Figures 3(i) and 3(j); Supplementary Fig. 6B and 7).

To further elucidate the influence of lnc-TMPO-AS1 on AD development as a downstream effector of ALKBH5 in vivo, we implemented a gene-interference-function study in AngII-infused C57BL/6N mice. First, 1×10^{12} viral genome particles of adeno-associated virus 9 (AAV9), including AAV9-LV-NC, AAV9-LV-ALKBH5, AAV9-LV-ALKBH5/pcDNA-TMPO-AS1, AAV9-sh-NC, AAV9-sh-ALKBH5, or AAV9-sh-ALKBH5/si-TMPO-AS1 in $100\,\mu$l of saline were randomly injected through the tail vein to C57BL/6N mice. At 28 days after AngII infusion, the incidence of AD and the survival time of mice in multiple groups were counted and analyzed. The results indicated that lnc-TMPO-AS1 upregulation could partly reduce the stimulating effect of ALKBH5 overexpression on the incidence of AD in AngII-infused mice, while its knockdown could partly counteract the impact of ALKBH5 knockdown on this index (Figure 3(k)). Consistent with the above results, lnc-TMPO-AS1 could prolong the survival time of mice and partly counteract the effect of ALKBH5 (Figure 3(l)). Taken together, our findings revealed that lnc-MPO-AS1 is a downstream target for ALKBH5 to exert its influence on AD progression in vitro and vivo.

(a)

(b)

(c)

(d)

(e)

(f)

Figure 4: Continued.

(g)

(h)
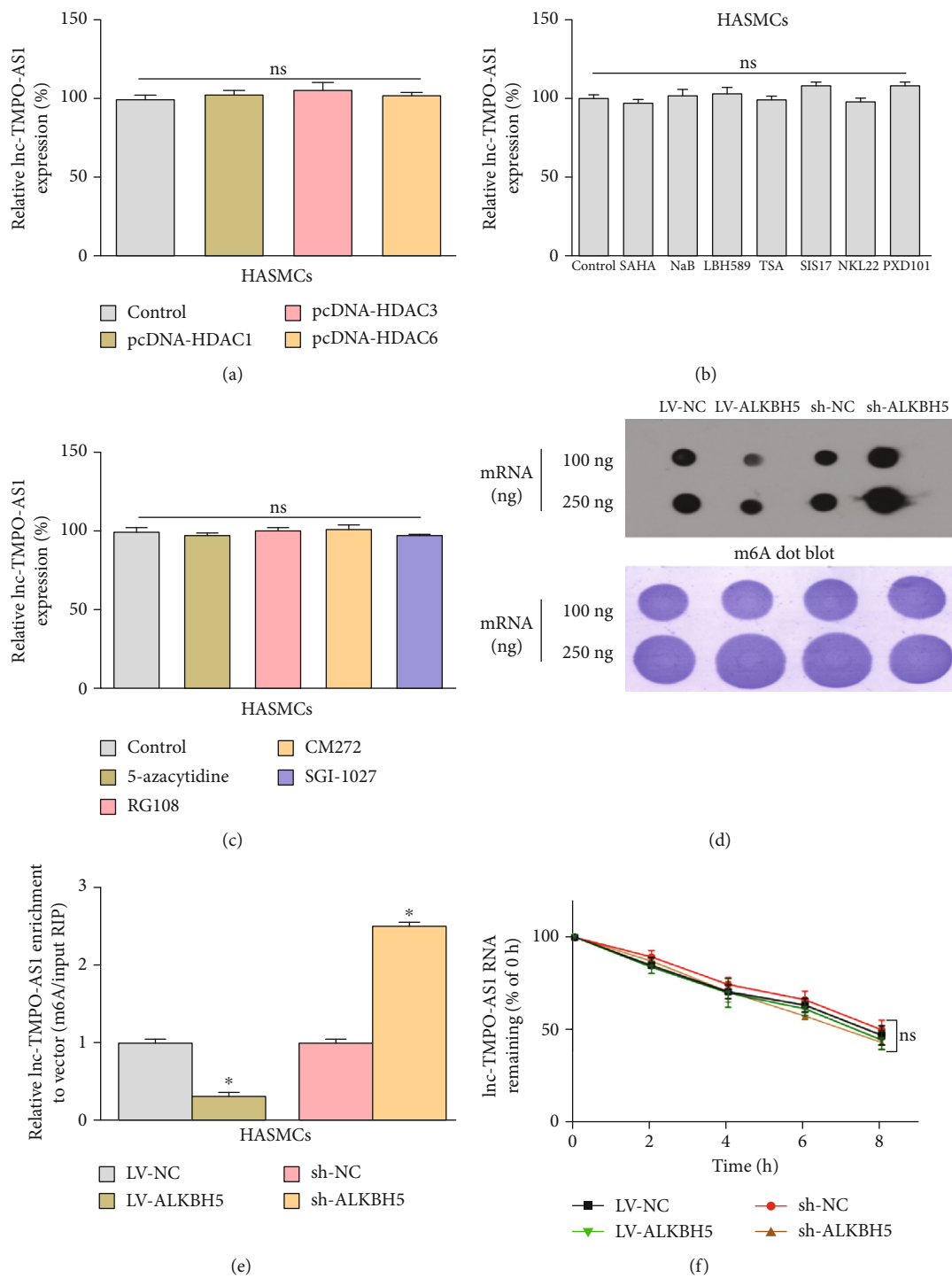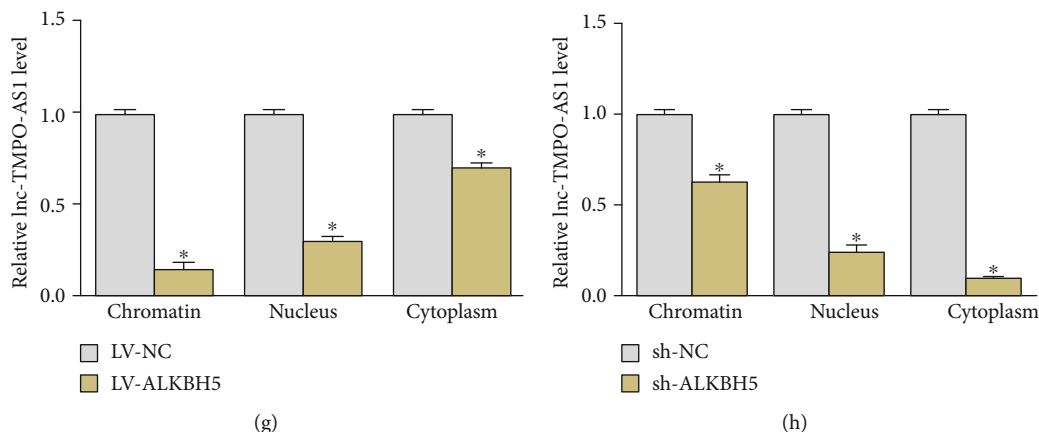
Figure 4: ALKBH5 downregulates lncRNA TMPO-AS1 through m6A demethylation in HASMCs. (a) DNA methylation might not be related to the lnc-TMPO-AS1 expression level in HASMCs. (b, c) Histone acetylation had no significant influence on the lnc-TMPO-AS1 level in HASMCs. (d) M6A dot blot assay revealed that overexpression of ALKBH5 markedly reduced m6A level while silencing ALKBH5 increased this level in HASMCs. (e) M6A RIP-qPCR analysis showed 0.3- and 2.5-fold enrichment in m6A antibody levels of lnc-TMPO-AS1 in ALKBH5-overexpressing and ALKBH5 knockdown cells, respectively. (f) The level changes of ALKBH5 had no significant influence on the half-life of lnc-TMPO-AS1. (g, h) Subcellular fractionation analysis indicated that ALKBH5 overexpression could apparently decrease the localization of lnc-TMPO-AS1 to chromatin while ALKBH5 knockdown enhance its accumulation in chromatin. Data represented the mean ± SEM from three independent experiments, $*P < 0.05$; ns represents no statistical difference between groups.

3.4. ALKBH5 Downregulates lncRNA TMPO-AS1 through m6A Demethylation in HASMCs. Recent progress in epigenetic regulation has revealed the involvement of m6A modification in various RNAs, including lncRNAs [5–7]. We then wondered whether ALKBH5 also regulated lnc-TMPO-AS1 by m6A modification and therefore began to explore the underlying epigenetic mechanisms responsible for lnc-TMPO-AS1 downregulation. Firstly, to investigate whether DNA methylation was involved in lnc-TMPO-AS1 downregulation, we treated HASMCs with multiple DNA methyltransferase inhibitors, including RG108, CM272, SGI-1027, and 5-azacytidine. Then, their effects on lnc-TMPO-AS1 expression level were examined, whereas no significant results were observed, suggesting that DNA methylation might not be related to the lnc-TMPO-AS1 expression level in HASMCs (Figure 4(a)). Moreover, since it had been previously reported that histone acetylation could regulate lncRNA expression [8, 9], we investigated its role in lnc-TMPO-AS1 expression via treating HASMCs with various histone deacetylase (HDAC) inhibitors, including SAHA, NaB, LBH589, TSA, SIS17, NKL22, and PXD101. The data revealed that these HDAC inhibitors had no significant influence on the lnc-TMPO-AS1 level in HASMCs (Figure 4(b)). This conclusion was further confirmed by results that indicated that overexpression of HDAC, such as HDAC1, HDAC3, and HDAC6, also had no impact on lnc-TMPO-AS1 expression in HASMCs (Figure 4(c)).

Subsequently, to identify whether ALKBH5 depends on m6A demethylation to reduce the expression of lnc-TMPO-AS1 in HASMCs, we first determined the effect of ALKBH5 on m6A level using m6A dot blot assay and found that the overexpression of ALKBH5 markedly reduced m6A level, while silencing ALKBH5 increased this level in HASMCs (Figure 4(d)). Meanwhile, m6A RIP-qPCR analysis showed 0.3- and 2.5-fold enrichment in m6A antibody levels of lnc-

TMPO-AS1 in ALKBH5 overexpressing and ALKBH5 knockdown cells, respectively (Figure 4(e)). These data revealed that ALKBH5 downregulates lnc-TMPO-AS1 expression via reducing its m6A level in HASMCs.

We then explored the deeper potential mechanisms associated with the m6A-mediated expression of lnc-TMPO-AS1 in HASMCs. By treating HASMCs with Act-D to terminate transcription, we observed that the level changes of ALKBH5 had no significant influence on the half-life of lnc-TMPO-AS1 (Figure 4(f)). In the following subcellular fractionation analysis, we found that ALKBH5 overexpression could apparently decrease the localization of lnc-TMPO-AS1 to chromatin while ALKBH5 knockdown enhance its accumulation in chromatin (Figures 4(g) and 4(h)), which might be attributed to the cause that ALKBH5 can reduce the stability of nascent lnc-TMPO-AS1. Collectively, these findings indicated that ALKBH5-mediated m6A demethylation is involved in the downregulation of lnc-TMPO-AS1, not by decreasing the stability of its transcript but possibly by decreasing the stability of nascent lnc-TMPO-AS1.

3.5. lncRNA TMPO-AS1 Exhibits Its Biological Roles in HASMCs via Regulating IRAK4. As is well known, lncRNA can regulate gene expression at the epigenetic, transcriptional, or posttranscriptional levels [10]. To elucidate the regulatory role of lnc-TMPO-AS1 in HASMCs, we first screened out genes whose expression was affected by lnc-TMPO-AS1 using an RNA-sequencing analysis. As shown in Figure 5(a), the expression levels of a large number of genes changed significantly after the lnc-TMPO-AS1 knockdown. Subsequently, through extensive literature review, nine of these genes that may be associated with inflammation and apoptosis were selected to validate RNA-seq results. IRAK4 attracted our attention not only because it has been reported as an important molecule in many inflammatory

(a)

(b)

(c)

(d)

(e)

(f)

(g)

Figure 5: Continued.

(h)

(i)

(j)

(k)

(l)

(m)

(n)
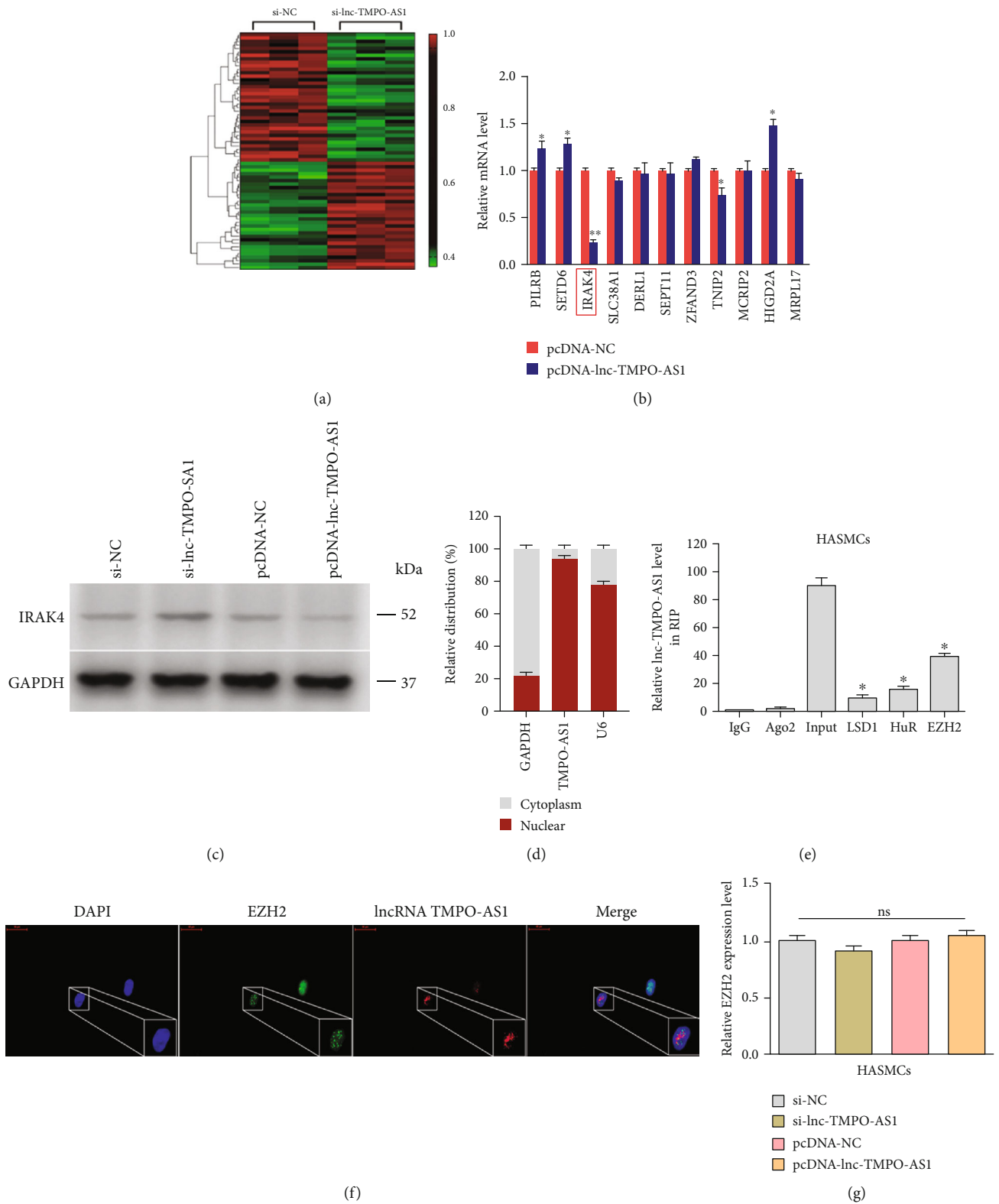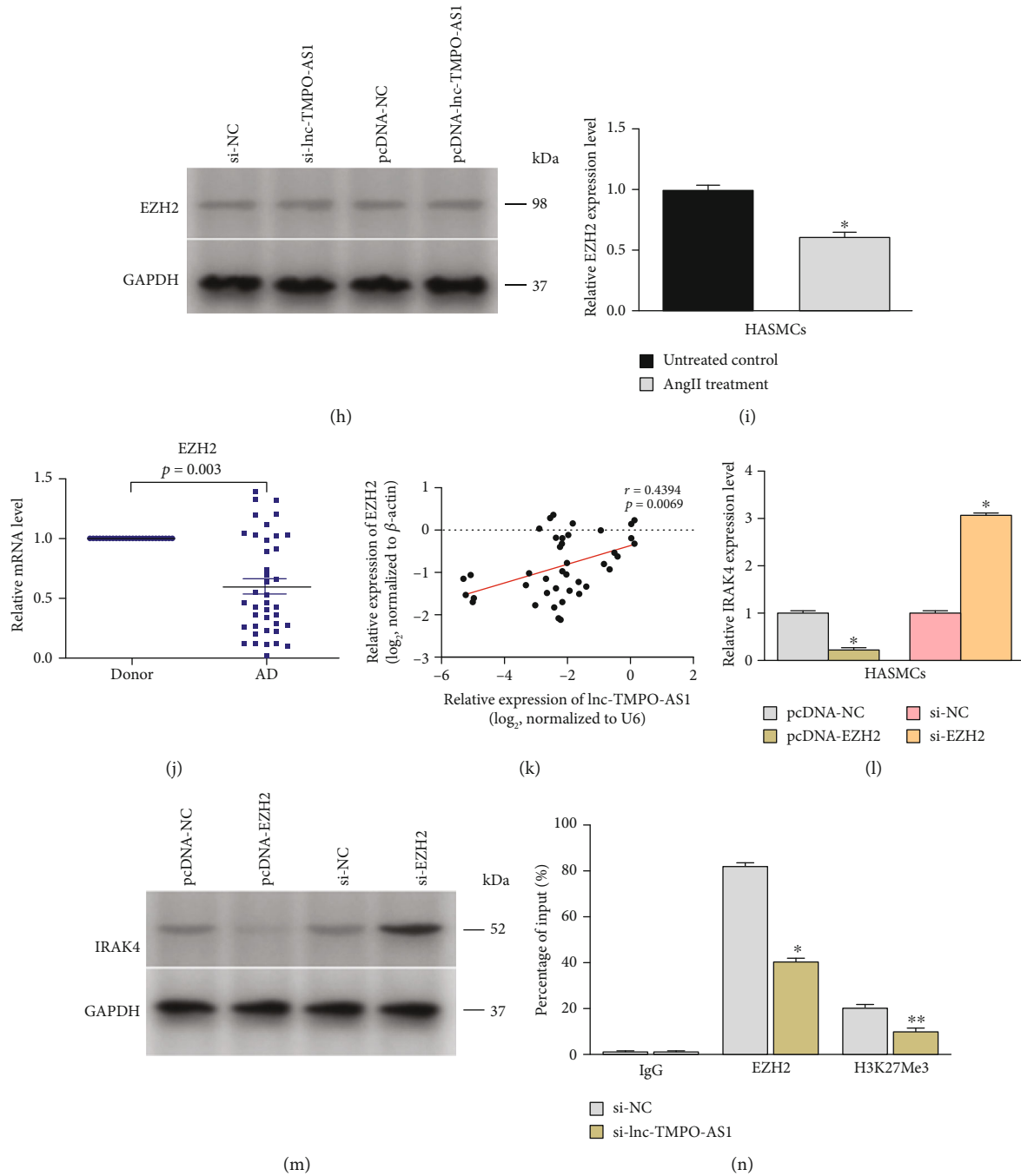
FIGURE 5: lncRNA TMPO-AS1 exhibits its biological roles in HASMCs via regulating IRAK4. (a) The expression levels of a large number of genes changed significantly after the lnc-TMPO-AS1 knockdown. (b) IRAK4 had the most dramatic expression change when lnc-TMPO-AS1 was overexpressed. (c) The protein level of IRAK4 was negatively regulated by lnc-TMPO-AS1. (d) The result of subcellular fractionation analyses indicated that lnc-TMPO-AS1 was predominantly located in the nucleus. (e) RIP assay revealed that lnc-TMPO-AS1 can combine with HuR, LSD1, and EZH2, with the strongest binding to EZH2. (f) The signals of lnc-TMPO-AS1 and EZH2 were confirmed to be colocalized in HASMCs by FISH and immunofluorescence. (g, h) No significant changes in EZH2 expression appeared in both pcDNA-TMPO-AS1 and si-TMPO-AS1 cells compared to the negative control. (i) EZH2 was downregulated in the AngII treatment group. (j, k) The expression of EZH2 was also reduced in aortas from AD patients and exhibited a positive correlation with lnc-TMPO-AS1 expression ($r = 0.4769$, $P = 0.0339$). (l, m) EZH2 knockdown significantly enhanced the mRNA and protein levels of IRAK4. (n) ChIP assays demonstrated that lnc-TMPO-AS1 knockdown reduced the binding of EZH2 and H3K27Me3 levels at the promoters of IRAK4. Data represented the mean ± SEM from three independent experiments; $^*P < 0.05$, $^{**}P < 0.01$.

and apoptotic pathways [11, 12] but also because it had the most dramatic expression change when lnc-TMPO-AS1 was overexpressed (Figure 5(b)). Western blot subsequently

confirmed at the protein level that IRAK4 was negatively regulated by lnc-TMPO-AS1 (Figure 5(c) and Supplementary Fig. 8). To elucidate explicitly how lnc-TMPO-AS1

(a)

(b)

(c)

(d)

(e)
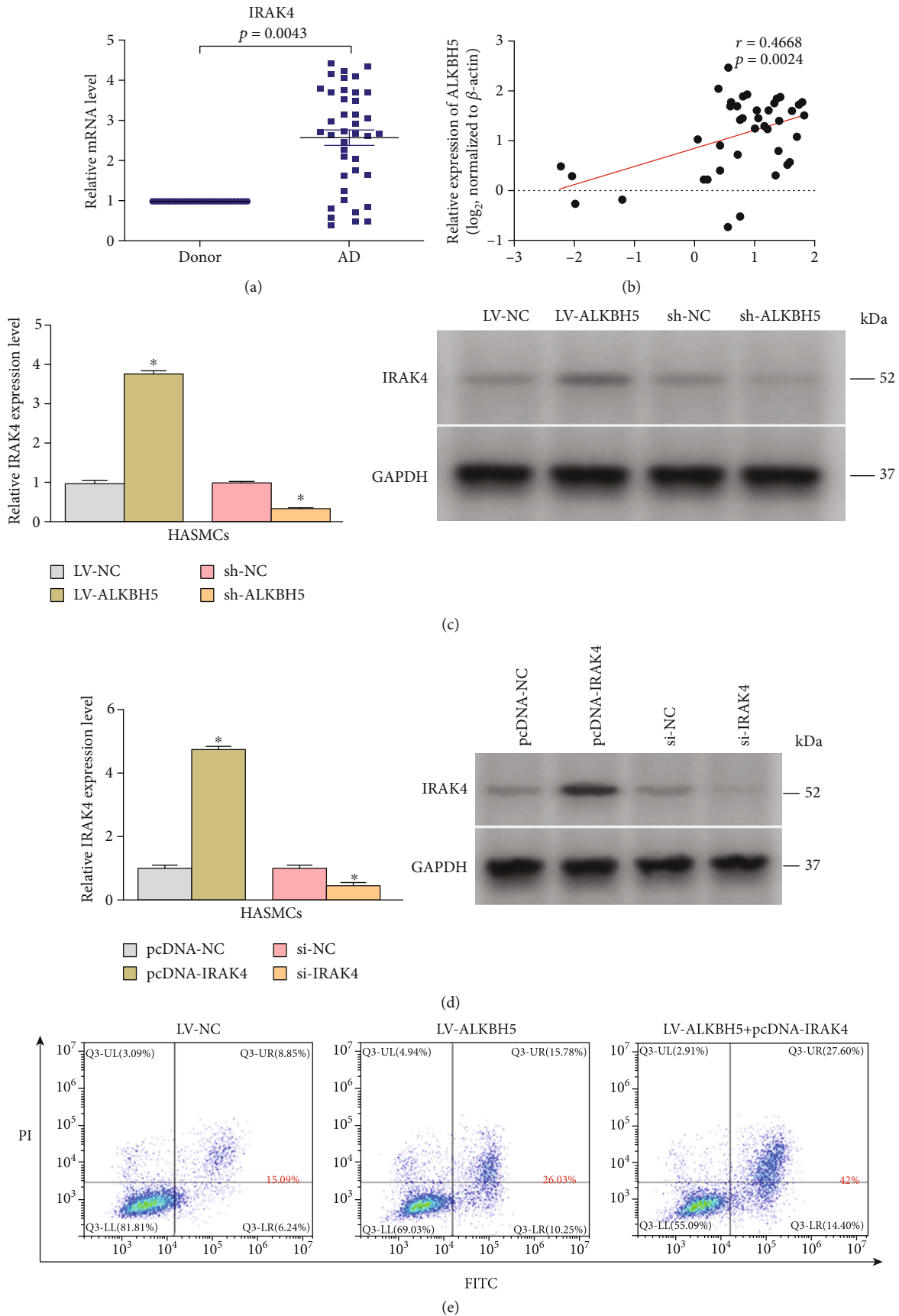
Figure 6: Continued.

(f)

(g)
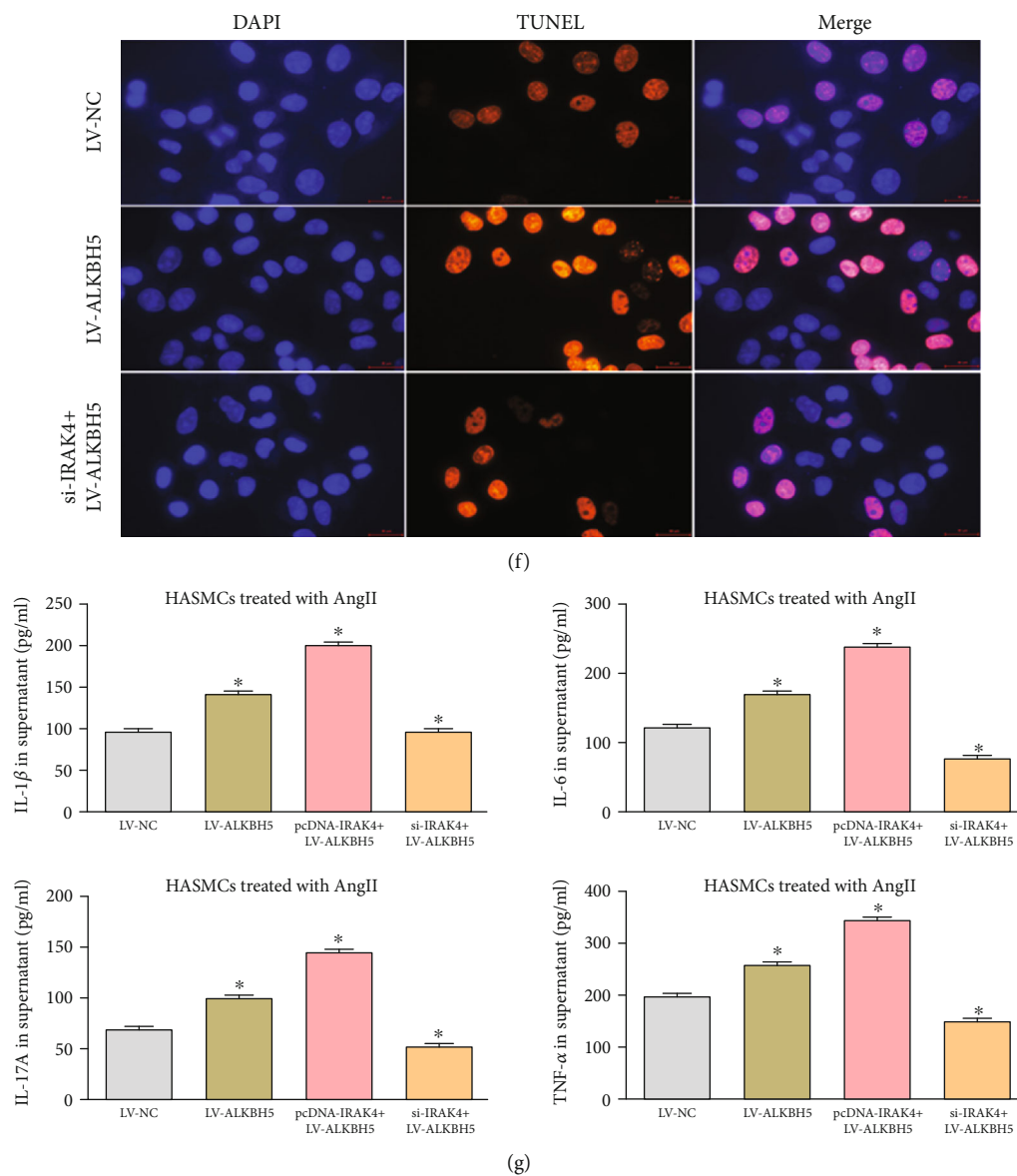
Figure 6: Continued.

(h)
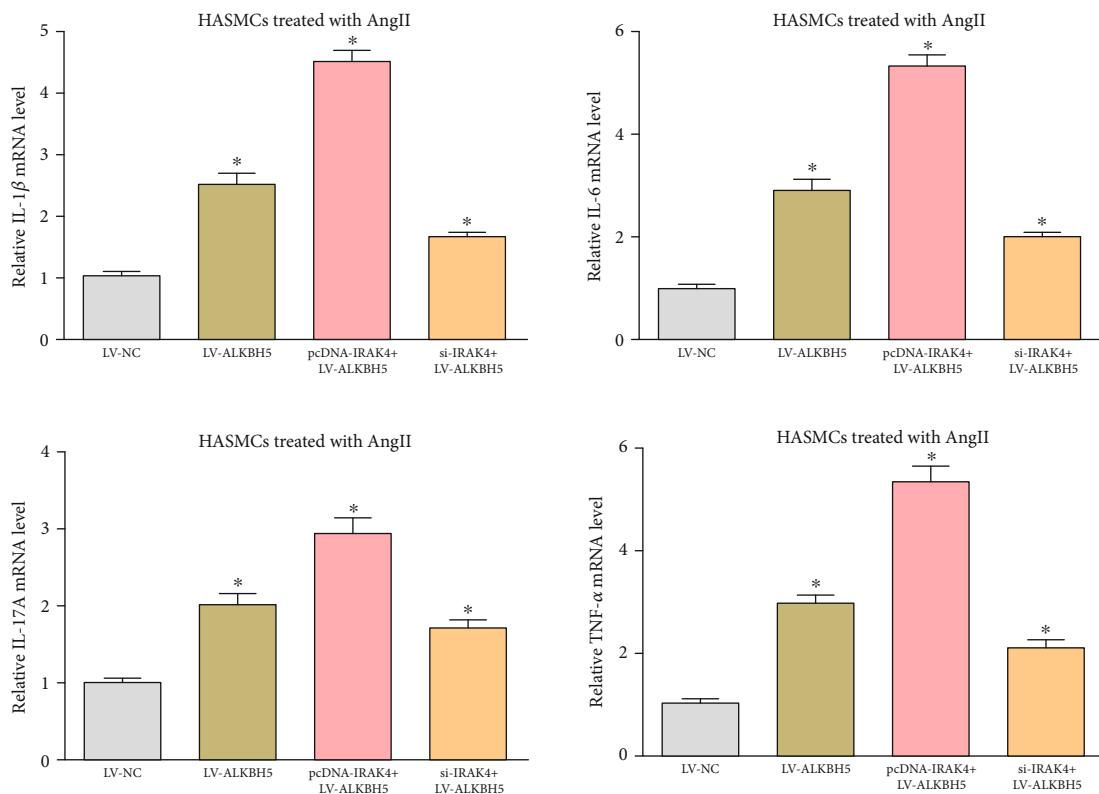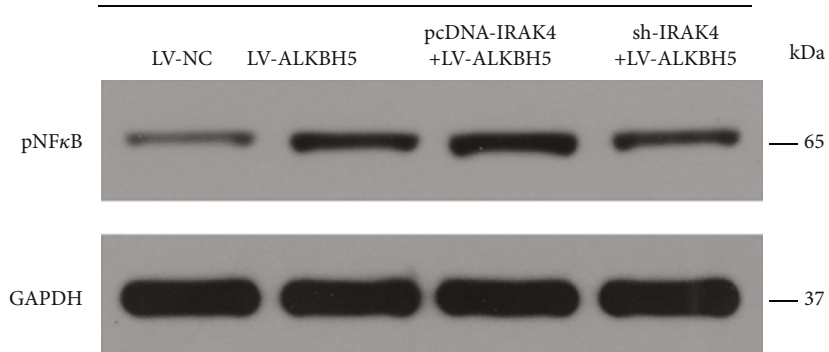
(i)

FIGURE 6: Continued.

(j)

(k)
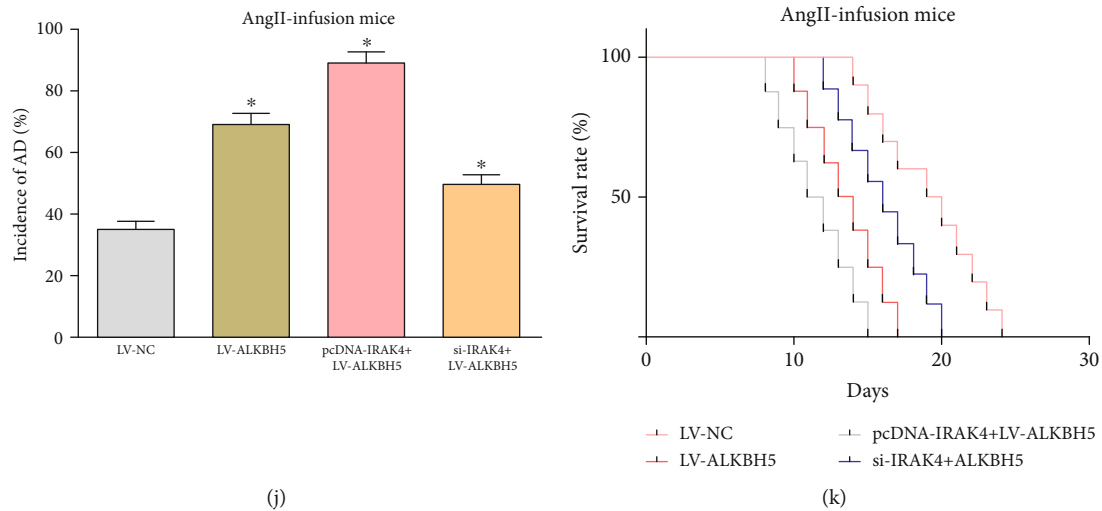
FIGURE 6: IRAK4 is positively correlated with ALKBH5 in terms of expression level and biological function. (a, b) The expression level of IRAK4 in 40 pairs of aorta tissues from AD patients and donors was measured and confirmed its negative correlation with ALKBH5 expression by Pearson's correlation coefficient analysis ($r = 0.7048$, $P = 0.0005$). (c) Overexpressing ALKBH5 promoted the expression of IRAK4 while ALKBH5 knockdown suppressed it. (d) The effects of interference on mRNA and protein levels of IRAK4 were confirmed. (e, f) IRAK4 could further promote AngII-induced HASMC apoptosis increased by ALKBH5 overexpression, while IRAK4 knockdown partly counteracted the proapoptotic effect caused by the overexpression of AKLBH5. (g, h) Overexpression of IRAK4 enhanced the hypersecretion of inflammatory cytokines and the high expression of inflammation-related genes caused by ALKBH5 overexpression while silencing IRAK4 could partially offset the proinflammatory effect of ALKBH5. (i) The level of pNFκB was upregulated by ALKBH5, and this effect could be further enhanced by the overexpression of IRAK4 or weakened by its knockdown. (j, k) IRAK4 overexpression or knockdown enhanced or partly offset the influences of ALKBH5 upregulation on the incidence of AD and survival time in mice. Data represented the mean ± SEM from three independent experiments, $^*P < 0.05$.

downregulates IRAK4 in HASMCs, we performed the following mechanistic analysis.

Given that the regulatory function of lncRNA is closely related to its intracellular distribution, we detected the distribution of lnc-TMPO-AS1 in HASMCs using subcellular fractionation analyses. The result indicated that lnc-TMPO-AS1 was predominantly located in the nucleus (Figure 5(d)), suggesting that lnc-TMPO-AS1 may function as a regulator at the epigenetic or transcriptional levels. Previous studies have reported that lncRNA can activate the transcription of its nearby genes in *cis* by promoting chromatin cyclization from transcriptional enhancers [13, 14]. We, therefore, searched the database for the location of lnc-TMPO-AS1 on chromosomes and identified several adjacent transcripts, including RUN4-41P, SNORA53, ADAF1, SLC25A3, IKBIP, ANKS1B, and AC008055.2 (Supplementary Fig. 9). The expression level detection of these genes showed no significant difference between the lnc-TMPO-AS1 overexpression or knockdown group and the control group (Supplementary Fig. 10A–B). Hence, the biological roles of lnc-TMPO-AS1 in HASMCs may not be involved in the *ris* regulatory mechanism.

Recent findings have revealed that lncRNAs can also regulate the expression of downstream genes via interacting with RNA binding proteins (RBPs), such as HuR, LSD1, and EZH2 [15, 16]. To confirm whether lnc-TMPO-AS1 regulates the downstream targets via binding RBPs, RIP was performed and revealed that lnc-TMPO-AS1 can combine with HuR, LSD1, and EZH2, with the strongest binding to EZH2 (Figure 5(e)). Furthermore, as shown in Figure 5(f),

the result that signals of lnc-TMPO-AS1 and EZH2 were confirmed to be colocalized in HASMCs by FISH and immunofluorescence, reinforced both the conclusion of the RIP assay (Figure 5(e)) and the results of subcellular fractionation analyses (Figure 5(d)). To further investigate the interaction between lnc-TMPO-AS1 and EZH2, we examined the expression changes of EZH2 after interfering with the level of lnc-TMPO-AS1 and no significant changes appeared in both pcDNA-TMPO-AS1 and si-TMPO-AS1 cells compared to the negative control (Figures 5(g) and 5(h)).

Enhancer of zeste homolog 2- (EZH2-) mediated trimethylation of histone 3 lysine 27 (H3K27Me3) is vital for the negative regulation of immunity intestinal inflammation [17]. To determine whether EZH2 is also involved in the regulation of AngII-induced HASMC inflammation and apoptosis, we first measured the expression level of EZH2 in HASMCs untreated and treated with AngII and observed that EZH2 was downregulated in the treatment group (Figure 5(i)). Consistently, in a subsequent qRT-PCR analysis between AD and normal aorta tissues, the expression of EZH2 was also reduced in aortas from AD patients and exhibited a positive correlation with lnc-TMPO-AS1 expression (Figures 5(j) and 5(k); $r = 0.4769$, $P = 0.0339$). More importantly, we observed that EZH2 knockdown significantly enhanced the mRNA and protein level of IRAK4, while the opposite results occurred when EZH2 was overexpressed (Figures 5(l) and 5(m)). Subsequently, we performed ChIP assays and demonstrated that EZH2 could bind directly to the promoter regions of IRAK4 and cause H3K27 trimethylation (H3K27Me3),
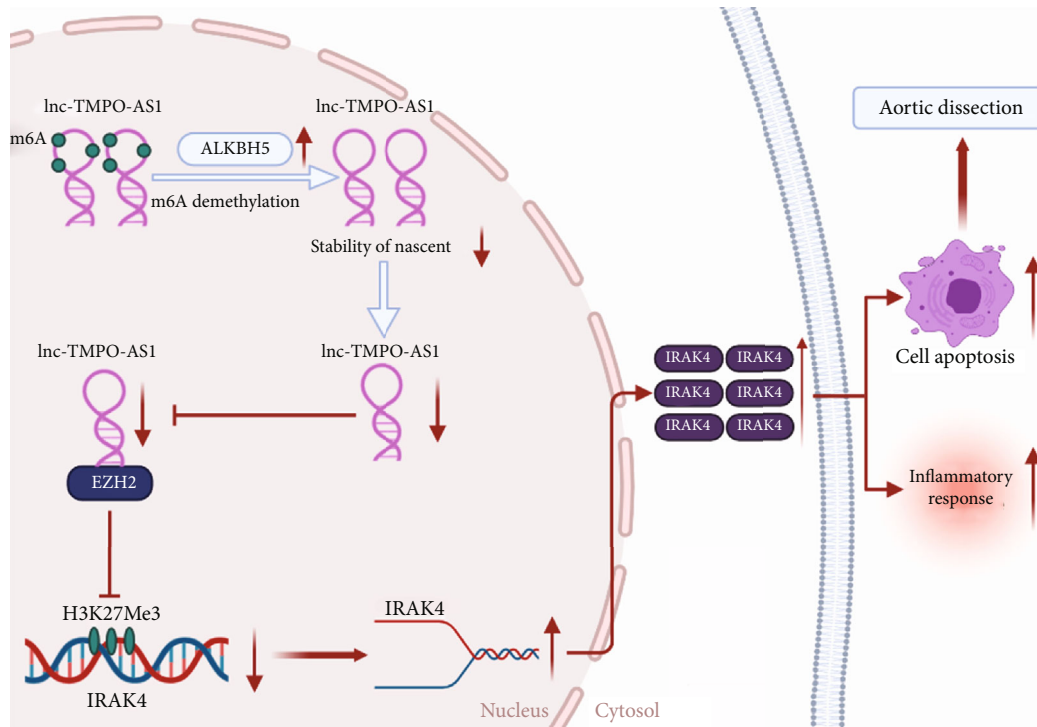
FIGURE 7: Schematic diagram of the mechanisms revealed in this study. ALKBH5 could aggravate AngII-induced inflammation response as well as apoptosis of HASMCs and increase the incidence of AD in AngII-infused mice through regulating lnc-TMPO-AS1/EZH2/IRAK4 signals in an m6A modification manner.

which results in the suppression of gene expression. Moreover, lnc-TMPO-AS1 knockdown reduced the binding of EZH2 and H3K27Me3 levels at the promoters of IRAK4 (Figure 5(n)). Taken together, these data indicated that lnc-TMPO-AS1 exhibits its functions in AngII-induced HASMC inflammation and apoptosis, at least partly, through downregulating IRAK4 at the epigenetic level by combining with EZH2.

3.6. IRAK4 Is Positively Correlated with ALKBH5 in terms of Expression Level and Biological Function. Since we had elucidated the regulatory relationship between ALKBH5 and lnc-TMPO-AS1, coupled with between lnc-TMPO-AS1 and IRAK4, we next investigated the relationship between ALKBH5 and IRAK4. Firstly, we measured the expression level of IRAK4 in 40 pairs of aorta tissues from AD patients and donors using qRT-PCR and confirmed its negative correlation with ALKBH5 expression by Pearson's correlation coefficient analysis (Figures 6(a) and 6(b); $r = 0.7048$, $P = 0.0005$). To determine whether this negative correlation was due to IRAK4 being regulated by ALKBH5, we detected the expression change of IRAK4 after interfering with ALKBH5. The results revealed that overexpressing ALKBH5 promoted the expression of IRAK4 while ALKBH5 knockdown suppressed it (Figure 6(c)). Furthermore, to explore the relationship between IRAK4 and ALKBH5 in terms of biological function, we elevated the IRAK4 level using pcDNA-IRAK4 or attenuated it with si-IRAK4 in ALKBH5-overexpressing HASMCs and a series of restoration assays were performed. The effects of interference on

mRNA and protein levels of IRAK4 were shown in Figure 6(d). Flow cytometry and TUNEL assay revealed that upregulation of IRAK4 could further promote AngII-induced HASMC apoptosis increased by ALKBH5 overexpression, while IRAK4 knockdown partly counteracted the proapoptotic effect caused by the overexpression of AKLBH5 (Figures 6(e) and 6(f) and Supplementary Fig. 11). Consistently, ELISA and qRT-PCR confirmed that the overexpression of IRAK4 enhanced the hypersecretion of inflammatory cytokines and the high expression of inflammation-related genes caused by ALKBH5 overexpression while silencing IRAK4 could partially offset the proinflammatory effect of ALKBH5 (Figures 6(g) and 6(h)). Moreover, we also found that the level of pNFκB was upregulated by ALKBH5 and this effect could be further enhanced by the overexpression of IRAK4 or weakened by its knockdown. (Figure 6(i) and Supplementary Fig. 12). In in vivo experiments, IRAK4 overexpression or knockdown enhanced or partly offset the influences of ALKBH5 upregulation on the incidence of AD and survival time in mice (Figures 6(j) and 6(k)). To sum up, these results identified that IRAK4 is positively correlated with ALKBH5 in terms of expression level and biological function in HAMSCs.

4. Discussion

Nowadays, with the maturation of m6A sequence technology, m6A modification has become a hotspot for research in RNA regulation-related fields [23]. Recently, accumulating evidence has revealed the pivotal roles of m6A modification

in noncoding RNAs in a series of physiological and biochemical processes, including cell proliferation and apoptosis, stem cell self-renewal, fate, and functions of lncRNAs, maturation of pri-miRNA, and RNA-protein interactions [24, 25]. However, most of the above findings are confined to tumor research, and studies in the cardiovascular system remain quite lacking. In this study, our results revealed that ALKBH5, a major m6A demethylase, could exacerbate AngII-induced inflammation damage and apoptosis of HASMCs. As far as we know, this is the first in-depth study on the involvement of ALKBH5 in AD progression through regulating the m6A modification of lncRNAs.

We firstly identified the high expression of ALKBH5, in AD tissues and HASMCs treated with AngII. Then, we demonstrated that ALKBH5 could exacerbate AngII-induced HASMC inflammatory response as well as apoptosis and increase the incidence of AD in AngII-infused mice. Mechanistically, we explored the interrelationship between ALKBH5 and noncoding RNAs and finally identified lncRNA TMPO-AS1 as a downstream signaling target of ALKBH5 in HASMCs. More importantly, we further explored the specific way for ALKBH5 to downregulate lnc-TMPO-AS1 in an m6A modification manner. We first experimentally excluded the involvement of DNA methylation and histone acetylation in this regulatory process and then confirmed that ALKBH5 did not downregulate lnc-TMPO-AS1 though decreasing the stability of its transcript. Finally, we demonstrated that ALKBH5-mediated m6A demethylation is involved in the downregulation of lnc-TMPO-AS1 by decreasing the stability of nascent lnc-TMPO-AS1.

Subsequently, a series of mechanistic studies were conducted to further investigate the downstream effectors of the ALKBH5-lncRNA TMPO-AS1 axis and their regulatory mechanisms. It is well known that lncRNAs are defined as a class of functional noncoding RNA transcripts with more than 200 nucleotides in length and widely engaged in diverse biological processes. Although they cannot directly encode proteins, they can regulate gene expression at various levels, including the epigenetic, transcriptional, posttranscriptional, and translational levels [26]. Given a fact found by subcellular fractionation analyses and FISH assay that lnc-TMPO-AS1 is predominantly distributed in the nucleus of HASMCs, we inferred that lnc-TMPO-AS1 may function as a regulator at the epistatic or transcriptional level. Subsequently, we confirmed that lnc-TMPO-AS1 can directly combine with EZH2, an RNA binding protein, by RIP assay and revealed that EZH2 can bind directly to the promoter regions of IRAK4 and cause H3K27Me3, which leads to the suppression of gene expression through using ChIP assay. To enhance the preciseness of the regulatory pathway in this study, we directly investigated the direct relationship between ALKBH5 and IRAK4, the most downstream effectors in the pathway, in terms of expression level and biological functions and ultimately confirmed the positive correlation between them. Collectively, our data confirm our inference and demonstrated that the ALKBH5-lncRNA TMPO-AS1 axis exhibits its functions in AngII-induced HASMC inflammation and apoptosis, at least partly, through downregulating IRAK4 at the epigenetic level via combining with EZH2.

Despite our best efforts to design and experiment rigorously, the present study still has some limitations. One limitation is that the clinical tissue sample size needs to be further expanded, which could reduce the possibility of bias, such as age bias and gender bias. The main obstacle to obtaining a larger sample size is that normal aorta tissues are derived from donations in China and the number of heart donors declared brain dead is in short supply. Another limitation is that the regulation mechanism of m6A modification on lncRNA expression is still scarce and at the exploratory stage. Therefore, in addition to the regulation manner confirmed in this study, whether ALKBH5 also modulates lnc-TMPO-AS1 in other ways remains to be more comprehensively explored. Moreover, when we look for downstream targets of ALKBH5, we found that lncRNA TMPO-AS1 and MEG3 were remarkably downregulated after ALKBH5 overexpression. Interestingly, however, when ALKBH5 was silenced, only the expression of lncRNA TMPO-AS1 was markedly enhanced, while the level of MEG3 was almost unchanged. The underlying mechanism leading to this interesting phenomenon still needs to be further revealed by subsequent studies.

5. Conclusion

In summary, we demonstrated that ALKBH5 could aggravate AngII-induced inflammation response as well as apoptosis of HASMCs and increase the incidence of AD in AngII-infused mice through regulating lnc-TMPO-AS1/EZH2/IRAK4 signals in an m6A modification manner (Figure 7). Our findings reveal for the first time the role of m6A modification in AD progression and may shed some new light on searching for novel therapeutic approaches to improve the health of patients fighting AD or other cardiovascular diseases.

Data Availability

The data used to support the findings of this study are available from the corresponding author upon request.

Conflicts of Interest

The authors declare that they have no potential conflicts of interest.

Authors' Contributions

Peng Wang and Min Zhang contributed equally to this work. P.W. designed the project plan, completed the main experiment, and drafted the manuscript. Z.W.W. devoted to the resources and supervised the implementation of the whole project. M.Z. organized experimental data and revised the manuscript. Q.W. and F.S. established the AngII-infusion animal model. S.Y. completed the bioinformatics analysis. All authors have read and approved the final version of the manuscript.

Acknowledgments

Supplementary Materials

Supplementary Figure 1: quantitative analysis of Figure 1(b) in the main text. Supplementary Figure 2: quantitative analysis of Figure 1(d) in the main text. Supplementary Figure 3: quantitative analysis of Figure 2(k) in the main text. Supplementary Figure 4: quantitative analysis of Figure 2(l) in the main text. Supplementary Figure 5: the interference effects of pcDNA-lnc-TMPO-AS1 and si-lnc-TMPO-AS1 in HASMCs were detected by qRT-PCR. Supplementary Figure 6: quantitative analysis of Figures 3(g) and 3(i) in the main text. Supplementary Figure 7: the effect of lnc-TMPO-AS1 downregulation on the inflammatory response was examined. Supplementary Figure 8: quantitative analysis of Figure 5(c) in the main text. Supplementary Figure 9: the location of lnc-TMPO-AS1 on chromosomes and several adjacent transcripts were identified. Supplementary Figure 10: the expression of some genes whose transcripts are close to lnc-TMPO-AS1 on chromosomes. Supplementary Figure 11: quantitative analysis of Figure 6(f) in the main text. Supplementary Figure 12: quantitative analysis of Figure 6(i) in the main text. (Supplementary Materials)

References

[1] C. A. Nienaber, R. E. Clough, N. Sakalihasan et al., "Correction: aortic dissection," *Nature Reviews. Disease Primers*, vol. 2, no. 1, p. 16071, 2016.

[2] J. Gawinecka, F. Schnrath, and A. von Eckardstein, "Acute aortic dissection: pathogenesis, risk factors and diagnosis," *Swiss Medical Weekly*, vol. 147, p. w14489, 2017.

[3] A. Karimi and D. M. Milewicz, "Structure of the elastin-contractile units in the thoracic aorta and how genes that cause thoracic aortic aneurysms and dissections disrupt this structure," *The Canadian Journal of Cardiology*, vol. 32, no. 1, pp. 26–34, 2016.

[4] D. M. Milewicz, S. K. Prakash, and F. Ramirez, "Therapeutics targeting drivers of thoracic aortic aneurysms and acute aortic dissections: insights from predisposing genes and mouse models," *Annual Review of Medicine*, vol. 68, no. 1, pp. 51–67, 2017.

[5] D. M. Milewicz, K. M. Trybus, D. C. Guo et al., "Altered smooth muscle cell force generation as a driver of thoracic aortic aneurysms and dissections," *Arteriosclerosis, Thrombosis, and Vascular Biology*, vol. 37, no. 1, pp. 26–34, 2017.

[6] W. Ren, Z. Wang, J. Wang et al., "IL-5 overexpression attenuates aortic dissection by reducing inflammation and smooth muscle cell apoptosis," *Life Sciences*, vol. 241, p. 117144, 2020.

[7] S. L. Berger, "Histone modifications in transcriptional regulation," *Current Opinion in Genetics & Development*, vol. 12, no. 2, pp. 142–148, 2002.

[8] H. Akhavan-Niaki and A. A. Samadani, "DNA methylation and cancer development: molecular mechanism," *Cell Biochemistry and Biophysics*, vol. 67, no. 2, pp. 501–513, 2013.

[9] W. A. Cantara, P. F. Crain, J. Rozenski et al., "The RNA modification database, RNAMDB: 2011 update," *Nucleic Acids Research*, vol. 39, no. Database issue, pp. D195–D201, 2010.

[10] R. Desrosiers, K. Friderici, and F. Rottman, "Identification of methylated nucleosides in messenger RNA from Novikoff hepatoma cells," *Proceedings of the National Academy of Sciences of the United States of America*, vol. 71, no. 10, pp. 3971–3975, 1974.

[11] K. D. Meyer, Y. Saletore, P. Zumbo, O. Elemento, C. E. Mason, and S. R. Jaffrey, "Comprehensive analysis of mRNA methylation reveals enrichment in $3'$ UTRs and near stop codons," *Cell*, vol. 149, no. 7, pp. 1635–1646, 2012.

[12] D. Dominissini, S. Moshitch-Moshkovitz, S. Schwartz et al., "Topology of the human and mouse m6A RNA methylomes revealed by m6A-seq," *Nature*, vol. 485, no. 7397, pp. 201–206, 2012.

[13] H. Song, X. Feng, H. Zhang et al., "METTL3 and ALKBH5 oppositely regulate m6A modification ofTFEBmRNA, which dictates the fate of hypoxia/reoxygenation-treated cardiomyocytes," *Autophagy*, vol. 15, no. 8, pp. 1419–1437, 2019.

[14] I. A. Roundtree, M. E. Evans, T. Pan, and C. He, "Dynamic RNA modifications in gene expression regulation," *Cell*, vol. 169, no. 7, pp. 1187–1200, 2017.

[15] S. Lin, J. Choe, P. Du, R. Triboulet, and R. I. Gregory, "The m6A methyltransferase METTL3 promotes translation in human cancer cells," *Molecular Cell*, vol. 62, no. 3, pp. 335–345, 2016.

[16] T. Lan, H. Li, D. Zhang et al., "KIAA1429 contributes to liver cancer progression through N6-methyladenosine-dependent post-transcriptional modification of GATA3," *Molecular Cancer*, vol. 18, no. 1, p. 186, 2019.

[17] J. Zhang, S. Guo, H. Y. Piao et al., "ALKBH5 promotes invasion and metastasis of gastric cancer by decreasing methylation of the lncRNA NEAT1," *Journal of Physiology and Biochemistry*, vol. 75, no. 3, pp. 379–389, 2019.

[18] P. Wang, Z. Wang, M. Zhang, Q. Wu, and F. Shi, "Lnc-OIP5-AS1 exacerbates aorta wall injury during the development of aortic dissection through upregulating TUB via sponging miR-143-3p," *Life Sciences*, vol. 271, p. 119199, 2021.

[19] W. Liu, B. Wang, T. Wang et al., "Ursodeoxycholic acid attenuates acute aortic dissection formation in angiotensin II-infused apolipoprotein E-deficient mice associated with reduced ROS and increased Nrf2 levels," *Cellular Physiology and Biochemistry*, vol. 38, no. 4, pp. 1391–1405, 2016.

[20] P. Wang, Y. Deng, and X. Fu, "miR-509-5p suppresses the proliferation, migration, and invasion of non-small cell lung cancer by targeting YWHAG," *Biochemical and Biophysical Research Communications*, vol. 482, no. 4, pp. 935–941, 2017.

[21] Q. Wu, J. Hong, Z. Wang et al., "Abnormal ribosome biogenesis partly induced p53-dependent aortic medial smooth muscle cell apoptosis and oxidative stress," *Oxidative Medicine and Cellular Longevity*, vol. 2019, Article ID 7064319, 19 pages, 2019.

[22] S. Mitchell, J. Vargas, and A. Hoffmann, "Signaling via the NFκB system," *Wiley Interdisciplinary Reviews. Systems Biology and Medicine*, vol. 8, no. 3, pp. 227–241, 2016.

[23] J. Cai, Z. Chen, J. Wang et al., "circHECTD1 facilitates glutaminolysis to promote gastric cancer progression by targeting

miR-1256 and activating β-catenin/c-Myc signaling," *Cell Death & Disease*, vol. 10, no. 8, p. 576, 2019.

[24] Y. Fu, D. Dominissini, G. Rechavi, and C. He, "Gene expression regulation mediated through reversible m^{6}A RNA methylation," *Nature Reviews. Genetics*, vol. 15, no. 5, pp. 293–306, 2014.

[25] G. Cao, H.-B. Li, Z. Yin, and R. A. Flavell, "Recent advances in dynamic m6A RNA modification," *Open Biology*, vol. 6, no. 4, article 160003, 2016.

[26] F. Kopp and J. T. Mendell, "Functional classification and experimental dissection of long noncoding RNAs," *Cell*, vol. 172, no. 3, pp. 393–407, 2018.

Research Article

Effects of Chronic Supplementation of L-Arginine on Physical Fitness in Water Polo Players

Jessica Gambardella [1,2,3] Antonella Fiordelisi,[1] Luca Spigno,[4] Lorenzo Boldrini,[4]
Giulia Lungonelli,[4] Eugenio Di Vaia,[1] Gaetano Santulli [1,2,3] Daniela Sorriento [1,5]
Federica Andrea Cerasuolo,[6] Valentina Trimarco [5,6] and Guido Iaccarino [1,5]

[1]*Department of Advanced Biomedical Sciences, Federico II University of Naples, Italy*
[2]*Department of Medicine, Wilf Family Cardiovascular Research Institute, Einstein-Institute for Aging Research, Albert Einstein
College of Medicine, New York, NY 10461, USA*
[3]*Department of Molecular Pharmacology, Fleischer Institute for Diabetes and Metabolism (FIDAM), Einstein-Mount Sinai Diabetes
Research Center (ES-DRC), Albert Einstein College of Medicine, New York, NY 10461, USA*
[4]*Clinical and Sports Nutrition Service, Villa Montallegro Hospital, Genova, Italy*
[5]*CIRIAPA Interdepartmental Center for Research on Arterial Hypertension and Associated Conditions,
Federico II University of Naples, Italy*
[6]*Department of Neurosciences, Federico II University of Naples, Italy*

Correspondence should be addressed to Guido Iaccarino; guiaccar@unina.it

Background. Ergogenic nutritional supplementation is sought by professional athletes for improving physical performance; nevertheless, scientific evidence to support the chronic use of L-Arginine among water polo players is missing. *Methods.* Seventeen male professional water polo players were randomly assigned to assume 5 grams per day of L-Arginine ($n = 9$) or placebo ($n = 8$) for 4 weeks. The players' fitness level was assessed in the maximal speed swimming test. Ear lobe blood samples taken before and after the effort for serum lactate content were analyzed. A speed-to-lactate ratio was generated at the baseline and after 4 weeks of treatment. We also tested the effects of L-Arginine *in vitro*, measuring NO production, mitochondrial respiration, and gene expression in human fibroblasts. *Results.* L-Arginine did not modify BMI, muscle strength, and maximal speed at 200 meters after 4 weeks. However, L-Arginine ameliorated oxidative metabolism to exercise as suggested by the statistically significant lower lactate-to-speed ratio, which was not observed in placebo-treated controls. *In vitro*, L-Arginine induced the expression of a key regulator of mitochondrial biogenesis (PGC1α) and genes encoding for complex I and increased the production of nitric oxide and the maximal oxygen consumption rate. *Conclusions.* Chronic L-Arginine is safe and effective in ameliorating the oxidative metabolism of professional water polo players, through a mechanism of enhanced mitochondrial function.

1. Introduction

The amino acid L-Arginine contributes to the regulation of energetic metabolism in cells, by participating in the Krebs cycle after conversion in citrulline [1]. In this reaction, the signaling molecule nitric oxide (NO) is also produced, which can participate in the contractility and metabolism of muscles, as well as in the potentiation of neuronal activity and immune response [2]. NO induces vasodilation and increases tissue perfusion, thus ameliorating the delivery of oxygen and nutrients for the production of ATP. Indeed, NO availability improves muscle mitochondrial respiration and biogenesis [3, 4].

Some studies associate these biological features of NO with the amelioration of muscle force production and endurance performance and recovery [5, 6]. Indeed, the nutritional

supplementation of dietary nitrates in adults engaged in leisure activities has been associated with amelioration of the physical performance, as reported by reduced oxygen cost of submaximal exercise and resistance to high-intensity exercises [7, 8]. Interestingly, in elite athletes, the chronic effects of nitrate administration have never been investigated [9].

Professional water polo represents an interesting setup to study muscular and physical adaptations to mixed training characterized by high-intensity bouts alternated to lower intensity efforts [10].

Nutrition participates greatly in the development of endurance and power capabilities in response to training [11]. The use of products containing L-Arginine among athletes is diffuse, although the effects on performance are not clear and still controversial [12, 13]. The physiological concentrations of L-Arginine are generally sufficient to saturate endothelial nitric oxide synthase; nevertheless, acute effects of 6 grams of arginine have been demonstrated to increase the performance [14]. In particular, dietary supplementation of nitrates in recreationally active athletes leads to a reduction in the oxygen cost and improves tolerance to high-intensity exercise [15]. Interestingly, in elite athletes, the effects of nitrate supplementation are less evident, and almost all of the studies are concordant on the neutral effects on maximal performance [16]. It has to be noted, though, that most of the studies in elite athletes are referred to acute supplementation, and the effects of chronic supplementation of L-Arginine in elite athletes are far less explored.

The present study investigates the effects of 4-week, 5 grams per day, dietary L-Arginine supplementation on serum biochemistry and exercise performance in elite water polo players. Furthermore, in an *in vitro* model, we evaluated the effects of chronic exposure to increased L-Arginine concentration on parameters of mitochondrial biogenesis and function.

2. Methods

2.1. Water Polo Players. Seventeen male water polo players participating in the top-level division of the Italian Championship took part in the single-blind, placebo-controlled, parallel-group, randomized study. They were randomly assigned to the L-Arginine (Bioarginina Farmaceutici Damor®, $n = 9$) or placebo ($n = 8$) parallel groups. The anthropometric features are described in Table 1. Informed consent was obtained by all players before testing, and the experimental protocol was approved by the Ethical Committee of the Federico II University of Naples, Italy. The trial is registered in (NCT04626375).

2.2. Procedures. The players' fitness level was assessed in the maximal speed swimming test. After 10 min standardized warm-ups, participants swam 200 meters in an indoor, 25 m swimming pool at maximum speed. Ear lobe blood samples were taken before and after the effort and analyzed for serum lactate content using the reflectance photometric enzymatic reaction method (Accusport, Boehringer, Germany). A speed-to-lactate ratio was generated. Further assessment implied blood sampling for IGF1 and CK on

serum and dynamometer measurements of upper limb maximal power.

The above-described assessments were performed at baseline and after 4 weeks of treatment with either placebo or a daily dose of 5 grams of L-Arginine *per os*. During the time of intervention, athletes trained daily according to the training schemes of the regular season. The placebo tablets were indistinguishable from those of L-Arginine as per shape and packaging. Therefore, the athletes were unaware of being on the treatment or placebo group.

2.3. Cells. Human Embryonic Kidney (HEK-293) fibroblasts were cultured in Dulbecco's minimal essential medium (DMEM) as previously described, 25 mM, and supplemented with 10% fetal bovine serum (FBS) at 37°C in 95% air-5% CO_2. At 70% confluence, cells were treated with L-Arginine (a kind gift from Farmaceutici Damor, Italy) at a concentration of 500 μM or vehicle (water), for 24 hours. After incubation, the cells were lysed or used for specific analysis.

2.4. NO Production. NO production was determined as previously described [17]. Briefly, HEK-293 were seeded in 24-well plates and incubated with 10 μM DAF-FM Diacetate (Invitrogen) for 60 min at 37°C. After washing, the cells were incubated for an additional 15 min at room temperature to allow complete deesterification of the internalized probe. Raw fluorescence at 495/515 nm was registered every 10 sec using the Tecan Infinite 200 Pro plate reader. The fluorescence was corrected by the background signal derived from nonmarked cells.

2.5. Mitochondrial Respiration. Mitochondrial respiration was assessed as previously described [18], using the Seahorse Analyzer (Agilent Technologies, Santa Clara, CA, USA). We added carbonyl cyanide 4-(trifluoromethoxy)phenylhydrazone (FCCP, 0.5 μM, Merck KGaA) and antimycin A (both 1 μM, Merck KGaA) to each well. After each assay, cells were collected to quantify DNA using the QuantiFluor dsDNA System (Promega, Madison, WI, USA).

2.6. Real-Time PCR. Total RNA from HEK-293 cells was extracted using a TRIzol reagent (Invitrogen), and cDNA was synthesized using the ThermoScript RT-PCR System (Invitrogen), following the manufacturer's instruction. After reverse transcription reaction, real-time quantitative polymerase chain reaction (RT-qPCR) was performed with a SYBR Green real-time PCR master mix kit (Applied Biosystems, Foster City, CA, USA) as described [17] using StepOne instrument (Applied Biosystems). Primers for gene analysis are indicated in Table 2. All standards and samples were assayed in triplicate. Thermal cycling was initiated with an initial denaturation at 95°C for 5 min. After this initial step, 40 cycles of PCR were performed. Each RT-PCR cycle consisted of heating at 95°C for 15 seconds, 60°C for 30 seconds, and 72°C for 1 minute. The ratio of fold change was calculated using the Pfaffl method [19].

2.7. Statistical Analysis. According to the available literature [20], an average physical performance assessment based on the lactate-to-speed ratio for professional water polo players

TABLE 1: Anthropometric, physical, and biochemical characteristics of the study population.

| | Baseline | | 4 weeks | |
	Control	L-Arginine	Control	L-Arginine
Age (yrs)	29.3 ± 1.66	30.9 ± 1.31		
Height (cm)	191.5 ± 1.92	192.0 ± 1.78		
Weight (kg)	95.81 ± 2.19	100.7 ± 3.56	95.6 ± 2.22	100.0 ± 3.58
BMI (kg/m^2)	26.1 ± 0.46	27.2 ± 0.56	26.07 ± 0.48	27.2 ± 0.56
CPK (μL/L)	156.1 ± 25.1	170.0 ± 25.8	133.7 ± 13.1	184.0 ± 35.5
IGF1 (μM/L)	327.9 ± 19.3	295.0 ± 19.0	226.5 ± 7.81	215.0 ± 10.0
Dynamometer (N)	76.1 ± 3.33	78.6 ± 2.02	76.12 ± 2.76	78.2 ± 1.88
Time to 200 mt (sec)	121.6 ± 1.62	123.0 ± 1.82	122.0 ± 1.93	124.0 ± 1.32
Basal lactates (μU/L)	1.10 ± 0.10	1.04 ± 0.08	0.92 ± 0.08	0.83 ± 0.05
Postexercise lactates (μU/L)	9.86 ± 0.41	10.0 ± 0.40	11.4 ± 1.22	9.25 ± 0.53

BMI: body mass index; CPK: creatine phosphokinase; IGF1: insulin-like growth factor.

TABLE 2: List of primers used in real-time PCR.

Gene	Sense primer sequence	Antisense primer sequence
18 S	5$'$-GTAACCCGTTGAACCCCATT-3$'$	5$'$-CCATCCAATCGGTAGTAGCG-3$'$
Cyt B	5$'$-CCTAGGCGACCCAGACAATTAT-3$'$	5$'$-TCATTCGGGCTTGATGTGG-3$'$
SDHA	5$'$-CATACTGTTGCAGCAGCACAGG-3$'$	5$'$-CCACCAAATGCACGCTGATA-3$'$
UQCRC I	5$'$-CCTACGCACTCGAGAGCAC-3$'$	5$'$-AGGTGTGCCCTGGAATGCTG-3$'$
PGC-1α	5$'$-AAACTTGCTAGCGGTCCTCA-3$'$	5$'$-TGGCTGGTGCCAGTAAGAG-3$'$

Cyt B: cytochrome B; SDHA: succinate dehydrogenase complex flavoprotein subunit A; UQCRC I: ubiquinol cytochrome c reductase complex I; PGC-1α: proliferator-activated receptor gamma coactivator 1α.

is around 7 with a standard deviation of 1.2. We calculated that to observe a 20% amelioration as effect of treatment, which is statistically significant with a power of 80% and alpha error of 10%, 7 volunteers per group are needed. Data are expressed as the mean ± standard error. Analysis of variance or Student's t-test was used as appropriate for continuous variables; chi-squared analysis was used to assess differences in expected distributions. $P < 0.05$ is considered statistically significant. All statistical analysis was performed on SPSS 24.0 (IBM-Italia, Segrate, Italy).

3. Results

3.1. In Vivo Studies

3.1.1. Physical Performance.
Athletes from the two groups at the baseline were similar by age, BMI, and muscle strength (Table 1). Baseline performance measured as the maximal speed at the 200 meters was not different between the control and the L-Arginine groups. Similar values of IGF-1, CK, and resting and exercise serum lactate were also observed between the two groups (Table 1). After 4 weeks, all the above parameters were not affected (Table 1). As previously established [20], the lactate-to-speed ratio represents a way to assess tolerance to exercise. While at the baseline, there was no difference between controls and L-Arginine athletes, after one month, the L-Arginine group presented a significantly lower lactate-to-speed ratio as compared to controls, suggesting a better oxidative metabolism to exercise (Figure 1(a)). This difference appears to be generated by the expected worsening of performance due to the intensive season training that was more frequent among the controls compared with the L-Arginine group (Figure 1(b)).

3.2. In Vitro Studies

3.2.1. Mitochondrial Biogenesis.
To assess the changes in the energetic metabolism that are induced by chronic exposure to L-Arginine, we exposed fibroblasts for 24 h with the amino acid. This timing is enough to activate protein synthesis and therefore modify the cellular phenotype. L-Arginine induces the expression of the regulator of mitochondrial biogenesis (PGC1α) and genes encoding for complex I proteins such as Succinate Dehydrogenase A (SDHA), while genes of complex III (cytochrome B and ubiquinol cytochrome C1 reductase) were not affected (Figure 2).

3.2.2. NO and Mitochondrial Function.
24 hr of L-Arginine induced a significant increase in the production of nitric oxide, which appeared to be almost double compared to control conditions (Figure 3(a)). Also, the maximal oxygen consumption rate, a measure of mitochondrial function, increased in L-Arginine-treated cells compared with control cells (Figure 3(b)).

(a)

(b)
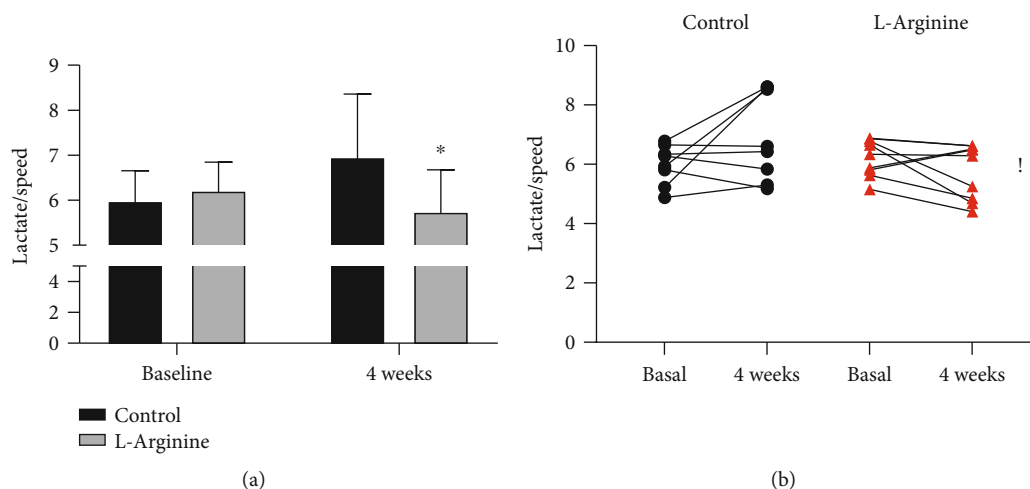
FIGURE 1: (a) Aerobic performance assessed as the serum lactate production to maximal speed on the 200 meters is similar between groups at the baseline, while significantly different after 4 weeks. (b) Evolution of lactate-to-speed ratio after 4 weeks in both groups. $^*P < 0.05$ vs. control, ANOVA; $^!P < 0.05$ vs. Control, chi-squared test.

(a)

(b)

(c)

(d)
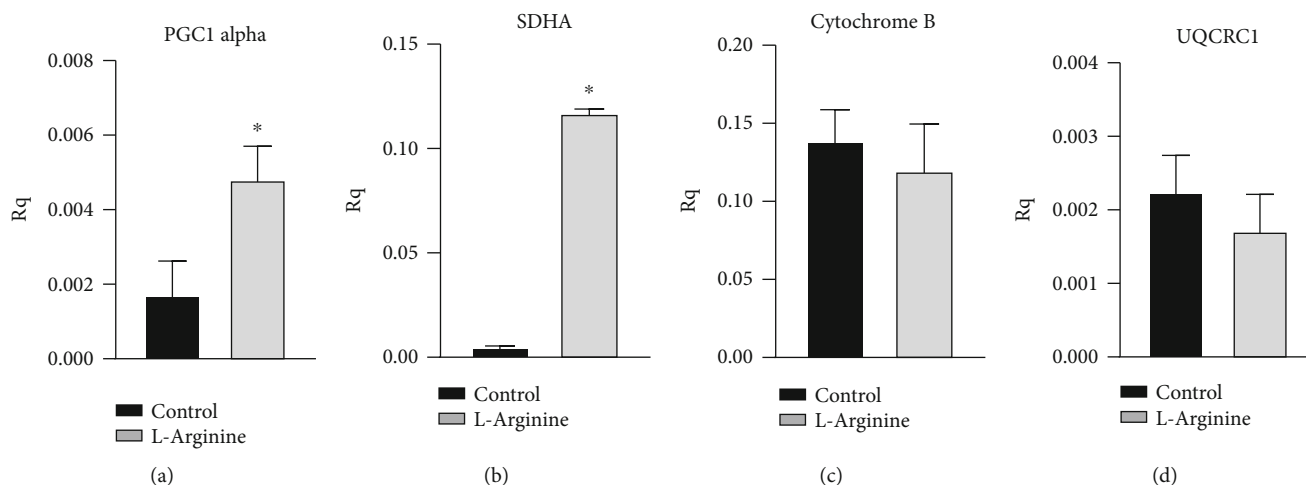
FIGURE 2: Gene expression in real time in L-Arginine vs. control-treated HEK-293 cells: (a) proliferator-activated receptor gamma coactivator 1α; (b) succinate dehydrogenase complex flavoprotein subunit A; (c) cytochrome B; (d) ubiquinol cytochrome c reductase complex I. $^*P < 0.05$ vs. control.

(a)

(b)
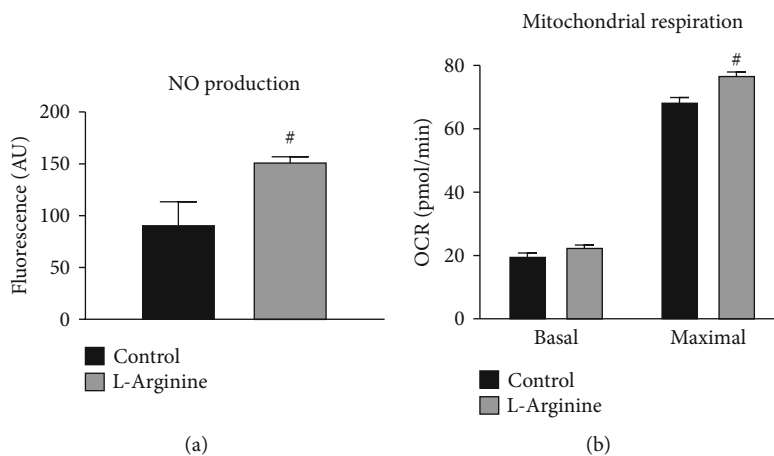
FIGURE 3: (a) Nitric oxide production in HEK-293 cells; (b) basal and maximal oxygen consumption rate (OCR) in HEK-293 cells. $^#P < 0.05$ vs. Control.

4. Discussion

Our results provide the first evidence that in elite water polo players, chronic L-Arginine supplementation ameliorates aerobic energy expenditure, possibly due to a positive effect on mitochondrial energetics. Chronic L-Arginine administration was tested before as a tentative enhancer of physical performance. In fact, only one group reported an amelioration in physical performance in healthy-untrained subjects [21]. On the other hand, chronic L-Arginine supplementation did not show statistical effects on time to exhaustion in running and cycling in endurance well-trained athletes [13, 22]. In swimmers, using a different NO donor, the root beer juice, a similar finding was observed by Pinna et al. who showed that 7-day supplementation reduced the anaerobic threshold, without enhancement in maximum workload achieved and/or VO_2max [23]. We confirm that we were unable to observe an amelioration of the physical performance of the examined athletes on average. Nevertheless, we verified that the physical response was achieved with lower production of lactates, thus suggesting the enhancement of the aerobic metabolism. Indeed, the *in vitro* study confirms the favorable effects of 24 hr exposure to L-Arginine on mitochondrial biogenesis and function.

Proteins and amino acids represent the most consumed ergogenic aids, with the esteem that at least one-third of athletes use them to maintain/potentiate athletic performance [11]. The consumption of amino acid supplements carrying vasodilatory properties is increasing in the sports field, due to the positive additional effect of vasodilation on muscle blood supply and athletic performance [24, 25]. In this scenario, the L-Arginine vasodilator effect has gained the favor of the athletes to improve their physical performance [14, 21, 26]. The perceived benefit of L-Arginine assumption, though, ailments the described arginine paradox, which has been described by Ignarro and coworkers; indeed, L-Arginine is a nonessential amino acid, synthesized in the small intestine from proline, glutamate, and glutamine, which is also abundant in diets with apparently no need for supplementation [27–29].

The vasodilator properties of L-Arginine reside in the fact that the amino acid is a substrate for nitric oxide synthases (NOS), a class of enzymes that share the ability to break arginine into citrulline and nitric oxide [30, 31]. Although its baseline plasma concentration is about 25- to 30-fold higher than the Michaelis-Menten constant Km of the isolated, purified endothelial NOS in vitro, further L-Arginine supplementation improves NO-mediated vascular function in vivo [32]. The possible mechanisms of action of L-Arginine supplementation might be identified in two main mechanisms. Indeed, being NO the most potent vasodilator produced in mammals, it has been shown to improve muscle performance by increasing blood flow, therefore inducing oxygen supplementation and carbon dioxide removal, and potentiation of mitochondrial biogenesis [33, 34]. The other possibility resides in the ability of citrulline to shift the energy metabolism to more anaerobic pathways and ameliorating mitochondria activity, through antioxidant properties [35]. Otherwise, L-Arginine has also been shown to stimulate the release of growth hormone (GH) [36, 37], which is a potent anabolic agent that favors cell growth and body energetics, which promotes muscle hypertrophy [38, 39]. Many effects of L-Arginine supplementation are also linked to improved carbohydrate oxidation and oxygen efficiency [40, 41], with reduced exercise-induced production of ammonia, lactate, fatty acids, and fat oxidation [42, 43].

In cells, we tested the ability of L-Arginine to interfere with energetic metabolism. We used L-Arginine to a μM concentration and for a time that is adequate to observe transcriptional adaptation. The amelioration of the energetic metabolism we observed in this setup appears to be due to an increase in mitochondrial effectiveness, possibly related to the increased expression of proteins of the complex I of the electron transport chain. Further studies are warranted for a more extensive investigation of the mechanisms of L-Arginine to regulate mitochondrial gene upregulation, and the current study represents the appropriate background.

Water polo players represent a unique setup for the study of energetic metabolism adjustments in response to mixed endurance and power training. Water polo alternates aerobic-anaerobic metabolic demand [10]. During a water polo game, high-intensity efforts occur several times [44]; thus, muscle recovery and oxygen-dependent processes between efforts, such as phosphocreatine replenishment and the removal of accumulated intracellular inorganic phosphates, are crucial for performance [10]. Therefore, aerobic fitness is important in water polo, to be achieved with appropriate training and also with nutritional, especially ergogenic, strategies [45]. Indeed, previous studies had evaluated the possible role of β-alanine supplementation on physical fitness and performance, showing that this nutritional strategy may not be effective. Given the pleiotropic effects of L-Arginine, the possibility that this amino acid can ameliorate the physical performance of high-intensity athletes are manifold. Our data provide evidence that the performance evaluated as speed by lactate production is indeed ameliorated and suggest that an enhancement of mitochondrial efficiency due to upregulation of mitochondrial biogenesis could be the putative mechanism.

Our results imply that in high-intensity training, the nutritional ergogenic approach with L-Arginine can ameliorate the physical training responses.

5. Conclusions

The administration of chronic L-Arginine to high-intensity athletes is safe and effective in ameliorating physical performance. A mitochondrial mechanism can be evoked by chronic L-Arginine supplementation.

Data Availability

Data are available at 10.6084/m9.figshare.13489977.

Conflicts of Interest

The authors declare that they have no conflicts of interest.

Acknowledgments

References

[1] R. Bescós, A. Sureda, J. A. Tur, and A. Pons, "The effect of nitric-oxide-related supplements on human performance," *Sports Medicine*, vol. 42, no. 2, pp. 99–117, 2012.

[2] W. Xu, S. Ghosh, S. A. A. Comhair et al., "Increased mitochondrial arginine metabolism supports bioenergetics in asthma," *The Journal of Clinical Investigation*, vol. 126, no. 7, pp. 2465–2481, 2016.

[3] S. K. Ferguson, D. M. Hirai, S. W. Copp et al., "Impact of dietary nitrate supplementation via beetroot juice on exercising muscle vascular control in rats," *The Journal of Physiology*, vol. 591, no. 2, pp. 547–557, 2013.

[4] A. Hernández, T. A. Schiffer, N. Ivarsson et al., "Dietary nitrate increases tetanic $[Ca^{2+}]i$ and contractile force in mouse fast-twitch muscle," *The Journal of Physiology*, vol. 590, no. 15, pp. 3575–3583, 2012.

[5] F. J. Larsen, E. Weitzberg, J. O. Lundberg, and B. Ekblom, "Effects of dietary nitrate on oxygen cost during exercise," *Acta Physiologica (Oxford, England)*, vol. 191, no. 1, pp. 59–66, 2007.

[6] A. Vanhatalo, S. J. Bailey, J. R. Blackwell et al., "Acute and chronic effects of dietary nitrate supplementation on blood pressure and the physiological responses to moderate-intensity and incremental exercise," *American Journal of Physiology. Regulatory, Integrative and Comparative Physiology*, vol. 299, no. 4, pp. R1121–R1131, 2010.

[7] F. J. Larsen, E. Weitzberg, J. O. Lundberg, and B. Ekblom, "Dietary nitrate reduces maximal oxygen consumption while maintaining work performance in maximal exercise," *Free Radical Biology & Medicine*, vol. 48, no. 2, pp. 342–347, 2010.

[8] R. Bescós, F. A. Rodríguez, X. Iglesias, M. D. Ferrer, E. Iborra, and A. Pons, "Acute administration of inorganic nitrate reduces V˙O2peak in endurance athletes," *Medicine and Science in Sports and Exercise*, vol. 43, no. 10, pp. 1979–1986, 2011.

[9] T. Haugen, S. Seiler, Ø. Sandbakk, and E. Tønnessen, "The training and development of elite sprint performance: an integration of scientific and best practice literature," *Sports medicine-open*, vol. 5, no. 1, p. 44, 2019.

[10] H. K. Smith, "Applied physiology of water polo," *Sports Medicine*, vol. 26, no. 5, pp. 317–334, 1998.

[11] I. Garthe and R. J. Maughan, "Athletes and supplements: prevalence and perspectives," *International Journal of Sport Nutrition and Exercise Metabolism*, vol. 28, no. 2, pp. 126–138, 2018.

[12] S. J. Bailey, P. G. Winyard, A. Vanhatalo et al., "Acute L-arginine supplementation reduces the O2 cost of moderate-intensity exercise and enhances high-intensity exercise tolerance," *Journal of Applied Physiology*, vol. 109, no. 5, pp. 1394–1403, 2010.

[13] T. S. Alvares, C. A. Conte-Junior, J. T. Silva, and V. M. F. Paschoalin, "L-arginine does not improve biochemical and hormonal response in trained runners after 4 weeks of supplementation," *Nutrition Research*, vol. 34, no. 1, pp. 31–39, 2014.

[14] H. U. Yavuz, H. Turnagol, and A. H. Demirel, "Pre-exercise arginine supplementation increases time to exhaustion in elite male wrestlers," *Biology of Sport*, vol. 31, no. 3, pp. 187–191, 2014.

[15] F. Husmann, S. Bruhn, T. Mittlmeier, V. Zschorlich, and M. Behrens, "Dietary nitrate supplementation improves exercise tolerance by reducing muscle fatigue and perceptual responses," *Frontiers in Physiology*, vol. 10, p. 404, 2019.

[16] A. M. Jones, "Influence of dietary nitrate on the physiological determinants of exercise performance: a critical review," *Applied Physiology, Nutrition, and Metabolism*, vol. 39, no. 9, pp. 1019–1028, 2014.

[17] J. Gambardella, M. de Rosa, D. Sorriento et al., "Parathyroid hormone causes endothelial dysfunction by inducing mitochondrial ROS and specific oxidative signal transduction modifications," *Oxidative Medicine and Cellular Longevity*, vol. 2018, Article ID 9582319, 18 pages, 2018.

[18] A. Lombardi, B. Trimarco, G. Iaccarino, and G. Santulli, "Impaired mitochondrial calcium uptake caused by tacrolimus underlies beta-cell failure," *Cell Communication and Signaling: CCS*, vol. 15, no. 1, p. 47, 2017.

[19] N. Regier and B. Frey, "Experimental comparison of relative RT-qPCR quantification approaches for gene expression studies in poplar," *BMC Molecular Biology*, vol. 11, no. 1, p. 57, 2010.

[20] P. G. Botonis, A. G. Toubekis, and T. I. Platanou, "Evaluation of physical fitness in water polo players according to playing level and positional role," *Sports (Basel)*, vol. 6, no. 4, p. 157, 2018.

[21] C. L. Camic, T. J. Housh, J. M. Zuniga et al., "Effects of arginine-based supplements on the physical working capacity at the fatigue threshold," *Journal of Strength and Conditioning Research*, vol. 24, no. 5, pp. 1306–1312, 2010.

[22] T. Abel, B. Knechtle, C. Perret, P. Eser, P. von Arx, and H. Knecht, "Influence of chronic supplementation of arginine aspartate in endurance athletes on performance and substrate metabolism - a randomized, double-blind, placebo-controlled study," *International Journal of Sports Medicine*, vol. 26, no. 5, pp. 344–349, 2005.

[23] M. Pinna, S. Roberto, R. Milia et al., "Effect of beetroot juice supplementation on aerobic response during swimming," *Nutrients*, vol. 6, no. 2, pp. 605–615, 2014.

[24] C. M. Kerksick, C. D. Wilborn, M. D. Roberts et al., "ISSN exercise & sports nutrition review update: research & recommendations," *Journal of the International Society of Sports Nutrition*, vol. 15, no. 1, p. 38, 2018.

[25] R. J. Maughan, L. M. Burke, J. Dvorak et al., "IOC consensus statement: dietary supplements and the high-performance athlete," *British Journal of Sports Medicine*, vol. 52, no. 7, pp. 439–455, 2018.

[26] N. Pahlavani, M. H. Entezari, M. Nasiri et al., "The effect of l-arginine supplementation on body composition and performance in male athletes: a double-blinded randomized clinical trial," *European Journal of Clinical Nutrition*, vol. 71, no. 4, pp. 544–548, 2017.

[27] J. Gambardella, W. Khondkar, M. B. Morelli, X. Wang, G. Santulli, and V. Trimarco, "Arginine and endothelial function," *Biomedicines*, vol. 8, no. 8, p. 277, 2020.

[28] G. Wu and S. M. Morris Jr., "Arginine metabolism: nitric oxide and beyond," *The Biochemical Journal*, vol. 336, no. 1, pp. 1–17, 1998.

[29] S. M. Morris Jr., "Arginine: beyond protein," *The American Journal of Clinical Nutrition*, vol. 83, no. 2, pp. 508S–512S, 2006.

[30] G. Lembo, G. Iaccarino, C. Vecchione et al., "Insulin modulation of an endothelial nitric oxide component present in the alpha2- and beta-adrenergic responses in human forearm," *The Journal of Clinical Investigation*, vol. 100, no. 8, pp. 2007–2014, 1997.

[31] G. Iaccarino, M. Ciccarelli, D. Sorriento et al., "AKT participates in endothelial dysfunction in hypertension," *Circulation*, vol. 109, no. 21, pp. 2587–2593, 2004.

[32] S. Bodeboger, F. Scalera, and l. Ignarro, "The L-arginine paradox: importance of the L-arginine/asymmetrical dimethylarginine ratio," *Pharmacology & Therapeutics*, vol. 114, no. 3, pp. 295–306, 2007.

[33] R. Domínguez, E. Cuenca, J. Maté-Muñoz et al., "Effects of beetroot juice supplementation on cardiorespiratory endurance in athletes. A Systematic Review," *Nutrients*, vol. 9, no. 1, p. 43, 2017.

[34] J. O. Lundberg, E. Weitzberg, and M. T. Gladwin, "The nitrate-nitrite-nitric oxide pathway in physiology and therapeutics," *Nature Reviews. Drug Discovery*, vol. 7, no. 2, pp. 156–167, 2008.

[35] C. Faure, B. Morio, P. Chafey et al., "Citrulline enhances myofibrillar constituents expression of skeletal muscle and induces a switch in muscle energy metabolism in malnourished aged rats," *Proteomics*, vol. 13, no. 14, pp. 2191–2201, 2013.

[36] J. A. Kanaley, "Growth hormone, arginine and exercise," *Current Opinion in Clinical Nutrition and Metabolic Care*, vol. 11, no. 1, pp. 50–54, 2008.

[37] S. C. Forbes, V. Harber, and G. J. Bell, "Oral L-arginine before resistance exercise blunts growth hormone in strength trained males," *International Journal of Sport Nutrition and Exercise Metabolism*, vol. 24, no. 2, pp. 236–244, 2014.

[38] B. Campbell, M. Roberts, C. Kerksick et al., "Pharmacokinetics, safety, and effects on exercise performance of l-arginine α-ketoglutarate in trained adult men," *Nutrition*, vol. 22, no. 9, pp. 872–881, 2006.

[39] E. Børsheim, Q. U. T. Bui, S. Tissier, H. Kobayashi, A. A. Ferrando, and R. R. Wolfe, "Effect of amino acid supplementation on muscle mass, strength and physical function in elderly," *Clinical Nutrition*, vol. 27, no. 2, pp. 189–195, 2008.

[40] S. C. Forbes, V. Harber, and G. J. Bell, "The acute effects of L-arginine on hormonal and metabolic responses during submaximal exercise in trained cyclists," *International Journal of Sport Nutrition and Exercise Metabolism*, vol. 23, no. 4, pp. 369–377, 2013.

[41] D. S. Rowlands, J. Clarke, J. G. Green, and X. Shi, "L-Arginine but not L-glutamine likely increases exogenous carbohydrate oxidation during endurance exercise," *European Journal of Applied Physiology*, vol. 112, no. 7, pp. 2443–2453, 2012.

[42] A. Schaefer, F. Piquard, B. Geny et al., "L-arginine reduces exercise-induced increase in plasma lactate and ammonia," *International Journal of Sports Medicine*, vol. 23, no. 6, pp. 403–407, 2002.

[43] P. H. Tsai, T. K. Tang, C. L. Juang, K. W. Chen, C. A. Chi, and M. C. Hsu, "Effects of arginine supplementation on post-exercise metabolic responses," *The Chinese Journal of Physiology*, vol. 52, no. 3, pp. 136–142, 2009.

[44] F. Tan, T. Polglaze, and B. Dawson, "Activity profiles and physical demands of elite women's water polo match play," *Journal of Sports Sciences*, vol. 27, no. 10, pp. 1095–1104, 2009.

[45] G. M. Claus, P. E. Redkva, G. M. P. Brisola et al., "Beta-alanine supplementation improves throwing velocities in repeated sprint ability and 200-m swimming performance in young water polo players," *Pediatric Exercise Science*, vol. 29, no. 2, pp. 203–212, 2017.

Research Article

Pleiotropic Properties of Valsartan: Do They Result from the Antiglycooxidant Activity? Literature Review and *In Vitro* Study

Kacper Maksymilian Mil [ID],[1] Małgorzata Ewa Gryciuk [ID],[1] Cezary Pawlukianiec [ID],[1] Małgorzata Żendzian-Piotrowska,[2] Jerzy Robert Ładny,[3] Anna Zalewska,[4] and Mateusz Maciejczyk [ID][2]

[1]*Students Scientific Club "Biochemistry of Civilization Diseases" at the Department of Hygiene, Epidemiology and Ergonomics, Medical University of Bialystok, 2c Mickiewicza Street, 15-233 Białystok, Poland*

[2]*Department of Hygiene, Epidemiology and Ergonomics, Medical University of Bialystok, 2c Mickiewicza Street, 15-233 Białystok, Poland*

[3]*1st Department of General Surgery and Endocrinology, Medical University of Bialystok, 24a M. Sklodowskiej-Curie Street, 15-274 Białystok, Poland*

[4]*Experimental Dentistry Laboratory, Medical University of Bialystok, 24a M. Sklodowskiej-Curie Street, 15-274 Białystok, Poland*

Correspondence should be addressed to Mateusz Maciejczyk; mat.maciejczyk@gmail.com

Valsartan belongs to angiotensin II type 1 (AT1) receptor blockers (ARB) used in cardiovascular diseases like heart failure and hypertension. Except for its AT1-antagonism, another mechanism of drug action has been suggested in recent research. One of the supposed actions refers to the positive impact on redox balance and reducing protein glycation. Our study is aimed at assessing the antiglycooxidant properties of valsartan in an *in vitro* model of oxidized bovine serum albumin (BSA). Glucose, fructose, ribose, glyoxal (GO), methylglyoxal (MGO), and chloramine T were used as glycation or oxidation agents. Protein oxidation products (total thiols, protein carbonyls (PC), and advanced oxidation protein products (AOPP)), glycooxidation products (tryptophan, kynurenine, N-formylkynurenine, and dityrosine), glycation products (amyloid-β structure, fructosamine, and advanced glycation end products (AGE)), and albumin antioxidant activity (total antioxidant capacity (TAC), DPPH assay, and ferric reducing antioxidant power (FRAP)) were measured in each sample. In the presence of valsartan, concentrations of protein oxidation and glycation products were significantly lower comparing to control. Moreover, albumin antioxidant activity was significantly higher in those samples. The drug's action was comparable to renowned antiglycation agents and antioxidants, e.g., aminoguanidine, metformin, Trolox, N-acetylcysteine, or alpha-lipoic acid. The conducted experiment proves that valsartan can ameliorate protein glycation and oxidation *in vitro* in various conditions. Available animal and clinical studies uphold this statement, but further research is needed to confirm it, as reduction of protein oxidation and glycation may prevent cardiovascular disease development.

1. Introduction

The formation of free radicals is an inevitable consequence of aerobic metabolism. As long as physiological mechanisms manage to eliminate reactive oxygen species (ROS), their adverse action on structural proteins, enzymes, membrane lipids, or nucleic acids may remain unseen [1]. However, the generation of ROS may exceed the capability of the organism to neutralize them. This situation is called redox imbalance and leads to oxidative damage to cellular biomolecules [2]. Indeed, ROS are not only proven to play a crucial role in many physiological processes [3, 4], but they are also a

vital factor in the pathogenesis of many diseases like obesity [5, 6], insulin resistance [7, 8], hypertension [9, 10], and chronic heart failure [11, 12].

ROS's role in the pathogenesis of hypertension is complicated and involves many different biochemical mechanisms [13–15]. ROS produced by nicotinamide adenine dinucleotide phosphate (NADPH) oxidases are responsible for nitric oxide (NO) depletion caused by its interaction with superoxide radical anions ($O_2^{-\bullet}$). This results in decreased endothelial nitric oxide synthase (eNOS) activity and leads to endothelial dysfunction, which is considered one of the essential pathogenetic factors [16, 17]. What is more, oxygen-free radicals can act on redox-sensitive genes in vascular smooth muscle cells and promote their mitogenic phenotype, stimulate fibrosis by inhibiting matrix metalloproteinases, or ameliorate an arterial wall calcification by activation of specific bone morphogenetic proteins (BMP). As an effect of this remodeling, stiffness of the vessel and peripheral resistance increase [9].

It is also reported that glycation of vascular proteins plays a vital role in hypertension development [5, 13, 14]. Interestingly, higher circulating levels of advanced glycation end products (AGE) correlate with increased arterial stiffness [18, 19]. Indeed, AGE accumulation in blood vessels impairs endothelial function by decreasing eNOS activity and reducing NO bioavailability [14, 20]. AGE also combine with a specific receptor (RAGE) to activate the transcription factor NF-κB (nuclear factor kappa-light-chain-enhancer of activated B cell). This not only stimulates ROS production but also activates many proinflammatory genes such as interleukins (IL-1b, IL-2, IL-6, and IL-8), adhesion molecules (vascular cell adhesion protein 1 (VCAM-1), intercellular cell adhesion protein 1 (ICAM-1)), growth and differentiation factors (vascular endothelial growth factor (VEGF), and transforming growth factor β2 (TGF-β2)) [20, 21]. Under these conditions, ROS production is intensified, which increases the already existing oxidative stress. Nevertheless, AGE also affect the activation of monocytes that overexpress the CD36 sweeping receptor. In this way, lipoproteins foam cells are formed, and atherosclerosis development is accelerated [20, 21]. Therefore, the use of antioxidants in cardiovascular diseases may have several positive effects [22].

According to recent studies, the drug which may potentially exhibit antioxidant and antiglycation activity is valsartan. Valsartan, (2S)-3-methyl-2-[pentanoyl-[[4-[2-(2H-tetrazole-5-yl)phenyl]phenyl]methyl]amino]butanoic acid, is a lipophilic, nonpeptide, tetrazole derivative, a selective antagonist of angiotensin II type 1 receptor (AT_1), which is widely used in many cardiovascular conditions like hypertension or chronic heart failure. The drug is administered orally, is characterized by rapid absorption and low bioavailability (25%), and is almost entirely bound to plasma proteins (94-97%) [23, 24]. The hepatic products of the metabolism of valsartan are mainly excreted with bile [25]. In comparison to other antihypertensives, valsartan is well tolerated and deprived of many side effects, like cough or angioedema, characteristic for angiotensin-converting enzyme inhibitors (ACEI). An occurrence of valsartan side effects in clinical studies was comparable to placebo, which confirms the

drug's safety [26]. Moreover, it has been proven to act nephroprotective in patients with diabetes mellitus and chronic renal failure and significantly reduce albuminuria [27, 28]. Some reports are claiming that valsartan may present additional mechanisms of action besides its AT_1 receptor antagonism. It was proven that patients treated with valsartan presented less urinary oxidative stress markers [29]. Similar outcomes were observed in mice where valsartan diminishes oxidative damage and acts nephroprotective [30].

However, it is still uncertain whether valsartan has antioxidant and antiglycation activity. Indeed, the impact of various glycating agents on protein oxidation/glycation in in vitro or in vivo models has not yet been evaluated. The effect of valsartan action was also not compared to other substances with recognized antioxidant properties. This is particularly important because confirmation of the antiglycooxidant activity of valsartan may result in a revision of the guidelines for the use of the drug in cardiovascular disease and diabetes, making it the first-line medication in patients with enhanced protein glycation. For this reason, we conducted a study to assess valsartan's effect on protein oxidation, glycation, and total antioxidant activity in in vitro model of oxidized bovine serum albumin (BSA). Either oxidizing (chloramine T) or glycating agents (glucose, fructose, ribose, glyoxal, and methylglyoxal), as well as antioxidants (Trolox, N-acetylcysteine, lipoic acid, and captopril) and protein glycation inhibitors (aminoguanidine and metformin), were used to compare the results of antiglycooxidant capabilities of valsartan [31–35]. We assessed the concentrations of protein oxidation products (total thiols, protein carbonyls, and advanced oxidation protein products (AOPP)), glycooxidation products (tryptophan, kynurenine, N-formylkynurenine, and dityrosine), levels of albumin glycation products (amyloid-β structure, fructosamine, and advanced glycation end products (AGE)), and antioxidant potential of albumin (total antioxidant capacity (TAC), DPPH assay, and ferric reducing antioxidant power (FRAP)). We have also made a detailed literature review on the antiglycooxidant properties of valsartan.

2. Methods

2.1. Reagents and Equipment.
All reagents (analytical grade) were purchased from Sigma-Aldrich (Nümbrecht, Germany, or Saint Louis, MO, USA). Solutions were sterilized by filtration through 0.2 mm membrane filters directly before use. The fluorescence and absorbance were evaluated using a microplate reader (M200 PRO multimode microplate reader; Tecan Group Ltd., Männedorf, Switzerland).

2.2. Experimental Model.
The glycated/oxidated BSA formation was implemented according to the previously published method [31–36]. BSA, of 96% purity, was dissolved in sodium phosphate buffer (1 M, pH 7.4), which contained 0.02% sodium azide as a preservative.

Chloramine T was used as an oxidation agent. 0.09 mM BSA and 1 mM valsartan were incubated with 20 mM chloramine T for 60 minutes [37, 38].

As glycating agents, sugars (glucose (Glu), fructose (Fru), and ribose (Rib)) and aldehydes (glyoxal (GO), and methylglyoxal (MGO)) were used. To assess the additives' effect on protein glycation, 0.09 mM BSA and 1 mM valsartan were incubated with 0.5 M Glu, Fru, and Rib for 6 days or 2.5 mM GO and MGO for 12 hours [31, 32, 39]. GO and MGO were used within a month after delivery, and solutions were prepared immediately before use [34].

Incubation was conducted in the closed vials, darkly, with continuous shaking (50 rpm) [31–35]. These conditions and concentrations of glycating agents were validated based on previously published kinetic studies [31, 34].

Captopril, Trolox, N-acetylcysteine (NAC), and lipoic acid (ALA) were used as protein oxidation inhibitors, while aminoguanidine and metformin as inhibitors of protein glycation [31–36, 38]. The concentration of all additives was 1 mM, which was based on the kinetic studies, in proportion to the high concentrations of the glycating agents [31, 32, 34, 35, 37, 39–41].

All experiments were performed three times, each time in duplicate.

2.3. Protein Oxidation Products.

Total thiols were detected using Ellman's reagent by the colorimetric method [42]. The absorbance was measured at 412 nm wavelength. Thiol groups' content was established based on a standard curve for N-acetylcysteine (NAC) [42].

The carbonyl groups' reaction with 2,4-dinitrophenylhydrazine (2,4-DNPH) was performed to examine protein carbonyl concentration in proteins that underwent oxidative damage. The absorbance of the products of this reaction was evaluated colorimetrically at 355 nm wavelength [43].

The concentration of advanced oxidation protein products was measured by spectrophotometric detection. $200 \mu L$ of examined solutions diluted with PBS in 1:5 ratio ($v:v$), chloramine T standard solutions (0-100 $\mu mol/L$), and $200 \mu L$ of blank PBS were placed in 96-well microplates. Then, $20 \mu L$ of acetic acid and $10 \mu L$ of 1.16 M potassium iodide were added to wells. Immediately after that, the absorbance was measured at 340 nm wavelength concerning blank ($200 \mu L$ PBS, $20 \mu L$ acetic acid, and $10 \mu L$ potassium iodide). Chloramine T solutions presented linear absorbance in the range of 0-100 $\mu mol/L$ [44].

2.4. Protein Glycooxidation Products.

Tryptophan, kynurenine, N-formylkynurenine, and dityrosine were evaluated by measuring emission and excitation at 95/340, 365/480, 325/434, and 330/415 nm, respectively. The samples were diluted with 0.1 M sulfuric acid in a 1:5 ratio ($v:v$). Results were standardized to the fluorescence of 0.1 mg/mL quinine sulfate in 0.1 M sulfuric acid [45].

2.5. Protein Glycation Products.

The assay was performed to measure fluorescence emitted when amyloid fibrils or oligomers are bound to amyloid-β structure. $10 \mu L$ of Thioflavin T and $90 \mu L$ of samples were mixed and transferred to a microplate; then, the fluorescence was assessed at 385/485 nm [46, 47].

The fructosamine content was detected colorimetrically with nitro blue tetrazolium (NBT) assay. The absorbance was measured at 525 nm using the monoformazan extinction coefficient (12.640 $M^{-1} m^{-1}$) [48].

All examined samples were diluted with 0.1 M sulfuric acid (1:5, $v:v$) [18]. Then, the content of advanced glycation end products (AGE) was measured using the spectrophotometric method at 440/370 nm at a 96-well microplate reader [44, 49]. AGE content was also analyzed with the ELISA method (UCSN, Life Science, Wuhan, China).

2.6. Antioxidant Activity.

TAC of each sample was measured according to Erel's method. For this purpose, 2,2-azinobis(3-ethylbenzene-thiazoline-6-sulfonate) (ABTS) radical cation decolorization assay was used. $ABTS^+$ was obtained by reacting ABTS with potassium persulfate and incubated for 12 hours at room temperature. After mixing $10 \mu L$ of samples with 1 mL of $ABTS^+$, the absorbance readings were taken at 735 nm. Results of decolorization were linear with increasing Trolox concentrations [50, 51].

The determination of free radicals scavenging activity was performed according to the Brand–Williams method. $10 \mu L$ of each sample and $390 \mu L$ methanolic diluted DPPH were mixed and placed on a 96-well microplate. The solutions were incubated in darkness at room temperature for 30 minutes. The absorbance was measured at 515 nm [52, 53].

The ferric reducing antioxidant power of each sample was measured following the Benzie and Strain method. FRAP reagent was prepared by mixing 25 mL acetate buffer, 2.5 mL $FeCl_3 \cdot 6H_2O$ solution, and 2.5 mL TPTZ solution and warming the solution to 37°C. $10 \mu L$ of sample and $300 \mu L$ of FRAP reagent were diluted with $30 \mu L$ of water and transferred to 96-wells microplate. The change of absorbance was calculated for each sample and related to the absorbance of Fe^{II} standard solution [54].

2.7. Statistical Analysis.

The statistical analysis was conducted using GraphPad Prism 8.3.0 (GraphPad Software, La Jolla, CA, USA). The results were expressed as a percentage of the corresponding control values (BSA + glycating/oxidizing agent). Differences between groups were assessed by one-way ANOVA followed by Tukey's post hoc test for multiple comparisons. $p < 0.05$ was considered statistically significant. Multiplicity adjusted p value was also calculated.

3. Results

3.1. The Impact of Valsartan and Other Additives on Protein Oxidation Products, Glycooxidation Products, and Glycation Products as well as Antioxidant Activity in Glucose- (Glu-) Induced Albumin Glycation.

The addition of glucose to the BSA solution led to increased protein oxidation products—PC and AOPP. Decreased levels of aforementioned parameters were noticed when BSA + Glu (control) were incubated with valsartan (84%, 79% compared to control, respectively), NAC (76%, 76% vs. control), ALA (69%, 76% vs. control), captopril (78%, 77% vs. control), or aminoguanidine (77%, 68% vs. control). Moreover, in samples containing

TABLE 1: The effects of valsartan, Trolox, NAC, ALA, captopril, aminoguanidine, or metformin addition to BSA + glucose solution on protein oxidation, glycooxidation, and antioxidant activity.

	BSA	BSA + Glu	BSA + Glu + valsartan	BSA + Glu + Trolox	BSA + Glu + NAC	BSA + Glu + ALA	BSA + Glu + captopril	BSA + Glu + aminoguanidine	BSA + Glu + metformin
Protein oxidation									
Total thiols	108 ± 5.50	100	103 ± 2.20	109 ± 4.30 *	119 ± 0.95 **	105 ± 1.10 **	110 ± 7.90	116 ± 4.50 **	102 ± 1.20
PC	68 ± 3.30 ****	100	84 ± 3.00 ***	101 ± 2.70	76 ± 2.10 ****	69 ± 1.80 ****	78 ± 3.70 ***	77 ± 5.50 **	98 ± 1.40
AOPP	66 ± 0.92 ****	100	79 ± 1.50 ****	66 ± 2.80 ****	76 ± 3.20 ***	76 ± 1.20 ****	77 ± 3.00 ***	68 ± 1.60 ****	97 ± 1.70
Protein glycooxidation									
Tryptophan	127 ± 3.10 ***	100	114 ± 2.20 ***	132 ± 6.30 ***	132 ± 6.30 ****	137 ± 1.60 ****	146 ± 0.43 ****	125 ± 3.40 ***	121 ± 2.00 ****
Kynurenine	67 ± 0.35 ****	100	70 ± 1.80 ****	64 ± 0.38 ****	71 ± 1.70 ****	75 ± 1.60 ****	72 ± 2.00 ****	56 ± 1.30 ****	79 ± 4.30 **
N-Formylkynurenine	66 ± 1.30 ****	100	71 ± 3.00 ****	65 ± 2.20 ****	82 ± 0.38 ****	80 ± 0.93 ****	72 ± 0.44 ****	44 ± 2.40 ****	65 ± 2.60 ****
Dityrosine	52 ± 5.90 ***	100	55 ± 2.00 ****	70 ± 1.60 ****	51 ± 4.80 ****	55 ± 5.20 ***	68 ± 2.70 ****	50 ± 5.40 ****	90 ± 3.30 **
Albumin glycation									
Amyloid-β structure	79 ± 1.50 ****	100	89 ± 1.30 ***	81 ± 0.91 ****	79 ± 2.00 ****	82 ± 0.87 ****	81 ± 1.50 ****	68 ± 0.45 ****	100 ± 1.50
Fructosamine	56 ± 2.40 ****	100	56 ± 1.20 ****	71 ± 1.70 ****	61 ± 5.10 ***	63 ± 4.40 ***	67 ± 2.30 ****	67 ± 2.00 ****	85 ± 2.10 ***
AGE	74 ± 0.82 ****	100	73 ± 1.90 ****	72 ± 0.83 ****	72 ± 1.2 ***	74 ± 1.6 ****	82 ± 1.60 ***	70 ± 0.56 ****	89 ± 3.20
Albumin antioxidant activity									
TAC	122 ± 2.70 ***	100	107 ± 2.90 *	102 ± 3.30	114 ± 2.40 ***	105 ± 3.70	99 ± 6.30	110 ± 4.10 *	103 ± 3.70
DPPH	118 ± 2.10 ***	100	109 ± 1.80 **	109 ± 0.14 ****	128 ± 1.40 ****	115 ± 4.30 **	111 ± 1.70 ***	111 ± 2.20 **	104 ± 3.70
FRAP	123 ± 3.20 ***	100	105 ± 2.00 *	113 ± 1.80 ***	122 ± 2.30 ****	111 ± 2.70 **	114 ± 0.80 ****	113 ± 0.37 ****	102 ± 1.10

Abbreviations: AGE: advanced glycation end products; ALA: alpha-lipoic acid; AOPP: advanced oxidation protein products; BSA: bovine serum albumin; DPPH: 2,2-di-phenyl-1-picrylhydrazyl radical scavenging capacity; FRAP: ferric reducing antioxidant power; Glu: glucose; NAC: N-acetylcysteine; PC: protein carbonyls; TAC: total antioxidant capacity; $*p < 0.05$ vs.control; $**p < 0.01$ vs. control; $***p < 0.001$ vs. control; $****p < 0.0001$ vs. control.

Trolox (109% vs. control), NAC (119% vs. control), ALA (105% vs. control), or aminoguanidine (116% vs. control), significantly higher values of total thiols were observed (Table 1).

The presence of glucose in the BSA sample caused a significant increase in kynurenine levels, N-formylkynurenine, and dityrosine due to albumin glycooxidation. In contrast, tryptophan concentration was lower in BSA + Glu compared to BSA alone. The addition of valsartan (70%, 71%, and 55% vs. control, respectively) and other additives resulted in decreased kynurenine contents, N-formylkynurenine, and dityrosine comparing to control. Moreover, statistically higher tryptophan (valsartan: 114% vs. control) in all investigated samples versus control was observed (Table 1).

Amyloid-β structure, fructosamine, and AGE contents were significantly higher in BSA incubated with glucose than BSA alone. All reviewed substances caused a significant decrease in parameters above (valsartan: 89%, 56%, and 73% vs. control, respectively), excluding sample with metformin in AGE measurement (Table 1).

Glucose was also responsible for a decreased antioxidant activity (TAC, DPPH, and FRAP). The analysis of these parameters showed significantly greater DPPH and FRAP in BSA + Glu + valsartan (109%, 105% vs. control, respectively), Trolox (109%, 113% vs. control), NAC (128%, 122% vs. control), ALA (115%, 111% vs. control), captopril (111%, 114% vs. control), or aminoguanidine (111%, 113% vs. control) comparing to control. Furthermore, the addition of valsartan (107% vs. control), NAC (114% vs. control), and aminoguanidine (110% vs. control) resulted in increased TAC compared to control (Table 1).

3.2. The Impact of Valsartan and Other Additives on Protein Oxidation Products, Glycooxidation Products and Glycation Products as well as Antioxidant Activity in Fructose- (Fru-) Induced Albumin Glycation.
Fructose-induced protein oxidation resulted in increased PC and AOPP levels and decreased total thiols level compared to BSA alone. All investigated agents caused a significant decrease in concentrations of PC and AOPP (valsartan: 81%, 58% vs. control, respectively), excluding BSA + Fru + metformin in AOPP concentration. Moreover, the addition of valsartan (105% vs. control), NAC (114% vs. control), ALA (107% vs. control), and aminoguanidine (105% vs. control) led to a higher concentration of total thiols compared to control (Table 2).

The results of protein glycooxidation products measurement showed significantly higher concentrations of kynurenine, N-formylkynurenine, and dityrosine in BSA + Fru comparing to BSA alone. However, the content of tryptophan decreased after fructose was added. In samples with all reviewed inhibitors, significantly lower kynurenine concentrations, N-formylkynurenine, and dityrosine (valsartan: 67%, 57%, and 65% vs. control, respectively) were observed (Table 2).

Moreover, the presence of fructose in the BSA solution resulted in greater concentrations of measured glycation products. The analysis showed significantly lower levels of amyloid-β structure, fructosamine, and AGE in samples with the addition of all investigated protein glycation and oxida-

tion inhibitors (valsartan: 88%, 53%, and 84% vs. control, respectively) comparing to control.

When BSA was incubated with fructose, significantly decreased TAC, DPPH, and FRAP were noticed. The addition of the antiglycooxidative agents such as NAC (146%, 129% vs. control, respectively), ALA (129%, 108% vs. control), and captopril (133%, 108% vs. control) resulted in higher levels of DPPH and FRAP. Antioxidant properties were shown by valsartan as well (DPPH: 126%, FRAP: 104% vs. control). Interestingly, a significantly decreased FRAP level in BSA + Fru + Trolox (95% vs. control) compared to BSA + Fru was observed (Table 2).

3.3. The Impact of Valsartan and Other Additives on Protein Oxidation Products, Glycooxidation Products, and Glycation Products as well as Antioxidant Activity in Ribose- (Rib-) Induced Albumin Glycation.
The addition of ribose to BSA solution resulted in lower total thiols level and higher PC and AOPP levels. All reviewed agents (valsartan: 68%, 76% vs. control, respectively) caused a significant decrease in PC and AOPP contents. Moreover, after inhibitors (valsartan: 105% vs. control) were added to BSA + Rib, statistically higher total thiols were noticed (Table 3).

Assays evaluating glycooxidation products revealed that ribose caused an increase of kynurenine, N-formylkynurenine, and dityrosine levels. Significantly greater concentrations of tryptophan were observed in comparison to BSA + Rib when BSA + Rib were incubated with valsartan (114% vs. control), Trolox (103% vs. control), NAC (105% vs. control), ALA (113% vs. control), captopril (106% vs. control), and aminoguanidine (118% vs. control). There were also significantly lower kynurenine values, N-formylkynurenine, and dityrosine in samples with agents above (valsartan: 83%, 76%, and 68% vs. control, respectively) (Table 3).

Regarding glycation products, the presence of ribose in BSA resulted in greater amyloid-β structure, fructosamine, and AGE compared to BSA alone. Furthermore, decreased levels of these parameters were noticed in samples with BSA + Rib and all investigated inhibitors (valsartan: 96%, 58%, and 66% vs. control, respectively), excepting metformin in amyloid-β structure level (Table 3).

Moreover, decreased antioxidant activity was present when ribose was incubated with BSA compared to BSA alone. The addition of antiglycooxidative agents (valsartan: 111%, 119%, and 106% vs. control), excluding metformin, resulted in significantly increased TAC, DPPH, and FRAP (Table 3).

3.4. The Impact of Valsartan and Other Additives on Protein Oxidation Products, Glycooxidation Products, and Glycation Products as well as Antioxidant Activity in Glyoxal- (GO-) Induced Albumin Glycation.
Glyoxal-induced protein oxidation resulted in increased PC and AOPP and decreased total thiols, similarly to carbohydrates described previously. Samples with all investigated agents were characterized by lower levels of PC and AOPP (valsartan: 68%, 40% vs. control, respectively). Significantly higher total thiols were observed in presence of valsartan (103% vs. control), Trolox (108% vs. control), NAC (118% vs. control), captopril (114% vs.

TABLE 2: The effects of valsartan, Trolox, NAC, ALA, captopril, aminoguanidine, or metformin addition to BSA + fructose solution on protein oxidation, glycooxidation, and antioxidant activity.

	BSA	BSA + Fru	BSA + Fru + valsartan	BSA + Fru + Trolox	BSA + Fru + NAC	BSA + Fru + ALA	BSA + Fru + captopril	BSA + Fru + aminoguanidine	BSA + Fru + metformin
					Protein oxidation				
Total thiols	114 ± 0.63 ****	100	105 ± 1.50 **	101 ± 4.80	114 ± 1.70 ***	107 ± 1.40 **	101 ± 1.30	105 ± 1.10 **	102 ± 2.10
PC	62 ± 3.70 ****	100	81 ± 1.40 ****	70 ± 5.10 ***	75 ± 4.70 ***	65 ± 7.50 **	60 ± 2.70 ****	56 ± 1.70 ****	90 ± 2.60 **
AOPP	22 ± 0.89 ****	100	58 ± 2.10 ****	49 ± 0.62 ****	39 ± 3.30 ****	39 ± 1.20 ****	45 ± 5.20 ****	36 ± 3.20 ****	95 ± 4.20
					Protein glycooxidation				
Tryptophan	238 ± 2.40 ****	100	100 ± 2.50	116 ± 12.00	103 ± 8.80	119 ± 12.00 *	158 ± 13.00 *	161 ± 3.60 ****	107 ± 9.20
Kynurenine	57 ± 1.80 ****	100	67 ± 1.80 ****	68 ± 1.10 ****	71 ± 3.10 ****	53 ± 9.10 ****	62 ± 2.90 ****	66 ± 0.26 ****	136 ± 3.40 ****
N-Formylkynurenine	21 ± 1.80 ****	100	57 ± 1.20 ****	53 ± 0.21 ****	59 ± 1.10 ****	45 ± 0.01 ****	71 ± 0.34 ****	28 ± 1.80 ****	187 ± 3.00 ****
Dityrosine	48 ± 1.50 ****	100	65 ± 1.90 ****	67 ± 0.23 ****	63 ± 1.20 ****	71 ± 1.20 ****	57 ± 0.78 ****	54 ± 0.98 ****	87 ± 1.00 ****
					Albumin glycation				
Amyloid-β structure	61 ± 0.13 ****	100	88 ± 2.60 **	87 ± 0.34 ****	86 ± 0.27 ****	81 ± 0.47 ****	81 ± 0.41 ****	80 ± 1.90 ****	108 ± 1.20 ***
Fructosamine	51 ± 1.80 ****	100	53 ± 3.50 ****	55 ± 4.00 ****	57 ± 4.00 ***	55 ± 7.60 ***	66 ± 3.90 ***	62 ± 1.20 ****	134 ± 2.80 ****
AGE	59 ± 1.10 ****	100	84 ± 1.60 ****	81 ± 0.69 ****	81 ± 0.29 ****	85 ± 2.20 ***	82 ± 0.58 ****	77 ± 2.50 ****	114 ± 2.10 ***
					Albumin antioxidant activity				
TAC	115 ± 1.10 ****	100	97 ± 2.40	86 ± 9.00	114 ± 3.20 **	89 ± 7.10	94 ± 4.60	93 ± 5.60	94 ± 4.50
DPPH	145 ± 4.60 ****	100	126 ± 2.40 ****	130 ± 3.00 ****	146 ± 3.10 ****	129 ± 8.40 ***	133 ± 3.00 ****	124 ± 3.70 ***	109 ± 3.20 **
FRAP	127 ± 2.30 ****	100	104 ± 1.80 *	95 ± 3.30 *	129 ± 3.00 ****	108 ± 1.80 **	108 ± 2.30 **	104 ± 2.40	98 ± 3.00

Abbreviations: AGE: advanced glycation end products; ALA: alpha-lipoic acid; AOPP: advanced oxidation protein products; BSA: bovine serum albumin; DPPH: 2,2-di-phenyl-1-picrylhydrazyl radical scavenging capacity; FRAP: ferric reducing antioxidant power; Fru: fructose; NAC: N-acetylcysteine; PC: protein carbonyls; TAC: total antioxidant capacity; $*p < 0.05$ vs. control; $**p < 0.01$ vs. control; $***p < 0.001$ vs. control; $****p < 0.0001$ vs. control.

TABLE 3: The effects of valsartan, Trolox, NAC, ALA, captopril, aminoguanidine, or metformin addition to BSA + ribose solution on protein oxidation, glycooxidation, and antioxidant activity.

	BSA	BSA + Rib	BSA + Rib + valsartan	BSA + Rib + Trolox	BSA + Rib + NAC	BSA + Rib + ALA	BSA + Rib + captopril	BSA + Rib + aminoguanidine	BSA + Rib + metformin
Protein oxidation									
Total thiols	128 ± 1.8 ****	100	105 ± 2.1 *	106 ± 2 **	107 ± 0.82 ***	104 ± 0.88 **	107 ± 2 **	109 ± 2.3 **	85 ± 2.9 ***
PC	65 ± 1.2 ****	100	68 ± 2.1 ****	82 ± 1.7 ****	69 ± 4.1 ***	86 ± 6.3 *	69 ± 4.9 ***	46 ± 1.7 ****	90 ± 2.2 **
AOPP	58 ± 1.5 ****	100	76 ± 2 ****	81 ± 2 ****	82 ± 1.5 ****	75 ± 1.3 ****	81 ± 2 ****	63 ± 2.9 ****	87 ± 2.7 ***
Protein glycooxidation									
Tryptophan	132 ± 1.9 ****	100	114 ± 1.4 ****	103 ± 1.2 *	105 ± 0.1 ****	113 ± 0.86 ****	106 ± 1 ***	118 ± 1.9 ****	102 ± 1
Kynurenine	46 ± 1.2 ****	100	83 ± 2.5 ***	87 ± 0.36 ****	77 ± 0.25 ****	85 ± 0.98 ****	86 ± 0.44 ****	75 ± 1.2 ****	96 ± 2.5
N-Formylkynurenine	44 ± 2.1 ****	100	76 ± 2.8 ***	81 ± 3.5 ***	64 ± 1.8 ****	76 ± 1.7 ****	65 ± 1.2 ****	63 ± 1.6 ****	68 ± 1.5 ****
Dityrosine	45 ± 4.2 ****	100	68 ± 1.9 ****	72 ± 1.6 ****	67 ± 1.6 ****	73 ± 1.9 ****	77 ± 0.04 ****	65 ± 1.2 ****	101 ± 4.8
Albumin glycation									
Amyloid-β structure	59 ± 2.2 ****	100	96 ± 1.7 *	96 ± 1.7 *	93 ± 1.4 **	95 ± 1.5 **	93 ± 1.2 ***	94 ± 1.2 ***	101 ± 4.2
Fructosamine	28 ± 2.4 ****	100	58 ± 1.8 ****	70 ± 8.6 **	75 ± 1.5 ****	78 ± 2.1 ****	60 ± 7 ***	59 ± 3.2 ****	94 ± 1.5 **
AGE	44 ± 1.8 ****	100	66 ± 1.1 ****	58 ± 1.1 ****	61 ± 1.7 ****	67 ± 1.7 ****	60 ± 1.1 ****	62 ± 1.2 ****	77 ± 0.68 ****
Albumin antioxidant activity									
TAC	132 ± 0.3 ****	100	111 ± 3.1 **	118 ± 5.4 **	129 ± 4.4 ***	104 ± 5.2	125 ± 3.6 ***	111 ± 3.6 **	104 ± 3.4
DPPH	150 ± 3.8 ****	100	119 ± 5.6 **	106 ± 0.89 ***	150 ± 6.1 ***	116 ± 8.1 *	108 ± 1.7 **	118 ± 0.93 ****	95 ± 5.7
FRAP	135 ± 2.2 ****	100	106 ± 0.54 ****	108 ± 2.4 **	117 ± 1.1 ****	110 ± 5 *	110 ± 1.6 ****	105 ± 1.3 **	78 ± 7 **

Abbreviations: AGE: advanced glycation end products; ALA: alpha-lipoic acid; AOPP: advanced oxidation protein products; BSA: bovine serum albumin; DPPH: 2,2-di-phenyl-1-picrylhydrazyl radical scavenging capacity; FRAP: ferric reducing antioxidant power; NAC: N-acetylcysteine; PC: protein carbonyls; Rib: ribose; TAC: total antioxidant capacity; $*p < 0.05$ vs. control; $**p < 0.01$ vs. control; $***p < 0.001$ vs. control; $****p < 0.0001$ vs. control.

TABLE 4: The effects of valsartan, Trolox, NAC, ALA, captopril, aminoguanidine, or metformin addition to BSA + glyoxal solution on protein oxidation, glycooxidation, and antioxidant activity.

	BSA	BSA + GO	BSA + GO + valsartan	BSA + GO + Trolox	BSA + GO + NAC	BSA + GO + ALA	BSA + GO + captopril	BSA + GO + aminoguanidine	BSA + GO + metformin
Protein oxidation									
Total thiols	123 ± 2.80 ***	100	103 ± 1.40 *	108 ± 3.00 *	118 ± 3.40 ***	98 ± 2.70	114 ± 3.70 **	114 ± 3.70 **	102 ± 1.30 *
PC	64 ± 1.10 ****	100	68 ± 2.20 ****	89 ± 2.80 **	56 ± 4.10 ****	85 ± 5.40 **	67 ± 1.40 ****	67 ± 1.40 ****	86 ± 2.80 ***
AOPP	32 ± 2.00 ****	100	40 ± 1.60 ****	52 ± 3.50 ****	32 ± 4.10 ****	41 ± 4.00 ****	50 ± 1.60 ****	33 ± 2.40 ****	64 ± 1.70 ****
Protein glycooxidation									
Tryptophan	126 ± 1.30 ****	100	113 ± 1.50 ***	126 ± 3.40 ***	113 ± 1.90 ***	111 ± 2.80 **	112 ± 5.00 *	107 ± 1.60 **	103 ± 1.70 *
Kynurenine	65 ± 3.60 ****	100	83 ± 2.20 ***	82 ± 1.90 ****	78 ± 2.00 ****	96 ± 2.90	75 ± 4.30 ***	62 ± 0.40 ****	98 ± 0.48 **
N-Formylkynurenine	16 ± 2.30 ****	100	42 ± 2.80 ****	47 ± 3.60 ****	38 ± 1.60 ****	59 ± 2.20 ****	37 ± 4.50 ****	36 ± 3.00 ****	65 ± 3.90 ***
Dityrosine	25 ± 1.20 ****	100	72 ± 1.50 ****	55 ± 2.30 ****	46 ± 1.40 ****	68 ± 1.00 ****	42 ± 0.78 ****	26 ± 2.20 ****	68 ± 1.70 ****
Albumin glycation									
Amyloid-β structure	69 ± 0.72 ****	100	71 ± 1.80 ****	68 ± 0.79 ****	66 ± 1.50 ****	75 ± 1.80 ****	62 ± 1.30 ****	63 ± 1.90 ****	83 ± 1.80 ****
Fructosamine	66 ± 2.60 ****	100	87 ± 2.90 **	92 ± 4.30 *	75 ± 3.40 ***	86 ± 2.70 ***	76 ± 2.60 ****	85 ± 3.20 **	95 ± 3.40
AGE	23 ± 2.00 ****	100	52 ± 1.60 ****	68 ± 5.00 ***	40 ± 1.80 ****	61 ± 1.80 ****	37 ± 4.80 ****	35 ± 3.40 ****	47 ± 3.20 ****
Albumin antioxidant activity									
TAC	154 ± 7.20 ***	100	116 ± 3.70 **	108 ± 0.97 ***	156 ± 3.00 ****	119 ± 2.30 ***	108 ± 3.10 *	133 ± 4.20 ***	111 ± 3.00 **
DPPH	152 ± 2.00 ****	100	115 ± 2.10 ***	128 ± 8.40 **	146 ± 3.50 ****	130 ± 2.90 ****	110 ± 6.80	133 ± 2.70 ****	105 ± 1.40 **
FRAP	159 ± 5.50 ****	100	118 ± 2.30 ***	104 ± 5.30	117 ± 1.10 ****	107 ± 1.00 ***	88 ± 2.30 **	124 ± 2.40 ****	78 ± 7.00 **

Abbreviations: AGE: advanced glycation end products; ALA: alpha-lipoic acid; AOPP: advanced oxidation protein products; BSA: bovine serum albumin; DPPH: 2,2-di-phenyl-1-picrylhydrazyl radical scavenging capacity; FRAP: ferric reducing antioxidant power; GO: glyoxal; NAC: N-acetylcysteine; PC: protein carbonyls; TAC: total antioxidant capacity; $*p < 0.05$ vs. control; $**p < 0.01$ vs. control; $***p < 0.001$ vs. control; $****p < 0.0001$ vs. control.

control), aminoguanidine (114% vs. control), and metformin (102% vs. control) (Table 4).

The glycooxidation products analysis revealed that glyoxal addition increased kynurenine, N-formylkynurenine, and dityrosine concentrations in BSA + GO samples. Furthermore, all reviewed inhibitors caused a significant increase in the aforementioned parameters (valsartan: 83%, 42%, and 72% vs. control, respectively). However, concentrations of tryptophan were higher in the presence of all substances compared to control (valsartan: 133% vs. control) (Table 4).

The presence of glyoxal in BSA solution resulted in higher glycation product content. Moreover, decreased amyloid-β structure, fructosamine, and AGE concentrations in all investigated samples versus control were observed (valsartan: 71%, 87%, and 52% vs. control, respectively), excepting sample with metformin (Table 4).

Regarding total antioxidant potential assays, the BSA + GO sample was characterized by significantly lower TAC, DPPH, and FRAP parameters than the BSA alone sample. Significantly greater TAC and DPPH values in all investigated samples, excluding DPPH in a sample with captopril, were observed. The addition of valsartan (118% vs. control), NAC (117% vs. control), ALA (107% vs. control), and aminoguanidine (124% vs. control) caused an increase of FRAP compared to control. On the other hand, the presence of captopril (88% vs. control) and metformin (78% vs. control) led to significantly lower FRAP value (Table 4).

3.5. The Impact of Valsartan and Other Additives on Protein Oxidation Products, Glycooxidation Products, and Glycation Products as well as Antioxidant Activity in Methylglyoxal- (MGO-) Induced Albumin Glycation. Methylglyoxal induced oxidative damage and significantly greater PC and AOPP levels in BSA samples. All investigated substances (valsartan: 66%, 55% vs. control, respectively) diminished this action and decreased the parameters above (except metformin). Moreover, significantly higher total thiols concentrations were noticed when valsartan (106% vs. control), Trolox (107% vs. control), NAC (109% vs. control), captopril (107% vs. control), and aminoguanidine (105% vs. control) were added (Table 5).

The presence of methylglyoxal resulted in a significant decrease in tryptophan concentration and an increase of kynurenine, N-formylkynurenine, and dityrosine concentrations. Significantly higher tryptophan levels were observed after inhibitors were added (valsartan: 107% vs. control). The majority of investigated substances (valsartan: 87%, 74%, and 72% vs. control, respectively) caused a significant decrease of kynurenine, N-formylkynurenine, and dityrosine concentrations (except ALA and metformin) (Table 5).

Furthermore, a decrease of amyloid-β structure, fructosamine, and AGE concentrations was observed due to methylglyoxal addition to the BSA sample. All used inhibitors (valsartan: 66%, 38%, and 56% vs. control, respectively) were responsible for the decrease of given parameters (Table 5).

Methylglyoxal was also the cause of decreased TAC, DPPH, and FRAP values compared to BSA alone. All the investigated samples (valsartan: 144%, 113%, and 132% vs. control, respectively), except metformin, were characterized by significantly higher TAC levels in comparison to control (Table 5).

3.6. The Impact of Valsartan and Other Additives on Protein Oxidation Products, Glycooxidation Products, and Glycation Products as well as Antioxidant Activity in Chloramine T-Induced Albumin Glycation. Markers of oxidative damage (PC and AOPP) were significantly greater in the presence of chloramine T compared to BSA alone. In all investigated samples (valsartan: 71%, 56% vs. control, respectively), significantly decreased levels of the parameters above versus control were observed. In addition, all used inhibitors (valsartan: 110% vs. control) caused a significant increase of total thiols level (Table 6).

Glycooxidation of proteins induced by chloramine T resulted in greater kynurenine concentrations, N-formylkynurenine, and dityrosine together with a lower concentration of tryptophan. The addition of valsartan (89%, 69% vs. control, respectively) and other substances led to decreased amounts of given parameters compared to control. In contrast, all the additives (excluding aminoguanidine) caused higher tryptophan concentrations in comparison to control (Table 6).

Chloramine T-induced glycation resulted in significantly higher levels of amyloid-β structure, fructosamine, and AGE. The analysis showed significantly lower concentrations of fructosamine and AGE when all investigated inhibitors were added. Moreover, a statistically decreased amount of amyloid-β structure in samples with valsartan (95% vs. control), NAC (87% vs. control), and captopril (95% vs. control) was noticed. However, the BSA + chloramine T + metformin sample presented a significantly higher amyloid-β structure than the control (Table 6).

Significantly decreased antioxidant activity markers were observed when BSA was incubated with chloramine T. The addition of valsartan (106%, 119%, and 133% vs. control, respectively) and other investigated agents, except metformin, caused a significant increase of TAC, DPPH, and FRAP value (Table 6).

4. Discussion

Cardiovascular diseases (CVD) are the most common cause of death worldwide. Many factors are involved in the pathogenesis of such diseases, but the role of oxidative stress seems to be crucial [55–58]. Oxidative stress, which is defined as excessive production of reactive oxygen species (ROS) and disproportion of oxidants over antioxidants, causes myocardial remodeling by activating hypertrophy-signaling kinases and stimulating cardiac fibroblasts to proliferate. ROS also affect myocardial calcium handling and lead to cellular dysfunction by inducing changes in intracellular pathways [59, 60]. Moreover, in dysfunctional myocardium, enhanced ROS production is observed, and the antioxidant mechanism's exhaustion leads to disease progression [61, 62]. Oxidative stress likewise participates in the pathogenesis of hypertension. ROS decrease the availability of nitric oxide (NO), causing vasoconstriction and lead to modification of low-density lipoprotein (LDL), increasing its uptake by

TABLE 5: The effects of valsartan, Trolox, NAC, ALA, captopril, aminoguanidine, or metformin addition to BSA + methylglyoxal solution on protein oxidation, glycooxidation, and antioxidant activity.

	BSA	BSA + MGO	BSA + MGO + valsartan	BSA + MGO + Trolox	BSA + MGO + NAC	BSA + MGO + ALA	BSA + MGO + captopril	BSA + MGO + aminoguanidine	BSA + MGO + metformin
Protein oxidation									
Total thiols	118 ± 0.3 ****	100	106 ± 0.95 ***	107 ± 1.1 ***	109 ± 1.5 ***	100 ± 1.4	107 ± 1.7 **	105 ± 1.1 **	97 ± 2
PC	57 ± 2.9 ****	100	66 ± 1.8 ****	71 ± 3.5 ***	63 ± 1.5 ****	58 ± 3.2 ****	51 ± 2.5 ****	48 ± 4 ****	79 ± 4.4 **
AOPP	25 ± 1.2 ****	100	55 ± 1.4 ****	62 ± 2.5 ****	55 ± 3.4 ****	57 ± 0.71 ****	53 ± 1.7 ****	57 ± 1.8 ****	90 ± 6.4
Protein glycooxidation									
Tryptophan	128 ± 1.1 ****	100	107 ± 1.4 **	102 ± 0.16 ****	100 ± 0.25	110 ± 0.31 ****	103 ± 0.39 ***	111 ± 0.15 ****	102 ± 0.9 **
Kynurenine	41 ± 2.2 ****	100	87 ± 2 ***	95 ± 0.14 ****	95 ± 1.3 **	99 ± 1.2	95 ± 3	76 ± 1.3 ****	102 ± 0.25 ***
N-formylkynurenine	13 ± 1.7 ****	100	74 ± 1.9 ****	60 ± 5.7 ***	62 ± 4.1 ****	93 ± 5.2	70 ± 7.1 **	46 ± 5.3 ****	165 ± 6.1 ****
Dityrosine	25 ± 3.9 ****	100	72 ± 1.2 ****	68 ± 4.6 ***	65 ± 2.8 ****	78 ± 5.6 **	70 ± 3.6 ***	63 ± 2.5 ****	102 ± 5.6
Albumin glycation									
Amyloid-β structure	32 ± 2.3 ****	100	66 ± 1.9 ****	86 ± 0.86 ****	62 ± 1.2 ****	50 ± 3 ****	67 ± 2.2 ****	52 ± 4.9 ****	65 ± 1.3 ****
Fructosamine	29 ± 1.2 ****	100	38 ± 2.9 ****	52 ± 5.2 ****	30 ± 0.45 ****	60 ± 6.1 ***	40 ± 0.59 ****	31 ± 6 ****	39 ± 4.7 ****
AGE	34 ± 3.5 ****	100	56 ± 1.6 ****	42 ± 2.5 ****	42 ± 2.9 ****	55 ± 3.2 ****	46 ± 4 ****	49 ± 6.2 ****	80 ± 5.7 ****
Albumin antioxidant activity									
TAC	219 ± 1.4 ****	100	144 ± 0.93 ****	107 ± 3.3 *	137 ± 7 ***	137 ± 8.7 **	148 ± 3.7 ****	141 ± 2.7 ****	129 ± 6.3 **
DPPH	143 ± 4.4 ****	100	113 ± 2.8 **	110 ± 3.1 **	127 ± 2.9 ****	116 ± 8.2 *	106 ± 1.5 **	121 ± 2.9 ***	104 ± 4.3
FRAP	150 ± 2.2 ****	100	132 ± 1.7 ****	105 ± 2.3 *	127 ± 3 ****	127 ± 3.6 ***	127 ± 4.9 ****	123 ± 5.8 **	99 ± 4.2

Abbreviations: AGE: advanced glycation end products; ALA: alpha-lipoic acid; AOPP: advanced oxidation protein products; BSA: bovine serum albumin; DPPH: 2,2-di-phenyl-1-picrylhydrazyl radical scavenging capacity; FRAP: ferric reducing antioxidant power; MGO: methylglyoxal; NAC: N-acetylcysteine; PC: protein carbonyls; TAC: total antioxidant capacity; $*p < 0.05$ vs. control; $**p < 0.01$ vs. control; $***p < 0.001$ vs. control; $****p < 0.0001$ vs. control.

Table 6: The effects of valsartan, Trolox, NAC, ALA, captopril, aminoguanidine, or metformin addition to BSA + chloramine T solution on protein oxidation, glycooxidation, and antioxidant activity.

	BSA	BSA + chloramine T	BSA + chloramine T + valsartan	BSA + chloramine T + Trolox	BSA + chloramine T + NAC	BSA + chloramine T + ALA	BSA + chloramine T + captopril	BSA + chloramine T + aminoguanidine	BSA + chloramine T + metformin
Protein oxidation									
Total thiols	126 ± 0.36 ****	100	110 ± 2.00 ***	104 ± 1.10 **	111 ± 1.40 ***	110 ± 0.64 ****	113 ± 1.40 ****	110 ± 1.20 ***	115 ± 1.80 ***
PC	57 ± 1.80 ****	100	71 ± 2.40 ***	64 ± 2.50 ****	57 ± 4.70 ****	58 ± 2.90 ****	51 ± 3.50 ****	54 ± 3.40 ****	56 ± 6.90 ***
AOPP	31 ± 0.63 ****	100	56 ± 2.10 ****	58 ± 2.80 ****	31 ± 0.77 ****	31 ± 1.10 ****	64 ± 1.70 ****	56 ± 5.60 ***	85 ± 2.90 *
Protein glycooxidation									
Tryptophan	130 ± 0.58 ****	100	101 ± 1.20 ****	102 ± 0.12 ****	104 ± 0.66 ***	107 ± 0.58 ****	97 ± 0.66 **	101 ± 1.30	97 ± 1.20 *
Kynurenine	36 ± 1.20 ****	100	89 ± 2.00 ****	88 ± 1.30 ***	50 ± 1.90 ****	78 ± 2.70 ***	53 ± 1.20 ****	91 ± 1.90 **	81 ± 2.40 ***
N-Formylkynurenine	12 ± 1.80 ****	100	69 ± 1.40 ****	62 ± 1.80 ****	46 ± 2.00 ****	51 ± 0.74 ****	54 ± 1.40 ****	93 ± 2.00 **	47 ± 1.90 ****
Dityrosine	46 ± 0.28 ****	100	77 ± 1.40 ****	82 ± 1.30 ****	42 ± 1.20 ****	53 ± 1.20 ****	64 ± 1.30 ****	82 ± 1.30 ****	84 ± 1.90 ***
Albumin glycation									
Amyloid-β structure	81 ± 0.41 ****	100	95 ± 0.83 **	84 ± 1.30	87 ± 2.50 ***	98 ± 1.10	95 ± 0.67 ***	99 ± 0.94	112 ± 1.80 ***
Fructosamine	61 ± 3.40 ****	100	86 ± 0.43 ****	66 ± 3.90 ***	57 ± 1.30 ****	79 ± 1.60 ****	69 ± 3.50 ***	87 ± 1.30 ****	66 ± 2.60 ****
AGE	44 ± 1.00 ****	100	74 ± 2.60 ****	74 ± 0.85 ****	76 ± 1.70 ****	79 ± 1.90 ****	62 ± 0.05 ****	91 ± 2.80 **	86 ± 0.97 ****
Albumin antioxidant activity									
TAC	124 ± 2.90 ***	100	106 ± 3.40 ***	111 ± 1.40 ***	116 ± 1.00 ****	125 ± 3.60 ***	116 ± 0.85 ****	105 ± 2.90 *	103 ± 2.70
DPPH	157 ± 4.60 ****	100	119 ± 3.00 ***	157 ± 4.00 ****	158 ± 2.70 ****	137 ± 2.10 ****	146 ± 4.20 ****	113 ± 3.00 **	108 ± 2.90
FRAP	150 ± 2.20 ****	100	133 ± 3.20 ****	134 ± 3.80 ****	167 ± 4.00 ****	127 ± 5.10 ***	126 ± 7.10 ***	122 ± 5.30 ***	107 ± 1.20

Abbreviations: AGE: advanced glycation end products; ALA: alpha-lipoic acid; AOPP: advanced oxidation protein products; BSA: bovine serum albumin; DPPH: 2,2-di-phenyl-1-picrylhydrazyl radical scavenging capacity; FRAP: ferric reducing antioxidant power; NAC: N-acetylcysteine; PC: protein carbonyls; TAC: total antioxidant capacity. $*p < 0.05$ vs. control; $**p < 0.01$ vs. control; $***p < 0.001$ vs. control; $****p < 0.0001$ vs. control.

macrophages. As a result, the so-called foam cells are formed. Those cells take a very important part in atherosclerosis's pathogenesis, which is a well-known factor of hypertension and other diseases, such as coronary artery disease [16]. Oxidative stress is also a proven link between diabetes mellitus (DM) and CVD [63]. Furthermore, in patients diagnosed with DM, elevated levels of advanced glycation end products (AGE) are observed. This, along with oxidative stress, may explain the pathogenesis of cardiovascular complications of DM [64–67]. AGE are also a proven factor leading to heart failure and other CVD [11, 68–71].

Valsartan is a potent and specific angiotensin II receptor antagonist used to treat hypertension and chronic heart failure. Many clinical studies confirm the effectiveness of the drug, especially in combination with sacubitril [72, 73]. What is interesting, it is also proven that the therapy with valsartan significantly increases the long-term quality of life in patients with chronic heart failure [74], which is a result of biochemical, echocardiographic, and clinical improvements [75]. Simultaneously, the drug remains safe in patients with many comorbidities, especially in chronic kidney disease [76]. In patients with hypertension, the use of valsartan is also associated with the reduction of the risk of organ complications, including left ventricular hypertrophy [77, 78]. Due to the valsartan's pleiotropic properties, it is believed that the mechanism of drug action is not fully understood.

The research about the antioxidant properties of valsartan is especially limited. Nevertheless, the majority of accessible papers uphold the hypothesis of the drug's positive impact on the redox homeostasis *in vivo* [29, 79–90] (Table 7). Experiments conducted on animals show a statistically significant decrease in oxidative stress parameters and inflammatory and cellular damage markers. Valsartan also causes an increase in antioxidant enzymes' activities and decrease concentrations of adhesive and chemotactic factors. What is important, results of clinical studies remain consistent with the animal model results (Table 7). However, there are no data on the antiglycation activity of valsartan. Only Komiya et al. revealed a statistically significant decrease in blood AGE concentration in diabetic and hypertensive patients treated with valsartan [86]. This may suggest a potential antiglycation role, but there is no more available evidence to support this statement.

Despite all the facts that stand for valsartan as the antioxidant potential, some limitations are worth mentioning regarding this research. Available clinical studies were conducted in relatively small groups of patients, making it more challenging to perform a reliable statistical prediction. In some studies, patients continued the treatment with previously prescribed drugs before administering valsartan. It is unclear if these drugs had no known impact on cellular redox balance and interfere with the trial's results. There is also even more limited information regarding the influence of valsartan on protein glycooxidation. Thus, it is necessary to evaluate the effect of valsartan on protein oxidative damage by measuring the oxidation rate of thiol and carbonyl groups, aromatic amino acid residues, or assessing the extent of early and late protein glycation products.

Our study is the first to assess valsartan's antiglycation properties with respect to various glycating and oxidizing agents. Using an *in vitro* model, we have shown that valsartan strengthens the antioxidant barrier and inhibits oxidation and albumin glycation comparable to recognized ROS scavengers (Trolox, N-acetylcysteine, lipoic acid, and captopril) and protein glycation inhibitors (aminoguanidine and metformin). Considering the key role of oxidative stress in CVD pathology, valsartan's pleiotropic activity may result from its antioxidant and antiglycation properties.

Albumin, the main plasma protein, has a crucial role in the human organism. It is responsible for the transport of various substances such as hormones or drugs and maintaining blood pH or colloid-oncotic pressure. Albumin can also bind transition metal ions which explains its antioxidative properties [94–96]. Due to its high plasma concentration, long half-life, and high content of arginine, cysteine, and lysine, albumin can be easily glycated and oxidized *in vivo* [97, 98]. Albumin glycation involves nonenzymatic addition of reducing sugar to its amino groups. This process is subdivided into several phases. During the early ones are formed, the first Maillard reaction produces the Schiff base and the Amadori products. At the final stage, the advanced glycation end products (AGEs) are produced—including carboxymethyl lysine (CML), furyl-furanyl-imidazole (FFI), pentosidine, and pyralin [68, 70, 82, 98]. The glycation process occurs simultaneously with oxidation, by which they are collectively referred to as glycooxidation. The final products of protein oxidation are advanced oxidation protein products (AOPP). AOPPs originate from the accumulation of oxidized residue of arginine, cysteine, dityrosine, and tryptophan [69, 99, 100].

Our research demonstrated that valsartan ameliorates protein oxidation ($\uparrow$total thiols, $\downarrow$PC, and $\downarrow$AOPP), reduces albumin glycooxidative damage ($\uparrow$tryptophan, $\downarrow$kynurenine, $\downarrow$N-formylkynurenine, and $\downarrow$dityrosine), prevents glycation ($\downarrow$amyloid-beta structure, $\downarrow$fructosamine, $\downarrow$and AGE), and enhances the antioxidant activity of albumin ($\uparrow$TAC, $\uparrow$DPPH, and $\uparrow$FRAP). These results are similar in every investigated glycating or oxidizing agent combined with the drug. However, some differences in the drug's action are distinguishable between sugars and aldehydes. Generally, the antiglycooxidant properties of valsartan are more marked in samples containing GO or MGO and valsartan, where the parameters decrease or increase even more in comparison to the sugars samples (e.g., AGE content is lower in BSA + GO/MGO + valsartan than in BSA + Glu/Fru/Rib + valsartan). Nevertheless, it is worth mentioning that the oxidation and glycation substances used in the research were at greater concentrations than physiological levels that might impact the experiment's outcome [31, 32]. However, our model is kinetically validated and allows us to evaluate unknown substances' antiglycooxidative properties rapidly [31, 34]. There were no prominent differences between used sugars, as given results in their samples were comparable. Interestingly, valsartan exhibited antioxidant and antiglycooxidant properties in chloramine T presence, but glycation inhibition was not so potent as in the case of sugars or aldehydes.

TABLE 7: The pleiotropic properties of valsartan in experimental and clinical studies.

Valsartan properties	Study design	Measured parameters	Results	References
Valsartan presenting antioxidant properties in myocardial ischemia and myocardial infarction model in rats	Seven male albino rats pretreated intraperitoneally (i.p.) with valsartan (10 mg/kg) before left anterior descending artery (LAD) ligation vs. rats which undergo the same intervention, but with no pretreatment or saline i.p. injection	Cardiac troponin T (cTnT) in heart blood plasma	↓cTnT concentration in valsartan-pretreated group vs. control ($p < 0.001$)	Hadi et al. 2015 [79]
		Malondialdehyde (MDA) and reduced glutathione (GSH) in heart blood serum	↓MDA concentration in valsartan-pretreated group vs. control ($p < 0.001$)	
		Tumor necrosis factor (TNF), interleukin 6 (IL-6), interleukin 10 (IL-10), caspase 3, and BAX protein in cardiac tissue	↓TNF, ↓IL-6, ↓IL-10 ↓caspase 3, ↓BAX concentrations in valsartan-pretreated group vs. control ($p < 0.001$)	
		Histopathological study of cardiac tissue	Histopathological injure improvement in valsartan-pretreated rats vs. control (14.3% of the group had no signs of injury; $p < 0.001$)	
	16 male Sprague-Dawley rats treated with p.o. valsartan (10 mg/kg/d, 2 weeks) after ligation of LAD vs. 16 not pretreated rats that undergone the same procedure	Plasma MDA, superoxide dismutase (SOD) activity, and TNF-α	↓MDA, ↑SOD after 4 h of reperfusion vs. ischemia-reperfusion control group ($p < 0.05$)	Wu et al. 2013 [80]
		Myocardial nicotinamide adenine dinucleotide phosphate (NADPH) oxidase and nuclear factor–kappa B (NF-κB)	↓TNF-α in 60 min, 120 min, and 240 min after reperfusion vs. ischemia-reperfusion control ($p < 0.05$)	
			↓NADPH oxidase activity, ↓NF-κB expression vs. ischemia-reperfusion control ($p < 0.05$)	
	2 groups of 6 male Wistar rats premedicated with valsartan 50 mg/kg or 100 mg/kg for 14 days and then treated with isoproterenol (ISO) to induce MI	Total antioxidant activity (TAC) and nitric oxide (NO) in serum	↓1.6x/2.03x TAC (VAL 50/100, $p < 0.01$/$p < 0.001$) vs. MI-control	Imran et al. 2019 [81]
			↓1.58x NO (VAL 100, $p < 0.01$)	
		Catalase, SOD, glutathione peroxidase (GPX), glutathione reductase (GR), glutathione S-transferase (GST), thiobarbituric acid-reactive substances (TBARS) in cardiac tissue	↑ CAT (VAL 100, $p < 0.05$)	
			↑ SOD (VAL 100, $p < 0.01$)	
			↑2.7x/3.45x GPX (VAL 50/100, $p < 0.05$/$p < 0.05$)	
			↑2.26x/2.42x GR (VAL 50/100, $p < 0.05$)	
			↑1.86x/2.11x GST (VAL 50/100, $p < 0.05$/$p < 0.01$)	
			1.86x/2.29x ↓TBARS (VAL 50/100, $p < 0.05$/$p < 0.01$)	
		Histopathological study of cardiac tissue	A few inflammatory cells and vacuolization in VAL 50 myocardium	
			Muscle fibers with no significant changes except for larger nucleus in VAL 100	
Valsartan ameliorates cardiac hypertrophy resulting from cardiac pressure overload in rats	4 groups of Sprague-Dawley rats (sham ($n = 16$), vehicle ($n = 26$), valsartan ($n = 29$), sacubitril/valsartan ($n = 28$)) undergoing aortic banding to induce cardiac pressure overload	Left ventricular weight	No significant change of left ventricular weight in VAL group vs. vehicle ($p = 0.04$)	Nordén et al. 2021 [91]
		Mean arterial pressure (MAP)	↓16% MAP in VAL group vs. sham	

TABLE 7: Continued.

Valsartan properties	Study design	Measured parameters	Results	References
Reduction of oxidative damage of kidneys with valsartan in streptozotocin-induced diabetes in rats	8 male Wistar rats with streptozotocin-induced diabetes treated with p.o. valsartan (100 mg/kg/d, 1 month) vs. 8 diabetic, nontreated rats	Atrial and brain natriuretic peptide (ANP, BNP)	↑ANP, BNP in VAL group vs. sham ($p < 0.05$)	Sanajou et al. 2019 [82]
		Histopathological study of cardiac tissue	↑Expression of collagen 1, 3, and metalloproteinase-2 of cardiac tissue in VAL group	
		MDA, SOD, GPX, renal TNF-α-mRNA, renal TGF-β-mRNA, renal IL-6, NAD/NADH ratio in renal tissue homogenate	↓TNF-α-mRNA, ↓IL-6, ↓urine IL-6, ↓TGF-β-mRNA, ↑NAD/NADH ratio vs. diabetic rats control group ($p < 0.001$)	
		IL-6 in urine	↓Renal MDA, ↑renal GPX, ↑renal SOD vs. diabetic rats control group ($p < 0.001$)	
		Histopathological study of renal tissue	Significant reduction of collagen deposition in the tubulointerstitial area	
Antiatherogenic effect of valsartan in cholesterol-fed rabbits	Male rabbits fed with normal ($n = 4$), cholesterol ($n = 6$), or cholesterol + valsartan ($n = 5$) diet (1 mg/kg, subcutaneously)	Systolic and diastolic blood pressure (SBP, DBP)	No significant change of SBP or DBP in VAL group vs. cholesterol-fed	Li et al. 2004 [92]
		Total cholesterol and triglycerides (TC, TG)	No significant change of TC in VAL group vs. cholesterol-fed	
		Serum ACE activity	↓TG in VAL group vs. cholesterol-fed ($p < 0.05$)	
		Morphology and histopathological studies of aorta	↓Of atherosclerotic lesion area in VAL group, but not statistically significant	
Inflammation and vascular remodeling attenuation in valsartan-treated diabetic and hyperlipidemic swine	24 diabetic and hyperlipidemic swine divided into three groups (early and late); placebo ($n = 4$), valsartan 320 mg daily ($n = 4$), valsartan + simvastatin 320 mg/40 mg ($n = 4$)	Progression of atherosclerotic lesions	Slower progression of atherosclerotic plaques vs. placebo	Chatzizisis et al. 2009 [93]
		Histopathological studies	↓area of inflammation in plaques in VAL group vs. placebo ($p = 0.041$)	
		Expression of extracellular matrix metalloproteinases (MMP-2, MMP-9)	↓MMP-9 ratio in plaques with expansive remodeling in VAL group ($p = 0.1$)	
		Expression of tissue inhibitors of metalloproteinases (TIMP-1, TIMP-2)	↓MMP/TIMP ratio in plaques with expansive remodeling in VAL group ($p = 0.01$)	
Antioxidant action of valsartan in high-glucose-cultured rat mesangial cells	HBZY-1 rat mesangial cells cultured with high glucose (30 mmol/lLconcentration and valsartan (10 μmol/L) vs. cells cultured in high-glucose only vs. osmotic pressure control group (25 mmol/L of mannitol, 5 mmol/L of glucose)	SOD activity, nitric oxide (NO), and malondialdehyde (MDA) contents in supernatant	↑SOD activity and ↑NO, ↓MDA contents in valsartan + high-glucose group vs. high-glucose only group (after 24 hrs of incubation)	Liu et al. 2016 [83]
Oxidative stress parameters in type 2 diabetic and hypertensive patients treated with valsartan	33 patients with type 2 diabetes and hypertension treated with valsartan (80 mg/d) for 24 weeks (no other antihypertensive drugs 2 weeks before the screening date)	Nitrotyrosine in blood	↓Nitrotyrosine after 24 weeks of treatment (0.68 ± 0.59 nmol/L vs. 0.38 ± 0.39 nmol/L, $p < 0.007$)	Kim et al. 2017 [84]
	26 patients with hypertension (>140/90 mmHg) and mild diabetes (HbA$_{1c}$ < 9%) treated	Blood inflammatory markers (hs-CRP, IL-6, IL-18, VCAM-1, L-selectin)	↓hs-CRP (0.231 vs. 0.134, $p = 0.043$)	Kuboki et al. 2007 [85]

Table 7: Continued.

Valsartan properties	Study design	Measured parameters	Results	References
	with 40 or 80 mg/kg valsartan for 3 months, all previously taken drugs were continued		↓VCAM-1 (471.1 vs. 403.2, $p = 0.012$)	
			↑IL-6, IL-18, L-selectin (but statistically insignificant)	
		8-Isoprostane and 8-OHdG in urine	↓8-OHdG after treatment (12.12 vs. 8.07, $p = 0.001$)	
			↑8-Isoprostane after treatment (283.5 vs. 302.0, but statistically insignificant)	
	15 patients with type 2 diabetes treated with 40 mg/d valsartan (in 6 patients dose increased to 80 mg/d after 6 months) for 1 year	AGE in blood	↓AGE (2.71 ± 0.62 vs. 2.29 ± 0.28, $p = 0.021$)	Komiya et al. 2008 [86]
		Urine 8-isoprostane	↓8-Isoprostane (347 ± 215 vs. 205 ± 122, $p = 0.025$)	
	25 patients with hypertension (>140/90 mmHg) treated with 80 or 160 mg/d valsartan depending on basal arterial pressure	Urine 8-isoprostane and 8-hydroxy-2′-deoxyguanosine (8-OHG)	55% ↓urine 8-isoprostane and 30% ↓8-OHdG after 12 months of treatment ($p < 0.05$)	Hirooka et al. 2008 [29]
Valsartan ameliorated oxidative stress in patients with hypertension	17 patients with hypertension (>140/90 mmHg) treated with 40 or 80 mg/d valsartan if BP did not decrease below 140/90 mmHg	Serum levels of lipoperoxidation (LPO)	↓LPO after 6 months, when pretreatment LPO levels were ≥1.5 pg/mL (2.12 ± 0.23 vs. 1.15 ± 0.31, $p < 0.05$)	Miyajima et al. 2008 [87]
	8 patients with hypertension and hyperlipidemia treated with 80 mg/d valsartan for 2 months	Plasma TBARS	↓TBARS after the treatment (33.0 ± 2.8 vs. 26.6 ± 1.8, $p < 0.05$)	Hussein et al. 2002 [88]
		Lag time required for the initiation of LDL oxidation	↑Lag time after the treatment (57 min ± 3 vs. 70 min ± 6, $p < 0.05$)	
Valsartan improved an atherosclerotic lesion in mice by oxidative stress improvement	Male apoE-deficient mice on standard or high-cholesterol diet (HCD) treated with 0.5 mg/kg valsartan i.p. in osmotic minipump	Expression of NADPH oxidase subunit p47[phox]	58% ↓p47[phox] in HCD + valsartan group vs. HCD-only ($p < 0.05$)	Suzuki et al. 2006 [89]
		The area of the atherosclerotic lesion in the aorta	2% of area in HCD + valsartan group vs. 5% in HCD group ($p < 0.05$)	
		Protein carbonyls (PC), 8-OHdG, 13-hydroxyoctadecadienoic acid (13-HODE), hs-CRP in plasma	No change in PC (0.17 ± 0.01 before and after, but statistically insignificant)	
Effect of valsartan on redox balance in hemodialysed patients with end-stage renal disease	19 patients with end-stage renal disease treated with 320 mg/d valsartan for 6 weeks		19.5% ↓ 8-OHdG (2.97 ± 0.22 vs. 2.38 ± 0.15, $p < 0.05$)	Aslam et al. 2006 [90]
			14.4% ↓13-HODE (428.3 ± 26.8 vs. 366.87 ± 15.8, but statistically insignificant)	
		Glutathione disulfide: reduced glutathione ratio (GSSG:GSH) in whole blood	↑hs-CRP (0.84 ± 0.36 vs. 1.33 ± 0.5, but statistically insignificant)	
			79% ↓GSSG: GSH (2.9 ± 3.1 vs. 0.6 ± 0.1)	

Although our study does not explain it, valsartan's anti-glycooxidant properties may be due to the molecule's chemical structure. It can be speculated that the -NH₂ group in valsartan competes with the amino residues of proteins for the attachment of reactive carbonyl groups. Thus, it protects the lysine and arginine residues of proteins from their gly-cooxidative modifications. Therefore, future investigations are necessary to validate conclusions that can be drawn from this study. The next phase of research is the *in vivo* analysis of antiglycooxidant activity and optimal dosage of valsartan in

animal and human models. However, the pleiotropic properties of valsartan may also be due to its other *in vivo* activities. Angiotensin II is a major effector peptide of the renin-angiotensin-aldosterone system, and it is generated from angiotensin I by the angiotensin-converting enzyme. Moreover, angiotensin II by acting on the AT_1 receptor stimulates NADPH oxidase activation (Nox) and increases expression of Nox subunits leading to ROS overproduction [101]. Importantly, blockade of the renin-angiotensin system with blockers of AT_1 receptors (ARBs) (such as valsartan) can reduce oxidative stress due to inhibition of the processes mentioned above. It was also shown that valsartan causes increased SOD expression, which transforms superoxide radicals into hydrogen peroxide and oxygen in a disproportionate reaction [102]. It is also speculated that ARBs can decrease protein oxidation via free radical scavenging and transition metal chelation [103].

Inhibition of protein glycation by valsartan may be of particular importance in patients with diabetic cardiomyopathy. AGE generated under hyperglycemic conditions increase ROS overproduction, which impairs the activity of ion pumps and mitochondria, disrupts the transport of calcium ions between cellular compartments, and initiates apoptosis. Extracellular matrix collagen also undergoes glycation, increasing cardiac stiffness and decreasing diastolic capacity and nerve impulse conduction velocity [61, 62]. It can be speculated that valsartan may inhibit the synthesis of AGE by directly neutralizing reactive dicarbonyl compounds by combining drug amino group with the α-dicarbonyl group of methylglyoxal. Nevertheless, these hypotheses require confirmation in further studies.

Overall, conducted research showed that valsartan can reduce oxidation and glycation damage and improve the albumin's antioxidant properties. The valsartan's activity was recorded against various oxidizing and glycating agents. What is more, the drug's action is comparable to many renowned antioxidants or is even more pronounced. The pleiotropic properties of valsartan may be due to its antiglycooxidant activity. Inhibition of protein glycation/oxidation in patients with CVD and DM may be crucial, given the significant contribution of oxidative and carbonyl stress to the development of cardiometabolic complications. Further studies considering this subject may be revolutionary for the treatment of cardiovascular diseases. Confirmation of the antiglycating effect of valsartan in human studies could result in a revision of clinical guidelines for the use of hypotensive drugs. Valsartan could be a first-line medicine in patients with heart disease and diabetes. Modifications to the chemical structure of valsartan should also be considered. The introduction of $-NH_2$ groups (as in polyamide compounds) could increase the antiglycation activity's potency.

Data Availability

The article contains complete data used to support the findings of this study.

Conflicts of Interest

The authors declare no conflict of interest.

Authors' Contributions

Conceptualization was done by M.M. Data curation was done by C.P., E.M.G, K.M.M., and M.M. Formal analysis was done by M.M. Funding acquisition was done by A.Z. and M.M. Investigation was done by M.M. Methodology was done by C.P., E.M.G, K.M.M., and M.M. Project administration was done by M.M. Resources was handled by A.Z. and M.M. Software was handled by M.M. Supervision was done by A.Z., M.Z.-P., and M.M. Validation was done by M.M. Visualization was done by M.M. Writing—original draft—was done by C.P., E.M.G, K.M.M., and M.M. Writing—review and editing—was done by A.Z. and M.M. All authors have read and agreed to the published version of the manuscript.

Acknowledgments

References

[1] B. Choromańska, P. Myśliwiec, M. Łuba et al., "Impact of weight loss on the total antioxidant/oxidant potential in patients with morbid obesity—a longitudinal study," *Antioxidants*, vol. 9, no. 5, p. 376, 2020.

[2] H. Sies, "Oxidative stress: a concept in redox biology and medicine," *Redox Biology*, vol. 4, pp. 180–183, 2015.

[3] E. Rendra, V. Riabov, D. M. Mossel, T. Sevastyanova, M. C. Harmsen, and J. Kzhyshkowska, "Reactive oxygen species (ROS) in macrophage activation and function in diabetes," *Immunobiology*, vol. 224, no. 2, pp. 242–253, 2019.

[4] J. Qiao, J. F. Arthur, E. E. Gardiner, R. K. Andrews, L. Zeng, and K. Xu, "Regulation of platelet activation and thrombus formation by reactive oxygen species," *Redox Biology*, vol. 14, pp. 126–130, 2018.

[5] B. Choromańska, P. Myśliwiec, M. Łuba et al., "The impact of hypertension and metabolic syndrome on nitrosative stress and glutathione metabolism in patients with morbid obesity," *Oxidative Medicine and Cellular Longevity*, vol. 2020, 1057510 pages, 2020.

[6] B. Choromańska, P. Myśliwiec, M. Łuba et al., "A longitudinal study of the antioxidant barrier and oxidative stress in morbidly obese patients after bariatric surgery. Does the metabolic syndrome affect the redox homeostasis of obese people?," *Journal of Clinical Medicine*, vol. 9, no. 4, p. 976, 2020.

[7] M. Maciejczyk, J. Matczuk, M. Żendzian-Piotrowska et al., "Eight-week consumption of high-sucrose diet has a prooxidant effect and alters the function of the salivary glands of rats," *Nutrients*, vol. 10, no. 10, p. 1530, 2018.

[8] F. Giacco and M. Brownlee, "Oxidative stress and diabetic complications," *Circulation Research*, vol. 107, no. 9, pp. 1058–1070, 2010.

[9] T. J. Guzik and R. M. Touyz, "Oxidative stress, inflammation, and vascular aging in hypertension," *Hypertension*, vol. 70, no. 4, pp. 660–667, 2017.

[10] N. Sinha and P. Dabla, "Oxidative stress and antioxidants in hypertension–a current review," *Current Hypertension Reviews*, vol. 11, no. 2, pp. 132–142, 2015.

[11] A. Klimiuk, A. Zalewska, R. Sawicki, M. Knapp, and M. Maciejczyk, "Salivary oxidative stress increases with the progression of chronic heart failure," *Journal of Clinical Medicine*, vol. 9, no. 3, p. 769, 2020.

[12] Q. M. Chen, S. Morrissy, and J. S. Alpert, "Oxidative stress and heart failure," in *Comprehensive Toxicology: Third Edition*, Elsevier Science, Amsterdam, The Netherlands, 2018, ISBN 9780081006122.

[13] M. Maciejczyk, K. Taranta-Janusz, A. Wasilewska, A. Kossakowska, and A. Zalewska, "A case-control study of salivary redox homeostasis in hypertensive children. Can salivary uric acid be a marker of hypertension?," *Journal of Clinical Medicine*, vol. 9, no. 3, p. 837, 2020.

[14] P. M. Vanhoutte, H. Shimokawa, E. H. C. Tang, and M. Feletou, "Endothelial dysfunction and vascular disease," *Acta Physiologica*, vol. 196, no. 2, pp. 193–222, 2009.

[15] N. Escobales and M. Crespo, "Oxidative-nitrosative stress in hypertension," *Current Vascular Pharmacology*, vol. 3, no. 3, pp. 231–246, 2005.

[16] M. Korsager Larsen and V. V. Matchkov, "Hypertension and physical exercise: the role of oxidative stress," *Medicina*, vol. 52, no. 1, pp. 19–27, 2016.

[17] K. A. Ahmad, D. Yuan Yuan, W. Nawaz et al., "Antioxidant therapy for management of oxidative stress induced hypertension," *Free Radical Research*, vol. 51, no. 4, pp. 428–438, 2017.

[18] K. Prasad and M. Mishra, "Do advanced glycation end products and its receptor play a role in pathophysiology of hypertension?," *International Journal of Angiology*, vol. 26, pp. 1–11, 2017.

[19] B. Gryszczyńska, M. Budzyń, B. Begier-Krasińska et al., "Association between advanced glycation end products, soluble RAGE receptor, and endothelium dysfunction, evaluated by circulating endothelial cells and endothelial progenitor cells in patients with mild and resistant hypertension," *International Journal of Molecular Science*, vol. 20, no. 16, p. 3942, 2019.

[20] C. Ott, K. Jacobs, E. Haucke, A. Navarrete Santos, T. Grune, and A. Simm, "Role of advanced glycation end products in cellular signaling," *Redox Biology*, vol. 2, pp. 411–429, 2014.

[21] E. Schulz, T. Gori, and T. Münzel, "Oxidative stress and endothelial dysfunction in hypertension," *Hypertension Research*, vol. 34, no. 6, pp. 665–673, 2011.

[22] K. Drygalski, K. Siewko, A. Chomentowski et al., "Phloroglucinol strengthens the antioxidant barrier and reduces oxidative/nitrosative stress in nonalcoholic fatty liver disease (NAFLD)," *Oxidative Medicine and Cellular Longevity*, vol. 2021, 18 pages, 2021.

[23] G. Flesch, P. Müller, and P. Lloyd, "Absolute bioavailability and pharmacokinetics of valsartan, an angiotensin II receptor antagonist, in man," *European Journal of Clinical Pharmacology*, vol. 52, no. 2, pp. 115–120, 1997.

[24] N. Siddiqui, A. Husain, L. Chaudhry, S. S. Alam, M. Mitra, and P. S. Bhasin, "Pharmacological and pharmaceutical profile of valsartan: a review," *Journal of Applied Pharmaceutical Science*, vol. 1, pp. 12–19, 2011.

[25] N. Perico, D. Spormann, E. Peruzzi, F. Bodin, A. Sioufi, and F. Bertocchi, "Efficacy and tolerability of valsartan compared with lisinopril in patients with hypertension and renal insufficiency," *Clinical Drug Investigation*, vol. 14, no. 4, pp. 252–259, 1997.

[26] J. N. Cohn and G. Tognoni, "A randomized trial of the angiotensin-receptor blocker valsartan in chronic heart failure," *The New England Journal of Medicine*, vol. 345, no. 23, pp. 1667–1675, 2001.

[27] G. Viberti and N. M. Wheeldon, "Microalbuminuria reduction with valsartan in patients with type 2 diabetes mellitus: a blood pressure-independent effect," *Circulation*, vol. 106, no. 6, pp. 672–678, 2002.

[28] J. Martin and H. Krum, "Role of valsartan and other angiotensin receptor blocking agents in the management of cardiovascular disease," *Pharmacological Research*, vol. 46, no. 3, pp. 203–212, 2002.

[29] Y. Hirooka, Y. Kimura, Y. Sagara, K. Ito, and K. Sunagawa, "Effects of valsartan or amlodipine on endothelial function and oxidative stress after one year follow-up in patients with essential hypertension," *Clinical and Experimental Hypertension*, vol. 30, no. 3-4, pp. 267–276, 2009.

[30] G. Zhou, A. K. Cheung, X. Liu, and Y. Huang, "Valsartan slows the progression of diabetic nephropathy in db/db mice via a reduction in podocyte injury, and renal oxidative stress and inflammation," *Clinical Science*, vol. 126, no. 10, pp. 707–720, 2014.

[31] I. Sadowska-Bartosz, S. Galiniak, and G. Bartosz, "Kinetics of glycoxidation of bovine serum albumin by glucose, fructose and ribose and its prevention by food components," *Molecules*, vol. 19, no. 11, pp. 18828–18849, 2014.

[32] I. Sadowska-Bartosz, I. Stefaniuk, S. Galiniak, and G. Bartosz, "Glycation of bovine serum albumin by ascorbate in vitro: possible contribution of the ascorbyl radical?," *Redox Biology*, vol. 6, pp. 93–99, 2015.

[33] S. Galiniak, G. Bartosz, and I. Sadowska-Bartosz, "Is iron chelation important in preventing glycation of bovine serum albumin in vitro?," *Cellular and Molecular Biology Letters*, vol. 20, pp. 562–570, 2015.

[34] I. Sadowska-Bartosz, S. Galiniak, and G. Bartosz, "Kinetics of glycoxidation of bovine serum albumin by methylglyoxal and glyoxal and its prevention by various compounds," *Molecules*, vol. 19, no. 4, pp. 4880–4896, 2014.

[35] I. Sadowska-Bartosz, S. Galiniak, J. Skolimowski, I. Stefaniuk, and G. Bartosz, "Nitroxides prevent protein glycoxidation in vitro," *Free Radical Research*, vol. 49, pp. 113–121, 2014.

[36] I. Zieniewska, A. Zalewska, M. Żendzian-Piotrowska, J. R. Ładny, and M. Maciejczyk, "Antioxidant and antiglycation properties of seventeen fruit teas obtained from one manufacturer," *Applied Sciences*, vol. 10, no. 15, p. 5195, 2020.

[37] E. Grzebyk and A. Piwowar, "The Tibetan herbal medicines Padma 28 and Padma Circosan inhibit the formation of advanced glycation endproducts (AGE) and advanced oxidation protein products (AOPP) in vitro," *BMC Complementary and Alternative Medicine*, vol. 14, no. 1, 2014.

[38] C. Pawlukianiec, M. E. Gryciuk, K. M. Mil, M. Żendzian-Piotrowska, A. Zalewska, and M. Maciejczyk, "A new insight into meloxicam: assessment of antioxidant and anti-glycating activity in in vitro studies," *Pharmaceuticals*, vol. 13, no. 9, pp. 240–219, 2020.

[39] I. Sadowska-Bartosz and G. Bartosz, "Effect of glycation inhibitors on aging and age-related diseases," *Mechanisms of Ageing and Development*, vol. 160, pp. 1–18, 2016.

[40] L. Lv, X. Shao, H. Chen, C. T. Ho, and S. Sang, "Genistein inhibits advanced glycation end product formation by trapping methylglyoxal," *Chemical Research in Toxicology*, vol. 24, no. 4, pp. 579–586, 2011.

[41] A. Meeprom, W. Sompong, C. Chan, and S. Adisakwattana, "Isoferulic acid, a new anti-glycation agent, inhibits fructose- and glucose-mediated protein glycation in vitro," *Molecules*, vol. 18, no. 6, pp. 6439–6454, 2013.

[42] G. L. Ellman, "Tissue sulfhydryl groups," *Archives of Biochemistry and Biophysics*, vol. 82, no. 1, pp. 70–77, 1959.

[43] A. Z. Reznick and L. Packer, "Oxidative damage to proteins: spectrophotometric method for carbonyl assay," *Methods in Enzymology*, vol. 233, pp. 357–363, 1994.

[44] J. Škrha, M. Prázný, J. Hilgertová, J. Kvasnička, M. Kalousová, and T. Zima, "Oxidative stress and endothelium influenced by metformin in type 2 diabetes mellitus," *European Journal of Clinical Pharmacology*, vol. 63, no. 12, pp. 1107–1114, 2007.

[45] C. L. Hawkins, P. E. Morgan, and M. J. Davies, "Quantification of protein modification by oxidants," *Free Radical Biology & Medicine*, vol. 46, no. 8, pp. 965–988, 2009.

[46] S. A. Hudson, H. Ecroyd, T. W. Kee, and J. A. Carver, "The thioflavin T fluorescence assay for amyloid fibril detection can be biased by the presence of exogenous compounds," *The FEBS Journal*, vol. 276, no. 20, pp. 5960–5972, 2009.

[47] H. Levine, "Thioflavine T interaction with synthetic Alzheimer's disease β-amyloid peptides: detection of amyloid aggregation in solution," *Protein Science*, vol. 2, no. 3, pp. 404–410, 1993.

[48] S. D. Sharma, B. N. Pandey, K. P. Mishra, and S. Sivakami, "Amadori product and age formation during nonenzymatic glycosylation of bovine serum albumin in vitro," *Journal of Biochemistry, Molecular Biology, and Biophysics*, vol. 6, pp. 233–242, 2002.

[49] G. Münch, R. Keis, A. Wessels et al., "Determination of advanced glycation end products in serum by fluorescence spectroscopy and competitive ELISA," *Clinical Chemistry and Laboratory Medicine*, vol. 35, no. 9, pp. 669–678, 1997.

[50] O. Erel, "A novel automated direct measurement method for total antioxidant capacity using a new generation, more stable ABTS radical cation," *Clinical Biochemistry*, vol. 37, no. 4, pp. 277–285, 2004.

[51] O. Erel, "A new automated colorimetric method for measuring total oxidant status," *Clinical Biochemistry*, vol. 38, no. 12, pp. 1103–1111, 2005.

[52] W. Brand-Williams, M. E. Cuvelier, and C. Berset, "Use of a free radical method to evaluate antioxidant activity," *LWT-Food science and Technology*, vol. 28, no. 1, pp. 25–30, 1995.

[53] R. Scherer and H. T. Godoy, "Antioxidant activity index (AAI) by the 2,2-diphenyl-1-picrylhydrazyl method," *Food Chemistry*, vol. 112, no. 3, pp. 654–658, 2009.

[54] I. F. F. Benzie and J. J. Strain, "The ferric reducing ability of plasma (FRAP) as a measure of "antioxidant power": the FRAP assay," *Analytical Biochemistry*, vol. 239, pp. 70–76, 1996.

[55] T. Münzel, G. G. Camici, C. Maack, N. R. Bonetti, V. Fuster, and J. C. Kovacic, "Impact of oxidative stress on the heart and vasculature: part 2 of a 3-part series," *Journal of the American College of Cardiology*, vol. 70, no. 2, pp. 212–229, 2017.

[56] H. Tsutsui, S. Kinugawa, and S. Matsushima, "Oxidative stress and heart failure," *American Journal of Physiology-Heart and Circulatory Physiology*, vol. 301, no. 6, pp. H2181–H2190, 2011.

[57] L. Zuo, C.-C. Chuang, B. T. Hemmelgarn, and T. M. Best, "Heart failure with preserved ejection fraction: defining the function of ROS and NO," *Journal of Applied Physiology*, vol. 119, no. 8, pp. 944–951, 2015.

[58] S. Rubattu, M. Forte, and S. Raffa, "Circulating leukocytes and oxidative stress in cardiovascular diseases: a state of the art," *Oxidative Medicine and Cellular Longevity*, vol. 2019, 9 pages, 2019.

[59] T. Senoner and W. Dichtl, "Oxidative stress in cardiovascular diseases: still a therapeutic target?," *Nutrients*, vol. 11, no. 9, p. 2090, 2019.

[60] T. Xu, W. Ding, X. Ji et al., "Oxidative stress in cell death and cardiovascular diseases," *Oxidative Medicine and Cellular Longevity*, vol. 2019, 11 pages, 2019.

[61] A. van der Pol, W. H. van Gilst, A. A. Voors, and P. van der Meer, "Treating oxidative stress in heart failure: past, present and future," *European Journal of Heart Failure*, vol. 21, no. 4, pp. 425–435, 2019.

[62] L. A. Kiyuna, R. P. Albuquerque, C. H. Chen, D. Mochly-Rosen, and J. C. B. Ferreira, "Targeting mitochondrial dysfunction and oxidative stress in heart failure: Challenges and opportunities," *Free Radical Biology and Medicine*, vol. 129, pp. 155–168, 2018.

[63] J. S. Moon and K. C. Won, "Oxidative stress: link between hypertension and diabetes," *The Korean Journal of Internal Medicine*, vol. 32, no. 3, pp. 439–441, 2017.

[64] K. Nowotny, T. Jung, A. Höhn, D. Weber, and T. Grune, "Advanced glycation end products and oxidative stress in type 2 diabetes mellitus," *Biomolecules*, vol. 5, no. 1, pp. 194–222, 2015.

[65] J. Koska, A. Saremi, S. Howell et al., "Advanced glycation end products, oxidation products, and incident cardiovascular events in patients with type 2 diabetes," *Diabetes Care*, vol. 41, no. 3, pp. 570–576, 2018.

[66] K. Luc, A. Schramm-Luc, T. J. Guzik, and T. P. Mikolajczyk, "Oxidative stress and inflammatory markers in prediabetes and diabetes," *Journal of Physiology and Pharmacology*, vol. 70, pp. 809–824, 2019.

[67] O. M. Ighodaro, "Molecular pathways associated with oxidative stress in diabetes mellitus," *Biomedicine & Pharmacotherapy*, vol. 108, pp. 656–662, 2018.

[68] P. Yang, J. Feng, Q. Peng, X. Liu, Z. Fan, and M. Luca, "Advanced glycation end products: potential mechanism and therapeutic target in cardiovascular complications under diabetes," *Oxidative Medicine and Cellular Longevity*, vol. 2019, 12 pages, 2019.

[69] M. Rasool, A. Malik, T. T. Butt et al., "Implications of advanced oxidation protein products (AOPPs), advanced glycation end products (AGEs) and other biomarkers in the development of cardiovascular diseases," *Saudi Journal of Biological Sciences*, vol. 26, no. 2, pp. 334–339, 2019.

[70] A. Geronikaki, A. Gavalas, V. Dislian, and G. Giannoglou, "Inhibition of renin-angiotensin system and advanced glycation end products formation: a promising therapeutic approach targeting on cardiovascular diseases,"

Cardiovascular & Hematological Agents in Medicinal Chemistry, vol. 5, pp. 249–264, 2007.

[71] A. Klimiuk, A. Zalewska, M. Knapp, R. Sawicki, J. R. Ładny, and M. Maciejczyk, "Salivary gland dysfunction in patients with chronic heart failure is aggravated by nitrosative stress, as well as oxidation and glycation of proteins," *Biomolecules*, vol. 11, no. 1, p. 119, 2021.

[72] Y.-H. Lee, W.-R. Chiou, C.-Y. Hsu et al., "Different left ventricular remodelling patterns and clinical outcomes between non-ischaemic and ischaemic aetiologies in heart failure patients receiving sacubitril/valsartan treatment," *European Heart Journal – Cardiovascular Pharmacotherapy*, 2020.

[73] R. Rettl, T.-M. Dachs, F. Duca et al., "What type of patients did PARAGON-HF select? Insights from a real-world prospective cohort of patients with heart failure and preserved ejection fraction," *Journal of Clinical Medicine*, vol. 9, no. 11, p. 3669, 2020.

[74] Y. Khariton, G. C. Fonarow, A. Hellkamp et al., "Heterogeneity of health status treatment response with sacubitril/valsartan: insights from the CHAMP-HF registry," *ESC Heart Failure*, vol. 8, no. 1, pp. 710–713, 2021.

[75] G. Romano, G. Vitale, L. Ajello et al., "The effects of sacubitril/valsartan on clinical, biochemical and echocardiographic parameters in patients with heart failure with reduced ejection fraction: the "hemodynamic recovery"," *Journal of Clinical Medicine*, vol. 8, no. 12, p. 2165, 2019.

[76] A. Heyse, L. Manhaeghe, E. Mahieu, C. Vanfraechem, and F. Van Durme, "Sacubitril/valsartan in heart failure and end-stage renal insufficiency," *ESC Heart Failure*, vol. 6, no. 6, pp. 1331–1333, 2019.

[77] M. Picca, F. Agozzino, and G. Pelosi, "Effects of losartan and valsartan on left ventricular hypertrophy and function in essential hypertension," *Advances in Therapy*, vol. 21, no. 2, pp. 76–86, 2004.

[78] C. N. Bang, E. Gerdts, G. P. Aurigemma et al., "Systolic left ventricular function according to left ventricular concentricity and dilatation in hypertensive patients: the losartan intervention for endpoint reduction in hypertension study," *Journal of Hypertension*, vol. 31, no. 10, pp. 2060–2068, 2013.

[79] N. R. Hadi, F. G. Al-Amran, Y. A. Hussien, I. K. Al-Yasiri, and M. Al-Turfy, "The cardioprotective potential of valsartan in myocardial ischaemia reperfusion injury," *Central European Journal of Immunology*, vol. 2, no. 2, pp. 159–166, 2015.

[80] B. Wu, R. Lin, R. Dai, C. Chen, H. Wu, and M. Hong, "Valsartan attenuates oxidative stress and NF-κB activation and reduces myocardial apoptosis after ischemia and reperfusion," *European Journal of Pharmacology*, vol. 705, no. 1-3, pp. 140–147, 2013.

[81] M. Imran, M. Q. Hassan, M. S. Akhtar, O. Rahman, M. Akhtar, and A. K. Najmi, "Sacubitril and valsartan protect from experimental myocardial infarction by ameliorating oxidative damage in Wistar rats," *Clinical and Experimental Hypertension*, vol. 41, pp. 62–69, 2018.

[82] D. Sanajou, A. Ghorbani Haghjo, H. Argani et al., "Reduction of renal tubular injury with a RAGE inhibitor FPS-ZM1, valsartan and their combination in streptozotocin-induced diabetes in the rat," *European Journal of Pharmacology*, vol. 842, pp. 40–48, 2019.

[83] D. Liu, Y. Liu, J. J. Yao et al., "Anti-oxidative stress role of valsartan and fluvastatin in rat mesangial cells cultured with high glucose," *International Journal of Clinical and Experimental Medicine*, vol. 9, pp. 4016–4022, 2016.

[84] H. J. Kim, S. J. Han, D. J. Kim et al., "Effects of valsartan and amlodipine on oxidative stress in type 2 diabetic patients with hypertension: a randomized, multicenter study," *The Korean Journal of Internal Medicine*, vol. 32, no. 3, pp. 497–504, 2017.

[85] K. Kuboki, K. Iso, E. Murakami et al., "Effects of valsartan on inflammatory and oxidative stress markers in hypertensive, hyperglycemic patients: an open-label, prospective study," *Current Therapeutic Research*, vol. 68, pp. 338–348, 2007.

[86] N. Komiya, H. Hirose, Y. Saisho, I. Saito, and H. Itoh, "Effects of 12-month valsartan therapy on glycation and oxidative stress markers in type 2 diabetic subjects with hypertension," *International Heart Journal*, vol. 49, no. 6, pp. 681–689, 2008.

[87] K. Miyajima, S. Minatoguchi, Y. Ito et al., "Reduction of QTc dispersion by the angiotensin II receptor blocker valsartan may be related to its anti-oxidative stress effect in patients with essential hypertension," *Hypertension Research*, vol. 30, no. 4, pp. 307–313, 2007.

[88] O. Hussein, J. Shneider, M. Rosenblat, and M. Aviram, "Valsartan therapy has additive anti-oxidative effect to that of fluvastatin therapy against low-density lipoprotein oxidation: studies in hypercholesterolemic and hypertensive patients," *Journal of Cardiovascular Pharmacology*, vol. 40, no. 1, pp. 28–34, 2002.

[89] J. Suzuki, M. Iwai, M. Mogi et al., "Eplerenone with valsartan effectively reduces atherosclerotic lesion by attenuation of oxidative stress and inflammation," *Arteriosclerosis, Thrombosis, and Vascular Biology*, vol. 26, no. 4, pp. 917–921, 2006.

[90] S. Aslam, T. Santha, A. Leone, and C. Wilcox, "Effects of amlodipine and valsartan on oxidative stress and plasma methylarginines in end-stage renal disease patients on hemodialysis," *Kidney International*, vol. 70, no. 12, pp. 2109–2115, 2006.

[91] E. S. Nordén, B. A. Bendiksen, H. Andresen et al., "Sacubitril/valsartan ameliorates cardiac hypertrophy and preserves diastolic function in cardiac pressure overload," *ESC Heart Failure*, vol. 26, 2021.

[92] J. Li, N. Hirose, M. Kawamura, and Y. Arai, "Antiatherogenic effect of angiotensin converting enzyme inhibitor (benazepril) and angiotensin II receptor antagonist (valsartan) in the cholesterol-fed rabbits," *Atherosclerosis*, vol. 143, no. 2, pp. 315–326, 1999.

[93] Y. S. Chatzizisis, M. Jonas, R. Beigel et al., "Attenuation of inflammation and expansive remodeling by valsartan alone or in combination with simvastatin in high-risk coronary atherosclerotic plaques," *Atherosclerosis*, vol. 203, no. 2, pp. 387–394, 2009.

[94] A. Farrugia, "Albumin usage in clinical medicine: tradition or therapeutic?," *Transfusion Medicine Reviews*, vol. 24, no. 1, pp. 53–63, 2010.

[95] G. Fanali, A. Di Masi, V. Trezza, M. Marino, M. Fasano, and P. Ascenzi, "Human serum albumin: from bench to bedside," *Molecular Aspects of Medicine*, vol. 33, no. 3, pp. 209–290, 2012.

[96] G. J. Quinlan, G. S. Martin, and T. W. Evans, "Albumin: biochemical properties and therapeutic potential," *Hepatology*, vol. 41, no. 6, pp. 1211–1219, 2005.

[97] J. Anguizola, R. Matsuda, O. S. Barnaby et al., "Review: glycation of human serum albumin," *Clinica Chimica Acta*, vol. 425, pp. 64–76, 2013.

[98] A. Arasteh, S. Farahi, M. Habibi-Rezaei, and A. A. Moosavi-Movahedi, "Glycated albumin: an overview of the in vitro

models of an in vivo potential disease marker," *Journal of Diabetes and Metabolic Disorders*, vol. 13, no. 1, 2014.

[99] W. Feng, K. Zhang, Y. Liu et al., "Advanced oxidation protein products aggravate cardiac remodeling via cardiomyocyte apoptosis in chronic kidney disease," *American Journal of Physiology-Heart and Circulatory Physiology*, vol. 314, no. 3, pp. H475–H483, 2018.

[100] A. Kural, A. Toker, H. Seval et al., "Advanced glycation end-products and advanced oxidation protein products in patients with insulin dependent diabetes mellitus and first degree relatives," *Medical Journal of Bakırkoy*, vol. 7, pp. 130–135, 2011.

[101] S. Masi, M. Uliana, and A. Virdis, "Angiotensin II and vascular damage in hypertension: role of oxidative stress and sympathetic activation," *Vascular Pharmacology*, vol. 115, pp. 13–17, 2019.

[102] E. L. Schiffrin, "Vascular and cardiac benefits of angiotensin receptor blockers," *The American journal of medicine*, vol. 113, no. 5, pp. 409–418.

[103] T. Miyata, C. Van Ypersele De Strihou, Y. Ueda et al., "Angiotensin II receptor antagonists and angiotensin-converting enzyme inhibitors lower in vitro the formation of advanced glycation end products: biochemical mechanisms," *Journal of the American Society of Nephrology*, vol. 13, no. 10, pp. 2478–2487, 2002.

Research Article

Inhibiting Cardiac Mitochondrial Fatty Acid Oxidation Attenuates Myocardial Injury in a Rat Model of Cardiac Arrest

Peng Wang,[1,2] **Fan Zhang,**[3] **Liming Pan,**[3] **Yunke Tan,**[1,2] **Fengqing Song,**[1,2] **Qiulin Ge,**[1,2] **Zitong Huang,**[1,2] **and Lan Yao** [3]

[1]*Department of Emergency Medicine, Sun Yat-sen Memorial Hospital, Sun Yat-sen University, Guangzhou, China*
[2]*Institute of Cardiopulmonary Cerebral Resuscitation, Sun Yat-sen University, Guangzhou, China*
[3]*Department of Emergency Medicine, The Fifth Affiliated Hospital, Sun Yat-sen University, Zhuhai, China*

Correspondence should be addressed to Lan Yao; yaolan2@mail.sysu.edu.cn

Mitochondrial fatty acid oxidation (FAO) is involved in myocardial damage after cardiopulmonary resuscitation (CPR). This study is aimed at investigating the effect of inhibiting mitochondrial FAO on myocardial injury and the underlying mechanisms of postresuscitation myocardial dysfunction. Rats were induced, subjected to 8 min of ventricular fibrillation, and underwent 6 min of CPR. Rats with return of spontaneous circulation (ROSC) were randomly divided into the Sham group, CPR group, and CPR + Trimetazidine (TMZ) group. Rats in the CPR + TMZ group were administered TMZ (10 mg/kg) at the onset of ROSC via the right external jugular vein, while rats in the CPR group were injected with equivalent volumes of vehicle. The sham rats were only administered equivalent volumes of vehicle. We found that the activities of enzymes related to cardiac mitochondrial FAO were partly improved after ROSC. TMZ, as a reversible inhibitor of 3-ketoacyl CoA thiolase, inhibited myocardial mitochondrial FAO after ROSC. In the CPR + TMZ group, the levels of mitochondrial injury in cardiac tissue were alleviated following attenuated myocardial damage and oxidative stress after ROSC. In addition, the disorder of cardiac mitochondrial metabolism was ameliorated, and specifically, the superfluous succinate related to mitochondrial reactive oxygen species (ROS) generation was decreased by inhibiting myocardial mitochondrial FAO with TMZ administration after ROSC. In conclusion, in the early period after ROSC, inhibiting cardiac mitochondrial FAO attenuated excessive cardiac ROS generation and preserved myocardial function, probably by alleviating the dysfunction of cardiac mitochondrial metabolism in a rat model of cardiac arrest.

1. Introduction

Sudden cardiac arrest is a leading cause of mortality worldwide. Despite the development of cardiopulmonary resuscitation (CPR) science and the increased rate of return of spontaneous circulation (ROSC), the survival rate in patients with sudden cardiac arrest after hospital discharge remains less than 10% [1, 2]. Deaths within the first 24 h of ROSC are typically associated with multiorgan system failure, especially due to postresuscitation myocardial dysfunction [3, 4]. It is now widely believed that oxidative stress damage in the process of global myocardial ischemia/reperfusion after ROSC is the main factor linking cardiac arrest to postresuscitation myocardial dysfunction [5, 6]. Although many studies

have focused on how to mitigate cardiac oxidative injury after ROSC, there remains no effective therapy for clinical application.

The generation of mitochondrial reactive oxygen species (ROS) is the main source of ROS and a crucial early driver of ischemia/reperfusion injury after ROSC [7, 8]. Uncontrolled ROS formation from the mitochondrial electron transport chain (ETC) was founded during the ischemia/reperfusion process when electrons leaking from the respiratory chain react with oxygen, especially in the hearts containing large numbers of mitochondria [9, 10]. A large body of experimental literature supports that mitochondrial ETC inhibitors appear to attenuate myocardial oxidative injury during ischemia/reperfusion [11, 12]. Our previous study found that

carbon monoxide-releasing molecules decrease the generation of cardiac mitochondrial ROS and alleviate myocardial dysfunction through mildly uncoupling mitochondrial respiration in a rat model of cardiac arrest [13]. Furthermore, some studies found that excessive succinate as the substrate of mitochondrial complex II is the major source of leaking electrons and leads to extensive mitochondrial ROS formation [10, 14]. Decreasing succinate accumulation or inhibition of complex II attenuates ischemia/reperfusion oxidative injury [15]. As an intermediate substance of the citric acid cycle (CAC), succinate is affected by changes in mitochondrial metabolism. After ischemia/reperfusion, mitochondrial fatty acid and glucose utilization are damaged at different levels, while fatty acid remains the main metabolism substrate of cardiac mitochondria [16]. In some *in vitro* experiments, it was demonstrated that suppressing mitochondrial fatty acid metabolism ameliorated oxidative stress injury after ischemia/reperfusion, but the underlying mechanism is not completely deciphered [17, 18]. According to the above research results, we considered that the inhibition of mitochondrial fatty acid oxidation (FAO) may attenuate myocardial oxidative damage after ROSC by regulating mitochondrial respiratory chain substrate production, subsequently decreasing the generation of cardiac mitochondrial ROS. To investigate this, we used a rat model of cardiac arrest to examine the effect of inhibiting mitochondrial FAO on myocardial oxidative injury and the underlying mechanisms of postresuscitation myocardial dysfunction.

2. Materials and Methods

2.1. Animal Preparation and Cardiac Arrest Model. Forty-two male Sprague-Dawley rats (370-420 g) were purchased from the Medical Experimental Animal Center of Guangdong Province (Guangzhou, China). Animals were cared for in accordance with the Chinese Guidance Suggestions for the Care and Use of Laboratory Animals and with the approval of the Animal Care and Use Committee of Sun Yat-sen University.

Rats were subjected to 8 min of ventricular fibrillation (VF) and underwent 6 min of CPR. Cardiac arrest was induced by VF. Briefly, animals were anesthetized with pentobarbital sodium (45 mg/kg), and anesthesia was maintained throughout the whole experimental procedure by the additional injection of 10 mg/kg intraperitoneal pentobarbital sodium when necessary. The trachea was orally intubated with a 14-G catheter. The left femoral artery was cannulated with a polyethylene (PE) 50 catheter for blood pressure measurement. A 4F PE catheter was advanced from the right external jugular vein to the right atrium for the electrical induction of VF. During this process, cardiac rhythm and hemodynamic data were recorded using a WinDaq data acquisition system (DataQ, Akron, USA). Rectal temperature was maintained at $36.5 \pm 0.5°C$. After the operation, VF was induced by a 3 mA current delivered to the right ventricular endocardium through a guidewire inserted from the right external jugular vein to the right ventricle. The current flow lasted for 3 min to prevent the spontaneous reversal of VF. Following 8 min of untreated VF, the animal was mechani-

cally ventilated (tidal volume 0.6 mL/100 g, ventilation rate 60 breaths/min, 100% oxygen), and 6 min of CPR was initiated with chest compression at a rate of 250 beats/min. After 4 min of CPR, epinephrine (0.02 mg/kg) was administered, and 3-J biphasic waveform shocks were attempted after 6 min of CPR. If VF persisted, another 3-J shock was administered after another 2 min of chest compression. Successful ROSC was defined as an organized rhythm with a mean aortic pressure (MAP) exceeding 60 mmHg for at least 10 min. If the animals had no ROSC after 10 min of CPR, unsuccessful resuscitation was declared. After ROSC, mechanical ventilation was continuously provided with 100% oxygen for 30 min and 50% oxygen for another 30 min, followed by 21% oxygen for 3 h.

2.2. Experimental Procedure. Trimetazidine (TMZ), a reversible inhibitor of 3-ketoacyl CoA thiolase (3-KT), was used to inhibit cardiac mitochondrial FAO. A total of 36 rats with successful ROSC were randomly divided into the CPR ($n = 18$) and CPR + TMZ ($n = 18$) groups. Rats in the CPR + TMZ group were administered TMZ (MedChemExpress, USA; 10 mg/kg, 10% dimethyl sulfoxide as a vehicle) at the onset of ROSC via the right external jugular vein, while those in the CPR group were injected with equivalent volumes of vehicle. The sham rats ($n = 6$) were only administered equivalent volumes of vehicle. Rats in the CPR and CPR + TMZ groups were again randomly divided into three subgroups according to the time of ROSC (1, 3, and 6 h after ROSC). Myocardial injury, oxidative stress, and cardiac mitochondrial metabolism and function were evaluated. The experimental procedure is shown in Figure 1.

2.3. Measurement of Serum Cardiac Troponin I and Myocardial Function. Cardiac troponin I (CTNI) levels in serum were detected using a Rat CTNI ELISA kit (CUSABIO, China). An M-mode echocardiograph was performed to detect the left ventricular ejection fraction (EF) to evaluate myocardial function.

2.4. Determination of Malondialdehyde in Myocardial Tissue and Cardiac Mitochondrial ROS. Malondialdehyde (MDA) is an evaluation indicator of oxidative stress indicators. The level of MDA in myocardial tissue was measured using a tissue MDA determination kit (GENMED, Boston, MA, USA). Cardiac mitochondria were isolated by differential centrifugation of the heart homogenates. Fresh cardiac mitochondria were loaded with a reagent containing the fluorescent probe (CM-H$_2$DCFDA) for 15 min. Fluorescence was measured using a fluorescence spectrophotometric enzyme mark instrument (SpectraMax M5, San Francisco, CA, USA) following the manufacturer's instructions for the mitochondrial ROS testing kit (GENMED).

2.5. Measurement of Mitochondrial Oxidative Phosphorylation and Respiration Enzyme Activities. The mitochondrial P/O ratio was used to evaluate the coupling of mitochondrial oxidative phosphorylation by a Clark-type oxygen electrode at 25°C. Fresh cardiac mitochondria were added to the respiration buffer (GENMED, Boston, MA, USA). Mitochondrial respiration was initiated using
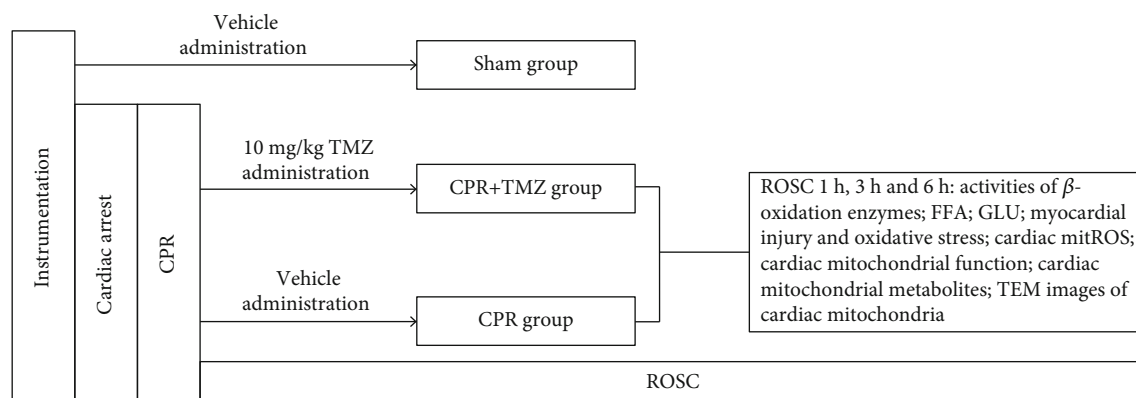
FIGURE 1: Experimental procedure. CPR: cardiopulmonary resuscitation; TMZ: trimetazidine; FFA: free fat acid; GLU: glucose; ROSC: return of spontaneous circulation; mitROS: mitochondrial reactive oxygen species; TEM: transmission electron microscope.

2 mmol/L pyruvate +5 mmol/L malate. State 3 respiration was induced by the addition of 0.5 mmol/L adenosine diphosphate (ADP). The ADP to O ratio was calculated based on the oxygen consumption during state 3 respiration. The activities of complexes I and II were measured using a mitochondrial respiratory enzyme activity determination Kit (GENMED, Boston, MA, USA). Complex I and II activities were assayed to monitor the dynamic change in transmittance from the oxidation of NADH to NAD^+ and $FADH_2$ to FAD^+.

2.6. Detection of FAO-Related Enzyme Activities.
Isolated mitochondria from the heart were suspended in 24-well plates. The rate of mitochondrial FAO was evaluated by using a fatty acid β-oxidation Assay kit (GENMED, Boston, Massachusetts). The activities of carnitine palmitoyltransferase 1 (CPT1), acyl-CoA dehydrogenase (ACDH), 3-OH-ACDH (HADH), and 3-KT as important enzymes in mitochondrial FAO were measured using their respective commercial enzyme activity determination kits (GENMED, Boston, Massachusetts).

2.7. Metabolite Analysis.
Sample preparations for targeted GC-MS metabonomic analysis were established as previously reported [19]. Then, 30 mg of left ventricle tissue from each mouse in the sham, CPR, and CPR + TMZ groups at 6 h of ROSC was mixed with 1 mL of methanol and ultrasonically ground for 30 min. The supernatant was then added to 2 mL of 1% sulfuric acid methanol solution. After methylation for 30 min at 80°C, the mixture was extracted with 1% hexane and washed with 5 mL of pure water. The supernatant (500 μL) was then collected for GC-MS metabolomics analysis. In parallel, 37 kinds of fatty acid methyl ester standards were proportionally mixed as the standard for target analysis of medium- and long-chain fatty acids. A quality control (QC) sample was prepared by mixing equal volumes (10 μL) of ventricle homogenate from each of the 18 samples. One in every six QC samples were analyzed to monitor the stability and reproducibility of the analysis. The samples were separated using an Agilent DB-WAX capillary column (30 m $\times$ 0.25 mM $\times$ 0.25 μM). The initial temperature of the

capillary column was maintained at 50°C for 3 min, raised to 220°C at 10°C/min, and then kept at this temperature for 20 min. The carrier gas (helium) was constantly supplied at a flow rate of 1.0 mL/min. GC-MS analysis was carried out using an Agilent 7890a/5975c gas chromatography mass spectrometer (Agilent, USA). The temperature of sample inlet, transmission line, and ion source temperature were 280°C, 250°C, and 230°C, respectively. The electron energy was set to 70 eV. The peak area and retention time data were extracted using the MSD ChemStation software. The levels of targeted medium- and long-chain fatty acids were calculated according to the total ion current picture of fatty acid standards.

To detect the content of metabolites mainly in CAC and glycolysis by targeted GC-MS metabolomic analysis, the samples were separated using an Agilent 1290 infinity liquid chromatography ultraperformance system. A QC sample from the experimental samples at each interval was established to detect and evaluate the stability and repeatability of the system. A standard mixture of substances from the sample queue was used to correct the chromatographic retention time. The samples were analyzed using a 5500 qtrap mass spectrometer (AB SCIEX) in negative ion mode. The detection settings were as follows: source temperature 450°C, ion source gas 1 45, ion source gas 2 45, culture gas 30, and floating voltage -4500 V. The MRM mode was used to detect ion pairs. Metabolite identification and retention time correction were performed according to the data of the standard mixture of substances. The peak area and retention time were extracted and calculated using the MultiQuant software.

The levels of free fatty acids (FFAs) and glucose in serum were estimated using an FFA Quantification Colorimetric/-Fluorometric Kit (BioVision, Milpitas, CA, USA) and a Rat Glucose Quantification Kit (CUSABIO).

2.8. Pathological Examination of Myocardial Tissue.
Left ventricular tissue was embedded in paraffin and cut into 6 μM thick sections following hematoxylin and eosin staining. Myocytolysis and organization of myocardial fibers were observed under a microscope by an experienced pathologist.

TABLE 1: Baseline characteristics before inducing cardiac arrest.

	Sham	CPR groups			CPR + TMZ groups		
		1 h	3 h	6 h	1 h	3 h	6 h
Body weight, g	392.3 ± 14.7	386.8 ± 14.8	392.3 ± 21.2	395.7 ± 16.3	394.7 ± 12.9	390.3 ± 15.1	393.2 ± 14.9
MAP, mmHg	110.3 ± 9.8	114.5 ± 11.5	111.2 ± 11.1	111.8 ± 10.1	112.5 ± 9.8	107.3 ± 11.3	108.2 ± 15.5
Heart rate, bpm	392.7 ± 11.4	395.0 ± 9.4	392.7 ± 11.5	393.3 ± 11.2	394.2 ± 7.4	393.0 ± 11.9	391.8 ± 12.2
Time of animal preparation, min	61.8 ± 5.4	63.7 ± 7.3	65.3 ± 6.0	62.7 ± 8.5	57.0 ± 6.4	61.8 ± 7.5	60.7 ± 9.7

2.9. Transmission Electron Microscopy. Apex tissue ($3 \times 1 \times 1$ mM) was prefixed in 2.5% glutaraldehyde and then added to 1% osmium tetroxide for continuous fixation and dehydrated in a gradient concentration of acetone series. After infiltration and embedding, the sample was sliced into ultrathin sections stained with both uranyl acetate and lead citrate. Samples were examined using a transmission electron microscope (Tecnai G2 Spirit Twin, FEI, USA).

2.10. Statistical Analysis. Statistical analyses were performed using the SPSS 21.0 software (SPSS, Chicago, IL, USA). Data are presented as the mean ± SEM. One-way analysis of variance was performed to compare more than two groups. The unpaired two-sample t-test was used for two-group comparison. Values of $p < 0.05$ were considered statistically significant.

3. Results

3.1. Baseline Characteristics and Hemodynamic Data before Inducing Cardiac Arrest. A total of 36 successfully resuscitated rats were randomly assigned to the Sham, CPR, or CPR + TMZ groups. The baseline and resuscitation characteristics of the rats were recorded. There was no significant difference in body weight, heart rate, MAP, or time of animal preparation in any group (Table 1).

3.2. TMZ Inhibited Myocardial Mitochondrial FAO after ROSC. The activities of enzymes related to mitochondrial FAO were evaluated in the heart. 1 h after ROSC, the activities of 3-KT (Figure 2(a)), CPT1 (Figure 2(b)), and ACDH (Figure 2(c)) were markedly elevated compared with the Sham group. Additionally, 3 h after ROSC, the activity of CPT1 (Figure 2(b)) remained higher, but there was no significant difference in the activities of 3-KT and ACDH (Figures 2(a) and 2(c)). Although the CPR group exhibited slightly increased activity of each related enzyme 6 h after resuscitation, there were no statistically significant differences between the sham and CPR groups. The activity of HADH (Figure 2(d)) did not obviously change after ROSC. In the TMZ group, TMZ, a reversible inhibitor of 3-KT, remarkably decreased the activity of 3-KT (Figure 2(a)) in the heart after ROSC compared with the CPR group. Meanwhile, the administration of TMZ evidently decreased the activity of CPT1 (Figure 2(b)) at 3 h and increased the activity of HADH (Figure 2(d)) in the heart at 6 h following ROSC, leading to the enzymatic activity being nearly restored to the levels of the Sham group. Together, these observations

indicated that myocardial energy metabolism was abnormally mobilized, and myocardial mitochondrial FAO was relatively accelerated after ROSC. TMZ effectively inhibited myocardial mitochondrial FAO during the early stage of ROSC due to the decrease in some key enzyme activities.

3.3. Inhibition of Mitochondrial FAO Attenuated Myocardial Injury after ROSC. After cardiac arrest, the levels of CTNI (Figure 3(a)) were significantly higher than those in the sham group. Rats in the CPR group showed a decrease in MAP (Figure 3(b)) and EF (Figure 3(c)) compared with sham rats. At 1, 3, and 6 h after ROSC, TMZ reduced the content of CTNI (Figure 3(a)) in blood serum as well as elevated MAP (Figure 3(b)) and EF (Figures 3(c) and 3(d)) in the CPR + TMZ group compared with the CPR group. At 6 h following ROSC, myocytolysis and disorganization occurred in the CPR group (Figure 3(e)). The ROSC rats treated with TMZ significantly alleviated myocytolysis and disordered myocardial fibers in the CPR + TMZ group (Figure 3(e)). These findings revealed that inhibition of mitochondrial FAO mitigated myocardial injury and improved myocardial performance after resuscitation.

3.4. Inhibition of Mitochondrial FAO Decreased Myocardial Oxidative Stress after ROSC. Cardiac mitochondria, as the main site of energy production, are also the main source of ROS after cardiac arrest. In the CPR group, the generation of ROS in cardiac mitochondria significantly increased 1 and 6 h after ROSC compared with the Sham group (Figure 4(a)). However, TMZ led to less ROS production in cardiac mitochondria in the CPR + TMZ group than in the CPR group (Figure 4(a)). Moreover, the levels of MDA in the CPR group were significantly higher than those in the sham group (Figure 4(b)). Moreover, 1, 3, and 6 h after ROSC, TMZ reduced the content of MDA in the heart (Figure 4(b)).

3.5. Inhibition of Mitochondrial FAO Preserved Mitochondrial Function after ROSC. To further evaluate the coupling of mitochondrial oxidative phosphorylation and the activities of respiratory enzymes related to mitochondrial ROS production, the ADP/O ratio and the activities of complexes I and II were detected. First, 1 and 6 h following ROSC, the ADP/O of cardiac mitochondria in the CPR group was markedly decreased compared with those of the Sham group (Figure 5(a)). Inhibition of mitochondrial FAO with TMZ treatment improved ADP/O after ROSC in the TMZ group (Figure 5(a)). Meanwhile, there was a significant
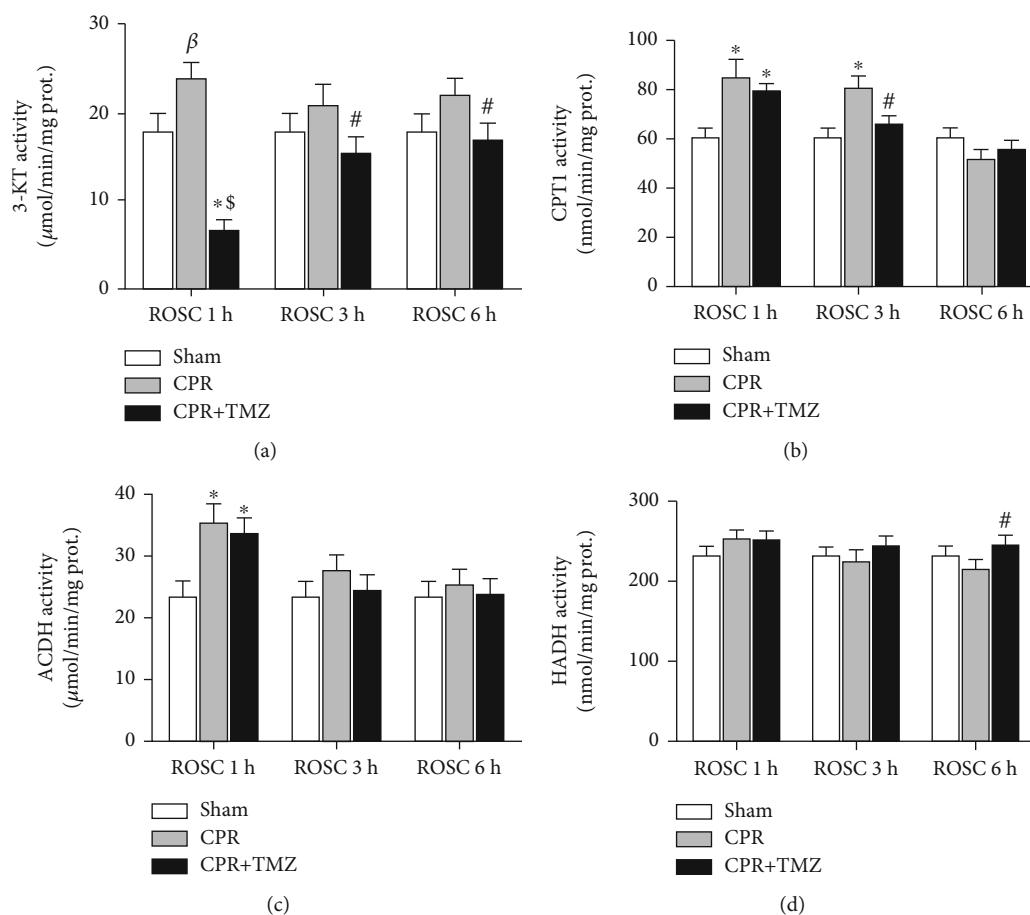
Figure 2: The enzyme activities of mitochondrial fatty acid oxidation in rat heart tissue at 1, 3, and 6 h following return of spontaneous circulation (ROSC) in the CPR and CPR+ Trimetazidine (TMZ) groups compared with the Sham group: (a) 3-ketoacyl CoA thiolase (3-KT) activity; (b) carnitine palmitoyltransferase 1 (CPT1) activity; (c) acyl-CoA dehydrogenase (ACDH) activity; (d) 3-OH-acyl CoA dehydrogenase (HADH) activity. $^{\beta} p < 0.05$, $^{*}p < 0.01$ versus Sham group; $^{\#}p < 0.05$, $^{\$}p < 0.01$ versus CPR group.

decline in the activities of complexes I and II 1 and 6 h after ROSC (Figures 5(b) and 5(c)). In the TMZ group, TMZ significantly alleviated the damage to complex I (Figure 5(b)) and complex II activities (Figure 5(c)) after ROSC. Transmission electron microscopy showed cardiac mitochondrial morphology in the CPR group was represented as mitochondrial swelling and unclear intima 6 h after ROSC (Figure 5(d)). Inhibition of mitochondrial FAO in the CPR + TMZ group obviously mitigated cardiac mitochondrial injury in the electron microscope image compared with the CPR group (Figure 5(d)).

3.6. Inhibition of Mitochondrial FAO Ameliorated the Disorder of Cardiac Mitochondrial Metabolism after ROSC. We found that the concentrations of FFAs (Figure 6(a)) and glucose (Figure 6(b)) in serum significantly increased after ROSC. TMZ treatment decreased FFA (Figure 6(a)) and glucose (Figure 6(b)) levels compared with CPR rats. Targeted metabolomics analysis of medium- and long-chain fatty acids and energy metabolites in heart tissue was carried out 6 h after ROSC. We found that the levels of five fatty acids were evidently decreased, while four metabolites were upregulated significantly in the heart tissue of CPR rats compared with that of sham rats. The lengths of the five

decreased fatty acids were in the range of C12-C22, closely related to mitochondrial FAO. Three elevated metabolites (succinate, fumarate, and citrate) were the main intermediate products of CAC, and succinate was the substrate of the ETC bound to mitochondrial ROS generation. Elevated phosphoenolpyruvate was the main metabolite of glycolysis. In the TMZ group, these changed metabolites were normalized to some extent through the inhibition of mitochondrial FAO (Table 2). These results showed that inhibiting mitochondrial FAO after ROSC restored the balance of cardiac mitochondrial metabolism.

4. Discussion

In this study, we showed that the inhibition of myocardial mitochondrial FAO attenuates myocardial injury and protects cardiac mitochondrial function after ROSC. The underlying mechanism is that FAO inhibition in cardiac mitochondria ameliorates the mitochondrial metabolism disorder and abnormal generation of ETC substrates, subsequently leading to the decrease in excessive ROS production in cardiac mitochondria after ROSC. Several findings in the present study support this conclusion. First, we found that the activities of some key FAO enzymes in
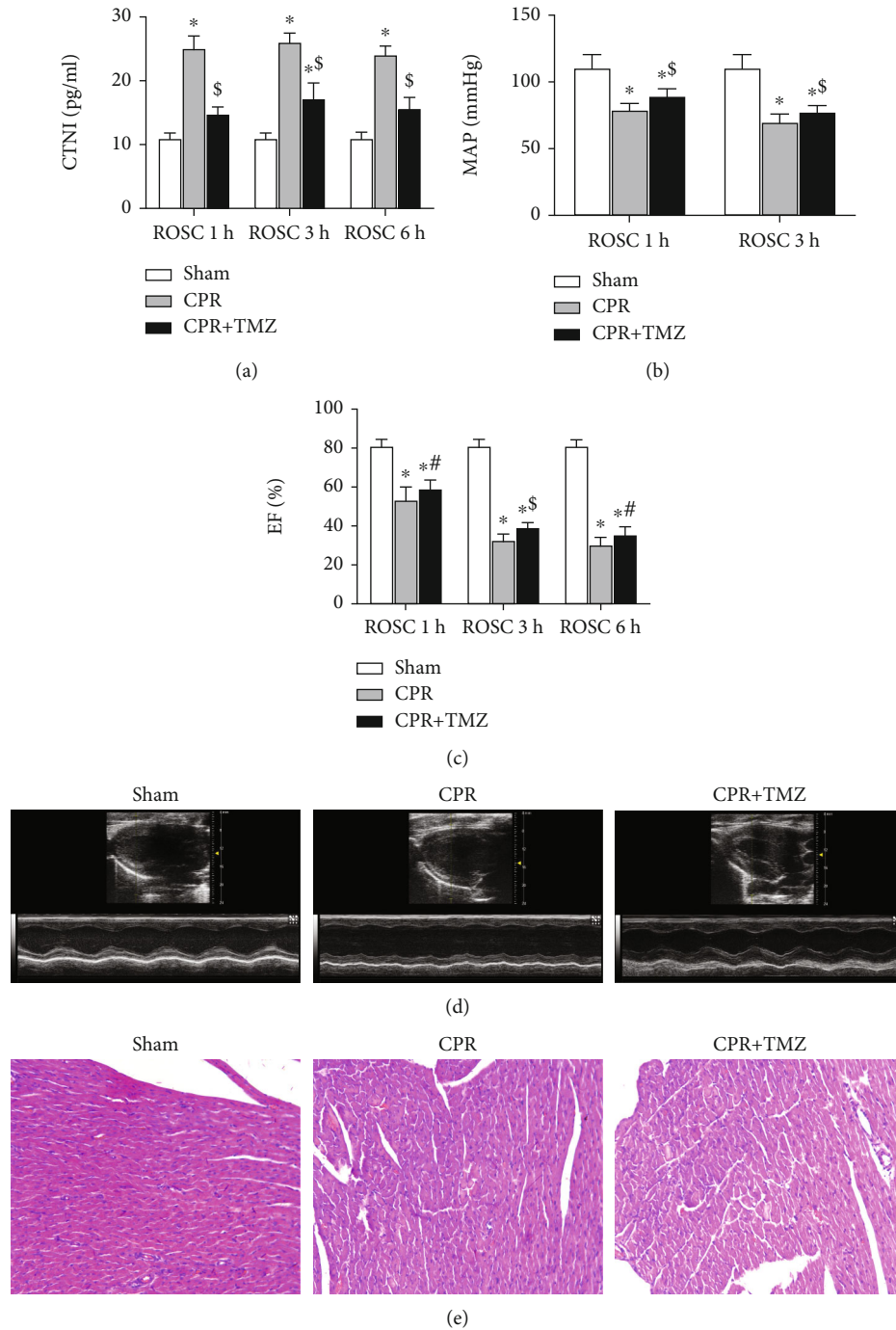
(a)

(b)

(c)

(d)

(e)

FIGURE 3: Myocardial injury at 1, 3, and 6 hours following return of spontaneous circulation (ROSC) in the CPR and CPR + Trimetazidine (TMZ) groups compared with the Sham group: (a) cardiac troponin I (CTNI); (b) mean aortic pressure (MAP); (c) left ventricular ejection fraction (EF); (d) representative echocardiograms in three groups at 6 hours following ROSC; (e) pathological examination of myocardial tissue in three groups at 6 hours following ROSC. Magnification ×200. $^{\beta}$ $p < 0.05$, $^{*}p < 0.01$ versus Sham group; $^{\#}p < 0.05$, $^{\$}p < 0.01$ versus CPR group.

cardiac mitochondria were elevated, and the levels of fatty acids in serum were markedly increased at the early stage of ROSC. 3-KT inhibitor TMZ repressed abnormal FAO in cardiac mitochondria and improved myocardial performance in ROSC rats. These results indicated that the suppression of activated FAO attenuated postresuscitation injury in the heart. Second, the excessive production of cardiac mitochon-

drial ROS significantly decreased following treatment with TMZ after ROSC. The alleviation of mitochondrial dysfunction was also found in the CPR + TMZ group. These findings demonstrated that the inhibition of cardiac FAO decreased mitochondrial ROS generation to mitigate cardiac oxidative injury and protected mitochondrial function after ROSC. Third, the anomalous level of succinate as an important
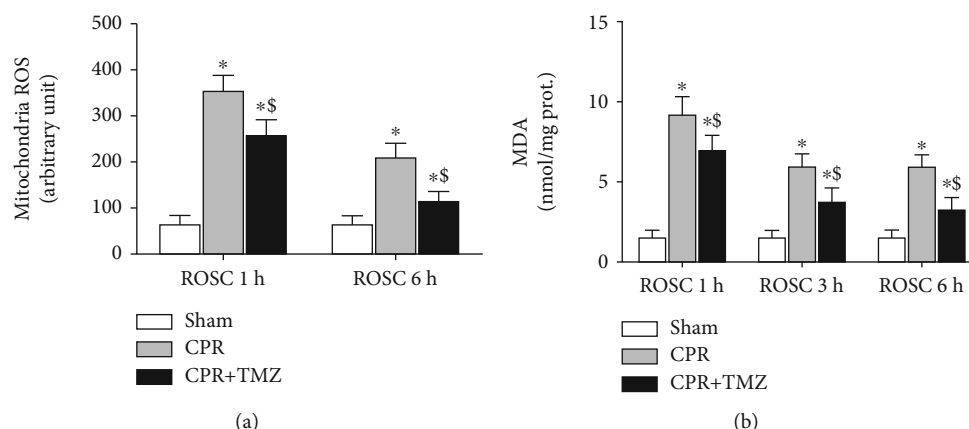
FIGURE 4: Cardiac mitochondrial oxidative stress at 1 and 3 hours following return of spontaneous circulation (ROSC) in the CPR and CPR + Trimetazidine (TMZ) groups compared with the Sham group: (a) cardiac mitochondrial reactive oxygen species (ROS); (b) malondialdehyde (MDA). $^*p < 0.01$ versus Sham group; $^\$p < 0.01$ versus CPR group.

ETC substrate in heart tissue, which is evidently related to excessive mitochondrial ROS generation, was reduced after ROSC with TMZ treatment. The abnormalities of fatty acid metabolism in cardiac mitochondria after cardiac arrest were reversed to some extent by the inhibitor TMZ. Simultaneously, the injury of glycometabolism in cardiac mitochondria was mitigated. These results indicated that the inhibition of FAO at the early stage of ROSC decreased mitochondrial ROS generation by reduction of abnormal mitochondrial metabolites. Several previous studies have demonstrated that inhibition of myocardial FAO attenuates ischemia/reperfusion injury by affecting AMPK and ERK signaling pathways, activating pyruvate dehydrogenase, and so on [17, 20]. However, there have been no studies involving to the effects of FAO inhibition on abnormal ROS generation in the cardiac mitochondria of cardiac arrest models and the underlying mechanism. Thus, this study showed that inhibition of myocardial FAO in the early stage of ROSC attenuates excessive ROS generation in cardiac mitochondria by decreasing the levels of abnormal mitochondrial substrates and modulating mitochondrial metabolism, leading to the mitigation of myocardial injury after ROSC.

In the normal heart, cardiac mitochondria are the main source of energy supply, and fatty acid β-oxidation is responsible for 60-80% of ATP production [3, 21]. After ischemia/reperfusion, although impaired mitochondrial oxidative phosphorylation results in a decline in ATP supply, fatty acid β-oxidation remains the dominant process of mitochondrial oxidative metabolism due to compensatory catecholamine discharge, accelerated adipose tissue lipolysis, increased plasma concentrations of FFA, etc. [16, 22]. Similar to the results of previous studies, we identified elevated activities of CPT1, 3-KT, and ACDH as the key enzymes of FAO in the heart tissue and increased levels of FFAs in ROSC rats. This suggests that fatty acid β-oxidation plays an important role in cardiac mitochondrial metabolism after ROSC. To further determine the effect of β-oxidation, we used a reversible 3-KT inhibitor, TMZ, to intervene in fatty acid β-oxidation at the early stage of ROSC. In the CPR + TMZ group, TMZ not only decreased the activities of 3-KT and CPT1 as

well as FFA levels after ROSC but also mitigated cardiac dysfunction and myocardial injury in cardiac arrest rat models. Strong evidence of this lay in improved EF and MAP following a reduced concentration of CTNI compared with the CPR group. The reduction of FAA in TMZ group may result from gradually rebalanced metabolism and reduced compensation of adipose tissue lipolysis after ROSC [21]. Furthermore, the MDA content of cardiac tissue was markedly lower in the CPR + TMZ group. It was known that oxidative injury is one of the most important pathological mechanisms in myocardial damage after ROSC [23, 24]. These results indicated that the inhibition of fatty acid β-oxidation attenuates myocardial oxidative damage to preserve cardiac function after ROSC. The consistent viewpoint was found in some researches on heart failure, myocardial hypertrophy, etc. [25].

Cardiac mitochondria, the main site of ATP production, are also the major source of ROS in the hearts subjected to ischemia/reperfusion injury [23]. Moreover, excessive ROS leads to cardiac mitochondrial dysfunction, which results in increased ROS generation in cardiac mitochondria and decreased ATP generation, forming a vicious cycle [26]. Several recent studies showed that mitochondrial ROS generation in pathological conditions is closely related to the disorder of mitochondrial metabolism [25, 27]. In our study, rats in the CPR + TMZ group showed elevated ADP/O of cardiac mitochondria and partial restoration of complex I and II activities compared with the CPR group. It was known that complexes I and II are the main sites of ETC accepting electrons to form ATP and ROS both in normal and pathological conditions [10, 27]. Attenuation of complex I and II damages led to a decrease in excessive ROS generation in cardiac mitochondria, probably due to less electron leakage and increased ATP production in ROSC rats with TMZ treatment. These findings showed that the inhibition of fatty acid β-oxidation mitigated excessive ROS generation in cardiac mitochondria and preserved their function, resulting in the attenuation of myocardial oxidative stress after cardiac arrest in a rat model. Previous studies supported abnormal ROS production in cardiac mitochondria plays an important role in oxidative injury
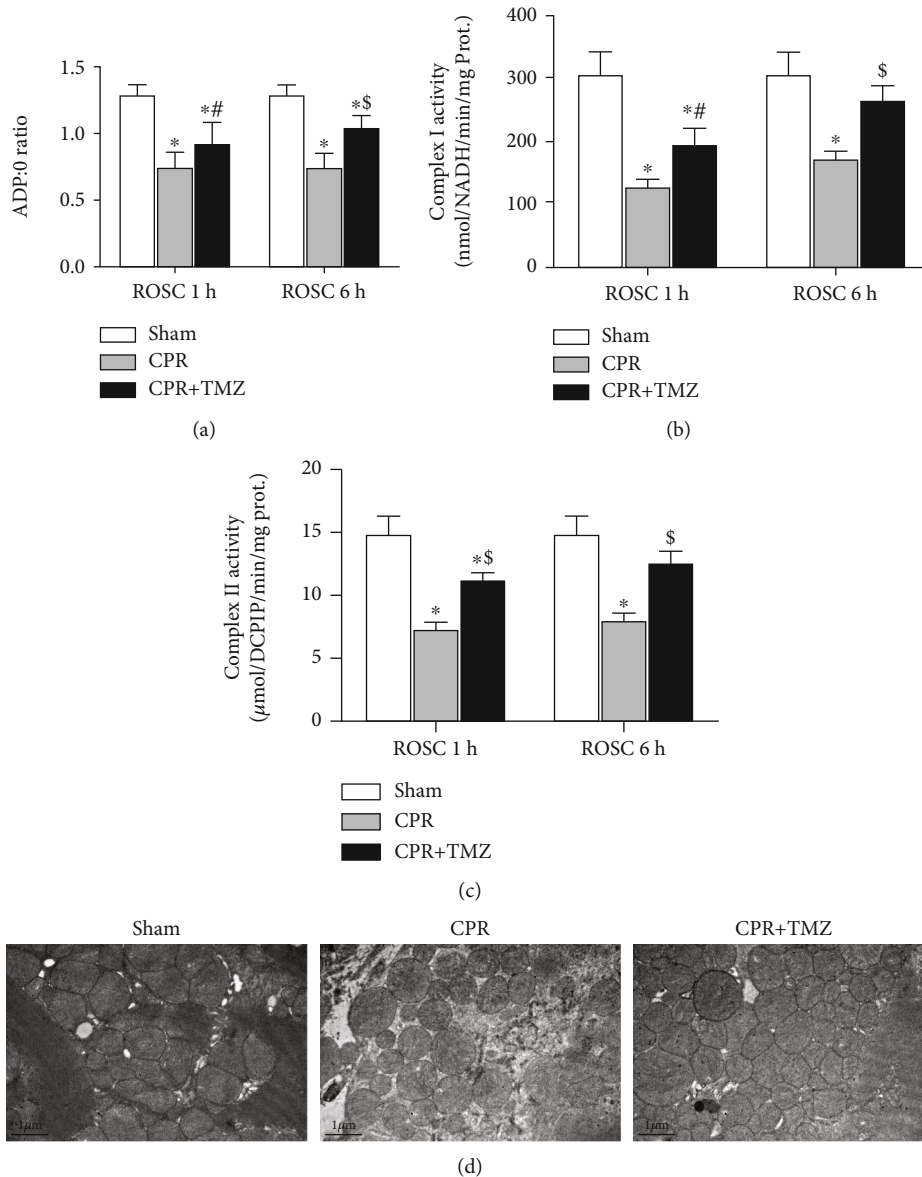
(a)

(b)

(c)

(d)

Figure 5: Cardiac mitochondrial function at 1 and 3 hours following return of spontaneous circulation (ROSC) in the CPR and CPR + Trimetazidine (TMZ) groups compared with the Sham group: (a) ADP/O ratio; (b) mitochondrial complex I activity; (c) mitochondrial complex II activity; (d) representative transmission electron microscope images of cardiac mitochondria at 6 hours following ROSC. $^{\beta}$ $p < 0.05$, $^{*}p < 0.01$ versus Sham group; $^{\#}p < 0.05$, $^{\$}p < 0.01$ versus CPR group.

in pathological conditions [26, 28]. It is well known that the excessive ROS generation is caused by the abnormal electron leak of the ETC related to mitochondrial dysfunction and aberrant metabolism in the pathological state of myocardia [29].

In this study, we found that the concentration of succinate, as the substrate of complex II, increased 6 h after ROSC in cardiac tissue, with an improved level of its subsequent metabolite fumarate in CAC. These observations indicate that superfluous succinate mismatches the acceptance of injured mitochondria in cardiac tissue, resulting in ETC electron leak and excessive ROS production after ROSC [11, 14]. In view of CAC metabolites mainly stemming from mitochondrial fatty acids and glucose metabolism, the levels of other metabolites and some key enzymes were also detected.

In the hearts of CPR rats, it was found that the content of five fatty acids (C12-C22) decreased, while phosphoenolpyruvate as the intermediate of glycolysis increased significantly 6 h after ROSC. In addition, the key enzyme activities of FAO, including CPT1, ACDH, and 3-KT, were elevated during the early postresuscitation period. These results prompted the hypothesis that excessive succinate formation in the heart after ROSC is related to comparatively elevated FAO. Some previous researches showed that partial inhibition of FAO mitigates the damage of cardiac cells and mitochondria in some pathological conditions, although the underlying mechanism is currently unclear [25]. To investigate the effect of elevated cardiac FAO in CPR rats, we used TMZ to suppress FAO and detected mitochondrial metabolism after ROSC. In the CPR + TMZ group, we found that the levels
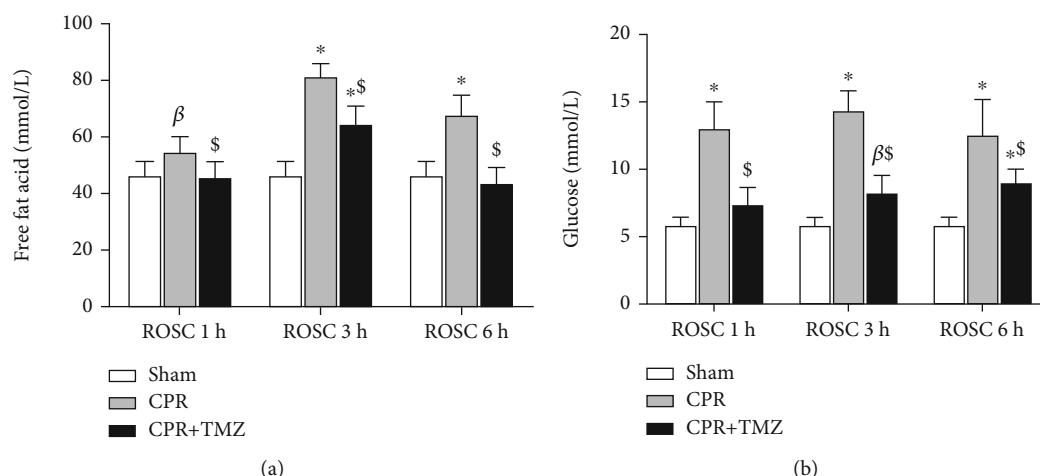
(a)

(b)

FIGURE 6: The levels of free fat acid and glucose in serum at 1, 3, and 6 hours following return of spontaneous circulation (ROSC) in the CPR and CPR + TMZ groups compared with the Sham group: (a) the level of free fat acid; (b) the level of glucose. $^\beta$ $p < 0.05$, $^*p < 0.01$ versus Sham group; $^\#p < 0.05$, $^\$p < 0.01$ versus CPR group.

TABLE 2: The change of cardiac mitochondrial metabolites at 6 hours following return of spontaneous circulation.

Mitochondrial metabolites	Sham group	CPR group	CPR + TMZ group
Lauric acid (μg/g)	0.56 ± 0.13	$0.05 \pm 0.03^*$	$0.33 \pm 0.15^{*,\$}$
Myristic acid (μg/g)	23.54 ± 10.58	$7.29 \pm 0.98^*$	$17.58 \pm 2.44^\#$
Palmitoleic acid (μg/g)	81.54 ± 31.97	$25.98 \pm 9.47^*$	$53.15 \pm 13.35^{\beta,\#}$
Elaidic acid (μg/g)	1245.51 ± 302.98	$394.61 \pm 55.86^*$	$779.61 \pm 219.82^{*,\$}$
Docosadienoic acid (μg/g)	3.22 ± 0.85	$1.28 \pm 0.52^*$	$2.96 \pm 0.78^\$$
Succinate (AU)	97601.71 ± 12955.30	$131530.6593 \pm 16054.71^*$	$103200.39 \pm 10078.42^\$$
Phosphoenolpyruvate (AU)	$9510787.49 \pm 5590095.37$	$21573980.98 \pm 5517056.59^*$	$15001059.54 \pm 2808820.31^\#$
Fumarate (AU)	865263.39 ± 210253.45	$2111186.90 \pm 627354.51^*$	$1565341.13 \pm 290282.39^{\beta,\#}$
Citrate (AU)	111084.32 ± 16644.73	$179985.21 \pm 32520.83^*$	$114157.36 \pm 38654.61^\$$

Values are means $\pm$ SE; $^\beta$ $p < 0.05$, $^*p < 0.01$ versus Sham group; $^\#p < 0.05$, $^\$p < 0.01$ versus CPR group.

of succinate and fumarate were reduced while the content of five fatty acids increased with the alleviation of ROS injury in cardiac tissue 6 h after ROSC. Moreover, the level of phosphoenolpyruvate simultaneously decreased to that of the Sham group. These findings indicated that the inhibition of abnormal FAO prompted the optimization of impaired mitochondrial metabolism and mitigated ROS injury in cardiac tissue during the early stage of ROSC, potentially due to the decrease of unsuitable ETC substrates offering excessive electrons to form ROS. Some studies also supported that the reduction of abnormal succinate may decrease ROS generation in ischemia-reperfusion injury [14, 30].

There are still some limitations in the current study. First, we only investigated the relationship between abnormal mitochondrial metabolism and excessive ROS production in the early stages of ROSC. Regarding postresuscitation cardiac damage and oxidative injury lasting several days, the long-term effect of abnormal FAO on cardiac oxidative stress requires determination. Second, in our study, we focused on the effect of abnormal FAO on unsuitable mitochondrial FAO and glycolysis metabolites and superfluous ROS gener-

ation in cardiac mitochondria after ROSC in rats. Other pathways of cardiac mitochondrial metabolism, such as amino acid metabolism, have not been studied.

5. Conclusion

The inhibition of cardiac mitochondrial FAO mitigates abnormal cardiac ROS production and myocardial injury as well as effectively improves cardiac function, in part, by alleviating the mitochondrial metabolism disorder and uncoupled mitochondrial oxidative phosphorylation in a rat model of cardiac arrest.

Data Availability

The data used to support the findings of this study are available from the corresponding author upon request.

Conflicts of Interest

The authors declare that they have no conflicts of interest in the studies described.

Authors' Contributions

Acknowledgments

References

[1] S. S. Virani, A. Alonso, E. J. Benjamin et al., "Heart disease and stroke statistics-2020 update: a report from the American Heart Association," *Circulation*, vol. 141, no. 9, pp. e139–e596, 2020.

[2] F. Xu, Y. Zhang, and Y. Chen, "Cardiopulmonary resuscitation training in China: current situation and future development," *JAMA Cardiology*, vol. 2, no. 5, pp. 469-470, 2017.

[3] J. C. Jentzer, M. D. Chonde, and C. Dezfulian, "Myocardial dysfunction and shock after cardiac arrest," *BioMed Research International*, vol. 2015, Article ID 314796, 14 pages, 2015.

[4] D. Stub, S. Bernard, S. J. Duffy, and D. M. Kaye, "Post cardiac arrest syndrome: a review of therapeutic strategies," *Circulation*, vol. 123, no. 13, pp. 1428–1435, 2011.

[5] B. Ibáñez, G. Heusch, M. Ovize, and F. Van de Werf, "Evolving therapies for myocardial ischemia/reperfusion injury," *Journal of the American College of Cardiology*, vol. 65, no. 14, pp. 1454–1471, 2015.

[6] T. R. Matsuura, J. A. Bartos, A. Tsangaris et al., "Early effects of prolonged cardiac arrest and ischemic postconditioning during cardiopulmonary resuscitation on cardiac and brain mitochondrial function in pigs," *Resuscitation*, vol. 116, pp. 8–15, 2017.

[7] C. Penna, M. G. Perrelli, and P. Pagliaro, "Mitochondrial pathways, permeability transition pore, and redox signaling in cardioprotection: therapeutic implications," *Antioxidants & Redox Signaling*, vol. 18, no. 5, pp. 556–599, 2013.

[8] Y. Ma, W. Wang, T. Devarakonda et al., "Functional analysis of molecular and pharmacological modulators of mitochondrial fatty acid oxidation," *Scientific Reports*, vol. 10, no. 1, pp. 1450–1463, 2020.

[9] E. Murphy and C. Steenbergen, "Mechanisms underlying acute protection from cardiac ischemia-reperfusion injury," *Physiological Reviews*, vol. 88, no. 2, pp. 581–609, 2008.

[10] R. Moreno-Sánchez, L. Hernández-Esquivel, N. A. Rivero-Segura et al., "Reactive oxygen species are generated by the respiratory complex II–evidence for lack of contribution of the reverse electron flow in complex I," *The FEBS journal*, vol. 280, no. 3, pp. 927–938, 2013.

[11] E. T. Chouchani, V. R. Pell, E. Gaude et al., "Ischaemic accumulation of succinate controls reperfusion injury through mitochondrial ROS," *Nature*, vol. 280, no. 3, pp. 927–938, 2014.

[12] Q. Chen, A. K. Camara, D. F. Stowe, C. L. Hoppel, and E. J. Lesnefsky, "Modulation of electron transport protects cardiac mitochondria and decreases myocardial injury during ischemia and reperfusion," *American Journal of Physiology. Cell Physiology*, vol. 292, no. 1, pp. 137–147, 2007.

[13] L. Yao, P. Wang, M. Chen et al., "Carbon monoxide-releasing molecules attenuate postresuscitation myocardial injury and protect cardiac mitochondrial function by reducing the production of mitochondrial reactive oxygen species in a rat model of cardiac arrest," *Journal of Cardiovascular Pharmacology and Therapeutics*, vol. 20, no. 3, pp. 330–341, 2014.

[14] T. N. Andrienko, P. Pasdois, G. C. Pereira, M. J. Ovens, and A. P. Halestrap, "The role of succinate and ROS in reperfusion injury - a critical appraisal," *Journal of molecular and cellular cardiology*, vol. 110, pp. 1–14, 2017.

[15] J. Xu, H. Pan, X. Xie, J. Zhang, Y. Wang, and G. Yang, "Inhibiting succinate dehydrogenase by dimethyl malonate alleviates brain damage in a rat model of cardiac arrest," *Neuroscience*, vol. 393, no. 21, pp. 24–32, 2018.

[16] M. Heger, M. J. Reiniers, and R. F. van Golen, "Mitochondrial metabolomics unravel the primordial trigger of ischemia/reperfusion injury," *Gastroenterology*, vol. 148, no. 5, pp. 1071–1073, 2015.

[17] A. Nsiah-Sefaa and M. McKenzie, "Combined defects in oxidative phosphorylation and fatty acid beta-oxidation in mitochondrial disease," *Bioscience reports*, vol. 36, article e003113, 2016.

[18] D. Bargiela, S. P. Burr, and P. F. Chinnery, "Mitochondria and hypoxia: metabolic crosstalk in cell-fate decisions," *Trends in Endocrinology and Metabolism*, vol. 29, no. 4, pp. 249–259, 2018.

[19] R. Sun, D. Xu, Q. Wei et al., "Silybin ameliorates hepatic lipid accumulation and modulates global metabolism in an NAFLD mouse model," *Biomedicine & pharmacotherapy*, vol. 123, article 109721, 2020.

[20] R. C. Rabinovitch, B. Samborska, B. Faubert et al., "AMPK maintains cellular metabolic homeostasis through regulation of mitochondrial reactive oxygen species," *Cell Reports*, vol. 21, no. 1, pp. 1–9, 2017.

[21] G. D. Lopaschuk, J. R. Ussher, C. D. Folmes, J. S. Jaswal, and W. C. Stanley, "Myocardial fatty acid metabolism in health and disease," *Physiological Reviews*, vol. 90, no. 1, pp. 207–258, 2010.

[22] M. M. Adeva-Andany, N. Carneiro-Freire, M. Seco-Filgueira, C. Fernández-Fernández, and D. Mouriño-Bayolo, "Mitochondrial β-oxidation of saturated fatty acids in humans," *Mitochondrion*, vol. 46, pp. 73–90, 2019.

[23] R. W. Neumar, J. P. Nolan, C. Adrie et al., "Post-cardiac arrest syndrome: epidemiology, pathophysiology, treatment, and prognostication. A consensus statement from the International Liaison Committee on Resuscitation (American Heart Association, Australian and New Zealand Council on Resuscitation, European Resuscitation Council, Heart and Stroke Foundation of Canada, InterAmerican Heart Foundation, Resuscitation Council of Asia, and the Resuscitation Council of Southern Africa); the American Heart Association Emergency Cardiovascular Care Committee; the Council on Cardiovascular Surgery and Anesthesia; the Council on Cardiopulmonary, Perioperative, and Critical Care; the Council on Clinical Cardiology; and the Stroke Council," *Circulation*, vol. 118, no. 23, pp. 2452–2483, 2008.

[24] N. Goguadze, E. Zhuravliova, D. Morin, D. Mikeladze, and T. Maurice, "Sigma-1 receptor agonists induce oxidative stress in mitochondria and enhance complex I activity in physiological condition but protect against pathological oxidative stress," *Neurotoxicity Research*, vol. 35, no. 1, pp. 1–18, 2019.

[25] J. S. Jaswal, W. Keung, W. Wang, J. R. Ussher, and G. D. Lopaschuk, "Targeting fatty acid and carbohydrate oxidation–a novel therapeutic intervention in the ischemic and failing heart," *Biochimica et Biophysica Acta (BBA)-Molecular Cell Research*, vol. 1813, no. 7, pp. 1333–1350, 2011.

[26] J. L. Pohjoismaki and S. Goffart, "The role of mitochondria in cardiac development and protection," *Free radical biology & medicine*, vol. 106, pp. 345–354, 2017.

[27] S. Cadenas, "Mitochondrial uncoupling, ROS generation and cardioprotection," *Biochimica et biophysica acta Bioenergetics*, vol. 1859, no. 9, pp. 940–950, 2018.

[28] J. Jezek, K. F. Cooper, and R. Strich, "Reactive oxygen species and mitochondrial dynamics: the yin and yang of mitochondrial dysfunction and cancer progression," *Antioxidants*, vol. 7, no. 1, pp. 13–37, 2018.

[29] D. A. Chistiakov, T. P. Shkurat, A. A. Melnichenko, A. V. Grechko, and A. N. Orekhov, "The role of mitochondrial dysfunction in cardiovascular disease: a brief review," *Annals of Medicine*, vol. 50, no. 2, pp. 121–127, 2018.

[30] V. R. Pell, E. T. Chouchani, C. Frezza, M. P. Murphy, and T. Krieg, "Succinate metabolism: a new therapeutic target for myocardial reperfusion injury," *Cardiovascular Research*, vol. 111, no. 2, pp. 134–141, 2016.

Research Article

Effect of Hypovitaminosis D on Lipid Profile in Hypothyroid Patients in Saudi Arabia

Awad S. Alsamghan,[1] Safar A. Alsaleem,[1] Mohammed A. S. Alzahrani,[2] Ayyub Patel,[3] Ayaz K. Mallick,[3] and Salah A. Sheweita [ID][3,4]

[1]*Department of Family and Community Medicine, King Khalid University, Abha, Saudi Arabia*
[2]*Department of Medicine, King Khalid University, Abha, Saudi Arabia*
[3]*Department of Clinical Biochemistry, Faculty of Medicine, King Khalid University, Abha, Saudi Arabia*
[4]*Department of Biotechnology, Institute of Graduate Studies and Research, Alexandria University, Egypt*

Correspondence should be addressed to Salah A. Sheweita; ssheweita@yahoo.com

Background. Hypothyroidism is believed to be associated with dyslipidemia and is considered a risk factor for the development of atherosclerotic cardiovascular diseases (ASCVD). Vitamin D, due to its steroid hormone action, retains cell function and controls the metabolism of lipids. Therefore, the present study was carried out to show the association of the risk factors of ASCVD and deficiency of thyroid hormones and vitamin D levels since no previous studies have been performed on Saudi patients before. *Methodology.* A retrospective cohort study was carried out on 400 hypothyroid patients. Medical records of those patients were followed up and were classified as normal and hypothyroid patients according to their thyroid-stimulating hormone levels. TSH, vitamin D, and lipid profiles were determined using the ELISA technique. *Result.* Total cholesterol, triglyceride, and low-density lipoprotein cholesterol levels were significantly higher in hypothyroid patients than those in the normal group. We have found a significant correlation between TSH levels and the risk factors of ASCVD (total cholesterol, triglycerides, and LDL-C). Moreover, a significant correlation between vitamin D levels and the risk factors of ASCVD (total cholesterol, triglycerides, and LDL-C) has been found. In addition, there is a correlation between deficiency of Vit D and low-TSH levels (95% CI 1.092–4.05) indicating a higher risk for the development of ASCVD among those patients. *Conclusion.* Hypothyroid and vitamin D-deficient patients must be screened regularly at an early stage to predict and also to prevent cardiovascular diseases. Moreover, an adequate supply of vitamin D and TH should be given to those patients to prevent cardiovascular diseases at an early stage.

1. Introduction

Vitamin D insufficiency is associated with cardiometabolic risk factors such as obesity, insulin resistance, hypertension, dyslipidemia, and type 2 diabetes mellitus (DM) [1–3]. Vitamin D deficiency is a global issue occurring in about 30-50 percent of the population of varying age groups [4, 5]. In United States, Canada, and Australia, the mean serum vitamin D levels ranged between 20 and 30 ng/mL pointing towards vitamin D insufficiency [5]. In Brazil, the prevalence of hypovitaminosis D ranged between 5.7% and 52.9% in men over 18 years of age [4]. However, in spite of being a global concern, the reference values for assessment of vita-

min D status are controversial. The Brazilian Society of Endocrinology and Metabolism [4] and the Endocrine Society [6] define adequate vitamin D levels at 30 ng/mL, whereas the Institute of Medicine [7] defines it at 20 ng/mL. Apart from this, occupational practices also affect the vitamin D levels as lower levels were reported in night shift workers [8, 9].

Hypothyroidism is known to affect 4-10% of the population, and its incidence is stated to be as high as 10% [10–12]. It is characterised by low levels of thyroid hormones and elevated levels of thyroid-stimulating hormone (TSH). Reduced circulating thyroid hormones have various effects on the cardiovascular system such as decreased cardiac function due to

impaired activation of vascular smooth muscles and reduced supply of endothelial nitric oxide. This causes increased vascular resistance [13]. Triiodothyronine (T3) also stimulates the synthesis of renin substrate, hence influencing the renin-angiotensin-aldosterone pathway which in turn may increase the diastolic blood pressure [10].

Dyslipidemia is a chronic metabolic disorder with a negative impact not only on public health but also on the expenses of health care system [14]. Dyslipidemia is one of the leading causes of morbidity and mortality worldwide due to induction of atherosclerotic cardiovascular disease (ASCVD) [15]. It has been found that ASCVD alone is responsible for over 17 million deaths worldwide making it the most common cause of deaths [16]. Following this worldwide trend, the prevalence of dyslipidemia in Saudi Arabia is increasing since it has been reported that between 20 and 40% of Saudi population are dyslipidemic [17]. Numerous factors, such as sociodemographic, nutritional, and economic development and lifestyle patterns, are known to influence the metabolism of lipids and lipoproteins [18]. Thyroid hormones are believed to affect all major metabolic pathways, including lipid oxidation and metabolism control. They regulate the endothelial functions via thyroid hormone receptor- (THR-) 1 and THR-β. Activation of THR-α1 increases coronary blood flow, decreases coronary resistance in experimental models, and increases the development of nitric oxide in both the endothelial and vascular smooth muscle cells [18].

Downregulation of low-density lipoprotein cholesterol (LDL-C) receptor and iodination of high-density lipoprotein cholesterol (HDL-C) in subclinical hypothyroidism along with elevated total cholesterol significantly alters lipoprotein metabolism, leading to ASCVDD development [15, 19]. Also, decreased LDL-C receptor and cholesterol-α-monooxygenase production results in decreased LDL clearance [20].

Hypothyroidism and deficiency of vitamin D lead to hyperlipidemia, thereby raising the risk of cardiovascular diseases. Therefore, this study was performed to investigate the association of dyslipidemia with hypothyroid and/or hypovitaminosis D in Saudi patients since no previous studies have been shown on such relationships. Furthermore, the aim of this study is to focus on early identification of cardiovascular disease risk factors that could be prevented and/or alleviated by hypothyroidism treatment and/or vitamin D dietary supplementation.

2. Material and Methods

2.1. Study Design and Sample Size. This retrospective cohort study was planned and carried out in the Aseer region of the Kingdom of Saudi Arabia between March 2020 and April 2020 following the approval of the Institutional Ethical Committee. Six centres operated by thyroid clinics have been selected as the data collection source. The sample size for the study was determined to maintain a reasonable α error of 5% and β error of 0.80 (study power of 80%) with a confidence interval of 95 percent, which was estimated to be 400 cases. Diagnosis of hypothyroidism was conducted on the basis of clinical symptoms of hypothyroidism and serum thyroid-stimulating hormone (TSH) levels greater than 4.5 mIU/L. Newly diagnosed patients that have been in the clinic for the past year were randomly picked. In order to prevent the bias of the investigator, one resident, unaware of the study goals, was assigned to each centre to collect the necessary data from the patient file. Detailed scrutiny of patients with a history of diabetes mellitus, hypertension, renal disorders, and lipid-lowering medicines and vitamin D supplementation was removed from the study. The case records were followed from the time of diagnosis till the collection of data. Their last serum TSH, vitamin D, and fasting lipid profile were reported. Based on their TSH levels, they were classified into two groups: the euthyroid group with serum TSH between 0.5 and 4.5 mIU/L and the hypothyroid group with serum TSH greater than 4.5 mIU/L.

2.2. Grouping of the Participants. Based on the lipid profile of all participants, patients in the euthyroid and hypothyroid classes were further divided into two categories: a low- and a high-risk group. The basis for this classification was the LDL-C concentration as it has been identified as the primary therapeutic target for ASCVD by the National Cholesterol Education System–Adult Treatment Plan (NCEP-ATP) as set out in the guidelines provided by the American Heart Association (AHA) [21]. According to their guidelines, five categories have been defined, i.e., $LDL - C < 100$ mg/dL as ideal, 101–129 mg/dL as above optimum, 130 to 159 mg/dL as moderately high, 160 to 189 mg/dL as high, and 190 mg/dL as very high. In this study, all participants were divided into two groups for the convenience of statistical analysis. Participants with LDL-C up to 129 mg/dL were classified as low risk as this range was within the ideal range, and those with 130 mg/dL and above were at high risk for ASCVD. Similarly, based on the concentration of vitamin D, the participants were divided into two classes according to the recommendations laid down by the Endocrine Society's clinical guidelines [6]. Participants with vitamin D less than 29 ng/mL were classified as a vitamin D deficiency group and those above 30 ng/mL were classified as an adequate vitamin D group. The vitamin D deficiency category included both vitamin D deficiency (>20 ng/mL) and vitamin D insufficiency (21–29 ng/mL).

2.3. Biochemical Analysis. Serum total cholesterol (TC), serum triglyceride (TG), and high-density lipoprotein cholesterol (HDL-C) were determined by an enzymatic approach using commercially available kits and an automated analyser. Low-density lipoprotein cholesterol (LDL-C) was calculated using the Friedewald formula. Total vitamin D (25(OH) vitamin D) and serum TSH levels were determined using an electrochemiluminescence method.

2.4. Statistical Analysis. All the data obtained were collected and analysed using Statistical Package for Social Sciences (SPSS) version 25.0 (SPSS/PC; SPSS-25.0, Chicago, USA). Parameters of lipid profile, TSH, and vitamin D concentration were expressed as mean (SD). Significance of mean was studied using independent "t" test. Correlation between vitamin D and parameters of lipid profile in hypothyroid

patients was determined using Pearson's coefficient. Relative risk with 95% confidence interval was determined in order to study the effect of vitamin D deficiency on lipid profile among hypothyroid patients. A P value less than 0.05 was considered significant.

3. Results

Medical records of 400 patients were followed up, and based on their serum TSH levels, they were divided into two groups, the euthyroid group with 186 patients and the hypothyroid group with 214 patients. As seen in Table 1, the hypothyroid group consisted of 69.2% (148) females and 30.8% (66) males having a combined mean ± SD age of 45.09 ± 15.54 years as compared to 43.78 ± 15.63 years in the euthyroid group. The body mass index (BMI) was significantly higher in hypothyroid patients in comparison to euthyroid patients ($P < 0.001$). No clinical or statistical difference was seen in the systolic and/or diastolic blood pressure of euthyroid and hypothyroid patients (Table 1). The total serum cholesterol, serum triglyceride, LDL-C, and serum TSH levels were elevated in hypothyroid patients whereas the HDL-C was decreased compared to the euthyroid group. All these changes were statistically significant ($P < 0.05$) (Table 1). Hypothyroid male and female had an increased total cholesterol, serum triglyceride, serum LDL, LDL/HDL ratio, and serum TSH levels in comparison to euthyroid females which was statistically significant ($P < 0.05$) (Table 1). On comparing the vitamin D levels in males and females, it was found that females had a lower vitamin D levels in both the euthyroid ($P < 0.041$) and hypothyroid group ($P < 0.009$) whereas in males, it was comparable (Table 1). Comparisons of lipid profile with vitamin D and/or TSH levels in hypothyroid male and female patients were done and are summarized in Figures 1 and 2.

Gender-based correlation study on TSH and vitamin D with parameters of lipid profile was done in hypothyroid male and female patients (Figures 1 and 2). In order to study the correlation strength, Pearson correlation coefficient (r) was determined. Male hypothyroid patients showed a stronger positive correlation between TSH and total cholesterol ($r = 0.457$, $P < 0.001$) (Figure 1(a)), serum triglyceride ($r = 0.319$, $P = 0.009$) (Figure 1(b)) and LDL (0.481, $P < 0.001$) (Figure 1(c)). Hypothyroid females also showed a positive correlation between TSH and total cholesterol ($r = 0.375$, $P < 0.001$) (Figure 1(d)), serum triglyceride ($r = 0.303$, $P < 0.001$) (Figure 1(e)), and LDL (0.378, $P < 0.001$) (Figure 1(f)). In males, the Pearson correlation coefficient between vitamin D with total cholesterol, serum triglyceride, and LDL were -0.336 ($P = 0.006$), -0.320 ($P = 0.009$), -0.344 ($P = 0.005$) and -0.271 ($P = 0.028$) (Figures 2(a), 2(b), and 2(c)) as compared to -0.335 ($P < 0.001$), -0.226 ($P = 0.006$), -0.362 ($P < 0.001$) and -0.265 ($P = 0.001$) (Figures 2(d), 2(e), and 2(f)) respectively in females. A moderate to weak inverse but significant correlation was observed in male patients between vitamin D and increasing TSH (Figure 3(a)) and in females (Figure 3(b)). Interestingly, all these correlations were not found between these

parameters in either euthyroid male or female patients (Table 2).

In order to study the risk of ASCVD due to hypovitaminosis D in hypothyroid patients, relative risk was calculated. Based on the concentration of LDL-C on the basis of NCEP-ATP classification, the participants were divided into two groups: the low-risk group for ASCVD with LDL-C up to 129 mg/dL and the high risk group for ASCVD having a serum LDL-C greater than 130 mg/dL. The distribution of hypothyroid and euthyroid patients based on their LDL-C concentration is summarized in Table 3. As depicted in Table 3, 79.4% (170) hypothyroid patients had serum vitamin levels of less than 29 ng/mL and were classified either as either insufficient or deficient as compared to 78% (145) of the euthyroid group. Association of vitamin D deficiency and dyslipidemia in hypothyroid patients was evaluated by determining the relative risk ratio which was found to be 2.103 (95% CI 1.092 to 4.050) indicating that hypothyroid patients with lower vitamin D concentration was more likely to develop dyslipidemia.

4. Discussion

Endothelium, the target tissue of thyroid hormones, is adequately responsive to the changes in the level of thyroid hormones [22]. Cardiovascular disease (CVD) is caused by both clinical and subclinical hypothyroidism by disrupting healthy endothelial function by various mechanisms such as inflammation, triggering lipid disorders and oxidative stress [23–25]. In the present study, a strong correlation was observed between increasing TSH and the parameters of lipid profile. The levels of total cholesterol, triglyceride, and LDL-C were higher in the hypothyroid patients which might be due to inhibition of hepatic low-density lipoprotein (LDL) receptors and cholesterol alpha-monooxygenase activity, resulting in decreased clearance of LDL and total cholesterol [26]. Similar dyslipidemia patterns have recently been reported in conjunction with the current research [27, 28]. The decrease in clearance of LDL and total cholesterol in hypothyroid patients might be due to binding of T3 with the sterol regulatory element binding proteins (SREBP), which upregulate the synthesis of LDL receptors along with the regulatory enzymes of cholesterol synthesis, i.e., hydroxymethyl glutaryl CoA (HMG CoA). Therefore, in the absence of T3, the reduction of LDL-C receptors results in an increase in their circulatory levels [29]. In addition, hypothyroidism affects the expression and action of vasorelaxant and vasoconstrictor molecules which control the production of nitric oxide (NO) [24, 30, 31].

The mechanism of increase in the triglyceride level in hypothyroid patients might be attributed to the inhibition of lipoprotein lipase (LPL) activity, a triglyceride hydrolysing enzyme present in the capillary walls of adipose tissue [32–34]. Apart from LPL, a low level of thyroid hormones was found to decrease the activity of hepatic lipase (HL) and cholesterol ester transfer proteins (CETP) which play a crucial role in the reverse cholesterol pathway involving the anti-atherogenic HDL-C [32, 33].

TABLE 1: Changes in lipid profile, vitamin D, and thyroid stimulating hormone in hypothyroid male and female patients.

| | Male | | | Female | | |
	Euthyroid ($n = 61$)	Hypothyroid ($n = 66$)	Significance	Euthyroid ($n = 125$)	Hypothyroid ($n = 148$)	Significances
Age (years)	46.9 ± 17.35	46.5 ± 15.60	NS (0.90)	42.27 ± 14.56	44.45 ± 15.36	NS (0.233)
BMI	26.06 ± 2.41	29.37 ± 1.71	<0.001	27.07 ± 2.06	29.71 ± 1.94	<0.001
Systolic BP (mmHg)	125.88 ± 14.58	127.60 ± 14.26	NS (0.529)	122.21 ± 14.06	121.88 ± 16.43	NS (0.87)
Diastolic BP (mmHg)	73.88 ± 9.87	76.42 ± 9.87	NS (0.18)	73.09 ± 9.33	71.05 ± 9.65	NS (0.09)
Total cholesterol (mg/dL)	174.16 ± 40.40	193.94 ± 50.86	0.017	169.56 ± 32.20	185.34 ± 40.74	<0.001
Serum triglyceride (mg/dL)	131.80 ± 47.07	149.71 ± 66.17	NS (0.08)	122.29 ± 48.84	147.05 ± 58.93	<0.001
HDL-C (mg/dL)	43.97 ± 8.35	42.26 ± 8.82	0.265	45.14 ± 8.07	43.28 ± 9.49	NS (0.09)
LDL-C (mg/dL)	103.87 ± 34.91	121.74 ± 43.62	0.012	100.02 ± 29.58	112.67 ± 36.93	0.002
LDL/HDL ratio	2.42 ± 0.85	3.00 ± 1.23	0.003	2.286 ± .76	2.75 ± 1.13	<0.001
Vitamin D (ng/mL)	25.17 ± 15.73	24.00 ± 13.64	0.654	20.89 ± 11.96	19.26 ± 11.51	NS (0.65)
TSH mIU/L	1.98 ± 0.92	19.07 ± 14.32	<0.001	2.22 ± 1.01	15.79 ± 13.18	<0.001

(a)

(b)

(c)

(d)

(e)

(f)
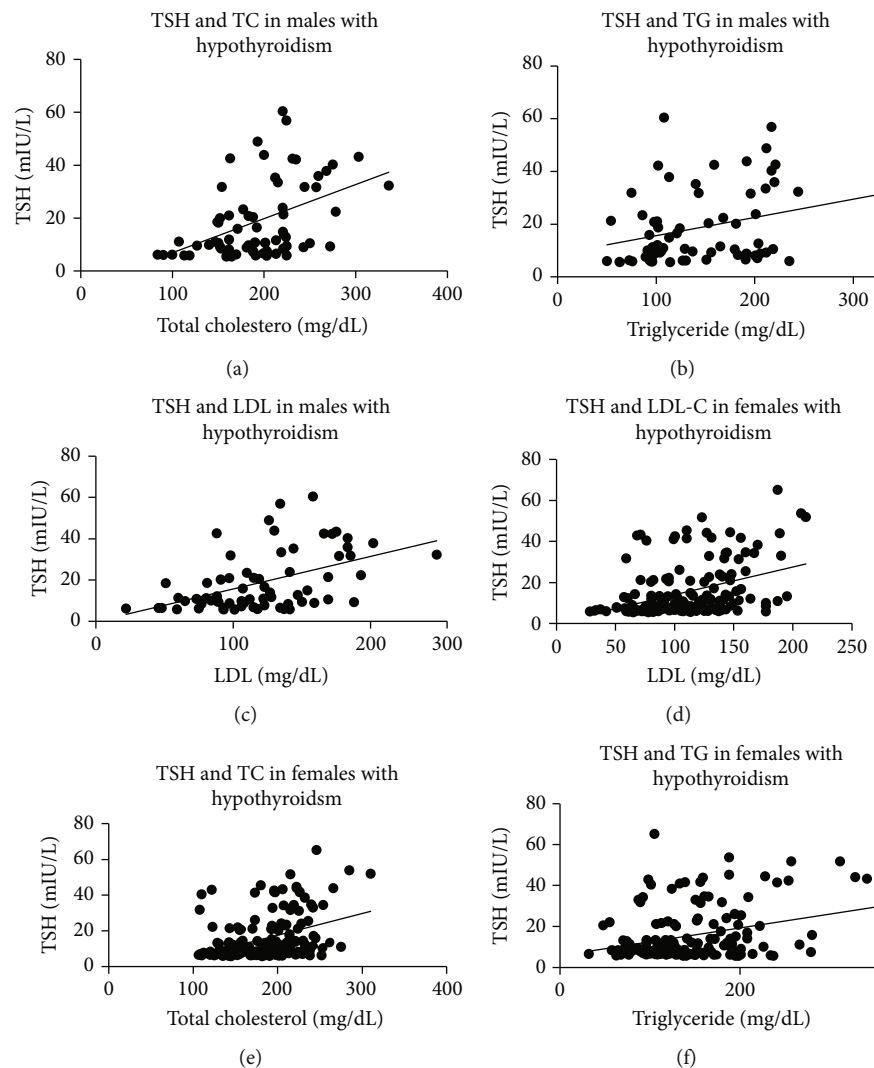
FIGURE 1: Correlations between thyroid stimulating hormone and lipid profile in hypothyroid male and female patients.
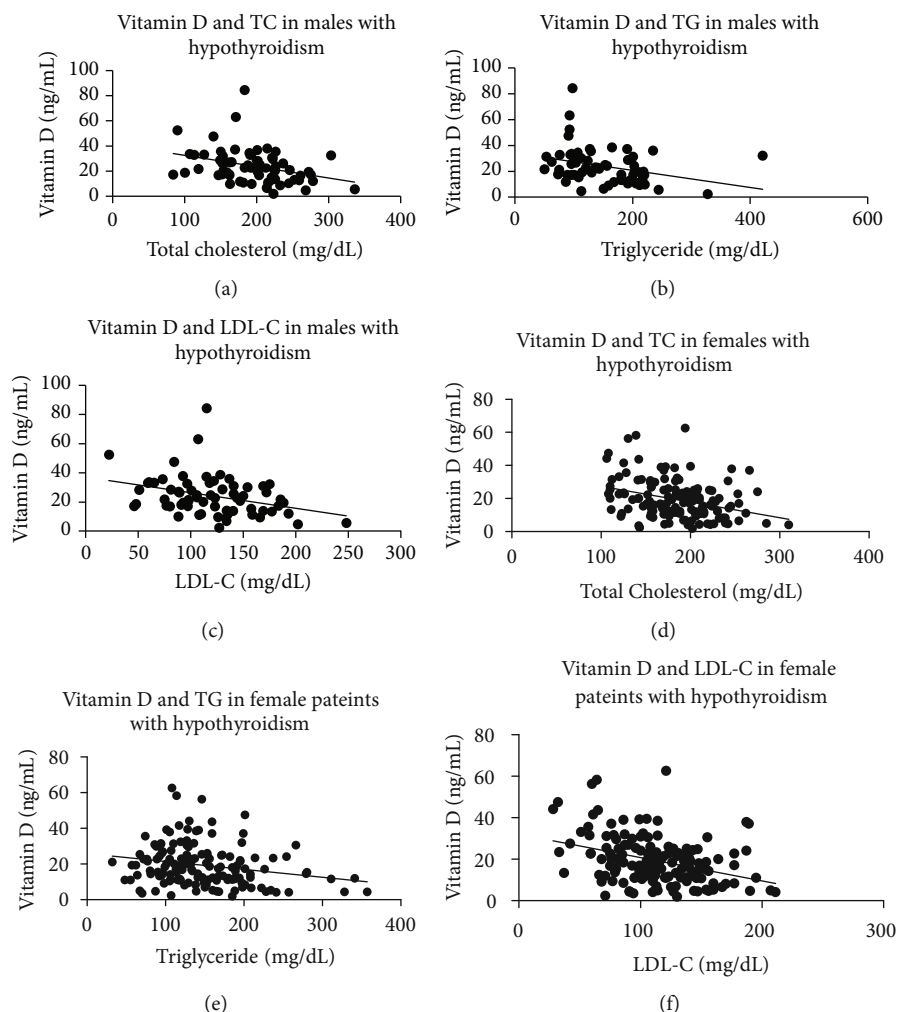
FIGURE 2: Correlations between vitamin D and lipid profile in hypothyroid male and female patients.

Various studies have shown a correlation between hypothyroidism and higher prevalence of obesity [35, 36]. Major weight gain has been associated with even a mild to moderate decrease in thyroid function. In regulating basal metabolism, thyroid hormones play a crucial role, thereby controlling the metabolism of glucose and lipids, the two key fuels for the body. BMI is categorized as healthy weight (BMI 18.5 to 24.9), overweight (BMI 25.0 to 29.9), and obese (BMI 30.0 and above) [37, 38]. In hypothyroid patients, various studies have reported contradictory results about BMI [39]. In this study, the hypothyroid patients had a significantly higher ($P < 0.005$) BMI in comparison to euthyroid patients. Although the exact mechanism by which hypothyroidism causes weight gain is still a matter of investigation, several hypotheses such as increased activity of deiodinase, role of leptin, inflammatory mediators from adipocytes have been postulated [40]. Therefore, obesity resulting from hypothyroidism itself may be a risk factor for development of CVD.

In the current study, vitamin D levels have been found to be lower and inversely correlated with the lipid profile, as vitamin D levels in both euthyroid and hypothyroid patients were below the normal range. Our results are in line with other published studies [41]. The mechanisms of the detri-

mental effect of reduced vitamin D levels on the lipid profile have been shown by numerous studies in particular on LDL-C and triglycerides [41]. Some of the mechanisms by which vitamin D provides cardioprotective action could be due to foam cell growth prevention, which could lead to rapid relaxation of cardiac myocytes after calcium efflux and nitric oxide release [42]. In support of our results, low vitamin D levels are associated with an increased risk of cardiovascular disease (CVD) and mortality in people with elevated lipid levels [43]. It was also observed that vitamin D inhibited the intracellular NF-κB pathway and in vitro renin synthesis and attenuated the progression of coronary artery disease [44–48]. This inhibition has been shown to reduce cardiovascular disease growth [49–51]. In addition, Al-Rasheed et al. showed that cholecalciferol administration significantly attenuated the production of induced cardiac hypertrophy in mice [52]. Vitamin D also controls cytokine levels, including interleukins (IL-6, IL-8, IL-17A, IL-10) and TGF, and inhibits the pathway of prostaglandins by reducing their receptors and reducing the expression of COX-2 [53]. The cardioprotective function of vitamin D, however, remains controversial, considering all these proposed mechanisms [54]. An inverse relationship between vitamin D and parathyroid hormone
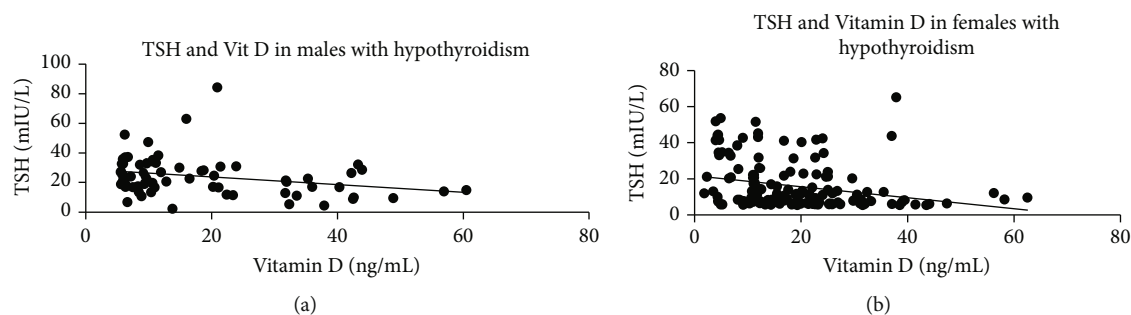
(a)

(b)

FIGURE 3: Correlations between TSH and vitamin D in hypothyroid male and female patients.

TABLE 2: Correlations between lipid profile and vitamin D and thyroid stimulating hormone in euthyroid male and female patients.

| | Male | | Female | |
	Pearson co-efficient (r)	P value	Pearson coefficient (r)	P value
TSH and total cholesterol	0.18	NS (0.16)	-0.05	NS (0.52)
TSH and serum triglyceride	-0.99	NS (0.19)	0.03	NS (0.73)
TSH and LDL-C	0.93	NS (0.13)	-0.01	NS (0.88)
TSH and vitamin D	-0.17	NS (0.89)	-0.11	NS (0.22)
Vitamin D and total cholesterol	-0.05	NS (0.68)	-0.04	NS (0.68)
Vitamin D and serum triglyceride	-0.24	NS (0.06)	-0.02	NS (0.812)
Vitamin D and LDL-C	-0.08	NS (0.55)	-0.02	NS (0.86)

TABLE 3: A cross-tabulation showing number of participants and relative risk with a 95% confidence interval between vitamin D deficiency and development of high-risk dyslipidemia among the euthyroid and hypothyroid groups.

| Vitamin D levels | Dyslipidemia | | Relative risk | 95% confidence interval |
	High risk	Low risk		
Euthyroid group (n = 186)				
Deficiency (n = 145)	22	123	0.622	0.32–1.20
Sufficient (n = 41)	10	31		
Hypothyroid group (n = 214)				
Deficiency (n = 170)	65	105	2.10	1.09–4.05
Sufficient (n = 44)	8	36		

(PTH) indicates that hypovitaminosis D may have an indirect effect on CVD. PTH could play a very relevant role in the production of CVD because PTH receptors are abundantly present in cardiac cells and vessels [54].

While conflicting conclusions have been recorded in several observational studies, there appears to be a correlation between vitamin D deficiencies and hypothyroidism. The fact that hypovitaminosis D results in the formation of cytokines and antibodies against thyroid receptors has explained this conflict [55]. It was found in this study that both euthy-

roid and hypothyroid patients had vitamin D levels below the normal range. The goal of this study was to investigate the increased risk of ASCVD in hypothyroid patients with hypovitaminosis D because both hypothyroidism and vitamin D deficiency are risk factors for hyperlipidemia development. In this study, it was observed that decreases in vitamin D were correlated with increases in total cholesterol, serum triglycerides, and LDL-C in hypothyroid patients, thus signifying their role in CVD development. Although the intensity of the association was mild and statistically relevant, these results are important since hypothyroid patients are already at risk for CVD. Since LDL-C is the primary objective of the National Cholesterol Education Program Adult Treatment Plan (NCEP ATP) for the treatment of dyslipidemia, participants were classified as a high-risk group ($LDL - C > 130$ mg/dL) and those below 130 mg/dL were classified as a low-risk group. As shown in the present study, the relative risk of ASCVD for the hypothyroid community with hypovitaminosis D (2.103, 95% CI 1.092-4.050) was greater than that of the euthyroid group and significantly increased the risk of ASCVD among hypothyroid patients.

5. Conclusion

Hypothyroidism and hypovitaminosis D are known as independent risk factors for the development of cardiovascular diseases. Hypothyroidism and hypovitaminosis D are associated and correlated with total cholesterol, triglycerides, and low-density lipoprotein in Saudi patients. It is also recommended that vitamin D deficiency be checked in hypothyroid

patients and that appropriate supplementation may be given if needed. Furthermore, for early detection and/or prediction of cardiovascular disease, screening of thyroid hormone and vitamin D levels should be undertaken at an early stage.

Data Availability

All data are available and included in the text.

Conflicts of Interest

The authors declare that they have no conflicts of interest.

References

[1] A. Gul, S. Ozer, R. Yılmaz et al., "Association between vitamin D levels and cardiovascular risk factors in obese children and adolescents," *Nutrición Hospitalaria*, vol. 34, no. 2, pp. 323–329, 2017.

[2] A. Mousa, N. Naderpoor, M. P. de Courten, R. Scragg, and B. de Courten, "25-Hydroxyvitamin D is associated with adiposity and cardiometabolic risk factors in a predominantly vitamin D-deficient and overweight/obese but otherwise healthy cohort," *The Journal of Steroid Biochemistry and Molecular Biology*, vol. 173, pp. 258–264, 2017.

[3] L. C. Milagres, N. P. Rocha, M. S. Filgueiras et al., "Vitamin D insufficiency/deficiency is associated with insulin resistance in Brazilian children, regardless of body fat distribution," *Public Health Nutrition*, vol. 20, no. 16, pp. 2878–2886, 2017.

[4] S. S. Maeda, V. Z. C. Borba, M. B. R. Camargo et al., "Recomendações da Sociedade Brasileira de Endocrinologia e Metabologia (SBEM) para o diagnóstico e tratamento da hipovitaminose D," *Arquivos Brasileiros de Endocrinologia & Metabologia*, vol. 58, no. 5, pp. 411–433, 2014.

[5] D. Wahl, C. Cooper, P. Ebeling et al., "A global representation of vitamin D status in healthy populations," *Archives of Osteoporosis*, vol. 7, no. 1-2, pp. 155–172, 2012.

[6] M. F. Holick, N. C. Binkley, H. A. Bischoff-Ferrari et al., "Evaluation, treatment, and prevention of vitamin D deficiency: an Endocrine Society clinical practice guideline," *The Journal of Clinical Endocrinology & Metabolism*, vol. 96, no. 7, pp. 1911–1930, 2011.

[7] A. C. Ross, J. E. Manson, S. A. Abrams et al., "The 2011 report on dietary reference intakes for calcium and vitamin D from the Institute of Medicine: what clinicians need to know," *The Journal of Clinical Endocrinology & Metabolism*, vol. 96, no. 1, pp. 53–58, 2011.

[8] E. Alefishat and R. A. Farha, "Determinants of vitamin D status among Jordanian employees: focus on the night shift effect," *International Journal of Occupational Medicine and Environmental Health*, vol. 29, no. 5, pp. 859–870, 2016.

[9] D. Sowah, X. Fan, L. Dennett, R. Hagtvedt, and S. Straube, "Vitamin D levels and deficiency with different occupations: a systematic review," *BMC Public Health*, vol. 17, no. 1, p. 519, 2017.

[10] I. Klein and S. Danzi, "Thyroid disease and the heart," *Circulation*, vol. 116, no. 15, pp. 1725–1735, 2007.

[11] S. Razvi, A. Shakoor, M. Vanderpump, J. U. Weaver, and S. H. Pearce, "The influence of age on the relationship between subclinical hypothyroidism and ischemic heart disease: a metaanalysis," *The Journal of Clinical Endocrinology & Metabolism*, vol. 93, no. 8, pp. 2998–3007, 2008.

[12] N. Ochs, R. Auer, D. C. Bauer et al., "Meta-analysis: subclinical thyroid dysfunction and the risk for coronary heart disease and mortality," *Annals of Internal Medicine*, vol. 148, no. 11, pp. 832–845, 2008.

[13] M. Udovcic, R. H. Pena, B. Patham, L. Tabatabai, and A. Kansara, "Hypothyroidism and the heart," *Methodist DeBakey Cardiovascular Journal*, vol. 13, no. 2, pp. 55–59, 2017.

[14] S. Sheweita, H. Baghdadi, and A. Allam, "Role of genetic changes in the progression of cardiovascular diseases," *International journal of biomedical science: IJBS*, vol. 7, no. 4, pp. 238–248, 2011.

[15] X. Jiang, M. Peng, S. Chen, S. Wu, and W. Zhang, "Vitamin D deficiency is associated with dyslipidemia: a cross-sectional study in 3788 subjects," *Current Medical Research and Opinion*, vol. 35, no. 6, pp. 1059–1063, 2019.

[16] P. Balakumar, K. Maung-U, and G. Jagadeesh, "Prevalence and prevention of cardiovascular disease and diabetes mellitus," *Pharmacological Research*, vol. 113, no. Part A, pp. 600–609, 2016.

[17] S. al-Ghamdi, M. M. Shubair, A. Aldiab et al., "Prevalence of overweight and obesity based on the body mass index; a cross-sectional study in Alkharj, Saudi Arabia," *Lipids in Health and Disease*, vol. 17, no. 1, p. 134, 2018.

[18] S. Opoku, Y. Gan, W. Fu et al., "Prevalence and risk factors for dyslipidemia among adults in rural and urban China: findings from the China National Stroke Screening and Prevention Project (CNSSPP)," *BMC Public Health*, vol. 19, no. 1, p. 1500, 2019.

[19] L. H. Duntas and G. Brenta, "The effect of thyroid disorders on lipid levels and metabolism," *Medical Clinics of North America*, vol. 96, no. 2, pp. 269–281, 2012.

[20] A. Jabbar, A. Pingitore, S. H. Pearce, A. Zaman, G. Iervasi, and S. Razvi, "Thyroid hormones and cardiovascular disease," *Nature Reviews Cardiology*, vol. 14, no. 1, pp. 39–55, 2017.

[21] A. K. Mallick and M. Ahsan, "Evaluation and interpretation of lipid profile based on the national cholesterol education programme adult treatment panel III guidelines," *Indian Journal of Medical & Health Sciences*, vol. 2, no. 2, pp. 129–135, 2016.

[22] T. Ichiki, "Thyroid hormone and vascular remodeling," *Journal of Atherosclerosis and Thrombosis*, vol. 23, no. 3, pp. 266–275, 2016.

[23] E. E. Türemen, B. Çetinarslan, T. Sahin, Z. Cantürk, and I. Tarkun, "Endothelial dysfunction and low grade chronic inflammation in subclinical hypothyroidism due to autoimmune thyroiditis," *Endocrine Journal*, vol. 58, no. 5, pp. 349–354, 2011.

[24] A. Kumar, D. Suresh, V. Annam, and R. Srikrishna, "Significance of early biochemical markers of atherosclerosis in subclinical hypothyroidism patients with normal lipid profile," *International Journal of Biological and Medical Research*, vol. 3, no. 4, pp. 2483–2486, 2012.

[25] E. Cebeci, F. Alibaz-Oner, M. Usta, S. Yurdakul, and M. Erguney, "Evaluation of oxidative stress, the activities of paraoxonase and arylesterase in patients with subclinical hypothyroidism," *Journal of Investigative Medicine*, vol. 60, no. 1, pp. 23–28, 2015.

[26] L. H. Duntas, "Thyroid disease and lipids," *Thyroid*, vol. 12, no. 4, pp. 287–293, 2002.

[27] A. Hussain, A. M. Elmahdawi, N. E.-H. Elzeraidi, F. Nouh, and K. Algathafi, "The effects of dyslipidemia in subclinical hypothyroidism," *Cureus*, vol. 11, no. 11, 2019.

[28] M. B. Hiregoudar, P. Mohantypm, S. Tripatys, A. Kerketta, U. K. Soren, and S. K. Sukla, "Clinical profile and lipid abnormalities in subclinical and overt primary hypothyroidism," *International Journal of Research in Medical Sciences*, vol. 7, pp. 2003–2008, 2019.

[29] C. Rizos, M. Elisaf, and E. Liberopoulos, "Effects of thyroid dysfunction on lipid profile," *The Open Cardiovascular Medicine Journal*, vol. 5, no. 1, pp. 76–84, 2011.

[30] A. L. de Castro, A. V. Tavares, R. O. Fernandes et al., "T3 and T4 decrease ROS levels and increase endothelial nitric oxide synthase expression in the myocardium of infarcted rats," *Molecular and Cellular Biochemistry*, vol. 408, no. 1-2, pp. 235–243, 2015.

[31] Y. Cai, M. M. Manio, G. P. Leung, A. Xu, E. H. Tang, and P. M. Vanhoutte, "Thyroid hormone affects both endothelial and vascular smooth muscle cells in rat arteries," *European Journal of Pharmacology*, vol. 747, pp. 18–28, 2015.

[32] R. Sabharwal, P. Mahajan, and A. Bhatia, "Association of subclinical hypothyroidism with dyslipidemia," *JK Science*, vol. 19, no. 2, pp. 81–84, 2017.

[33] M. D. S. Filgueiras, L. G. Suhett, M. A. Silva, N. P. Rocha, and J. F. de Novaes, "Lower vitamin D intake is associated with low HDL cholesterol and vitamin D insufficiency/deficiency in Brazilian children," *Public Health Nutrition*, vol. 21, no. 11, pp. 2004–2012, 2018.

[34] R. A. Sinha, B. K. Singh, and P. M. Yen, "Direct effects of thyroid hormones on hepatic lipid metabolism," *Nature Reviews Endocrinology*, vol. 14, no. 5, pp. 259–269, 2018.

[35] C. M. Moulin de Moraes, M. C. Mancini, M. E. de Melo et al., "Prevalence of subclinical hypothyroidism in a morbidly obese population and improvement after weight loss induced by Roux-en-Y gastric bypass," *Obesity Surgery*, vol. 15, no. 9, pp. 1287–1291, 2005.

[36] P. K. Nayak, S. Mitra, J. Sahoo, E. Mahapatra, S. Agrawal, and Z. Lone, "Relationship of subclinical hypothyroidism and obesity in polycystic ovarian syndrome patients," *Journal of Family Medicine and Primary Care*, vol. 9, no. 1, pp. 147–150, 2020.

[37] M. Ashwell, P. Gunn, and S. Gibson, "Waist-to-height ratio is a better screening tool than waist circumference and BMI for adult cardiometabolic risk factors: systematic review and meta-analysis," *Obesity Reviews*, vol. 13, no. 3, pp. 275–286, 2012.

[38] A. Chandrasekaran, "Body mass index-is it reliable indicator of obesity," *Journal of Nutrition & Weight Loss*, vol. 3, no. 1, p. 2, 2018.

[39] A. Milionis and C. Milionis, "Correlation between body mass index and thyroid function in euthyroid individuals in Greece," *ISRN Biomarkers*, vol. 2013, Article ID 651494, 7 pages, 2013.

[40] S. Longhi and G. Radetti, "Thyroid function and obesity," *Journal of Clinical Research in Pediatric Endocrinology*, vol. 5, Supplement 1, p. 40, 2013.

[41] A. M. Mackawy, B. M. Al-Ayed, and B. M. Al-Rashidi, "*Vitamin d deficiency and its association with thyroid disease. Int J Health Sci (Qassim)*," vol. 7, no. 3, pp. 267–275, 2013.

[42] P. Prasad and A. Kochhar, "Interplay of vitamin D and metabolic syndrome: a review," *Diabetes & Metabolic Syndrome: Clinical Research & Reviews*, vol. 10, no. 2, pp. 105–112, 2016.

[43] S. Savastio, E. Pozzi, F. Tagliaferri et al., "Vitamin D and cardiovascular risk: which implications in children?," *International Journal of Molecular Sciences*, vol. 21, no. 10, p. 3536, 2020.

[44] J. Sun, J. Kong, Y. Duan et al., "Increased NF-κB activity in fibroblasts lacking the vitamin D receptor," *American Journal of Physiology-Endocrinology and Metabolism*, vol. 291, no. 2, pp. E315–E322, 2006.

[45] Z. Janjetovic, M. A. Zmijewski, R. C. Tuckey et al., "20-Hydroxycholecalciferol, product of vitamin D3 hydroxylation by P450scc, decreases NF-κB activity by increasing IκBα levels in human keratinocytes," *PLoS One*, vol. 4, no. 6, p. ???, 2009.

[46] Y. Chen, J. Kong, T. Sun et al., "1,25-Dihydroxyvitamin D_3 suppresses inflammation-induced expression of plasminogen activator inhibitor-1 by blocking nuclear factor-κB activation," *Archives of Biochemistry and Biophysics*, vol. 507, no. 2, pp. 241–247, 2011.

[47] S. Chen, V. J. Swier, C. S. Boosani, M. M. Radwan, and D. K. Agrawal, "Vitamin D deficiency accelerates coronary artery disease progression in swine," *Arteriosclerosis, Thrombosis, and Vascular Biology*, vol. 36, no. 8, pp. 1651–1659, 2016.

[48] R. K. Al-Ishaq, P. Kubatka, M. Brozmanova, K. Gazdikova, M. Caprnda, and D. Büsselberg, "Health implication of vitamin D on the cardiovascular and the renal system," *Archives of Physiology and Biochemistry*, pp. 1–15, 2019.

[49] G. Valen, "Nuclear factor kappa-B and the heart," *Journal of the American College of Cardiology*, vol. 38, no. 2, pp. 307–314, 2001.

[50] C. C. Low Wang, C. N. Hess, W. R. Hiatt, and A. B. Goldfine, "Clinical update: cardiovascular disease in diabetes mellitus: atherosclerotic cardiovascular disease and heart failure in type 2 diabetes mellitus–mechanisms, management, and clinical considerations," *Circulation*, vol. 133, no. 24, pp. 2459–2502, 2016.

[51] H. Derakhshanian, A. Djazayery, M. H. Javanbakht et al., "Vitamin D downregulates key genes of diabetes complications in cardiomyocyte," *Journal of Cellular Physiology*, vol. 234, no. 11, pp. 21352–21358, 2019.

[52] N. M. al-Rasheed, N. M. al-Rasheed, Y. A. Bassiouni et al., "Vitamin D attenuates pro-inflammatory TNF-α cytokine expression by inhibiting NF-κB/p 65 signaling in hypertrophied rat hearts," *Journal of Physiology and Biochemistry*, vol. 71, no. 2, pp. 289–299, 2015.

[53] W. Liu, L. Zhang, H.-J. Xu et al., "The anti-inflammatory effects of vitamin D in tumorigenesis," *International Journal of Molecular Sciences*, vol. 19, no. 9, p. 2736, 2018.

[54] A. V. Pascale, R. Finelli, R. Giannotti et al., "Vitamin D, parathyroid hormone and cardiovascular risk: the good, the bad and the ugly," *Journal of Cardiovascular Medicine (Hagerstown, Md.)*, vol. 19, no. 2, pp. 62–66, 2018.

[55] G. Muscogiuri, G. Tirabassi, G. Bizzaro et al., "Vitamin D and thyroid disease: to D or not to D?," *European Journal of Clinical Nutrition*, vol. 69, no. 3, pp. 291–296, 2015.